Department of Precision and Microsystems Engineering

The design, build and verification of Forcesix: a measurement setup capable of observing low-level flow-induced vibration forces in 6-DOF.

A.A. de Wildt

Report no	:	MSD 2021.053
Coach	:	Dr. ir. J. Rommers
Professor	:	Prof. dr. ir. J.L. Herder
Specialisation	:	Mechatronic System Design
Type of report	:	Master Thesis
Date	:	24 August 2021

CONFIDENTIAL

The design, build and verification of the Forcesix measurement setup

capable of observing low-level flow-induced vibration forces in 6-DOF

by

Arjan de Wildt

in partial fulfillment of the requirements for the degree of

Master of Science

in Mechanical Engineering

at the Delft University of Technology,
to be defended publicly on August 24, 2021 at 12:00 AM.

Student number:	1319094	
Report number:	MSD 2021.053	
Thesis committee:	Prof. dr. ir. J.L. Herder,	Chairman
	Dr. ir. J. Rommers,	Supervisor
	Dr. ir. J.F.L. Goosen,	Reader

This thesis is confidential and cannot be made public until August 24, 2023.

Delft University of Technology

I dedicate this work to my mother, Annemieke.
Her willpower and optimism have inspired me beyond words.

Abstract

With the development of its innovative e-beam lithography tool -called Matrix- Mapper is pushing the boundaries of existing technology in many ways. Patterning by means of focused electron currents requires extreme precision and overlay characteristics on a scale almost unimaginable. With in-plane stage-stability requirements of approximately 1/100.000th of a human hair, every disturbance is problematic. To this end, a variety of cutting-edge solutions have been implemented that shield or correct for environmental influences.

A remaining issue for Mapper and motivation behind this project is a heat problem that arises in the process of scaling up the number of used electron beams. This generated heat limits node-size and throughput of the Matrix-tool, both of which are important for Mapper's technology to become viable. As a solution, water-cooled structures have been designed and implemented to remove the roughly 2.5 kW of excess heat. This turbulent water flow however, causes flow-induced-vibrations that again result in wafer error.

Flow-induced vibrations (FIV) is the phenomenon that couples the domains of fluid mechanics and vibration engineering. This makes it highly empirical and difficult to predict by means of model simulations. To get a good understanding of the full impact of these FIV, a tool is thus required that can perform verification measurements on relevant modules which are located inside the Metro-Optics Frame (MOF). *Therefore, the goal of this study is to develop a measurement setup that can accommodate these modules and accurately observe the induced cooling forces.*

Overall objective of this tool is to verify the stage-stability requirements set for the Matrix-machine with regards to FIV. This requires measuring in 6-DOF, over a wide frequency range (10 – 300 Hz) and at a very low noise level ($\approx 10^{-11} N^2/Hz$). Additionally, the measured force spectrum can be used to reduce the negative effect of FIV on patterning accuracy, by strategically modifying cooling geometries. Most challenging for this design is to be able to observe the FIV while in the presence of a variety of dominant environmental disturbances.

The first step in designing the measurement setup is to re-budget stage stability error tolerances based on cooling characteristics per module. Next, spectral force requirements are derived from these wafer error values by modeling relevant Matrix dynamics. *All further design choices are based on the design's ability to meet these requirements.*

To predict the effect of various interference sources on the accuracy of the design, they are quantified by performing environmental measurements. A dynamic error budgeting model is created and validated to simulate the effect of these floor accelerations, supply tubing induced flow vibrations and acoustical sound pressure levels, amongst others.

Based on the model results, strategic design choices are made that ensure sufficient:

- attenuation of floor vibrations
- shielding of environmental acoustics
- reduction of FIV in supply tubing
- signal ratio by a high axial stiffness train
- low spectral noise floor (at requirement level)

The final design "Forcesix" consists of a mass-optimized triple mass-spring-damper (MSD) system, weighting 828 kg. It uses six low-noise piezoelectric force transducers to observe the 6-DOF reaction-forces exerted by the modules. These modules under testing are supported by the piezos through custom designed stiff-flexible struts with a high axial/radial stiffness ratio. This improves measured signal and protects the piezos from damaging bending moments. This sensitive part of the measurement setup is isolated from floor vibrations by a double MSD Vibration Isolation (VI) platform (granite stones on airmounts). Acoustic shielding has been achieved by a custom designed enclosure that disconnects at the bottom granite stone. Flow vibrations in the supply tubing are discharged at various stages. Water flow is provided under constant pressure and flow rate by a hydrostatic pressure vessel. This prevents measuring distinct resonances from asynchronous motor characteristics inherent to a centrifugal pump. Verification measurements have been performed showing a noise floor characteristic at the level of the theoretically predicted effect of all disturbances combined ($2.5 \cdot 10^{-11} N^2/Hz$).

The main findings of this study are:

- when aiming to measure very low-level reaction forces ($\pm$ 0.35 μN-rms) in the presence of dominant disturbances that transmit through parasitic stiffnesses, quartz piezoelectric sensors proof to be a better solution when compared to (seismic) accelerometers.
- flow vibrations induced in supply tubing can have a significant impact on the measured signal, if the stiffness train that connects the sensor with the measurement setup is relatively low. An effective method to minimize this disturbance is to discharge the bulk of the input to different stages of the vibration isolation platform, if present.
- of all disturbances, environmental acoustics have shown to be most difficult to shield. The most effective means of reducing its effect is to fully enclose the sensitive part of the measurement setup and to rigidly connect this casing to a heavy mass with an attractive transfer path to the sensor e.g. the bottom stage of a two MSD VI platform.
- when measuring direct forces using sensitive piezoelectric sensors that cannot withstand transverse loading / bending moments, stiff-flexible support struts with a high axial/radial stiffness ratio (roughly $\geq$ 500) are found to be a solution.

Concluding, although the application for which Forcesix has been developed is highly specific, this research also contributes to scientific knowledge of experimental characterization of FIV in a broader sense. To the best of authors' knowledge, this is namely the first study that measures the 6-DOF reaction forces of complex geometries due to FIV, at a very low-noise level. Moreover, the design process detailed in this thesis describes a method on how to effectively design such a measurement system, while in the presence of a variety of disturbances. Generic design guidelines that can serve as a reference are listed in Appendix B-3.

"**This is the real secret to life** — to be completely engaged with what you are doing in the here and now. And instead of calling it work, realize it is play."

— *Alan Watts*

Acknowledgements

At last! My thesis is finished!

After a long and difficult period with many physical problems, I am now extremely happy and proud that I have managed to finish what seemed impossible at times. I could not have done this without the help of so many people for which I would like to express my gratitude.

My wife Anita, first and foremost. You have always been there for me and I cannot thank you enough for that! Your unwavering support and trust, even under very difficult conditions, has made all the difference. Thank you so much for your patience over the years and giving me the space to bring this to a successful end.

To my father and my brothers, thank you so much for your help over the years! You have really shown me what family actually means. In particular Wouter, for helping me get started again when I felt stuck - it gave me the kickstart I needed. Niek and Dani for helping out with Olivia whenever!

Special thanks to my supervisor Jelle, for sticking with me! Your daily support and positive feedback has helped me a lot! My professor, Just Herder, for keeping an open mind and allowing me to take an unconventional route.

Also I would like to thank Rogier Ellenbroek, my supervisor at the time at Mapper. Your feedback was always on-point and I have learned a lot from you. Dennis Lakerveld, colleague at the time, for helping me get on my way and continuing his research.

And lastly a big thanks to my friends, Emiel and Luc for the many in-depth discussions and reviewing.

Contents

III RESULTS

IV APPENDIX

Part I

BACKGROUND

Chapter 1

Introduction

1.1 Market Research

1.1.1 Semiconductor Industry

For decades, technological advancements have been progressing at an exponential rate. Only in recent years however, the effects of this growth have become more apparent (Kurzweil, 2006). All over the world and in virtually every area, innovations in technology are now taking place at an unprecedented level. Today's society has gotten used to this rate of progress and is craving for smaller, faster and cheaper electronics. With chips being at the heart of all phones, laptops and tablets, the pressure is on the industry to produce these integrated circuits (ICs) with increasingly greater resolution and smaller overlay (layer-to-layer alignment).

The Divide

The semiconductor industry can be divided in two parts. There is the high-end segment where major companies such as TSMC, Intel, Samsung and Global Foundries annually invest billions to create IC microprocessors and integrated memory chips(ets) for smart devices such as laptops and smartphones. Then for the less critical applications, companies like Micron, Toshiba, Sandisk and NXP produce the hardware required for Flash Logic, MEMS, CMOS and LED devices. The sub-division high- and low-end is made based on the feature size that is imaged on a die in order to produce transistors that make up a chip. The smaller these features, the faster and more energy-efficient an equal-sized chip will result. Clearly, smaller transistors are harder to manufacture and require a more complex and expensive machine to build. *This thesis focuses on a specific tool designed to operate in the high-end segment of the market and deals with a problem that arises when going to smaller feature sizes.*

Chip Production

The production of chips takes place in highly complex and expensive (10-20 B$) production facilities, so called fab's or foundry's (EETimes, 2017). These specialized mega factories accomodate hundreds of complex machinery, each of which performs a specific task in the process of making a chip. The most crucial step in this process is that of photolithography: the frequent exposure of thin silicium plates by a high-energy light source, alternated by chemical treatment of these wafers. Eventually, various different light patterns create three-dimensional structures called transistors. These are the basic building blocks that can be used to do calculations with, by passing a current through them. Once cleverly combined and stacked onto a small surface, billions of such transistors together form a chip - the brain of every intelligent device. The interested reader can learn more about this in Intel (2012).

Clearly, there are many more aspects besides patterning involved in the process of making a chip, such as deposition, etching, cleaning, doping, dicing and packaging. However the lithography step is most difficult and thus important to the fab's production volume and overall duration of the process - thereby determining the cost of the chip ("price per die"). The entire manufacturing process takes about 3 months for modern 7/10/14 nm nodes due to the high number of exposures required (LaPedus, 2017). This stresses the importance of *throughput* ("wafers per hour") and *reliability* ("percentage uptime") characteristics.

The new technology this thesis revolves around, experiences difficulty with both key factors.

ASML's Twinscan

A basic explanation of the lithography tools that are being developed by ASML would be that it is essentially a projection system. Light of a certain wavelength is passed through a blueprint of the pattern ("reticle") that needs to be imaged. With this pattern information now encoded in the light, it can be shrunk in size, focussed and projected onto a wafer. This process is repeated over and over until the desired 3D structure results.

For many years now, ASML has been world market leader when it comes to the production of litho tools that are used industry-wide. Up to the year 2000, Japanese competitors Nikon and Canon still had a significant market share (15-40%), but as technology progressed they couldn't keep up. Nowadays ASML dominates with an overall market share of about 85% across all production nodes - even supplying 100% for the high-end segment (Moody's, 2018). The change in market dominance occured as ASML introduced its TWINSCAN system with dual-stage technology in 2001. This allowed for parallel measuring, alignment and exposure of wafers by 193 nm light, produced by an ArF excimer laser. Not only is this deep ultraviolet (DUV) platform still in use today, it manufactures most of the semiconductor products available. This is the result of ASML's constant quest to being able to image smaller features with the same light source (ASML, 2019a). Today's NXT machines are able to image sub-13 nm patterns at a throughput of 275 Wph while keeping overlay requirements below 2.0 nm.

These numbers define the challenge for any newcomers on the market to be competitive.

Figure 1.1: Illustration of the ASML TWINSCAN NXT-series

1.1.2 Future Innovations

This subsection discusses one of the most important indicators of progress in the lithography sector. It presents how global innovation leader ASML aims to meet the goals that result from this. Also a new competitor in the market is introduced and its technology briefly explained.

Moore's Law

In order to meet market's demands, the lithography sector aims to keep up with a statement made in 1965 called "Moore's Law". Founder of Intel, Gordon Moore, observed that *"the size and price of transistors on a chip halves every two years"*. He predicted it would continue to do so which also meant that computational power of an equal-sized chip would double every two years. To date, ASML has succeeded in making this a reality through clever solutions such as multiple patterning, immersion- and computational lithography. With double -or even quadruple- patterning, two lines are closely printed together, making it possible to create smaller structures than the wavelength of light used. This however requires excellent overlay characteristics and significantly decreases throughput. Immersion lithography uses a layer of fluid to increase the refractive index from 1,0 (for air) to 1,44 (for water), thus operating below the diffraction limit of the lenses used for imaging (ASML, 2019b).

Despite these innovations, the boundaries of what can be achieved with 193 nm light at acceptable yield comes in sight. Therefore, improvements are also sought in process efficiency to help prolong the desired trend of fitting more transistors on a chip. Examples are complex architectural layouts (3D designs) and completely automated chip production. The latter requires barely any human presence on-site and is referred to as a "lights-out fab", as these factories can run "with the light out". Such a production facility only takes in raw materials and outputs finished products with a minimum of human interaction. An additional advantage of this mode of operation is that modern fab's are basically big cleanrooms where humans are a big source of contamination (Schweder, 2017).

ASML: EUV-technology

Experts have long predicted the decline of Moore's Law but ASML aims to prove them wrong with the development of a new platform that uses 13,5 nm EUV light. This reduction in wavelength by a factor 14 compared to Twinscan would make the system much more futureproof. However, this Extreme Ultra-Violet (EUV) light is close to X-ray and gets absorbed by pretty much everything from air to lenses. It took ASML many years to overcome these and other challenges, but the technology became prototype ready in 2010. However, achieving sufficient laser power and throughput was at the time of writing still a serious problem for EUV to supply to the high-end market.

Once evolved, the combination of EUV and DUV lithography can prove to be a very cost-effective method to produce advanced-node chips. The main advantage here being the fact that EUV takes out the need for multiple patterning, reducing exposures. Also, DUV litho is a very mature technology which has been developed and re-designed for decades. This offers great value/price for larger nodes when different layers of a chip are being printed on different tools.

Despite the potential of EUV, there will always be physical barriers related to the very nature of ASML technology, which uses light. This is where mapper aims to break ground.

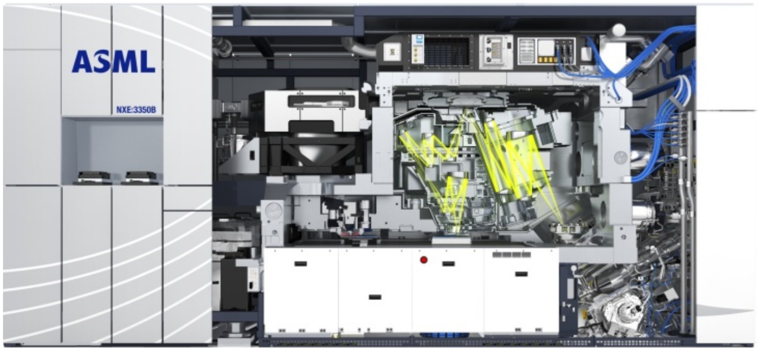

Figure 1.2: Illustration of the ASML EUV NXE-series

Mapper: E-beam lithography

New competitor on the market, Mapper Lithography, is developing a new way of writing patterns on a wafer by use of electron beams. The pattern information comes directly from the memory of a computer, rather than encoded in multiple expensive reticles, bringing down startup costs. Their technology can best be described as *'massive parallel e-beam lithography'* as it uses 13260 individually actuated electron bundles, all on the surface of a postage stamp.

Mapper Lithography was founded in 2000 and currently employs some 275 people. They aim to provide an alternative for optical lithography which is only financially attractive for bulk-production. For the past years, Mapper has survived solely on the promise of their concept, requiring investors and government subsidies to pay the bills. Current status of this 15 year-old startup is that proof-of-concept has been demonstrated and a prototype realized. Due to heating issues however, this prototype only works at ten percent of the total power, limiting production to 2 WPH. This is one of the major obstacles that needs to be overcome in order to scale up, get sufficient throughput and become viable. *The measurement setup designed in this thesis aims to assist in doing just that.*

If solutions for this heat problem are found, the next step for Mapper will be to make the challenging transformation from an R&D company to a fully fledged production facility. It's a long way to go but should this technology come to full fruition, it has the potential to drastically change the balance in the lithography sector. More detail about this in section 1.2.1.

Figure 1.3: Mapper's FLX-1200 prototype at LETI

1.1.3 Comparison ASML - Mapper

ASML and Mapper share the same goal, i.e. develop cost-effective tools for chip production, but their approach is quite different. Where ASML uses fotons of a certain wavelength (*light*) to image entire patterns at once, Mapper makes use of focussed electron beams (*currents*) to write a pattern line-by-line. Both approaches have their pros & cons but as ASML already has been discussed extensively, the unique selling points of Mapper will now be listed:

- **low startup costs**: maskless and available for small volume (batch) production
- **small fab footprint**: a unit requires just 1m^2 of (highly expensive) floorspace
- **unique chip designs**: each layer a custom design; opening doors to new markets
- **complex chip design**: shapes impossible with mask-based litho e.g. cutting patterns
- **high resolution at low exposure**: single-pass patterning to produce advanced-nodes
- **futureproof**: pushing back Moore's Law for decades with a 'pen tip' of 2Å in diameter

Despite these clear advantages of the technology, Mapper first has to survive as a company. This requires some key problems to be solved so first-generation tools can be shipped to customers. Initially these will be research institutes and universities. A next step would be to aim for higher node designs, still with low volume requirements. Only at a final stage it would be possible to compete with ASML for mass production of advanced-node chips.

1.2 Mapper Technology

1.2.1 The Mapper Machine

The Mapper Machine, called Matrix for the development phase, is a vertically aligned tool with a 1m^2 footprint. Current version is Matrix v1.1 which is one unit operating a 10% of its specified design power due to the presence of a heat issue. Once solved, full power operation will yield Matrix v1.10, which is able to produce some 18-20 WPH. In line with Mapper's commercial view, this is sufficient for the niche mentioned above.
Final version v10.10 will consists of ten identical v1.10 machines clustered as one, providing both high throughput as well as advanced logic / cutting capabilities. This tool should provide an alternative to the NXT/NXE-series of ASML, at lower costs and similar footprint.

Prototype of Matrix v1.1 is called FLX-1200 and roughly consists of the following sub-systems:

- *Metro-Optics Frame (MOF)* - This leaf-spring suspended box is supported by the base frame and houses various modules. All modules work together to produce the electron beams that are used to write patterns on the wafer. The MOF operates in a high vacuum (10^{-11} Pa) for sake of the electron beams and to shield off acoustics.
- *Wafer Positioning System (WPS)* - A few micrometers below the Electron Optics (EO), the wafer stage module is located. As part of the WPS, its job is to clamp the wafer and position it relative to the optical column hovering over it.
- *Electronics* - All IT, electronics and facilities are located on top of Matrix, so as not to occupy any unnecessary fab floor space as this is most costly.

1.2.2 Method of Patterning

The mode of operation of Matrix is quite different in comparison to that of ASML. Where ASML has a strong focus on dynamics, resulting in extreme accelerations of both the reticle and the wafer, the Mapper machine works by slow and steady movements. Objective for the wafer is to gradually move underneath the MOF at a constant speed. To accomplish this, Mapper aims to create an as-silent-as-possible environment. This requires cancelling out relevant disturbances or at least reduce them to the point where the WPS can compensate for the remainder of them. In this way, the system is able to write patterns on the wafer 'line by line' in one single sweep from beginning to end as shown in the next illustrations:

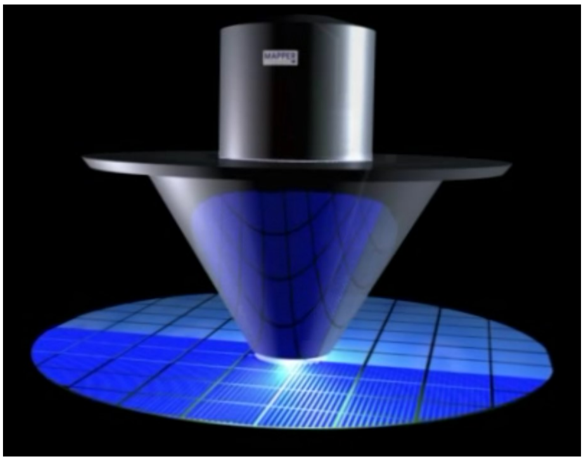

Figure 1.4: Scanning a Wafer (© Mapper)

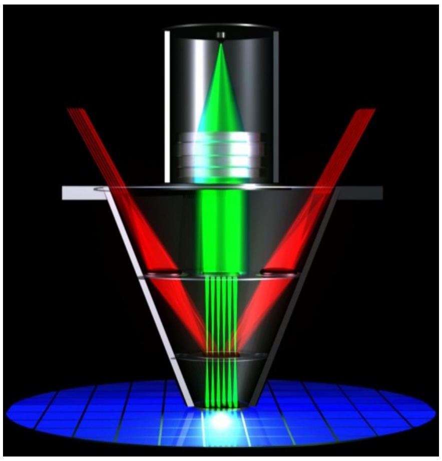

Figure 1.5: Electron Optics

1.2.3 Modular Design Approach

With a machine of this complexity, on which so many people are simultaneously working, strict separation of design processes is crucial. To that end, Mapper has adopted the *modularity in design* approach. This methodology divides the entire system in sub-systems, which in turn are split up into modules, sub-modules and parts.
All components of the total system have a well defined interface to their surroundings and an individual set of requirements. Each can thus be considered 'a separate machine'. Main advantage of this approach is that it allows for (sub)modules to be designed, tested and implemented in parallel. This reduces design cycle times as it enables hundreds of engineers to effectively work together. Another benefit is in the field of quality control. By verifying each component separately, functionality of the entire machine can be guaranteed up to the last nut and bolt. Should a machine fail during operation, the modular design ensures that only the faulty (sub)module needs to be replaced by a new (verified) one.

However effective, this way-of-work also brings about disadvantages. For instance alterations, which are inherently associated with iterative design, not only affect the (sub)module under consideration but often also related designs. To prevent time-consuming redesigns due to non-matching interfaces, ongoing communication between teams is required. In addition, comprehensive documentation strategies and good knowledge management are standard practice. Examples are interface-, performance-, reliability- and lifetime *requirements* as well as design-, build-, test-, verification- and integration *procedures*. Although necessary, this way-of-work brings about a significant administrative burden.

1.3 Motivation of the Project

1.3.1 Problem Statement

The motivation for doing this project relates to the heat problem as mentioned in section 1.2.1. More specifically, the issue for Matrix is that at full power a heat load of about 2.5 kW gets generated. This occurs in the process of creating beamlets, when electron currents dissipate on various (sub)modules in the Metro-Optics Frame (MOF). As heat constitutes physical vibration of molecules, this is analogous to an uncontrolled input of disturbance forces which results in poor overlay. As introduced in section 1.1.2, overlay is a key factor for good quality chips as many layers have to be printed on top of each other. Without good alignment (good overlay), poor contact results (Megens, 2007). This heat problem is especially difficult as Matrix largely operates in a high vacuum, rendering convective cooling impossible.

As a solution, water-cooled structures have been designed and implemented to remove the excess heat. This turbulent water flow however, causes flow-induced-vibrations (FIV) that again lead to inaccuracies when patterning. Nonetheless, there is a positive aspect to this transformation of the initial problem. The spectral distribution of FIV (frequencies at which the modules vibrate due to cooling) *can* namely be altered by modifying the cooling geometry. As will be detailed in section 2.1, the controller of the WPS has a sensitivity function that varies strongly with frequency. The FIV problem thus provides an opportunity to shift the main input to a frequency band where the controller has more influence. However, before any redesigns can take place, it is first needed to being able to observe the FIV acting over the whole range of operation of Matrix. *This is the challenge that drives the project.*

1.3.2 Previous Work

This thesis continues upon the work done by Dennis Lakerveld on the determination of direct disturbance forces (FIV) (Lakerveld, 2013). As part of his master thesis project, also conducted at Mapper Lithography, he has developed an experimental stand named *"Vibronix"*. Outcome of his research was the starting point of the design detailed in this thesis.

Research by Dennis Lakerveld

When Dennis Lakerveld began with his assignment, it was clear that the induced heat is problematic for accuracy. The extent to which this caused wafer error however, was not yet fully known. The objective for him was therefore set broadly to:

"Reduce the error in alignment between the electron optics and the wafer caused by the disturbances acting on the vibration isolation system to 1 nm 3σ RMS."

To this end, he investigated the Vibration Isolation (VI) & Dynamic Error Budgeting (DEB) at Mapper and built the Vibronix test setup. This tool is able to perform measurements in 1-DOF on the Aperture Array over 35 % of Matrix's frequency range relevant for cooling error compensation. The observed accelerations result from water supplied to the AA at nominal flow rate, thereby giving an indication of the amount of FIV generated by this sub-module.

Even though some of these results were known, the full thesis of Dennis Lakerveld was only finished in summer of 2013, whereas this project already took off in 2012. A clear transfer of insights and conclusions beforehand thus lacked. Therefore, significant effort has been put into properly establishing technical requirements for a new measurement tool. Chapter 2 discusses this along with a thorough analysis of the Vibronix setup.

Test Setup Vibronix

Vibronix measures FIV by observing accelerations in the 20-90 Hz frequency range (Lakerveld, 2013). This is done by suspending a water-cooled sub-module from flexible pendulums. Through Newton's Second Law, the forces related to these accelerating masses can be determined. By attenuating floor vibrations and acoustics using a granite plate, airmounts and an acoustical cage, an overall noise bottom of $3{\cdot}10^{-7}(\mathrm{m/s^2})/\sqrt{Hz}$ is achieved. As shown below, this setup theoretically resembles a passive two-stage VI system with acoustical shielding.

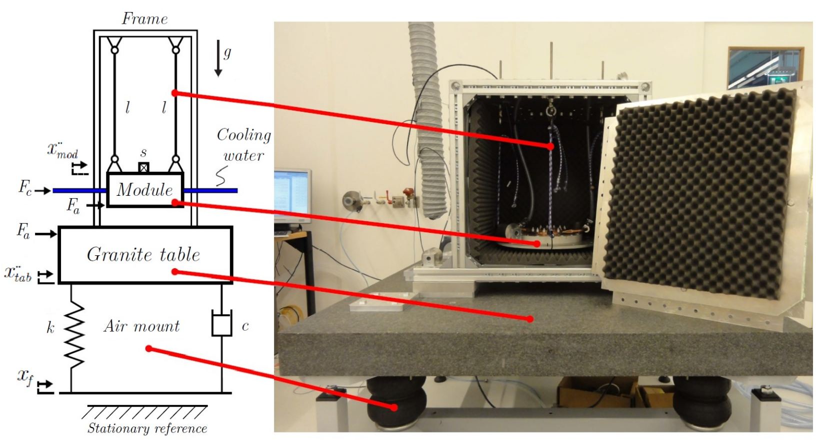

(a) Picture and schematic of the Vibronix test setup.

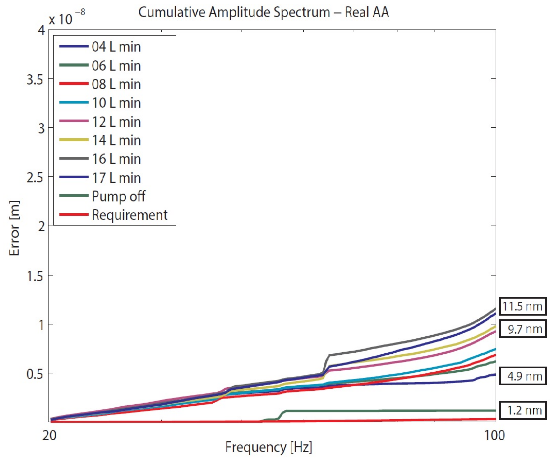

(b) Flow measurements on the AA-module.

Figure 1.6: Overview and results from Lakerveld (2013)

Preliminary Conclusions

The measurements performed on the Aperture Array (AA) over a limited frequency band, indicate that FIV are cause of significant wafer error. The line chart related to the AA's nominal flow conditions (13.8 L/min), namely shows a resulting wafer error of around 10 nm. This already exceeds the stage stability budget by a factor ten (1.3.2), whilst only a-third of the Matrix's rigid frequency range is observed. Even more, accelerations are measured in just one degree-of-freedom (DOF) and on one water-cooled sub-module. However, as the largest single contributor of FIV, the AA does provide a good idea of the overall magnitude of the induced cooling forces. Concluding, Vibronix has proven to be a valuable tool to obtain a first-order approximation of the present FIV, but a more sophisticated setup is required.

Interpretation of all test results lead Lakerveld (2013) to similar conclusions:

- *"The results from the Vibronix setup show that the forces to be expected are significantly larger than the available budget."*
- *"The main challenge can only be met if a solution is found for suppressing or eliminating the flow-induced forces."*
- *"The limiting factor for predicting and improving the system performance are the unknown direct disturbance forces."*
- *"The experimental research with the test setup is not conclusive in covering all the aspects related to the influence of using water-cooled components on an isolated load"*

1.3.3 Goal of the Study

Flow-induced vibrations (FIV) is the phenomenon that couples the domains of fluid mechanics and vibration engineering. This makes it highly empirical and difficult to predict by means of model simulations. To get a good understanding of the full impact of these FIV, a tool is thus required that can perform verification measurements on relevant modules located inside the MOF. These measurements should answer the question whether the wafer error that results from the coolant flow's input, is within spec. Therefore, the goal of this study is to:

"Design, build and verify a 6-DOF experimental setup, tailored to observe FIV, that is able to accommodate water-cooled Matrix-modules and perform measurements over their full operating range (10-300 Hz) at a resolution that allows for verification of the stage stability budgets."

Achieving this goal requires being able to differentiate between FIV input and noise originating from the environment. An important aspect is thus to map all present parasitic disturbances that can influence the measured signal. This also demands good insight of the system's dynamics and transfer paths through which disturbance forces are transmitted. These aspects will be thoroughly analyzed in chapters 2 & 3 and should ensure knowing what is being measured, which is essential to the trustworthiness of the measurement setup. These observations are consistent with conclusions of Lakerveld (2013), where it is stated on p. 48: *"Without a correct approximation of the acting force disturbances no realistic prediction of the system performance can be obtained."*

1.4 Research Objectives

Following on the the goal of the study, the research objectives will now be discussed. This is done by first defining the main research question and related sub-questions. After that the project scope is listed and lastly the academical contribution mentioned.

1.4.1 Research Question

The main research question, illustrating the overall problem that drives the project, can be formally phrased as follows:

"Are the cooling forces, induced in the modules and exerted onto the MOF, resulting in exceedances of the stage-stability error budgets?"

Related sub-questions:

- how do FIV translate to wafer error?
- inversely reasoned, what would be an 'acceptable level' of the FIV spectrum given the stage stability error budgets?
- upon identification of miscellaneous disturbance forces (acoustics, floor vibrations, etc); is it possible to shield them off or mitigate their effects?
- what modules contribute most to wafer error and what can be done to reduce their effects?
- in what DOFs is the Matrix-system most susceptible to disturbance input and are there means of utilizing the most resilient DOFs?

1.4.2 Project Scope

The project scope is a valuable prioritization- and planning tool that can be used to effectively achieve the set goals and to answer the main research question. It provides an overview of the key project objectives, requirements and deliverables and links these to tangible milestones. This scope definition assists in getting a clear overview upfront of the work needed to successfully meet the project objectives. Even more important than stating what is *in-scope*, are the activities and deliverables decided upon to be *out-of-scope* - which turned out to be little. *In hindsight it can be said that this part of the project has not gone well at all.*

Top-level Requirements

The high-level requirements are that the design should be able to accommodate three-of-the-four main modules under study: BSW, ABC, POS (shown in section 2.1). These should be spatially constrained in the same way as by the MOF -in Matrix- and receive flow supply at their nominal flow rates. Detailed requirements are presented in section 2.4.
Based on initial analysis it became clear that incorporating the Beam Generator (BG) module in the design would severely complicate matters. Given the separate cooling system for this module it was decided to leave it out.

Main Deliverables

The main deliverable of this project is a physical machine that can perform flow measurements at specifications in accordance with the above requirements. A theoretical model with performance simulations must accompany this design to prove its functionality prior to construction. Input to this model should come from an internal- & external literature review, supplemented with empirical measurement data. This literature study is a separate deliverable.

Furthermore, in terms of documentation the following deliverables can be expected:

- Forcesix - Requirements Sheet v01-05
- Forcesix - Concept Design File v01-02
- Forcesix - Detailed Design File v01-06
- Forcesix - Inventory List - v01-s05
- Forcesix - Assembly Procedure v01-06
- Forcesix - Build Sheet v03-10
- Forcesix - Verification Procedure v01-01
- Forcesix - Measurement Plan v02-01

Note that the final design of the measurement setup created in this project, goes by the name of '**Forcesix**', referring to the measurement of **Force**s in **Six** degrees of freedom.

Key Milestones

Chronologically, the milestones related to this research are as follows:

- conduct an external literature study on relevant topics such as vibration isolation, flow-induced vibrations, dynamic error budgeting, acoustics and low-noise design (App. A)
- perform an internal literature study to gain understanding of the workings and dynamics of the Mapper machine (2.1)
- analyze the Vibronix measurement setup, perform characterization measurements and draw conclusions (2.2)
- re-budget stage stability error tolerances based on cooling characteristics (2.3)
- establish technical requirements necessary for the new design (2.4)
- select measurement principle and devise concept solutions using DEB (3.1)
- quantify disturbance sources (DS) by performing environmental measurements (3.2)
- create Matlab models to simulate the effects of DS on the measured signal (3.4)
- create a 3D CAD model of the final design in Solidworks (3.5)
- construct detailed drawings and order all components, hardware and sensors (3.5)
- assemble all materials and build the measurement setup
- calibrate and perform verification measurements to establish a noise bottom (4.2)
- perform flow measurements on particular (sub)modules at their nominal flow rates (4.2)
- write processing scripts, convert the sensor data, plot results
- analyze the measured response and draw conclusions (5.1)
- provide recommendations on how to reduce the effect of FIV (5.2)

1.4.3 Scientific Significance

The Matrix-machine developed by Mapper is a complex tool that is highly sensitive to external disturbance forces. It's massive parallel e-beam technology must be shielded from or corrected for environmental influences to prevent wafer error. Present disturbances include floor vibrations, magnetic- and electric fields, acoustics and temperature (variations). To this end, a variety of cutting-edge solutions have been implemented. Examples are ultra-high vacuum operation, turning the MOF into a Faraday cage and an advanced PID controlled wafer stage.

However, as explained in section 1.3.1, heat dissipation inside the (high vacuum) MOF remains an issue. It has been attempted to solve this problem by implementing water-cooled structures. Unfortunately, the water flow inside these elements produces flow-induced vibrations (FIV - 1.3.3) that in turn cause inaccuracies. This problem is difficult for Mapper to circumvent as cooling capacity increases with turbulent flow, making FIV intrinsic to the method of cooling. Nonetheless, the negative effects of FIV on patterning accuracy can be reduced by modifying the cooling geometries. Objective of this approach is to shift the spectral distribution of the unwanted force input to a frequency region where the WPS controller has more influence. *This however requires a unique measurement setup that is able to observe these induced cooling forces, motivating this project.*

Currently, no such tool exists as a commercial fit-to-purpose solution. This is due to the specificity of the problem and because fluid mechanics is a highly theoretical domain where analytically explaining the phenomena is of primary importance. Therefore, experimental setups described in literature mostly relate to standardized situations where they are used for validation purposes (Kaneko et al., 2008). Such studies are generally aimed at observing behavior related to specific key figures and do not observe global reaction forces over a broad frequency spectrum. Think of internal flow characteristics of a pipe line (Veerapandi et al., 2019) or vibrations induced by cross-flow over a cylinder (Wong and Zhao, 2018). An example of a key figure under study can be establishing the maximum velocity at which fluids or gas can be transported before turbulence (FIV) occurs. Moreover, many such research focuses on applications in the oil and gas industry, where operation takes place at a much bigger scale. Therefore, even when external reaction forces are considered, their magnitudes are much larger and can be measured quite straightforward. This in contrary to the problem described in this thesis, which also entails more than flow-vibration measurement alone. *This challenge is set apart from experimental setups found in literature due to the following aspects:*

- the design must be tailored for the modules under study, mimicking Matrix's interface requirements in terms of stiffness and directional constraints.
- the need for a custom designed floor vibration isolation system, significant low-frequency acoustical attenuation and a mechanical design optimized for low-stiffness connections.
- flow should be supplied at nominal speeds and pressure as specified per module, whilst making sure the pump does not inject pressure pulses or causes noise (cavitation/eddies).
- the induced FIV are of low magnitude ($\pm$ 3.5 μN-rms), which makes it difficult to observe them especially in the presence of dominant environmental disturbances.
- multi-DOF broadband dynamic force measurement at a very low-noise level, requiring specific electronics and data processing (contrary to static 1-DOF force measurement).

The above overview shows the difficulty and novelty of this mechanical design challenge. It also argues for modeling and simulation using FEM which would seem a simpler approach than physically developing the experimental setup. Yet, this theoretical option has already been explored prior to the start of the project detailed in this thesis.

In 2009, TNO investigated the most relevant cooling geometry, the Aperture Array (AA) and performed analyses on vibrations caused by turbulence in the cooling channels. Their results are detailed in two reports that were thoroughly analyzed and summarized in appendix A.1 as part of this thesis's literature review. Most relevant outcome of this study is that turbulence

I.P.

ther modeling and simulation does not seem the best way forward. A logical next step is thus to develop a custom experimental setup with realistic connections and sufficient tubing length.

There was some urgency related to the design of this tool as Mapper Lithography struggled to pay the bills. In order to become viable and survive as a company, several technical obstacles needed to be overcome of which the heating problem addressed in this thesis was an important one. The impact of a solution could therefore be far reaching.

Besides benefiting Mapper, this research also contributes to scientific knowledge of experimental characterization of FIV in a broader sense. To develop a FIV measurement tool namely requires operating on the interface of the domains of fluid dynamics and mechanical design. This has been done by combining theoretical knowledge with environmental data through a dynamical model. *Therefore, the design process detailed in this thesis describes a method on how to effectively design a measurement setup for low-noise reaction forces due to FIV.* This could be valuable to other companies and research institutes that focus on high-tech applications suffering from FIV. In particular those that are dealing with complex geometries which are difficult to simulate using FEM, may benefit.

Lastly, the world at large is able to profit from results obtained in this study as it could lead to competition on the chip production market which is currently dominated by ASML (1.1.1) Especially in the high-end segment, where ASML has a market monopoly, the technology developed by Mapper has the potential to be disruptive. Alternative means of production will inherently lead to lower chip prices and thus to cheaper consumer electronics. This would benefit the general public which illustrates the overall significance of this study.

1.5 Research Approach

This section discusses the research approach used in the design of the Forcesix measurement setup. First, the adopted design methodology is addressed. After that, the objective of chapter 2 is stated and steps taken to establish technical requirements are summarized. Lastly, an outline of this thesis is given which provides the reader with an overview of its structure.

1.5.1 Design Methodology

Forcesix has been developed by the same modular design approach as used by Mapper (1.2.3). This subdivision of the entire system into smaller (sub)modules and parts yields a variety of intermediate deliverables for this design, as listed in section 1.4.2. Advantage of this way of work is that after having established global requirements, it is possible to divide the design into multiple independent sub-designs. Each of these can then be individually devised, modeled and constructed after which the total design is made up by the assembly. In particular, splitting up requirement budgets per component is advantageous as it allows for focused selection and optimization until standards are met.

This modular design approach is part of a larger system engineering methodology which is represented well by the V-model (Schmidt et al. (2011) - page 25). Basically the V-model means going from big (system) to small (parts) and back whilst iteratively performing checks to ensure functionality. Benefit of this systematic approach is that it goes hand in hand with a work-breakdown structure, which allowes for prioritization using the **MoSCoW** method. This organizes objective using a '**M**ust have', '**S**hould have', '**C**ould have' and '**W**on't have' logic. The identified sub-problems for this design can be found in §3.1.1 where they are solved one after the other. Effectively applying the V-model requires good understanding of interface requirements and ongoing communication with other design teams. Therefore, as part of the internal literature review, 11 interviews were conducted with members of the five different design teams to which Forcesix interfaces. One of the major outcomes of these meetings was that due to its weight, the Beam Generator (BG) module is not accounted for in the design. It is therefore labeled as a *'won't have'* in the scope. On the other hand, performing noise-bottom measurements on Forcesix once completed is a *'must have'*, as it is necessary to meet the project goal of verifying the setup (1.3.3).
There are also aspects that are not essential for this study but which would be valuable to Mapper. An example is actually testing the three modules suffering from FIV, which is therefore considered a *'should have'*. However, processing and analyzing this measurement data to make statements about the resulting wafer error, is optional i.e. a *'could have'*. This design methodology has been applied to all deliverables and its division can be found in *'Forcesix - Requirement Sheet v01-05'*. Throughout the design process, the design leaders of the three teams responsible for the modules under study were kept in close contact to coordinate design changes and ensure compatibility upon integration.

1.5.2 Establishing Design Requirements

Objective of chapter 2 is to determine the design requirements for the Forcesix measurement setup. This requires going back to the principle objective of the Forcesix design which is to verify whether Matrix meets its stage stability error budget in terms of FIV. However this is not straightforward as Matrix requirements have been specified as *wafer error values* only (e.g. "max 1.8 nm overlay in XY"), whereas the generated FIV consist of an unknown *force-vibration spectrum* which is frequency-dependent.

Since neither the shape nor the magnitude of these cooling forces is known on forehand, it is necessary to reason backwards from the Matrix budgets. This requires a good understanding of how FIV spectrums (6-DOF) translate into singular wafer error values (3-DOF).
The great difficulty with this transformation though, is that differently shaped FIV spectra can result in equal wafer error values (in nm). Therefore, it is important to get a good idea of the expected spectral shape of these cooling vibrations first. This is done by examining a variety of measurement performed on similar geometries. Only then, Force Requirement Spectra (FRS) can be established by computing the related magnitudes that result in each module's error budget. It is important for these noise level requirements to be set as accurately as possible since their correctness can only be confirmed by actual testing afterwards (upon completion of Forcesix). Moreover, improper bounds between system noise bottom and sensor range, would result in a tool that is useless for Matrix in terms of verification purposes. Therefore, all aspects related to the generation of FIV, their transformation into wafer error and the formulation of the stage stability budgets must be thoroughly investigated.

The illustration in fig. 1.7 shows the steps involved in extracting technical design requirements for Forcesix on a global level. This regards the calculations for 1-DOF (e.g. X or Y) without cross-talk. In the model, these have been repeated for all six degrees-of-freedom (6-DOF), whilst accounting for cross-talk from one DOF to all others.

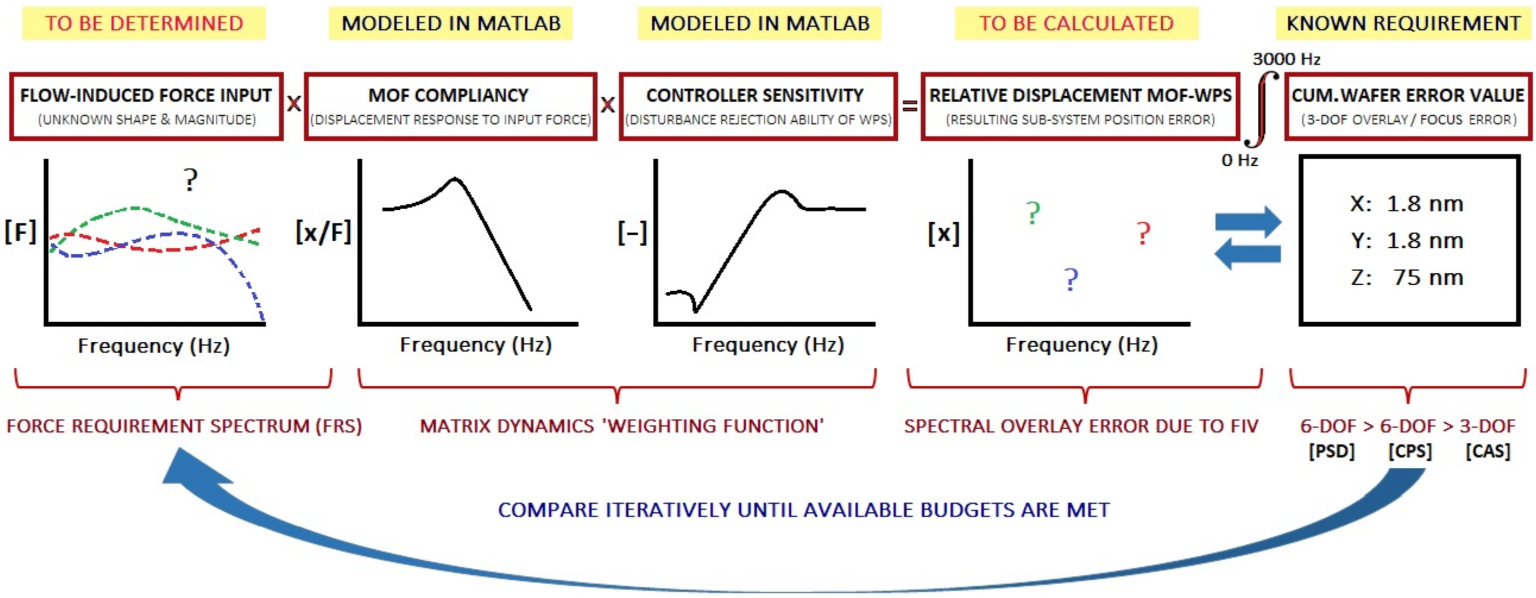

Figure 1.7: Overview of the calculations that are detailed in chapter 2.

<u>From left-to-right, the following charts can be seen:</u>

- possible force-vibration spectrums, induced by coolant flowing through small channels. This unknown disturbance is what Forcesix aims to quantify. To accomplish this, Force Requirement Spectrums (FRS) need to be established for every water-cooled module.
- two-of-the-three dynamical transfer functions that make up the 'weighting function' which will be presented in §2.1.3. This function translates FIV to wafer error.
- the unknown resulting relative spectral overlay between the MOF & WPS sub-system.

- the rightmost circled block is the cumulative wafer error that follows from integration of the previous graph over the entire operating range of matrix (0-3000 Hz). It is important to note that calculations include all 6-DOF, whereas final Matrix requirements have only been set in 3-DOF. Therefore, rotational input is translated- and added to translations.

1.5.3 Thesis Outline

This report details the development of the Forcesix measurement setup which has been designed for Mapper Lithography. A synopsis of all chapters will now be given.

Chapter 1 starts by providing context of the semiconductor industry and explaining the origin of this project. This is followed by the problem statement and a definition of the goal of the study. Related milestones are then listed in the project scope which provides a good overview of the main steps in the design process. The introduction ends with a description of the applied design methodology.
Chapter 2 describes how the design requirements for the Forcesix measurement setup have been determined. This includes a detailed description of the Mapper Machine ("Matrix") and the Vibronix test setup that resulted from previous research. Also performed flow measurements will be discussed along with (a redistribution of) the available error budgets. Outcomes of this chapter are thus requirements for the (sub) modules for which the setup will be designed next. *As the process to establish these technical requirements is quite comprehensive, it has been visually summarized in section 1.5.2.*
Chapter 3 details the design of the measurement setup. This is done by identifying functionalities, devising concepts and mapping environmental disturbances. A DEB model created in Matlab and validated using acceleration measurements then combines these disturbances to arrive at a theoretical performance estimate of these concepts. Result of this chapter is the final design ("Forcesix") along with a corresponding modeled residual noise level.
Next, ***Chapter 4*** shows the construction process of Forcesix and its experimental verification. Most important outcomes of this chapter are design specifications i.e. quantified requirements. Section 4.2 will present the results that have been achieved through the applied design methodology. These flow measurements are interpreted in the discussion section to answer the research question stated in chapter 1, thereby closing the loop.
Lastly, ***Chapter 5*** draws conclusions based on these results and makes recommendations for further study. In the appendices, the literature study (A) can be found as well as additional results (B), design details (C), Matlab code (D), technical drawings (E), Forcesix documentation (F) and datasheets (G).

Part II

METHODOLOGY

Chapter 2

Establishing Technical Requirements

To provide the reader with a bird's-eye view of how technical requirements are established in this chapter, an overview of its structure will now be given. Section 2.1 begins with an overview of the architectural layout of Matrix and its global systems. This is followed by its most relevant dynamical transfer functions and a description of each (sub)module's functionality. These should provide a good overview of the Matrix system and insight into its dynamics. After that, characterization measurements that were performed on Vibronix will be discussed and interpreted (2.2). This is done to determine the best means of supplying flow during testing and to derive insights that may be useful in the design of Forcesix. Additionally, these measurements provide an indication of the generic shape of the FIV spectrum. This information is then used in section 2.3 as part of a three-step approach to define the Force Requirement Spectrums (FRS). Yet this section starts by discussing the stage stability budgeting document and redistributing its values based on dissipated power and relating flow speeds/turbulence. From these new error tolerances, technical requirements are deduced. The chapter closes with an overview of all functional design requirements.

As the process of establishing technical requirements is quite comprehensive, it has been globally summarized in the research approach (1.5.2).

2.1 Matrix Architecture

This chapter can be seen as an 'internal literature review' aimed at all relevant aspects of the Mapper technology. Gained insights from this study, combined with performed measurements and model simulations result in the project requirements that are presented in section 2.4.1.

2.1.1 Machine Overview

Schematic Layout

Figure 2.1a shows the Mapper Machine ("Matrix) on the left. Due to its ultra-high vacuum operation it basically looks like a solid metal cube from the outside. Since cleanroom floorspace is most valuable, this 5.5 tons weighting tool is vertically aligned with all electronics & facilities located in metal boxes on top. Matrix therefore only has a footprint of about 1m^2.

Based on a variety of internal Mapper documents and conversations with Design Leaders, the schematic overview on the right (fig. 2.1b) has been created to provide insight into its construction and general layout. This is focused on a the mechanics of the machine.

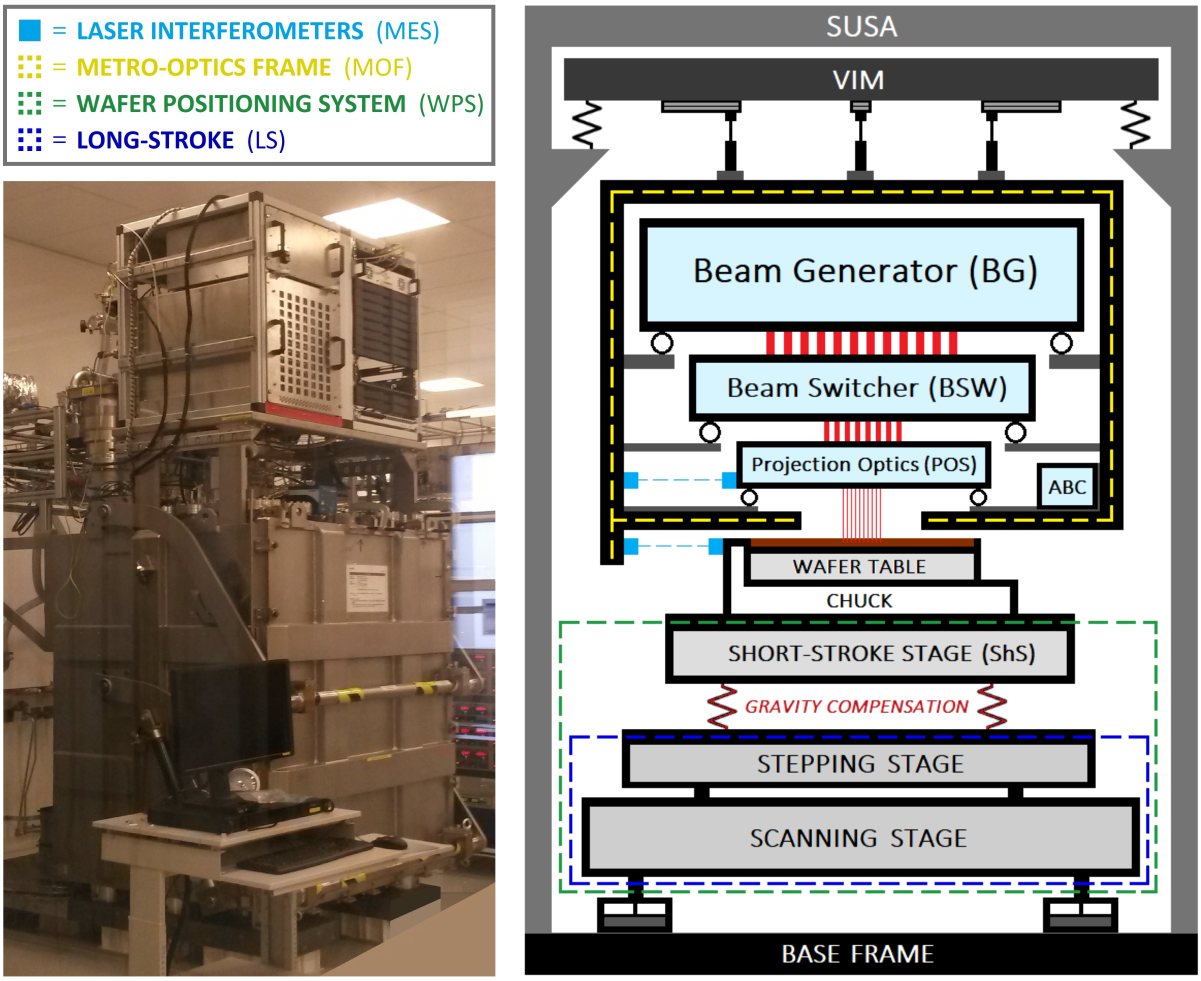

(a) Matrix S007 in the Mapper Cleanroom. (b) Schematic illustrating Matrix's main systems & modules.

Figure 2.1: Overview and construction of the Mapper Machine

The main subsystems relevant for this thesis i.e. the Metro-Optics Frame (MOF) and the Wafer-Positioning System (WPS), are indicated by dashed colored lines. Also the four (sub)modules of interest inside the Metro-Optics-Frame (MOF) are marked (in lightblue). These will be discussed individually hereafter.

Metro-Optics Frame

The Metro-Optics-Frame (MOF) is a metal Faraday cage that accommodates the modules that make up the Electron Optics (EO) and purify this system. The MOF weighs about 400 kg and is suspended from the Vibration-Isolation Module (VIM) which in turn is located in an even bigger sub-system responsible for alignment: SUpport Subsystem Alignment (SUSA). Each of these layers of additional (sub)systems help shield external disturbances and/or reduce their effect on stage stability. Surrounding all structures is the SUpport Subsystem Vacuum (SUSV) which reduces pressure to 10^{-11} Pa (not shown in schematic).

Objective of MOF is to produce the electron beams needed to write nanometer size patterns on the wafer below, supported by the Wafer-Positioning-System. To this end, various (sub)modules each perform a specific task in the overall process of generating and accelerating electrons, turning them into beams and shrinking/focusing them on the wafer. Specific functionalities of the four main modules located inside the MOF will be discussed in section 2.1.2.

The three modules relevant for this research are the ones suffering most from heat dissipation as mentioned in the Project Scope (1.4.2): BSW, POS & ABC.

As can be seen in fig. 2.1b, the entire MOF is passively supported from the VIM by three thin metal rods that connect to metal leaf springs. This means of suspension is equivalent to a pendulum where the weight of the MOF acts *as mass* and the stiffness of the leaf spring *as the spring*. The first translational- and rotational eigenfrequencies of the leaf springs from which MOF is suspended are as follows:

Figure 2.3: Overview of the module's interfaces to MOF

With regards to dynamics, weight restrictions on the modules combined with the stiff interface towards MOF makes sure that dynamical decoupling does not take place below 585 Hz for the heaviest module (BG: 185 kg). Together with the requirement that all modules must have their first eigenfrequency above 200 Hz, this means the whole MOF acts as a rigid body when subject to disturbance forces. *Hence, no internal resonances will occur when (sub)modules are subject to cooling vibrations within the 0-200 Hz frequency range.*

Wafer-Positioning System

The Wafer-Positioning System (WPS) is designed to position the wafer under the Projection Optics (POS) module. Its objective is to bring the relative positioning error within tolerance set for stage stability: 1,8 nm (XY) & 75,0 nm (Z). As shown in fig. 2.1b, the WPS is made up by the Long-Stroke stage (LS) and Short-Stroke Stage (ShS). These work as follows:

- **The LS stage** is supported by airmount isolators and performs the coarse positioning. This is done by means of stepping with piezo actuators and scanning with a rotational drive along a linear guide. This first stage operates in the order of micrometers.

- **The ShS stage** does the fine positioning by means of magnetic actuation in six degrees-of-freedom. The used Lorentz sensors have a low stiffness which reduce the effect of floor vibrations on stage stability. Combined with the gravity compensator that carries the weight of the chuck, the ShS is able to achieve nanometer precision.

- **The Chuck** is mounted on top of the ShS and holds the Wafer Table that clamps the wafer. Optical positioning takes place with respect to this Chuck.

This dual-stage control system moves relative to the stationary electron beams to pattern the wafer whilst correcting for residual movement of the MOF. To achieve this, WPS is dependent on data from the *Metrology Sub-System (MES)* which has the following sensors at its disposal:

- **Interferometry** - as can be seen in fig. 2.1b, laser interferometers are used to measure

I.P.

- the interferometers take over.

- **Accelerometry** - additionally, accelerometers mounted on the MOF provide information about its absolute motion which can be used to improve accuracy (feedforward) and further characterize system transfer functions.

Ultimately, stage stability positioning specs that have been achieved with this system are the required 1,8 nm in-plane with 0,5 nm alignment repeatability w.r.t. MOF. *This is however the case when no cooling vibrations are present as these result in 30-70 nm error.*

Cooling Geometries

The design of the cooling channels present in the three modules relevant for this study are shown in fig. 2.4. Due to volumetric constraints inside Matrix, these geometries are quite complex. Moreover, their small dimensions and high pressures / flow velocities make it difficult to accurately predict flow behavior. *Particularly the fact that both the desired cooling capacity as well as the unwanted Flow-Induced Vibrations (FIV) increase as flow becomes more turbulent, makes this a difficult engineering problem.* In fact, turbulent flow is a necessity to achieve sufficient cooling power in the current design. Therefore, rather than trying to minimize FIVs, the objective has been set to try and control the spectral region in which these vibrations occur, so as to mitigate their effect on overall performance.

However, as adviced by TNO (Lemmen et al. (2009)), the total cross-sectional area of the cooling channels has been kept at a constant value throughout the design (fig. 2.4a bottom-right). This is done to prevent pressure drops due to flow velocity reducing to laminar flow. Such pressure variations could result in local vortices that unnecessary increase (low-frequency) vibration levels.

Figure 2.4: Renders of channel layout in the modules under study: POS, BSW & ABC.

Computing the effect of Cooling Forces It has been mentioned in section 1.5.2 that the cumulative wafer error is computed by integrating over the entire operating range of matrix (0-3000 Hz). It should be noted that this does not conflict with the objective of Forcesix which is to observe cooling forces over a 10-300 Hz band. This is because the interface of the modules to the MOF has been designed to decouple dynamically around 200 Hz already.
After this resonance, the compliancy response decays rapidly i.e. limiting transmission from applied forces to MOF displacements. Therefore, higher frequency input affect wafer error mainly through excitation of higher-order resonances causing structural deformation of modules (mode shapes). This is a different problem for which separate budgets are available, therefore focusing on the 10-300 Hz range is adequate.

2.1.2 Module Functionalities

The combined objective of the modules is to generate electrons, separate them in 649.740 individual beamlets that are controlled by 13260 separate arrays in order to write patterns on a wafer 'pixel-by-pixel'. This is done by different stages that sequentially manipulate the small current flows. This process will now be detailed.

Beam Generator (BG)

The Beam Generator (BG), part of the illumination optics (ILO) subsystem, is the top module and source of all electrons. It generates the free electrons needed for wafer imaging and feeds them to the BSW module located underneath. Upon creation, the (charged) electrons have a tendency to spread out evenly in all directions. Through magnetic actuation with double octupole magnets, the diverging source is turned into a more parallel stream. This is done by electrical fields as conventional optical lenses do not have the desired effect on what are basically 'current-streams'. Additionally, the electrons are accelerated further whilst adjusting for global deviations. The final stage of the BG is a collimator lense, which focuses the electron cloud in preparation for BSW.

The processes in the BG generate about 16.3 % of the total induced heat.

Beam Switcher (BSW)

Objective of the Beam-SWitcher (BSW) module is to turn the collimated electron beam into bundles of arrays that can each be switched on- and off at will. Furthermore, it's target is to shrink these bundles in preparation for the final stage: the Projection OpticS (POS). The BSW consists of multiple sub-modules, each tasked with a specific assignment. The measurement setup as developed in this thesis, takes various aspects of BSW's sub-modules into account. To provide enough context to substantiate the design decisions, these sub-modules will now be discussed top to bottom.

The combined stages of the BSW module generate about 58.1 % of the total induced heat.

Aperture Array The top-most sub-module of BSW is the Aperture Array (AA), a copper

Individual Beam Corrector (IBC) is located that adjusts all 13260 electron bundles individually by means of electrostatic lenses. These alterations ensure they are well organized in a matrix-like configuration.

Condensor Lense As all electrons are negatively charged, they naturally repel each other. This causes parallel bundles to diverge over time / distance, thus requiring corrections at every stage. In the BSW module, the Condensor Lense (CL) sub-module refocuses the arrays whilst shrinking them by another factor. Again this is process that generates heat which needs to be cooled away. *Therefore at the bottom of the CL, another cooling array is present*

Beam Blanker Yet another level down the Beam Blanker (BLK) is found which takes the 13260 separate arrays and splits each of them into 49 individual electron beamlets. Next, the BLK's responsibility is to switch each of the 13260 arrays either on- or off by means of electrostatic deflection. This switching information comes from the Pattern Streamer (PS), providing data at 3.2 Gbit/s (Wieland, 2017).

This binary approach makes sense as the patterns that will be written on a wafer with this machine come straight from a computer memory and are written 'line by line'. This in contrary to the means of imaging by masks ('negatives') in classical lithography. At this micrometer-level stage, the arrays that consist of 49 beamlets thus either pass on untouched or are deflected sideways to dissipate on the Beam Stop Array.

Projection Optics (POS)

The bottom-most module regards the Projection Lense (PL) which is part of the Projection-OpticS (POS) sub-system. As the PL cannot be taken out individually, this sub-system is considered as a whole for the design of the measurement setup this thesis details. POS consists top-to-bottom of the Beam Stop (BS) Array, the Beam Deflector (BD) Array and lastly the Projection Lense (PL) Array. Purpose of POS is to shrink and manipulate the remaining electron beams from a micro-to-nano level. POS is located directly under the BSW module and hovers only micrometers above the wafer stage. The electrons that are switched-off by the BLK dissipate on this first stage: the Beam Stop. The remaining electron beams ("switched-on") are now individually actuated by the Beam Deflector allowing for patterns to be written with a resolution of one electron beam.

A second objective of the BD is to provide the remaining beamlets with yet another sweeping motion, deflecting 2 microns at high frequency, to be able to image a larger surface more effectively when moving over the wafer (Pil, 2015). Apart from applying corrections and interfacing to the Pattern Streamer that allows for raw data to be modulated onto the electron bundles, the POS sub-system outputs beamlets in the order of nanometers. This brings it within the required range for commercial (high-end) purposes. After this final stage, the roughly 650K bundles have been reduced to the point where they can all pass through the EO slit. This parallel slotted element measures only 10x26 mm, about the size of a postage stamp, and identical to the imaged field in an optical stepper.

The POS module generates about 2.1 % of the total induced heat.

Advanced Beam Cleaner

The ABC sub-module is responsible for producing gas to clean the EO in between exposures. It suffers from induced heat that requires water cooling, thus generating FIV that contribute to wafer error as it is rigidly bolted to the MOF. Therefore this sub-module is incorporated in the design of the measurement setup and will also be tested.

The ABC module generates about 24.4 % of the total induced heat.

CH. 2.1

Matrix Architecture

(continued)

2.1.3: Matrix Dynamics

MAPPER lithography

Detailing transfer functions important to understand Matrix's system dynamics

1-MSD representation of the Metro-Optics-Frame (MOF)

This sub-section explains the most important transfer functions needed to accurately model and understand the system dynamics of the Matrix tool. These are based on a MathCad calculation used by Mapper and have been modeled in Matlab to be able to simulate the effect of environmental measurements on the design of the measurement setup.

Assuming a single Mass-Spring-Damper (MSD) representation of a system, as illustrated below, the compliance function describes the relation between force on an object and its resulting spectral displacement (x/F). On the next slide the compliance response for each of MOF's six degrees-of-freedom (DOF) will be detailed, when subject to disturbance forces. This is based on the same MSD model which is a realistic representation as the MOF is suspended like a pendulum on which cooling vibrations are exerted (see Fig 2.1). Moreover, it has been designed to behave as a rigid body up to 200 Hz.

Similarly, the transmissibility function describes the dynamic response of a suspended mass to base movements. These floor vibrations can either be expressed as displacements, velocities or accelerations. Ideally, resonance is at a low frequency as this causes the mass to isolate from its suspension early on, thus limiting its response to higher frequency input.

All graphs that follow in this report use a log-log scale showing magnitude at increasing frequency [Hz]. It is good to note that a straight line in such graphs signifies an exponential relation. Also, the step size between orders expressed on the horizontal- and vertical axis is not linear.

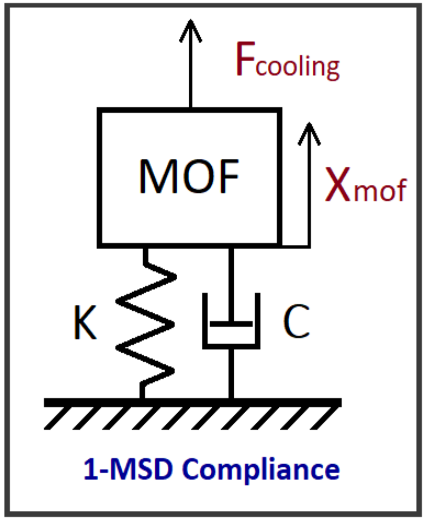

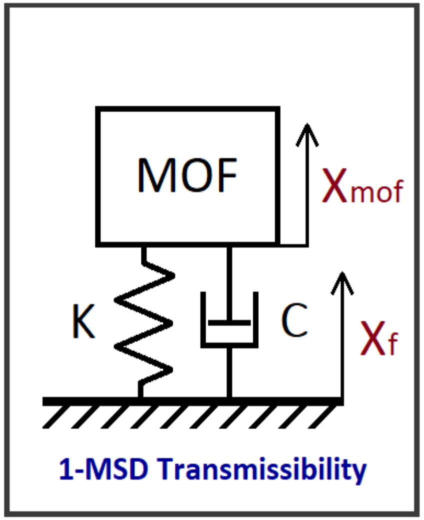

2.1.3: Matrix Dynamics

MAPPER lithography

Detailing transfer functions important to understand Matrix's system dynamics

MOF – Compliance Function (no crosstalk)

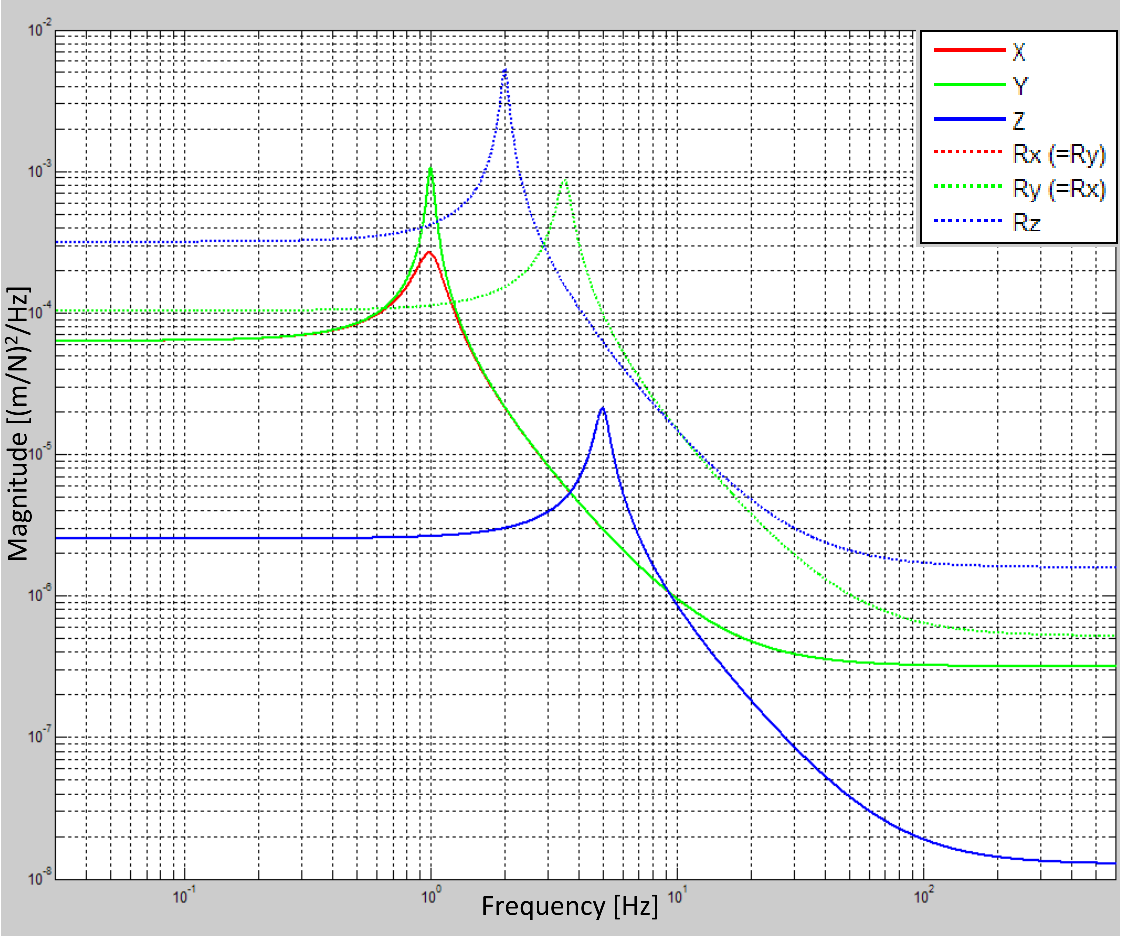

- the compliancy function shows the response of the MOF for each of the six degrees of freedom when subject to disturbance forces.
- ideally, the resonance peak is at an as low as possible frequency, transferring as few as possible disturbance forces to movement (i.e. low magnitude ratio).
- both X and Y resonate around 1 Hz after which the magnitude of the response drops off with a -2 slope (-40 dB/dec). This results in lesser response when subject to higher frequency input.
- although the dynamics of the MOF for Z, Rx, Ry and Rz is less desirable, the vertical motion does not result in significant error as it is out of focus by a factor 10.

2.1.3: Matrix Dynamics

Detailing transfer functions important to understand Matrix's system dynamics

MOF – Compliance Function (with crosstalk)

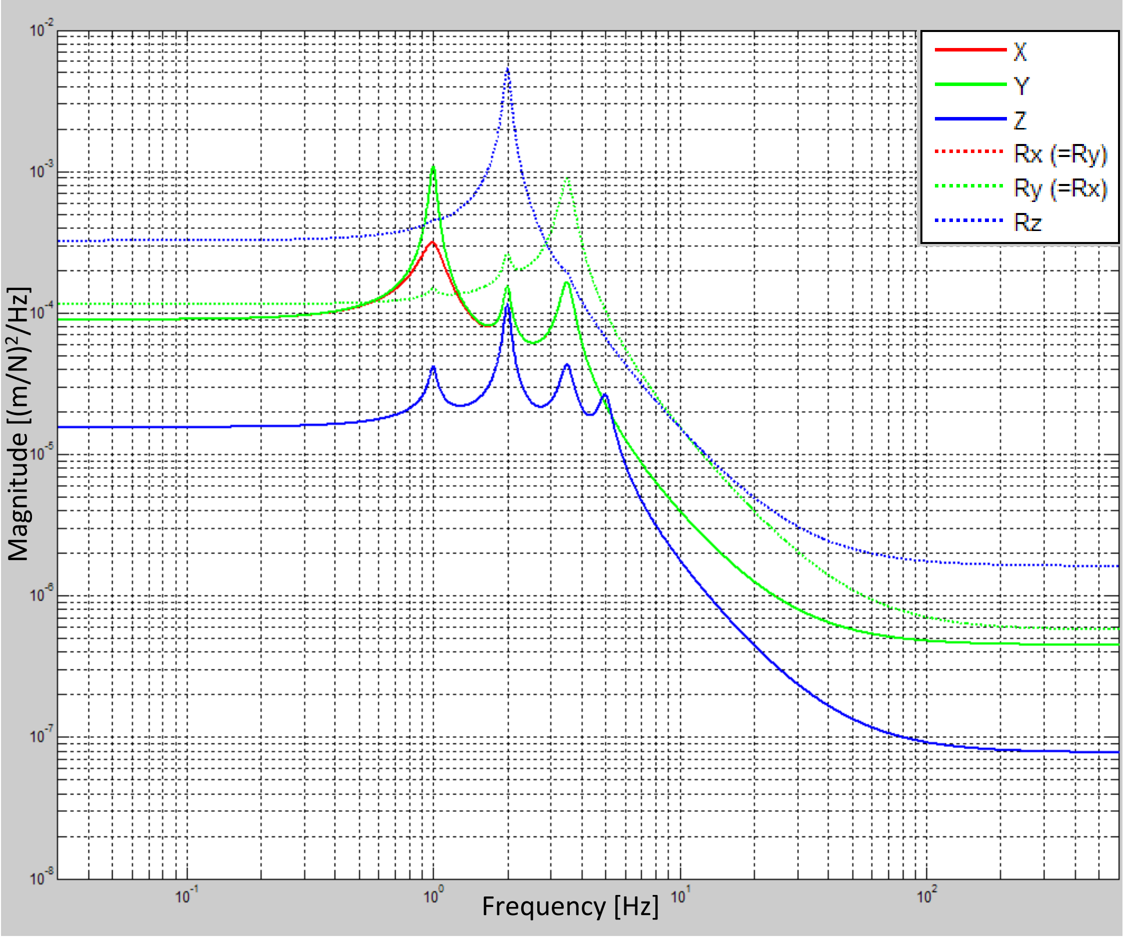

- ideally, the compliancy function is as shown on the previously slide (all DOFs uncoupled). In reality however there is significant cross-talk, mostly from the rotations to the linear movements.
- for each degree-of-freedom, 2% crosstalk to all others has been assumed with the exception of Rx to y & Ry to x where this value has been set to 16% because of a greater arm. Since Rx and Ry have identical behavior only five responses are visible.
- the effect of the crosstalk is that some curves are elevated, their area of resonance widened, and drop-off occurs at a higher frequency. This effect is most significant for Z, as all rotations contribute. Again, as the converging electron beams cause errors in Z to be out-of-focus, the effect this has on overlay (wafer error in XY) is limited.

2.1.3: Matrix Dynamics

MAPPER lithography

Detailing transfer functions important to understand Matrix's system dynamics

WPS – Controller Sensitivity Function

- the controller actuates the wafer stage and aims to minimize the error from relative motion between MOF and the chuck.
- the FRF of the PID controller shows how well its able to do so in the freq. range 0 – 10kHz. Wherever curves that represent the 6-DOFs are below the black horizontal line, errors are reduced; above it they are amplified.
- at the level of the horizontal line ($10^0 = 1$) the controller has no effect on the error (input = output). The unity-gain cross-over frequency is seen to be around 40 Hz. The corresponding phase chart (not shown) indicates closed-loop stability as the phase remains below -180 degrees at this frequency. The Matrix system has an effective BW of ≈ 75 Hz after which error amplification increases further. **Therefore the controller is most susceptible to disturbances acting between 40 – 300 Hz.**

2.1.3: Matrix Dynamics

Detailing transfer functions important to understand Matrix's system dynamics

MATRIX – Weighting Function

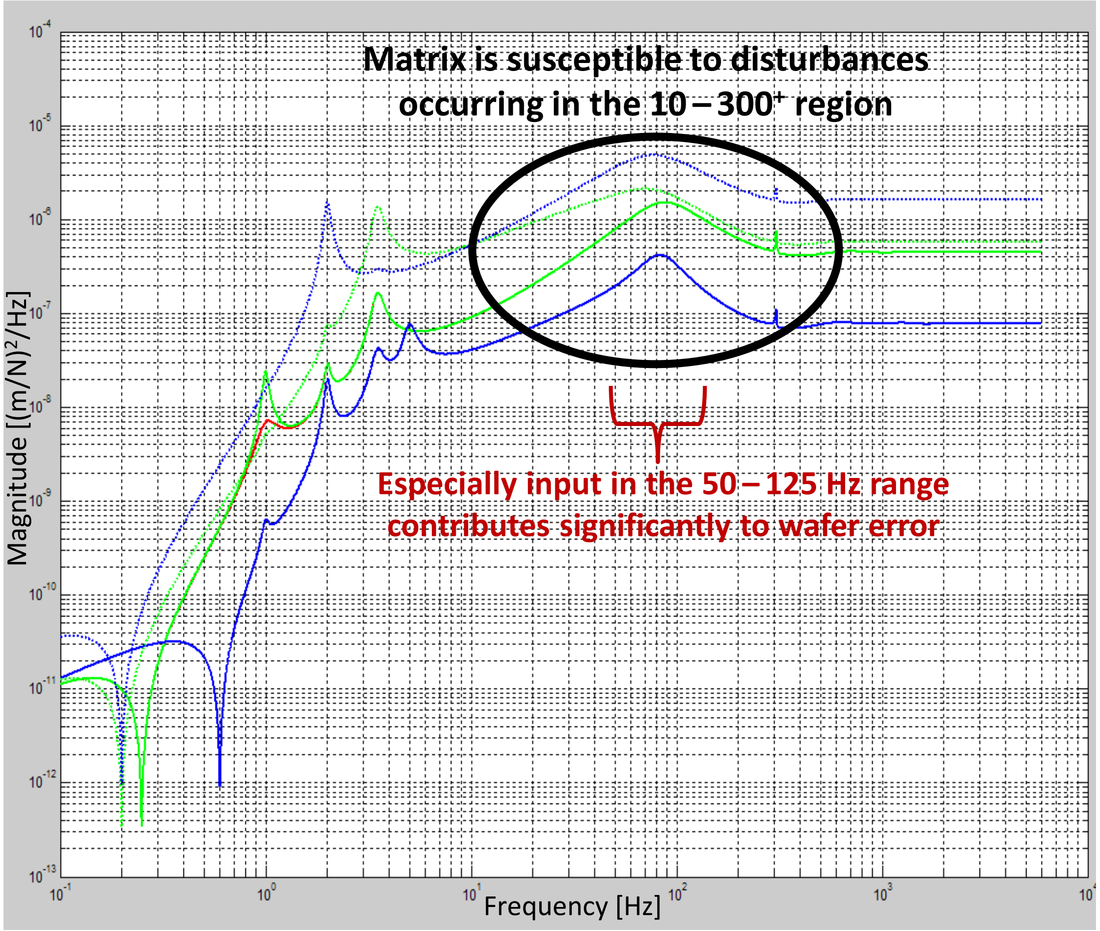

- this graph shows the 6-DOF weighting function which is the combination of the compliancy function (with crosstalk), filtered by the controller sensitivity transfer function.
- in essence, it describes the relation between potential disturbance forces acting directly on the suspended mass (MOF) and the resulting error on the wafer.
- **it can be seen that Matrix is most susceptible to disturbances occurring in the 10 – 300 Hz range.** This is largely due to the controller's sensitivity function crossing unity-gain around 40 Hz, causing diminished disturbance rejection for higher frequencies because of the waterbed effect (Schmidt, 2011). Despite the limited control BW, Matrix is designed to operate over the full range. Precise measurement of the magnitude and spectral distribution of flow vibrations inside the cooled modules is thus essential to be able to re-design channel geometries with this sensitivity in mind.

CH. 2.2

Characterization Measurements

2.2.1: Objective & Method

Gaining insight in how best to supply flow to the new design

Testing with the Vibronix Tool

The Vibronix test setup as introduced in Chapter 1 (see Fig. 1.6) is the result of the previous work by Dennis Lakerveld. This test setup will be used here to investigate the best means of supplying flow to the new design. This means: delivering water at a pre-set, constant flow rate to the modules under testing, without creating turbulence or injecting longitudinal pressure waves that interfere with the measurement. Also the effect of tubing / clamping on Helmholtz resonances is explored.

The difficulty is to being able to differentiate between measured error due to the actual cooling vibrations induced in the object that is tested and measured error due to noise inherent to the Vibronix test-setup, e.g. by the way flow is supplied.

<u>To achieve this, two sets of characterization measurement have been performed:</u>

The first set of characterization measurements looks at the difference when measuring the same module under the exact same conditions, only with a difference in flow supply, to decide which ‘pump’ can be used best. The tested options are:

- standard (centrifugal) pump as used by Vibronix
- Ultra-Pure Water (UPW) cooler pump used by Mapper to supply flow to Matrix (“the mapper machine”)
- a large pressure vessel specifically selected as an alternative to minimize input through hydrostatic flow

The second set of characterization measurements takes the method of flow supply that proved to be most effective above, and applies it to three general structures often used when measuring FIV. These structures are:

- straight flexible tubing (PVC)
- straight rigid tubing (metal)
- the Aperture Array (AA) sub-module onto which most of the heat in Matrix gets dissipated

2.2.1: Objective & Method

Gaining insight in how best to supply flow to the new design

.. continued ..

The objective of all characterization measurements is to help answer the questions:

- How can flow be supplied best to the modules under study?
- What kind of flow-induced vibrations (FIV) spectrum can be expected for different geometries?
- What kind of weaknesses can be identified in the design of Vibronix to prevent in the new design? (Appendix A-5)

Additionally, the measurements provide an indication of:

- the effect of acoustics on the observed accelerations (measurement with open cover)
- the effect of floor vibrations on the observed accelerations (measurement with -partially- deflated airmounts)
- the occurance of helmholtz resonances (measurements with different lengths & types of tubing)

Some background about the methods used to supply flow at a rate of 13.8 L/min:

- **the standard pump** that was used by Vibronix is expected to generate a relatively high input since its not at all designed to operate silently. Moreover, distinct resonances are expected to its centrifugal nature with an asynchronous motor.
- **the UPW cooler pump** supplies water flow to the modules inside Matrix. This device is custom designed by Mapper to operate quietly and to keep flow rates and temperature within narrow bounds using PID control. This 'ideal candidate' is however very expensive, in high demand and located fixed in the cleanroom, some 80 m from the labspace where testing takes place. Clearly, this is not a realistic option but it does provide a good reference of what can be achieved.
- **a large pressure vessel** of 120 liters will be tested as an alternative means of providing hydrostatic flow during a test. This carbon wrapped tank is filled with water and then pressurized by inflating the rubber balloon inside. At a pressure of 8 bar, the max flow rate that can be attained is 18 L/min - which meets Matrix demands. Its large volume contains sufficient water to perform batch measurements of 2 min without pressure or flow rate reducing noticeably.

2.2.1: Objective & Method

Gaining insight in how best to supply flow to the new design

Overview of the Vibronix test setup and the Aperture Array (AA) sub-module

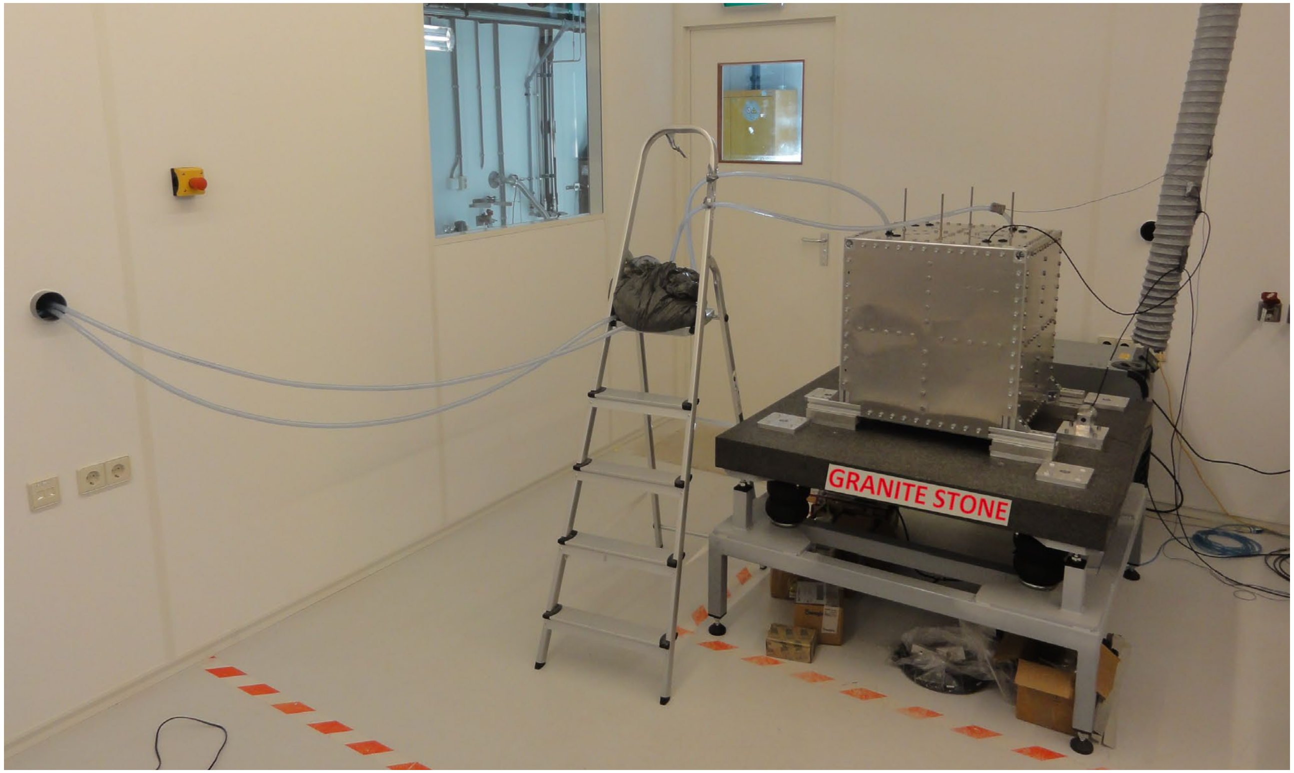

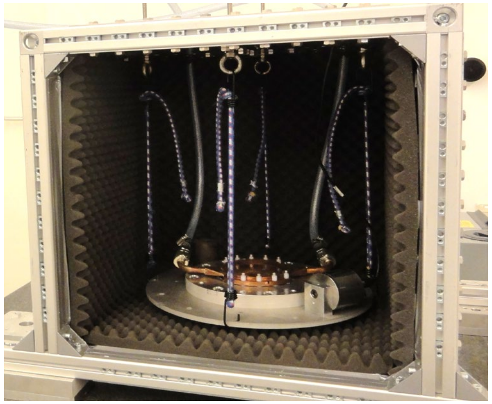

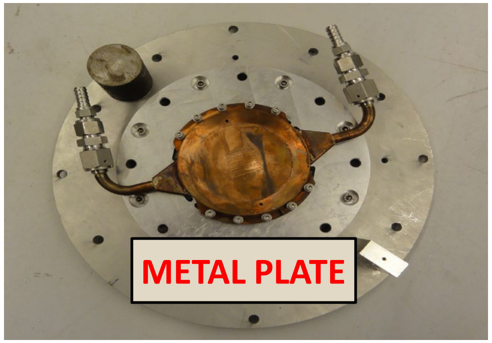

Picture of the Vibronix Test Setup in the lab-space at the Rotterdamseweg in Delft
Tubes supplying water in closed-loop can be seen fed through the wall (pump not visible)
A sand bag aims to prevent unwanted vibrations. It can be seen that tests performed on the Vibronix test setup are quite cumbersome. ***Vibronix performance is detailed in App. A-4.***

The Aperture Array sub-module
mounted on the metal plate that is supported by pendulums inside the acoustic casing of Vibronix

2.2.1: Objective & Method

Gaining insight in how best to supply flow to the new design

Overview of the sensors used for the measurements

Endevco M86 piezoelectric accelerometer

For the low-level accelerations of the pendulum *plate*, located inside the acoustic casing, the seismic-grade Endevco sensor has been used, depicted on the right. This sensor has excellent low noise characteristics but lacks bandwidth as build up towards its first resonance already starts at 90 Hz. A second Endevco sensor has also been mounted rigid to the granite *stone*. **This means that both the red and blue lines in the results presented next are only reliable until 90 Hz.**

BruelKjaer BK 8344 & 4513-002 deltatron accelerometers

To distinguish Helmholtz resonances and other input specifically generated *inside the supply tubing* a light-weight BK sensor has been mounted on the tubing. The noise level of this sensor is much higher than the Endevco sensor but that is compensated by a 1000 Hz bandwidth. Apart from its low weight, this sensor has been selected as helmholtz resonances generally occur at distinct frequencies which results in sharp resonance peaks that should be observable.

Data Acquisition

All measurements have been performed using the IEPE protocol on a NI-4472 DAQ installed for these tests, shown on the right.

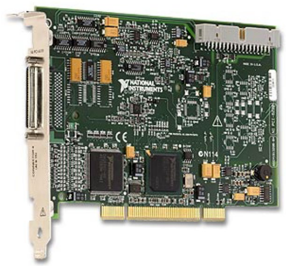

Lessons that can be learned from Vibronix for the new design are summarized in Appendix A-5. Moreover, based on the obtained results a *"to be expected"* generic force baseline will be derived that will be used in the requirement setting process in § 2.3.

2.2.2: Investigating Flow Supply

MAPPER lithography

2.2.2.1: Overview of **first set** of tests – *performed on the Aperture Array*

Normal Pump
(centrifugal)

Average PSD vibrations

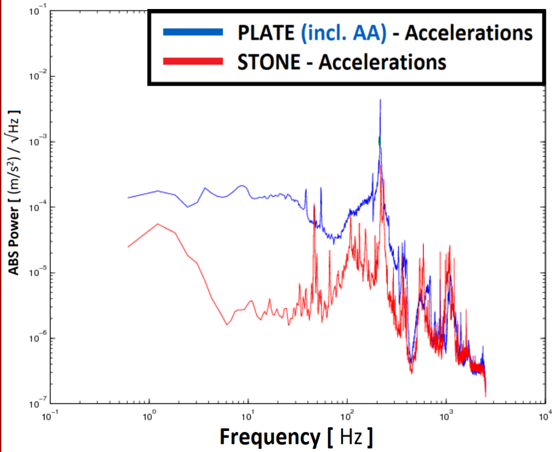

UPW-cooler
(PID controlled)

Average PSD vibrations

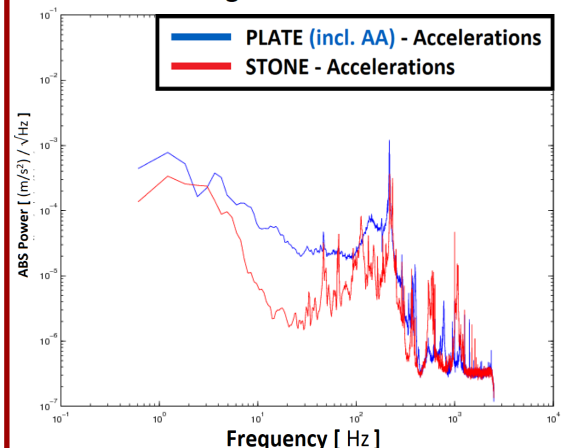

Pressure Vessel
(hydrostatic)

Average PSD vibrations

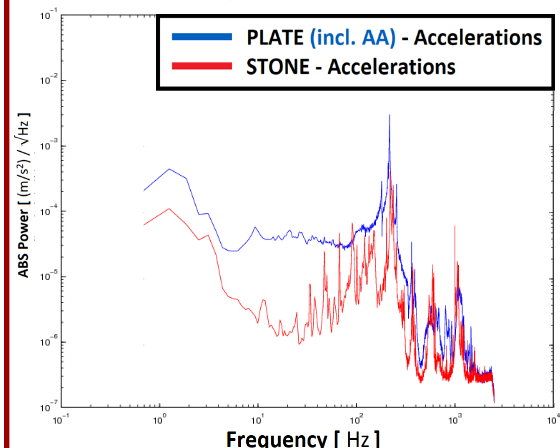

2.2.2: Investigating Flow Supply

2.2.2.2: Interpretation of the **first set** of measurements

Global Analysis

The graphs on the previous slide show flow measurements performed on the Aperture Array (AA) under identical conditions and at nominal flow rate as specified for Matrix (13.8 L/min). The only variable is a difference in the means of flow supply. All measurements have been performed in batch and then averaged out to limit the effect of anomalies. The Endevco sensors used are accelerometers (type M86) with excellent low frequency characteristics, but limited to 90 Hz. This explains the build-up of the large resonance, peaking at 110 Hz. The blue lines show data from the sensor mounted on the same metal plate that holds the AA, and the red lines show the data from the sensor mounted on the granite stone (damping floor vibrations).

When comparing the three measured accelerations, the 50 Hz resonance present in the sensor signal related to the granite stone stands out. This peak is visible in all three measurements, but most dominant when flow is supplied by the centrifugal pump. This resonance is expected to be caused by a Helmholtz resonance in the supply tubing, which was predicted to occur in this frequency region by TNO (see App. A1). Since the magnitude of the elevated stone accelerations at 50 Hz relate to the magnitude of the measured acceleration of the plate, it is most likely that the induced Helmholtz resonances in the tubing are exciting a structural eigenmode that is present in the Vibration-Isolation (VI) system – and not the other way around. This is in congruence with the fact that floor vibrations are a generally a relatively constant disturbance source.

It can be observed that the input generated by the centrifugal pump is much higher than that of the UPW pump (about a factor 10 in the 10 – 90 Hz range). Also, the pressure vessel is able to supply water at a much lower noise level. The fact that turbulence generated by the hydrostatic flow is only a factor 2 higher than the UPW pump is impressive given that this is a custom designed, PID controlled tool costing € 58.000 – contrary to the pressure vessel which only costs € 90.

Conclusions

From these first tests it can be concluded that hydrostatic water flow is a good alternative to the UPW cooler and that both trump the centrifugal pump. Given its availability and low cost price, the pressure vessel is best suited to supply flow to the modules in the new design. **The measurement results are individually analyzed in detail in Appendix A-6, providing insight in the origin of the present resonances.**

2.2.3: Hydrostatic Testing

MAPPER lithography

2.2.3.1: Overview of **second set** of tests – *water supplied by the pressure vessel*

Flexible Tubing
(PVC, Ø 10 mm)

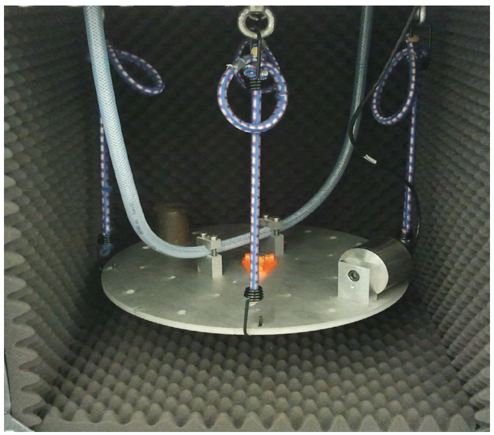

Average PSD vibrations

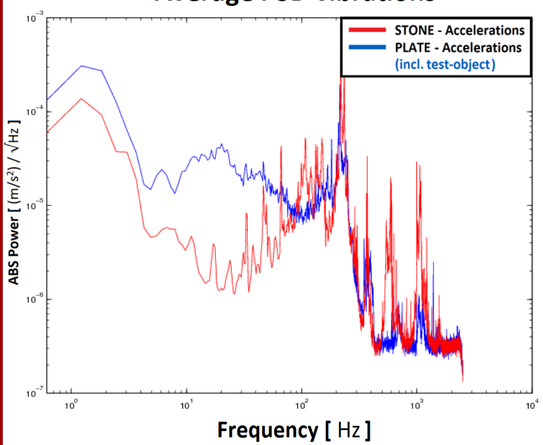

Rigid Connector
(metal pipe, Ø 10 mm)

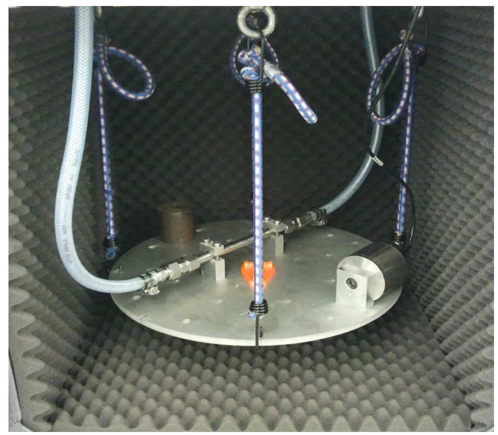

Average PSD vibrations

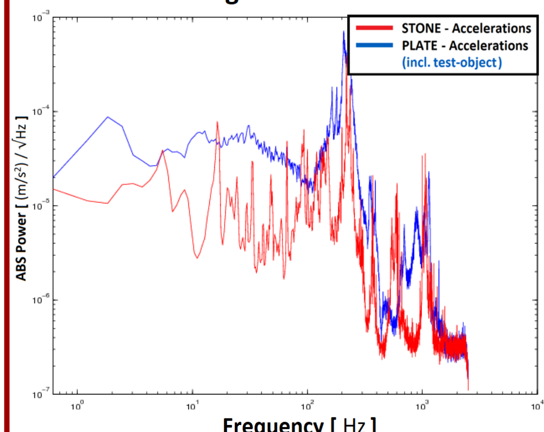

Aperture Array
(complex geometry)

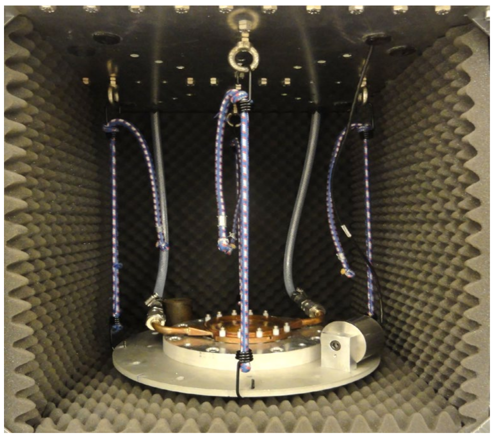

Average PSD vibrations

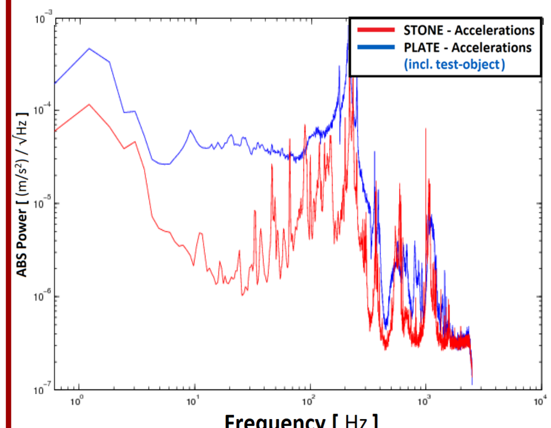

MAPPER lithography

2.2.3.2: Interpretation of the **second set** of measurements

Global Analysis

The three graphs on the previous slide show the measurement results for the tested geometries that are displayed above. In the 0 – 50 Hz range, the rigid connector and Aperture Array (AA) display a higher average power than the looped tubing. Especially in the low-frequency range where Flow-Induced Vibrations (FIV) would be expected to occur given the dimensions of the complex cooling channel geometries in the Aperture Array, higher input is indeed observed. Further investigation is however required to the origin of this turbulence.

When comparing the flexible and rigid tubing, the straight connector shows more input for higher frequencies. This could be explained by the fact that the flexible tubing surrounding the straight connector becomes a source for Helmholtz resonances as indicated by the TNO research (App. A-1). Another explanation could be that separation occurs at the swagelok connector edges. Knowing this, the type of tubing, its length, and the applied flow speed and pressure should be accounted for in the new design. Combined with the hydrostatic flow supply, this should result in a measurement system that is able to observe FIV as induced in the testing geometry, without introducing additional input by the pump or supply tubing.

Conclusions

From this second set of tests it can be concluded that complex structures yield a response that is elevated over the whole measurement range. From the comparison of the flexible tubing and rigid connector it is concluded that the supply tubing should ideally consists of one piece without connectors which could result in vortex shedding. Accounting for potential Helmholtz resonances is of importance, when clamping tubing or using connector pieces.

These measurement results are individually analyzed in detail in Appendix A-6, providing insight in the origin of the present resonances.

CH. 2.3

Determining Force Requirement Spectra

2.3.1: Stage Stability Document

MAPPER lithography

Distributing error values over all Mapper sub-modules

What is it and how does it work?

The Matrix stage stability budgeting document (Ellenbroek, 2013) is a comprehensive list of requirements that aims to ensure dynamic stability on a system level. To this end, all known disturbances have been given budgets i.e. allowed contributions to the global position error. This should lead to a overall stage stability of 1,8 nm in-plane (XY) and 75 nm out-of-plane (Z), which is sufficiently accurate to pattern wafers for high-end nodes.

To accomplish this, the system has been split up in sub-systems, modules, sub-modules and parts that are each alotted an acceptable deviation from a pre-determined reference. These references come in a variety of physical quantities that cannot easily be compared or distributed. Therefore, the stage stability document expresses all requirements in wafer error values i.e. nanometers. This allows each design team to transform their problem back into this universal quantity.

Initially, all water-cooled modules have been given the same portion of the cumulative error that could result from FIV. This is not a very realistic approach given the vast differences that exist between the (sub)modules in terms of cooling power. The BSW module for instance cools away 1468 W whereas the PL only takes up 30W of total heat load. With such vast differences, equal distribution of the wafer error values makes it impossible to verify the PL, whereas BSW has it way too easy. Therefore, as part of the literature study of this thesis, a small study has been carried out to re-budget these values to a more fair and logical distribution.

The used method and parameters will be presented next and § 2.3 closes off with an overview of the new values that will serve as basis for the requirements for the design.

2.3.1: Stage Stability Document

Distributing error values over all Mapper sub-modules

Initial budgeted error per (sub)module

Obviously, positioning is actually done in six degrees-of-freedom (6-DOF) and not just three (XYZ). Rotations are however attributed to these translational coordinates by taking their momentum over the EO slit (opening through which the electron beams are projected onto the wafer). From these global stability criteria it becomes clear that the system is much more forgiving for out-of-plane errors. This is due to the narrow vertical focus that reduces the effect of errors in Z, scaling them favorably. **In-plane requirements (XY) are thus the most stringent, which makes sense from an overlay perspective** (§ 1.3.1)**.** For clarity, these are the directions that are used and presented by default.

Another reason why it makes sense to re-budget these values is that all modules interface in the same way to the inside of MOF which, up to its first resonance, acts as a rigid body. This means that it is irrelevant where forces are exerted: as long as it is within the frequency range 0 – 200 Hz, their effect on the resulting spectral displacement will be equal.

Initially, the budget that was available for all sources of cooling vibrations i.e. the four water-cooled modules and SUSA supply tubing was **<0.70**, **0.70**, **4.0 nm> (XYZ**). These values were divided evenly over all sources in a quadratic fashion:

sub-system	*module*	*sub-module*	*X-budget* [nm]	*Y-budget* [nm]	*Z-budget* [nm]
ILO	BG		0.35	0.35	2.00
PBB	BSW		0.35	0.35	2.00
POS			0.35	0.35	2.00
CON		ABC	0.35	0.35	2.00

Next, a new division will be presented ("re-budgeted error").

2.3.2: Redistributing Error Budgets

2.3.2.1: Incorporated Parameters

Method

Based on a variety of parameters, and insights gained from the TNO study that established a relation between expected acoustic source characteristics and flow rate, computations have been made specifically for the modules that will be tested in the new design (see App. B-1). Based on these outcomes, a shift in center frequency and scaling of the source amplitude is predicted for which the requirements will be adjusted (custom specs per module).

Input Parameters:

- Flow rates [m³/s]
- Pressure [bar]
- Heat dissipation [W]
- Dimensions channel geometries [m]
- Number of channels [n]
- Length of channel [m]

Output Parameters:

- Reynolds number i.e. turbulence indication [-]
- Flow velocity [m/s]
- Expected source amplitude [Hz]
- Expected shift of center frequency *(bulk of generic shape)* [-]
- Weighting function – *(50% relative tube length, 50% fractional flow velocity & amplitude)* [-]

relation between acoustic **source amplitude** and **flow rate**

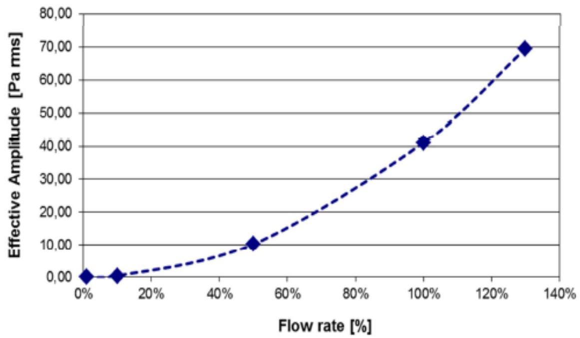

relation between **acoustic source center frequency** and **flow rate**

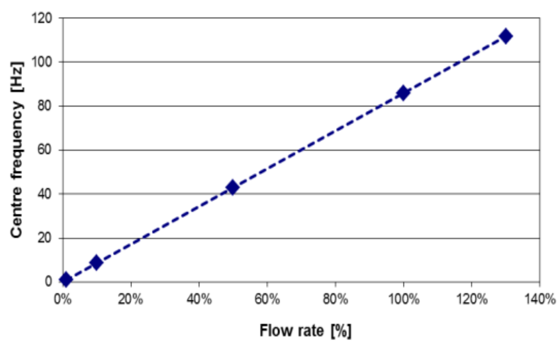

Graphs from the TNO research report for Mapper: "Flow induced pulsation analysis inside cooling channels of Aperture Array"

2.3.2: Redistributing Error Budgets

MAPPER lithography

2.3.2.2: Re-budgeted Error Values

Distributing wafer error contribution based on process parameters

Based on the parameters mentioned before, an overview will now be given of the applied weighting factor and the resulting (re-budgeted) error values. The latter will be used as basis to determine the Force Requirement Spectra (FRS) needed for the design. The applied distribution is not based solely on dissipative power of the modules or the flow rate at which coolant circulates to remove this heat (App. B-1). This is because it is inevitable for the cooling channels to become increasingly smaller, as modules get closer to the wafer (and the electron beams have shrunk). Therefore channel length, geometry and pressure have been incorporated as well. The resulting factors used to weigh each module's FIV contribution to nanometer wafer error are:

sub-system	module	sub-module	*flow rate* [l/min]	*dissipated power* [W]	*Weighting factor* for source amplitude exponential graph TNO	*(AVG: tube length / 50% flow speed)*		*Predicted Shift* for center frequency linear graph TNO	*(base line from prediction TNO study on AA)*
ILO	BG	AA			-			-	Hz
ILO	BG	COL			**14,99%**			-1,4	Hz
PBB	BSW	CL+IBC (CLBC)			34,90%	**59,60%**	= ∑ BSW	-	Hz
PBB	BSW	MAA / BLK			24,70%			-	Hz
POS	PL				**15,14%**			16,75	Hz
CON		ABC			**10,27%**			-6,03	Hz
		Total flow rate UPW:	[illegible]	∑ Power: [illegible]					

I.P.

Re-budgeted error per (sub)module:

sub-system	*module*	*sub-module*	*X-budget* [nm]	*Y-budget* [nm]	*Z-budget* [nm]
ILO	BG		0.16	0.16	0.94
PBB	BSW		0.65	0.65	3.75
POS			0.17	0.17	0.95
CON		ABC	0.11	0.11	0.65

2.3.3: Extracting Force Functions

2.3.3.1: **STEP 1** – Presumed Spectral Shape of FIV

Comparison differently shaped FRS – scaled to meet budget

Motivation
Before, the expected force spectrum used by Mapper, was an educated guess and an overall downward trending shape was used **(blue curve)**. The right figure shows the new spectrum that has been constructed based on available measurement data that is reliable up to 90 Hz **(red curve)**.

This graph has been adjusted based on the process parameters mentioned in § 2.3.2.1 and hydrostatic measurement data showing that complex geometries (AA) can expect higher FIV input in the 80–150 Hz regime. Also, center frequency has been shown to depend on flow rate for which adjustments are made per module. This results in force spectra that are *lower overall* due to the peak in sensitivity of Matrix's weighting function (§ 2.1.3). *Designing the tool based on this red curve is more conservative as it poses a stricter requirement on the performance of Forcesix.*

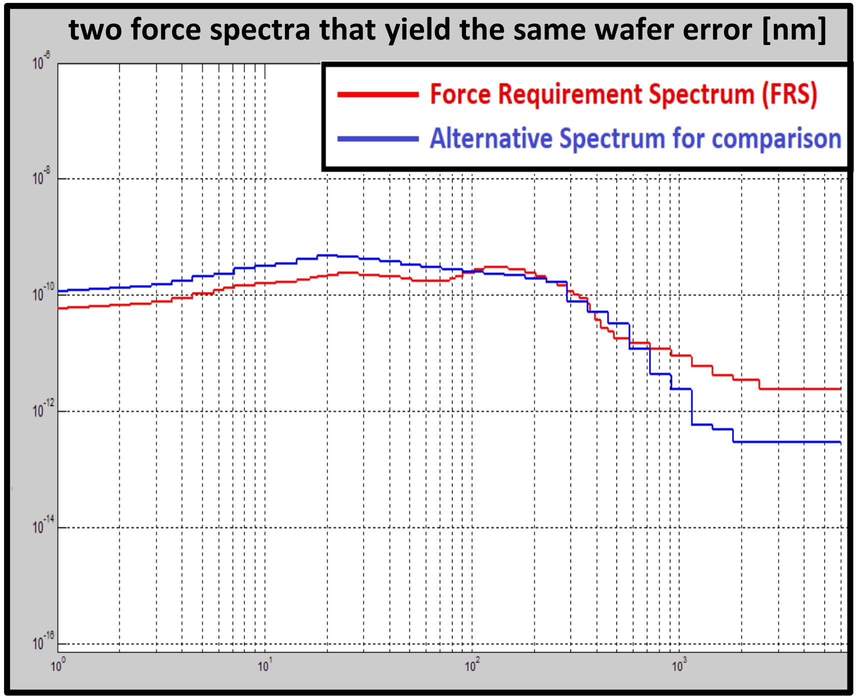

Conclusion
Forcesix will be designed to observe dynamic forces in the frequency range 10 – 300 Hz with its required noise level shaped as the red spectrum. In magnitude however, this requirement is placed *an order lower* than the level corresponding to re-budgeted wafer error values (different for each module). This is done to account for limited resolution w.r.t. the different DOFs that need to be measured, e.g. due to different sensor angles. This approach allows for focus on the most stringent requirement (XY) only, based on which design choices can be made.

Note: differences that can be seen in step size for higher frequencies are due to logarithmic scaling.

2.3.3: Extracting Force Functions

2.3.3.2: **STEP 2** – Converting FIV to Wafer Error

As illustrated by Figure 1.7 and shown here below, converting FIV to wafer error is not straightforward and requires a number iterative computations. To achieve this a Matlab script has been written which can be found in Appendix D.

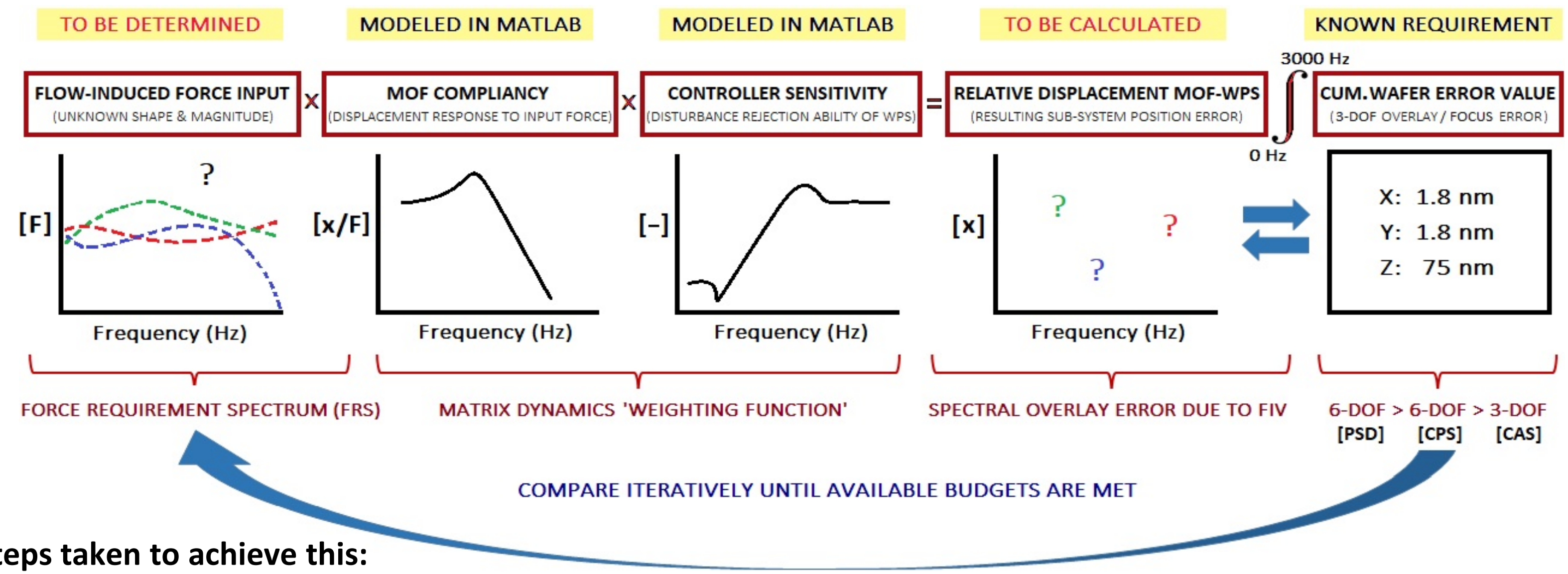

The steps taken to achieve this:

- establish a generic FIV shape based on real-life measurement on a realistic structure (Vibronix > Aperture Array)
- compute deviations from this shape based on theoretical insights from the TNO study (source amplitude & center freq)
- model the compliance of MOF and its controller sensitivity characteristics (i.e. create a ‘weighting function’)
- starting at a low magnitude: write a multiplicative script that combines the above functions (per terts band)
- integrate the resulting spectral overlay error due to FIV over the whole Matrix BW (0 – 3000 Hz)
- compare the cumulative wafer error value with the re-budgeted values presented in § 2.3.2.2
- If not met: increase the magnitude of the base shape by 0,1 % and loop the calculations; repeat until budgets are met

2.3.3: Extracting Force Functions

2.3.3.3: **STEP 3** – Filtering the Expected Response

The last 4 steps mentioned on the previous slide indicate how the expected response can be 'filtered' into a final wafer error value that can be compared against the available budgets. Objective of that approach is to arrive at a four different force requirement spectra, one for each module that will be tested, that together make up the total portion of the stage stability error budget, alotted to cooling vibrations.

The next challenge will be to select a sensor who's bounds between noise level and range are sufficient to not only verify the force requirement spectrum, but also observe FIV that well exceed that level. This will be investigated in the next chapter.

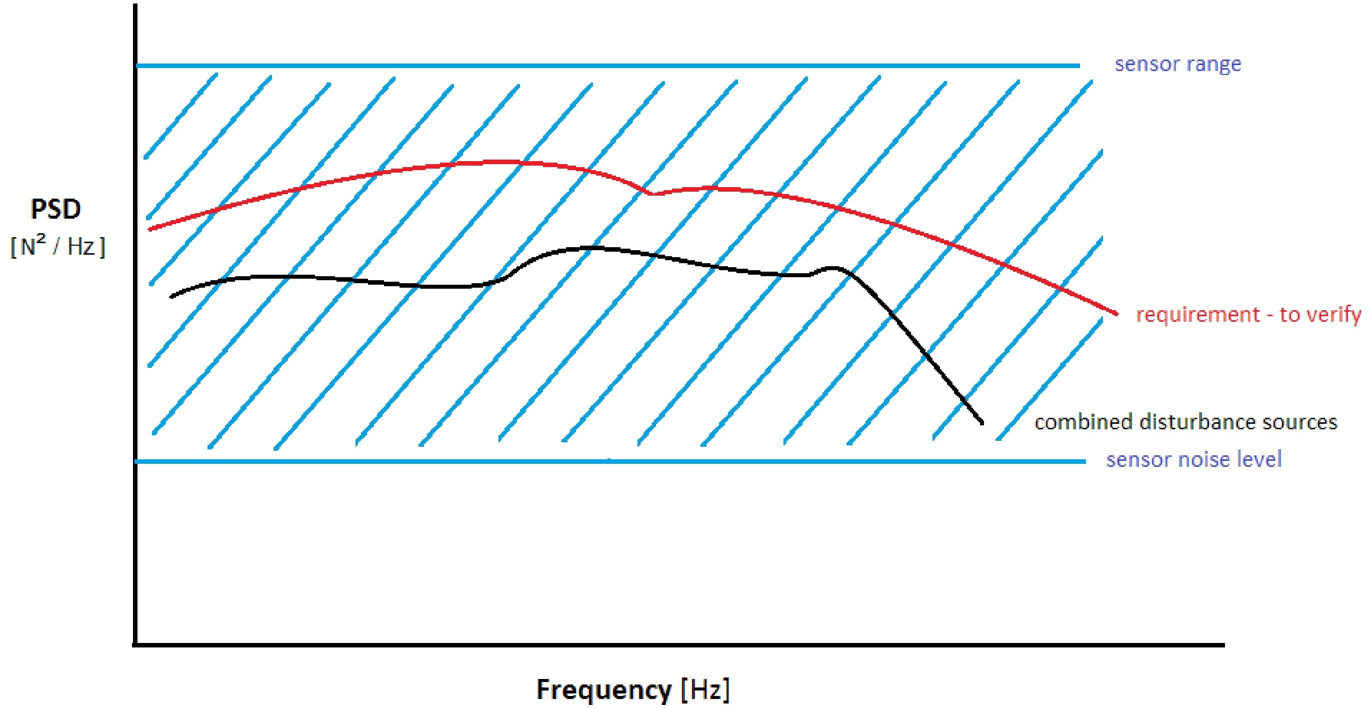

CH. 2.4

Design Requirements

Functional Requirements

Key Indicators

TECHNICAL

The PSD of the Force Requirement Spectra (FRS) that the new design should be able to measure in order to verify the matrix modules, is shown below. **This requirement has been set for all six degrees-of-freedom in the ratio: < 1, 1, 10, 2, 2, 10 >** i.e. < X, Y, Z, Rx, Ry, Rz >. This is based on Matrix system dynamics, with only the most stringent direction shown here (XY – in plane).

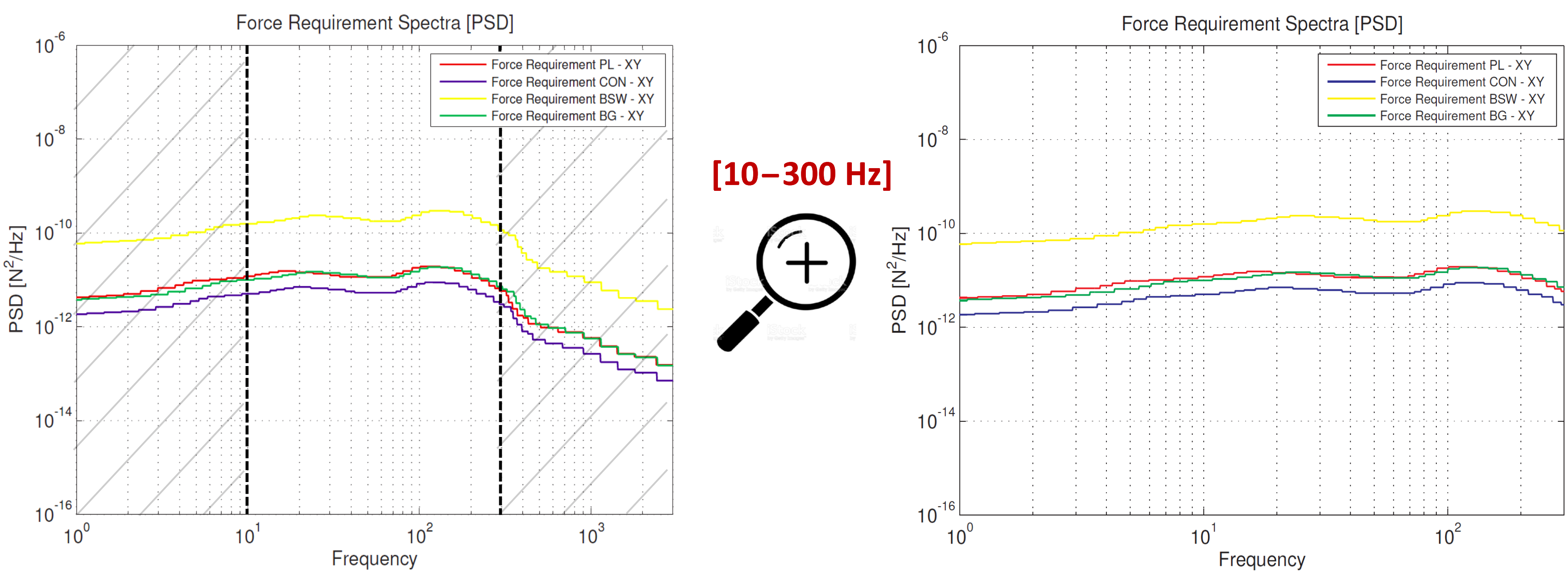

This left plot shows the FRS computed over the total BW for Matrix (3 kHz), see § 2.3.3.2. The right plot zooms in on the section from (10 – 300 Hz); the requirement for *this design*. A difference in horizontal alignment between different requirements can be observed. This is the result of the presumed spectral shape calculations as detailed in § 2.3.3.1. It can be seen that the required noise level is extremely low, being in the order of 10^{-11} [N²/Hz], which corresponds to a RMS force level of 0,35 µN [XY].

Functional Requirements

Key Indicators

This poses a design challenge as it is difficult to find sensors that can observe such small forces. Second, to incorporate them in a mechanical design where this noise level is not overshadowed through a variety of disturbances (e.g. mechanical vibrations).

The graph on the right shows the scaling of the Force Requirement Spectra (FRS) over the different DOFs, in the ratio as mentioned on the previous slide. This is displayed for the POS module with XY at the level of the FRS presented. Note that this graph is a CAS representation [N/$\sqrt{Hz}$], whereas the global requirements regard Power Spectral Density [PSD] functions in units [N^2/Hz].

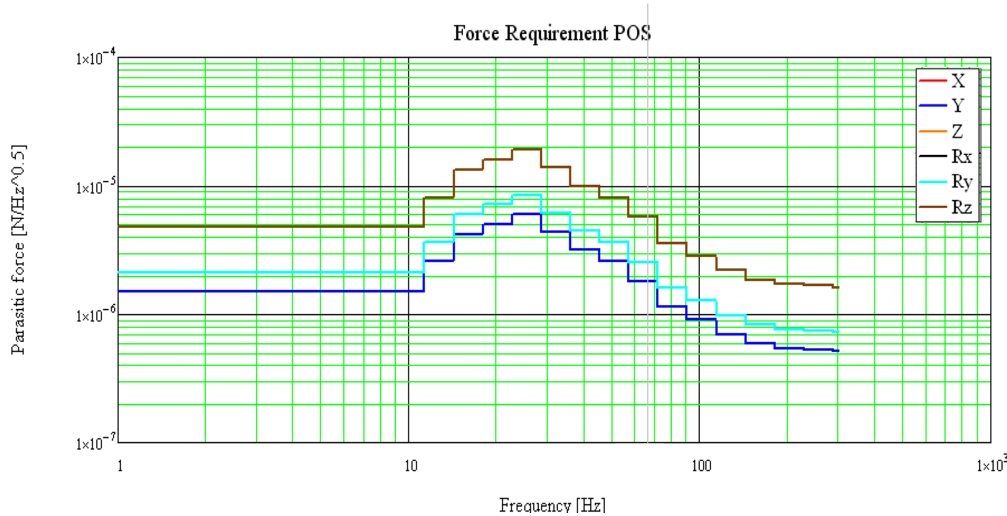

INTERFACE

The design should have a interface comparable to that of the module when integrated in the MOF. This in terms of center position, interface stiffness, contact mount (Hertzian) and with similar pre-tension. In Matrix this is achieved through Ø 15 mm ceramic balls. Lastly, its orientation should be the same w.r.t the global coordinate frame used by Mapper.

TESTING

All facilities and procedures for testing should be devised in such a way that it can be executed repetitely and accurately. This means supplying sufficient water flow under near constant pressure and flow velocity for the during of multiple batch measurements, so they can be averaged out. Also, installation and verification steps should be documented in a procedure.

Chapter 3

Designing the Measurement Setup

Chapter Outline

Chapter 3 is set up as follows:

- in § 3.1, the design is split in independent sub-designs and concepts are devised that meet the required functionalities.
- to gain an understanding of the challenges in this design, the present disturbances are calculated and measured in § 3.2.
- using this input, the above design questions are answered individually in § 3.3, yet on a global level.
- in § 3.4, the dynamics of the selected concept and the Dynamic Error Budgeting (DEB) model used to combine all disturbances sources are explained. After validation, the model predicts the expected performance of the winning concept. This is a clear indication of the concept's ability to meet the requirements that were set in chapter 2.
- lastly, § 3.5 describes the final design in detail, giving more insight in the sub-functionalities used to solve the design questions listed in § 3.1.

Note that even though the chapter starts off by showing different concepts in § 3.1, for readability the rest of the chapter only shows the results for the winning concept. All calculations and simulations have however been conducted for both concepts, based on which a winning concept has been selected. These additional results can be found in Appendix B-2.

CH. 3.1

Concepts

3.1.1: Defining sub-functionalities

Applying the modular design approach i.e. splitting the design in independent sub-designs

To ensure feasible concepts, the following functionalities should be present:

1. **Isolate the setup from floor vibrations** present at the location where the design will be placed
2. **Shield the setup from acoustics** present at the location where the design will be placed
3. **Supply flow to the modules** that are held by the design to mimic conditions in the Mapper machine (Matrix)
4. **Decouple internal FIV** in supply tubing from flow-vibrations induced in the modules
5. **Prevent Helmholtz resonances** from occurring in the supply tubing i.e. don't create additional input
6. **Select a quantity to measure** i.e. what physical property can be used best to answer the RQ
7. **Measurement principle choice** i.e. given the outcome of (6) what principle is most effective
8. **How to suspend the modules** i.e. keep them isolated from the environment, limiting disturbance transmission
9. **Choose a sensor configuration** i.e. how many sensors / orientation / angle etc. is feasible and most (cost) effective
10. **Design a generic interface** that can be used to mount the modules to the setup, referenced w.r.t. Matrix coordinates

These 10 design questions each bring about sub-problems that can be solved using a variety of sub-solutions. Different combinations of these sub-solutions resulted in different concepts of which the most promising two will be presented next.

The concepts discussed are already a selection from a meta-analysis from which the choice was made to aim for a robust passive system (i.e. not actively actuated). This to reduce costs but also to limit complexity given the stringent requirements posed on the various Mapper modules that have to be tested, in terms of allowable magnetic- and electric fields present.

This objective and the steps taken to prevent Helmholtz resonances (5) are treated integrally in *§ 3.3.3 and § 3.3.4* *therefore no separate page is present.*

3.1.2: Concept A

Absolute **Acceleration** Measurement

Using 6 accelerometers

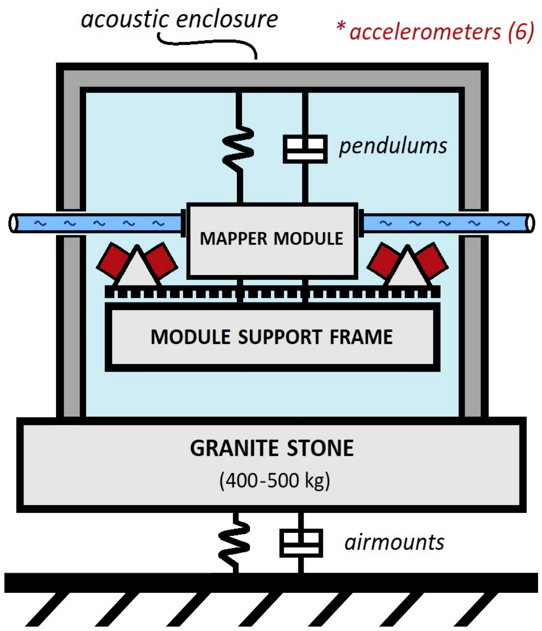

Concept A uses six acceleration sensors to observe movement of the module under testing in 6-DOF. These accelerations result from cooling water flowing through the Mapper module, thereby inducing vibrations. The illustration on the right gives a general overview of the components, not a definitive configuration.

In this setup, the Mapper module is passively suspended as a pendulum (mass hanging from an ideally frictionless pivot) by which a very low eigenfrequency can be achieved. This is beneficial as it can therefore act as the second stage of the VI platform. The low stiffness interface does however go at the expense of the system's disturbance rejection ability, making the design prone to outside disturbances.

An advantage of this concept is that all FIV generated forces result in acceleration of the suspended module, with negligible transfer to the first stage. The downside of measuring low-level accelerations is that noise levels scale with mass, which calls for a light design. This is challenging since the seismic sensors alone weigh about six kilos. Also, this mass restriction limits the allowed stiffness of the pendulum suspension, to ensure a low enough resonance to start FV attenuating from 10 Hz on. The following aspects make creating the silent world necessary to measure absolute accelerations, difficult to bring into practice:

- creating a reliable pendulum suspension without hysteresis or large static sag *(but with a low 1st resonance)*
- a low resonance frequency for the most stringent DOFs *(X, Y, Rx, Ry)*
- uncoupled DOFs of suspended module *(the pendulums overconstrain the concept vertically)*
- symmetric design, accounting for offsets in COM of modules *(remain level w.r.t. the horizon)*

3.1.2: Concept A

Absolute **Acceleration** Measurement

Properties selected accelerometer

The selected seismic accelerometers are from the brand Wilcoxon, type M731A (picture bottom-right). This sensor has an effective range of 0.05 – 450 Hz and is normally used to monitor seismic activity. Its *spectral acceleration noise level* (**red line**) is therefore very low. This is a necessity given the incredibly small forces that need to be measured to meet the stringent *Force Requirement Spectrum* (FRS: **black line** ≈ 10^{-11} – 10^{-12} N^2/Hz).

It can be seen that the sensor's PSD noise level scales with mass squared. To meet the design objective of being able to verify the FRS over the frequency range 10 – 300 Hz, the maximum allowed mass of the payload is 25,4 kg (level in between **purple** – **yellow line**). Included in this weight are the Module Support Frame (MSF), optical breadboard, Mapper module, six sensors, and supply tubing w/water.

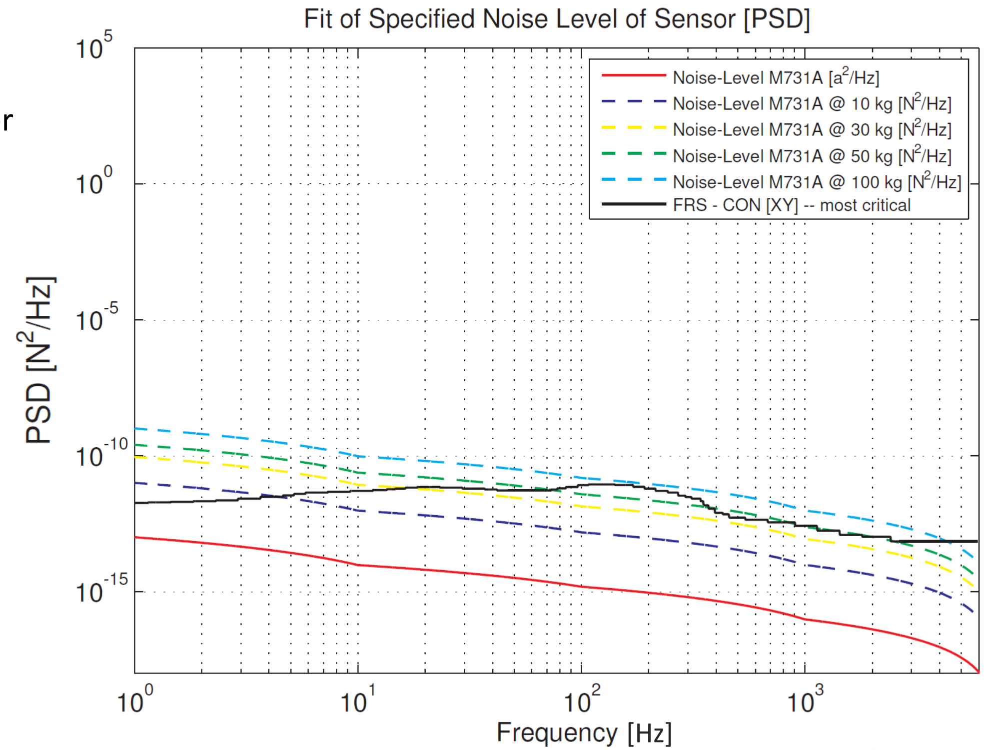

Apart from having a low enough noise level, the M731A has been chosen because of its high sensitivity of 10 V/g (i.e. 1,02 V/[m/s²]) providing good resolution and a narrow uncertainty band. Other advantages are a first resonance at 750 Hz and a low sensitivity to electromagnetic interference (20 µg/gauss). The former ensures trustworthy measurement until 300 Hz (contrary to behavior seen in the Endevco sensor in Vibronix) and the latter minimizes AC mains pickup. A disadvantage is the high temperature sensitivity of 0,343 %/°C which can cause thermal drift under lab space operating conditions (± 3,4 % output variation at ± 5°C).

3.1.3: Concept B

Reaction **Force** Measurement

Using 6 piëzo sensors

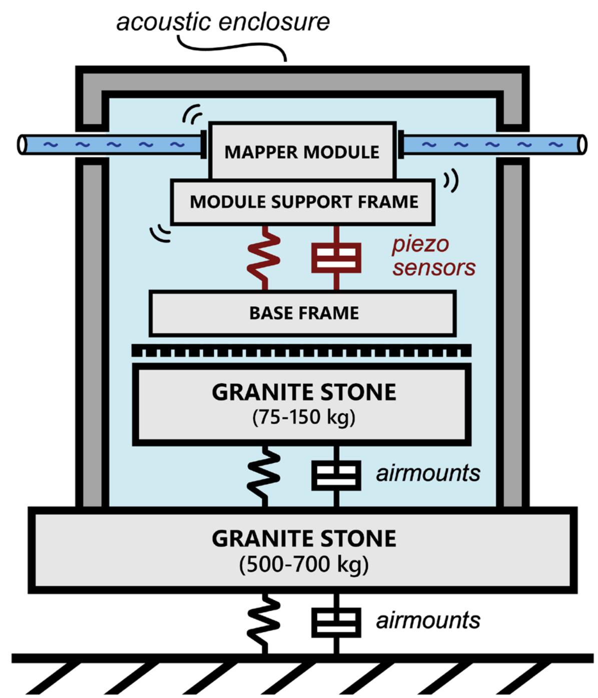

As illustrated, **concept B uses 6 piezoelectric force sensors to observe forces exerted by the tested module on its environment in 6-DOF.** These reaction forces result from cooling water flowing through the Mapper module, thereby inducing vibrations.

In this design, the module is rigidly connected to the 2nd stage of the VI platform through the high stiffness of the six piëzos. This is possible as the quartz crystals only measure dynamic forces, allowing the sensors to be subject to small static loads (thus measuring in compression). This means of support effectively turns the setup into a triple mass-spring-damper system, which is advantageous from a dynamics point-of-view. Once the airmounts have fully decoupled, there is good isolation from floor vibrations. However, for passive systems this normally goes at the cost of the disturbance rejection ability of the suspended mass (seen when observing payload accelerations). Yet now, the stiff interface makes the tested module much less sensitive to direct disturbances entering the system through parallel stiffnesses (e.g. pressurized tubing, cabling).

Contrary to the acceleration concept, this configuration is able to circumvent the fundamental trade-off of passive VI. This as dynamic measurement takes place in the frequency range *after* resonance of the VI system and *well before* the piëzos start to decouple. Here, the response is dominated by the stiffness of the piezo sensors i.e. the combined 'spring line' and dependent on relative displacement instead. The effect this has on the ratio measured force/exerted force, will be investigated in § 3.4.4.1.

Another advantage of this design is that connecting the module in this way, will ensure it remains perfectly level i.e. the DOFs uncoupled. This is due to the high axial stiffness of the piëzos ($4 \cdot 10^8$ N/m) that comes from pre-loading the used quartz crystal in a metal enclosure. This value is comparable to a steel rod of 20 cm long and one cm in diameter. (Schmidt et al, 2011)

3.1.3: Concept B

Reaction **Force** Measurement

Properties selected piëzo sensor

The selected sensors are dynamic force transducers from the brand PCB, model 209C11 (picture bottom-right). This piezo has an effective range of 5 – 6000 Hz and can be used to measure unidirectional transient forces perpendicular to its impact cap. It has a built-in signal conditioner that transforms the high-impedance signal to a low-impedance voltage which is ideal for low-noise measurements. More detail can be found in § 3.5.6.

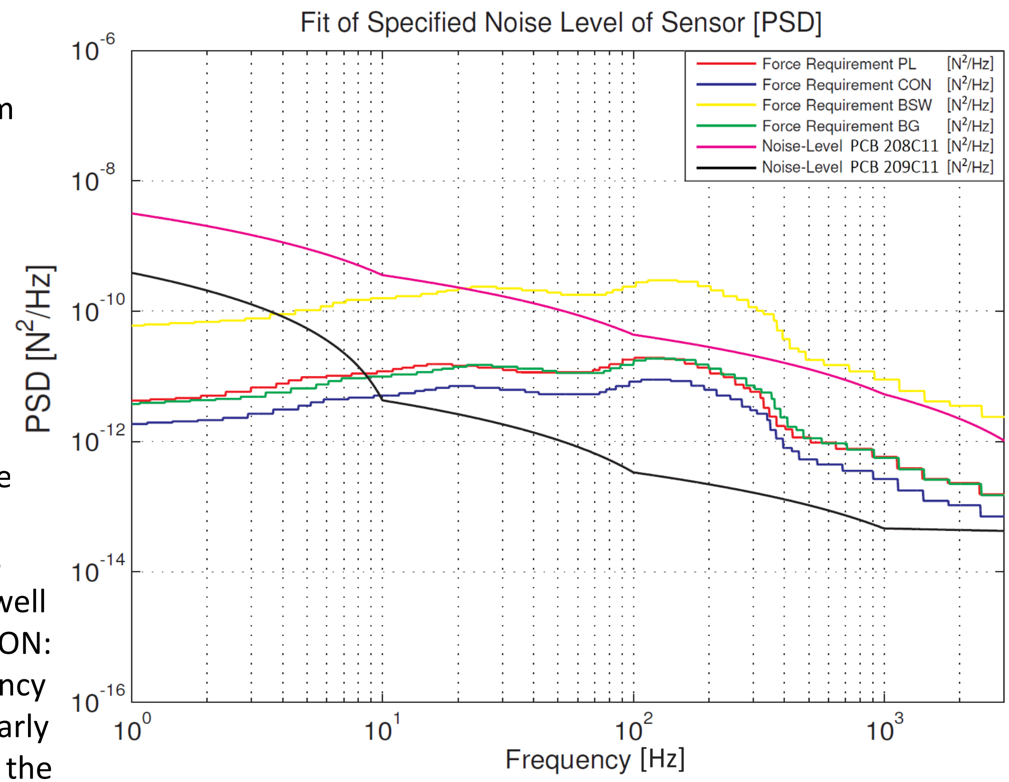

The graph on the right shows the *force noise level* of the sensor, indicated by the **black line,** alongside the *Force Requirement Spectra (FRS)* of the four Mapper modules that must be verified. It can be seen that the sensor is well able to observe even the most stringent requirement (CON: **blue line** ≈ $6 \bullet 10^{-12}$ [N²/Hz]) over the 10 – 300 Hz frequency range. In fact, the sensor noise characteristic is particularly low in the critical frequency range of 80 – 120 Hz, where the Matrix metrology system is unable to adequately correct for errors due to a peak in controller sensitivity.

This advantage of a very low broadband resolution ($9 \bullet 10^{-5}$ N-rms) which is independent of the mass it supports, comes at the price of a limited static load tolerance of 48,9 N per sensor. This restricts the angle under which the sensors can be placed as they have to carry the module to be tested. The **pink line** is the noise floor of the best alternative sensor (PCB-208C11) that has a higher static load tolerance. This piezo is only able to verify the BSW module and therefore not a viable option. Light design is thus key.

3.1.4: General Comparison

MAPPER lithography

Acceleration Concept (A) vs Force Concept (B)

Fundamental trade-off of passive vibration isolation

Measuring **accelerations** instead of **reaction forces** using *passive* floor vibration isolation brings about the fundamental trade-off of such a system. This means that until the resonance frequency, the stiffness of the spring can resist direct-disturbances acting on the body well, as spring forces dominate the response. However, base accelerations are transmitted one-on-one through this same spring connection giving poor isolation from floor-vibrations (**graph 1**). Conversely, above resonance floor accelerations are well attenuated but DDF cannot be opposed as now frequency-dependent inertia forces dictate the response.

This becomes visible when plotting the normalized, dimensionless compliance (double derivative i.e. accelerance) together with the acceleration-based transmissibility (**graph 2**). It can be seen that the two functions are linked together through the (complementary) sensitivity function (**graph 3**) i.e at every frequency except ω_n, they add up to 1. Therefore, shifting the resonance frequency left or right by increasing mass or decreasing stiffness will benefit one, but only by going at the expense of the other. Moreover, this can cause practical issues such as static sag and decreased disturbance rejection ability in terms of displacements (compliance, **graph 4**)

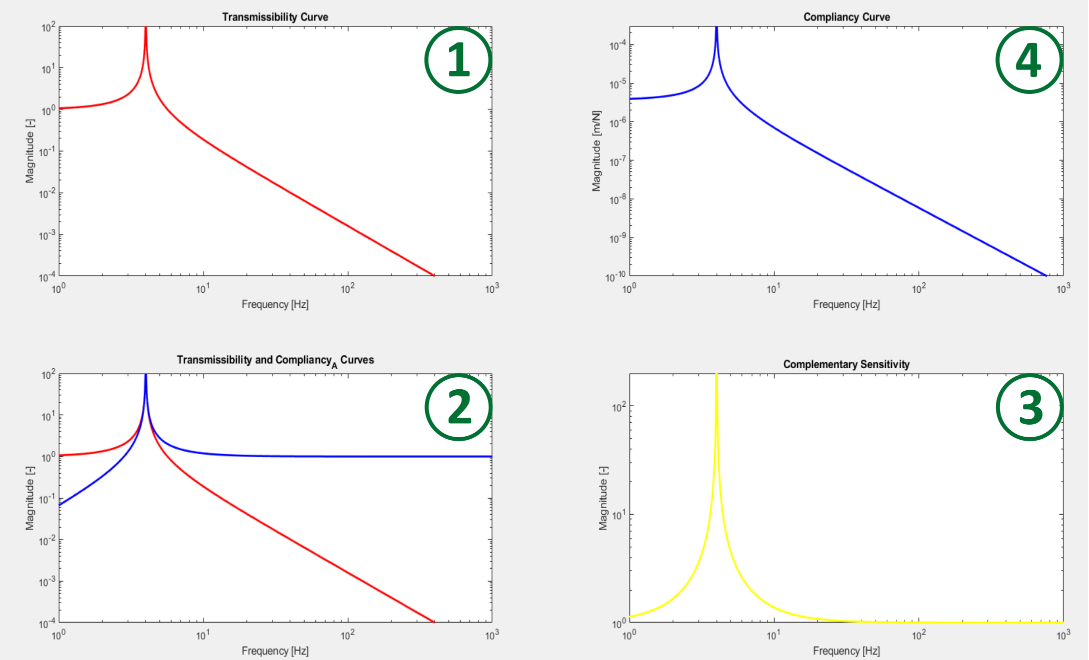

As the design will be placed in Mapper's lab space there is a need for significant suppression of floor vibrations. **This favors the force concept as the acceleration concept is particularly prone to outside disturbances at frequencies above the resonance frequency of the VI system (≈ 3-5 Hz).**

3.1.4: Concept Selection

MAPPER lithography

Acceleration Concept (A) vs Force Concept (B)

Pros & Cons

The main requirement for both concepts to work is that the module under study is properly isolated from FV and shielded from DDF. As will be detailed in § 4.1, a double MSD system is required to sufficiently suppress base accelerations as well as a physical enclosure to shield environmental acoustics, both of which would otherwise dominate sensor output.

Also both concepts require airmount damping values to be kept low to prevent the transmissibility chart from 'hinging up' after resonance. This as high damping causes roll-off at a -1 slope instead of a standard -2 slope resulting in more throughput for higher frequencies, which is unwanted.

The figure below gives an overview of the pros and cons for both concepts. Based on this comparison, it was not possible to make a choice between concept A and B. This as the requirement that needs to be verified (FRS) is very low level and it was unclear what the effect would be the various disturbance sources on the sensor signal. Hence, both concepts have been fully simulated and only then the conclusion could be drawn that **Concept B is the only one concept that is able to meet the requirement.**

Therefore, this is the concept that will be presented in the body of this document. For readability, all simulation results of Concept A (acceleration) can be found in Appendix B-2.

	CONCEPT A *acceleration measurement*	**CONCEPT B** *reaction-force measurement*
PROS	- low noise sensor - high sensitivity	- low noise sensor - high axial stiffness (good dist. rejection) - light-weight sensors - easier to uncouple DOFs - low thermal sensitivity sensor
CONS	- scaling sensor noise with mass - sensitive to parallel stiffnesses - big and heavy sensor (x6) - large static sag pendulums - high coupling between DOFs (≠ level) - high thermal sensitivity sensor - heavy sensors must be placed away from COM for angular resolution increasing moment of inertia	- low static force tolerance - mounting challenging (no bending moment) - sensitivity sensor lower

CH. 3.2

Disturbance Sources

3.2.1: Overview

3.2.1.1: Measurement Uncertainty

Interfering and modifying error

Objective of this paragraph is to map all present disturbance sources that have an impact on the signal that is measured by the two concepts. Ideally this 'idle noise level' is close to zero. In practice it never is and the challenge is to bring remnant parasitic noise down to an level that is acceptable for the purpose of the measurement setup. Note that for the current designs, crosstalk levels can be computed as these relate to used sensors, cables and data processing equipment. However, the effects of (measured) interference sources on the sensor signal strongly depend on design-dependent parasitic stiffnesses. As their influence is generally dominant, these are modelled in detail in § 3.4.

The below schematic shows that any every level of a measurement system, disturbances can enter as either an interfering error (i.e. adding) or a modifying error (i.e. multiplying). Here, the total measurement uncertainty is the difference between the true value (often not known) and the measured value (sensor signal). Besides calibration, properly mapping all disturbances beforehand is key in order to end up with a design that meets its requirements but also to know its uncertainty (Bentley, 2005).

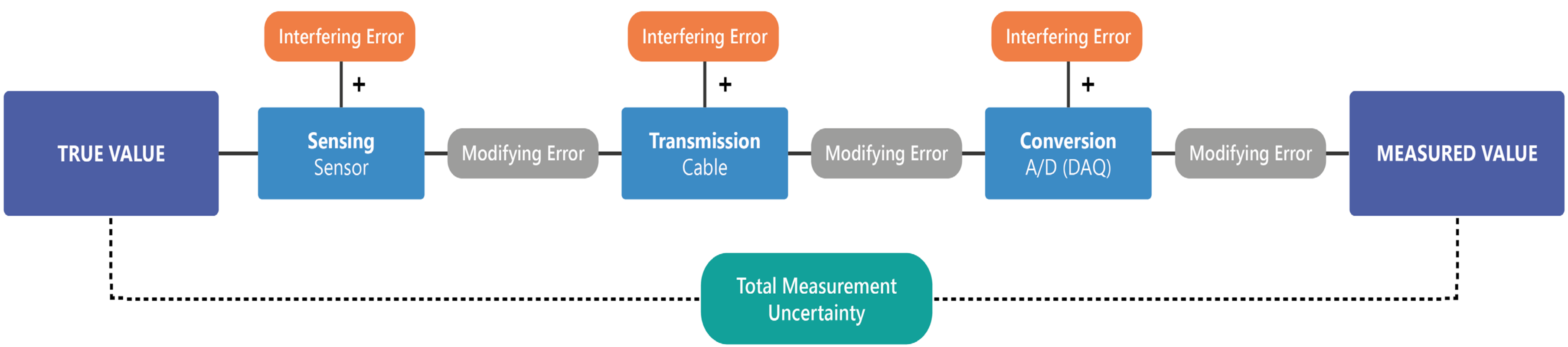

MAPPER lithography

3.2.1.2: General subdivision

Interfering and modifying error

A first step in preventing measurement error and eventually determining the total uncertainty is to map out all different error sources. From various literature sources, multiple different error sources have been identified. These can be split up into **interference** or **crosstalk** i.e. coming from *outside* the measurement setup, or being generated *within*. Distinguishing what is what is essential as both require a different mitigation/attenuation approach. The general sub-division that can be made between error sources, and their respective deterministic/random nature, has been summarized in the following figure:

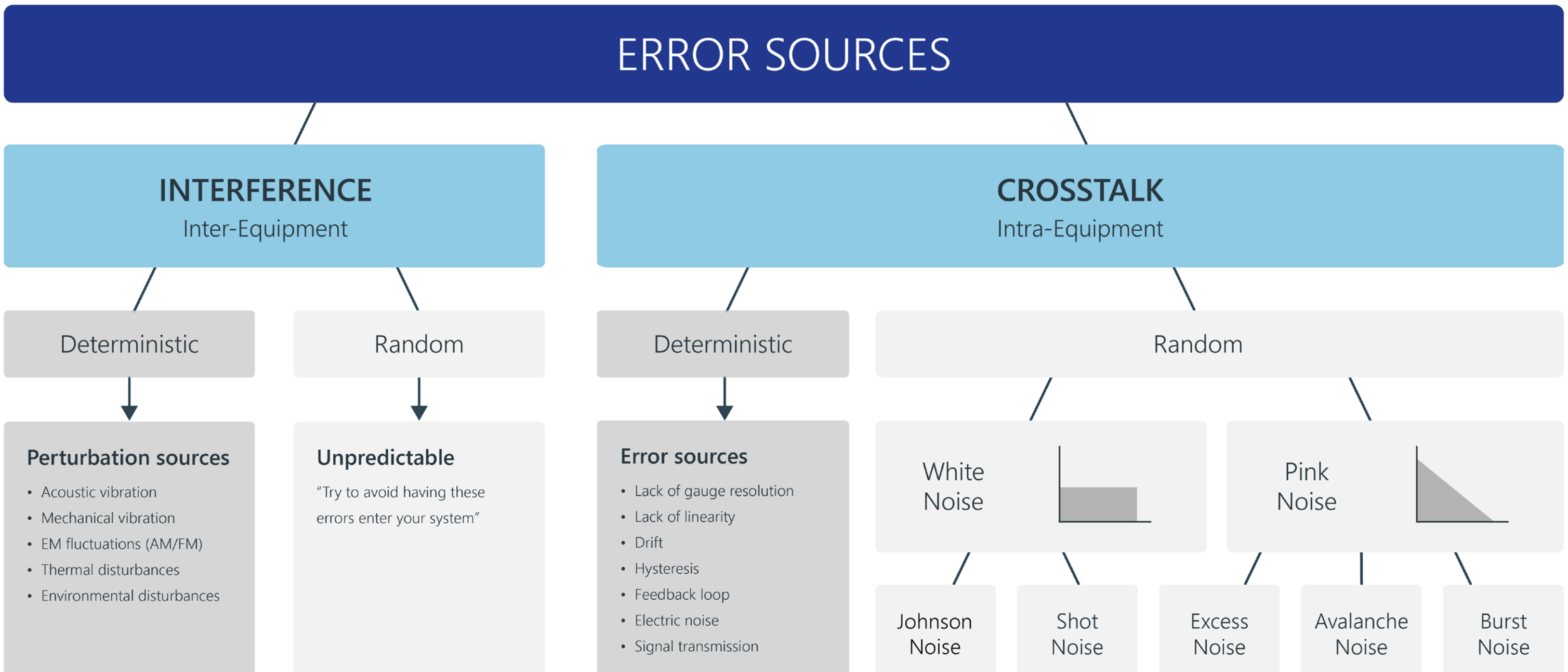

Measurement in Engineering (WB2303-10) – lectures 8 & 9 (M. van Spengen)

3.2.1.3: Design Specific Categorization

Mechanical / thermal / electrical disturbances

The general sub-divide shown on the previous slide can be made design-specific by mapping out all error sources that are expected to be present in a design. This has been done for both concepts.

The overview on the right-hand side shows the identified deterministic and random error sources for concept B (reaction force measurement).

In the schematic, all sources of interference and crosstalk have been categorized in **mechanical**, **thermal** and **electronical** disturbances. The ten sub-solutions discussed in the following section that make up the final design, take these disturbances as a basis and propose a solution (*shield / mitigate / accept*). This decision is often made by modeling the effect that the measured disturbance has on the measured sensor signal.

Using this error source overview, generic design guidelines have been established that can serve as a reference when others are designing a measurement system in the presence of dominating disturbances (Appendix B-3)

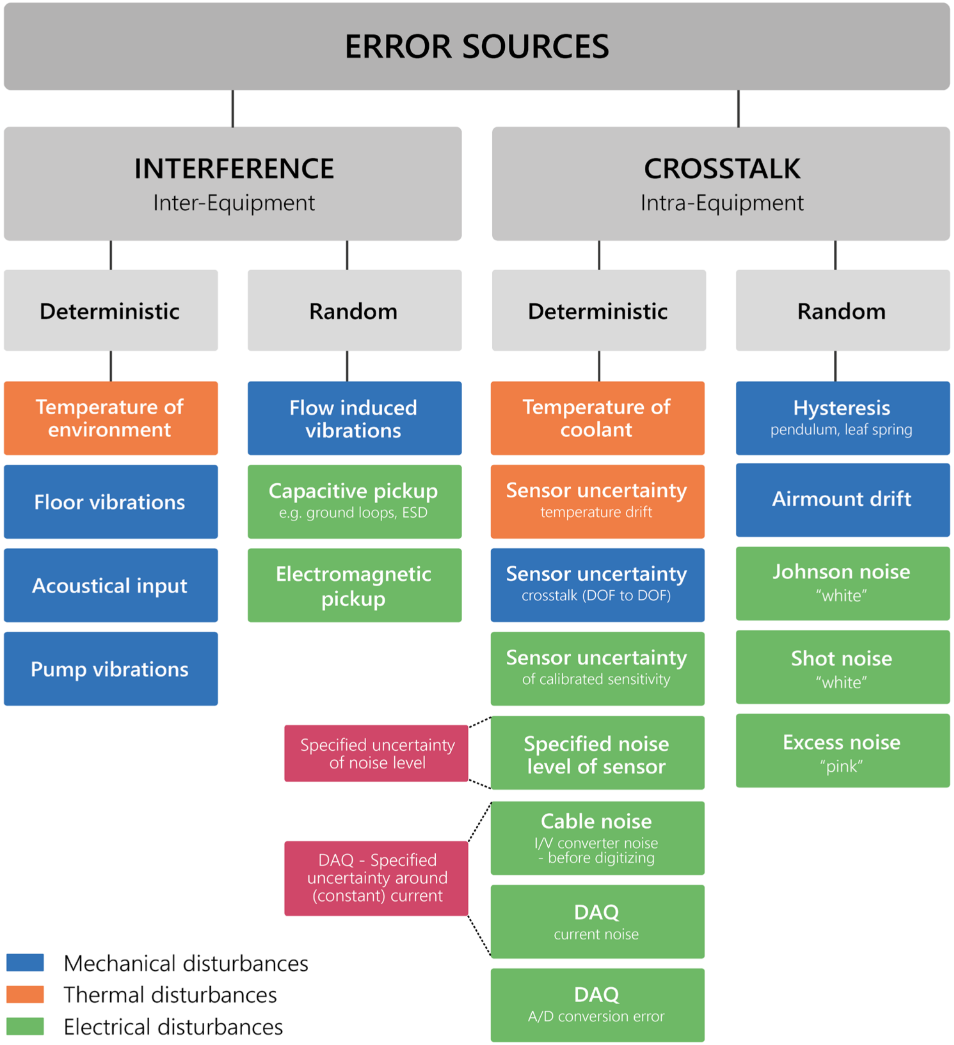

3.2.2: Measuring Interference

3.2.2.1: Floor-Vibration levels

Location: Mapper labspace Rotterdamseweg

Floor vibrations can greatly impact the performance of a sensitive measurement device. Especially the labspace of Mapper at the Rotterdamsweg where the design shall be placed, is notarious for ground movement as it is right next to the river “de Schie” with cargo ships regularly passing by. To prevent measurement error because of this, floor accelerations have been measured in 3-DOF at different times / locations using BK accelerometers mounted on a custom interface block with a high-stiffness ceramic connection to the ground. The background levels present at this location is quite different than was modeled by Mapper using standard VC spectra. Therefore, the generic background noise level shown on the right has been made which captures the expected floor vibrations, fitted for this specific location.

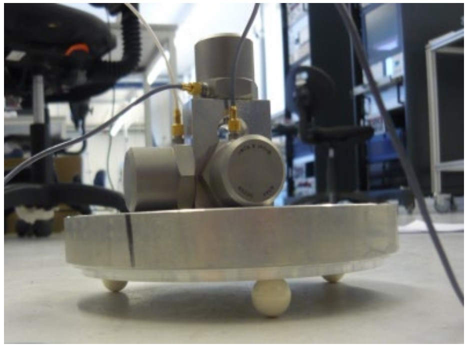

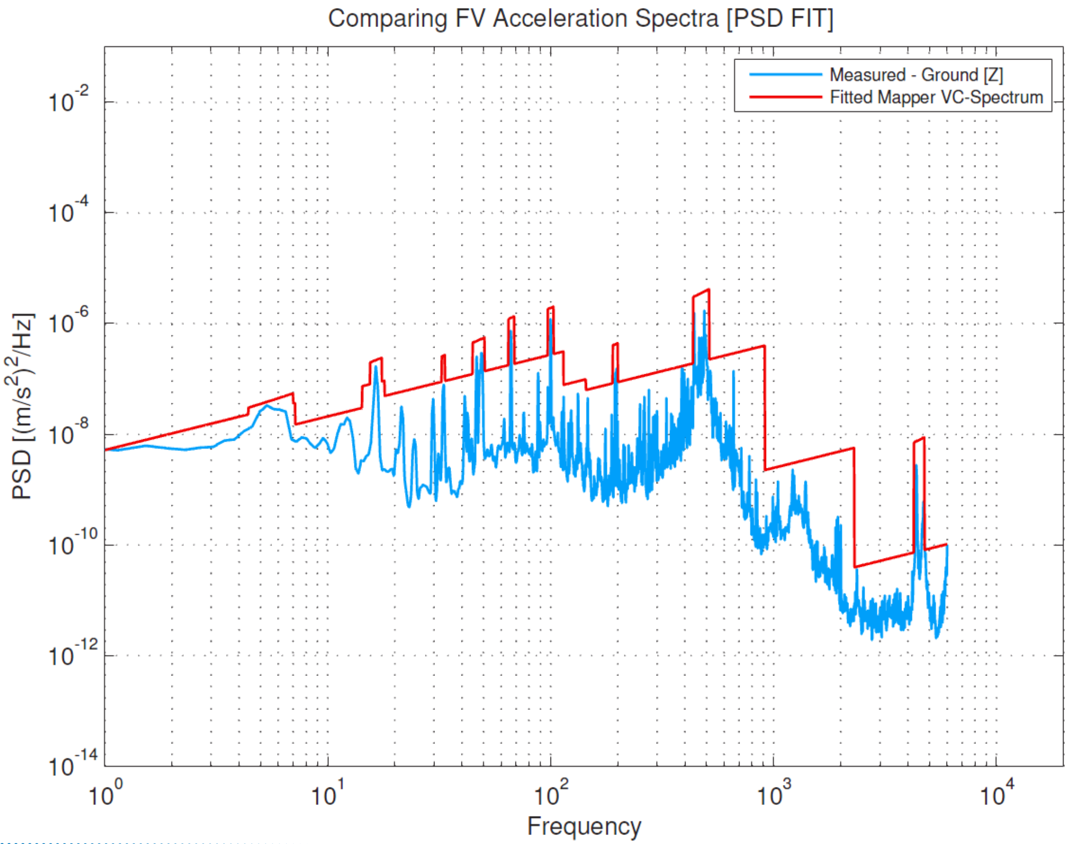

3.2.2.2: Acoustical Background

Location: Mapper labspace Rotterdamseweg

The research of Dennis Lakerveld, who created the Vibronix test setup, made clear that acoustical interference can have a large effect. To model the effect of acoustics for this design beforehand, the background acoustic sound pressure has been measured on various locations around the test setup, in different directions and at different times using a BruelKjaer Microphone (*type 4189 with pre-amplifier type 2671*). From this measurement data, a mean background noise level has been constructed (**"AC"**) that will be used in the Dynamic Error Budgeting (DEB) model presented in § 3.4. It looks as follows:

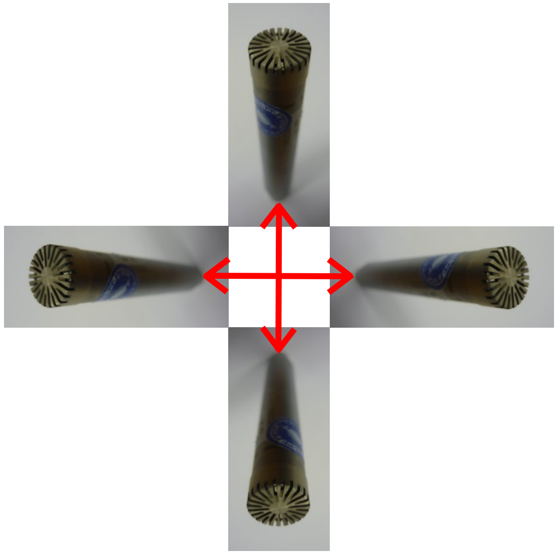

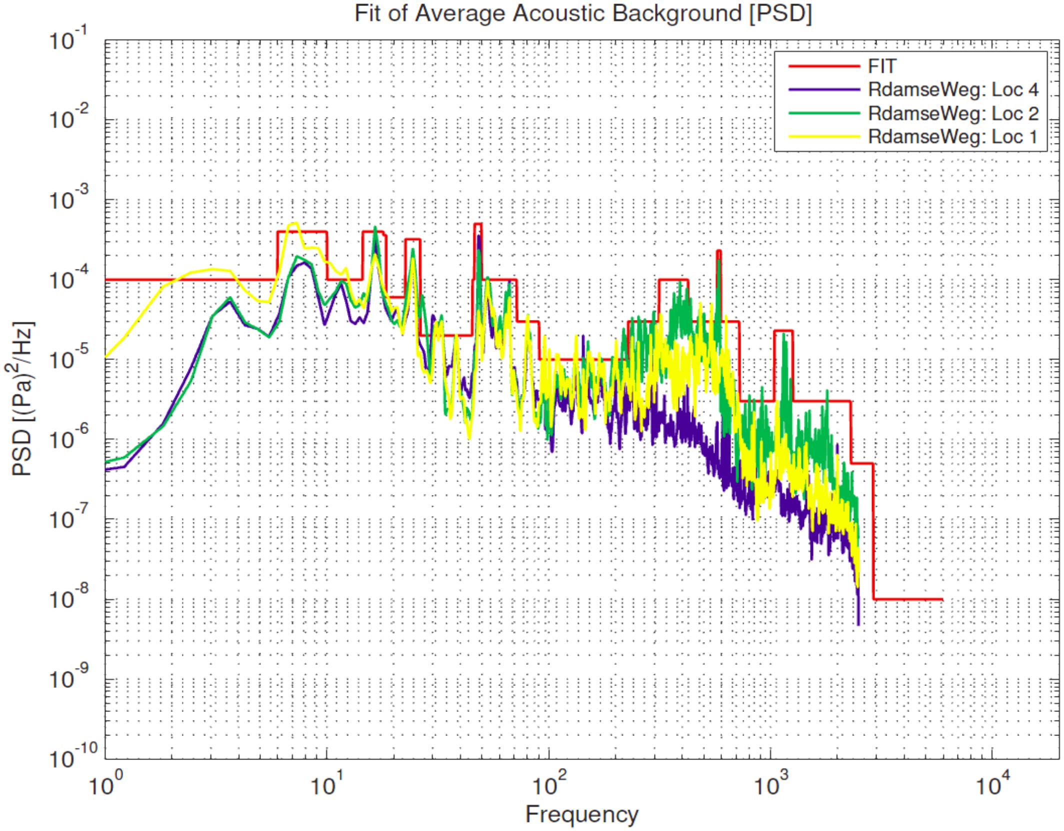

3.2.2: Measuring Interference

3.2.2.3: Internal Acoustics – *observed inside Vibronix*

Location: Mapper labspace Rotterdamseweg

Similar to the previous slide, the remnant acoustic sound pressure level inside the Vibronix test setup is of particular importance, as these sound waves act unfiltered on the sensitive part of the measurement device under design. Therefore, it has also been quantified through measurement at different times. For clarity: the measurements have been performed *in* the acoustic casing shown below, with the cover closed (through a hole in its roof).

From these sound measurements, a mean (attenuated) background noise level has been constructed: **"ACi"**. It will be used in the Dynamic Error Budgeting (DEB) model presented in § 3.4. It looks as follows:

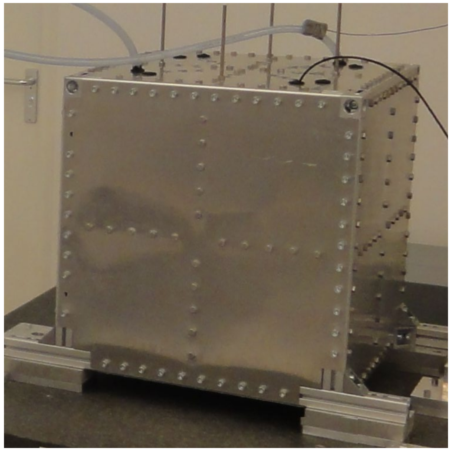

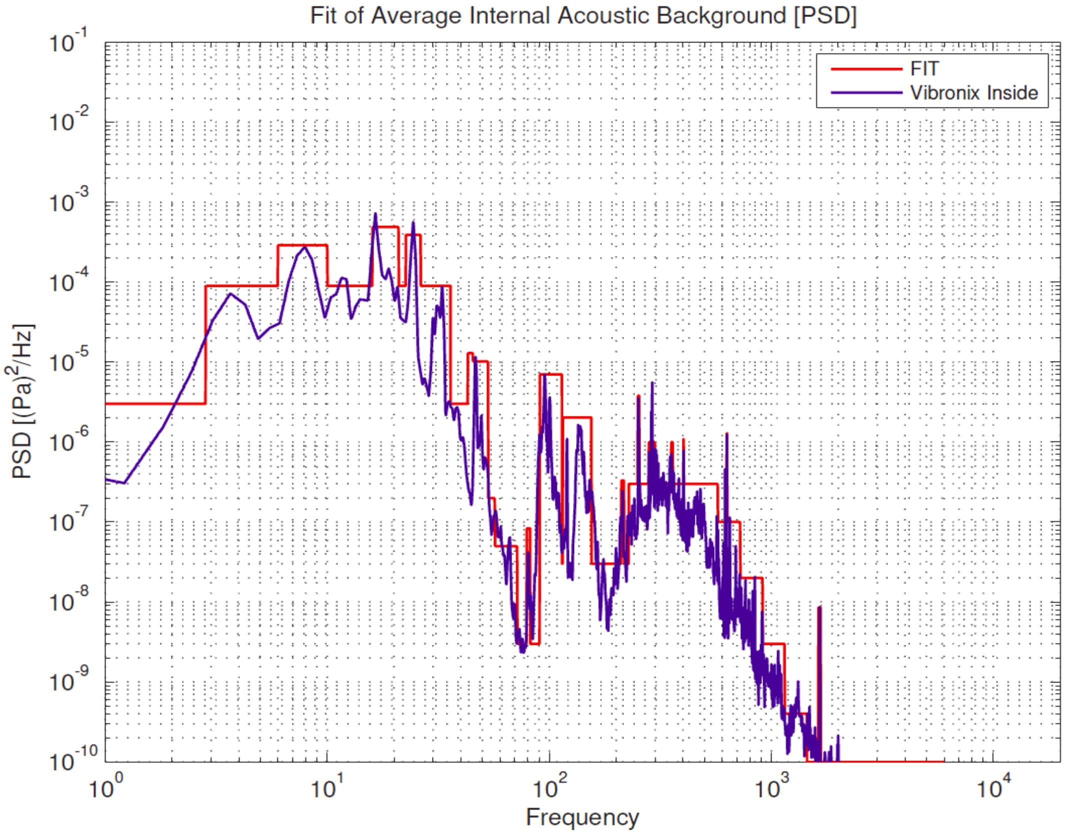

3.2.2: Measuring Interference

3.2.2.4: Flow-Induced Vibrations in Supply Tubing

Acceleration of straight flexible tubing – NO FLOW

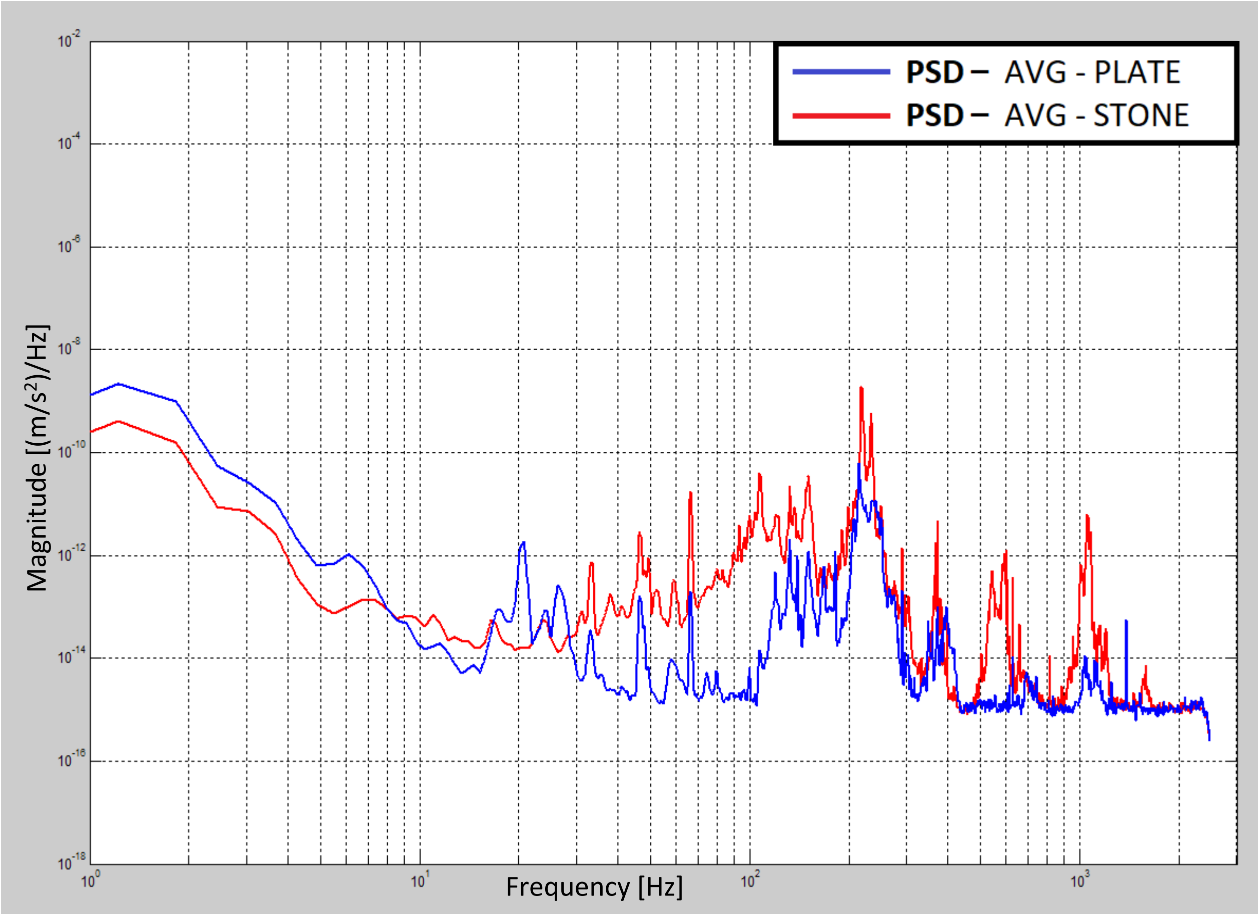

3.2.2: Measuring Interference

3.2.2.4: Flow-Induced Vibrations in Supply Tubing

Acceleration of straight flexible tubing – WITH FLOW @ nominal rate for AA (13.8 L/min)

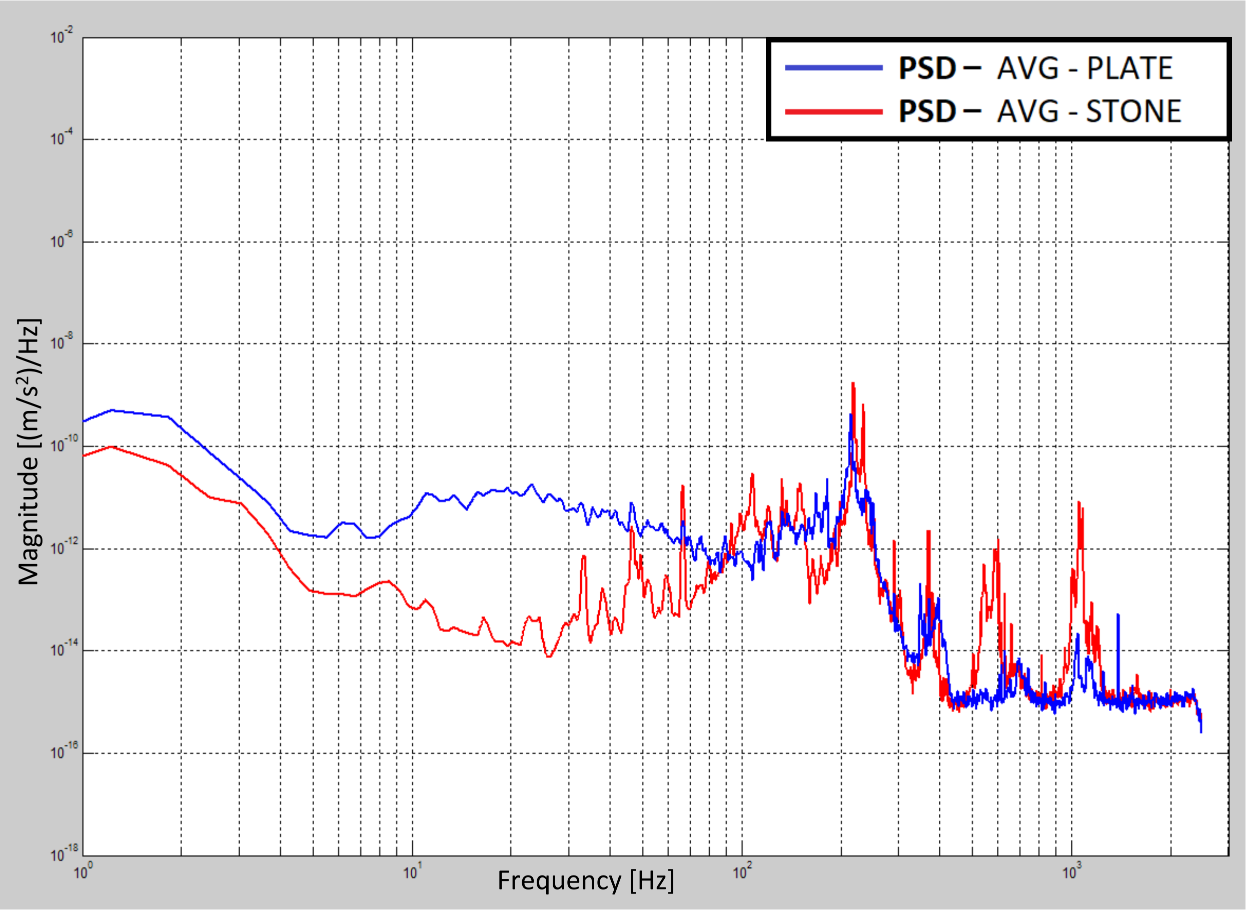

3.2.2.4: Flow-Induced Vibrations in Supply Tubing

Extrapolating Results – identified FIVi (0.3 m) and assumed FIVo (3.0 m)

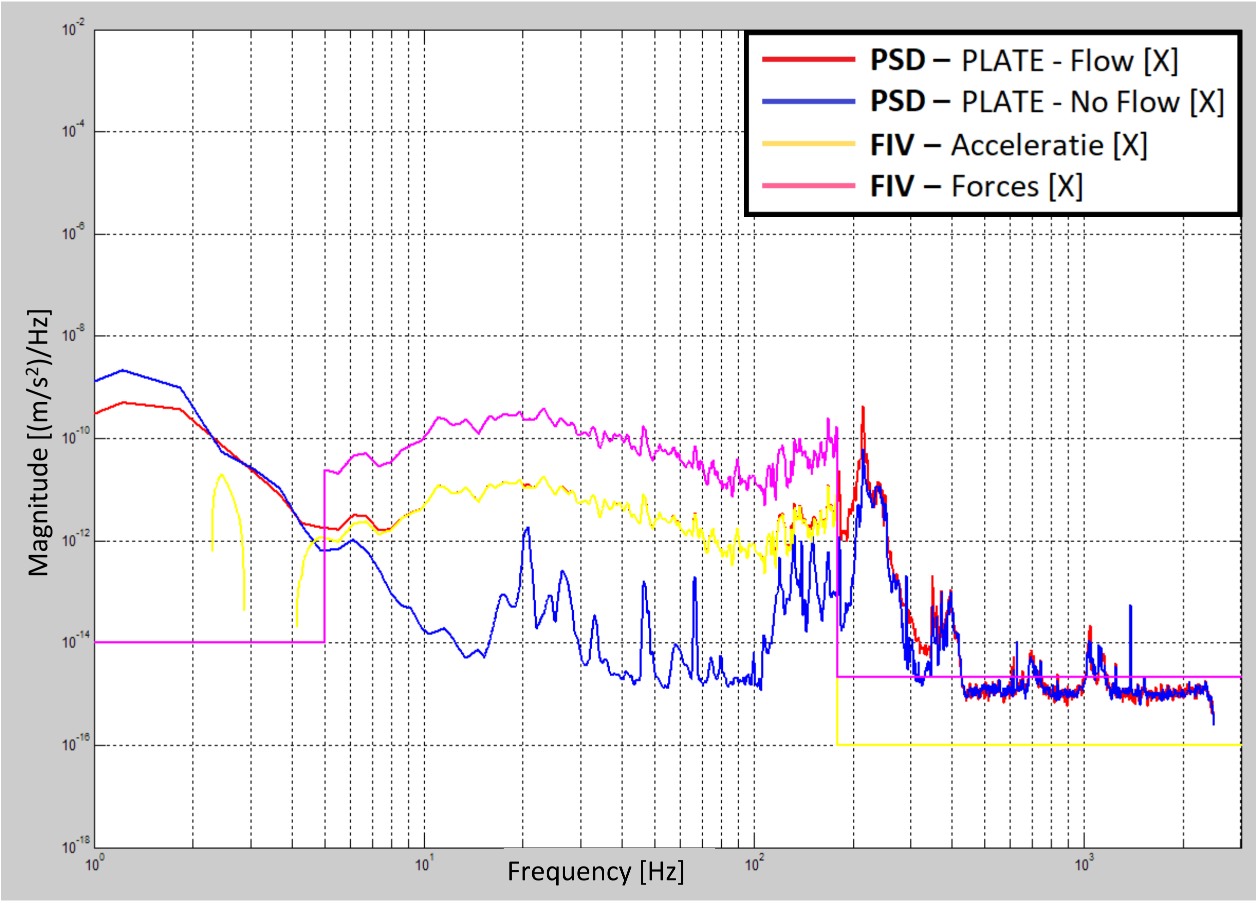

The measured accelerations due to flow vibrations induced in a tubing section of about 50 cm long are plotted in **yellow**. This is referred to as *FIVi*. Multiplied by the (squared) mass of the suspended pendulum + tubing, the resulting forces in X are obtained (**pink line**).

The tubing length *outside* the acoustic case of Vibronix is about 3-5 m. Hence this force spectrum (*FIVo*) is expected to be 10x stronger. Both will be used in DEB model presented in § 3.4.

3.2.3: Computing Crosstalk

MAPPER lithography

3.2.3.1: Formulae

Estimating noise levels inherent to the design

Many aspects of the general overview shown in § 3.2.1 can be circumvented by design, shielded of attenuated to acceptable levels. There is however an element that will always remain which is the *random part of crosstalk* (Hisland and Alciatore, 2012). This noise can either be 'white' (independent of frequency) or 'pink' (spectral power decreases at increasing frequency) but it is inherent to the use of currents and voltages in cables / sensors / DAQs to perform the measurement.

From different sources of literature, the below overview has been composed (**larger picture in Appendix A-3**). Using the below formulae, the spectral **Johnson Noise, Shot Noise** and **Excess Noise** levels have been calculated. The approximated effect of these crosstalk sources on the design is shown on the next slides, relative to the FRS level i.e. the requirement to verify.

White Noise

Pink Noise

Johnson Noise

Johnson Noise is the thermally induced random motion of charge carriers (e.g. electrons) that cause a fluctuating potential. Every dissipative element (e.g. resistors) suffers from this noise source which is also called 'thermal noise'. It is independent of current flow and can be modeled either as a voltage or as a current.

When modeled as a voltage, the thermal noise source is placed in series with an otherwise noiseless resistor:

PSD: $N_t = 4kTR$ [V²/Hz]

CAS: $V_{rms} = \sqrt{(4kTR*B)}$ [V]

When modeled as a current, the thermal noise source is placed in parallel with an otherwise noiseless resistor:

PSD: $N_t = 4kT/R$ [A²/Hz]

CAS: $I_{rms} = \sqrt{(4kTB/R)}$ [A]

k = 1.38 x 10^{-23} [J/°K] - Bolzmann's constant
R = Resistance in the device [Ω]
T = Absolute temperature of the device [°K]
B = Bandwidth (BW) over which voltage is measured

Shot Noise

Shot Noise is the noise due to random passage of individual charges across a potential barrier (e.g. a transistor junction). This effect becomes especially troublesome for very small currents due to the discretization of the flowing charges.

When measuring voltages, shot noise levels are calculated as follows:

PSD: $\varphi_{sv}(f) = 2I_n qR^2$ [V²/Hz]

CAS: $V_{rms} = \sqrt{(2I_n qR^2*B)}$ [V]

When measuring currents, shot noise levels are calculated as follows:

PSD: $\varphi_{si}(f) = 2I_n q$ [A²/Hz]

CAS: $I_{rms} = \sqrt{(2I_n q*B)}$ [A]

q = 1.59 x 10^{-19} [C] - Electron charge
R = Resistance in the device [Ω]
I_n = Nominal current flowing in the device [A]
B = BW over which voltage / current is measured

Excess Noise

Excess Noise, also called flicker noise or 1/f noise, indicating its decreasing spectral power at increasing frequency. This is the noise 'in excess' of Johnson and Shot Noise. It is caused by the non-constant conductivity of materials due to imperfect contacts. Excess noise is always associated with a DC current in the device and it is dominated by thermal noise if the current flow is low. Because of its 'pink nature', this noise source is especially troublesome at low frequencies.

It can be modeled as a voltage:

PSD: $N_e = Ke^2/f$ [V²/Hz]

CAS: $V\_rms = \sqrt{\int_0^{BW}(Ke^2/f^{\alpha})df}$ [V]

Or calculated as a current:

PSD: $N_e = Ki^2/f$ [A²/Hz]

CAS: $V\_rms = \sqrt{\int_0^{BW}(Ki^2/f^{\alpha})df}$ [A]

K = Process constant (application dependent)
α = 1/f characteristic (assumed 1)
f = frequency band under consideration

Avalanche Noise

Burst Noise, also called popcorn-noise, is the popping sound that is sometimes heard when a bad speaker plays low frequency sound (< 100 Hz). It is likely related to imperfections in semiconducor materials which lead to stepped transitions between voltage levels.

Not present in this design.

Burst Noise

Avalanche Noise is the noise produced in a junction diode when high voltages (strong electric fields) lead to discharging of energy.

Not present in this design.

Measurement in Engineering (WB2303-10) – lectures 8 & 9 (M. van Spengen) - https://web.mit.edu/dvp/Public/noise-paper.pdf - http://home.physics.leidenuniv.nl/~exter/SVR/noise.pdf

3.2.3: Computing Crosstalk

3.2.3.2: Sensor Noise

PCB209C11

This graph shows that the selected piezo-electric sensor is suitable as its specified spectral noise floor **(black line)** is well below the lowest requirement that it needs to verify (CON Module, **blue line**).

In addition, the sensor's dynamic range is 9,79 N in compression i.e. ≈ 10^{-2} N^2/Hz spectral over its bandwidth (not shown). This means the broadband resolution ($9 \bullet 10^{-5}$ N-rms) and this measurement range are separated by about 5 orders in magnitude which is a significant variation. Another indication that this range will suffice comes from the work of Dennis Lakerveld. He showed that at nominal flow rate (13.8 L/min), the Aperture Array sub-module will produce FIV in the order or 10^{-5} N^2/Hz in [Z] i.e. a factor 1000 less than the available range.

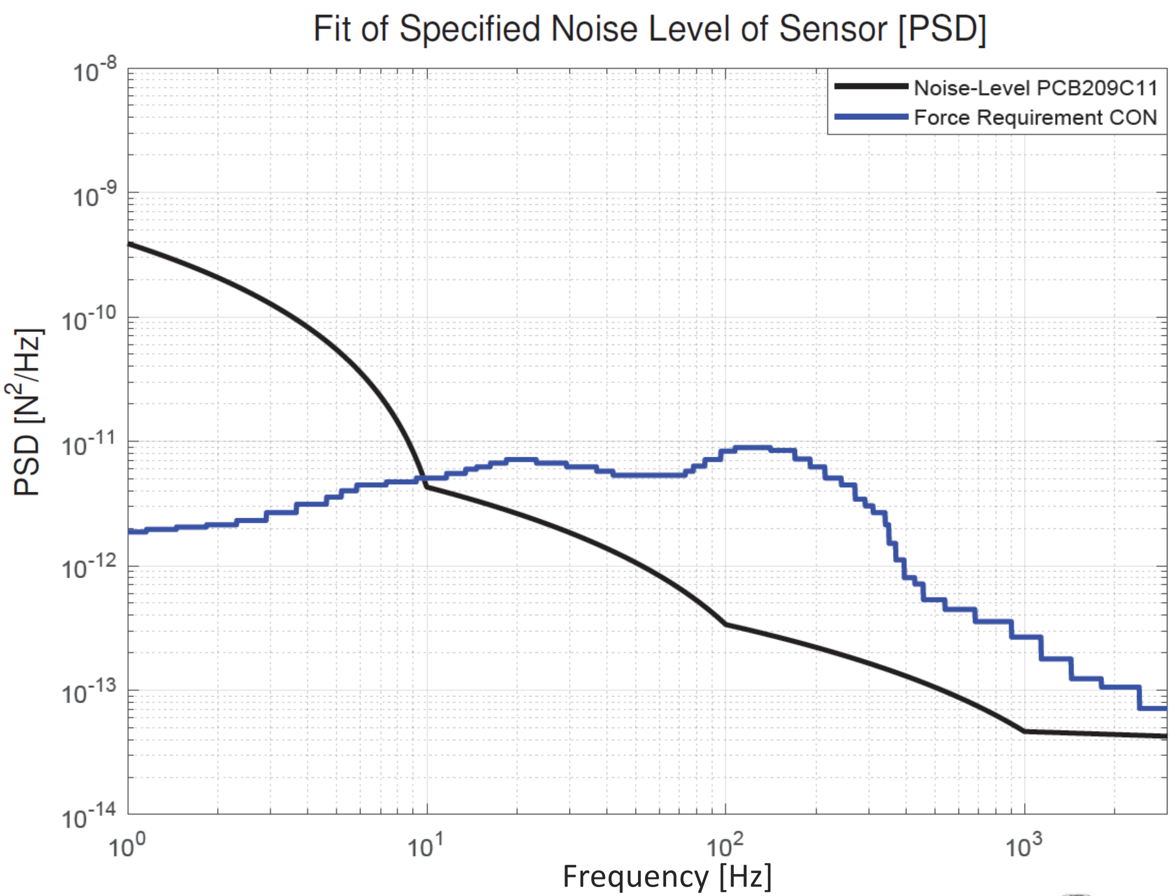

<u>In comparison:</u> if the cooling forces induced in the CON module are exactly at the level of its requirement, it is equivalent to a broadband resolution of ≈ $3{,}5 \bullet 10^{-7}$ N-rms, when integrated over the 10 – 300 Hz bandwidth. In other words, the dynamic force observed by the sensor is then equal to the weight of $\frac{1}{18}$ sugar grain (36 μg).

3.2.3.3: Cable Noise

Johnsson / Shot / Excess Noise

As explained on the previous slide, this is the remnant spectral noise level that cannot be reduced further without drastically changing the way the measurements have been set-up. The calculated levels are about a factor 10^3 – 10^5 lower than the FRS and will thus not affect the design. As can be seen, the Johnson- and Shot Noise levels are estimated to have a *'white spectrum'* i.e. independent of frequency, whereas the Excess Noise is typically known for its *'pink spectrum'* meaning that its magnitude decreases with increasing frequency.

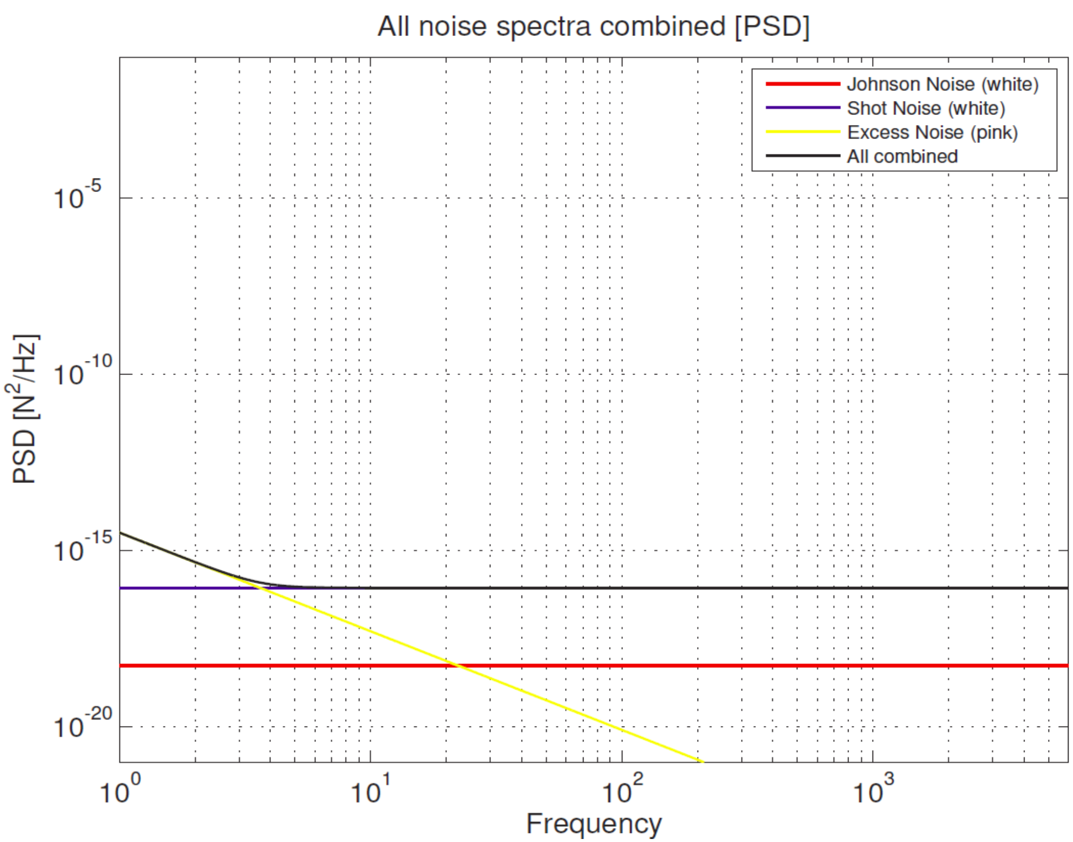

3.2.3: Computing Crosstalk

3.2.3.4: Data Acquisition (DAQ) Noise

Current / Quantization / Channel-to-Channel Noise

Related to the overview in 3.2.1.2 and derived from the formulae in 3.2.3.1, the resulting **Current Noise**, **Quantization Noise** and **Channel-to-Channel** (DAQ) **Noise** levels are shown below. From these calculations it became clear that the quantization noise level of the DAQ that was built-in the computer and had to be used for the measurements, was too high. This means it became too close to the level of the FRS (10^{-11} – 10^{-12} N^2/Hz) to be able to verify it with certainty. Therefore an alternative DAQ (NI 6229) has been selected which is 16-bit, has a high gain (100) and thus significantly reduced quantization noise. This is the noise level shown in the chart below, already translated from a current- or voltage deviation through the sensitivity into a force-spectrum PSD. *The achieved result is that these levels are now a factor ≈ 1000 lower than the FRS.*

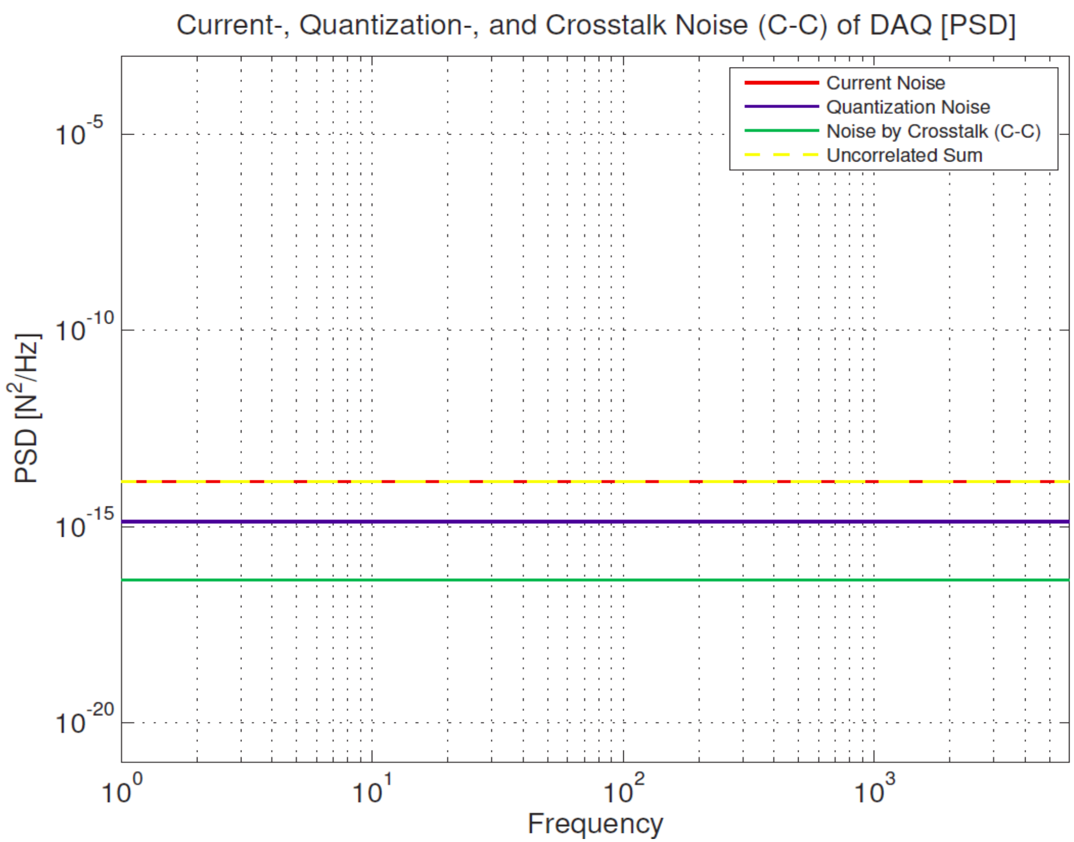

3.2.3: Computing Crosstalk

3.2.3.5: Combined Noise Level

Sensor Noise + Cable Noise [3] + DAQ Noise [3]

This slide combines all calculated noise levels presented individually on the previous slides, i.e. **Sensor Noise**, **Cable Noise** and **DAQ Noise.** This combined levels (left figure) are plotted alongside the noise level of the sensor which is now dominant. When compared to the Force Requirement Spectrum (FRS), right figure and objective of this design, it is to be expected that the remaining random part of crosstalk will not affect sensor resolution. *Note that, for scale, the axes do not align.*

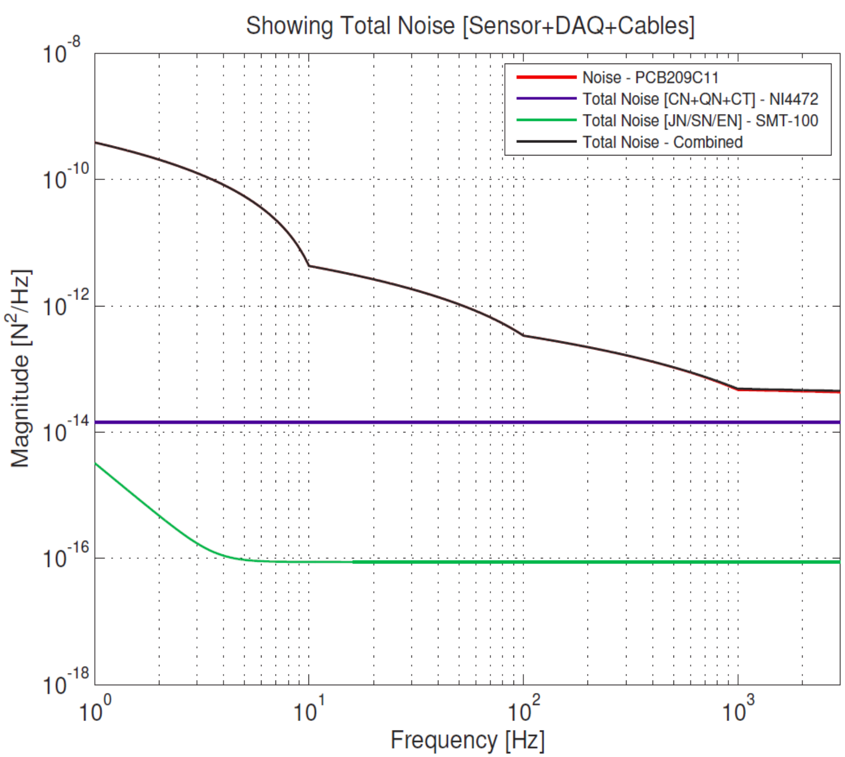

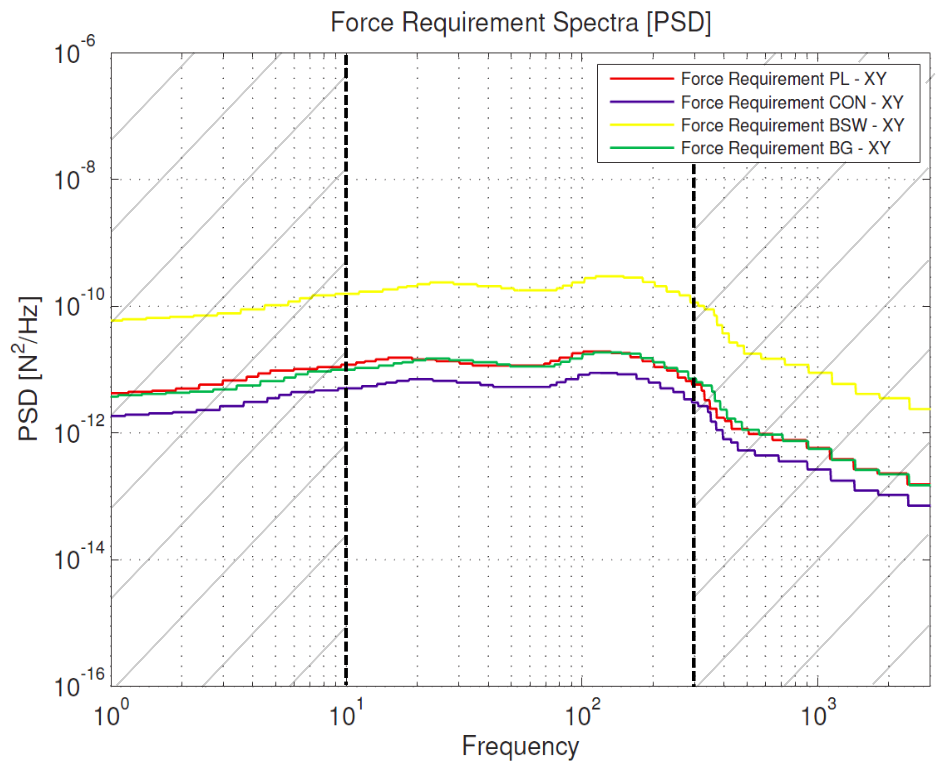

CH. 3.3

Concept
Sub-Solutions

3.3.1: Isolating Floor Vibrations

Sub-problem

- cleanroom space is unavailable, the designed tool will have to be placed at Mapper's Labspace (Rotterdamseweg, Delft)
- this is a location with higher than average floor acceleration levels, due to various equipment that is running 24/7 and because it is right next to the river 'de Schie' which has cargo ships regularly passing by. Vibrations from these heavy engines and propellor turbulence are effectively transmitted through the water, causing ground movement to be at levels higher than standard VC spectra (floor vibration levels, expressed as velocities)
- unattenuated, these vibrations can greatly impact the performance of a sensitive measurement device such as this one

Approach taken

- acceleration batch measurements have been performed in 3-DOF [XYZ] on different times and at different locations around the floor space designated for the design. This was done using three BK accelerometers (results here)
- a matlab script has been written that models the behavior of Concept B (force) in a 1-MSD system and a 2-MSD system
- the measurement data has been used to model the effect of these present floor accelerations on the forces measured if the selected sensor would be **a)** placed on the ground **b)** connected to the top mass of the 1-MSD system **c)** connected to the top mass of the 2-MSD system. These first-order results can be found in App. C.1.1. *Detailed modeling is necessary.*

Sub-solution

- the results show that a two mass-spring-damper system is necessary to sufficiently suppress floor accelerations to a level where the residual force that is measured because of it, remains below the level of the FRS from [10 – 300 Hz].
- to get a good transmissibility characteristic i.e. early airmount decoupling and a –2 slope for higher frequencies, the bottom mass in this configuration should weight approximately 500-700 kg and the top mass about 75-150 kg with max 8% damping.

3.3.2: Shielding Acoustics

Sub-problem

- labspace where the setup is to be installed has a high background acoustic noise level
- various machines running continuously; different sources, broadband spectrum
- sound pressure variations will exert harmonic forces on the measurement tool under design
- these forces migrate through the design through mechanical vibrations and are picked up by the sensor
- this acoustical interference compromises accuracy of the observed FIV forces; requirement cannot be met if unshielded

Approach taken

- a capacitive microphone has been selected to accurately observe the environmental sound pressure level
- batch measurements have been performed at various locations, times and in multiple directions
- a generic background noise level has been established and a matlab script written to model the effect of acoustics.
- the behavior of concept B (force) has been modeled for three situations : **a)** no acoustic enclosure present **b)** acoustic enclosure surrounding M3 and connecting ridigly to M2 (top stage of VI platform) **c)** acoustic enclosure surrounding M3 and connecting rigidly to M1 (bottom stage of VI platform) These first-order results can be found in App. C.1.2.

Sub-solution

- the results show that an acoustic enclosure is necessary to sufficiently reduce the effect of environmental acoustics, to ensure that the residual force that is measured because of it, remains below the level of the FRS from [10 – 300 Hz].
- this acoustic casing must be rigidly connected to M1 (not M2), contactlessly surrounding M3. Also it should be better constructed and have higher damping values than the cage used in Vibronix, especially for low frequencies [10 – 80 Hz].
- Detailed modeling is necessary, especially to determine the effect of the remnant acoustic sound pressure level *inside the enclosure* (ACi), as this disturbance acts directly on the sensitive part of the measurement setup. This is done in § 3.4.

3.3.3: Supplying Flow

MAPPER lithography

3.3.3.1: Selecting a Fluid Displacement Device

Sub-problem

Feeding water to the test setup requires a fluid displacement device as well as supply tubing. Both elements create FIV that can end up in the sensor signal which should be prevented as the goal is to only observe the flow vibrations induced *in the module.*

When using a regular (centrifugal) pump to supply flow the following unwanted input sources are generated:

- pressure fluctuations due to vortex shedding (turbulent flow)
- pump vibrations inserted as longitudinal pressure pulses through the fluid
- distinct resonances inherent to its asynchronous motor characteristics

Sub-solution

From performed measurements to test different means of flow supply, the following conclusion can be drawn:

- a hydrostatic pressure vessel is most effective to supply flow to Forcesix under constant pressure, flow rate and without introducing unwanted input (FIPs triggering Helmholtz resonances). When compared to a centrifugal pump, this results in an acceleration response of an identical geometry that is a factor 4.3 lower in overall magnitude. Moreover, static pressure prevents asynchronous motor characteristics to show up as distinct resonances in the measured response.
- various options were explored, a 120 L pressure vessel made from fiberglass with an polyethylene diaphragm proved best suitable to expel water at a high pressure and flow velocity (2.2.2.1). This solution also prevents contamination of the water, changing its viscosity and damaging the modules.
- measurements are executed in batch with their duration dependent on the sampling frequency to prevent aliasing (≈ 10 sec each, ≈ 2 min in total). Prior to every set of flow measurements, the water tank is filled with approximately 60 – 80 liters of water and then pressurized to 3.0 – 6.0 bar (varying per module). This provides a near constant flow rate and negligible pressure drop and is representative for the flow conditions provided by the UPW cooler to Matrix.

3.3.3: Supplying Flow

3.3.3.2: Selecting Supply Tubing

Sub-problem

FIV literature (Anagnostopoulos (2002) and Naudascher (1994)) and the TNO study that was analyzed (App. A-1) emphasize the importance of identifying and accounting for excitation mechanisms (**sources**) and local acoustical resonances (**responses**).

Therefore, the following aspects must be prevented when selecting tubing that is used to connect the pump with a module:

- **local aberations on the inside of the tubing wall** as these can strongly affect noise sources (Kaneko et al, 2008)
- **changes in cross-sectional shape or geometrical alterations that change impulse** (flats / restrictions / bends). This as abrupt transitions will cause pressure variations that dynamically excite the system's acoustic behavior
- **sharp connections by e.g. hose connectors and tubing adapters** as these cause boundary layer separation
- **low radial stiffness of tubing wall** as this causes Helmholtz resonances where the inertia of the fluid flow will start to oscillate on the radial stiffness of the tube wall. Additionally this determines the frequency range at which such resonances will occur when different stiffnesses are present along the length of the tubing.
- **clamping tubing over a relatively short distance** when rigidly connecting it to different stages of the VI platform to discharge FIV input. This is because a sequential flexible-stiff-flexible radial tubing stiffnesses will effectively cause the fluid flow to act as a mass in between two springs, only dampened by viscous forces. The shorter the clamping distance, the higher the frequency of the resulting helmholtz resonance which is undesired given the sensitivity characteristic of the controller. The TNO study indicated that the frequency of this fluid-resonance can also be reduced by either increasing the length- or decreasing the stiffness (wall thickness) of the flexible tubing elements.
- **changes in cross-sectional area (overall diameter)** as this determines flow speed at fixed flow rate and thus local pressure. Changes in flow rate will affect the flow's effective amplitude (exponentially) and center frequency (linearly). For most channels, turbulent flow is already a necessity to achieve sufficient cooling power, therefore keeping this as

3.3.3.2: Selecting Supply Tubing

constant as possible is important. This is substantiated by TNO research which indicates that turbulent boundary layer flow can act as a dominant sound source. Especially since the bulk of its sound power density will be located relatively low-frequency, which would impact the measurements most, preventing local vortices is key. [RD-06]

Sub-solution

To satisfy the above, the following tubing, connectors, fittings and adapters are used to connect the pump with the module:

- **an internally smooth Ariaform TPU polyurethane tubing** has been selected, preventing flow separation. An even better surface roughness could have been achieved using PFA tubing, however this fluoropolymer does not meet the criteria set for the Mapper modules that will be tested. To prevent contamination, the Ariaform TPU was the best alternative.
- **transitions from this flexible tubing to rigid RVS connectors are minimized**. Swagelok connectors, fittings and adapters are selected to match the internal tube diameter. Each is manually adjusted to take out sharp edges to not disturb the flow.
- **the radial stiffness of the Ariaform TPU tubing is low,** this can be determined as it is related to its wall thickness (2 mm). With regards to Helmholtz resonances, a lower radial stiffness is better as this reduces the center frequency. Other tubing (TPAF) was available with 25% less wall thickness, however this tubing was less smooth overall. As the pressurized stiffness in XYZ for the global structure is more important (≈ 50/50/200 N/m), it was opted for the Ariaform tubing. This as the tubing will connect to all masses (discharge at M1 and M2 and supply flow to M3) and thus act as a mechanical shortcut.
- **rigidly connect the flexible Ariaform TPU tubing by RVS casings that surround the tubing**, to prevent diametrical restrictions. To prevent the predicted Helmholtz resonance (62 Hz) from occurring in the most critical frequency range of the modules (50-125 Hz), the clamping distance has been increased to a maximum of 17 cm. This gives a 'flexible-rigid-flexible' ratio of 32 for tubing between M1 and M2 (2.72 m tubing), which should be sufficient to bring it down to 44-56 Hz. The occurrence of Helmholtz resonances is inevitable given the jump in impedances between the different tubing sections. However this is a deliberate choice as discharging the FIV to the granite stones is more important.

3.3.4: Decoupling Internal FIV

Sub-problem

- different (stage stability) budgets are allocated for FIV induced in supply tubing and FIV induced in modules
- aim of this research is to verify the latter, but this requires supplying flow to the module under testing, which inherently brings about additional input that should not be observed by the piezo sensors. The sub-solutions listed at § 3.3.3 limit the occurrence of induced flow vibrations as much as possible, however they cannot be prevented completely.
- theoretical estimates of these FIV levels are not reliable given the high spectral sensitivity of the WPS controller i.e. if input is predicted to occur a few Hz further left or right than is actually the case, this can have large implications
- therefore there is a need to decouple the ‘internal FIV’ induced in the supply tubing and to account for its (pressurized) stiffness as this parasitic stiffness will act as a mechanical shortcut between elements of the design (3-MSD system).

Sub-solution

- prior to the design, experiments have been performed on different types of supply tubing (materials, radial stiffness)
- an optimal solution was found in Ariaform TPU polyurethane tubing which remains flexible even when under pressure (max 8 bar). This tube will be used at a 10/14,5 mm diameter as this is the same internal diameter used in Matrix.
- the flow vibrations induced in the selected Ariaform tubing have been measured using very light weight accelerometers
- observed input induced in tubing with a length of 3 m will serve as in input for the **FIV generated outside** of the design
- input induced in tubing with a length of 0.3 m will serve as in input for the **FIV generated inside** the casing of the design
- various options have been modeled to determine the configuration that gives the least effect of these two interference source (FIV-o & FIV-i). This means rigidly connecting parts of tubing to one (or more) of the stages of the vibration isolation platform to discharge as much input as possible. The results of the first order estimate, and the four configurations that have been simulated can be found in Appendix C-1. The detailed simulation is presented in § 3.4.4.4

The piezoelectric effect

The design measures FIV forces by observing the voltage induced when the dynamic oscillating forces are exerted on a piezoelectric sensor (quartz crystal). This voltage is the result of a displacement of charges in response to applied pressure.

Quartz is a crystal with a honeycomb molecular structure in one of its lattice planes that holds opposing charges. These polar-bonded atoms are spatially oriented in such a way that the net sum of charges in the center of the spiraling hexagon is zero. When subject to pressure (force on an area) it deforms, thereby bringing some charges closer together while others are moving away. This causes the locations of the net positive- and net negative charge to shift away from each other. The result is a build up of positive and negative charge at the faces of the crystal, while its overall charge is still neutral. *This electrostatic potential can be utilized for measurements as it is directly proportional to the magnitude of the applied force.*

This phenomenon is known as the piezoelectric effect and it only occurs when a piece of SiO_2 is sliced under a specific angle. In the selected piezoelectric sensor, this quartz crystal is pre-loaded in a metal housing and sandwiched between two impact caps, which allows it to be used to as a dynamic force measurement tool. *With a high Young's modules of quartz ($E \approx 10^6$ N/m) further compressed, a very high axial stiffness is achieved ($4 \cdot 10^8$ N/m) which is essential for this design's intended application.*

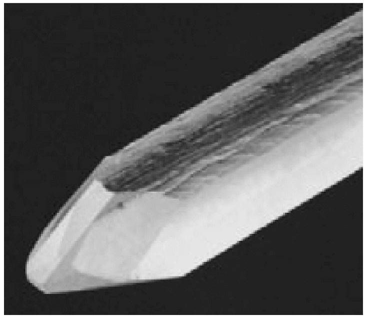

Cultured Quartz Crystal SiO_2

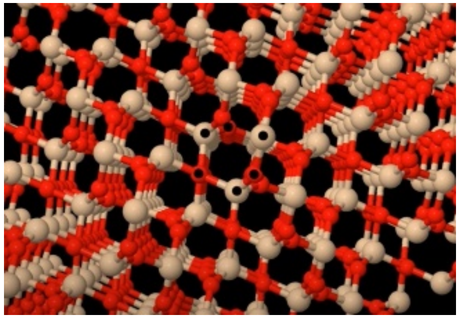

Repeating Hexagon Structure

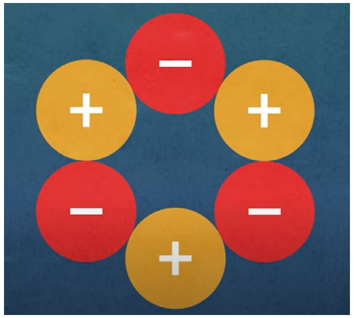

Oppositely charged Si & O_2 atoms

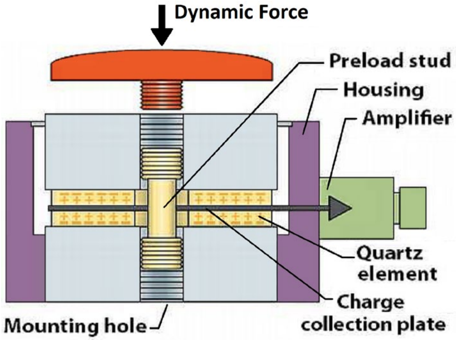

Schematic of selected sensor (PBC 209C11)

Fundamentals of Sensor Design (Dr. Suketu Naik) - https://www.meditronik.com.pl/doc/plus/pfscat.pdf - https://circuitglobe.com/piezo-electric-transducer.html

3.3.7: Measurement Principle

How the applied force is observed in the design

The 6 piezo sensors used in the design have a calibrated sensitivity of 0,495 V/N. *This means that when a force **F** is exerted on the sensor, the quartz crystal will elastically deform over distance **dL** thereby inducing an electrostatic potential **V** that is proportional to the magnitude of this applied force.* This relates to the material properties of the quartz as follows:

$$E = \frac{\sigma \ \text{"stress"}}{\varepsilon \ \text{"strain"}} \quad \sigma = \frac{F}{a}, \quad \varepsilon = \frac{dl}{l} \qquad E = \frac{F \cdot l}{a \cdot dl} \Rightarrow F = \frac{E \cdot a}{l} \cdot dl \quad \text{i.e.} \quad F = \left(k_{pre\text{-}load} + k_{piezo}\right) \cdot x_{piezo} \quad \text{with} \quad k_{piezo} = \frac{E \cdot a}{l}$$

In terms of the sensor's frequency response, measurement takes place in the linear region where spring stiffness dominates as illustrated by the figure on the right. The extremes of this dynamic response are determined by the piezo's Discharge Time Constant (DTC) and its first resonance. The DTC is the time required for the sensor to discharge a measured signal to 37% of its original value. This occurs as it is inevitable for electrostatic charges to leak away to zero, despite high insulation values. The selected sensor has a DTC of >1 sec and a specified dynamic range of [0.5 – 30.000 Hz]. Consequence of the former is that for very low frequencies (0.5 – 5 Hz), the crystal acts as a high-pass filter which reduces precision of the measurement (± 5%). The latter affects the high-frequency behavior as this is expected to be linear up to 20% of its resonant frequency of 30 kHz (App. F-1).

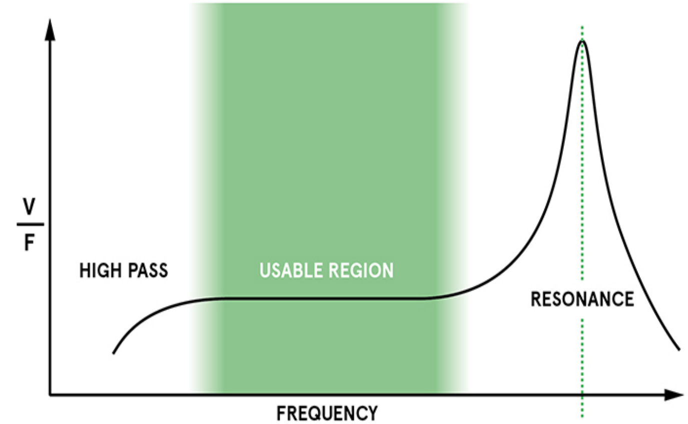

Figure showing the frequency response of a piezo-electric sensor (output voltage over applied force)

The effective range that can be utilized is therefore approximately (5 – 6000 Hz) which is sufficient to meet the requirement (10 – 300 Hz).

Tressler (2003) - https://www.avnet.com/wps/portal/abacus/solutions/technologies/sensors/pressure-sensors/core-technologies/piezoelectric/

3.3.8: Module Suspension

Isolating the module from its environment whilst measuring FIV forces

Sub-problem

Contrary to the acceleration concept (A) that uses a low stiffness pendulum support of the Mapper modules, this concept (B) aims to measure forces through the high stiffness interface of the selected piezo sensors. This gives a high disturbance rejection ability and reduces crosstalk between DOFs, but brings about the challenge of finding a suitable way to suspend the module. This is challenging as the selected piezos are very fragile and may only be used to measure axial forces; they cannot handle transverse loading as this will cause a bending moment. Therefore, a suspension platform needs to be designed that:

- provides a basis with a generic interface (§ 3.3.10) to which the Mapper modules can be mounted
- is level w.r.t. the horizon i.e. is a symmetric design with its COM in the geometrical center
- connects the modules to the sensors without pre-/overloading them (incl. installation procedure)
- has a very flat and parallel mount surface to prevent edge loading (0,001 TIR)
- has a maximum weight of 19,5 kg (incl. the module under testing i.e. ABC: 11,0 kg, BSW: 7,5 kg, POS: 3,5 kg)
- is dynamically stiff up to ≥ 300 Hz (pref. 400 – 450 Hz)

Sub-solution

The devised solution is a Base Frame (BF) to which the piezos rigidly connect, allowing them to carry a second mass. This Module Support Frame (MSF) then clamps the module under testing, together making up the top mass of the in total triple MSD system. Due to weight restrictions, the MSF will be designed to accommodate the three modules suffering most from FIV i.e. the ABC-, BSW- and POS module – and not the BG.

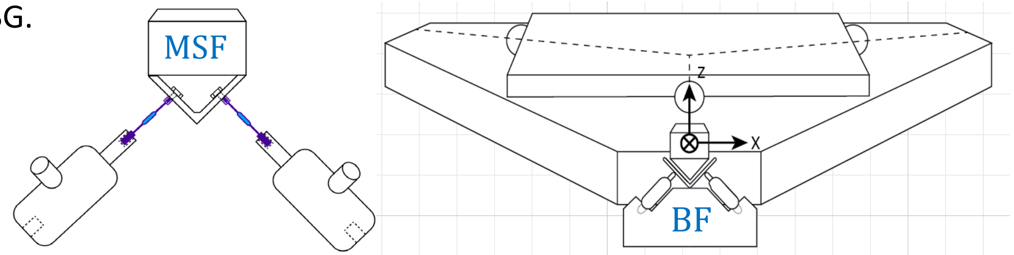

3.3.9: Sensor Orientation

MAPPER lithography

Measuring six degrees-of-freedom without overloading the fragile sensors

Sub-problem

- the sensors are very fragile and costly (13K), leaving no room for error and requiring a first-time-right mechanical design
- the piezos have a low static load tolerance, of 4,45 N (≈ 0,5 kg) in tension and 48,9 N (≈ 5 kg) in compression, limiting layout options
- the sensors cannot handle bending moments; transverse forces due to radial stiffnesses must be prevented
- when measuring 6-DOF, the sensor's transverse sensitivity results in crosstalk to other DOFs (not specified)
- a high *axial stiffness train* is necessary (≥ 10^7 N/m) for a good signal-noise ratio i.e. the ratio $F_{measured}/F_{applied}$ (§ 3.4.4.1)
- a high *global stiffness per DOF* is needed (≈ $10^7 – 10^8$ N/m) to attain sufficient resolution to verify the FRS for each DOF (§ 2.4) and to be able to withstand direct-disturbance forces that act through parallel stiffnesses
- the above sub-problems are interdependent and require simultaneous solving

Sub-solution

- the max static load of the sensors limits the angle under which the sensors can be placed to both support the module and observe the dynamic FIV forces that will be transmitted through the piezo's
- the limited static load tolerance of 48,9 N axial per sensor i.e. 293,4 N if all six sensors would be placed vertical, gives a maximum weight of the module of 29,9 kg. However, measurement of all six DOFs (X,Y,Z, Rx, Ry, Rz) is needed.
- the piezos are connected to the Module-Support Frame (MSF) through custom designed stiff-flexible struts. These connectors, extending the sensors, are optimized for the axial/radial stiffness ratio. By using a thickened middle section (Ø 4mm) and thinner diameters on the outsides (Ø 2mm), a low transversal stiffness of 5.4e4 N/m has been achieved, while maintaining a high axial stiffness of 4.6e7 N/m. This gives the strut a high axial/radial stiffness ratio of 693. The transitions have rounded edges to prevent peak stresses exceeding the yield stress; elastic deformation has been verified using Comsol (peak stress 13 MPa, yield stress 465 MPa). Axial- and radial stiffnesses are also in the same order.

3.3.9: Sensor Orientation

Measuring six degrees-of-freedom without overloading the fragile sensors

The 6 piezo sensors will be placed in a circular configuration in pairs of two and 120 degrees apart (i.e. 60^{0} externally rotated). These miniature quartz sensors (8 gram – 9,5 x 21 mm) are very delicate and each have a maximum static load capacity of 4,45 N (≈ 0,5 kg) in tension and 48,9 N (≈ 5 kg) in compression. As they are simultaneously used to support the module under testing, whilst measuring its transmitted forces, there is a limit to their mounting angle. The smallest angle under which the piezos could be placed depends thus depends on the weight of the Mapper Module that will come available for testing and the Module Support Frame (MSF), part of Forcesix's design. **The requirement set for this combination is a maximum of 19,5 kg i.e. 31,9 N static load per sensor which results in a minimum angle of 40,7^{0} w.r.t the horizon.** A smaller angle would improve the in-plane sensitivity (XY) as well as Rz, whereas as larger angle benefits the resolution of Z, Rx and Ry.

In this configuration, each piezo pair protects each other as the axial stiffness of one piezo is placed parallel to the transversal stiffness of its counterpart. The high stiffness ratio of each piezo then ensures that 99,8% of the shear force is carried axially by the opposing piezo *("the element with the least compliance, determines the total compliance"*, *Schmidt et al, 2011*). This is essential to the workings of the design as this transversal force would otherwise causes a bending moment which would impair performance (≥ 10^{-2} Nm) of damage the sensors (≥ 10^{-1} Nm). **Calculations and details can be found in Appendix C-3.**

RVS strut of 40 mm in length with a 32 mm thickened middle section

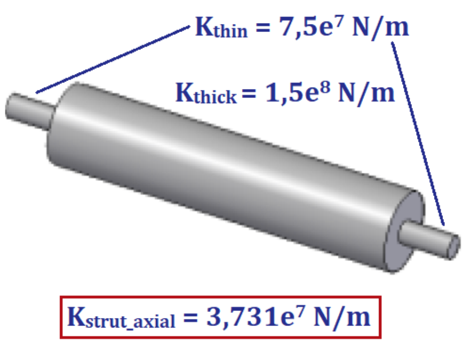

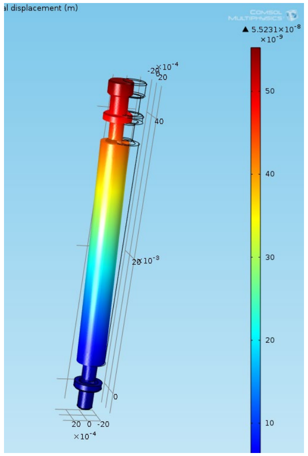

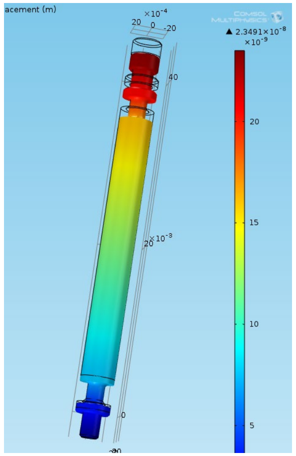

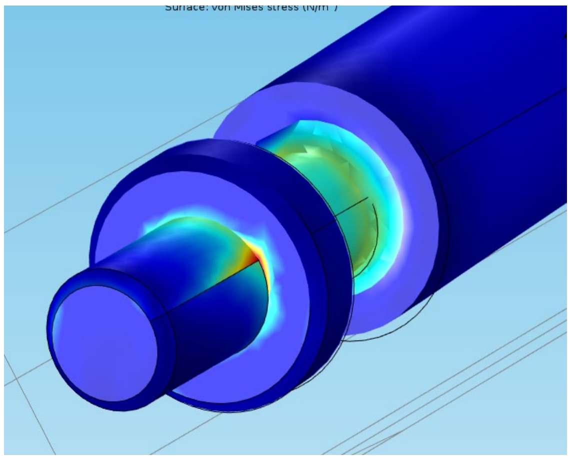

3.3.10: Generic Interface

Sub-problem and solution

Following the technical requirements mentioned in § 2.4, a custom frame will have to be designed and build that can support the Mapper module to be tested according to its interface requirements and to which the sensors can rigidly connect. This frame will have to be designed such that it is dynamically stiff up to 300 Hz but preferably 400 – 450 Hz as it would be valuable to know what goes on just outside the calibrated measurement range. This ensures that the modules and the measurement setup will act as a rigid body in the required frequency range.

Also, resonances can display build-up well before there eigenfrequency which could compromise accuracy. The below figure shows the concentric manner in which modules are placed on top of each other in Matrix. Note that each module has its own interface to the MOF using 15 mm Ø ceramic balls i.e. they are not touching each other. This is the interface connection that needs to be adhered to. They are clamped against a 1-DOF support plane to fixate but not to overconstrain. Hertzian contact stiffness is calculated using the calculator Hertzwin 1.2.2.

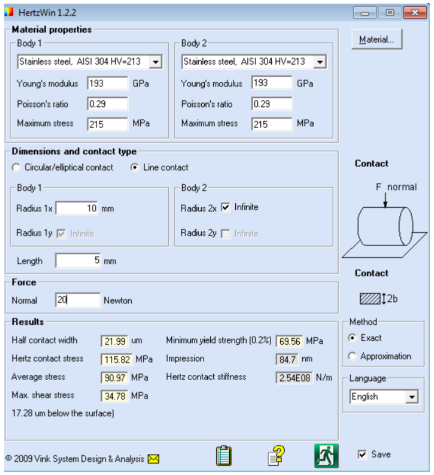

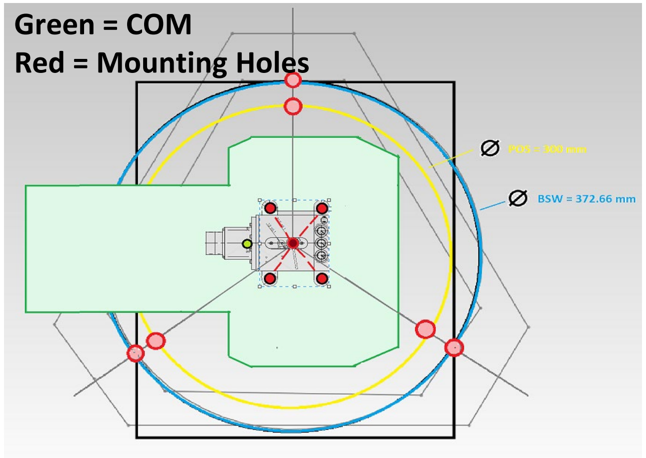

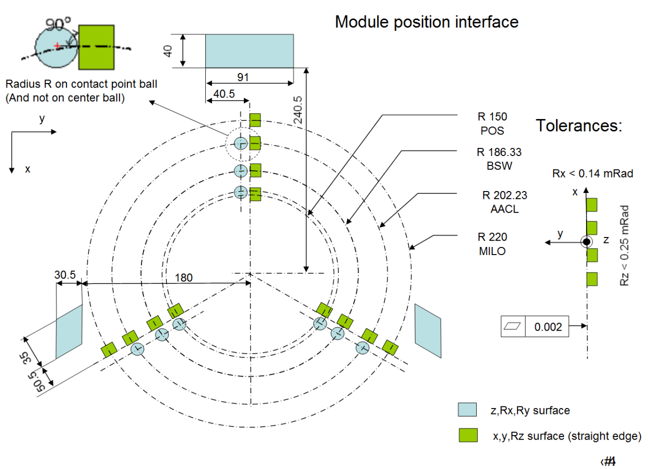

CH. 3.4

Theoretical Performance Estimate of Concepts

3.4.1: Multi-Body Dynamics

3.4.1.1: Modeled Configuration

Overview triple M-S-D system

To simulate the theoretical performance of the design (concept B), it will be modeled as a triple Mass-Spring-Damper (MSD) system. Its one-DOF layout is depicted here:

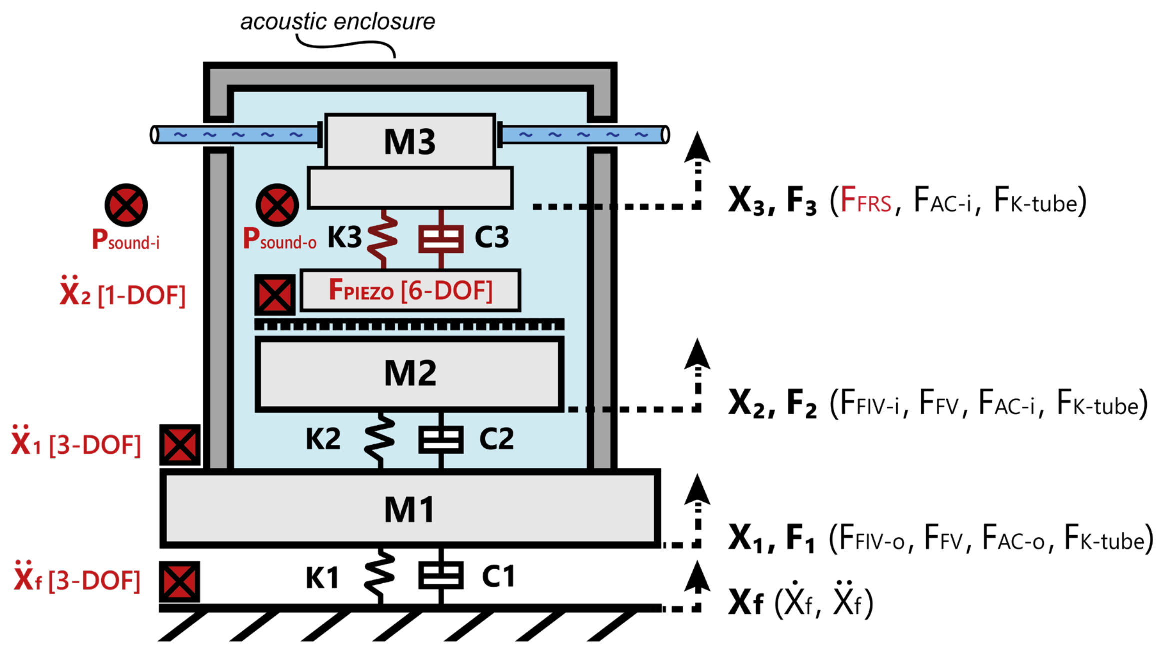

This setup consists of two granite plates (M1, M2) and one of the Mapper modules under testing (POS / BSW / ABC) connected to the MSF, together making up M3.

The six piezo sensors that carry M3 and rigidly connect it to M2 (up to 600-800 Hz) make up the largest part of the stiffness train that determines k3 (and c3). Other elements are RVS stiff-flexible support struts and unwanted parallel stiffnesses e.g. by supply tubing. At the bottom, k1, k2, c1 and c2 are determined by the SLM-3A (4x) and SLM-12A (4x) airmount isolators used to isolate the sensitive part of the setup from floor-vibrations. Since airmount damping is a function of the applied load (and not necessarily the k/m ratio), it will be iteratively updated in the model.

The disturbances characterized in § 3.2 are put in the model to predict their impact and for validation purposes. In the schematic, **red cubes** indicate acceleration sensors, measuring the floor (XYZ), bottom granite stone (XYZ) and accelerations of the second mass (Z). The **red circles** signify the microphones used to establish sound pressure levels: both environmental (Psound-i) and casing attenuated (Psound-o). At various levels of the design, **direct-disturbance forces** enter the system and act on one or more masses. The Dynamic Error Budgeting (DEB) model explained next, looks at the transfer paths of these forces and simulates how much of their input arrives at the sensors. Based on these insights, strategic design choices are made.

3.4.1: Multi-Body Dynamics

MAPPER lithography

3.4.1.2: Transfer Functions – *manually derived and verified using 20-SIM*

The following TFs have been determined and will be used for simulations (visuals are plotted in App. C-2)

(Transmissibility)

- Floor – M1: $x_1 / x_f = \ddot{x}_1 / \ddot{x}_f$ $x_1 / \ddot{x}_f$ i.e. A_f – to – X1 & A_f – to – A1
- Floor – M2: $x_2 / x_f = \ddot{x}_2 / \ddot{x}_f$ $x_2 / \ddot{x}_f$ i.e. A_f – to – X2 & A_f – to – A2
- Floor – M3: $x_3 / x_f = \ddot{x}_3 / \ddot{x}_f$ $x_3 / \ddot{x}_f$ i.e. A_f – to – X3 & A_f – to – A3
- M1 – M2: $x_2 / x_1 = \ddot{x}_2 / \ddot{x}_1$ $x_2 / \ddot{x}_1$ i.e. X1 – to – X2 & A1 – to – A2 & A1 – to – X2
- M1 – M3: $x_3 / x_1 = \ddot{x}_3 / \ddot{x}_1$ $x_3 / \ddot{x}_1$ i.e. X1 – to – X3 & A1 – to – A3 & A1 – to – X3
- M2 – M3: $x_3 / x_2 = \ddot{x}_3 / \ddot{x}_2$ $x_3 / \ddot{x}_2$ i.e. X2 – to – X3 & A2 – to – A3 & A2 – to – X3

(Compliance – Mobility – Accelerance)

- M1 – M1: x_1 / F_1 $\ddot{x}_1 / F_1$ i.e. F1 – to – X1 & F1 – to – A1
- M1 – M2: x_2 / F_1 $\ddot{x}_2 / F_1$ i.e. F1 – to – X2 & F1 – to – A2
- M1 – M3: x_3 / F_1 $\ddot{x}_3 / F_1$ i.e. F1 – to – X3 & F1 – to – A3
- M2 – M2: x_2 / F_2 $\dot{x}_2 / F_2$ $\ddot{x}_2 / F_2$ i.e. F2 – to – X2 & F2 – to – V2 & F2 – to – A2
- M2 – M3: x_3 / F_2 $\dot{x}_3 / F_2$ $\ddot{x}_3 / F_2$ i.e. F2 – to – X3 & F2 – to – V3 & F2 – to – A3
- M3 – M2: x_2 / F_3 $\dot{x}_2 / F_3$ $\ddot{x}_2 / F_3$ i.e. F3 – to – X2 & F3 – to – V2 & F3 – to – A2
- M3 – M3: x_3 / F_3 $\dot{x}_3 / F_3$ $\ddot{x}_3 / F_3$ i.e. F3 – to – X3 & F3 – to – V3 & F3 – to – A3

3.4.1: Multi-Body Dynamics

3.4.1.3: Vibration Attenuation

Relevant transfer functions to describe transmissibility characteristics

In § 3.3.1, the concept sub-solution to counter floor vibrations has been explored. From a first order estimate it was concluded that a **double** mass-spring-damper system is necessary to achieve sufficient attenuation (App. C.1.1). Here below, the most relevant FRFs related to the **floor vibration isolation** of Forcesix are shown. These have been manually derived and verified using Matlab and 20-SIM. These TFs will be used in the DEB model next and have been used to determine the influence of ground floor accelerations on the measured sensor signal. These model results can be found in App. C-2.

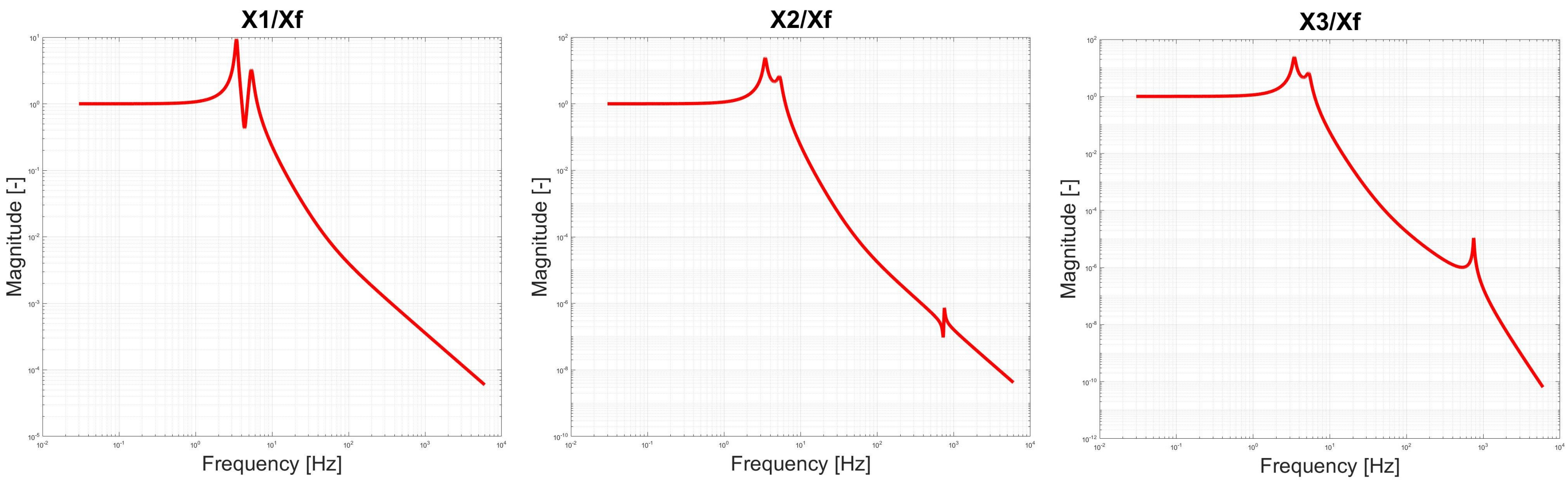

The above figures clearly show the double resonance of the two VI stages. In the transfer Xf/X2 an anti-resonance can be seen around 725 Hz. At this frequency, excitation from the ground (accelerations) that transmit through the airmounts, result in reduced motion of X2. This can be explained by M3 (light mass) oscillating in counterphase against M2.

3.4.1: Multi-Body Dynamics

3.4.1.4: Acoustic Damping

Measured – model expanded

Using the acoustic data gathered inside- and around Vibronix, the following sound pressure attenuation graph has been made. The **red curve** is the environmental sound level in the labspace, wheras the **blue curve** represents the pressure spectrum measured *inside Vibronix*. The black line shows the attenuation ratio w.r.t a unity spectral force.

It can be seen that the acoustic casing of Vibronix only becomes effective from 50 Hz on and that it does not do much between ≈ 80 – 160 Hz. This is something to consider when designing the new acoustic shielding. **However, for the model calculations that follow, this is the attenuation factor that will be used.** This should provide a conservative estimate of what noise floor can be achieved.

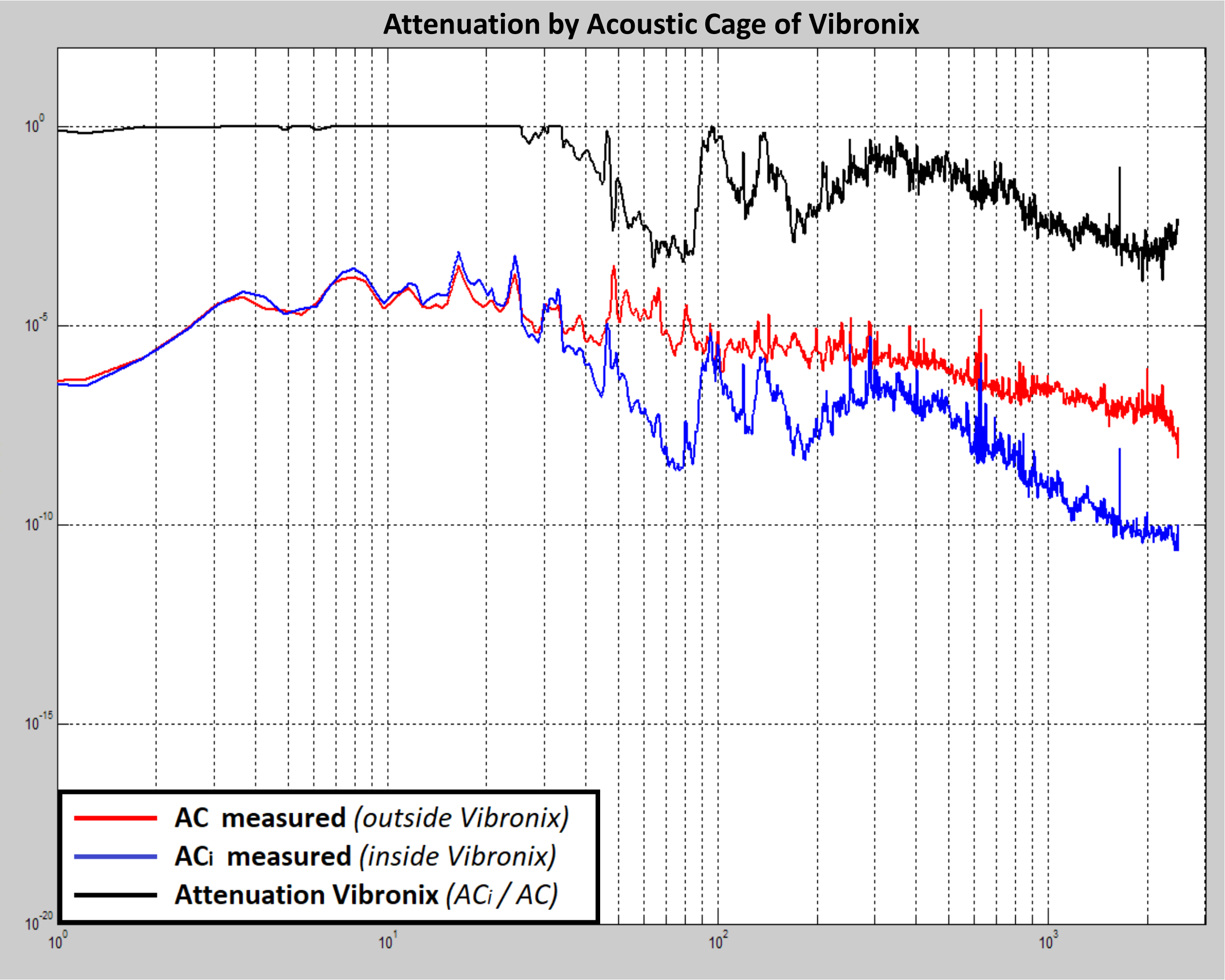

3.4.2: Dynamic Error Budgeting (DEB)

3.4.2.1: Framework

"Dynamic Error Budgeting is a method to combine various error sources that are present in a system"

To use DEB in a design process, it is required to first map all present disturbance sources and to characterize them according to the noise distribution scheme as presented in § 3.2.1. This overview might suggest that all systematic errors and random interference signals can be completely eliminated from a design. In practice however, this is not possible nor needed. The drift of the airmounts for example has not been characterized as it is not expected to be detrimental to the attained resolution.

The objective is to succeed in designing a measurement system where the overall noise level that remains is equal or less than the required resolution (Sydenham and Thorn, 1992). By modeling impact of disturbances during the design process, strategic choices can be made about what inputs will be attenuated (e.g. floor vibrations or acoustics) and up to what level.

Dynamic Error Budgeting is a tool that can be used to model the effect that stochastic disturbances have on the total error of a system. By using a frequency dependent description, the propagation of disturbances can be computed by multiplying the PSD functions with squared transfer functions (see § A-2 for comments on ASD, PSD, CPS or CAS power/amplitude functions). A good theoretical explanation why this works by mathematically deriving energy and power functions and linking them to statistical expressions, is given by Jabben (2006) and Lakerveld (2013). Assumptions that are made when applying DEB:

- the system is linear and time invariant
- the disturbances are stationary and uncorrelated
- the disturbances are ergodic stochastic, meaning that a long random sample is sufficient to derive statistical properties
- statistically, all disturbances combined will approach a normal distribution (in the limit)

For the disturbances that were measured in this study (floor vibrations, acoustics, FIV in supply tubing), this seems true. Therefore, their effect on the relative motion and ultimately measured error will be modeled using dynamic error budgeting. Care will be taken to ensure the measurements are executed long enough and in batch.

3.4.2: Dynamic Error Budgeting (DEB)

MAPPER lithography

3.4.2.2: Model Parameters

INPUTS:

- **Mass, damping, stiffness values** (configuration dependent – literature – calculated: see overview)
- **Mass ranges** (M1: < 500-700 kg > – M2: < 75-150 kg > M3: < 5.5-19.5 kg >)
- **Acceleration data** (vibronix [Z] – stone [XYZ] – ground [XYZ] – acoustics [-])
- **Transfer functions** (various configurations (§ 3.4.1.2 & App. C-2) – acceleration & force – matlab & 20-SIM verified)
- **Mitigation strategies** (FV: 2-MSD system – AC: case around M3 (to M1) – FIV: discharge to M2 & M3 i.e. Ktube: M2-M3)

OUTPUTS:

- **Model validation** (comparison modeled accelerations with isolated measured accelerations)
- **Mass optimization** (for: floor vibration isolation – disturbance rejection – ratio Fmeas/F3)
- **Simulated effect of disturbance sources on sensor signal** (comparison with Force Requirement Spectra {FRS})

	CON	ABC	BSW
M1	644.5	644.5	644.5
F1	4.2	4.2	4.2
Z1	0.0426	0.0426	0.0426
M2	113.65	113.65	113.65
F2	4.5	4.5	4.5
Z2	0.0467	0.0467	0.0467
M3	6.812	10.812	14.312
F3	550.9	633.9	798.6
Z3	0.0071	0.0081	0.0102

ABBREVIATIONS:

- **FRS –** Force Requirement Spectrum (noise level that needs to be observable)
- **FV –** Floor Vibrations
- **ACo –** Acoustics (outside) *i.e. environmental*
- **ACi –** Acoustics (inside) *i.e. casing attenuated*
- **FIVo –** Flow Induced Vibrations (outside) *i.e. environmental*
- **FIVi –** Flow Induced Vibrations (inside) *i.e. casing attenuated*
- **Noise Floor –** Sensor Noise + DAQ + Cable Noise

3.4.3: Model Validation

3.4.3.1: Method

"Validation is the process of checking the accuracy of the model's representation of the real system"

To ensure accuracy of the DEB model that is used to predict the impact of various disturbance sources (§ 3.2) on the signal measured by the proposed measurement tool (concept B: direct-force), it needs to be validated. Various elements of this model have already been checked individually, by means of 20-SIM, Comsol and manual estimates. However, an overall validation step is required to ensure the model simulations are a good description of how the proposed concept will behave.

This is done by making use of the Vibronix test setup shown below, which was introduced in § 2.3.2 as result of the previous work by Dennis Lakerveld. **The validation process draws a comparison between modeled- and measured accelerations of two test-objects:** the granite stone which is part of the vibration isolation platform & the metal disc supported by elastic bands ("pendulum") located inside the acoustical casing of Vibronix. To achieve this, a variety of acoustical & acceleration measurements have been performed which will be discussed next.

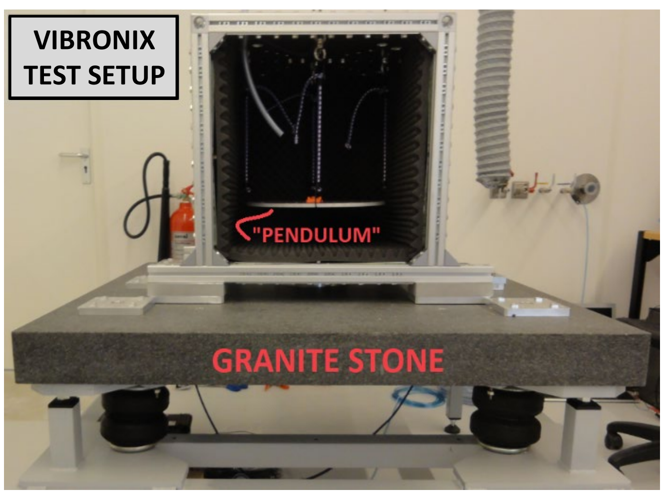

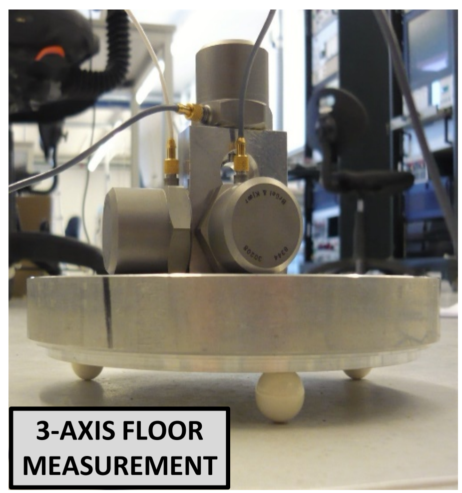

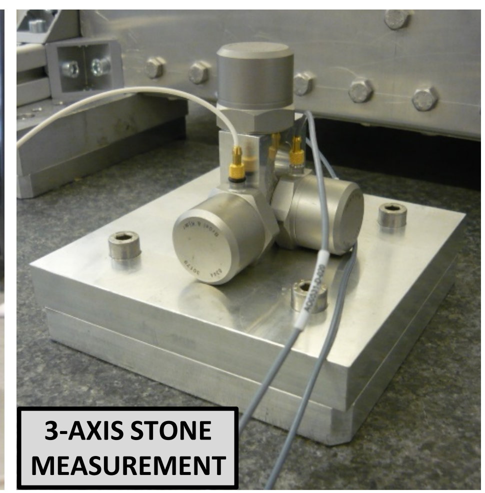

3.4.3: Model Validation

MAPPER lithography

3.4.3.1: Method

.. continued ..

The method used to validate the DEB model assumes that stone- and pendulum accelerations are purely a consequence of present acoustics and transmitted floor vibrations that are observed simultaneously in [Z].

Because component accelerations can be measured absolutely, and disturbance sources individually, a direct comparison can be drawn between actual vibrations and model predictions. Environmental acoustics is the dominant disturbance source, therefore its effect on the two mentioned structures will be examined in particular.

To this end, the following measurement data is required:

1. the background floor vibration levels [Z] at the labspace where Forcesix will be placed: **< FV >**
2. the mean acoustic sound pressure level *around* Vibronix: **< AC >**
3. the mean acoustic sound pressure level *inside* Vibronix i.e. attenuated by the casing: **< ACi >**
4. transfer paths from ground floor to the 1st (a) and 2nd stage (b) of the vibration isolation (VI) platform: **< TF_i >**
5. absolute accelerations [Z] of the granite stone suspending Vibronix (1st VI stage): **< STONE_acc >**
6. absolute accelerations [Z] of the pendulum suspended *inside* Vibronix (2nd VI stage): **< END_acc >**

The first three items regard interference sources that were measured in § 3.2.2. Next, transfer paths (4) have been identified in § 3.4.1.3. Absolute movement of the granite stone (5) has been determined using the BK accelerometers depicted on the previous slide. These sensors are mounted on a custom-made 3-axis tool with ceramic interface. Pendulum accelerations (6) could not be measured directly as these proved very low-level. To observe them, sensor blending has been applied. The constructed signal is shown in § 3.4.3.3 prior to comparison with modeled predictions.

3.4.3: Model Validation

3.4.3.1: Method

.. continued ..

Using this information, the following analysis has been performed:

- measured floor vibrations (1) are filtered by transmissibility characteristics of Vibronix (4a) to attain the component of stone accelerations that results from ground movement alone.
- reducing (5) with these modeled outcomes yields the stone accelerations due to *external* acoustics alone
- the effect of (2) acting on the granite stone and (3) on the metal disc is estimated (pressure on a surface)
- these spectral forces are respectively multiplied with their double derivative of compliance i.e. accelerance (a/F)
- the predicted stone accelerations by the model can now compared with the accelerations isolated above (shown next)

Outcomes are that the model initially overestimated the effect of acoustics for lower frequencies but was able to match the higher frequency accelerations. **After calibration, see Appendix B-4, the model is able to predict the magnitude & spectral trend of the stone accelerations due to acoustics reasonably well over the whole frequency range of interest (0 – 3000 Hz).**

As a sanity check, the analysis has been repeated for pendulum accelerations using (4b) & (6), as detailed in § 3.4.3.4, yielding similar results.

3.4.3.2: Comparison of Stone Accelerations [Z] – *excited by **external** acoustics*

Modeled VS Measured

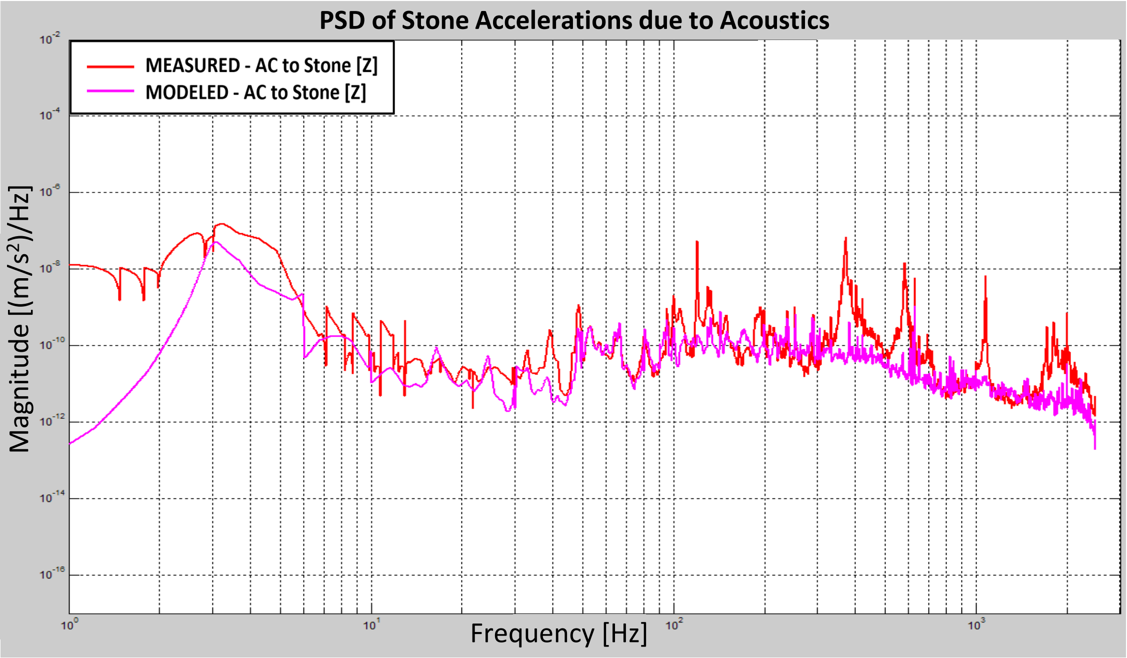

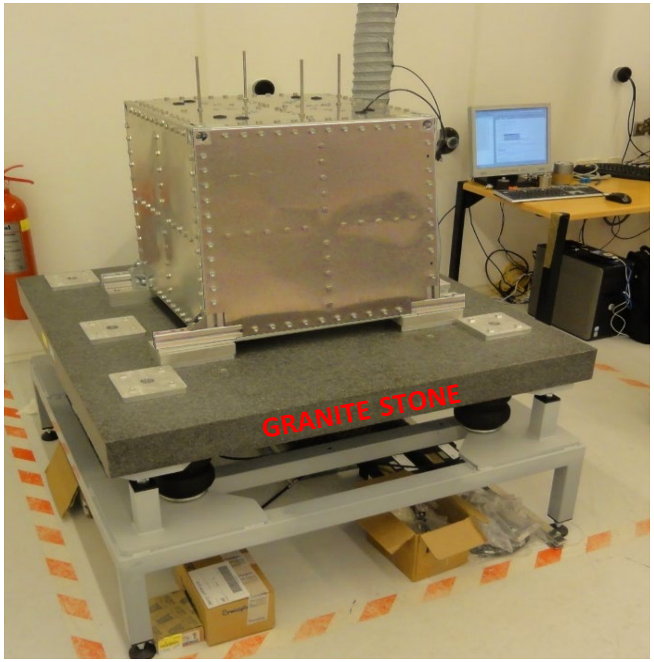

This figure shows the comparison between modeled and measured accelerations of the granite stone due to acoustics alone.

The response clearly shows the accelerance characteristic of Vibronix: peaking at the 3 Hz eigenfrequency of the airmounts that support the granite stone, then remaining relatively flat (slope = 0). The floor vibrations by which the measured response was reduced were of little influence to the overall magnitude and mostly result in capping of low-frequency resonance peaks.

Apart from five distinct resonance peaks, the model is able to predict the magnitude & spectral trend well over the whole frequency range of interest (0 – 3000 Hz). These outliers are investigated on the next slides and can be explained sufficiently to come to the conclusion that: **it is likely that model simulations of acoustics-induced object accelerations will be accurate.**

MAPPER lithography

3.4.3.2: Comparison of Stone Accelerations [Z] – *excited by **external** acoustics*

Detailed analysis of resonance peaks

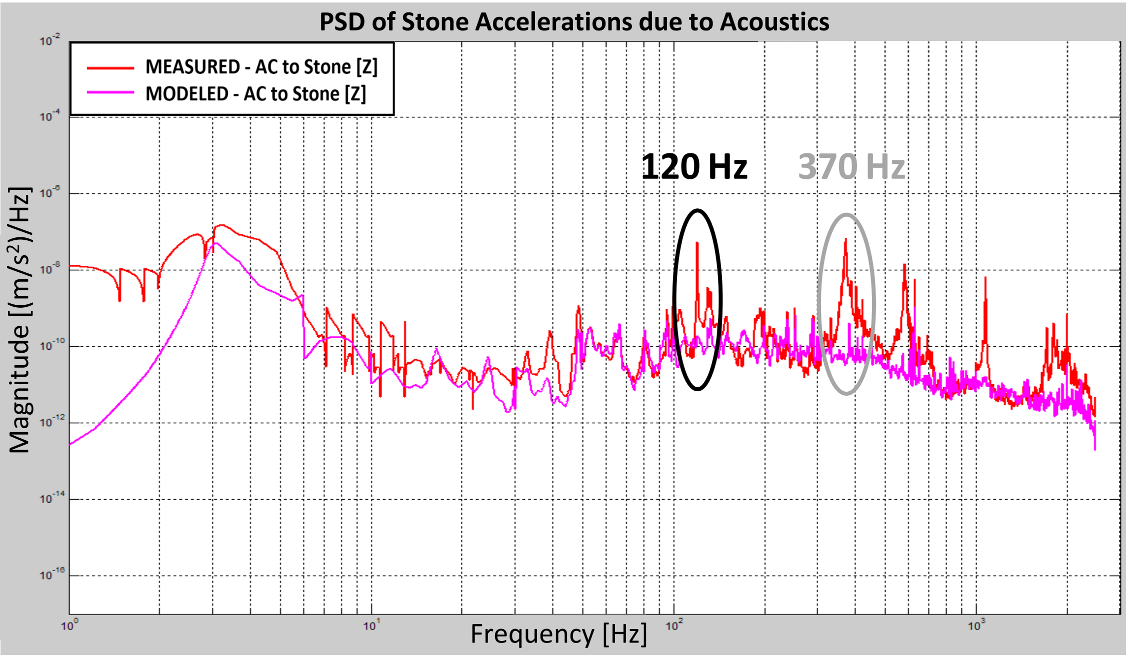

120 HZ – the first resonance peak for which the modeled prediction could not account, was initially thought to be due to *Mains Hum.* This is a form of electromagnetically induced acoustic noise and the phenomenon where the EM field of an alternating current source (here: the mains) causes environmental objects to vibrate, effectively turning them into a speaker. Because a time-varying magnetic field causes a changing electric field, these oscillations can occur in conductive elements and ferromagnetic materials, both of which were plenty present on site. The acoustic frequency induced is then twice that of the AC source creating it, since the magnetic flux density of an electric field peaks twice every cycle (Belmans and Binns, 2012). Should the 120 Hz resonance therefore be acoustic or origin, this would imply a 60 Hz American frequency; not European (50 Hz). This is plausible as there were several (American made) devices present in the lab space where the tests were performed that ran on 60 Hz using transformers. However, this graph represents the predicted effect of the environmental acoustics *measured in that same lab space* which should thus have been observed. To rule out sensor error, additional sound pressure measurements were performed but none could identify 120 Hz sources. This excluded the *'Mains hum hypothesis'* but did trigger closer investigation of the nearby American equipment. **One machine turned out to be running at an RPM of 120 Hz and likely caused interference through its AC magnetic field that got picked up by the BK sensor.** Important to note when interpreting this acceleration signal is that this outlier resonance thus does *not* represent physical movement. **Also: twisted cable pairs are a must for the new design.**

3.4.3: Model Validation

3.4.3.2: Comparison of Stone Accelerations [Z] – *excited by **external** acoustics*

Detailed analysis of resonance peaks

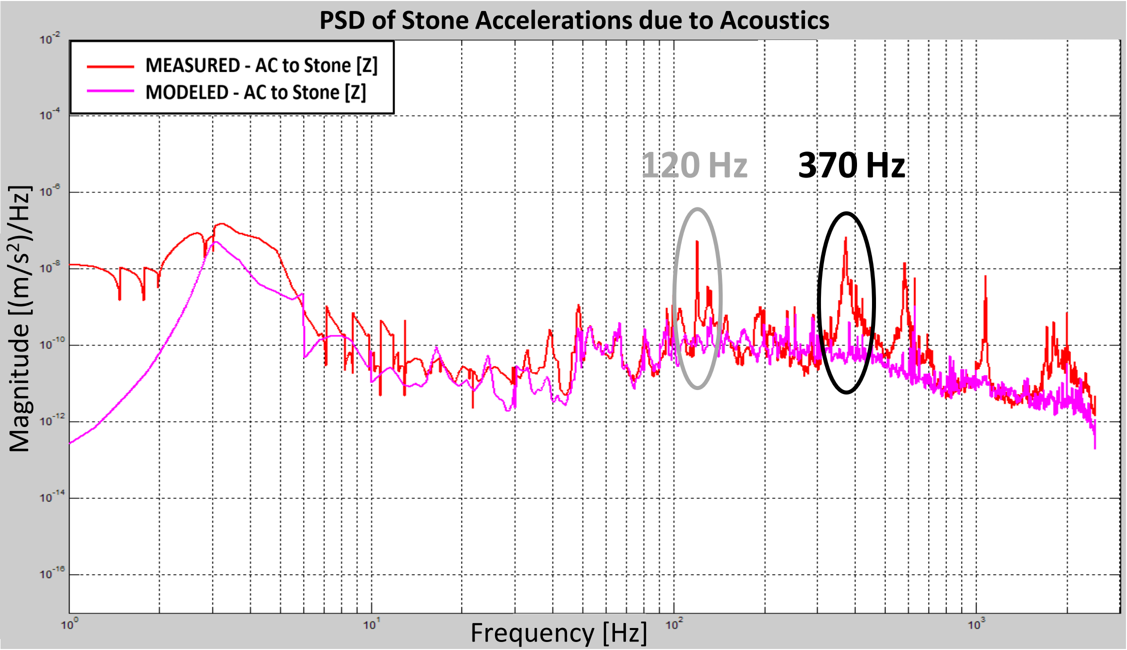

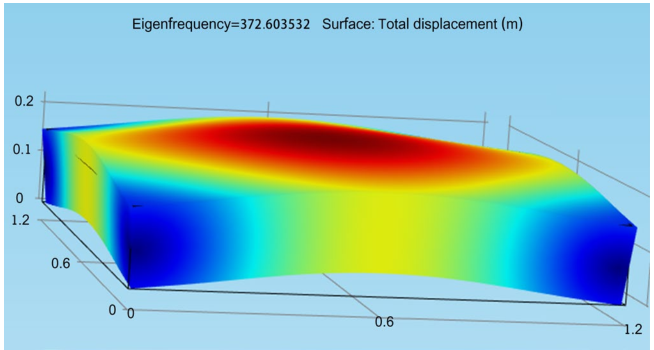

370 HZ – the second resonance that does not match with the modeled prediction can be linked to the internal eigenfrequency of the granite stone, part of Vibronix's VI platform. This heavy slab weighting 432 kg is supported by four airmount isolators tuned to a stiffness of 40,9 KN/m each. The result is a single VI stage that starts to reduce transfer of floor vibrations from 3 Hz on. This means of support, at the corners of the 1.2x1.2 m large plate, does however allow for symmetric out-of-plane bending; the plate's first *internal vibration mode.*

Using COMSOL, **this structural eigenmode has been determined to occur at a frequency of 372 Hz** (picture above)**.** It means that excitation of the system at this frequency results in amplified movement in Z, the direction of measurement. This explains why accelerations of the granite stone at 370 Hz are a factor 10^3 higher than indicated by the measured floor vibrations. The higher frequency resonances that stand out (**585 Hz**, **1075 Hz** & **2000 Hz**) could not be identified individually. These are expected to be caused by spurious modes in plating / connections and sensor cut-off. Having identified the cause of the relevant outliers, **the conclusion can be drawn that it is likely that model simulations of acoustics-induced object accelerations will be accurate.**

3.4.4: Model Simulations (concept B)

MAPPER lithography

3.4.4.1: Dynamical Response of Forcesix

Influence of mass variations on measured signal

Concept B can be represented by the triple mass-spring-damper system shown on the right (larger illustration here), whose behavior is simulated using the DEB model.

It can be seen that the bottom granite stone of the VI platform makes up **M1** (≈ 644 kg) together with the acoustical casing placed on top of it (contactlessly surrounding M2 & M3). The top granite stone, also part of the VI platform, together with the attached optical breadboard, Base Frame (BF) and piezo sensors determines the weight of **M2** (≈ 114 kg). Then, **M3** (6,8-14,3 kg) is made up by the Module Support Frame (MSF) and one of the modules it carries through the stiff-flexible RVS struts.

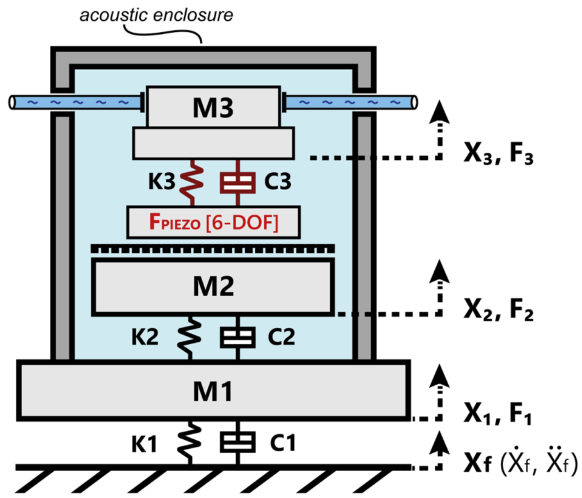

This very stiff (piezo) connection gives the module good force-disturbance rejection, whilst the double mass-spring-damper system beneath ensures good attenuation of floor accelerations. *However, as (reaction)forces have to pass through this stiff interface, thereby exciting the middle mass as well, slightly less of what is generated will be measured.* This drawback is inherent to the design but it can be improved by simultaneously optimizing mass ratios (m1:m2:m3) for signal ratio (force observed / force exerted), transmissibility (FV attenuation) and accelerance (DDF rejection). Moreover, an accurate description of this dynamic allows for correction afterwards when processing the measurement data.

The system can be described with a 6th order differential equation that consists of three coupled second-order differential equations. From this ODE, FRFs that describe the dynamical behavior of the concept in response to a variety of stimuli (in terms of compliance and transmissibility) have been determined. This has first been done through analytical derivation of the EOMs to gain optimal understanding of its workings, see App. C.2.2. The derived transfer functions have been verified using Matlab (eigenvalue decomposition) and 20-SIM, of which the most relevant ones will be presented in § 3.4.4.2.

First however, the optimization results of the measured signal will be presented on the next three slides.

3.4.4: Model Simulations (concept B)

MAPPER lithography

3.4.4.1: Dynamical Response of Forcesix

Influence of mass variations on measured signal

The following figure shows a 3D plot that is the result of an optimization for mass ratio between m1:m2:m3. **This is done with the intention of attaining sufficient resolution, by tuning the mass distribution.**

This strongly depends on the location of the (3rd) resonance peak as this affects the effective measurement range (i.e. the linear range). Aim is to get as close to unity as possible As this measured signal ratio depends not on one transfer but on two (x2/f3 – x3/f3), this means balancing the following objectives:

- **the weight of M2**. Ideally this mass is as heavy as possible as this results in a signal ratio closer to 1 (at fixed m1, m3) However the price to pay is that the the third resonace shifts left; causing build-up sooner and reducing the effective BW. Also there is a practical limit: how much weight the bottom granite plate can support (200 kg)
- **the weight of M1 & M2 together.** Both these masses are needed for FV attenuation and disturbance rejection. Therefore they cannot be moved outside the 75-150 kg and 500-700 kg range.
- **the weight of M3.** This mass is very important to the achieved signal ratio. A lower value results in a higher third resonance and a far better signal ratio. Unfortunately, the mass of the modules that will be tested is fixed. Therefore, the MSF has been designed as light as possible by removing mass everywhere it is not needed. This results in a dynamically stiff design with a mass of only 3.3 kg, while remaining rigid body up to 453 Hz (Ansys).
- **the stiffness train of the piezos.** Another option to get f3 higher is to increase k3 as this is present in the TF's numerator. This regards the stiffness in Z, which conflicts with the in-plane resolution that must be attained (FRS XY = 10x FRS Z).
- **the angle of the piezo pairs.** Deviating from the 45 degrees orientation is not possible as the axial stiffness one piezo must be fully available to protect the other piezo (in the same pair) from transverse loading as this would lead to a bending moment. Also there is a practicle preference to machine the base frame's support planes under 45 degrees.

Concluding, many practicle limitations and interdependency exist at and are ideally optimized at the same time (i.e. good disturbance rejection, good effective bandwidth (high res freq), good signal value (unity transfer as close to 1 and linear over the range 10-300 hz). On the following slide these will be 'visually' optimized by choosing M2 and then M1 (all at fixed M3).

3.4.4: Model Simulations (concept B)

MAPPER lithography

3.4.4.1: Dynamical Response of Forcesix

Influence of mass variations on measured signal

In the concept solution for floor vibrations, the mass range for M1 and M2 was set to respectively 500-700 kg and 75-150 kg (§ 3.3.1). Within this range, the granite stones used would be able to suppress floor vibrations well enough.

With this simulation, more precise value for M1 and M2 are determined, whilst accounting for the weight of M3 that influences the ratio Fmeas/F3. The graph on the right iterates M1 over the Z-axis as well as M2 values over the Y-axis, thereby observing the effect this has on the ratio Fmeas/F3. Based on this, the initial choice has been made for the weight of M2 (105 kg). The front view of this optimization is shown on the next slide, where the best value for M1 is established.

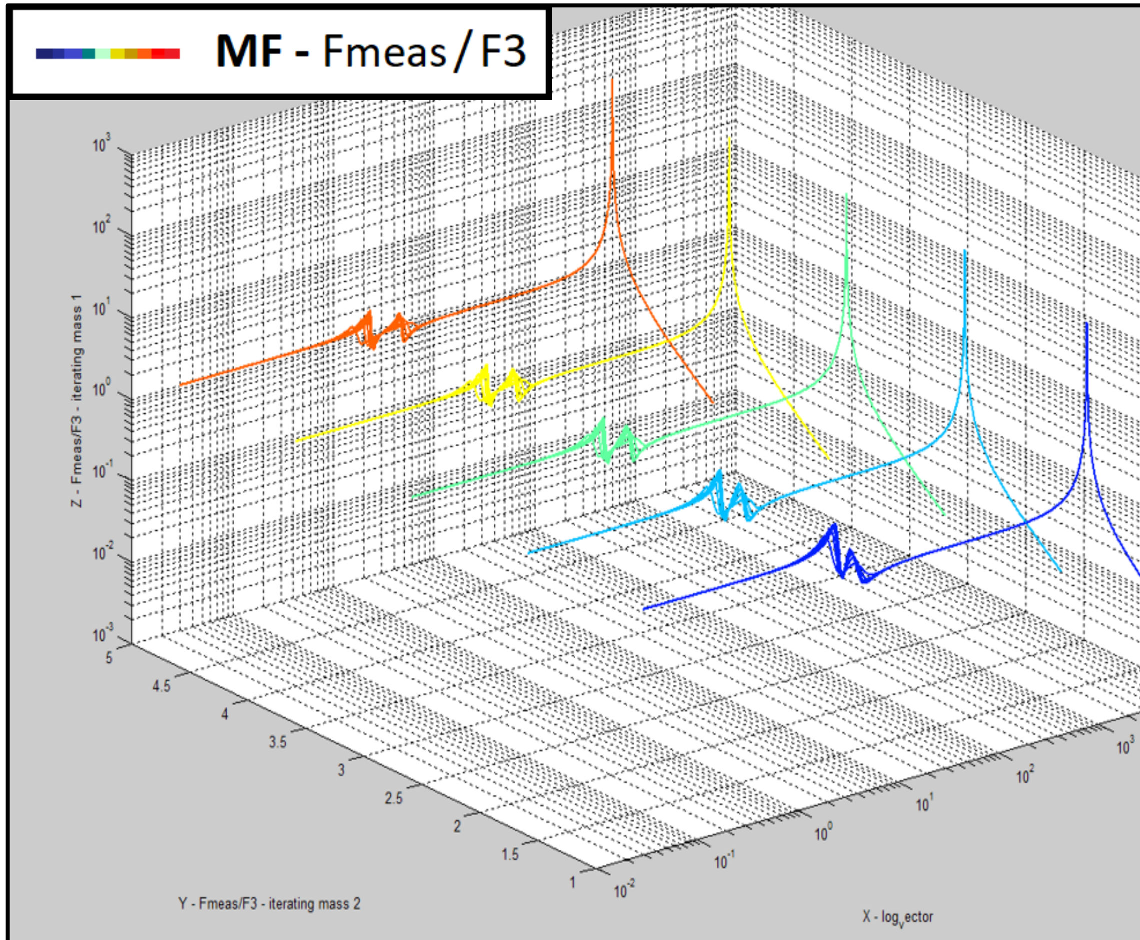

3.4.4: Model Simulations (concept B)

3.4.4.1: Dynamical Response of Forcesix

Influence of mass variations on measured signal

When viewing the location of the airmount resonances from the front, zoomed in, for a discrete number of M1 values (M2 has been determined on the previous slide and M3 is bound to module masses), the top left figure can be seen. It shows that the location and magnitude of the airmount resonances shift, depending on the value for M2. More importantly, the more spread out these resonances become (negatively affecting floor vibration isolation), the better the ratio Fmeas/F3 gets (the measured response shifts up towards unity). Based on the parameter optimization explained in 3.4.4.1, M2 is set to 660 kg.

Measured Force (MF) by the sensor

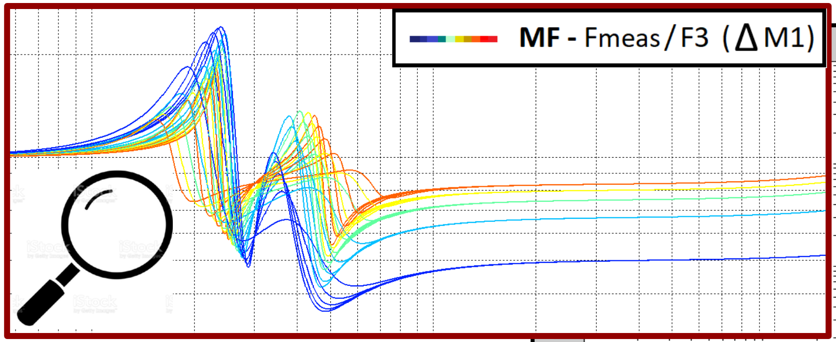

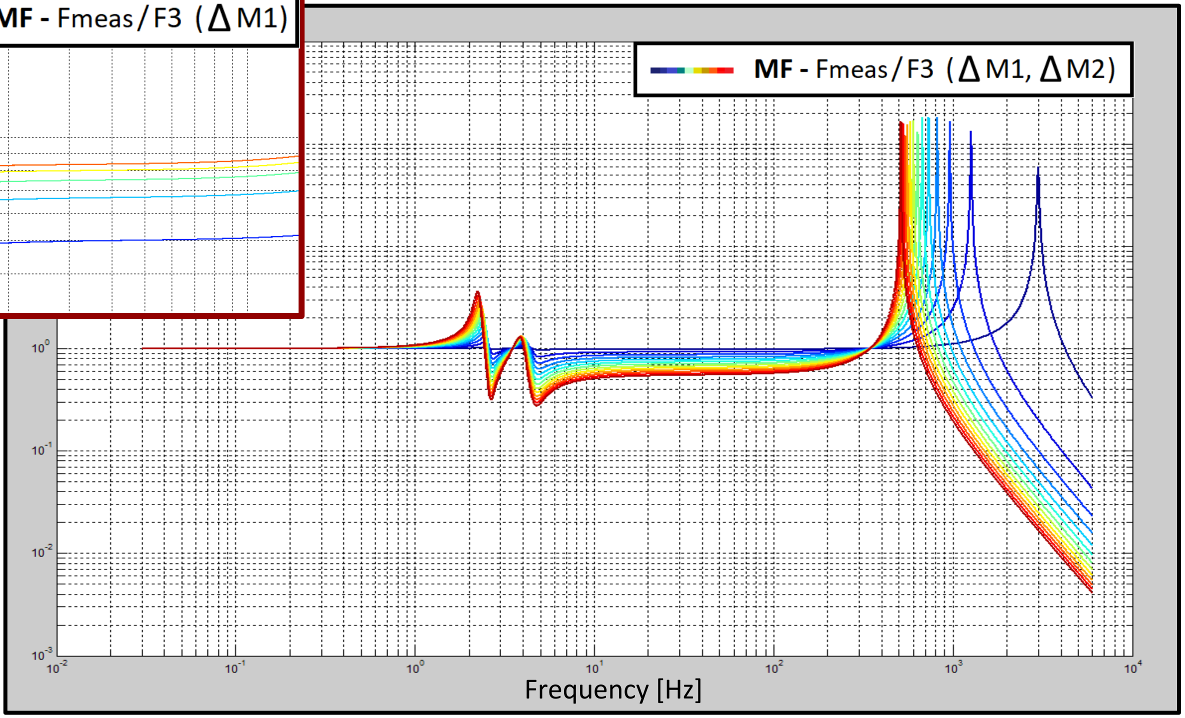

3.4.4: Model Simulations (concept B)

3.4.4.2: Dynamical Response of Forcesix – *relevant transfer functions*

At optimized mass distribution * 3.4.4.1

In the design, the Mapper module is supported by the piezos that connect it to the top mass of the VI platform. To determine the measured signal, the *relative motion* between M2 and M3 is of importance. This as the combined [Z] stiffness of the piezo sensors w/support struts relative to the total [Z] stiffness between the middle and the top mass (K3), determines how much of the force applied on M3 is transmitted through the piezos – and thus observed in [Z]. By determining the compliance response of the top granite plate relative to the DDF (X2/F3) and that of the module (X3/F3), this relative displacement can be calculated. These internal dynamics are described by the various transfer functions (TF) of the system which are derived in App. C.2.3. To help ease understanding, a more intuitive description using a complex plane representation is provided in App. C.2.4. The shapes of the four most relevant TFs that describe the effective measurement range of the integrated piëzos are shown below (full here).

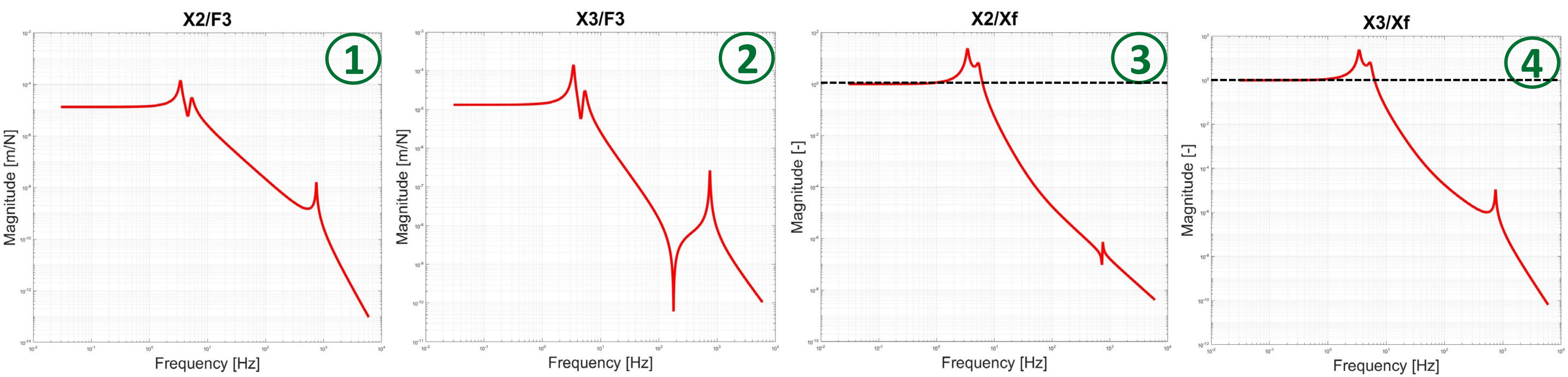

Both compliance functions (**graphs 1 & 2**) drop-off with a -2 slope after the 2nd resonance i.e. the top mass of the VI system, until the piezos decouple at 749 Hz. The displacement response of the module (**2**) encounters an antiresonance (standstill of M3) at 179 Hz before moving up again towards the piezo resonance. After that, the increased magnitude at similar slope indicates full detachment of M3 from M2. **Graph 3 & 4** show the transmissibility characteristic of M2 & M3 i.e. the floor vibration isolation capability of the system. Both masses drop of with a -4 slope after the 2nd resonance resulting in good attenuation ≥ 10 Hz on.

3.4.4: Model Simulations (concept B)

MAPPER lithography

3.4.4.2: Dynamical Response of Forcesix – *unity spectral force input*

At optimized mass distribution * 3.4.4.1

The below graph represents the dynamic response of Forcesix in [Z] when a spectral force of magnitude 1 is applied on M3 i.e. one of the modules, rigidly connected to the Module Support Frame (MSF). It shows the behavior of the system at optimized mass distribution and with the lightest module installed (MSF-POS: 6,81 kg). As explained in 3.3.7, measurement takes place from 10 – 300 Hz which is in the regime where spring forces dominate. It can be seen that the achieved response is mostly linear and close to unity (---), which is what was aimed for. Although damping is low (0.5 – 1.0%, Laman (2002)), build-up towards piezo resonance (749 Hz) starts from ≈ 175 Hz. For this module the ratio Fmeas / Fapplied has an average offset w.r.t. unity of ≈ 5%, with a maximum of 12.3% at 300 Hz. The heavier the module that is tested, the greater this offset becomes which can be seen in the table placed in the figure. This was known on forehand and is inherent to the design, which is why significant effort has been put into making the design as light and stiff as practically possible.

Since this characteristic is mostly linear and well known, the measurement data can be corrected for the offset.

Measured Force (MF) by the sensor

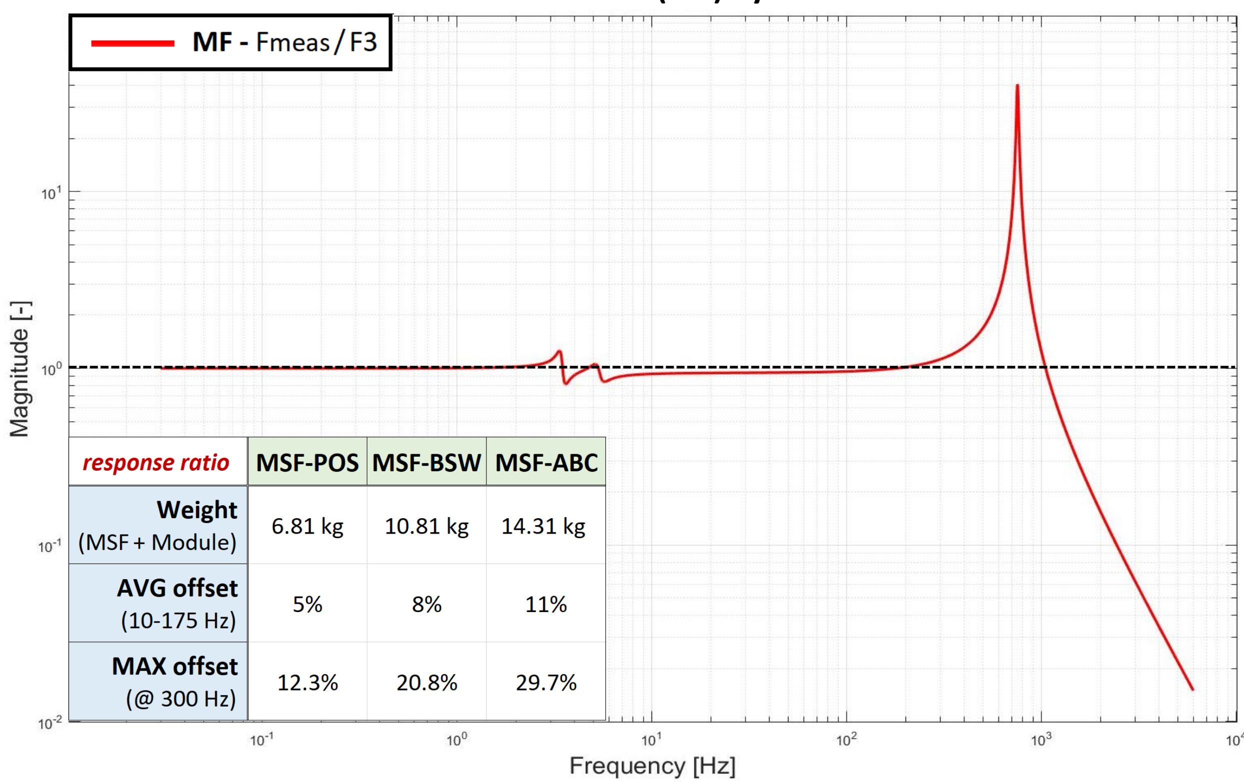

response ratio	MSF-POS	MSF-BSW	MSF-ABC
Weight (MSF + Module)	6.81 kg	10.81 kg	14.31 kg
AVG offset (10-175 Hz)	5%	8%	11%
MAX offset (@ 300 Hz)	12.3%	20.8%	29.7%

3.4.4.3: Predicted Sensor Signal – *force requirement spectrum as input*

At optimized mass distribution * 3.4.4.1

The below graph shows how much is measured when the Force Requirement Spectrum (FRS) serves as input (act as "F3"). This is relevant as the modules ideally exert this force spectrum since that satisfies their stage stability budgets. The same trend as could be observed with the unity force spectrum is visible in this chart too. Overall, the sensor signal follows the response well, with measured forces being slightly lower than exerted forces but this difference is almost constant from 10 – 200 Hz. This is the most important range as the modules are dynamically stiff up to 200 Hz.

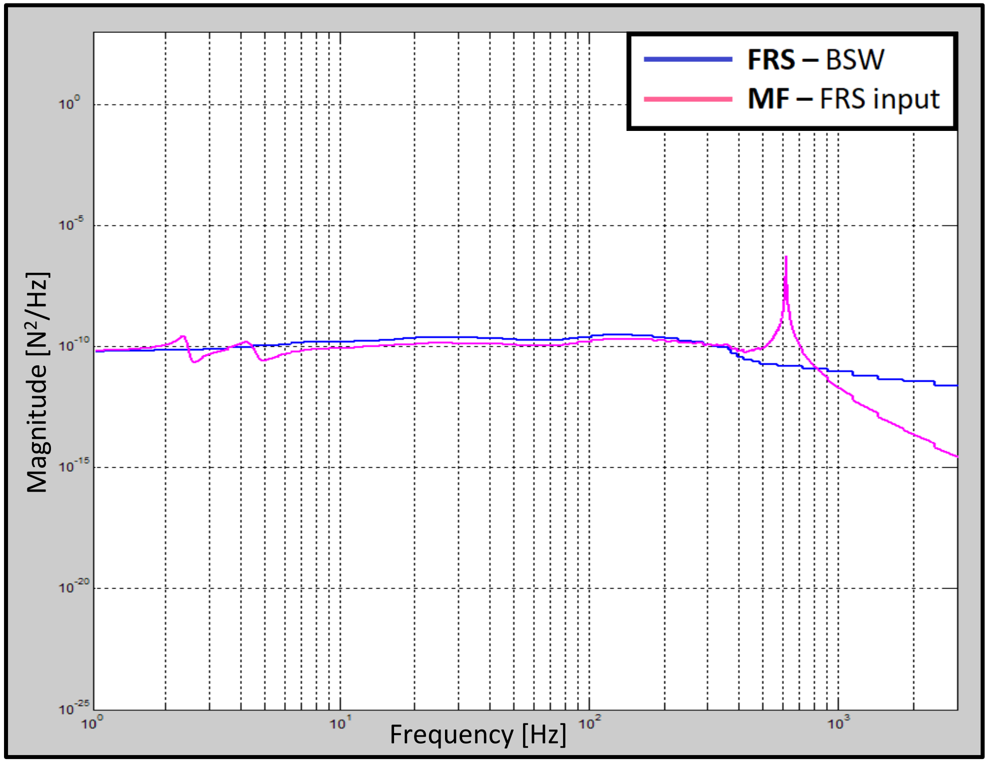

3.4.4: Model Simulations (concept B)

MAPPER lithography

3.4.4.4: Predicted Sensor Signal – *effect of interference on measured signal*

Modeled transmission through parasitic stiffnesses (freq. [Hz] **vs** magn. [N^2/Hz])

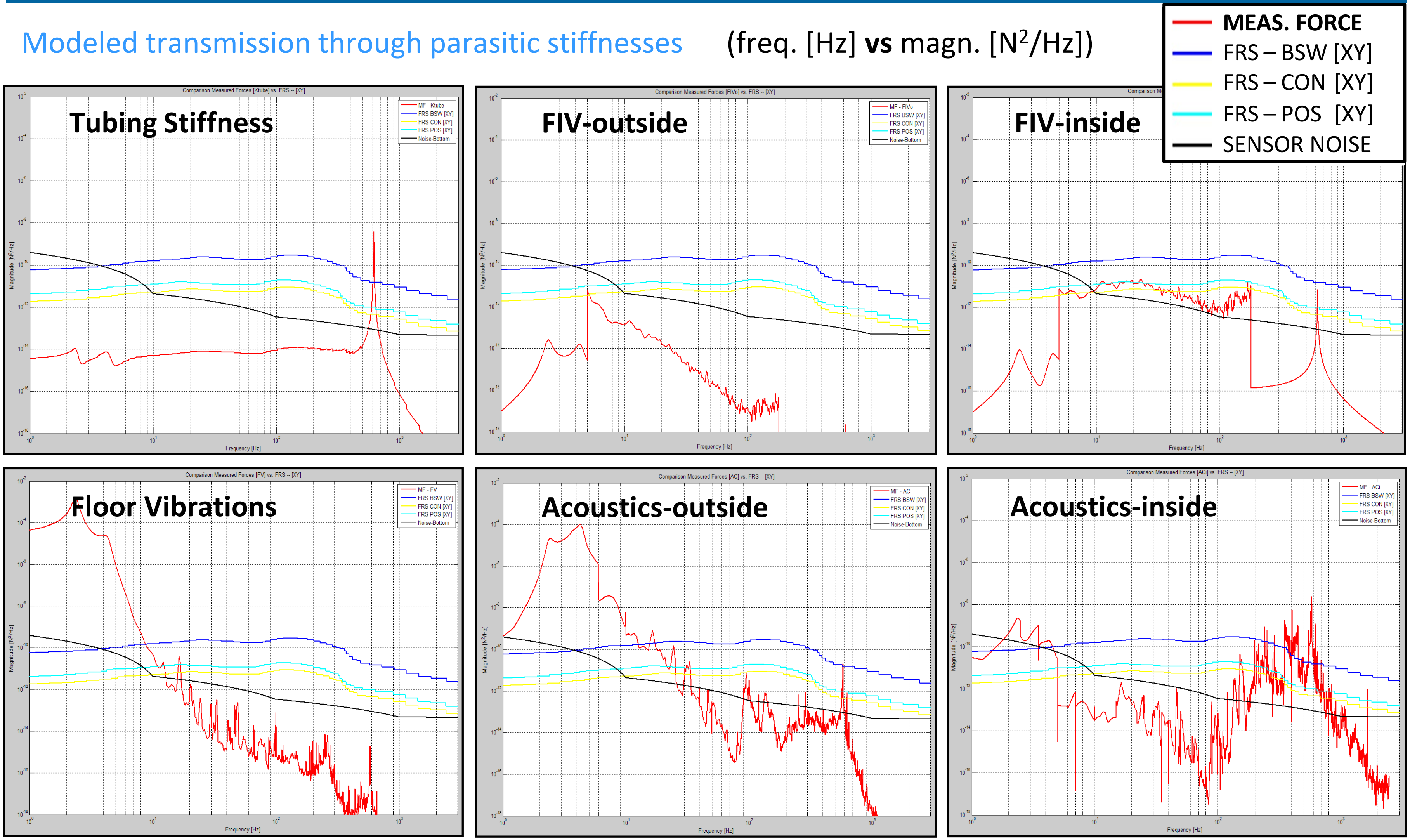

3.4.4: Model Simulations (concept B)

MAPPER lithography

3.4.4.4: Predicted Sensor Signal – *residual noise level of **all disturbances combined***

Floor Vibrations + Acoustics [2] + FIV Tubing [2] + Cable Stiffness + Sensor Noise + Cable Noise [3] + DAQ Noise

This graph is the final result of the DEB model, combining all simulations for concept B in one figure. It shows:

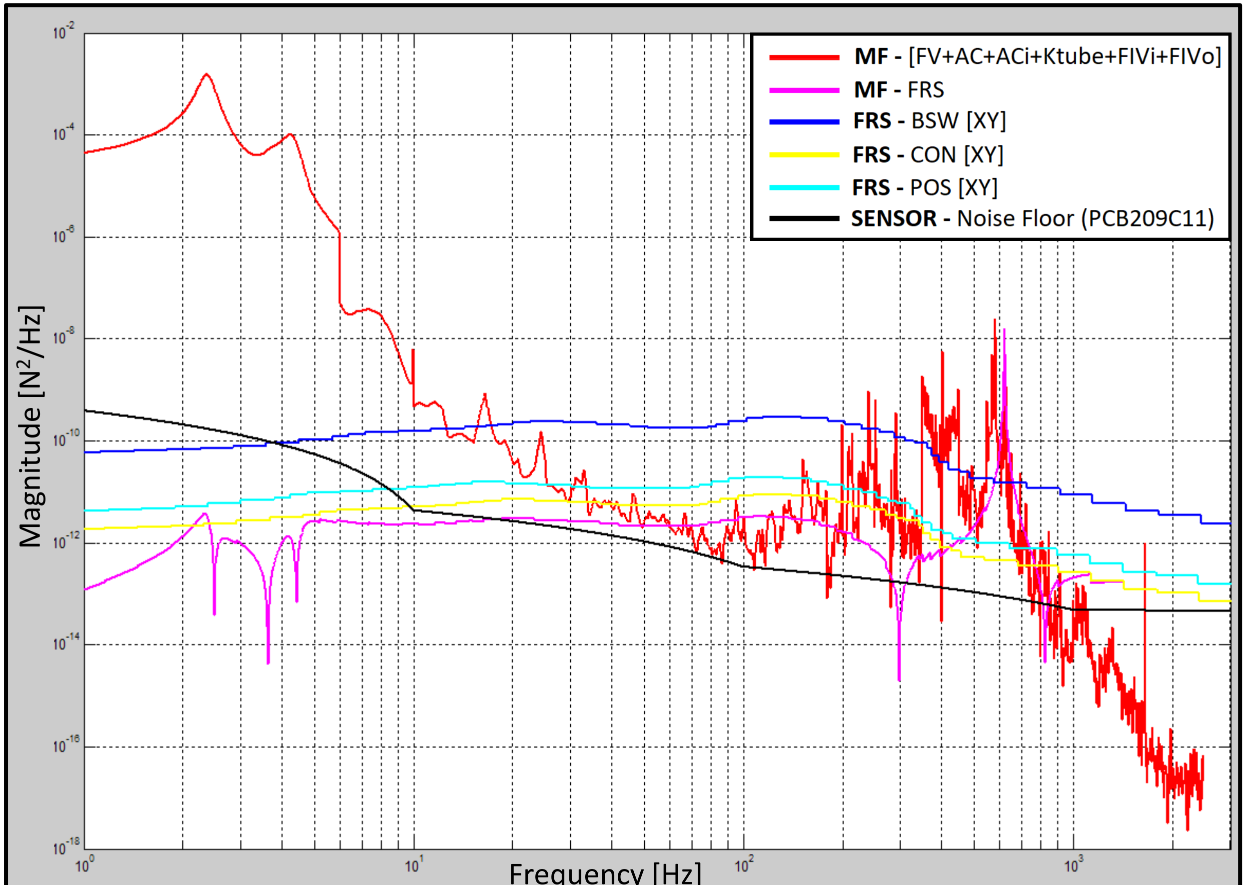

- the requirements (FRS) that need to be verified for the different Mapper modules (yellow-, turquoise-, **blue** line), with CON (ContaminatiON sub-system: Advanced Beam Cleaner [ABC] Module) requiring the lowest noise level.
- the signal that will be measured by the piezo sensors, if no disturbances are present and flow-vibrations inside the ABC Module are at the level of its desired FRS (pink link).
- the sum of all disturbances combined (interference, crosstalk, parasitic stiffnesses), at the level that remains after all the measures taken to prevent / shield / attenuate them, *in other words: the expected performance of the designed measurement tool.*

* simulations of alternative concept (**A:** acceleration-based) in Appendix B-2

3.4.4: Model Simulations (concept B)

3.4.4.5: Predicted Sensor Signal – *residual noise level of **all disturbances combined***

*simulations of alternative concept (**A:** acceleration-based) in Appendix B-2

Interpretation of the simulation results

<u>To restate the objective:</u> Forcesix should be able to observe the FRS over the frequency range 10 – 300 Hz.

It can be seen that with the current design, this range is not met. Overall, the sum of all disturbances combined (interference, crosstalk, parasitic stiffnesses) has been brought down to a very low level. However, the sensor signal is still disturbed until 30 Hz and above 200 Hz. When analyzing the individual contributions it becomes clear that in both cases, acoustics is the main culprit:

- **external acoustics**, i.e. environmental sound pressure levels in the labspace, causes the low-frequency input (10 – 30 Hz). This interference source acts on M1 and affects measurement through the transfers X3/F1 & X2/F1.
- **internal acoustics**, i.e. external acoustics filtered by *the acoustic enclosure of Vibronix*, is responsible for the higher-freq' elevation (200 – 300 Hz). This dampened source acts on M3 and affects measurement through the transfer X3/F3.

It is positive that this is timely identified (i.e. in the design phase and not after construction) and improvements can still be made. Note that these acoustic sound pressure levels are the result of measurements performed in- and around Vibronix. From testing, possibilities for improvement were already investigated. Its acoustic damping (§ 3.4.1.4) namely turned out to be very limited from ≈ 80 – 150 Hz and also started to decrease from ≈ 160 Hz up to 340 Hz. This can be explained by the small amount of mass on the outside of the cage, limited thickness of damping material and insufficient support of plating / construction elements. Besides limited attenuation, spurious mode decoupling of plating is expected to cause the high frequency spikes. Altogether, this gives confidence that the damping capabilities of the new acoustic enclosure's architecture can be sufficiently improved such that it will reduce the effect of internal acoustics with the necessary amount from 200 – 300 Hz (i.e. about a factor 100). For the low end of the spectrum (10 – 30 Hz), improvements are more difficult as this is the simulated effect of the *unfiltered* environmental acoustics on movement of the bottom granite stone. Since M1 has already been optimized for signal ratio, it can only be attempted to shift the first resonance left by lowering airmount pressure. This is not expected to remove the 10 – 30 Hz elevation completely, but fortunately lower frequencies contribute much less to overlay error than higher frequencies (Schmidt et al, 2011). Therefore, this remaining input is expected to have an effect, but not enough to significantly impair Forcesix's performance. The model simulations also show that discharging the FIV input from external (5m) and internal (0.5m) supply tubing to both stages of the VI platform has resulted in an average reduction of a factor 10^1-10^6 (§ 3.2.2.4 and § 3.4.4.4)

CH. 3.5

Final Design

Comments on Final Design

The final design goes by the name **Forcesix** (*"measuring forces in 6-DOF"*)

The theoretical solution will be presented next. This will be done by discussing each sub-solution individually. With regards to the outcome of the mass optimization discussed in § 3.4.4.1: the optimal theoretical distribution came to a total of 660 kg for M1 (bottom granite stone + acoustic cage) and 105 kg for M2 (top granite stone + optical breadboard + base frame). To get as close as possible to these values, the acoustical cage has been designed in CAD first to get a detailed breakdown of the used components. Next, various suppliers of granite stones have been contacted and the best fit in terms of dimensions, load capacity and total weight has been selected. **This came to a bottom granite stone of 576 kg and a top granite stone of 95 kg and a total mass for M1: 644,5 kg and M2: 113,7 kg.** The difference due to practicality is acceptable (≈ 10-15 kg)

3.5.1: Vibration Isolation Platform

Granite Stones – Airmounts – Optical Breadboard – Table Frame

Overview of theoretical design – *real life construction in [§ 4.1]*

The final design is illustrated below and is made up by two granite plates respectively weighting 576 kg and 95 kg, placed in a custom frame supported by two sets of 4 airmounts. This is the result of the mass optimization discussed in [§ 3.4.4.2]. *Together they make up a two-stage VI platform with eigen-frequencies at 3.3 Hz and 5,1 Hz.* The mass table on the right provides a detailed breakdown of all elements involved. Note that the calculated eigen-frequencies are assuming a 1-MSD system. Hence, integrated in the final design the achieved values are slightly different (as mentioned above).

SLM-3A	*max load per isolator:*	*136,1*	*kg*	
module mass (avg)	M3:	7,25	kg	(=BSW: 7,5 kg - CON-ABC: 11,0 kg - POS-PL: 3,5 kg)
module support frame		3,3	kg	(=excl. 4x SLA-12A airmounts)
base frame		6,2	kg	(=incl 4x SLM-3A + bouten)
optical breadboard		12,5	kg	(=incl insulation and bolts/nuts)
top granite plate		95	kg	>> **load per isolator: 31,1 kg**
total load on top 4 airmounts		**124,2**	**kg**	>> **% of max isolator load: 22,8 %**
	M2:	113,7	kg	>> **eigenfrequency 2nd trap: 4,5 hz**
SLM-12A	*max load per isolator:*	*544,3*	*kg*	
total top assembly		***124,2***	***kg***	
acoustic casing		65	kg	(=incl 6 piezos a 8,2 gr p/s, incl 3 support poles a 89 gr p/s
4x SLM-3A airmounts		3,5	kg	incl bottom plate, incl chambered structure ca 4,936 kg)
bottom granite plate		576	kg	
total load on bottom 4 airmounts		**768,7**	**kg**	>> **load per isolator: 192,2 kg**
	M1:	644,5	kg	>> **% of max isolator load 35,3 %**
				>> **eigenfrequency 1st trap: 4,2 hz**

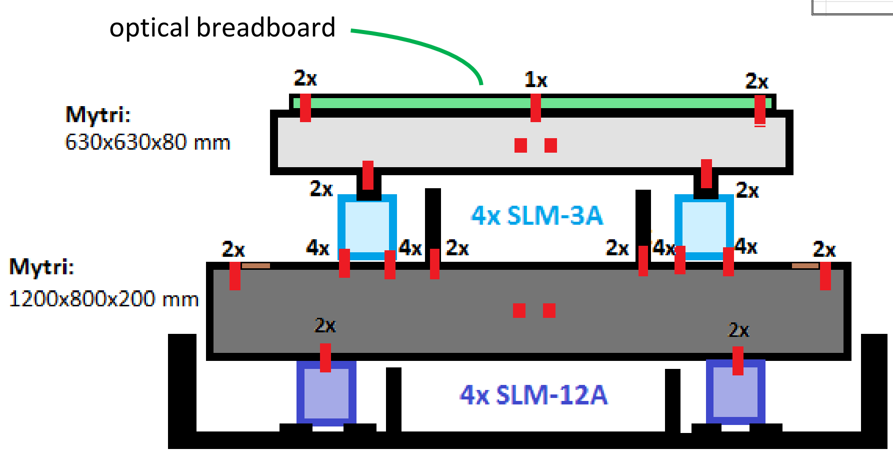

optical breadboard
(Newport M-SA2-22)

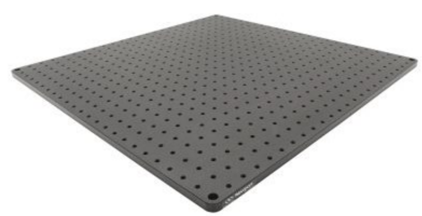

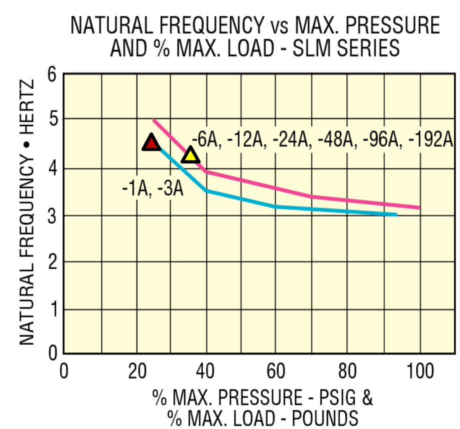

3.5.2: Acoustic Enclosure

MAPPER lithography

Coomach profiles – Akotherm D80 –Metal Plating, Stiff-Flexible Interface

Overview of theoretical design – *real life construction in* [*§ 4.1*]

- the acoustical casing has been carefully designed in terms of isolation thickness, shielding mass and connection methods to achieve high levels of reduction for input in the frequency range of interest. The fact that this regards relatively low frequencies, made it particularly challenging as longer wavelengths require significantly thicker insulation
- besides lowering sound levels, an additional challenge is that acoustical input gets absorbed by this casing and thus injected into the system. The only configuration that proved to be effective to dispose of these vibrations, is having the acoustic casing fully enclose the top MSD system without touching it and connect rigidly to the bottom MSD system. Resulting accelerations are then sufficiently reduced, since the bottom mass (M1) is a factor 5,7 heavier than the middle one (M2). Note that the actual measurement tool connects rigidly to the optical breadboard attached to the top of the VI platform shown on the second picture from left. In other words, it is free afloat in an acoustically isolated chamber.

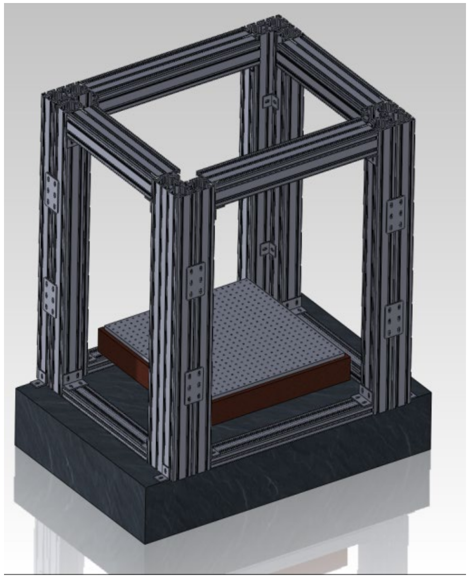

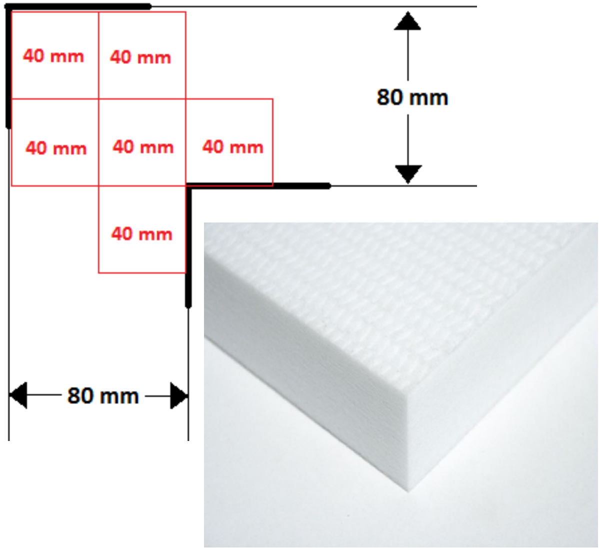

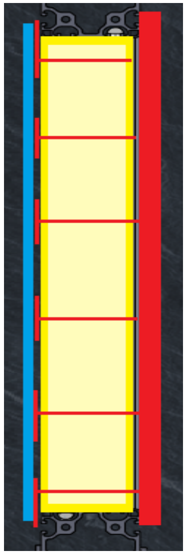

3.5.3: Module Support Frame (MSF)

ABC module attached to MSF and supported by 6 piezos that connect to the Base Frame (BF)

Overview of theoretical design – *real life construction in [§ 4.1]*

Objective of the module support frame (MSF) is to be able to mount various modules without pre-loading the pressure sensors that carry them. In turn these are supported by a solid ground plate which has been rigidly attached to the upper mass. Since granite is difficult to machine, an aluminum Newport Mounting plate with various tapped holes has been used in between for this purpose. Both the ground plate and MSF are triangular shaped blocks that will be machined out of aluminium and will weight approximately 3,3 kg. To increase the first eigenfrequency mass has been removed from the center of the MSF. The piezo sensors link the blocks at the corners through stainless steel struts. These struts have been electrically insulated with high resistance Loctive Hysol 9492 glue to prevent measurement error due to ground loops.

The MSF has been specifically designed to accommodate the three modules that suffer most from FIV; the ABC, BG and CON module. The same interface as is used in the MOF has been used as this was already present and is similar for all modules. The eigenmodes have been verified using Comsol and indicate that deflection happens at locations which minimizes impact on piezo measurements. One of the modules that the setup has been designed for can be seen mounted on the render (ABC module).

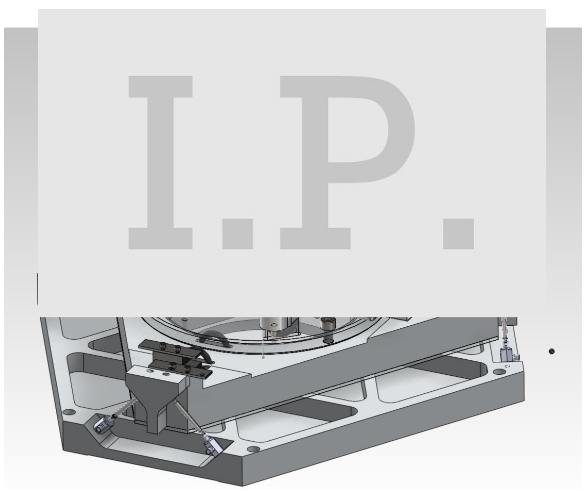

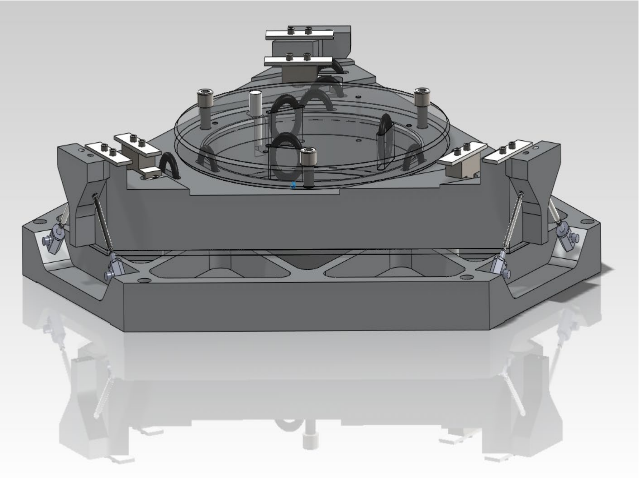

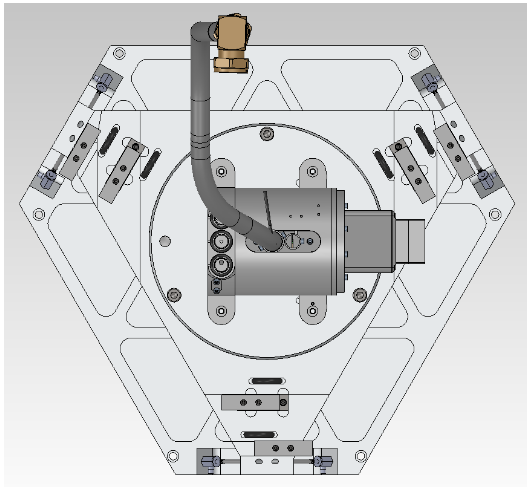

3.5.4: Sensor Configuration

Hexagon Layout (paired under 120 degrees)

Overview of theoretical design – *real life construction in [§ 4.1]*

The piezo sensors are very sensitive but very delicate, they are designed only to withstand and measure compressive loading and tolerate absolutely no tensile forces. Therefore the weight of the MSF acts as a static pre-load, causing a bias offset, that is filtered out by the data acquisition (DAQ) unit. Measuring the dynamic deviation on the static voltage output.

The chosen sensors were the only ones on the market that could measure within the required range. To prevent ground loops they too were insulated from the aluminum frame just like the metal struts (detail in [§ 4.1.4].)

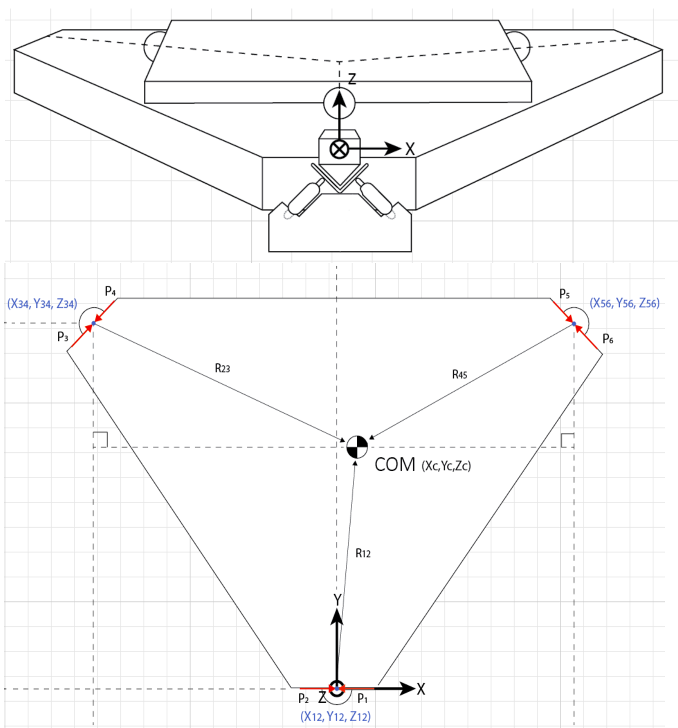

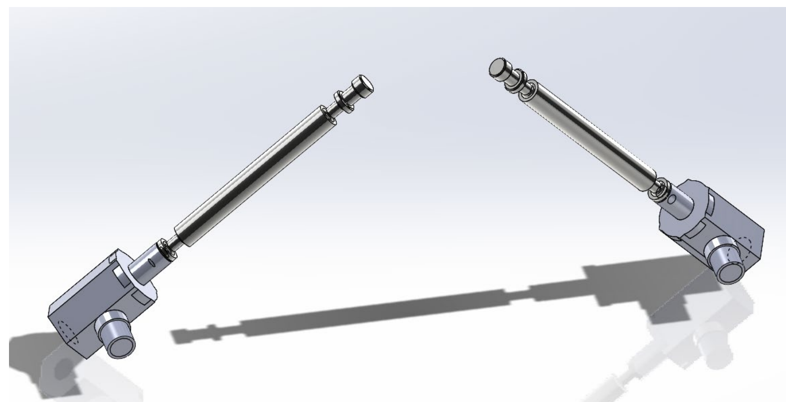

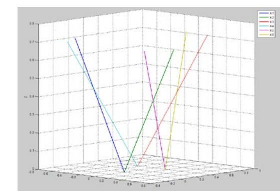

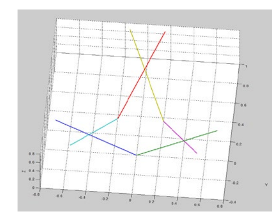

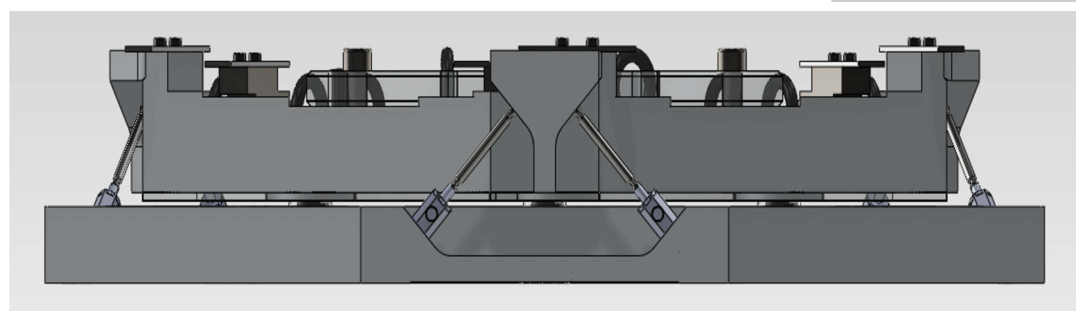

3.5.5: Supply Tubing (overview)

Feeding the supply tubing through the design – *discharging FIV through stone-mounting*

Overview of theoretical design – *real life construction in § 4.1*

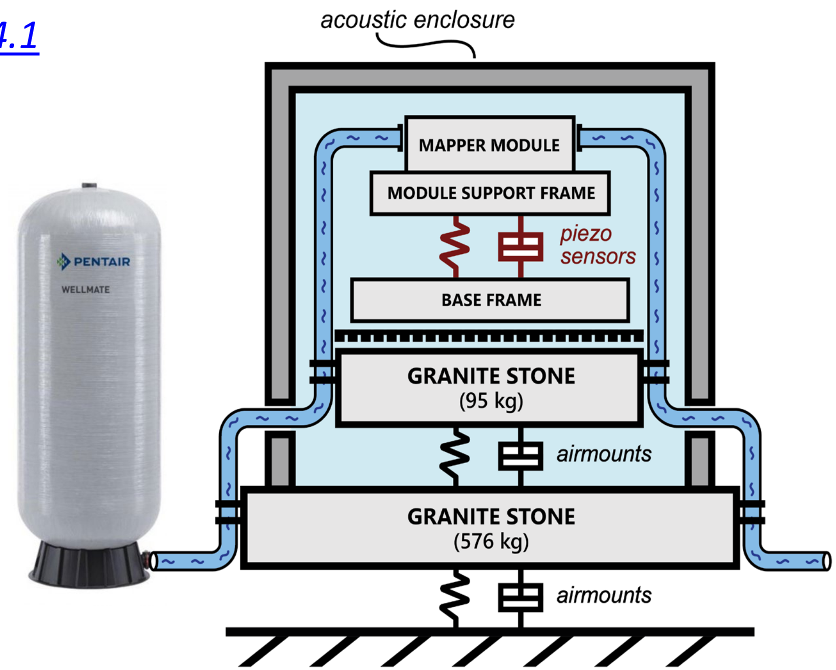

The picture on the top right-hand side shows the solution used in the final design to minimize interference due to supply tubing. To ensure the FIV induced in the supply tubing do not interfere with the measurements, they are connected rigidly to the granite plates of the VI platform. This is because the objective of Forcesix is to *only* measure FIV induced in the modules and not in the supply tubing as these have separate budgets. Also, the stiffness of the pressurized supply tubing (XYZ: 50/50/200 N/m) has been accounted for. An optimal solution has been found in the use of Ariaform TPU poly-urethane tubing, which remains relatively flexible even when under pressure (8 bar). At the same time the radial stiffness is low enough to expect the Helmholtz resonances to occur at a low frequency.

The used RVS clamps have been reworked on the inside to prevent diametrical restrictions from occurring. Also the majority of the vibrations induced in the tubing discharges at the largest granite stone (≈ 91%) which has a much more benifical transfer path to 'measured forces by the piezo sensors' than the top granite stone to which the remaining input (9%) is transferred.

Different means of connecting the supply tubing to the heavy granite slabs or acoustic enclosure have been modeled, at different stiffness values (100-1000 N/m) and accounting for parasitic resonances. The illustration on the bottom right shows these configurations.

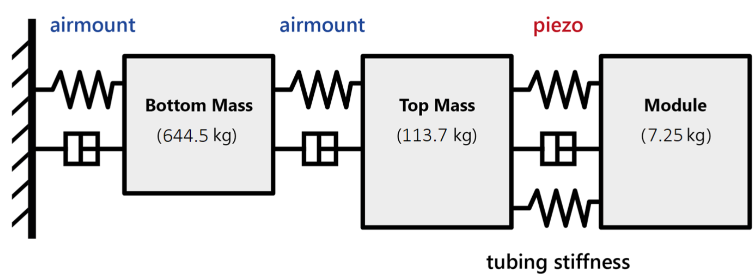

3.5.5: Supply Tubing (routing)

Showing: CAD design of acoustical enclosure, tubing- and cable feedthrough

Overview of theoretical design – *real life construction in [§ 4.1](#)*

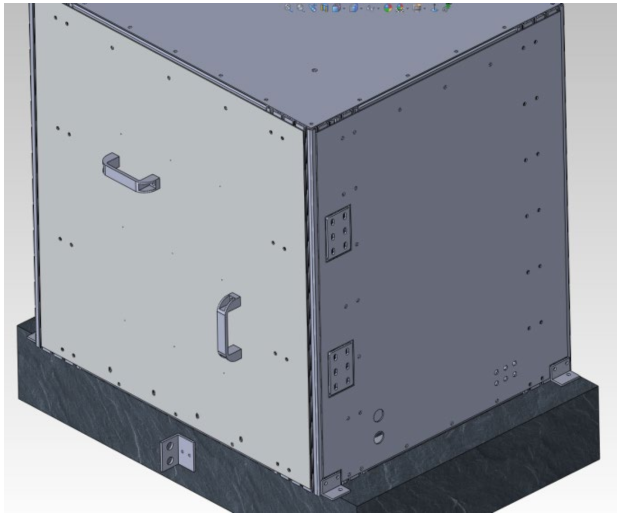

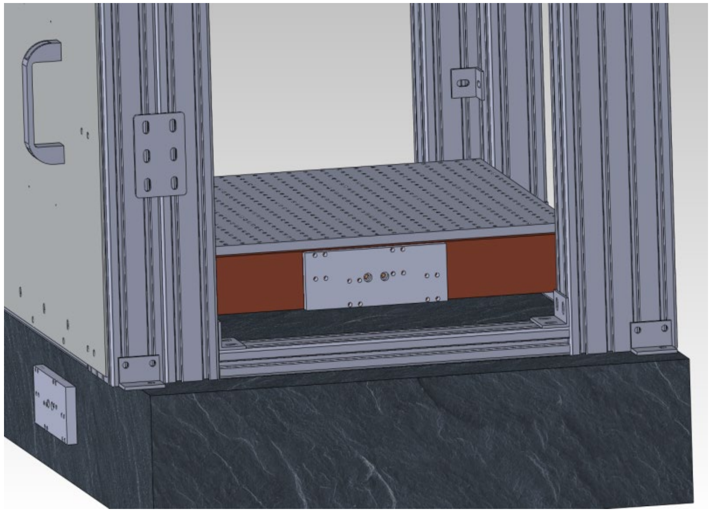

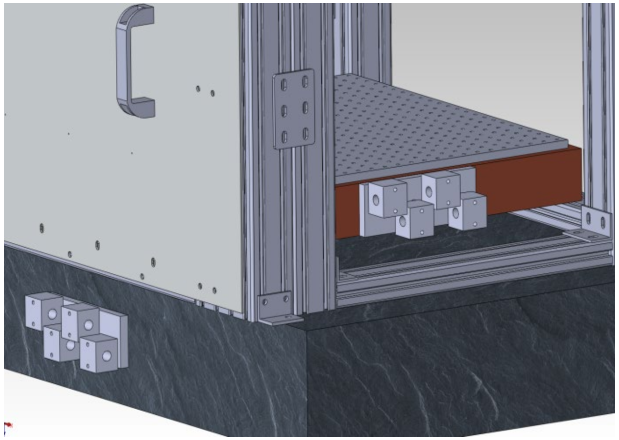

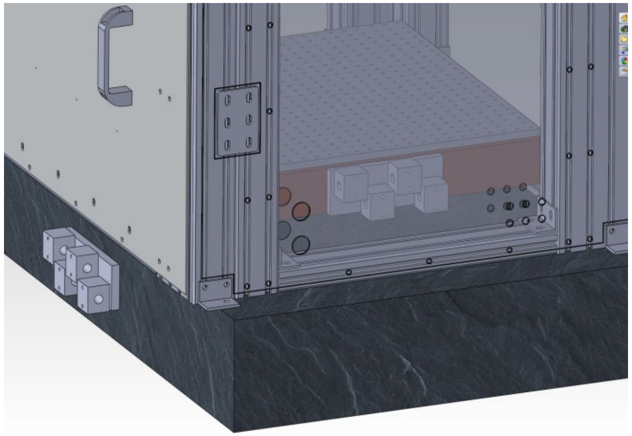

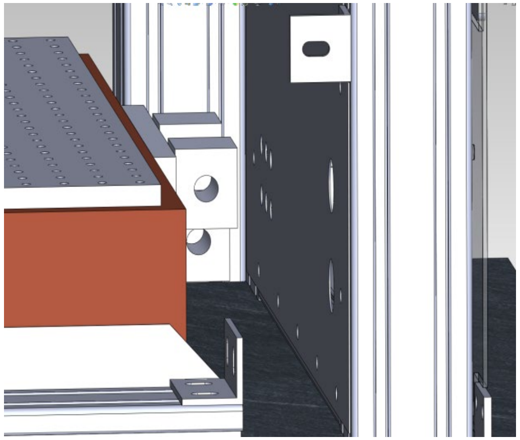

3.5.6: Data Acquisition

MAPPER lithography

Explanation voltage mode sensing at IEPE measurement

Overview of theoretical design – *real life construction in § 4.1*

The PCB209C11 miniature quartz sensor regards an Integrated Circuit Piezoelectric (ICP) transducer that operates using voltage mode output (and not charge mode). This means it has built-in electronics which conditions the high-impedance electrostatic charge output and converts it into a low-impedance voltage signal. This allows the sensor to be controlled by a constant-current source such as the IEPE type selected for this design (2-20 mA) while under 24 V compliance.

Advantage of the built-in MOSFET amplifier is that the created low-impedance signal can be used to transmit data over longer distances without loss of signal quality. Important to note its that the constant current value can cause more susceptibility to EM interference due to a higher output impedance; therefore the IEPE bias current has been set to 4 mA.

On the next slide, a schematic can be found that has been made to provide an overview of the various electronical components present in the sensor, cable and DAQ. It summarizes the transitions that take place from **SENSOR – AMPLIFIER – CABLE – DAQ – COMPUTER** when performing an IEPE measurement. Moreover, it shows how the applied force translates into an AC signal that is superimposed on the DC bias output voltage (PCB). The 60 pF blocking capacitor present in the used DAQ acts as a high pass filter from 3.4 Hz, removing the stationary component of the signal. This allows the dynamic AC variation to be processed by the computer (script). The selected coaxial cables are specific for low-noise measurement and have a 100 Ohm resistance.

In § 4.2.4.1, the various parameters that must be selected when performing an IEPE measurement are discussed. A step-by-step calculation is presented that can be used to prevent aliasing an optimize the signal in the frequency area of interest (i.e. prevent 'noisy results').

https://www.pcb.com/resources/technical-information/tips-from-techs/troubleshooting-using-bias-voltage

3.5.6: Data Acquisition

Data stream from sensors to computer

Overview of theoretical design – *real life construction in* *§ 4.1*

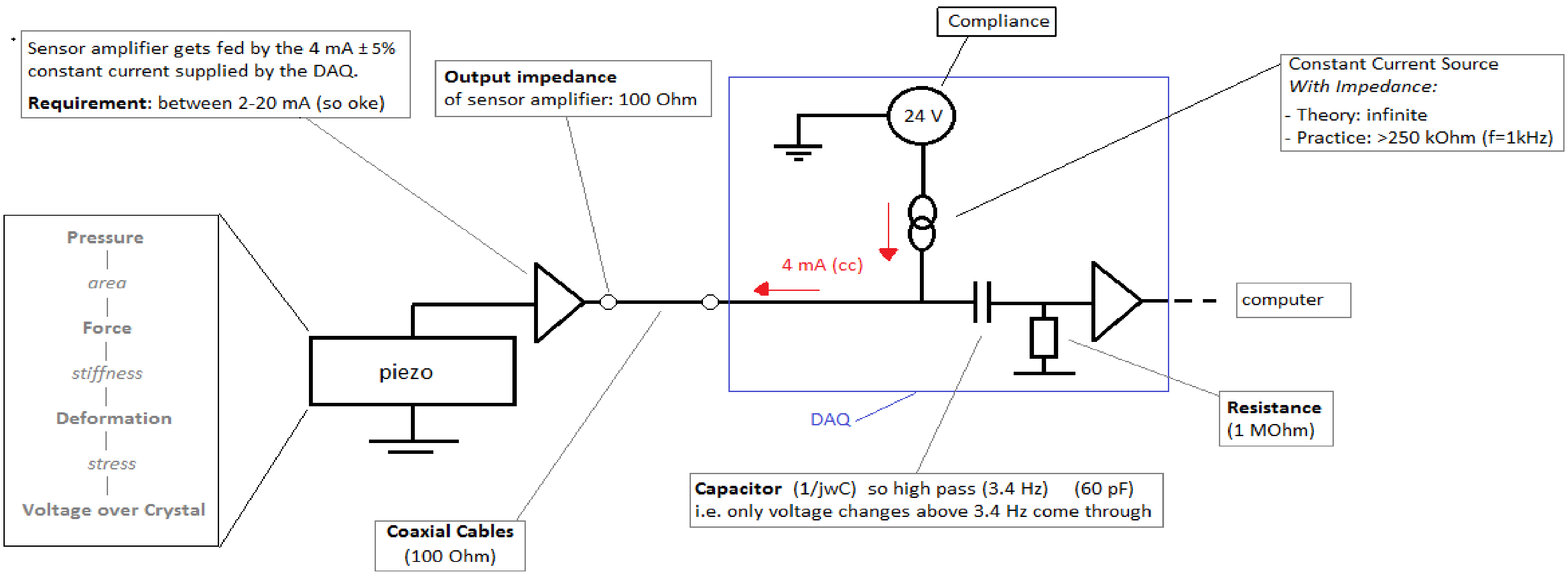

Chapter 4

Experimental Verification of the Final Design

CH. 4.1

The Final Design in Practice: **Forcesix**

4.1.1: Overview Final Design

Key Characteristics

Forcesix in 10 numbers

A total overview of the € 33.049 costing final design is shown below. Each sub-design element will be detailed on a separate slide.

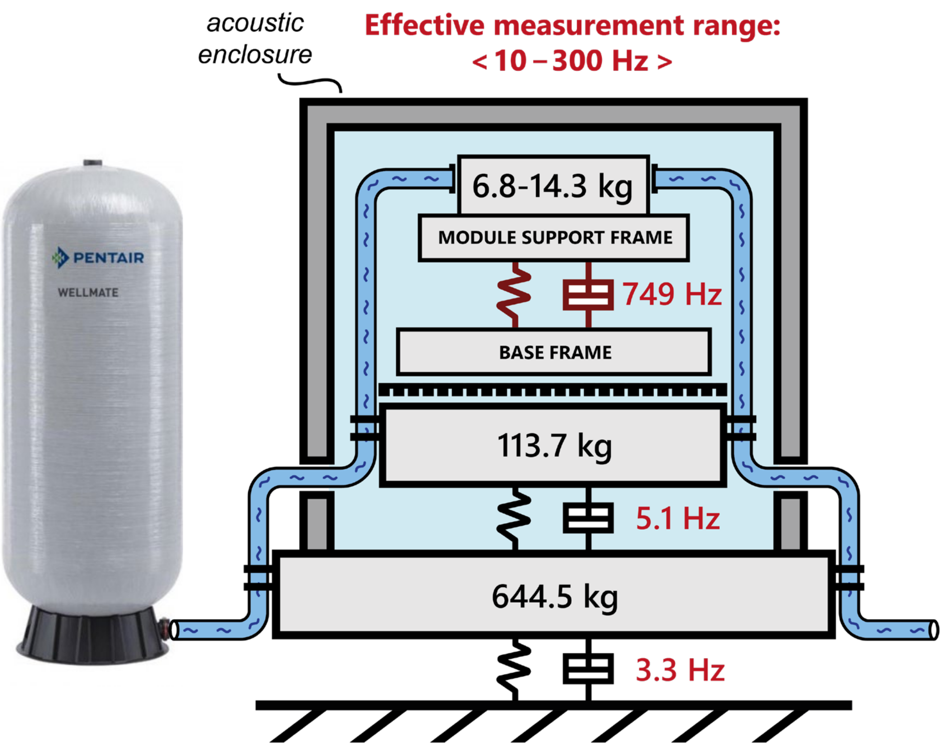

- **Sensing:** PCB209C11 Miniature Quartz Force Transducers (6x)
- **Signal-Conditioning:** Wilcoxon [PR710A] + NI BNC 2090A (1x)
- **Signal-Processing:** Integrated DAQ [NI PCI-6229] (1x)

4.1.2: Vibration Isolation Platform

Showing: the double mass-spring-damper system designed and build to attenuate FV

Practical implementation of the final design

What follows are pictures of all previously discussed elements of the theoretical design, only now in practice. The table frame, granite plates, airmounts and optical breadboard weight 828 kg together. More construction details in Appendix E.

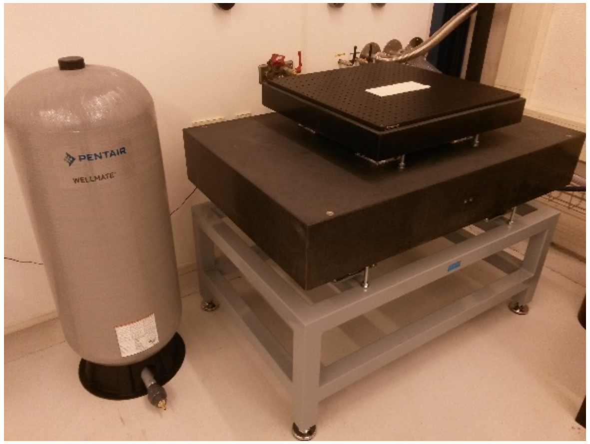

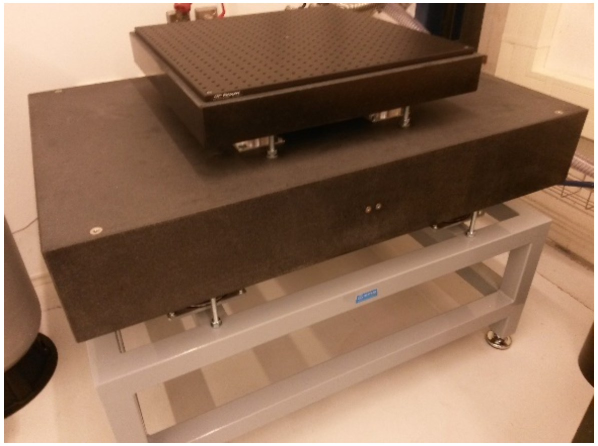

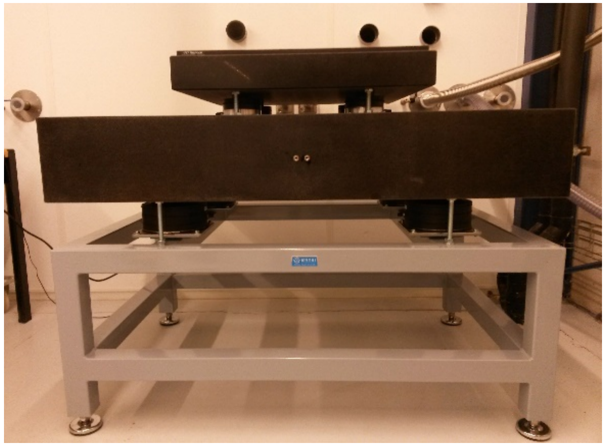

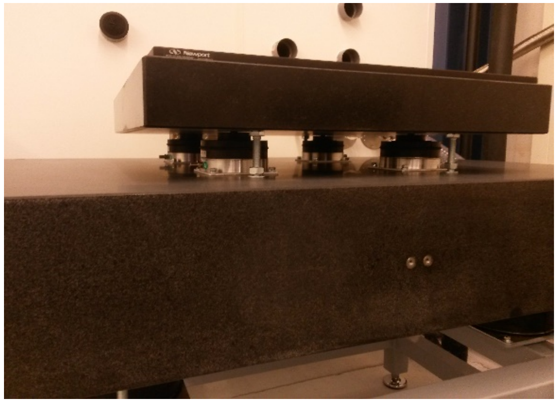

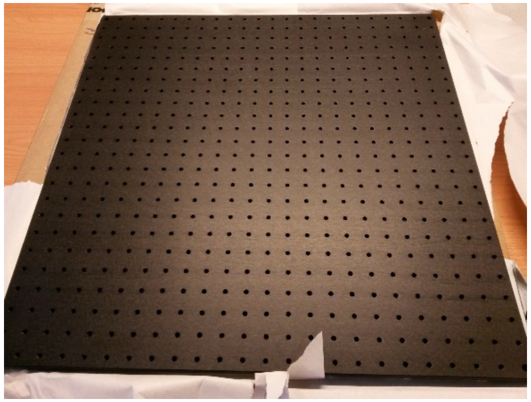

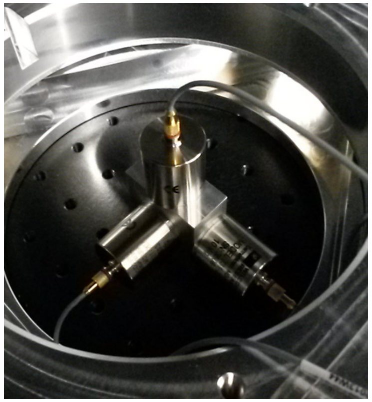

4.1.3: Acoustic Enclosure

Showing: the acoustical enclosure with and without front panel and with mic inside

Practical implementation of the final design

This casing has been custom designed for this measurement tool, with its dimensions, masses, eigenfrequency and support to prevent eigenmodes, tuned for the design. More construction details in Appendix E.

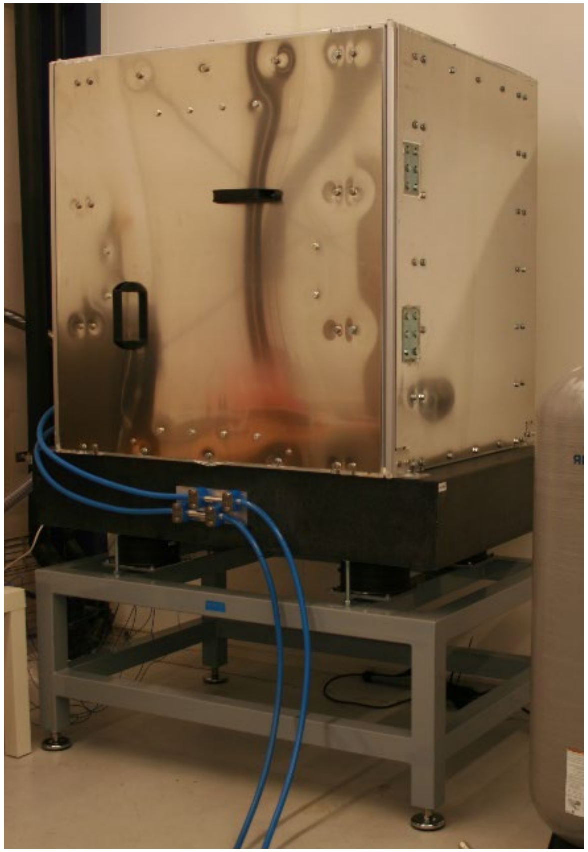

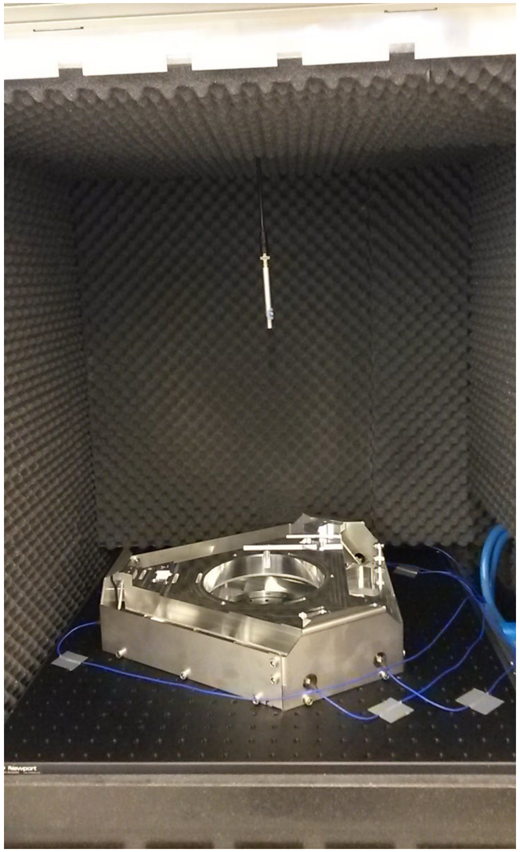

4.1.4: Module Support Frame (MSF)

MAPPER lithography

Showing: overview picture of Base Frame (BF) + piezos + MSF + protective casing

Practical implementation of the final design

This picture shows the design mounted on the top stage of the VI platform, inside the custom designed and build acoustical enclosure (front panel removed). On the right hand side, supply tubing can be seen entering and disconnecting at M2. The small rotation angle of the tubing indicates its flexibility. During testing it connects to the module (not present).

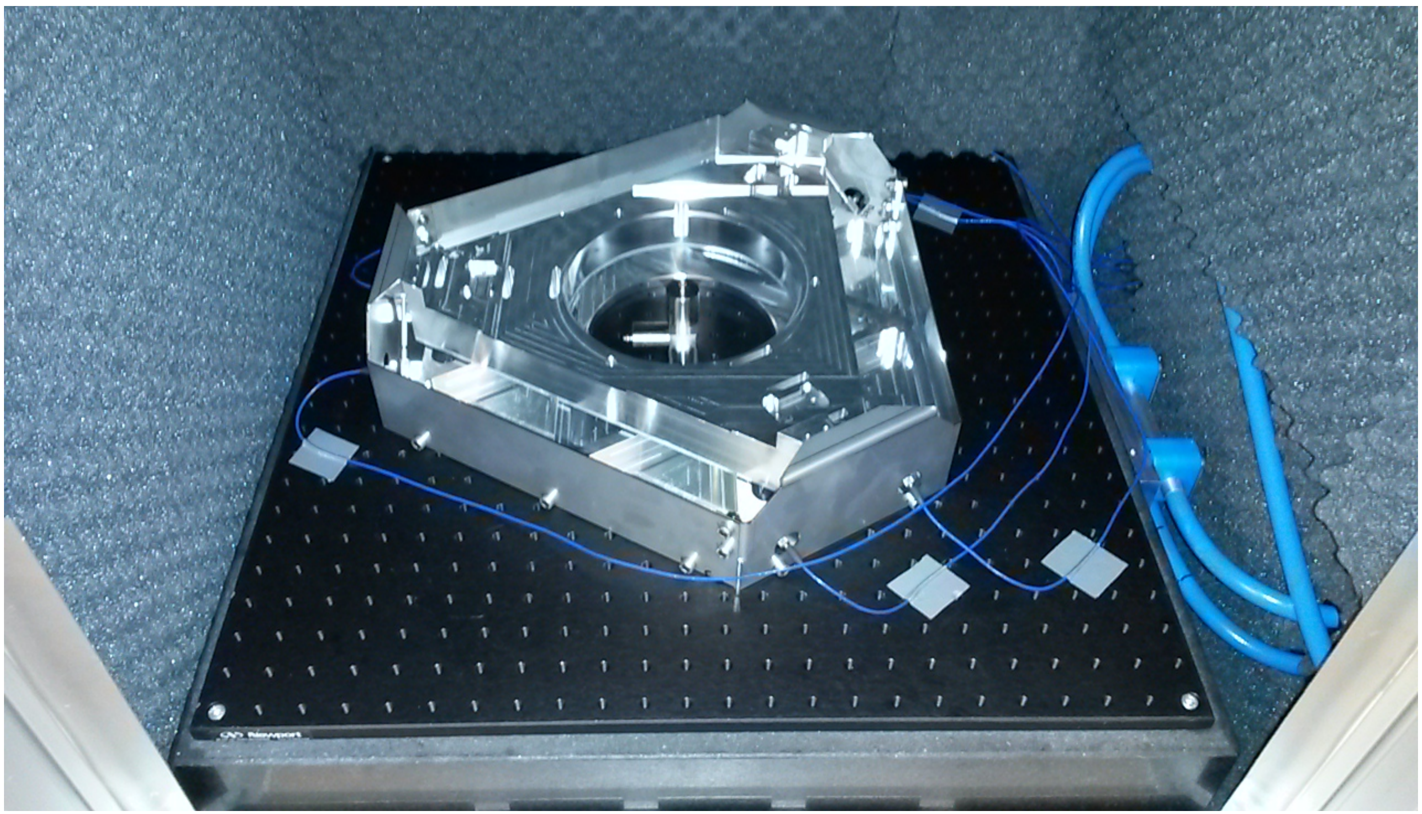

4.1.4: Module Support Frame (MSF)

Showing: MSF carried by 6 piezos, supported from BF, mounted rigid to optical breadboard

Practical implementation of the final design

To prevent **ground loops**, a film of electrical insulating material is used between the piezo and the base frame. The stiff-flexible support struts have been coated with a non-conducting glue and a nylon bolt is used to secure the piezo.

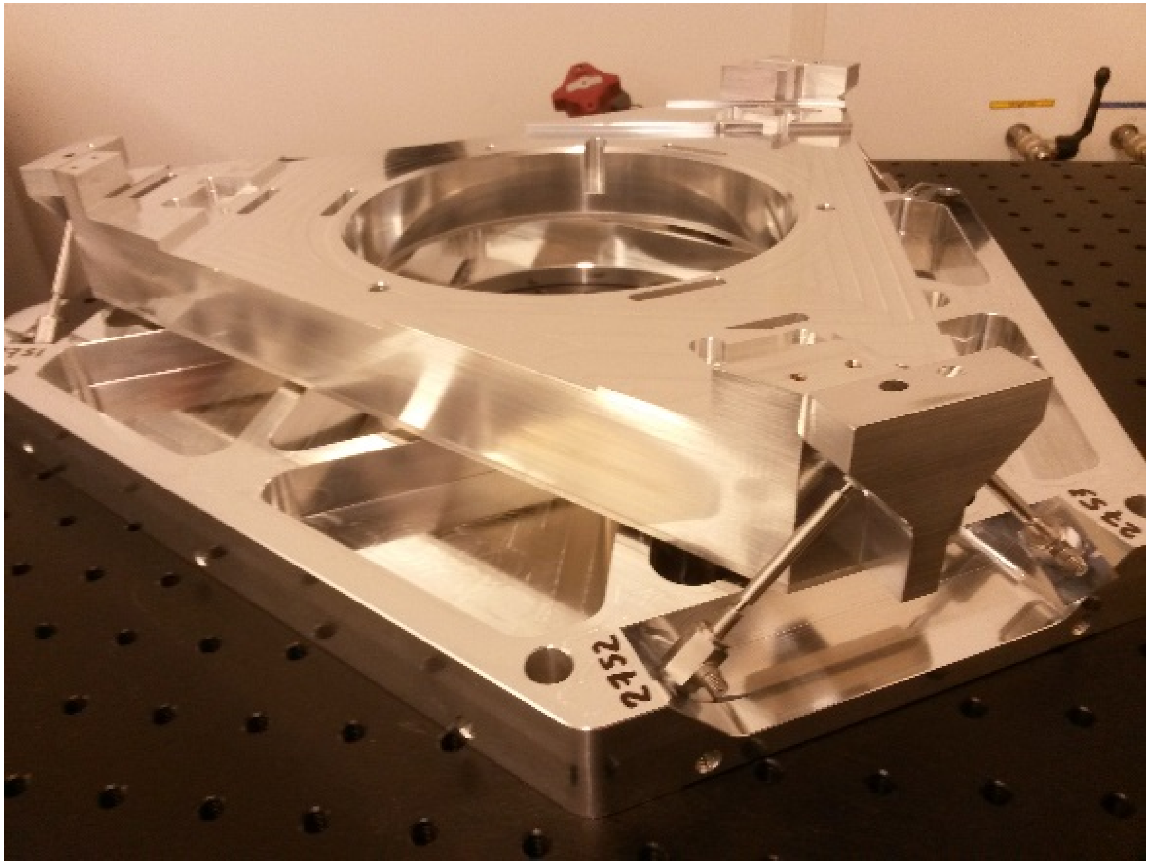

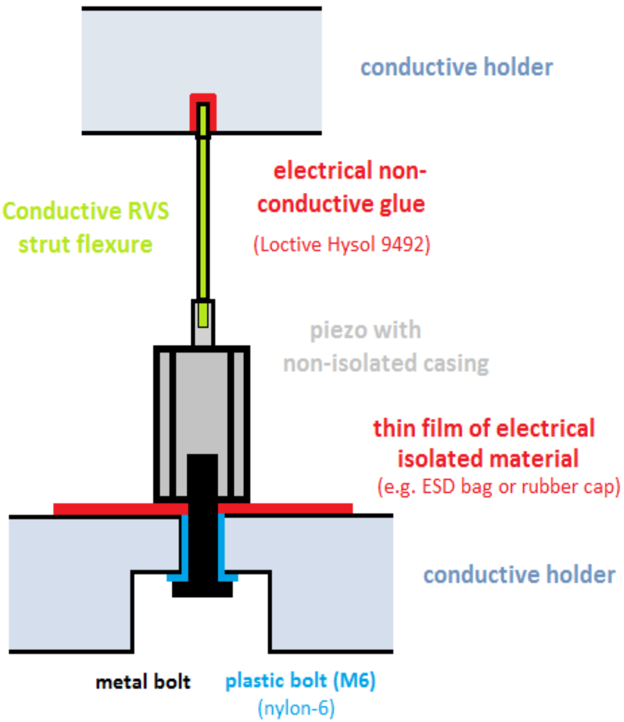

4.1.4: Module Support Frame (MSF)

Showing: separate elements of the MSF

Practical implementation of the final design

The construction of the MSF is shown here. It can be seen that as much mass as possible has been removed. Also the contact surface for the modules to interface through a ceramic ball can be seen in the bottom middle picture.

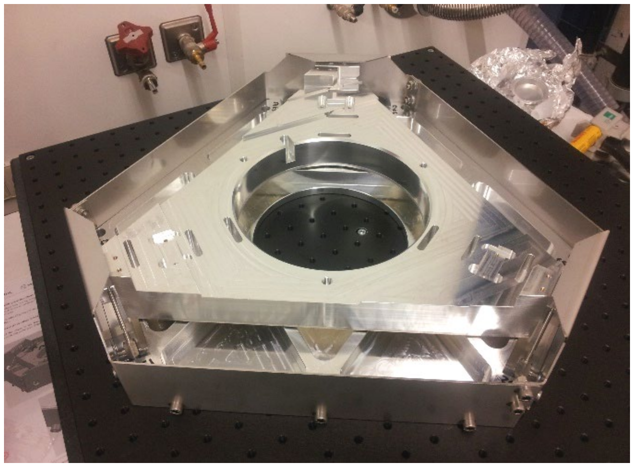

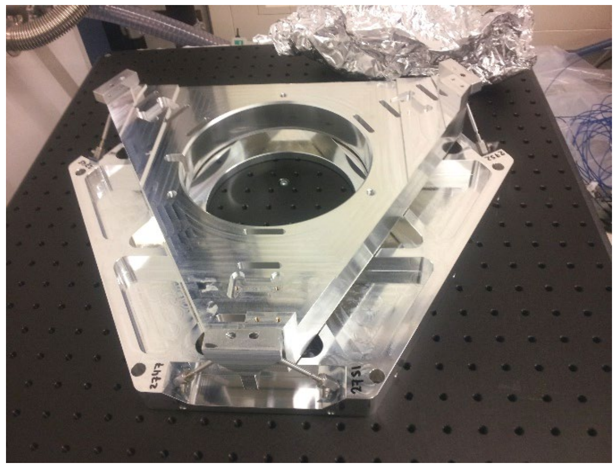

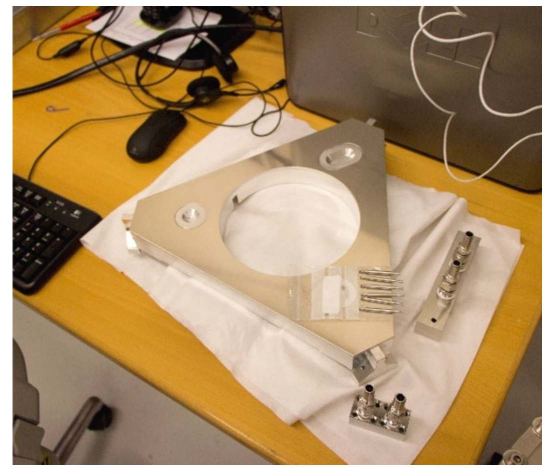

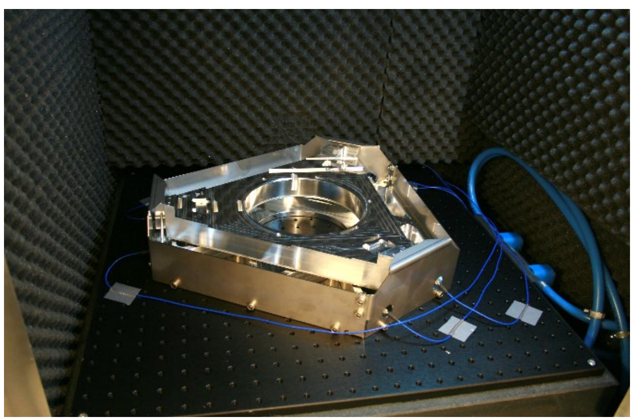

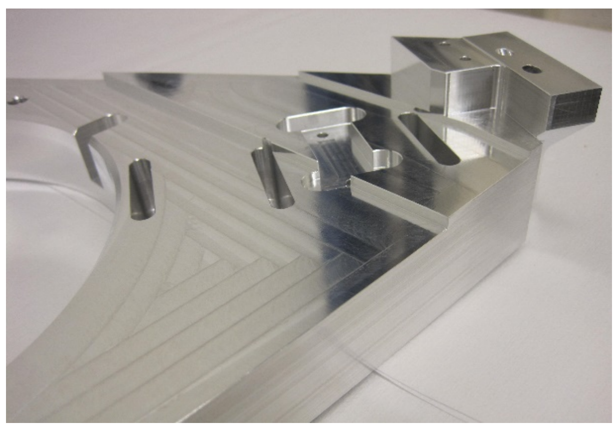

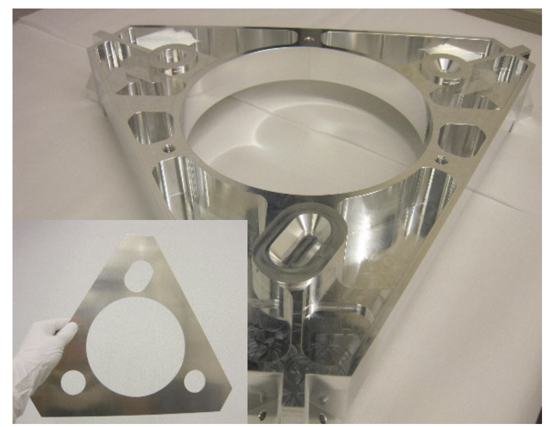

4.1.5: Piëzo Sensors

Showing: preventing ground loops and connecting the piezos with support struts

Practical implementation of the final design

This slide shows the (electric insulated) stiff-flexible support struts that were designed to achieve a high axial stiffness, whilst protecting the piezos from a bending moment through their 693 times lower, transverse stiffness. **Piezo:** 1cm & **strut:** 4 cm.
This is essential as the six PCB piezoelectric sensors are very costly (€ 12.600).

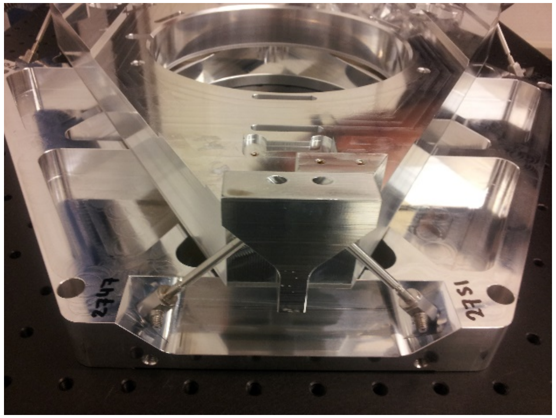
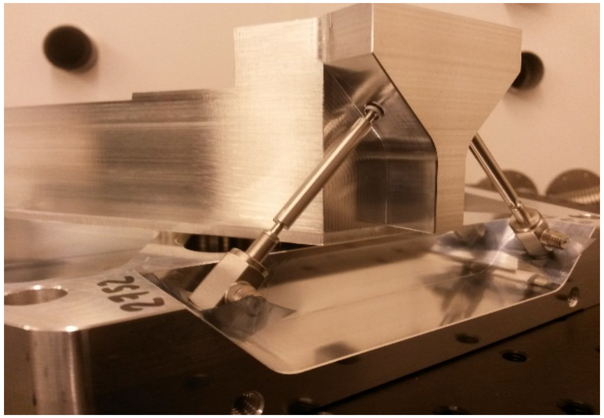

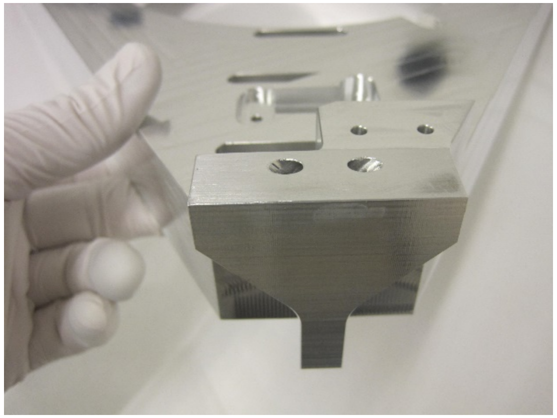
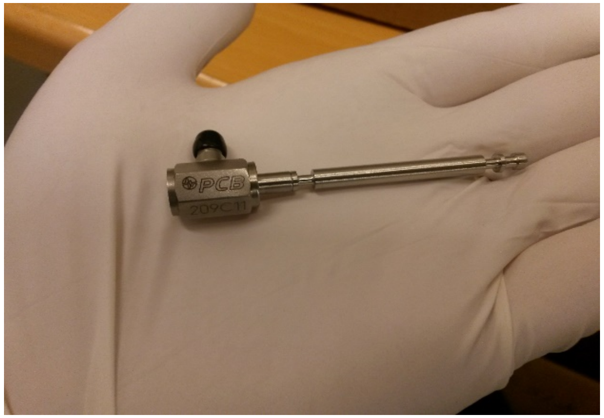

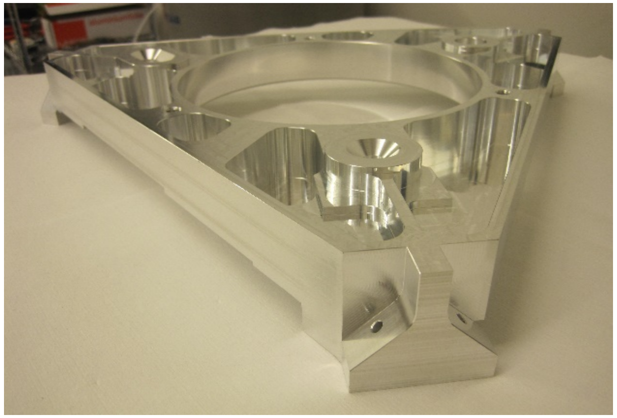

4.1.6: Supply Tubing (elements)

Showing: fiberglass pressure vessel, custom mounts to granite stones, connector flanges

Practical implementation of the final design


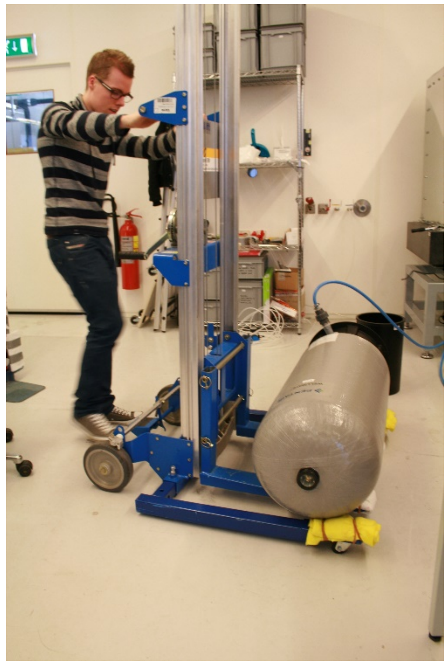
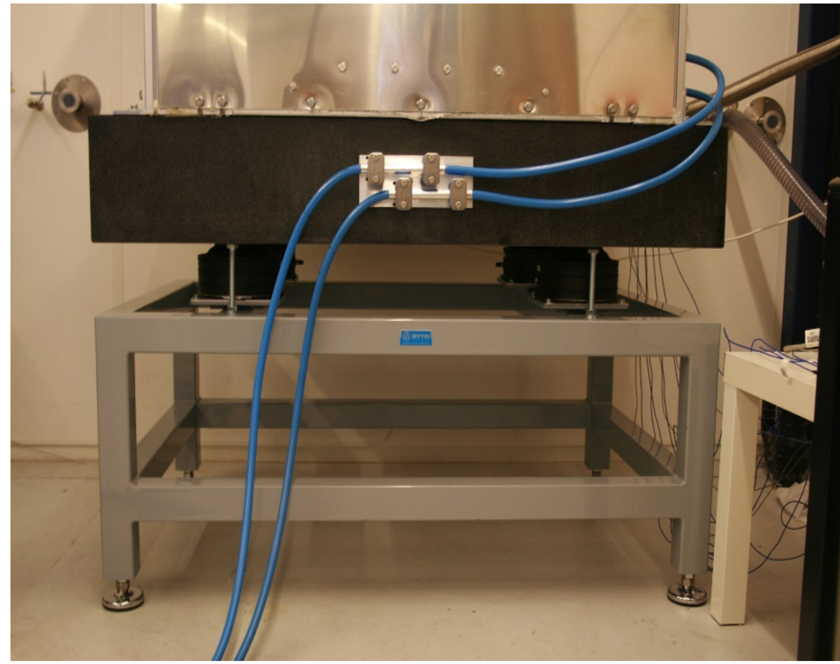



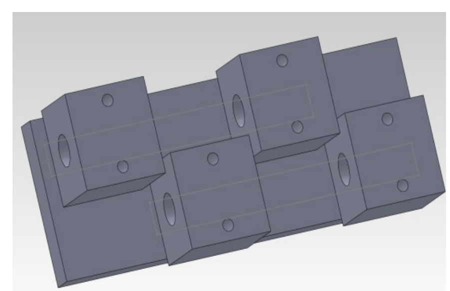


4.1.6: Supply Tubing (routing)

MAPPER lithography

Showing: tubing- and cable feedthrough

Practical implementation of the final design

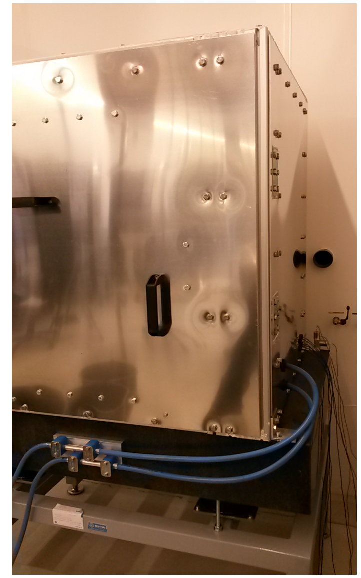

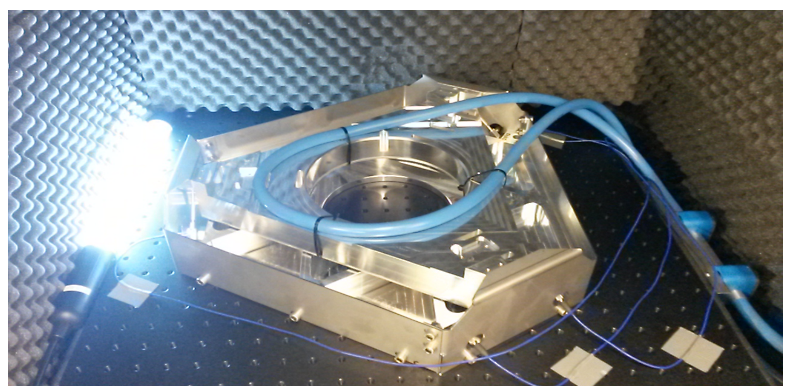

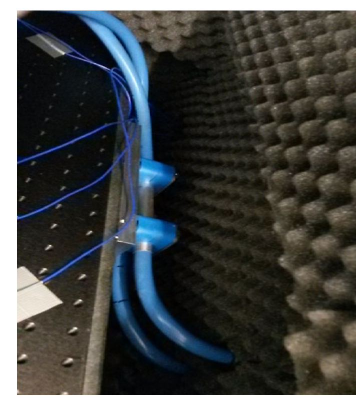

4.1.7: Data Acquisition

Practical implementation of the final design

Very low-noise SFTP cables are used (double twisted cable pair, individually foiled) with a minimum length required to make the connection. The braided wrapping cancels out EM interference as the magnetic/electric fields protect each other.

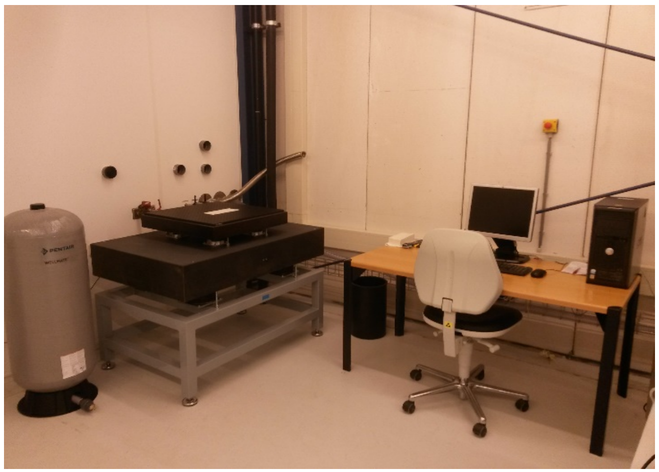

NI 6229

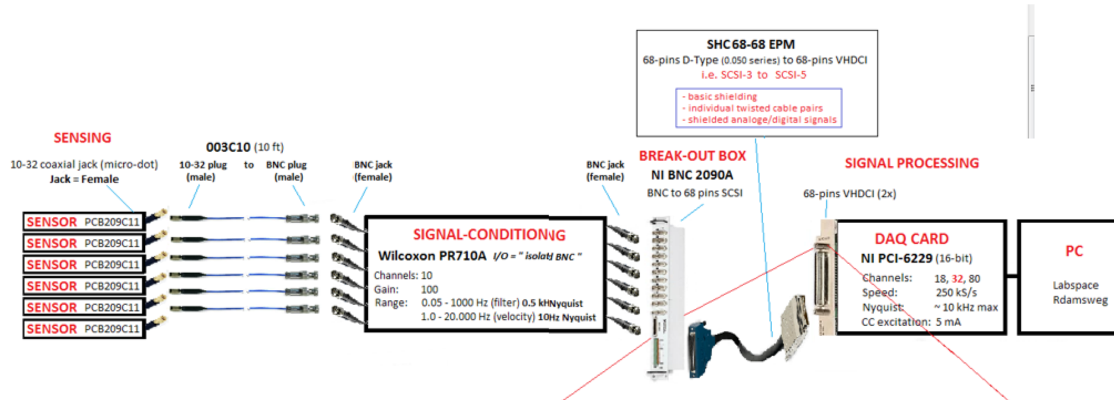

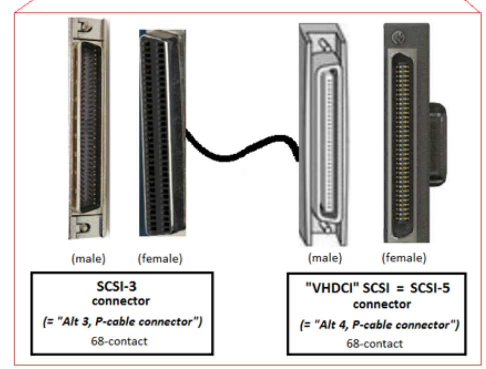

CH. 4.2

Forcesix Verification

Explanation Measurement Settings

Preventing aliasing by choosing the right parameters

To make sure measurements are free from digital distortion (e.g. aliasing, noisy signal) and that the required measurement time can be achieved using the hydrostatic pressure vessel, the IEPE parameters are calculated as follows:

- determine the **highest frequency of signal input** expected for the measurement (**Nyquist Frequency**)
- choose a **sampling frequency (Fsamp)** that is at least double this **nyquist frequency Fn)** i.e. ≥ 2x BW of interest
- choose a **frequency resolution (Fres)** suitable for the measurement (high Fres e.g. 0.01 results in noisy high freq behavior but gives a clear low freq response and vice versa for a low Fres of e.g. 0.5)
- calculate the required **number of samples per window N** **[**= 2^(round(log2(Fsamp/Fres)))**]**
- determine the **number of windows W over which the measurement shall be averaged**, accounting for the fact that the random white noise associated with the measurement will grow with √n (Sydenham, 2005), ergo higher is better. This is also important from a dynamic error budgeting point-of-view to ensure the disturbances are ergodic stochastic (3.4.2.1)
- calculate the **required total number of samples S** **[**= W • N **]**
- determine the **minimum measurement time** for batch measurement Mtime **[**= S/Fsamp**]**
- as a last step the **realized frequency resolution** can be computed by Frealized = Fsamp/N as well as the PSD frequency vector length **[**= (Fsamp/2) / Frealized + 1**]**

Objective for the verification was to measure accurately up to 10 kHz (SUSA SE), the following values have been used:

- **Fsamp:** 25.000 Hz (Nyquist Frequency is 12.5 kHz)
- **Fres:** 0.07 Hz (focus on clear low-frequency response but keep measurement time < 2 min)
- **N:** 262.144
- **W**: 10 (therefore S = 2.621.440)
- **Mtime:** 104.8 sec (performed in batch > averaged out; also a 4 min sensor warm up time to reduce impedance is scripted)

4.2.1: Acoustic Attenuation

Sound pressure measurements outside- and inside Forcesix

Evaluating Forcesix's real-life performance

The acoustical performance of Forcsix (outside & inside case) is shown in the below left plot. These results will be interpreted in the *discussion section*. Full measurements along with a comparison with the performance of the Vibronix cage (previous setup) in App. B-7 .

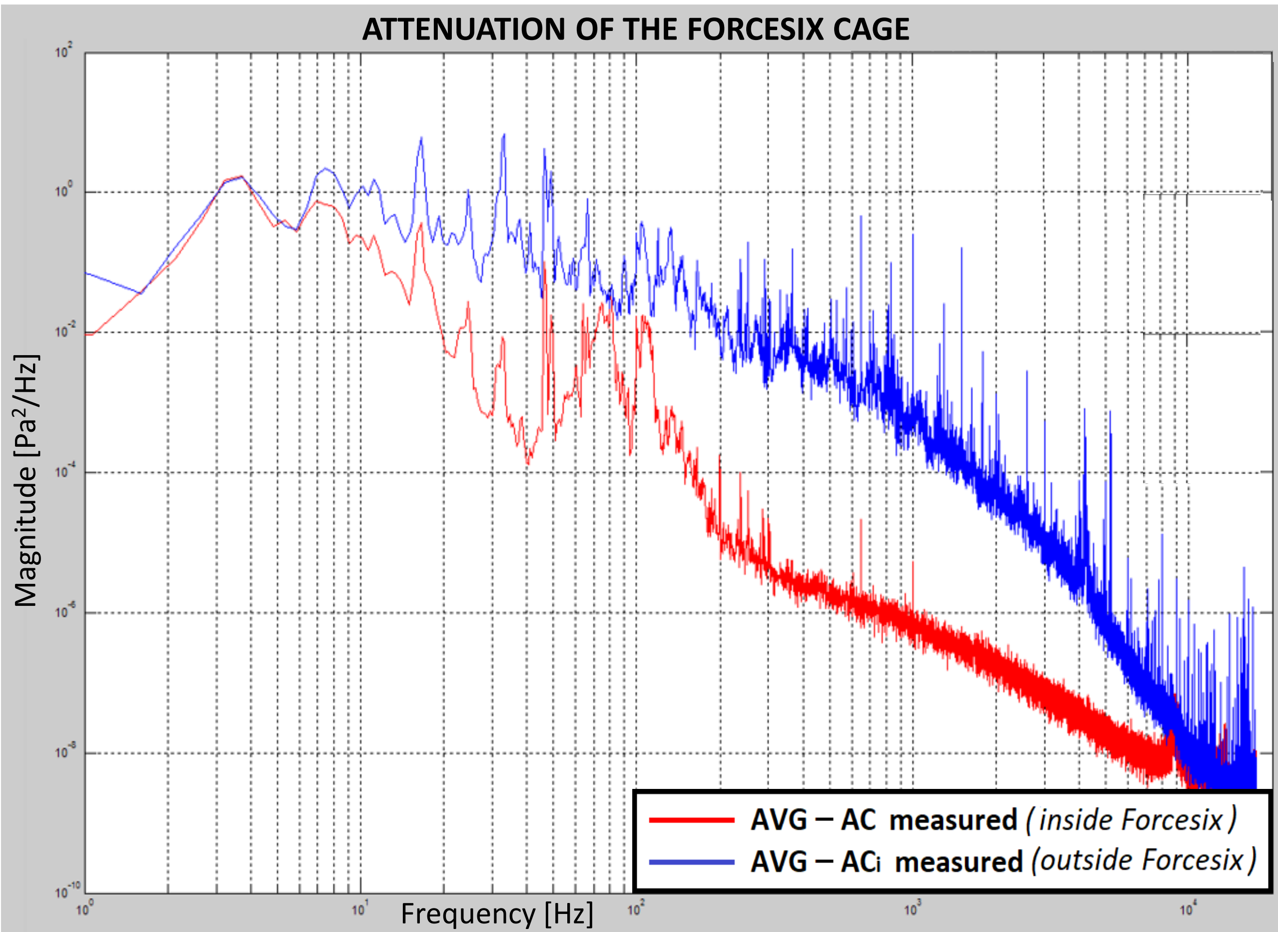

4.2.2: Measuring Background Noise

MAPPER lithography

Observed Spectral Noise Level – *no water flow*

Evaluating Forcesix's real-life performance

The noise bottom plot on the left shows good equal response for all sensors and comparable to the predicted signal (right plot). This is still uncorrected for sensitivity, gain, transformation matrix and unity spectral force characteristics. These measurements without flow give confidence that the setup works well.

Force sensor signal (time & freq. domain)

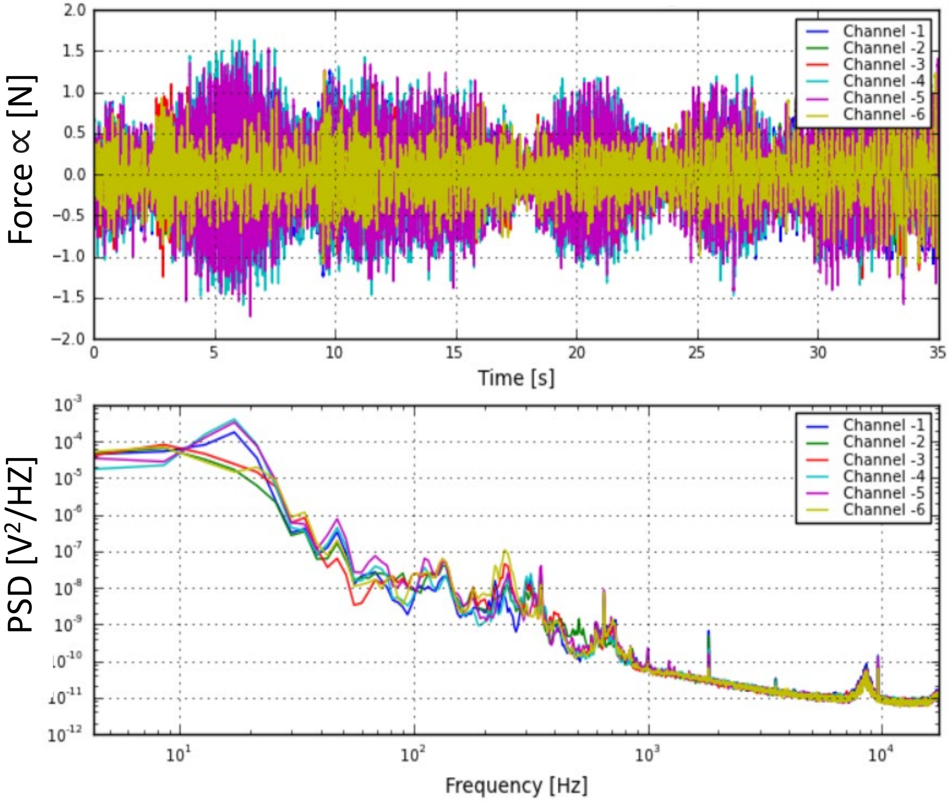

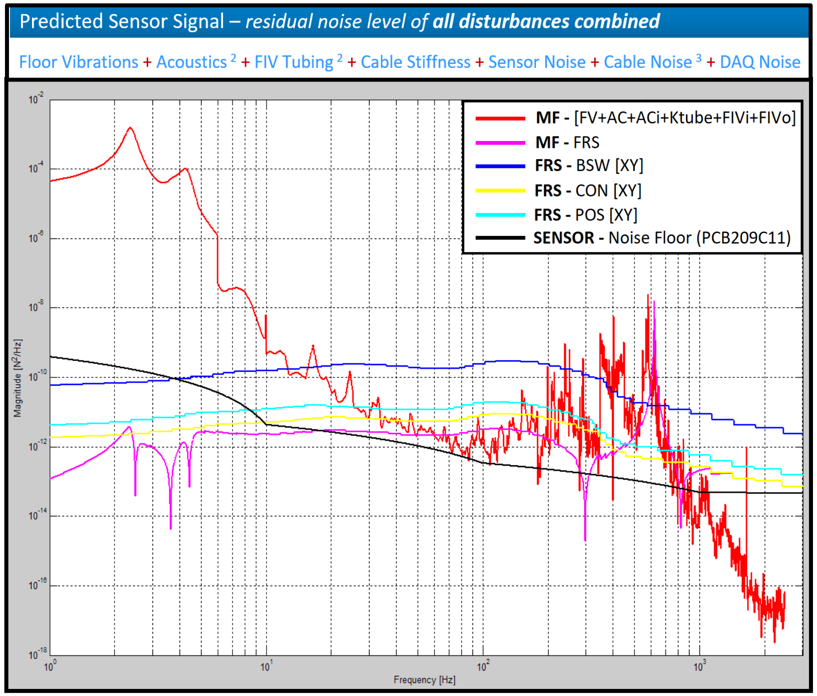

4.2.3: Flow Measurements

4.2.3.1: POS Module – *flow rate 0.1 L/min*

Hydrostatic water supply by means of pressure vessel

The below graph shows the initial flow measurement results at $^{1}/_{3}$ of the nominal flow rate for POS (0.33 L/min). This is still uncorrected for sensitivity, gain, transformation matrix and unity spectral force characteristics. The clear increase in input when measurements with flow are performed gives confidence that the setup can distinguish FIV forces from background noise.

Force sensor signal (time & freq. domain)

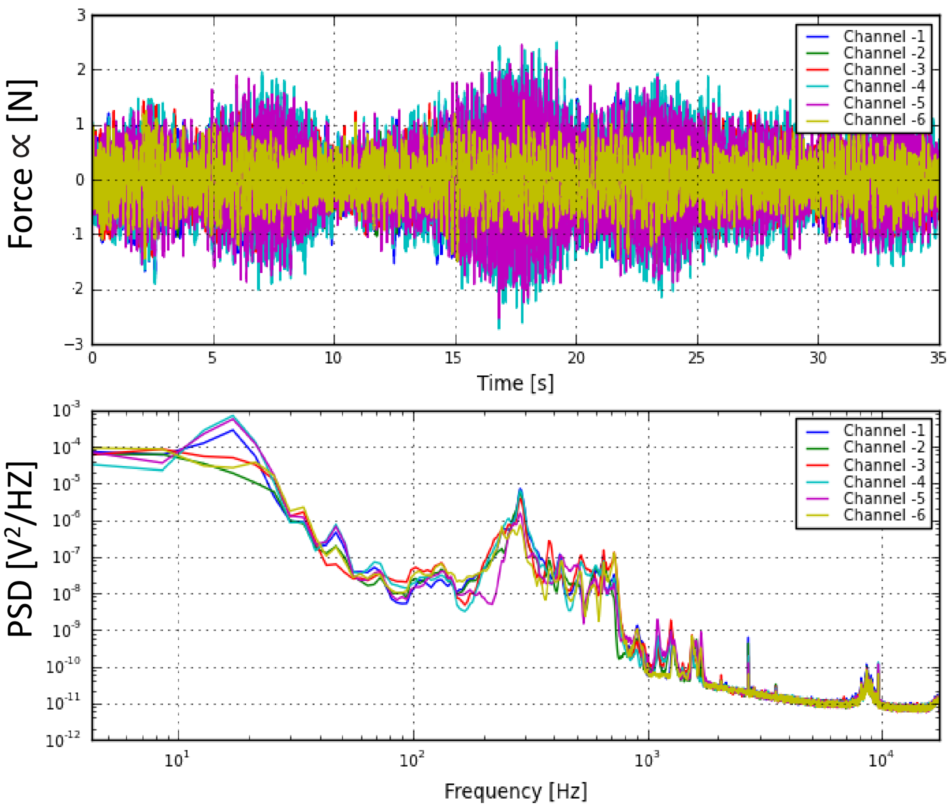

4.2.3: Flow Measurements

4.2.3.2: ABC Module – *flow rate 1.5 L/min*

Hydrostatic water supply by means of pressure vessel

The below graph shows the initial flow measurement results at half the nominal flow rate for ABC (3.0 L/min). This is still uncorrected for sensitivity, gain, transformation matrix and unity spectral force characteristics. The clear increase in input when measurements with flow are performed gives confidence that the setup can distinguish FIV forces from background noise.

Force sensor signal (time & freq. domain)

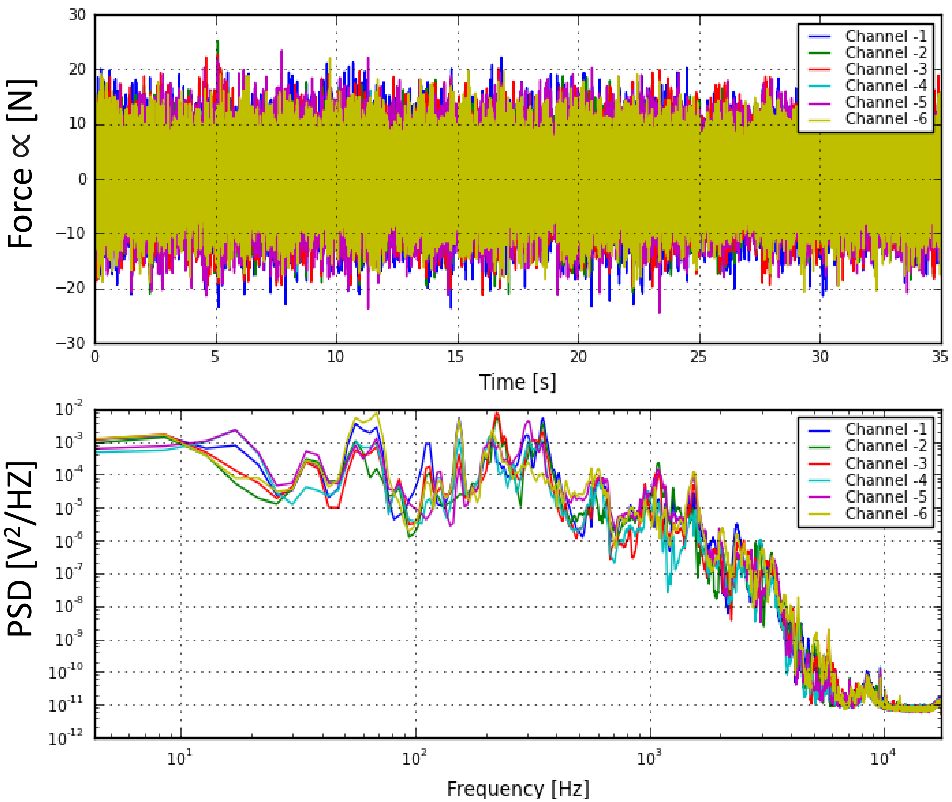

4.2.3: Flow Measurements

4.2.3.3: BSW Module – *flow rate 5.2 L/min*

Hydrostatic water supply by means of pressure vessel

The below graph shows the initial flow measurement results at nominal flow rate for BSW (CLBC). This is still uncorrected for sensitivity, gain, transformation matrix and unity spectral force characteristics. The clear increase in input at increasing flow rate is an indication that we know what is measured.

Force sensor signal (time & freq. domain)

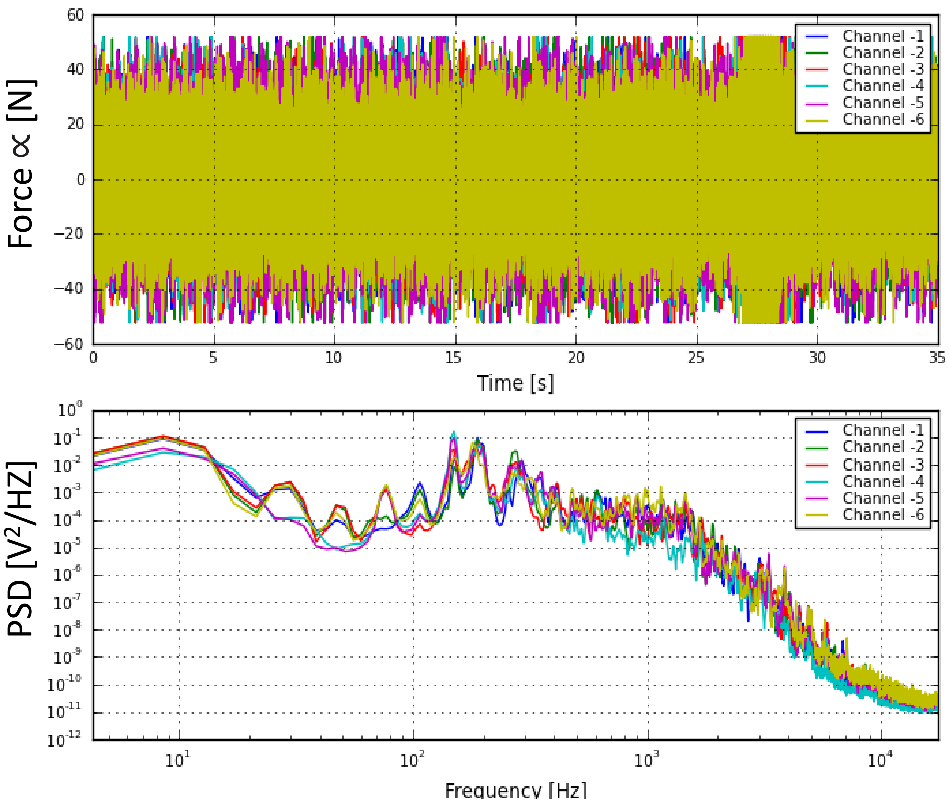

4.2.4: Data Processing

4.2.4.1: Transformation Matrix

Transforming six sensor signals into 6-DOF spectral forces

Manual derivation global stiffnesses (Kx, Ky, Kz)

Assuming similar axial compression- and tension stiffness values, and simplifying by setting θx to 0^o (a prerequisite for the bending moment), this design's global stiffness can be analytically expressed (sanity check) as:

$$\mathbf{K}_{\mathbf{X}\,6\text{piezos}} = 2\cos(\alpha)K_{axial} \bullet \text{abs}[(\cos(\beta) + \cos(\beta+60) + \cos(\beta+120)] + 2K_{transv.} \bullet \text{abs}[(\sin(\beta) + \sin(\beta+60) + \sin(\beta+120)]$$

$$\mathbf{K}_{\mathbf{Y}\,6\text{piezos}} = 2\cos(\alpha)K_{axial} \bullet \text{abs}[(\sin(\beta) + \sin(\beta+60) + \sin(\beta+120)] + 2K_{transv.} \bullet \text{abs}[(\cos(\beta) + \cos(\beta+60) + \cos(\beta+120)]$$

$$\mathbf{K}_{\mathbf{Z}\,6\text{piezos}} = 6\sin(\alpha)K_{axial}$$

Note that K_{axial} is the resulting *stiffness train value* of the piezo-strut combination ($3.73e^7$ N/m) and not K_{piezo} ($3.5e^8$ N/m). Furthermore, α is the angle that spans each sensor pair and β represents the external rotation from one pair to another.

For this design configuration α=45^o and β=0^o, yield an overall stiffness expressed as K_{axial} factor of **< 2.83, 2.45, 4.24 >** for **< K_X, K_Y, K_Z >** which corresponds well with the summation of [X] values of the inverse transformation matrix (respectively < 2.84, 2.47, 4.26 > • K_{axial}, as shown on the next slide.

The rotational stiffness values are < 0.57, 0.58, 0.87 > • K_{axial} for < K_{RX}, K_{RY}, K_{RZ} > which means that rotations can be measured a factor (6/0.57=10.5), (6/0.58=10.3) and (6/0.87=6.9) worse than the noise level of the sensor. This should be sufficient to meet the requirement as the required noise level to verify the modules (FRS) was set *an factor 10 lower* to account for this (§ 2.3.3.1). Additionally, this was based on the most stringent in-plane requirements (XY), which relate to the other DOFs in the ratio < 1, 1, 10, 2, 2, 10 > i.e. < X, Y, Z, Rx, Ry, Rz) > (§ 2.4).

The fact that these stiffnesses are non-symmetric is due to the orientation of the sensors, placed in-line with the circumference of the sphere surrounding the MSF. This is a consequence of the sensors inability to handle transverse loads, which does not allow them to be rotated inward i.e. directed more towards the COM.

4.2.4: Data Processing

4.2.4.2: Transformation Matrix

Transforming six sensor signals into 6-DOF spectral forces

Courtesy of Rogier Ellenbroek from Mapper, the following transformation matrix has been derived with Ansys. It matches the total XYZ stiffness that was manually computed on the previous slide. Also, the Z stiffness *per sensor* is correct as it corresponds with calculations.

Initially it was intended to analytically derive the transformation matrix using global- and local stiffness matrices to express the forces/moments by displacements/rotations as detailed in Cook (2005), but for sake of time this FEM description is used.

Transformation matrix from force/moment to sensor reaction force as obtained from ANSYS

	X	Y	Z	Rx	Ry	Rz
Sensor 1	0.10735	0.46779	0.23473	-1.02E-002	-2.2863	1.1479
Sensor 2	0.10743	-0.46733	0.23463	1.30E-002	-2.2871	-1.1477
Sensor 3	-0.45871	-0.14081	0.23538	1.9845	1.1381	1.1481
Sensor 4	0.35131	0.32659	0.23467	1.9716	1.1493	-1.1487
Sensor 5	0.35146	-0.3268	0.2348	-1.9727	1.1488	1.1484
Sensor 6	-0.45875	0.14068	0.23556	-1.9854	1.1383	-1.148

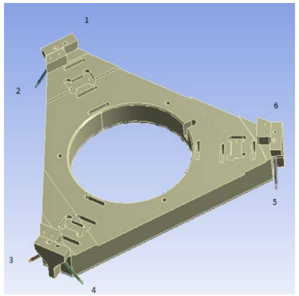

4.2.4: Data Processing

4.2.4.3: Stage Stability Contribution

Transforming 6-DOF spectral forces into 3-DOF Matrix overlay errors

Using the transformation matrix on the previous slide, the 6 sensors signals can be transformed into 6-DOF spectral forces, which the module that is being tested, exerts on its environment. The next step would then be to translate this to MOF movement inside Matrix (the Mapper machine), to see how these forces affect wafer error. This can be done using the same script written to establish requirements (§ 2.3.3.2). For sake of time this data processing step has not been performed.

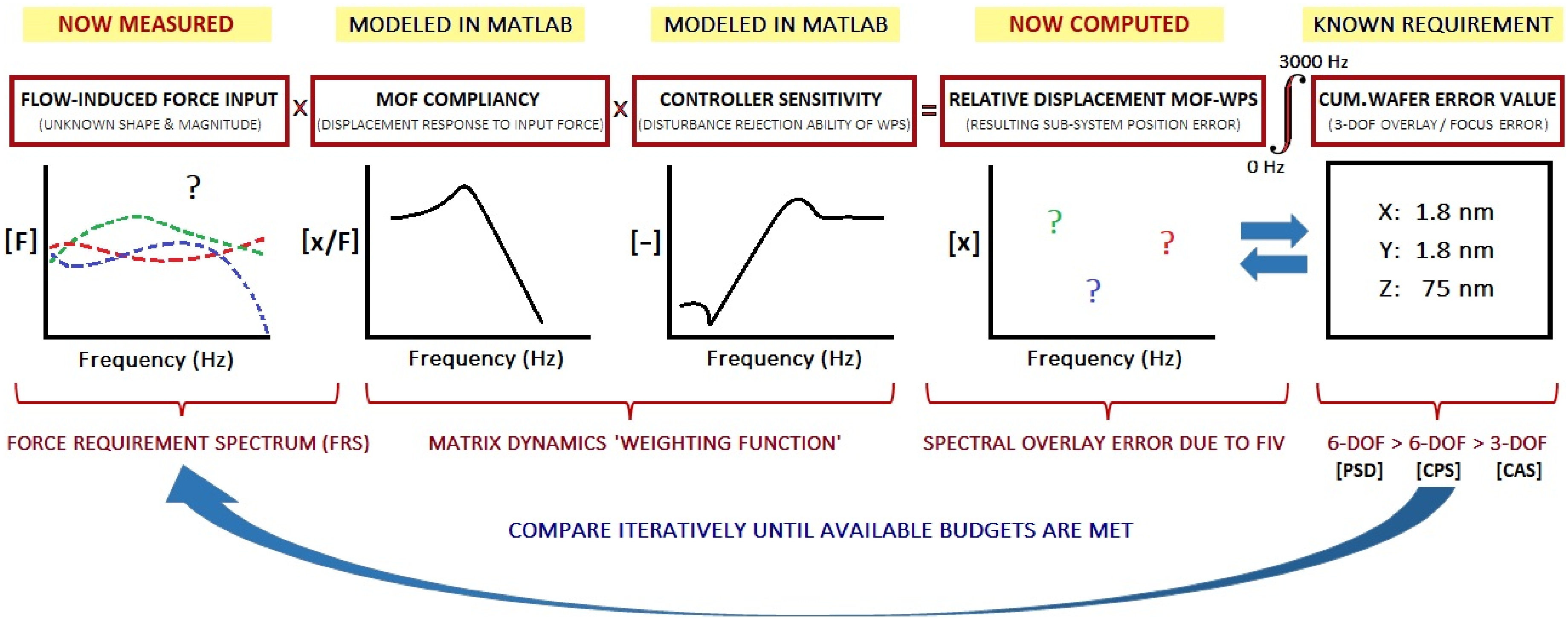

4.2.5: Applying a Known Force Input

MAPPER lithography

Injecting a calibrated signal and observing what is measured by Forcesix

Additional verification step performed by Mapper

One of this project's recommendations for future research was to perform an additional verification step with a calibrated actuator (e.g. an imbalanced microdrive) to objectively determine the correctness with which Forcesix is able to measure (flow-induced) vibration forces. After project completion, this test has in fact been executed by Mapper already and gives insight in the performance of Forcesix in terms of accuracy ("truthfulness of the measurement"). Although this test was not performed by the Author of this thesis, the outcome is too relevant not to be mentioned here. Courtesy of Rogier Ellenbroek:

> Nog even een beetje stimulerend nieuws:
> We hebben vorige week een test gedaan op Forcesix om even eenvoudig te controleren of de orde-grootte van de door ForceSix gemeten krachten klopt. We hebben dit gedaan met een heel klein motortje met een kleine onbalans (zoals dat ook in je telefoon zit, zie https://catalog.precisionmicrodrives.com/order-parts/product/304-015-4mm-vibration-motor-7mm-type).
> Resultaat hiervan was dat de krachten in X/Y binnen 10 a 20% overeen komen met de verwachtingen.
> Mooi werk!
>
> Groeten,
> Rogier

The above results are positive as it indicates that the setup works as designed, which could be expected from initial measurement results. Particularly interesting is the fact that the measured offset is 10 – 20%, which is in the same range was predicted based on the ratio Fmeas/F3 and inherent to the design (§ 3.4.4.2).

Given the good match between the expected response and these practical results, it can be said that Forcesix is expected to behave according to its design and it able to meet the demands as posed by Mapper to be able to use it as a verification tool for modules. **Therefore, it is concluded that Forcesix is verified and the measurement results are accurate and thus reliable.**

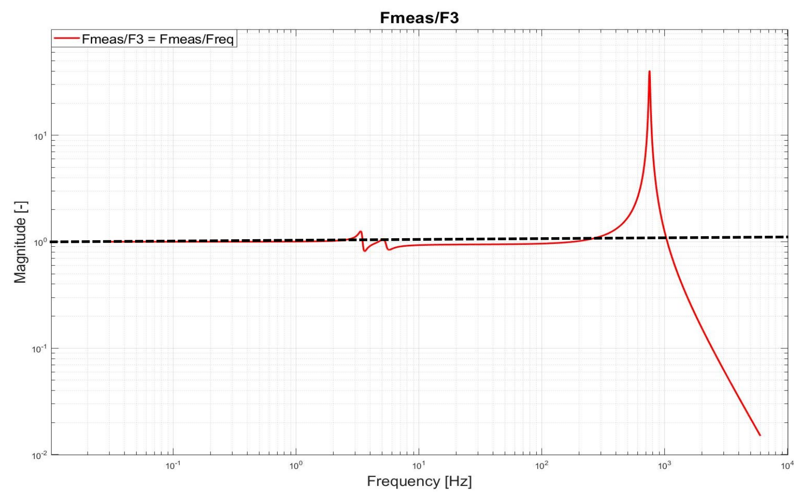

CH. 4.3

Discussion

Interpreting the Verification Results

MAPPER lithography

- the acoustical measurement results performed inside and outside the enclosure of Forcesix, show that it is more effective at shielding acoustics than the casing used with Vibronix, with significantly improvements below 50 Hz and above 175 Hz. In addition, the Vibronix cage only starts to attenuate from 50 Hz on and has very limited effect from 80 – 140 Hz. This has improved much with the Forcesix cage as attenuation starts as low a 7 Hz, with limited reduction only from 65 – 85 Hz.
- verification measurements on the final design from 10 – 300 Hz show a noise floor characteristic that is in accordance with the theoretically predicted effect of all disturbances combined (≈ $2.5e^{-11}$ N^2/Hz). The 15 Hz peak cannot be explained.
- performed flow measurements also indicate that the obtained results are reliable given a much higher average input signal (varying per module) than the background noise present. Specifically, the signal-to-noise ratio (**SNR**) ranges from **10^1** (POS) and **10^4** (ABC) to **10^5** (BSW).
- courtesy of Mapper it can be stated that this background force noise level corresponds to a wafer error of 0.10 nm (XY – POS) when transformed back through Matrix system dynamics (MOF compliance, WPS controller sensitivity) which is a factor 1.7 lower than its FRS (0.17 nm).

<u>These outcomes also suggest to answer the underlying Research Question (RQ) relevant for Mapper and driving the project:</u>

<< Are the cooling forces, induced in the modules and exerted onto the MOF, resulting in exceedances of the stage-stability error budgets? >> …. with *yes* given the significant difference in SNR between ‘no flow’ and ‘flow at a rate which is not even at nominal value’. However, to be able to say this with certainty, the measurements for the POS, ABC and BSW module at their exact nominal flow rates would have be processed and interpreted. <u>This requires correcting for the following aspects:</u>

- raw sensor data (6-SIGNAL ASD) [V/sqrt(hz)]
- order of connection [-] (6-SIGNAL ASD) [V/sqrt(hz)]
- calibrated sensitivities [-] (6-SIGNAL ASD) [N/sqrt(hz)]
- scaling with SUSA gain [-] (6-SIGNAL ASD) [N/sqrt(hz)]
- 6-DOF transformation matrix (6-DOF ASD) [N/sqrt(hz)]
- Turn into PSD (square it) (6-DOF PSD) [N^2/Hz]

Interpreting the Verification Results

MAPPER lithography

- unity input spectrum (correct for unity force spectrum)
- 6-DOF MOF compliancy (Matrix) (6-DOF PSD) [m^2/Hz] *"relative MOF movement"*
- 6-DOF Controller sensitivity (WPS) (6-DOF PSD) [m^2/Hz] *"relative wafer motion wrt MOF" i.e wafer error*
- 3-DOF EO-slit (mapping rotations to translations) (3-DOF PSD) [m^2/Hz] *"relative wafer movement wrt MOF"*
- 10 – 300 Hz integration and squaring to obtain CAS values (nm). (3-DOF CAS) [m] *"relative wafer movement wrt MOF"*
- this value should be expressed in nanometers and compared against the rebudgeted errors as established in § 2.3.2.2:

Re-budgeted error per (sub)module:

sub-system	*module*	*sub-module*	*X-budget* [nm]	*Y-budget* [nm]	*Z-budget* [nm]
ILO	BG		0.16	0.16	0.94
PBB	BSW		0.65	0.65	3.75
POS			0.17	0.17	0.95
CON		ABC	0.11	0.11	0.65

If done, this transforms the sensor's ASD values (V/√Hz) into 6-DOF exerted forces < X,Y,Z,Rx,Ry,Rz > PSD values (N^2/Hz) and then into the 6-DOF relative MOF motion <X,Y,Z,Rx,Ry,Rz > PSD values (N^2/Hz). Upon integration over the 10-300 Hz frequency range and squaring this eventually yields the intended 3-DOF wafer error <X,Y,Z> expressed as standard deviation (σ) CAS value [m].

Given the fact that IEPE measurments remove the bias (offset voltage), this signal has a mean value (μ) of 0 which means this σ would then be equal to the RMS expression.

If the XYZ wafer errors are indeed in exceedances of the budgets, this would not come as a surprise. This is because the nature of water cooling is that efficiency increases with turbulence, which correlates strongly with the source amplitude of FIV.
The main problem that lies at the root of wafer error is therefore the significant amount of heat generated (≈ 2.5 KW) in an environment that aims for stability at the sub-nanometer level. A redesign from first principles on the creation of beamlets would be a more fundamental solution for Matrix to generate less heat in the first place.

Chapter 5

Conclusion

& Recommendations

CH. 5.1

Conclusion

Conclusion of the Study

Has the goal of the study been accomplished?

Can we also answer the main research question, underlying and driving the project?

The goal of this study was to:

"Design, build and verify a 6-DOF experimental setup, tailored to observe FIV, that is able to accommodate water-cooled Matrix-modules and perform measurements over their full operating range (10 – 300 Hz) at a resolution that allows for verification of the stage stability budgets."

A mechanical design has been realized, called Forcesix, which:

- attenuates floor-vibrations using a mass-optimized triple MSD system that decouples at 3.3 Hz and 5.1 Hz (§ 3.5.1) and isolates from 8.5 Hz onwards (§ C-2.1). This mass distribution also ensures dynamical stiff behavior up to 749 Hz (POS).
- shields off acoustic interference with a physical enclosure that is rigidly connected to the bottom VI stage (644 kg). This results in significant reduction of the environmental sound pressure level by an average factor of 427 (10 – 300 Hz).
- decreases the effect of flow-vibrations induced in external- and internal supply tubing on the sensor signal by an average factor of 10^6 and 10^1 respectively, by discharging this input to both stages of the VI platform using custom clamps.
- has good disturbance rejection due to an achieved high axial stiffness train of $3.7 \bullet 10^7$ N/m. This also results in a dynamic response ratio of 95% w.r.t. a unity spectral force input (avg linear POS module § 3.4.4.2).
- carries the modules through custom designed RVS struts with an achieved axial/radial stiffness ratio of 693. This protects the six delicate piezo sensors and allows them to mounted in pairs under 45 degrees in a hexagon configuration.
- is based on design choices which have been substantiated by modeling the effects of measured environmental disturbances on various configurations. The DEB model predicting this theoretical performance estimate has been validated using separate acceleration measurements performed on Vibronix.

This results in an overall performance where:

- verification measurements on the final design from 10 – 300 Hz show a noise floor characteristic that is in accordance with the (theoretically) predicted effect of all disturbances combined (≈ $2.5e^{-11}$ N^2/Hz). Performed flow measurements also indicate that the obtained results are reliable given a much higher average input signal (varying per module) than the background noise present. Specifically, the signal-to-noise ratio (**SNR**) ranges from **10^1** (POS) and **10^4** (ABC) to **10^5** (BSW).

- this background force noise level corresponds to a wafer error of 0.10 nm (XY – POS) when transformed back through Matrix system dynamics (MOF compliance, WPS controller sensitivity) which is a factor 1.7 lower than its FRS (0.17 nm).

Based on these results, it is concluded that the goal of the study has been met.

The main findings of this study are that:

- redistribution of Mapper's stage stability error budgets based on flow rate, pressure, heat dissipation and channel dimensions resulted in more realistic force-requirements for Forcesix both in magnitude and spectral distribution.
- a hydrostatic pressure vessel proved most effective to supply flow to Forcesix under constant pressure, flow rate and without introducing unwanted input (FIPs triggering Helmholtz resonances). When compared to a centrifugal pump, this results in an acceleration response of an identical geometry that is a factor 4.3 lower in overall magnitude. Moreover, static pressure prevents asynchronous motor characteristics to show up as distinct resonances in the measured response.
- when aiming to measure low-level reaction forces in the presence of dominant disturbances that transmit through parasitic stiffnesses, quartz piezoelectric sensors proof to be a better solution when compared to (seismic) accelerometers.
- particularly flow vibrations induced in supply tubing can have a significant impact on the measured signal, if the stiffness train that connects the sensor with the measurement setup, is relatively low. An effective method to minimize this disturbance is to discharge the bulk of the input to different stages of the vibration isolation platform, if present.
- of all disturbances, environmental acoustics have shown to be most difficult to shield. The most effective means of reducing its effect is to fully enclose the sensitive part of the measurement setup and to rigidly connect this casing to a heavy mass with an attractive transfer path to the sensor e.g. the bottom stage of a two MSD VI platform.
- when measuring direct forces using sensitive piezoelectric sensors than cannot withstand transverse loading / bending moments, stiff-flexible support struts with a high axial/transverse stiffness ratio (roughly ≥ 500) are found to be a solution.

Conclusion of the Study

MAPPER lithography

.. continued ..

With regards to the underlying Research Question (RQ) relevant for Mapper and driving the project:

"Are the cooling forces, induced in the modules and exerted onto the MOF, resulting in exceedances of the stage-stability error budgets?"

The flow measurements performed on the POS, ABC and BSW module at their nominal flow rates and pressures have not been fully processed. Yet the preliminary verification results indicate that there is already a significant difference in **SNR** between *'no flow'* and *'flow at a relatively low rate'* (order: **10^4** ABC). Given the 0.10 nm wafer error that corresponds with the *'no flow'* level (Courtesy of Mapper), and the FRS of 0.11 nm (XY – ABC), it can be said with great certainty that the resulting wafer errors will likely exceed stage stability budgets.

If this is indeed the case, it would not come as a surprise as the nature of water cooling is that efficiency increases with turbulence, which strongly correlates with FIV source amplitude (§ 3.3.3). **The main problem that lies at the root of this wafer error is therefore the significant amount of heat generated (≈ 2.5 KW) in an environment that aims for stability at the sub-nanometer level. A redesign from first principles on the creation of beamlets would be a more fundamental solution for Matrix to generate less heat in the first place.**

Concluding, although the application for which Forcesix has been developed is highly specific, this research also contributes to scientific knowledge of experimental characterization of FIV in a broader sense. To the best of authors' knowledge, this is namely the first study that measures the 6-DOF reaction forces of complex geometries due to FIV, at a very low-noise level (≈ 10^{-11} N^2/Hz). Moreover, the design process detailed in this thesis describes a method on how to effectively design such a measurement system, while in the presence of a variety of disturbances. Generic design guidelines that can serve as a reference have been established and are listed in Appendix B-3.

CH. 5.2

Recommendations

Future Research Recommendations

MAPPER lithography

How can Forcesix be improved? Are there other options for Mapper to explore?

Forcesix

- further characterization of Forcesix is recommended. For instance: up to which frequency are the measurement results coherent? Does the setup reliably behave like the mass-spring-damper system as which it was modeled? In particular, precise determination of the ‘unity force spectrum’ (§ 3.4.4.2) by quantifying damping of the piezo-strut combination would be valuable. This regards its linear regime, percentage offset and the frequency at which build-up starts. This information can be used to more accurately correct the measurement data afterwards. *After project completion Mapper has already performed this additional verification step with an imbalanced microdrive that exerts a calibrated force (§ 4.2.5)*
- correct measurement data for the (ideally verified) unity input spectrum detailed in § 3.4.4.2 (post-processing).
- add more mass (preferably ‘thick mass’ e.g. sheets of bitumen or other high-density insulative material) on the outside of the acoustical case further improve its low-frequency performance in terms of acoustical attenuation.
- Investigate the steep reduction in damping at 47 and 50 Hz that can be seen in the graph displaying the measured sound pressure inside the constructed acoustical shielding. This is suspected to be due to a mechanical resonance and not electronical interference. More specifically, the inside- and outside plating of the enclosure might be coupled together through the Akotherm insulation that is used to dampen sound waves. This would cause them to oscillate in phase on their first bending mode. If this is indeed the case, it can be stopped by mounting stiff diagonal connectors against the inside plating.
- Investigate the resonances seen at 16 Hz in the verification (flow) measurements. As three (out of six) sensors suffer from this, it is expected to be mechanical of nature. Electronic noise e.g. by the used SUSA sensor electronics is unlikely to occur selectively and would come back in all signals. It is interesting that the measured floor accelerations [XYZ] in the Labspace show a high distinct peak at exactly 16 Hz, while the 1-MSD stone accelerations [XYZ] measured simultaneously display little response. This indicates that the vibration isolation platform worked well before. It could be possible that this 16 Hz behavior is caused by deflation of one (of the four) airmounts, exposing some sensors more to floor vibrations than others.
- BSW measurements show clipping of the acceleration levels (time domain). This indicates that the exerted forces are on the level of the maximum allowed signal. Possibly this can be improved by increasing the voltage limit of the DAQ.

Future Research Recommendations

How can Forcesix be improved? **Are there other options for Mapper to explore?**

Matrix (Mapper Machine)

- using Forcesix, perform 6-DOF measurements on the POS, BSW and ABC module and do a structural re-design of the cooling geometries, to shift the bulk of the input to a frequency range where the controller (WPS) has more influence. In other words, if the overall magnitude of the occurring FIV in modules cannot be reduced, try to move it to a region where the effect on wafer error (XYZ) is less. Especially the critical length of tubing and bellows requires attention.
- the main problem for Mapper that lies at the root of the cooling water induced wafer error is the significant amount of heat generated (≈ 2.5 KW) in an environment that aims for stability at the sub-nanometer level. A redesign from first principles on the creation of beamlets would be a more fundamental solution to generate less heat in the first place.
- if lower flow rates (less heat production) is not an option, investigate the use of different coolants. For example, visco-elastic fluids are a polymer-solvent blend that possess non-Newtonian characteristics as they are made by combining viscous- and elastic components. This might reduce turbulence of the fluid flow whilst maintaining cooling capacity.
- perform a thorough transfer path analysis to verify if the cooling forces are indeed transmitted as modeled by the weighting function (MOF compliance + WPS sensitivity). In particular determining how this idealized TF looks in practice could be valuable as it is unlikely to be as 'clean' as simulated.
- applying feedforward using accelerometer data from sensors mounted on the MOF could improve performance of the wafer stage. In addition, laser interferometers or capacitive sensors looking at the MOF could be used to obtain more information about its motion (not so much to improve resolution). This as accelerometers are not able to distinguish static components i.e. if the MOF is moving at constant velocity this is not observable.
- reducing relative motion by actively controlling the entire MOF with piezo actuators could be considered to stabilize this 'massive pendulum'. Note that this should be done relative to a fixed ground and not on the interface of the modules as the impulse would be transmitted regardless since MOF is passively suspended. To prevent mechanical shortcut, an actuator with a very low stiffness should be considered (essentially a parallel stage). If all the above is not sufficient to bring the wafer error down to acceptable levels: increase the budget for cooling vibrations and focus on improving other aspects of Matrix.

Appendix

Details & Literature

App. A

Literature Review

A-1: Analysis of the TNO study on the Aperture Array

Flow-Induced Pulsations (FIPs) – Helmholtz Resonances – Source & Response analysis

Commissioned by Mapper, TNO has investigated the design and manufacturability of the most relevant cooling geometry, the Aperture Array (AA). Their results and recommendations have been detailed in two reports totaling 200 pages (Lemmen et al., 2009), (van Osch and Smeulers,

I.P.

frequency where the WPS cannot correct well for it. Helmholtz resonance is the phenomenon where a medium (fluid in this case) acts as a spring with a certain stiffness, related to its density and the wall stiffness of the casing / tubing. When part of this medium is moving (flow of the fluid), its inertia causes it to act like a mass who's movement is only dampened out by viscous/elastic forces. Together, they form the equivalent of a mass spring-damper system which can be excited as an acoustical resonance. An example of a Helmholtz resonance is the high pitch sound that can be heard when blowing over the top of a beer bottle.

I.P.

A.1.2 Limitations and Simplifications

It is important to note that, in their analysis, TNO focused solely on resulting pressure forces and did not account for fluid-structure interaction. This is the case when FIV excite structural resonances which can then have an effect on the fluid dynamics. Incorporating structural dynamics through mechanical vibration analysis would be essential however to get the full picture. It is therefore stated in their report that *"these calculations are not exact and only provide a ROM estimate"*. As a next step, TNO took these simulated FIV levels and calculated what effect they would have on wafer error. To this end they used the assumed force spectrum shown below (fig. A.2), together with a visual of the Aperture Array.

I.P.

this study that should be thoroughly investigated to properly establish technical requirements.

Research detailed in chapter 2 of this thesis let to the conclusion that force requirements had to be set a factor $\pm 1 \cdot 10^5 - 1 \cdot 10^9$ lower than initially assumed by TNO (fig. A.2)

Other simplifications used in the analyses:

- boundaries are assumed to be reflection-free
- tubing walls are assumed to be infinite-stiff, allowing for ∞ wave propagation speed
- inlet- and outlet piping walls are assumed to be infinite-stiff while these transition areas could be cause of the biggest pressure forces due to geometrical restrictions (connectors)
- assumed low temperature increment of coolant which is unlikely given steep pressure drops

A.1.3 Conclusions

Altogether it can be concluded that the performed analyses give an estimate of the FIV, but should certainly not be considered definitive outcomes. The high turbulence, complex cooling geometries and significant supply tubing w/connectors make it very difficult to come up with more than a ROM indication. Moreover, discrepancies have been observed between

I.P.

to increase significantly with increased channel diameter. *Therefore, a logical next step to accurately determine the induced flow vibrations is to perform experimental tests with realistic connections and sufficient tubing length.*

I.P.

A.1.4 Gained Insights

Despite its limitations, the TNO report does contain valuable insights that help to develop a profound insight into the emergence of FIV. Key contributing factors specifically related to the FIV problem discussed in this thesis have been extracted and will be listed below:

- **flow velocity** (relates to power and spectral distribution)
- **cooling element geometry** (bends / turns / nozzles / connectors)
- **pressure fluctuations** due to transitions (channel splitting/joining & diametrical changes)
- **fluid-structure interaction** (structural resonances interacting with fluid dynamics)
- **wall friction** (surface roughness / aberrations)

In addition, several observations related to these key factors could be extracted. They are useful to consider in the design of the experimental setup detailed in this thesis. These observations will be summarized now:

- FIV source strength increases *quadratically* with increasing flow speed
- the center frequency of FIV input increases *linearly* with flow speed

- dead end branches, abrupt transitions and cross-sectional changes of the flow supply can cause Flow-Induced Pulsations (FIP) and must therefore be avoided
- motions due to forces inside the flexible hose may be reduced by supporting it or connecting the hose to a rigid frame by means of clamps. This is important as the diffusor inside the AA proved of lesser significance, with the supply tubing w/connectors doing most harm
- exact determination of acoustical resonances is paramount as slight variations in frequency can have a significant effect on resulting (computed) wafer error. Theoretically this cannot be predicted good enough, e.g. the calculated vs modeled Helmholtz were already 5% apart

A-2: Dynamic Error Budgeting (DEB)

MAPPER lithography

Explaining the amplitude & power functions often used with DEB

ASD – PSD – CPS – CAS

This schematic has been composed using information from different literature sources, i.a. Vasilescu (2006), Fish (1993), Schmidt (2011). It present the four most relevant functions that are important to understand when working with a Dynamic Error Budgeting model. Besides understanding the math, units and transformation of one function into another, knowing which one to use when and what their limitations are is essential. For example, it is a common mistake among mechatronic designers to evaluate system performance by looking at ASD. Similarly the CAS value is sometimes observed to determine the largest power contribution to the resulting error. Both approaches are wrong as explained in the comments below the functions.

PSD [SI^2 / Hz]

Power Spectral Density

Average power of a signal (random or periodic) as a function of frequency.

In theory, a PSD is computed from -f to f. When dealing with a single-sided function division should be by /T instead of /2T.

$\int$

CPS [SI^2]

Cumulative Power Spectrum

Most useful to determine the largest power contribution in a system and to compare performance against specifications.

For example, to determine the largest contribution to the total error, one should observe the CPS and not the CAS. This as taking the square root, visually enlarges the impact of low-frequency disturbances relative to the impact of disturbances at higher frequencies.

√

√

ASD [SI / √ Hz]

Amplitude Spectral Density

Often used by suppliers to indicate noise performance.

ASD cannot mathematically be transformed into CAS directly. Analytically, one can take out the square root and re-write the expression, which is the same as going from PSD > CPS > CAS

CAS [SI]

Cumulative Amplitude Spectrum

Not necessarily an amplitude! The CAS value is the standard deviation σ. Since Xrms = Xmean + σ, the CAS value can equals the RMS value (effective value), but only in case of a zero mean.

The CAS value is used to determine the final performance value of a design (often: resulting error) for instance due to disturbance PSDs that propagate through the system.

Important to remember is that, despite the build-up of a CAS graph, higher frequencies contribute significantly more to the total error as it costs much more energy to move something faster, even with a smaller amplitude.

A-3: Calculating (random) Crosstalk

MAPPER lithography

Detailed overview of formulae

Schematic constructed based on different literature sources

As discussed in [§ 3.2.3](), the below overview details the formulae that can be used to make an approximate calculation of the spectral Johnson-, Shot- and Excess noise levels present in the design.

White Noise → Johnson Noise, Shot Noise

Pink Noise → Excess Noise, Avalanche Noise, Burst Noise

Johnson Noise

Johnson Noise is the thermally induced random motion of charge carriers (e.g. electrons) that cause a fluctuating potential. Every dissipative element (e.g. resistors) suffers from this noise source which is also called 'thermal noise'. It is independent of current flow and can be modeled either as a voltage or as a current.

When modeled as a voltage, the thermal noise source is placed in series with an otherwise noiseless resistor:

PSD: $N_t = 4kTR$ [V²/Hz]

CAS: $V_{rms} = \sqrt{(4kTR*B)}$ [V]

When modeled as a current, the thermal noise source is placed in parallel with an otherwise noiseless resistor:

PSD: $N_t = 4kT/R$ [A²/Hz]

CAS: $I_{rms} = \sqrt{(4kTB/R)}$ [A]

k = 1.38 x 10^{-23} [J/°K] - Bolzmann's constant
R = Resistance in the device [Ω]
T = Absolute temperature of the device [°K]
B = Bandwidth (BW) over which voltage is measured

Shot Noise

Shot Noise is the noise due to random passage of individual charges across a potential barrier (e.g. a transistor junction). This effect becomes especially troublesome for very small currents due to the discretization of the flowing charges.

When measuring voltages, shot noise levels are calculated as follows:

PSD: $\varphi_{sv}(f) = 2I_n qR^2$ [V²/Hz]

CAS: $V_{rms} = \sqrt{(2I_n qR^2*B)}$ [V]

When measuring currents, shot noise levels are calculated as follows:

PSD: $\varphi_{si}(f) = 2I_n q$ [A²/Hz]

CAS: $I_{rms} = \sqrt{(2I_n q*B)}$ [A]

q = 1.59 x 10^{-19} [C] - Electron charge
R = Resistance in the device [Ω]
I_n = Nominal current flowing in the device [A]
B = BW over which voltage / current is measured

Excess Noise

Excess Noise, also called flicker noise or 1/f noise, indicating its decreasing spectral power at increasing frequency. This is the noise 'in excess' of Johnson and Shot Noise. It is caused by the non-constant conductivity of materials due to imperfect contacts. Excess noise is always associated with a DC current in the device and it is dominated by thermal noise if the current flow is low. Because of its 'pink nature', this noise source is especially troublesome at low frequencies.

It can be modeled as a voltage:

PSD: $N_e = Ke^2/f$ [V²/Hz]

CAS: $V\_rms = \sqrt{\int_0^{BW}(Ke^2/f^{\alpha})df}$ [V]

Or calculated as a current:

PSD: $N_e = Ki^2/f$ [A²/Hz]

CAS: $V\_rms = \sqrt{\int_0^{BW}(Ki^2/f^{\alpha})df}$ [A]

K = Process constant (application dependent)
α = 1/f characteristic (assumed 1)
f = frequency band under consideration

Avalanche Noise

Burst Noise, also called popcorn-noise, is the popping sound that is sometimes heard when a bad speaker plays low frequency sound (< 100 Hz). It is likely related to imperfections in semiconducor materials which lead to stepped transitions between voltage levels.

Not present in this design.

Burst Noise

Avalanche Noise is the noise produced in a junction diode when high voltages (strong electric fields) lead to discharging of energy.

Not present in this design.

[Measurement in Engineering (WB2303-10) – lectures 8 & 9 (M. van Spengen)]() - [https://web.mit.edu/dvp/Public/noise-paper.pdf]() - [http://home.physics.leidenuniv.nl/~exter/SVR/noise.pdf]()

A-4: Performance Analysis Vibronix

MAPPER lithography

A-4.1: Overview

Vibronix measures in 1-DOF – the new design must be able to observe all 6-DOFs

The Vibronix test setup as introduced in Chapter 1 (see Fig. 1.6) is the result of the previous work by Dennis Lakerveld. An overview of this practical tool to perform flow-tests is shown in the picture on the right. The hydrostatic pressure vessel (on the right) does not belong to Vibronix; it is the result of an investigation into the best means of flow supply performed for this thesis.

This test setup is able to perform measurements in 1-DOF on a specific sub-module (Aperture Array) from 20 – 90 Hz at an overall noise floor of ≈ $4 \cdot 10^{-7}$ (m/s^2) / √Hz.

This acceleration ASD value scales with mass and is not able to individually validate modules from the Mapper machine (Matrix), which is the goal of this study *(Appendix A-4, draws a performance comparison between Vibronix and the new design developed in this thesis.*

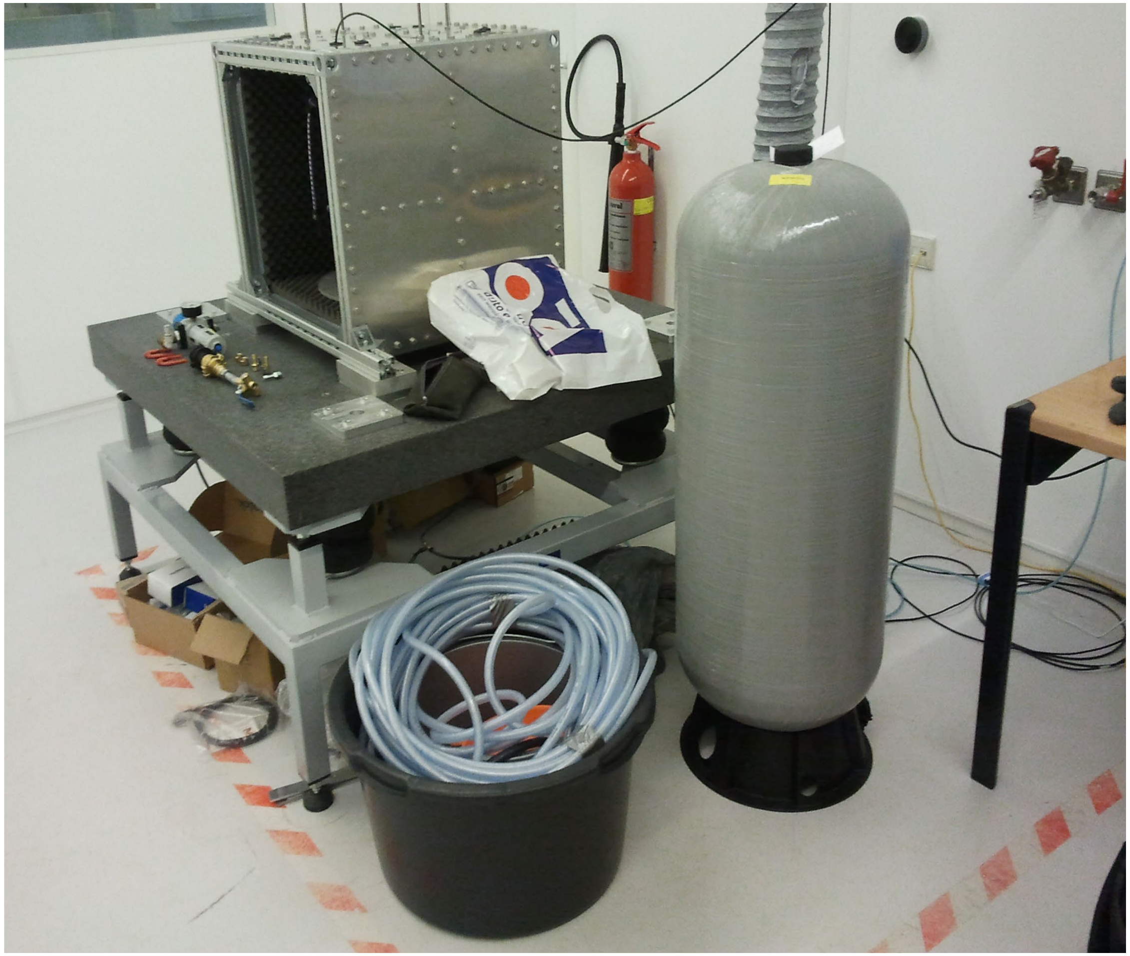

A-4: Performance Analysis Vibronix

A-4.2: Measurement range & resolution

The bottom left figure is taken from the Master Thesis of Lakerveld (2013) to compare with Forcesix (§ 3.4.4)

The bottom left figure shows that Vibronix has a PSD noise bottom of about $2 \cdot 10^{-13}$ $(m/s^2)^2$ / Hz which translates to a force noise floor of around 10^{-11} N^2 / Hz from 20 – 90 Hz as a 7.5 kg mass is installed (AA). However, major resonances can be seen from 40 – 50 Hz, at 65 and 80 Hz peaking up to about $10^{-6} – 10^{-7}$ N^2 / Hz and compromising measurement accuracy. **Compared to the performance of the new design (Forcesix, right figure), it can be seen that significant improvements have been made:**

The overall noise floor of Forcesix is at a level of ≈ 2,5e^{-11} N^2/Hz and independent of mass (measuring reaction-forces instead of accelerations). Also the effective bandwidth has been increased to 10 – 300 Hz for BSW. Especially since none of the major disturbances present in the 90 – 300 Hz range are able to come through, this is a good result. Since Vibronix only measures up to 90 Hz, these disturbances are not visible in the left plot but an example is environmental acoustics (see § 3.4.4.4).

Performance of Vibronix (result of thesis Dennis Lakerveld):

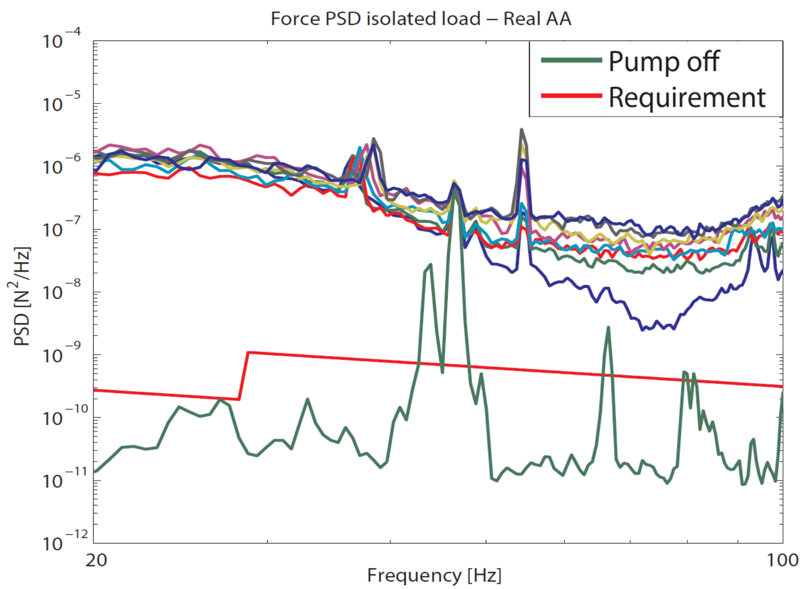

Theoretical performance of Forcesix (result of this thesis):

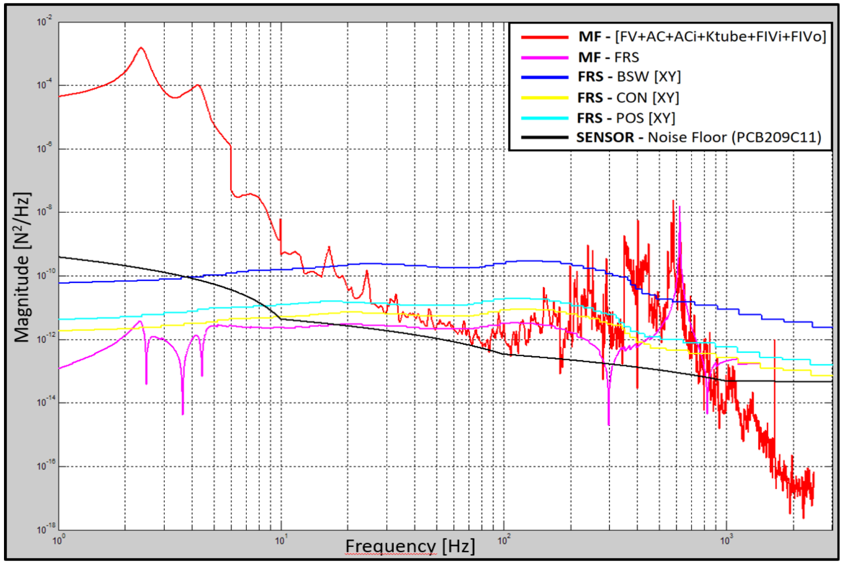

A-4: Performance Analysis Vibronix

MAPPER lithography

A-4.3: Dissecting a typical response

Analysis of the most relevant hydrostatic test result (performed on the Aperture Array)

Eigenfrequency pendulum (1 Hz)
>> also present without geometry / water flow

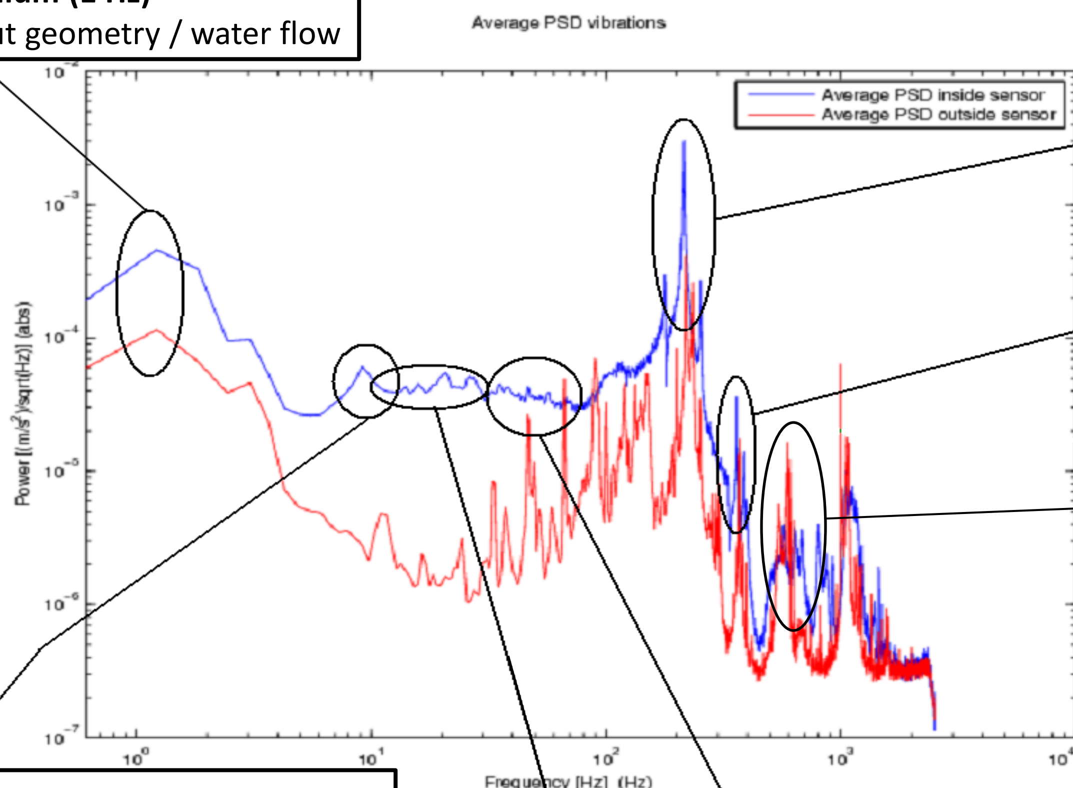

Endevco sensor resonance

Plate fundamentals?

Spurious mode decoupling?

Eigenfrequency airmounts (10 Hz)
>> also present without geometry / water flow

45 Hz removed (hydrostatically)
>> asynchronous motor characteristics of centrifugal pump

FIV input (AA geometry)

A-5: Practical Analysis of Vibronix

A-5.1: Design weaknesses – **mechanical**

Identified weak spots in the Vibronix design

- axial stiffness of elastics is not constant / hysteresis
- eigenfrequencies of tubing can be seen in measurement results
- limited compliance of tubing in measurements direction i.e. parasitic forces due to tubing stiffness present in results
- significant cross-coupling between DOFs due to in plane stiffness of elastics (i.e. currently not really measuring 1-DOF)
- heavy sensor is placed off-center, causing a shift in the COM, which affects the dynamics of the pendulum structure
- acoustic attenuation by casing is limited and only reduces sound pressure waves in some low frequency bands

A-5: Practical Analysis of Vibronix

A-5.2: Design weaknesses – **electronical**

Identified weak spots in the Vibronix design

- **Cables.** The used cables are not shielded and prone to electromagnetic pick-up. It is important for measurements to be performed at a suitable location away from lab equipment or TL bulbs which are notorious for EM interference (50 Hz). Specifically, pigtail connections (picture left below) should be avoided as they are sensitive to (high-freq) capacitive pick-up. In general, low-noise cables with an isolated outer shell and limited length should be selected.
- **DAQ card.** The DAQ card is currently not equipotential, thus susceptible to ground-loops. Circumvent by design.
- **Sensor.** The accelerometers require a 4 min warm up time to reduce their impedance. It should therefore be part of the measurement protocol that a constant current of 4 mA is supplied prior to any measurement sequence performed in batch. This was not done for Vibronix. Since measurements were pre-programmed, performed in batch and then averaged out, erroneous input will be part-of the measured accelerations and can no longer be observed individually [3]
- **Sensor range.** Datasheet for the Endevco sensor specifies its first resonance at 370 Hz, making it a good pick theoretically, as it also has excellent low frequency characteristics ($\approx 10^{-14}$). However, in practice, this peak is seen at 220 Hz, and build-up already starts at 90 Hz, thereby disturbing the measurement. To be able to measure accurately from 10 – 300 Hz, a different sensor needs to be selected.
- **Sensor connection force.** Too much momentum has been applied to mount the BruelKlaer accelerometers. This can cause pre-tension of the reference-mass which shifts the dynamical response and compromises accuracy.

A-5: Practical Analysis of Vibronix

A-5.3: Design weaknesses – **flow / tubing**

Identified weak spots in the Vibronix design

- Limited compliancy of tubing in measurements direction
- Test objects are linked to tubing through sharp edged connectors with varying diameters causing separation (vortices)
- The used regular -centrifugal- pump causes additional flow vibrations which result in significant accelerations
- Tubing has too much length inside Vibronix, introduces much unnecessary FIV input
- High radial stiffness of tubing shifts the Helmholtz resonances to higher frequencies (unwanted)
- Small acoustic chamber requires small bending angle of tubing (acoustic source)

A-5: Practical Analysis of Vibronix

MAPPER lithography

A-5.4: Lessons learned – **Main insights from tests on- and analysis of Vibronix**

Structural limitations for scaling up to 6-DOF and verifying Matrix modules

- measured accelerations due to stiffness of pressurized tubing too high in all directions
- cannot accommodate bigger / heavier modules (the sensor PSD noise level scales with mass squared)
- measurement range is limited to 20 – 90 Hz due to sensor (Endevco). Required: 10 – 300 Hz.
- transmitted disturbance levels are a factor 40 – 40.000 too high for requirement verification (peak disturbance with 12.5 kg suspended mass at 10^{-5} – 10^{-6} N^2/Hz). This is only from 20 – 90 Hz, from 90 – 300 Hz significant higher input can be expected.
- flow measurements over the 10 – 90 Hz range show significant input which, when filtered by Matrix's dynamics (earlier mentioned weighting function), results in about 10 nm wafer error (see picture below). This is in X-direction at nominal flow requirement (13.8 L/min). Whilst only observing one-third of the total specified frequency range (300 Hz), this already exceeds stage stability budget by a factor 5.
- vibronix measures only 1-DOF and using this pendulum suspension, is not possible to 'upgrade' to 6-DOF
- suitable for AA only, not easily upgradeable to heavier modules

Aspects to incorporate in the new design

- attenuating floor vibrations by means of a 1-2-3 MSD system has proven to be essential. The idea of using granite plates on airmount isolators has proven to be effective and practical. The various possible configurations will be considered, a dynamical analysis and mass optimization is something to incorporate in the new design, as well as means of support w.r.t. internal mode shapes.
- environmental acoustics are insufficiently attenuated, this can and must be improved in the new design. A redesign of the acoustical enclosure will be done as well as analysis how to best connect these
- prevent ground loops at sensors and DAQ by proper insulation

A-6: Detailed Analysis of Measurements performed on Vibronix

A-6.1: Investigating flow supply – **centrifugal pump**

Geometry under testing: **Aperture Array (AA)**

Detailed analysis of the measured response:

- This graph represents the measured accelerations due to water supplied by a normal -centrifugal- pump. It shows relatively high input in the 10 – 30 Hz range and distinct resonances occurring at 40, 50 and 55 Hz as indicated by the black circle.
- The 10 – 30 Hz disturbance is expected to be due to turbulence caused by the impellers that displace the water at a relatively high flow speed (13.8 $l min^{-1}$)
- The two striking resonances at 40 and 55 Hz that show up in both the plate sensor and tubing sensor are caused by the asynchronous motor characteristics of the centrifugal pump. This is clear since they are not present when using another flow supply method.
- The large 50 Hz resonance present in all signals is most likely caused by Helmholtz resonances induced in the long supply tubing and not the mains. Originally these were calculated by TNO to occur at 65 Hz (see App. A1) and it was predicted that doubling the tubing length would reduce it to about 45 Hz. Given the distant location of the pump, it is probable that this is indeed a Helmholtz resonance that also excites the VI system.

Average PSD vibrations

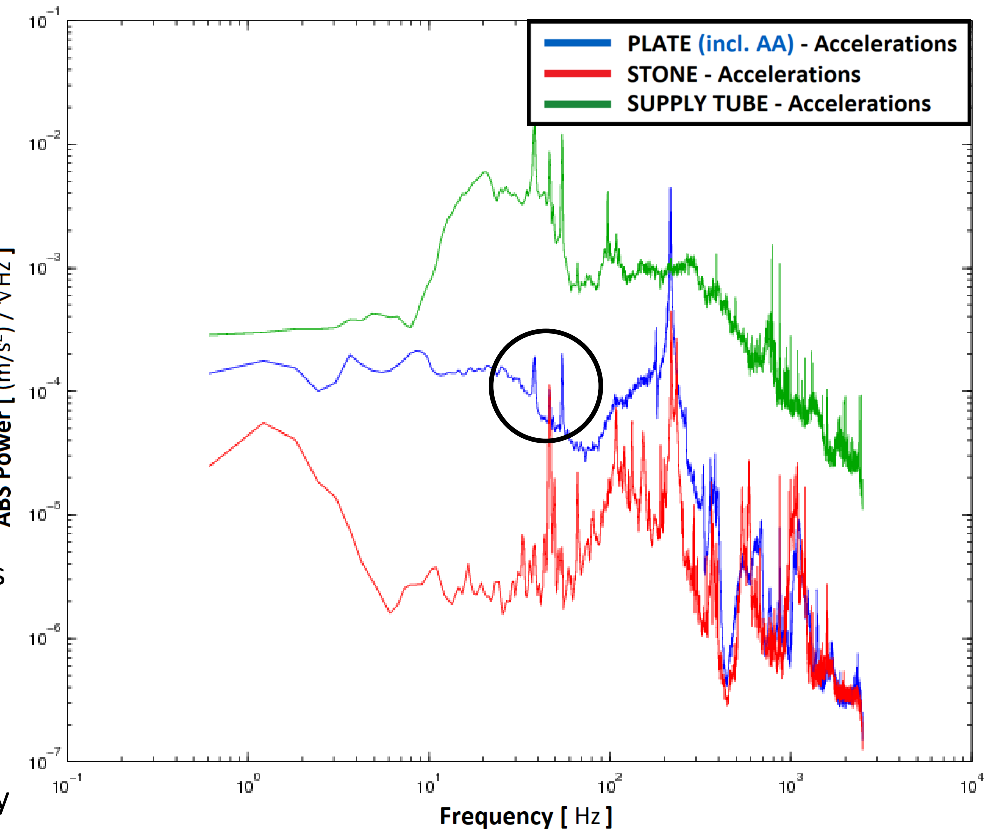

* measurements have been performed using an Endevco M86 piezoelectric accelerometer (BW: 90 Hz) that was mounted rigid to the pendulum *plate* and granite *stone*. For the tube: a light-weight BK4513 deltatron accelerometer has been used (BW: 1000 Hz)

A-6: Detailed Analysis of Measurements performed on Vibronix

A-6.1: Investigating flow supply – **Ultra-Pure Water** (UPW) **cooler pump**

Geometry under testing: **Aperture Array (AA)**

Detailed analysis of the measured response:

- In these measurements, flow is supplied to the AA by the UPW cooler. The results show a much lower average power distribution over the 10 – 90 Hz range which was to be expected.

- Distinct resonances in the (blue) graph are not present due to the well thought-out design of this low-noise, low-turbulence pump.

- In this graph the stone accelerations are a factor two higher than in the other measurements that took place under similar conditions. This can be explained by higher levels of floor vibrations as other lab equipment had started running during the second test (only). It is interesting to observe the correlation between these elevated stone accelerations and the resulting plate accelerations. Especially since the UPW cooler is the most low-noise pump possible, it suggests there is a strong coupling between this first VI stage of Vibronix and the pendulum. This should be improved and is something to account for in the new design.

Average PSD vibrations

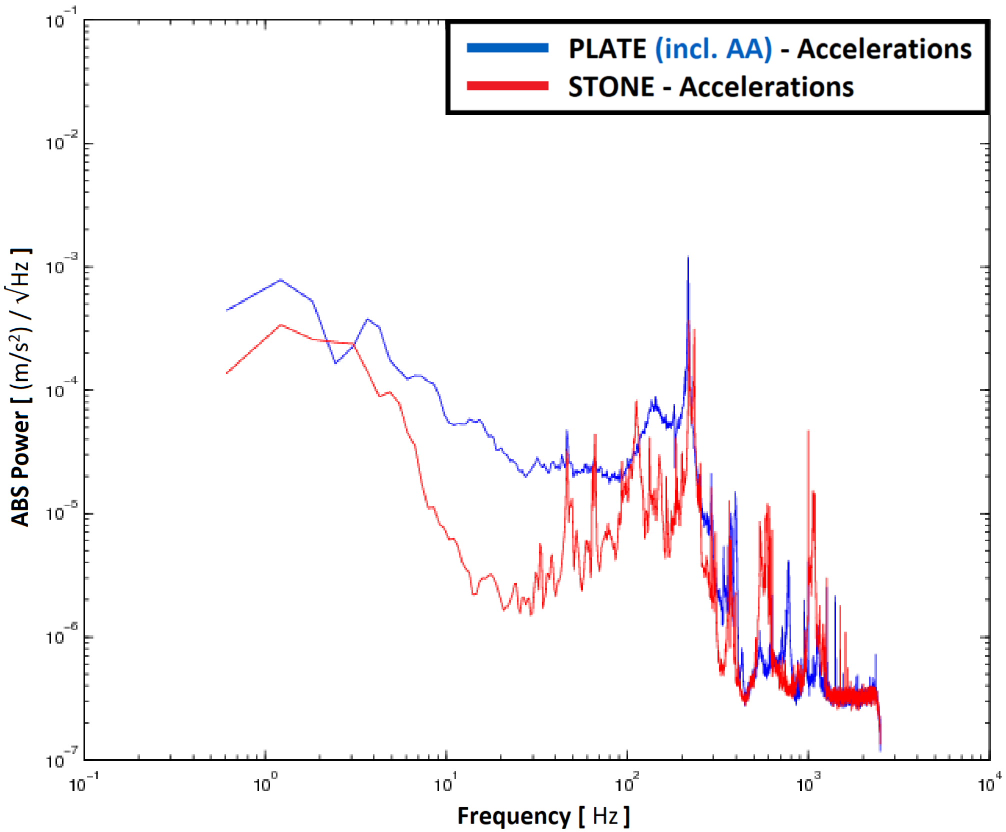

* measurements have been performed using an Endevco M86 piezoelectric accelerometer (BW: 90 Hz) that was mounted rigid to the pendulum *plate* and granite *stone*. For the tube: a light-weight BK4513 deltatron accelerometer has been used (BW: 1000 Hz)

A-6: Detailed Analysis of Measurements performed on Vibronix

A-6.1: Investigating flow supply – **hydrostatic pressure vessel**

Geometry under testing: **Aperture Array (AA)**

Detailed analysis of the measured response:

- The pressure vessel measurements show a relative calm spectrum compared to the normal pump's graph.
- No resonances are present and no clear correlation can be seen in the range of interest with regards to the red line ('stone acceleration'). This indicates that the system is uncoupled as floor vibrations do not impact flow measurements.
- Overall, the blue line is about a factor 1,5 higher when compared to the flat section of the 'UPW line'.
- Contrary to the normal pump and the UPW, the pressure vessel is not a closed-loop system, meaning that the water is discharged during a measurement, after which it needs refilling.
- A total of 10 meter of flexible tubing is used with the Aperture Array placed in between through the use of swagelok connectors that vary only slightly in diameter and a ball-valve sealing off the end.

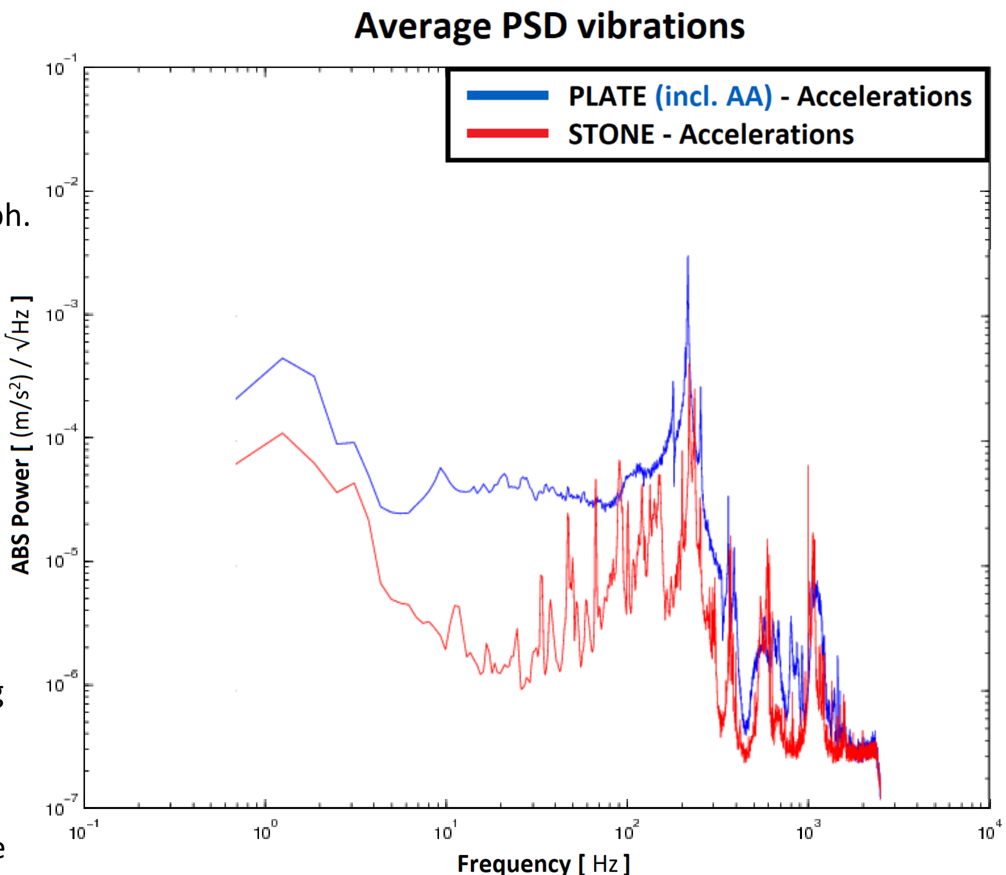

* measurements have been performed using an Endevco M86 piezoelectric accelerometer (BW: 90 Hz) that was mounted rigid to the pendulum *plate* and granite *stone*. For the tube: a light-weight BK4513 deltatron accelerometer has been used (BW: 1000 Hz)

A-6: Detailed Analysis of Measurements performed on Vibronix

A-6.2: Hydrostatic testing – **flexible tubing**

Water supplied by: **pressure vessel** (shown below)

Detailed analysis of the measured response:

- The response of the plate sensor shows input in the 10 – 30 Hz range but is overall low when compared to the other tested structures.
- The elevated bump (peaking at 20 Hz) could be caused by fluid-structure interactions in the tubing, where the transversal stiffness of the tubing interacts with the fluid flowing through it.

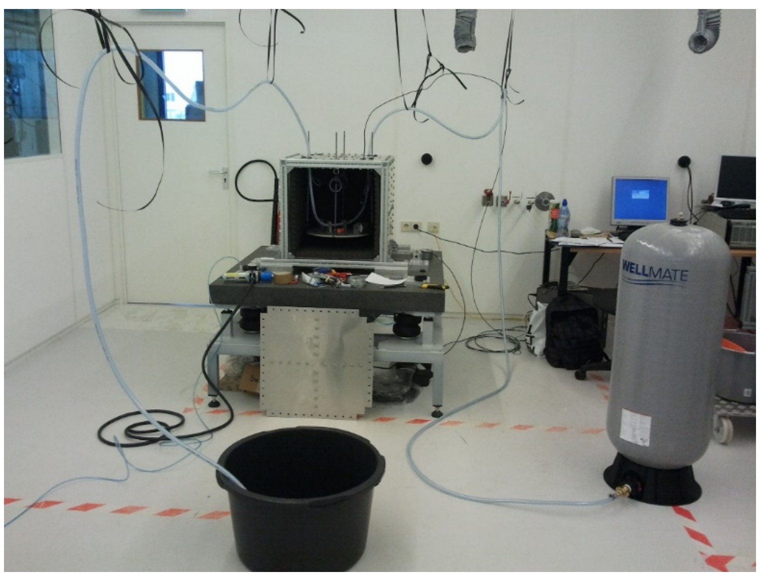

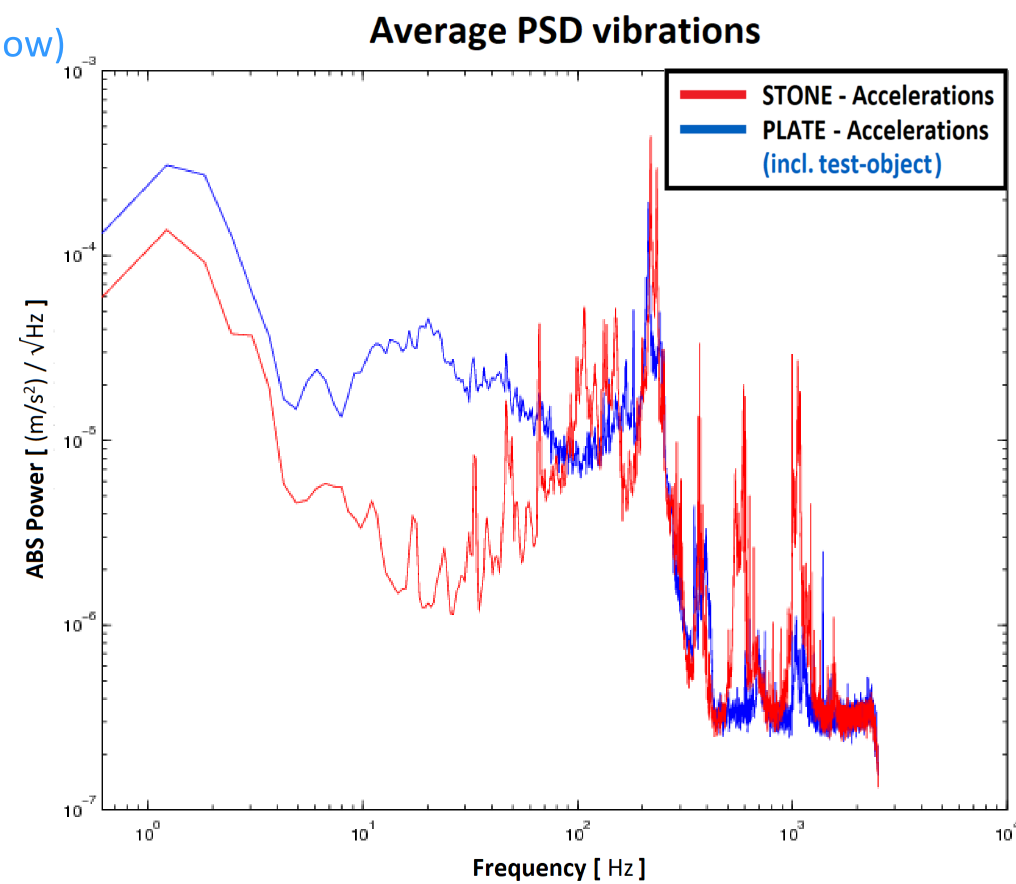

* measurements have been performed using an Endevco M86 piezoelectric accelerometer (BW: 90 Hz) that was mounted rigid to the pendulum *plate* and granite *stone*. For the tube: a light-weight BK4513 deltatron accelerometer has been used (BW: 1000 Hz)

A-6: Detailed Analysis of Measurements performed on Vibronix

A-6.2: Hydrostatic testing – **stainless-steel tubing**

Water supplied by: **pressure vessel**

Detailed analysis of the measured response:

- Overall the response of the plate sensor is elevated compared to accelerations generated by the flexible tubing
- The high frequency variation on the plate signal however is very calm with no resonance peaks standing out below the BW of the used sensor.
- Significant resonances *can* be observed in accelerations of the granite stone however (red line). This is caused by newly installed lab equipment which was running during the measurement and could not be switched off. Initially it was thought this could have compromised reliability of the measurement. Therefore, a reference measurement has been performed *without flow* in the evening when this machine was still running. It showed the same response for stone accerations, but much lower plate accelerations. This indicates that the second VI trap attenuates these floor vibrations well enough such that the blue line indeed shows the accelerations due to water flow in the stainless-steel tubing reliably.

Average PSD vibrations

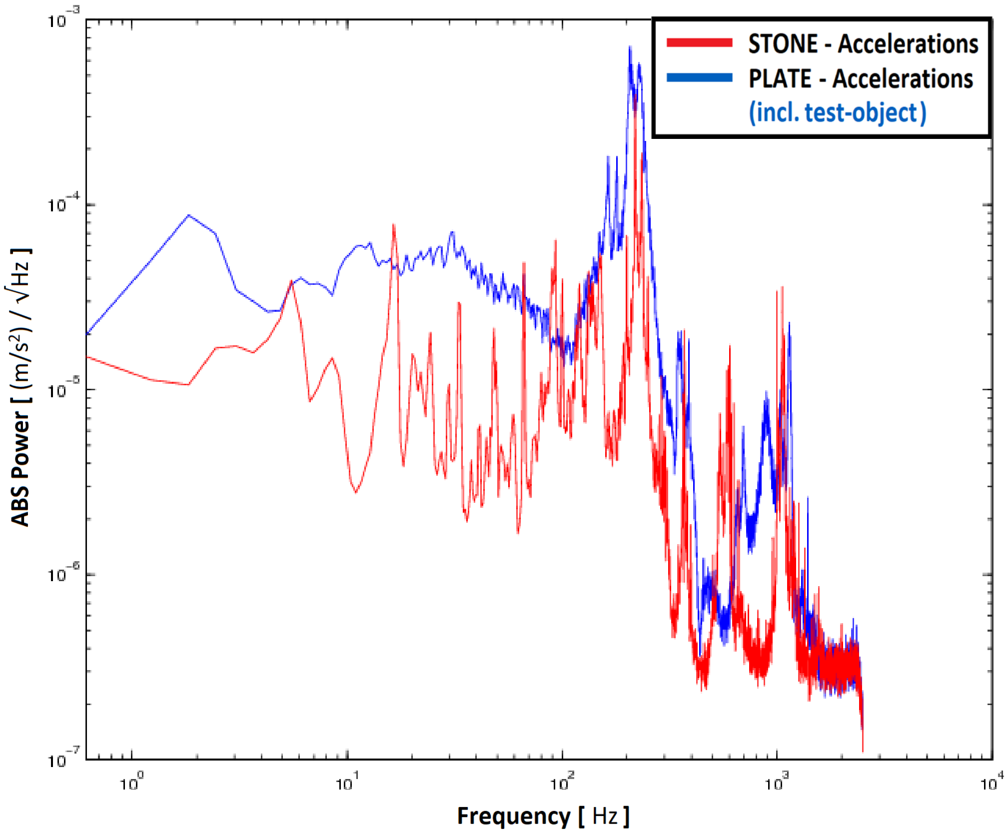

* measurements have been performed using an Endevco M86 piezoelectric accelerometer (BW: 90 Hz) that was mounted rigid to the pendulum *plate* and granite *stone*. For the tube: a light-weight BK4513 deltatron accelerometer has been used (BW: 1000 Hz)

A-6: Detailed Analysis of Measurements performed on Vibronix

A-6.2: Hydrostatic testing – **Aperture Array** (AA)

Water supplied by: **pressure vessel**

Detailed analysis of the measured response:

- The response of the plate sensor (blue line) shows an calm but elevated acceleration signal that is flat over the whole range up to the BW of the sensor
- Knowing that the Aperture Array in particular has been designed to generate as little as possible eddies due to separation, indicates that it is very difficult to prevent FIV when dealing with a complex structure.
- It is suspected that changes in the geometry of the small cooling channels are cause of high input over the whole measured range. Despite the fact that the cross-sectional area of these channels has been designed to remain constant, FIV due to turbulence is likely to occur when shapes change or bends force the fluid to change its direction.

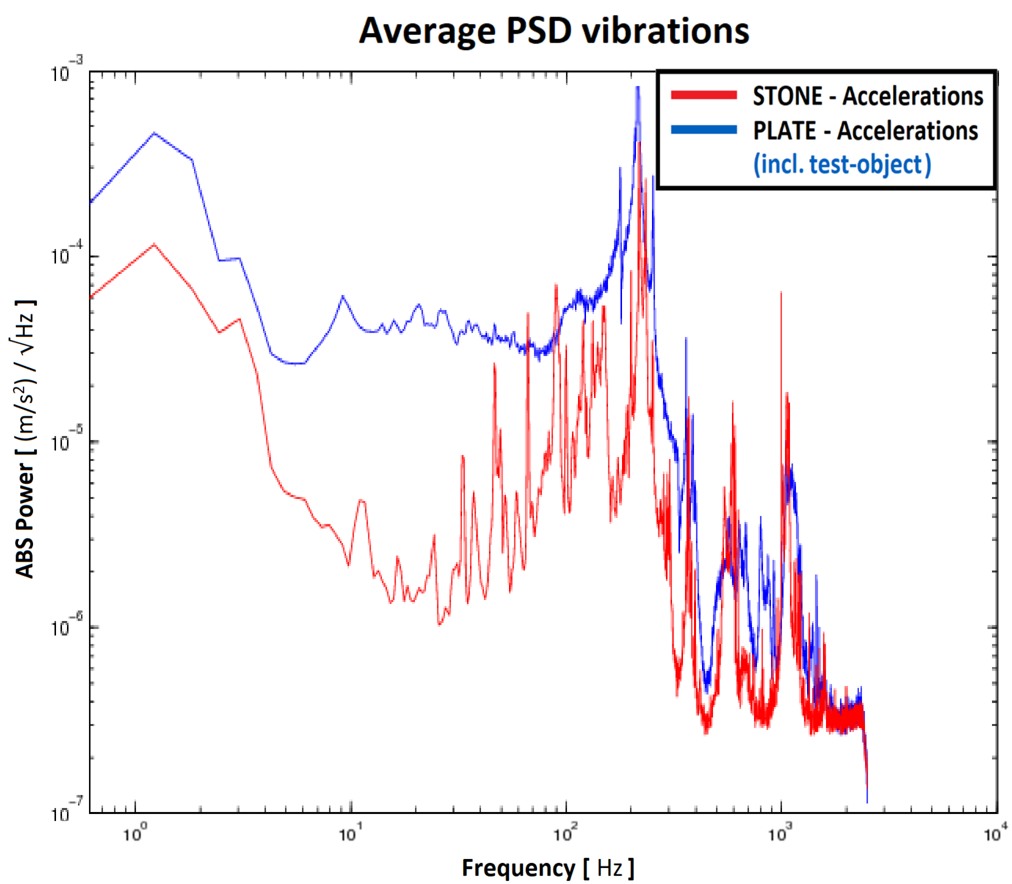

* measurements have been performed using an Endevco M86 piezoelectric accelerometer (BW: 90 Hz) that was mounted rigid to the pendulum *plate* and granite *stone*. For the tube: a light-weight BK4513 deltatron accelerometer has been used (BW: 1000 Hz)

App. B

Additional Results

B-1: Redistributing Error Budgets

MAPPER lithography

Compute scaling **source amplitude** & **center frequency** based on Matrix process parameters

Default base line (100 %) for calculations is the Aperture Array flow rate (13.8 L/min) as modeled by TNO

relation between acoustic **source amplitude** and **flow rate**

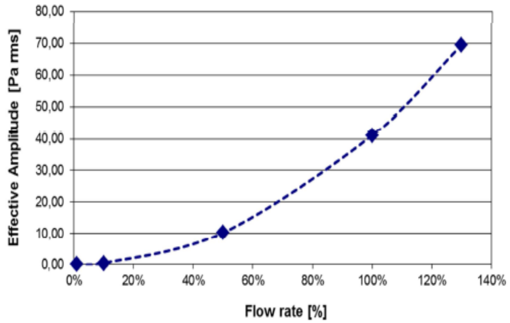

relation between **acoustic source center frequency** and **flow rate**

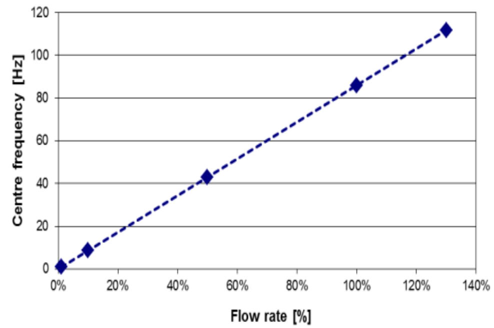

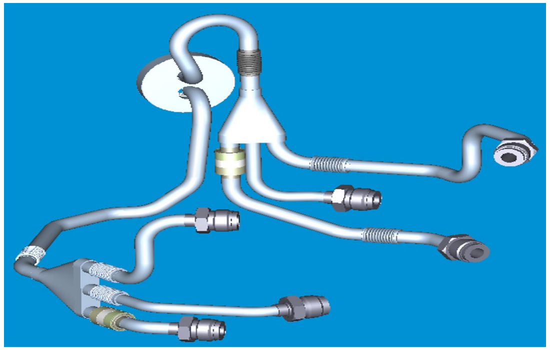

Cooling requirements new design [RD.04] Data from RD.08 or Design Files

sub-system	*module*	*sub-module*	*part*	*flow rate* [l/min]	*flow rate* [m^3/s]	*pressure* [bar]	*dissipated power* [W]	*% of total*	*∑ per module*
ILO	BG	AA						nvt	
ILO	BG	COL						15,30%	15,30%
PBB	BSW	CL+IBC (CLBC)						37,48%	54,53%
PBB	BSW	MAA / BLK						17,06%	
POS	PL		BS					2,08%	2,08%
CON		ABC						22,94%	22,94%
	Total flow rate UPW:								

Graphs from the TNO research report for Mapper: "Flow induced pulsation analysis inside cooling channels of Aperture Array"

B-1: Redistributing Error Budgets

MAPPER lithography

Compute scaling **source amplitude** & **center frequency** based on Matrix process parameters

Determined flow velocity through each channel, turbulence indication and % of effective amplitude

Tubing of Parts:

sub-system	module	sub-module	part	Width of a channel *if square* [m]	Height of a channel *if square* [m]	Hydraulic Diameter *if square channel* [m]	Diameter of a channel *if round* [m]	Crossectional Area of Channel [m^2]	# of channels for part [1]
								7,85E-05	= straight tube
ILO	BG	AA					2,50E-03	4,91E-06	8
ILO	BG	COL		1,69E-02	1,69E-02	1,69E-02		2,86E-04	1
PBB	BSW	CL+IBC (CLBC)		2,30E-03	9,00E-04	1,29E-03		2,07E-06	6
PBB	BSW	MAA + BLK		2,30E-03	9,00E-04	1,29E-03		2,07E-06	6
POS	PL		BS	1,00E-03	2,00E-04	3,33E-04		2,00E-07	6
CON		ABC					3,50E-03	9,62E-06	5

Total Length of all channels together [m]	Flow velocity through one/each channel [m/s]	Reynolds number [-]	Turbulence of flow	Sources
4,40E-01	5,85690	1,46E+04	TURBULENT	L_part from Water system for cooling Array presentation
6,91E-01	0,35013	5,89E+03	TURBULENT	Beam Generator Collimator Cooling Concept D=Dhydr=side (square) : 2*16.9*16.9/(2*16.9)=16.9
3,60E-01	6,97799	8,98E+03	TURBULENT	Titanium cooling array (clbc) Detailed design V01-02
6,00E-01	5,09930	6,56E+03	TURBULENT	Titanium cooling array (clbc) Detailed design V01-02
2,60E-01	4,58333	1,52E+03	LAMINAR	Feasibility study on beam stop cooling in the laminar flow regmine V01-01
4,51E-01	1,03938	3,62E+03	TURBULENT	RD.08

Rebudgeting:

sub-system	module	sub-module	part	Fraction TOTAL tubes length [%]		Fraction Flow Velocity of AA (100% in graph)[%]	Effective Amplitude	% of Eff. Amplitude
				2,3615E+00	(excl AA)	5,8569E+00	exp. graph above	
ILO	BG	AA		nvt		nvt		
ILO	BG	COL		29,26%		5,98%	1	0,73%
PBB	BSW	CL+IBC (CLBC)		15,24%		119,14%	75	54,55%
PBB	BSW	MAA + BLK		25,41%		87,06%	33	24,00%
POS	PL		BS	11,01%		78,26%	26,5	19,27%
CON		ABC		19,08%		17,75%	2	1,45%
			check	100,00%		sum:	137,5	check:

B-1: Redistributing Error Budgets

MAPPER lithography

Compute scaling **source amplitude** & **center frequency** based on Matrix process parameters

Resulting weighting factor of source amplitude and shift in center frequency per module

Relation Flow Rate [m^3/s] **- Flow Velocity** [m/s] *per module, geometry and number of channels taken into account, indicated per measured flow rates*

Legend	flow rate	flow velocity AA	flow vel COL	flow vel POS	flow vel ABC	flow vel BSW (1 & 2)
04 L min	4	1,70E+00	2,33E-01	5,56E+01	1,39E+00	5,37E+00
06 L min	5	2,12E+00	2,92E-01	6,94E+01	1,73E+00	6,71E+00
08 L min	6	2,55E+00	3,50E-01	8,33E+01	2,08E+00	8,05E+00
10 L min	8	3,40E+00	4,67E-01	1,11E+02	2,77E+00	1,07E+01
12 L min	10	4,24E+00	5,84E-01	1,39E+02	3,46E+00	1,34E+01
14 L min	12	5,09E+00	7,00E-01	1,67E+02	4,16E+00	1,61E+01
16 L min	14	5,94E+00	8,17E-01	1,94E+02	4,85E+00	1,88E+01
17 L min	16	6,79E+00	9,34E-01	2,22E+02	5,54E+00	2,15E+01
Pump off Requirement	17	7,22E+00	9,92E-01	2,36E+02	5,89E+00	2,28E+01

Weighting factor (= 0.5*tube_length+0.5*flow_velocity) *for amplitude of source*			**Predicted Shift from Center Frequency AA** *estimate for other modules based on perc of flow velocity* **linear graph above**	
			-	Hz
14,99%			-1,4	Hz
34,90%			-	Hz *(base line from prediction TNO study on AA)*
24,70%	59,60%	= ∑ BSW	-	Hz *(base line from prediction TNO study on AA)*
15,14%			16,75	Hz
10,27%			-6,03	Hz
100,00%				

Computation Shift Center Frequency *done in matlab*

- plot the theoretical prediction for AA - corrected for flow *velocity*
- take for each module the expected center frequency based on their corresponding flow velocity
- multiply with the difference between theoretical predicted shift and measured shift
- multiply for each module with the (radius_module_channel / radius_AA_channel) ratio, as the center frequency is expected to shift to the right (get higher) for smaller diameter channels that still have the same flow *velocity*. This as more higher frequent eddies can fit in (JvN) and also because TNO predicts that (linear shift with flow velocity)

B-2: Model Simulations (Concept A)

Alternative concept: acceleration-based – *computing crosstalk*

Noise levels different acceleration sensors

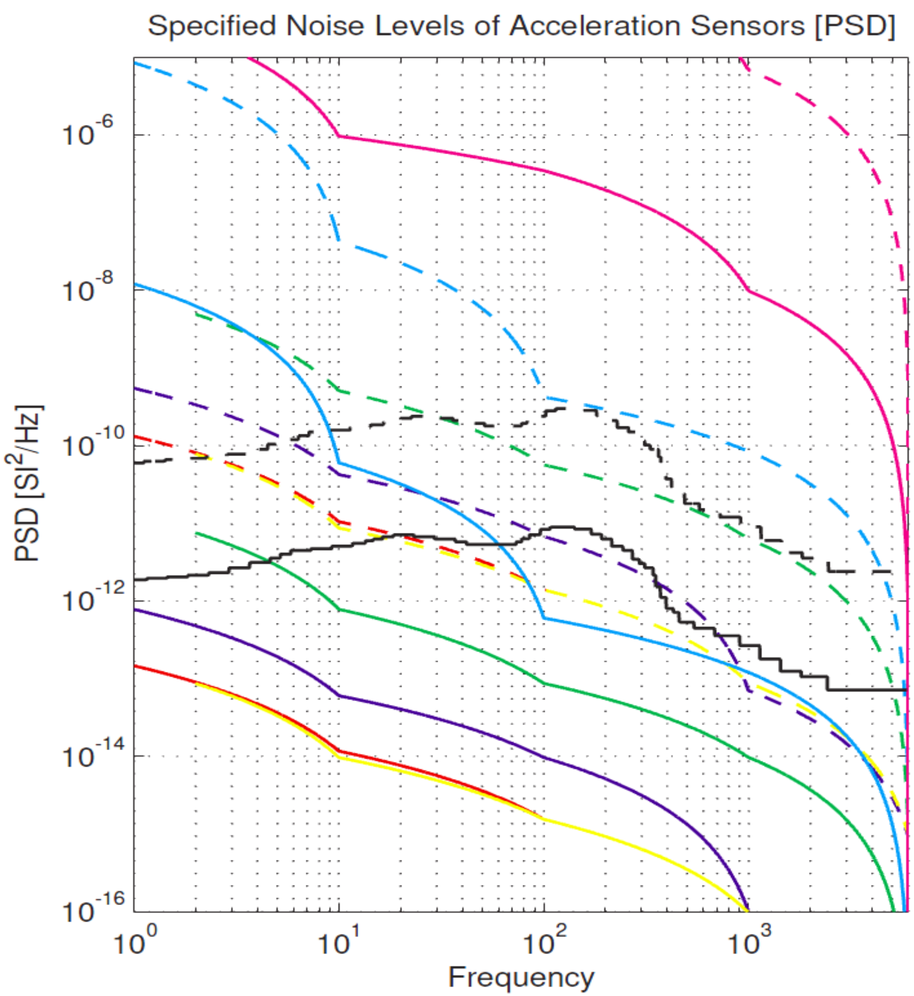

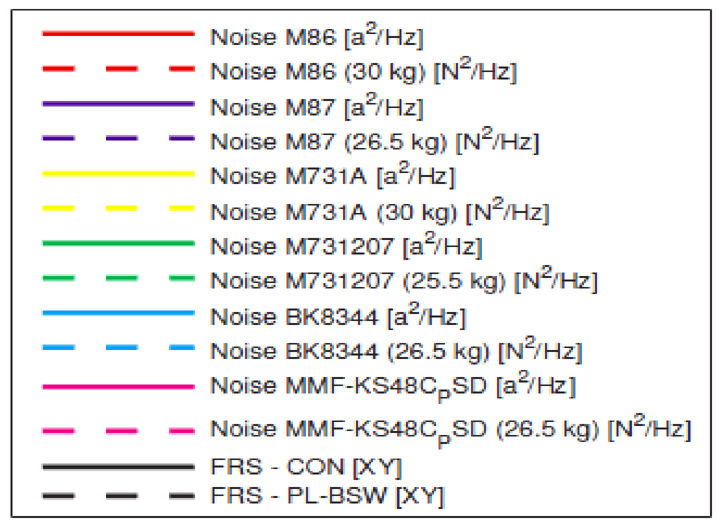

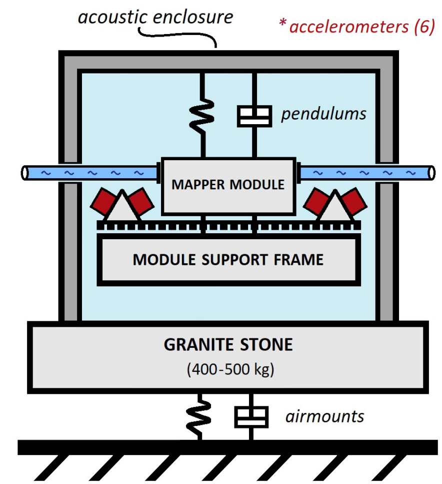

*simulations of winning concept (**B:** direct-force) in § 3.4.4

B-2: Model Simulations (Concept A)

MAPPER lithography

Alternative concept: acceleration-based – *computing crosstalk*

Comparing feasible sensors with the FRS

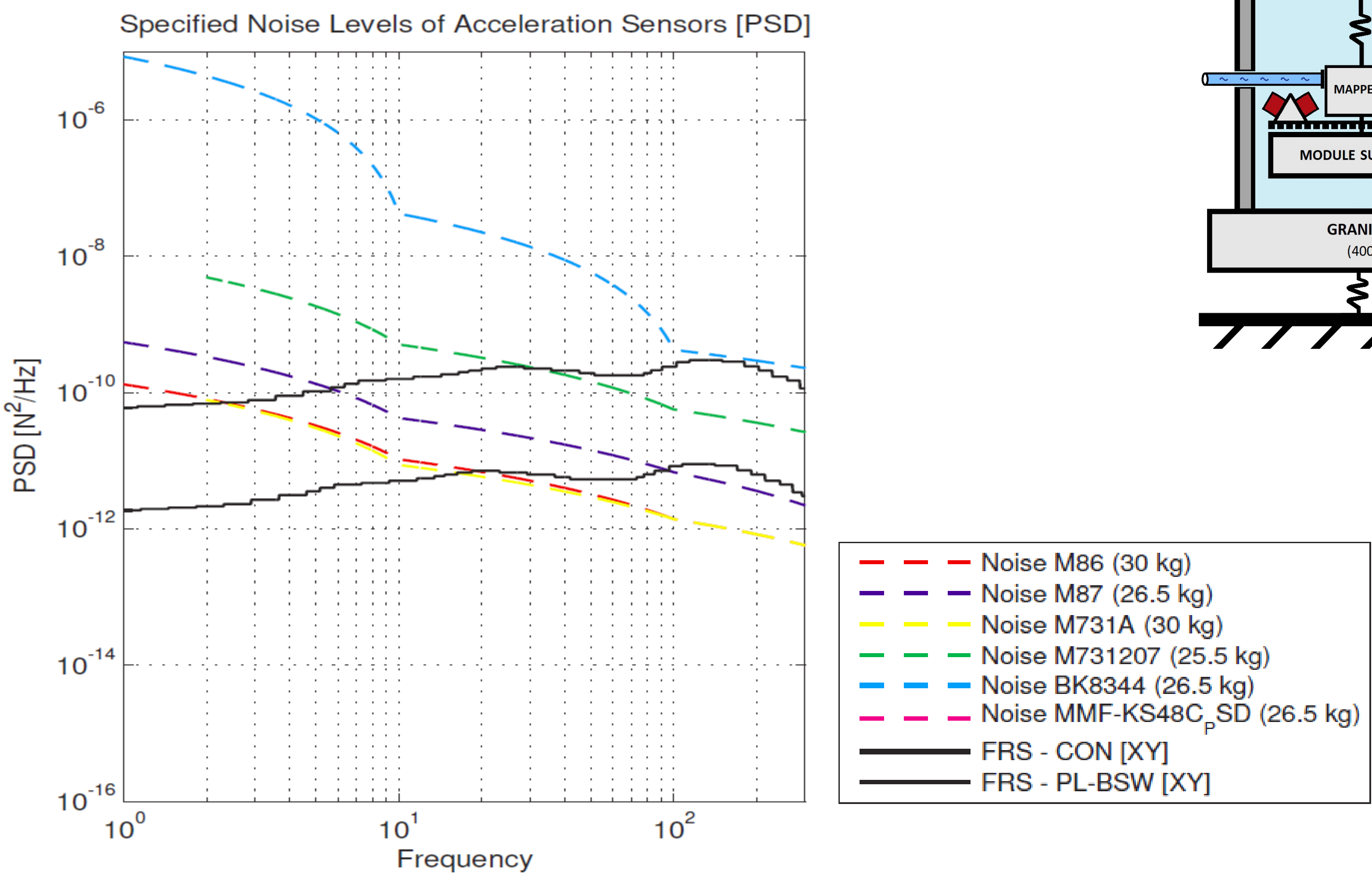

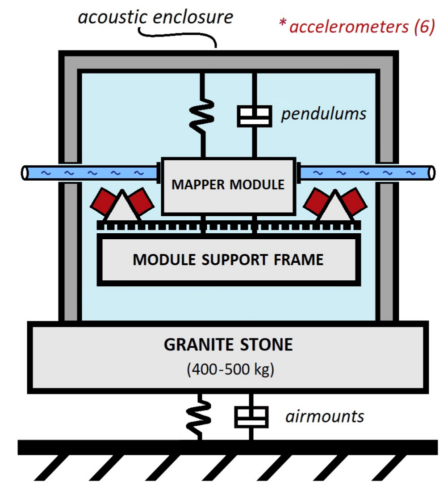

direct-force) in § 3.4.4

B-2: Model Simulations (Concept A)

MAPPER lithography

Alternative concept: acceleration-based – *computing crosstalk*

Noise levels cables

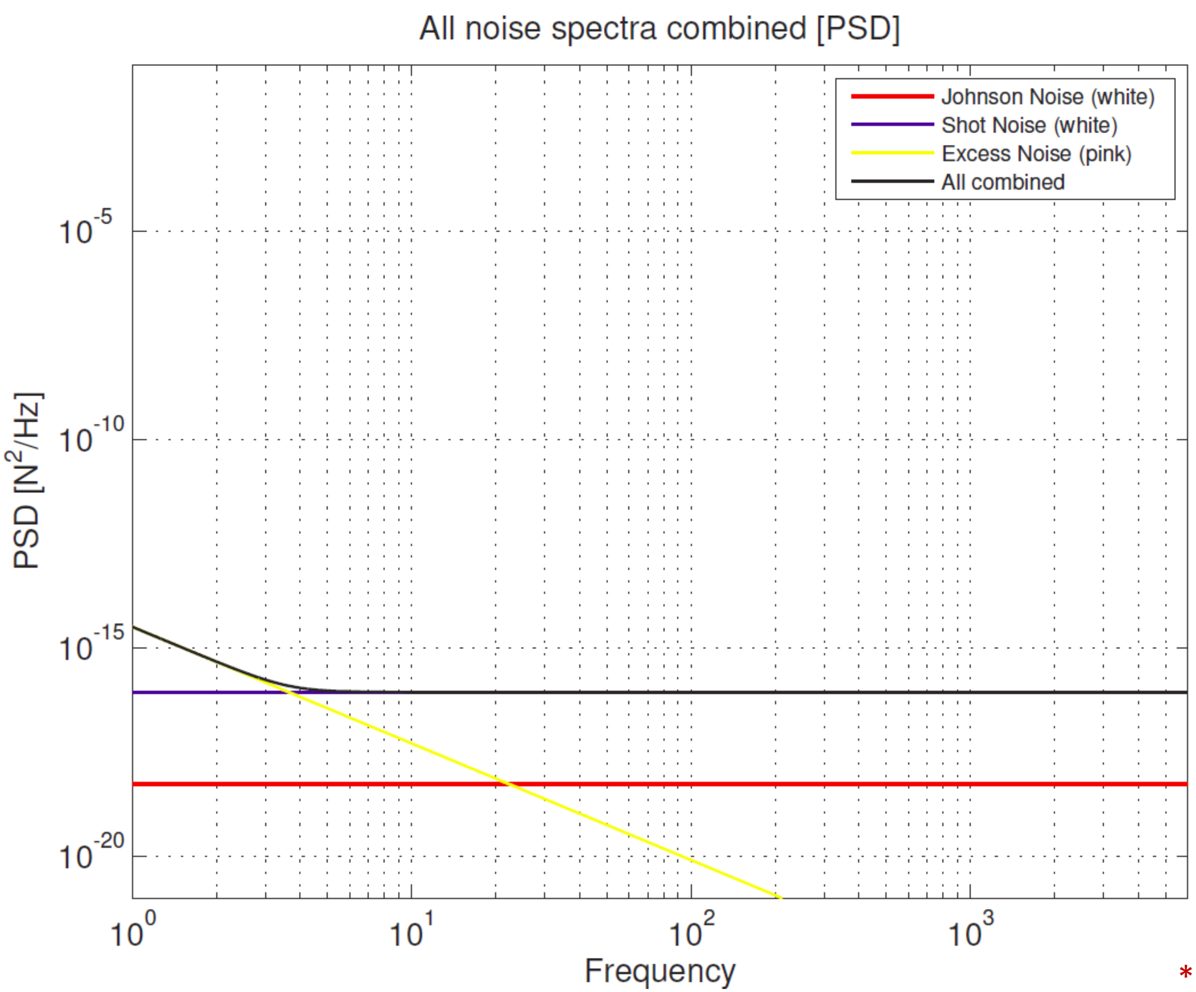

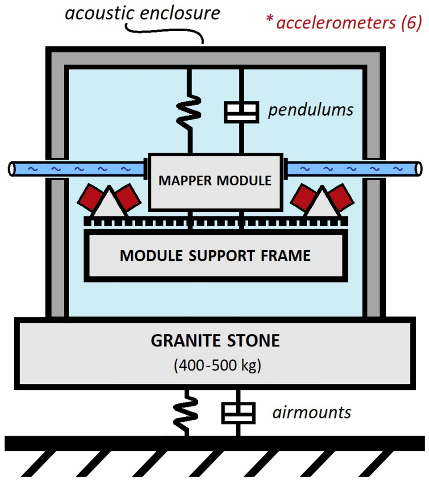

* simulations of winning concept (**B:** direct-force) in § 3.4.4

B-2: Model Simulations (Concept A)

Alternative concept: acceleration-based – *computing crosstalk*

DAQ noise levels

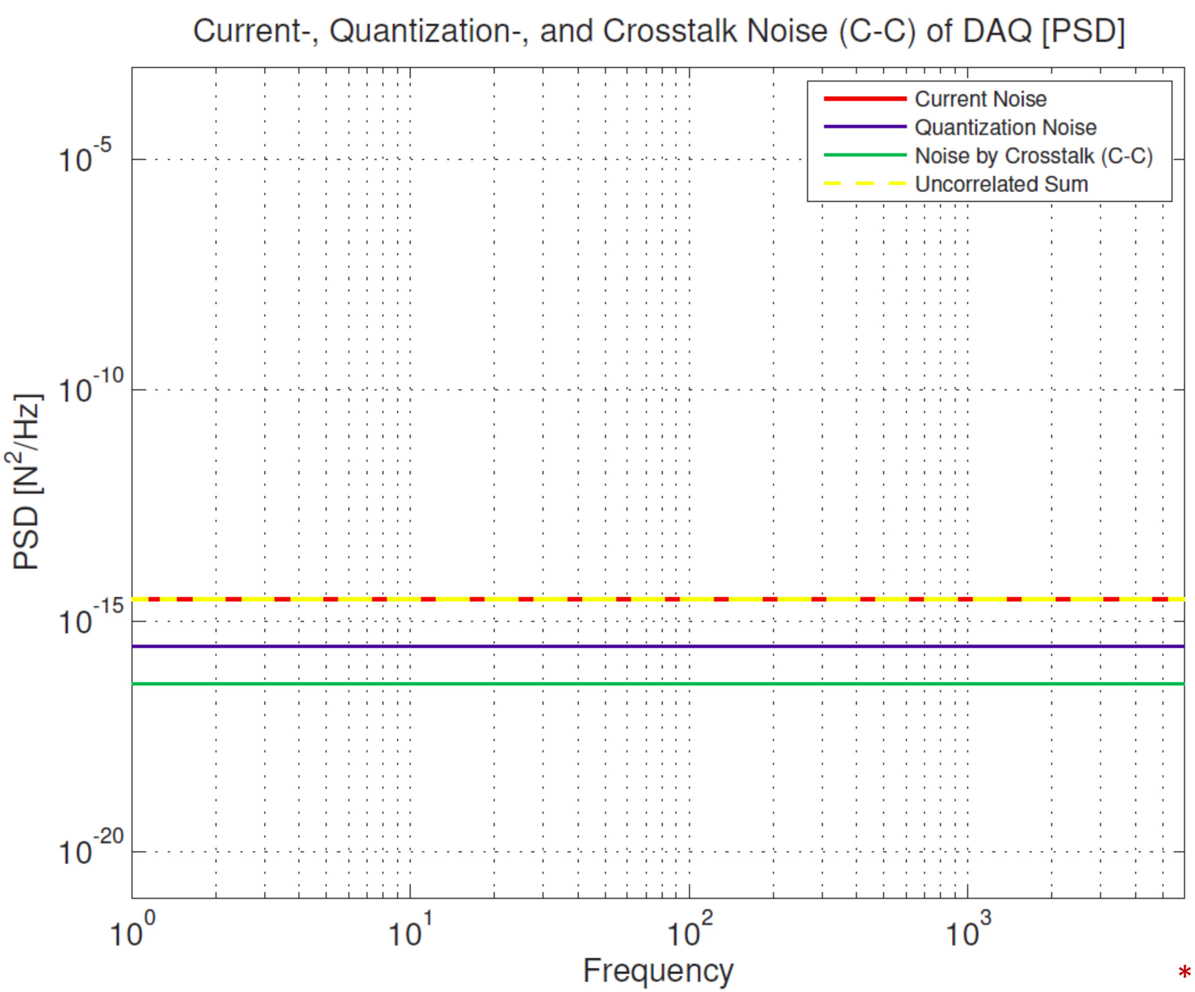

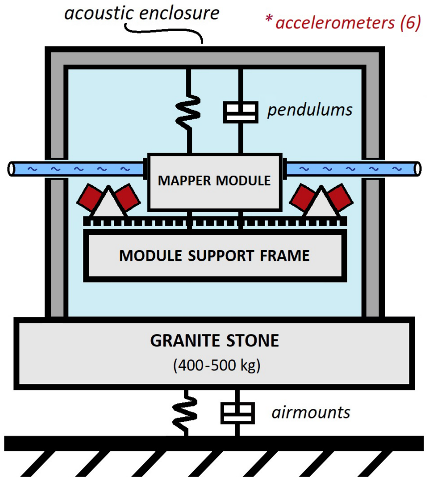

* simulations of winning concept (**B:** direct-force) in § 3.4.4

B-2: Model Simulations (Concept A)

Alternative concept: acceleration-based – *computing crosstalk*

Combined noise level: **sensor noise + cable noise [3] + DAQ noise [3]**

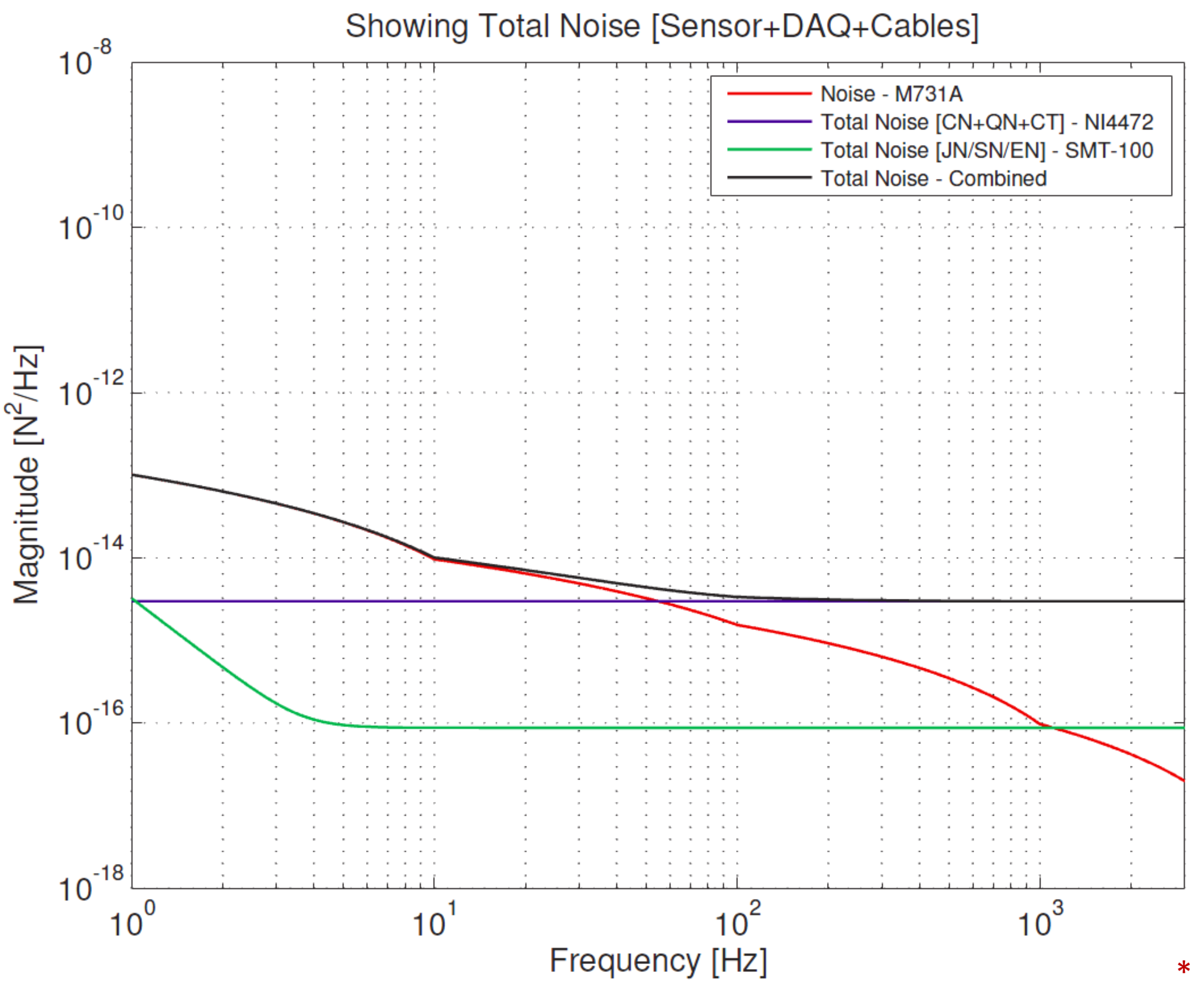

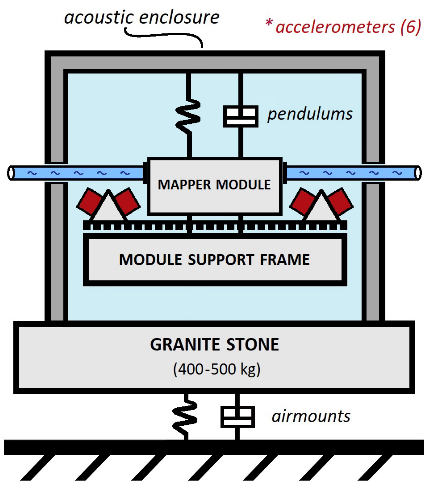

*simulations of winning concept (**B:** direct-force) in § 3.4.4

B-2: Model Simulations (Concept A)

MAPPER lithography

Alternative concept: acceleration-based – *effect of interference on measured signal*

Modeled transmission through parasitic stiffnesses

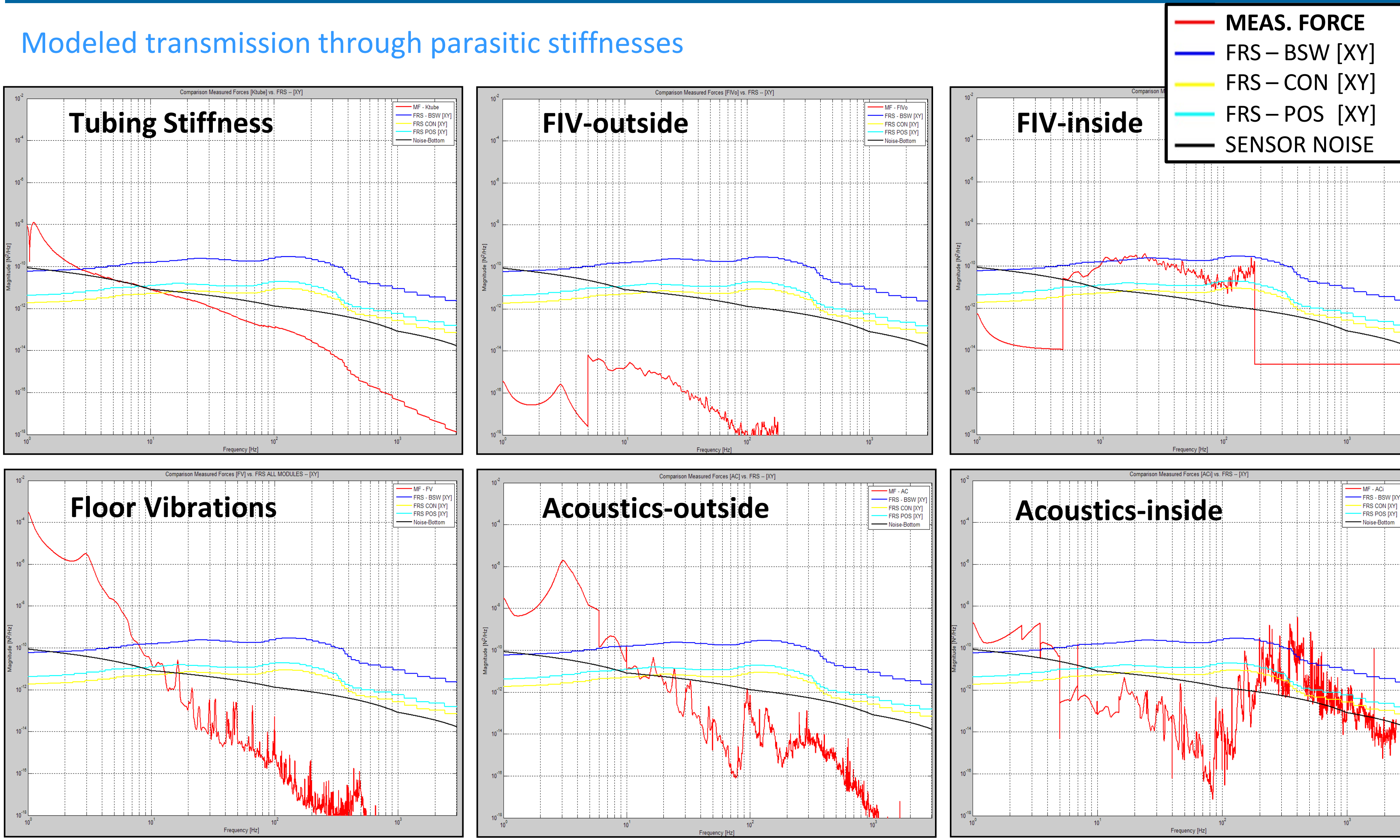

B-2: Model Simulations (Concept A)

Alternative concept: Predicted Signal – *residual noise level of **all disturbances combined***

Floor Vibrations + Acoustics [2] + FIV Tubing [2] + Cable Stiffness + Sensor Noise + Cable Noise [3] + DAQ Noise

This graph is the final result of the DEB model, combining all simulations for concept A in one figure. It shows:

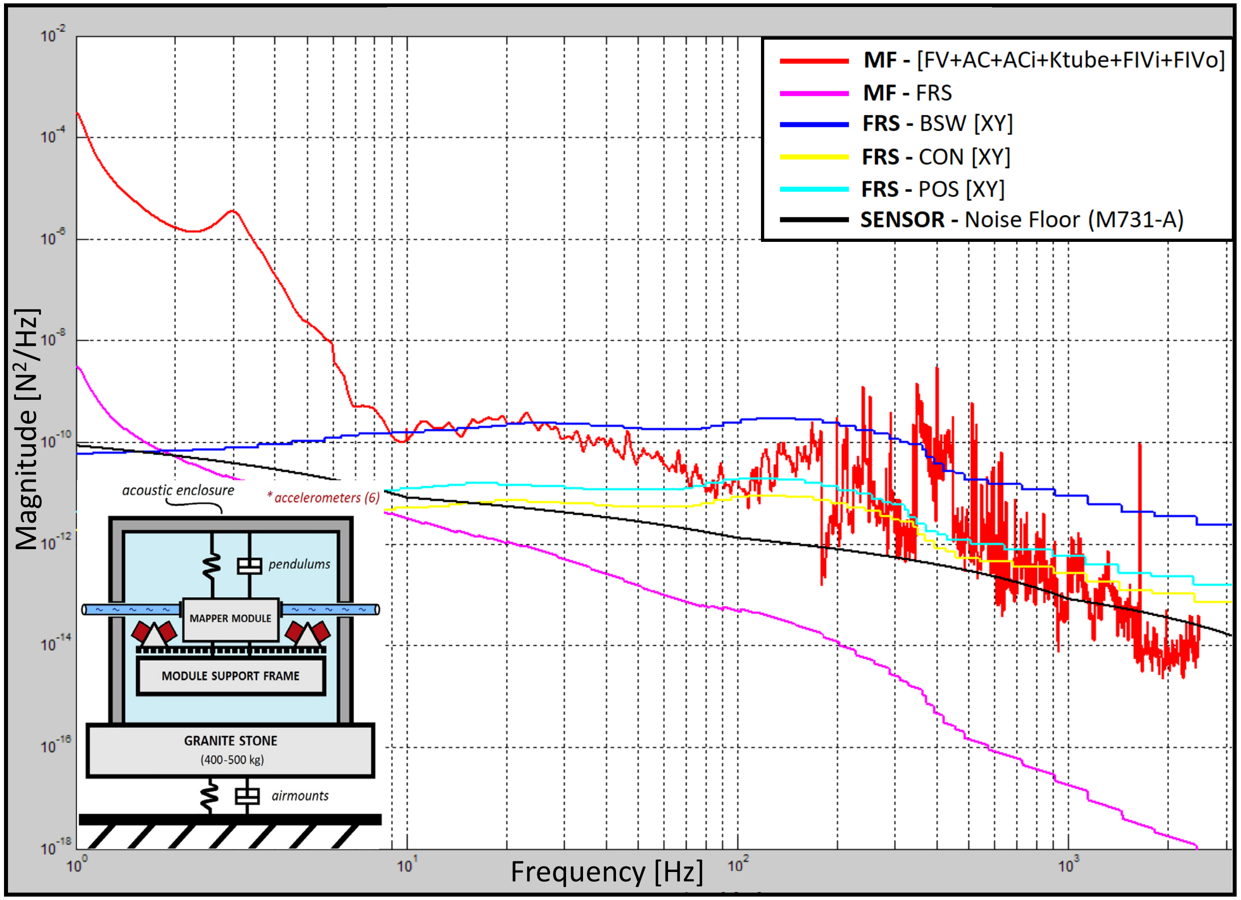

- the requirements (FRS) that need to be verified for the different Mapper modules (**yellow-**, **turquoise-**, **blue** line), with CON (ContaminatiON sub-system: Advanced Beam Cleaner [ABC] Module) requiring the lowest noise level.
- the signal that will be measured by the seismic grade accelerometers if no disturbances are present and flow-vibrations inside the ABC Module are at the level of its desired FRS (**pink** link).
- the sum of all disturbances combined (interference, crosstalk, parasitic stiffnesses), at the level that remains after all the measures taken to prevent / shield / attenuate them, *in other words: the expected performance of the designed measurement tool.*

B-2: Model Simulations (Concept A)

MAPPER lithography

Force concept (B): Predicted Signal – *residual noise level of* ***all disturbances combined***

Floor Vibrations + Acoustics [2] + FIV Tubing [2] + Cable Stiffness + Sensor Noise + Cable Noise [3] + DAQ Noise

This graph is the final result of the DEB model, combining all simulations for concept B in one figure. It shows:

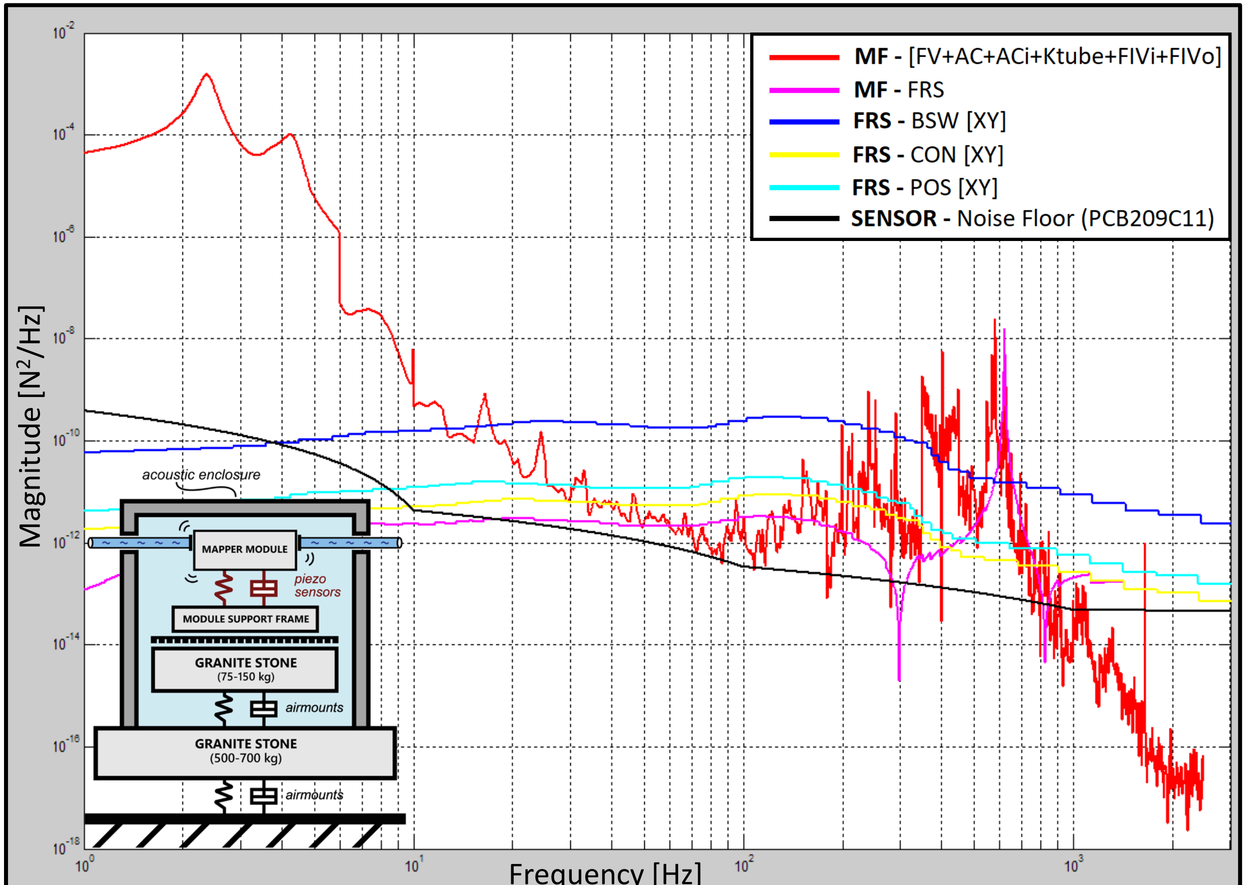

- the requirements (FRS) that need to be verified for the different Mapper modules (yellow-, turquoise-, **blue** line), with CON (ContaminatiON sub-system: Advanced Beam Cleaner [ABC] Module) requiring the lowest noise level.
- the signal that will be measured by the piezo sensors, if no disturbances are present and flow-vibrations inside the ABC Module are at the level of its desired FRS (**pink** link).
- the sum of all disturbances combined (interference, crosstalk, parasitic stiffnesses), at the level that remains after all the measures taken to prevent / shield / attenuate them, *in other words: the expected performance of the designed measurement tool.*

B-3: Generic Design Guidelines [1/2]

MAPPER lithography

The following general design guidelines can serve as a reference when designing a meas. tool

"how to effectively design a low-noise force measurement system while in the presence of dominant disturbances"

- identify all disturbances present in the concept design using the error overviews presented in § 3.2.1.
- map out all disturbances and create a categorization specific for the design under study.
- sub-divide in interference and crosstalk and categorize in mechanical / thermal / electrical domains. Aim is to prevent random (interference) sources from entering the system under design § 3.2.1.3.
- determine through measurement and modeling the degree to which deterministic error sources must be shielded or attenuated to meet the objective.
- compute the magnitudes of the random (crosstalk) sources that determine the remaining noise level and compare with requirement (select alternative elements if too high).
- identify the transfer paths towards the measured (sensor) signal. Dependent on the used measurement principle this will differ. For example piezoelectric sensors work on the applied pressure which is a function of displacement if part of the design's stiffness train. Accelerometers yield a signal proportional to accelerations which allows for suspension in a way that allows for free motion in all directions.
- determine the measures that need to be taken to attenuate floor vibrations (measure accelerations and transform in velocities [VC spectra] or displacements) to levels that are acceptable in the design under consideration. When designing a passive vibration isolation platform, measuring displacements is key to achieve good floor vibration isolation as well as a high payload disturbance rejection. If accelerations are to be observed, the fundamental trade-off for passive vibration isolation systems inhibits both to be good at the same time.
- tune mass, damping and stiffness values to shift the resonance frequency to a desired location, dependent on whether the design behaves more like a low-pass or a high-pass system. Account for the (modeled) effect this has on measured signal.

B-3: Generic Design Guidelines [2/2]

The following general design guidelines can serve as a reference when designing a meas. tool

"how to effectively design a low-noise force measurement system while in the presence of dominant disturbances"

- discharge unwanted FIV input on a heavy mass with an attractive (low throughput) transfer path towards the sensor signal. Generally speaking it is effective to unload the largest portion of supply tubing induced vibrations onto the mass element representing the first stage of a double VI platform.
- shield-off acoustic interference with a physical enclosure that is rigidly connected to a heavy VI stage. Note that this will most likely only be effective when using a double MSD vibration isolation platform. When using a single MSD system to attenuate floor vibrations, or when connecting casing to the top mass in case of a double MSD system, the effect is amplified which should be prevented.
- when selecting a method to apply pressure on the tubing, be aware of the impact that the workings of the pump has on the water flow it displaces (§ 3.3.3.1) For example, asynchronous motor characteristics of an centrifugal pump can show up as distinct resonances in the measured acceleration response of a geometry under testing. This can be prevented by using a hydrostatic pressure vessel to supply flow. This requires selecting a dimension that meets the type of batch measurement that will be executed to ensure sufficient duration of constant flow and pressure.
- when tubing is selected to supply flow to the geometry under testing, take the aspects listed in § 3.3.3.2 into account to prevent creating unnecessary acoustic sources and minimize their effect on local responses (e.g. the frequency at which Helmholtz like resonances occur; strongly depends on used geometry).

B-4: Model Calibration

Comparison of Stone Accelerations [Z] – *excited by **external** acoustics*

Calibrating the model for acoustic-induced accelerations

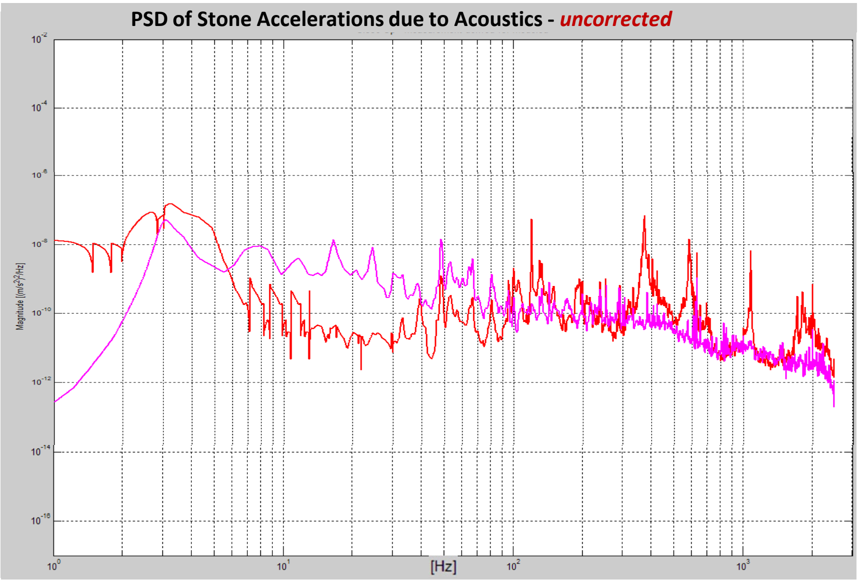

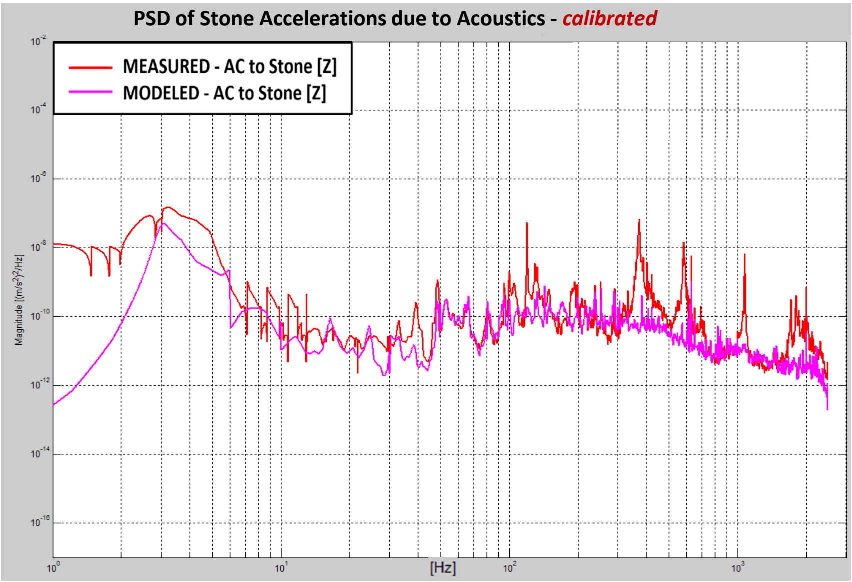

This slide details calibration of the Dynamic Error Budgeting model's prediction of acoustic influence on object accelerations.

When comparing the modeled accelerations of the stone due to environmental acoustics with those actually measured, it is clear that the model overestimates the resulting acceleration level for relatively low frequencies (above left Figure). For higher frequencies, the model's predictions are of the same order as the measured data.

Assumptions that were made regarding the transfer of acoustical pressure to forces on a surface, such as linearity and limited absorption by the granite, do not adequately explain the observed difference. The fact that sensitivity for force disturbances increases after the eigenfrequency also does not, as this is already incorporated through the used accelerance characteristic, describing Vibronix's acceleration response to an input force.

B-4: Model Calibration

Comparison of Stone Accelerations [Z] – *excited by **external** acoustics*

Physically, the background acoustic noise present at the lab space means that various sources of equipment cause longitudinal movement of air. It is these vibrations that produce pressure fluctuations that act on the exterior surface area of the Vibronix test setup (mounted to the granite stone) and result in acceleration of the air-mount suspended granite stone. **An explanation for this observed difference could be therefore be that for relatively low frequencies, i.e. frequencies where the wavelength of sound pressure waves are in the same order as the object on which it acts, the effect of phase is much less than for relative higher frequencies (shorter wavelengths).** This is because very long wavelengths cause a much more uniform pressure field as experienced by the mechanical objects on which they act (in this case: the granite stone of the Vibronix test setup supported by airmounts). As vertical acceleration of this granite stone is the consequence of the force that results from this net pressure, acting on the surface area, it is expected to be less for relatively low frequencies than for high frequencies. The picture on the next slide aims to illustrate this difference.

This means that the net pressure variation that results when multiple sound waves of the same frequency and magnitude but different phase, strike on an object is lower. Even though this hypothesis has not been thoroughly investigated, it would explain why the model initially overestimated the resulting accelerations of the granite stone due to external acoustics up to frequencies corresponding with the objects characteristic length. After these corrections, the predicted accelerations by the model correspond well with the actually measured accelerations (top right figure on previous slide).

This concludes the calibration process as, apart from five distinct resonance peaks, the DEB model is able to predict the magnitude & spectral trend well over the whole frequency range of interest (0 – 3000 Hz). These outliers are investigated in § 3.4.3.2 and can be explained sufficiently to come to the conclusion that: **it is likely that model simulations of acoustics-induced object accelerations will be accurate.**

B-4: Model Calibration

I.P.

B-5: Wafer Error Calculations

MAPPER lithography

Detailing the EO slit size that maps rotational errors to translational wafer error

I.P.

B-6: Floor Acceleration Measurements

Detailing acceleration measurement performed on the floor [XYZ] and stone [XYZ] **(1st VI stage)**

Floor Vibrations – full range [XYZ]

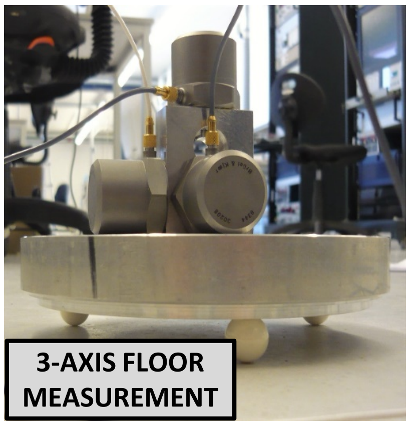

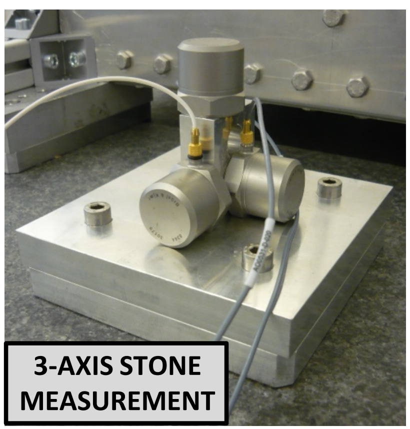

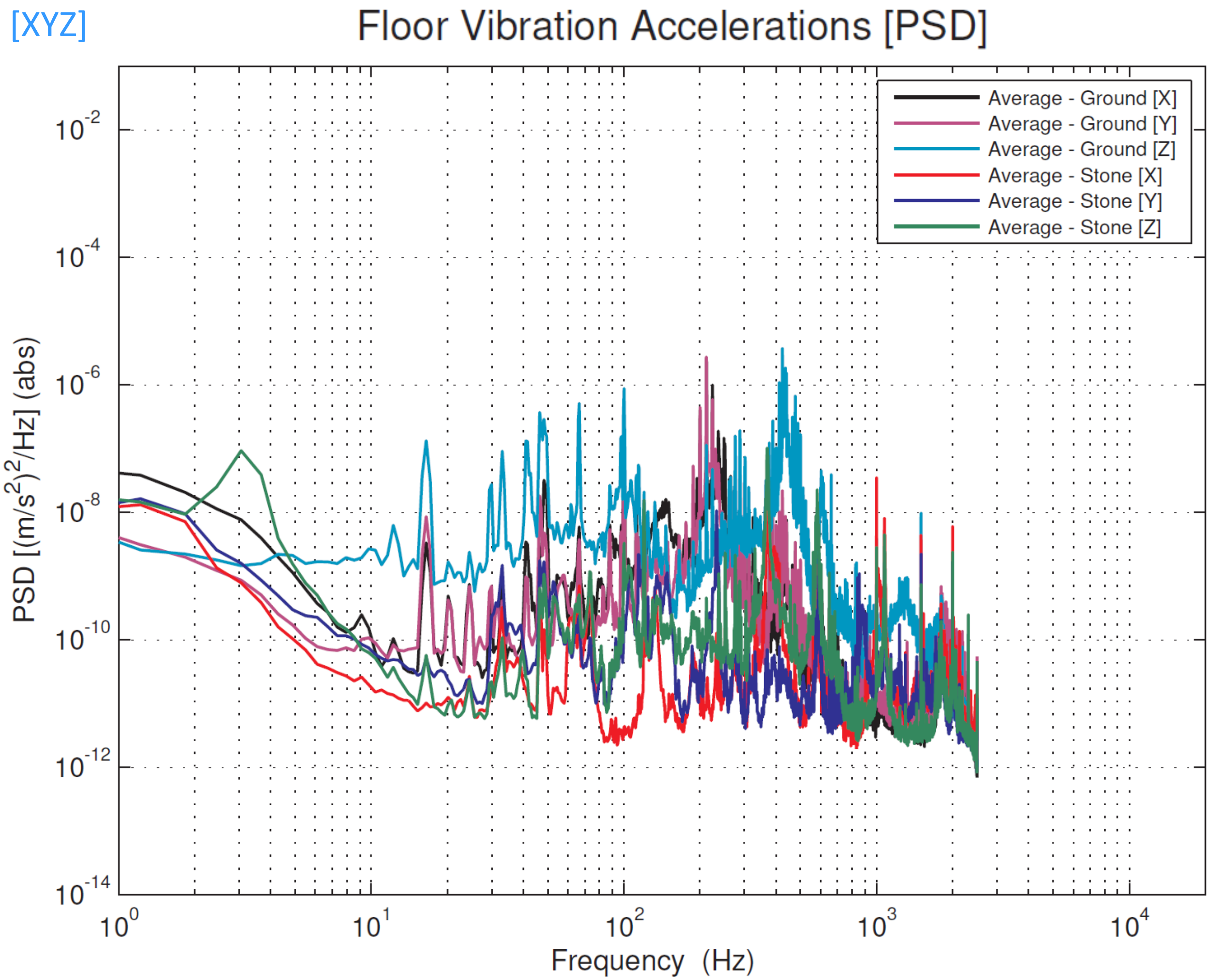

B-6: Floor Acceleration Measurements

MAPPER lithography

Detailing acceleration measurement performed on the floor [XYZ] and stone [XYZ] (1st VI stage)

Floor Vibrations – full range [X]

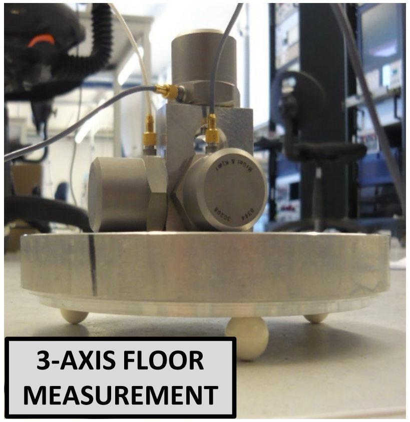

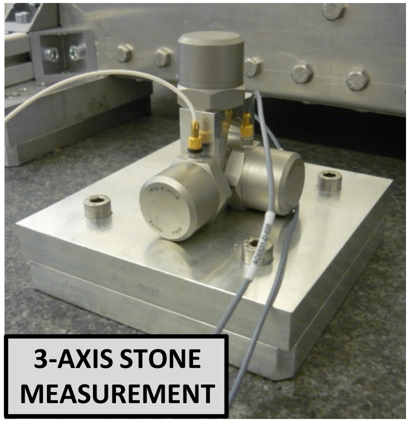

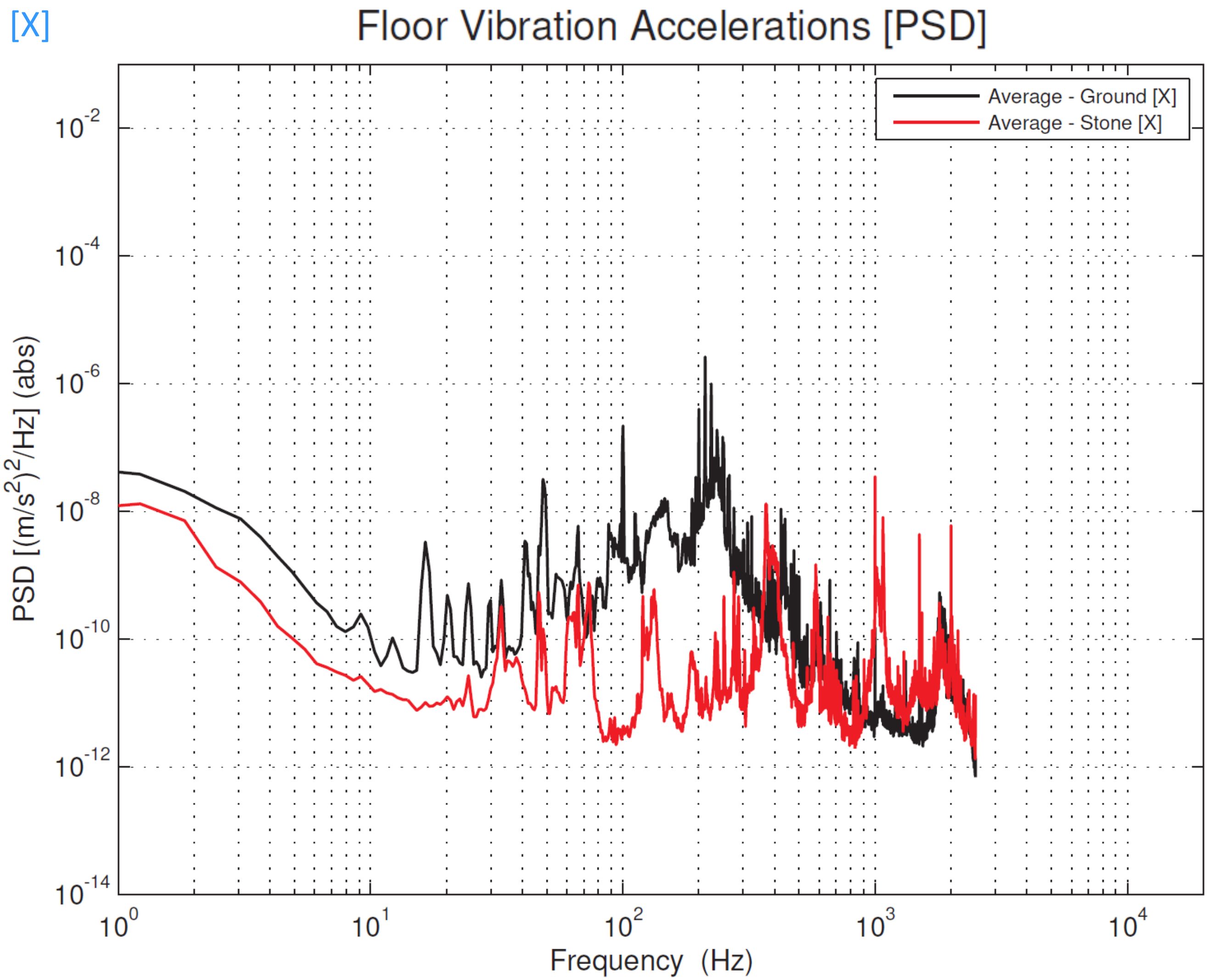

B-6: Floor Acceleration Measurements

Detailing acceleration measurement performed on the floor [XYZ] and stone [XYZ] **(1st VI stage)**

Floor Vibrations – full range [Y]

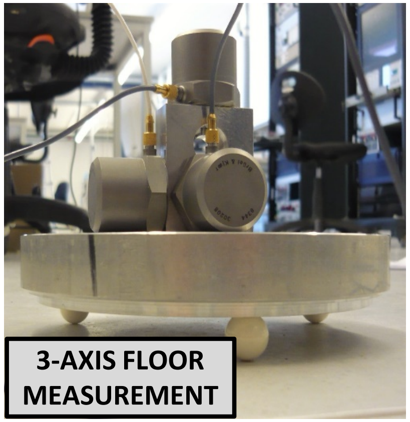

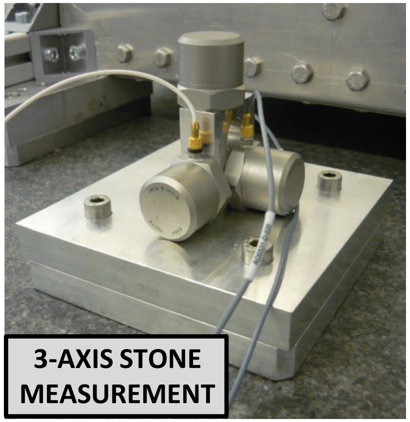

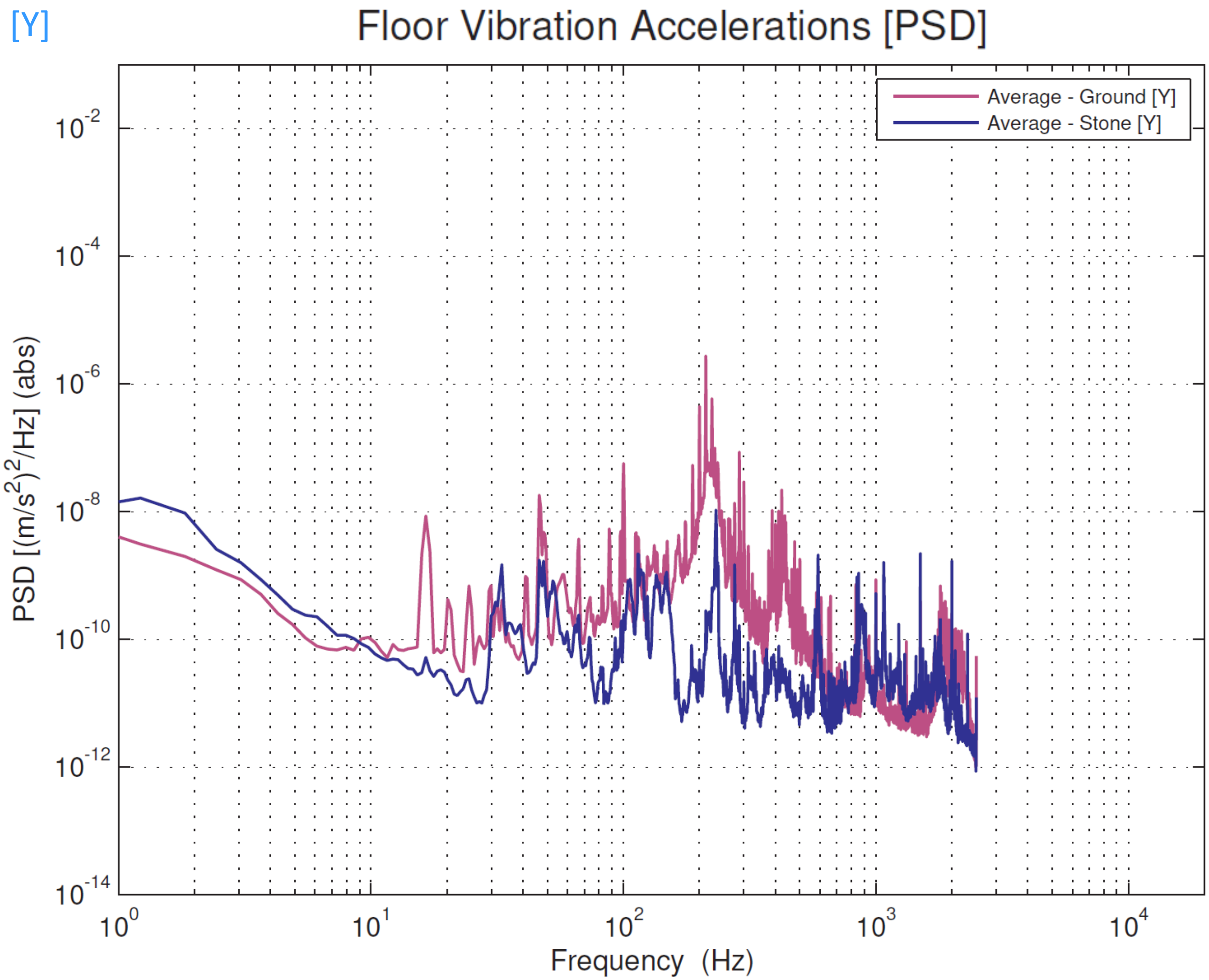

B-6: Floor Acceleration Measurements

Detailing acceleration measurement performed on the floor [XYZ] and stone [XYZ] (1st VI stage)

Floor Vibrations – full range [Z]

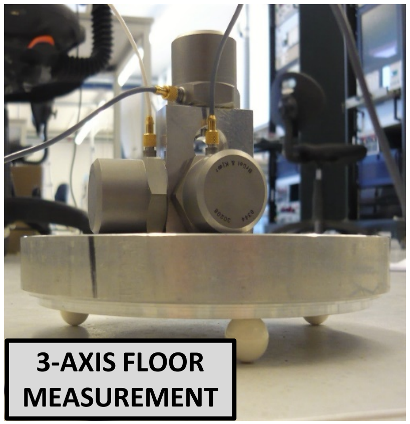

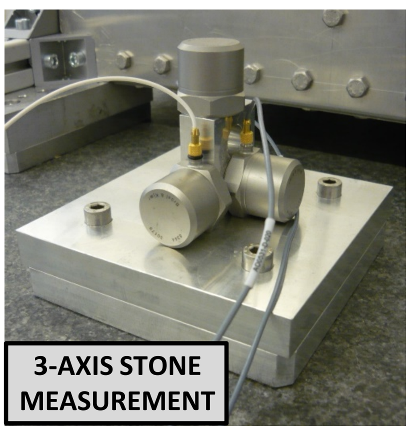

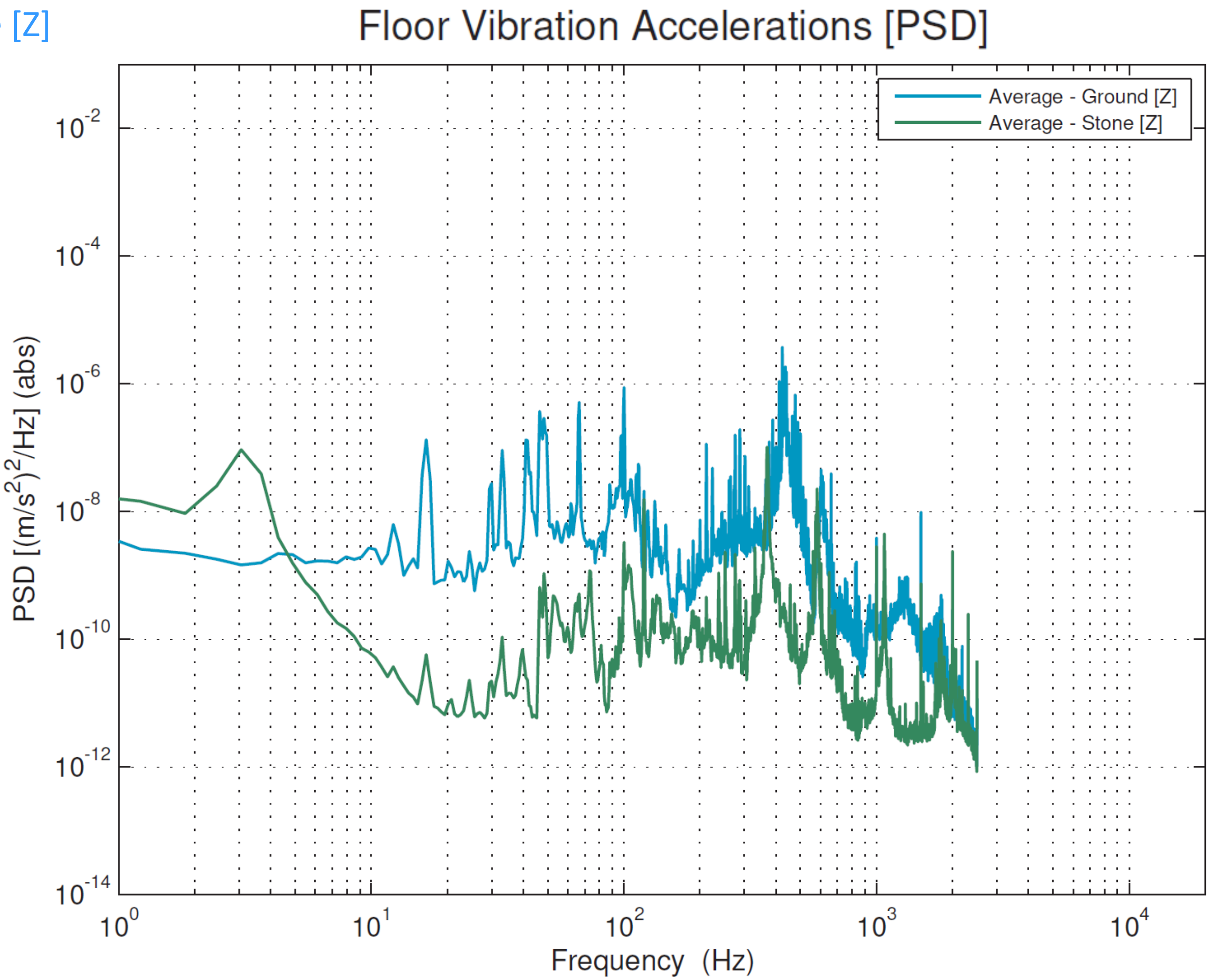

B-6: Floor Acceleration Measurements

Detailing acceleration measurement performed on the floor [XYZ] and stone [XYZ] (1st VI stage)

Floor Vibrations – design range [XYZ]

EXTRACT: [10 – 300 Hz]

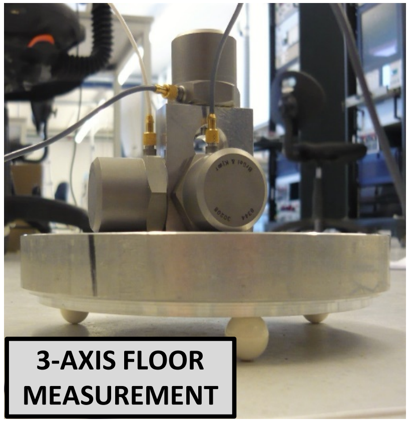

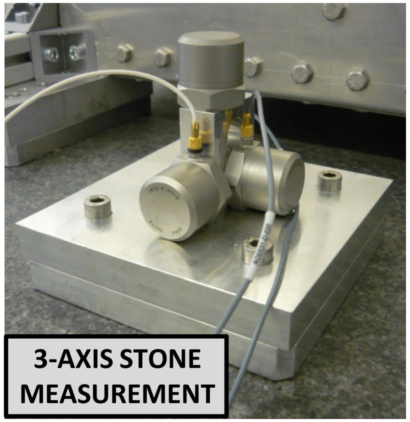

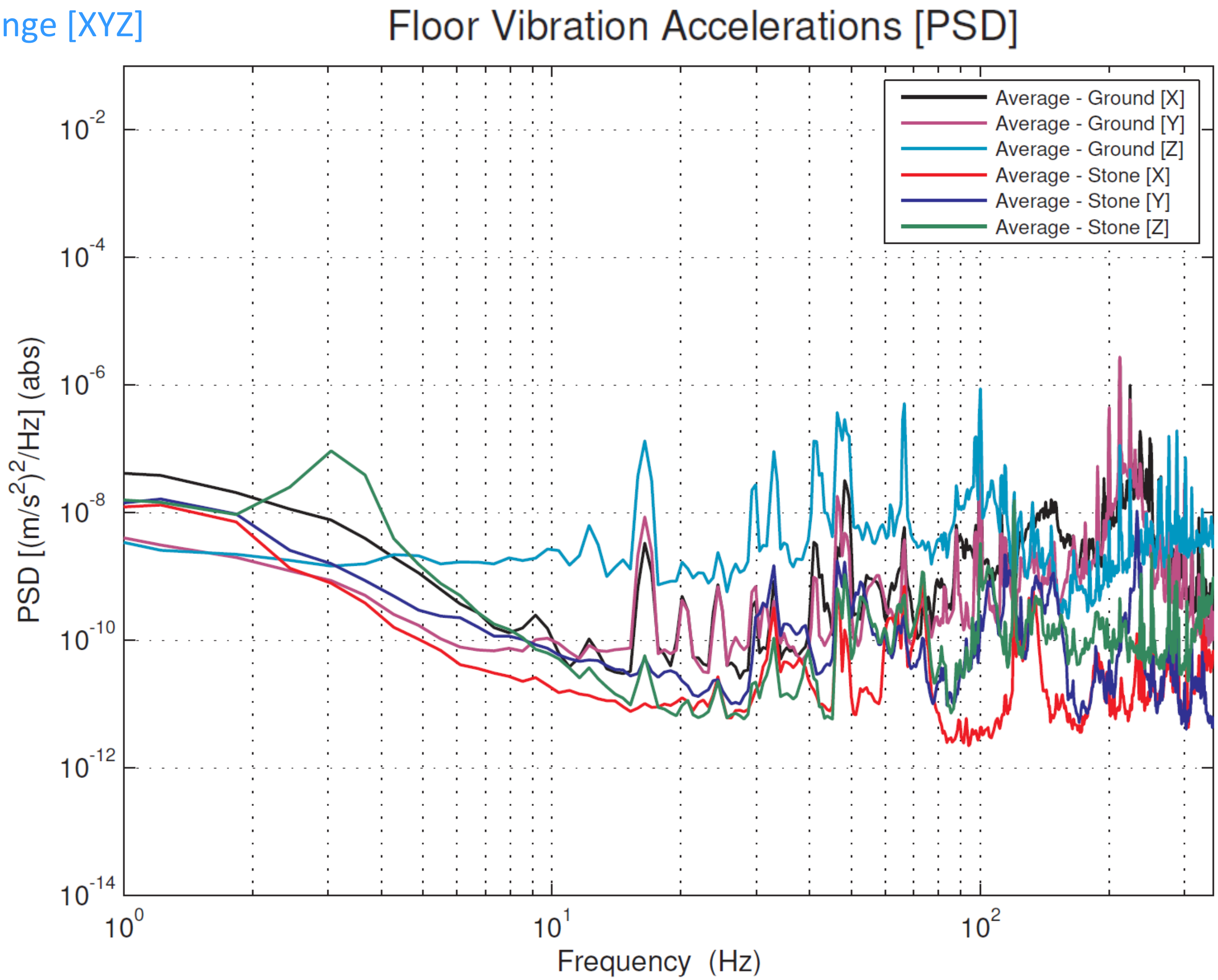

Detailing acceleration measurement performed on the floor [XYZ] and stone [XYZ] (1st VI stage)

Floor Vibrations – design range [X]

EXTRACT: [10 – 300 Hz]

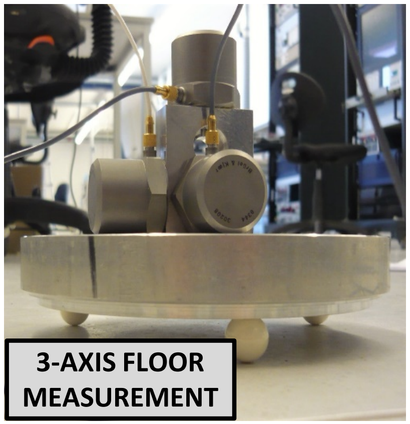

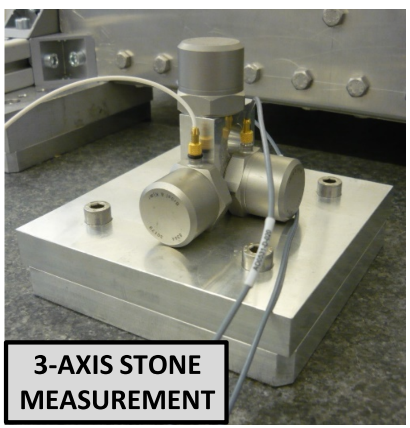

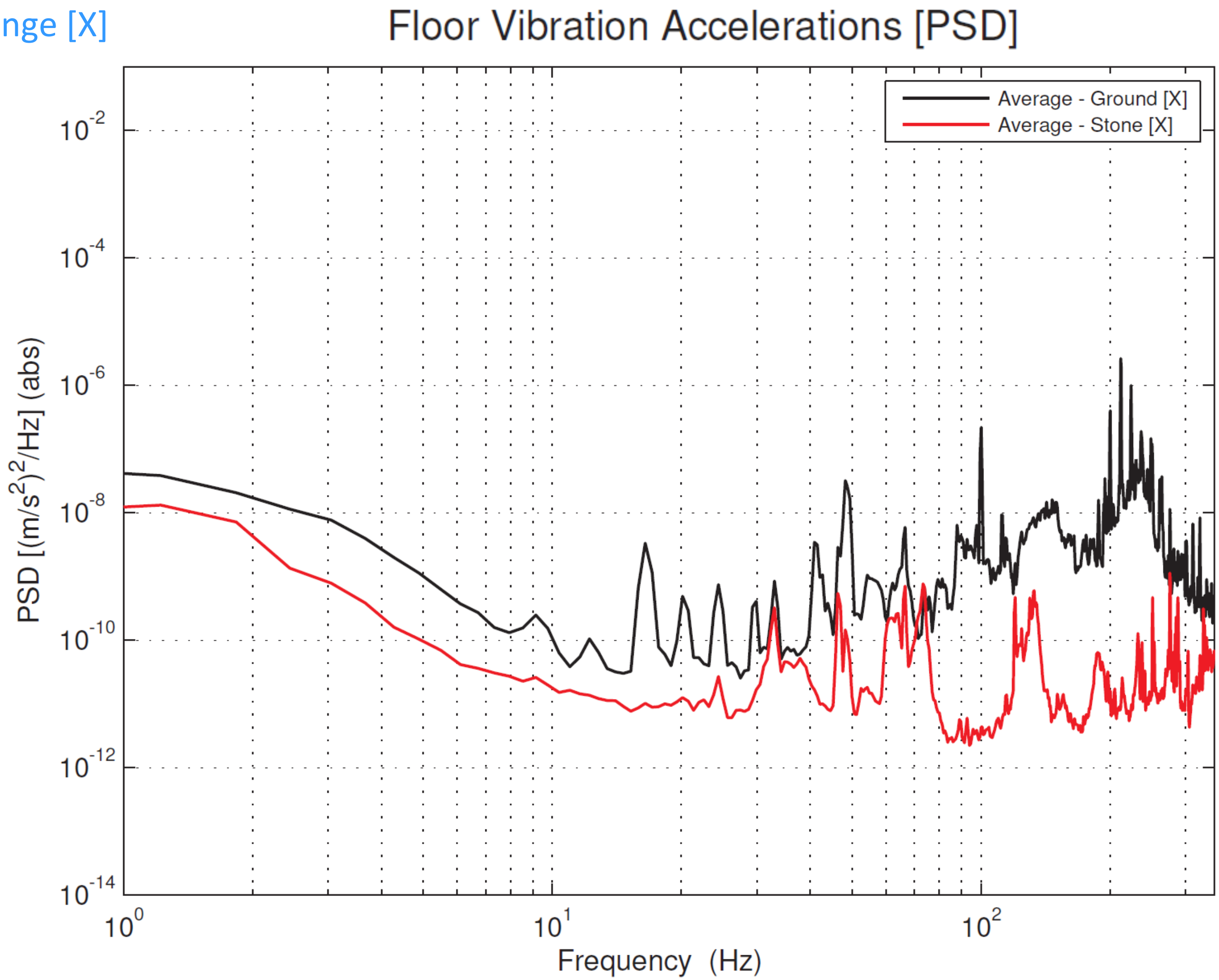

B-6: Floor Acceleration Measurements

Detailing acceleration measurement performed on the floor [XYZ] and stone [XYZ] (1st VI stage)

Floor Vibrations – design range [Y]

EXTRACT: [10 – 300 Hz]

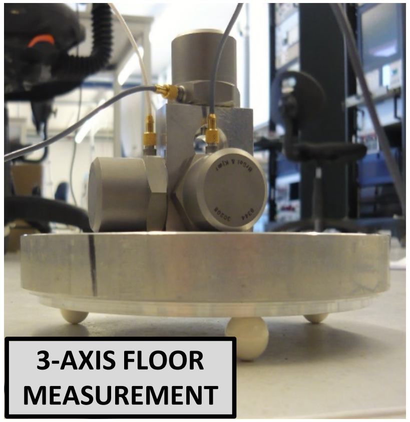

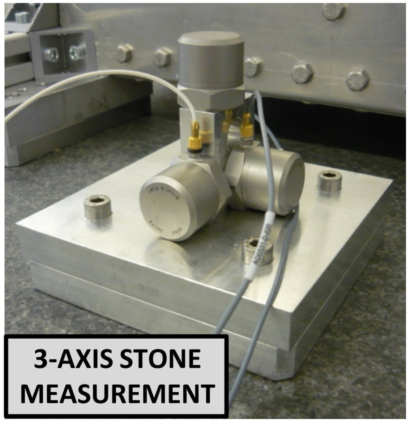

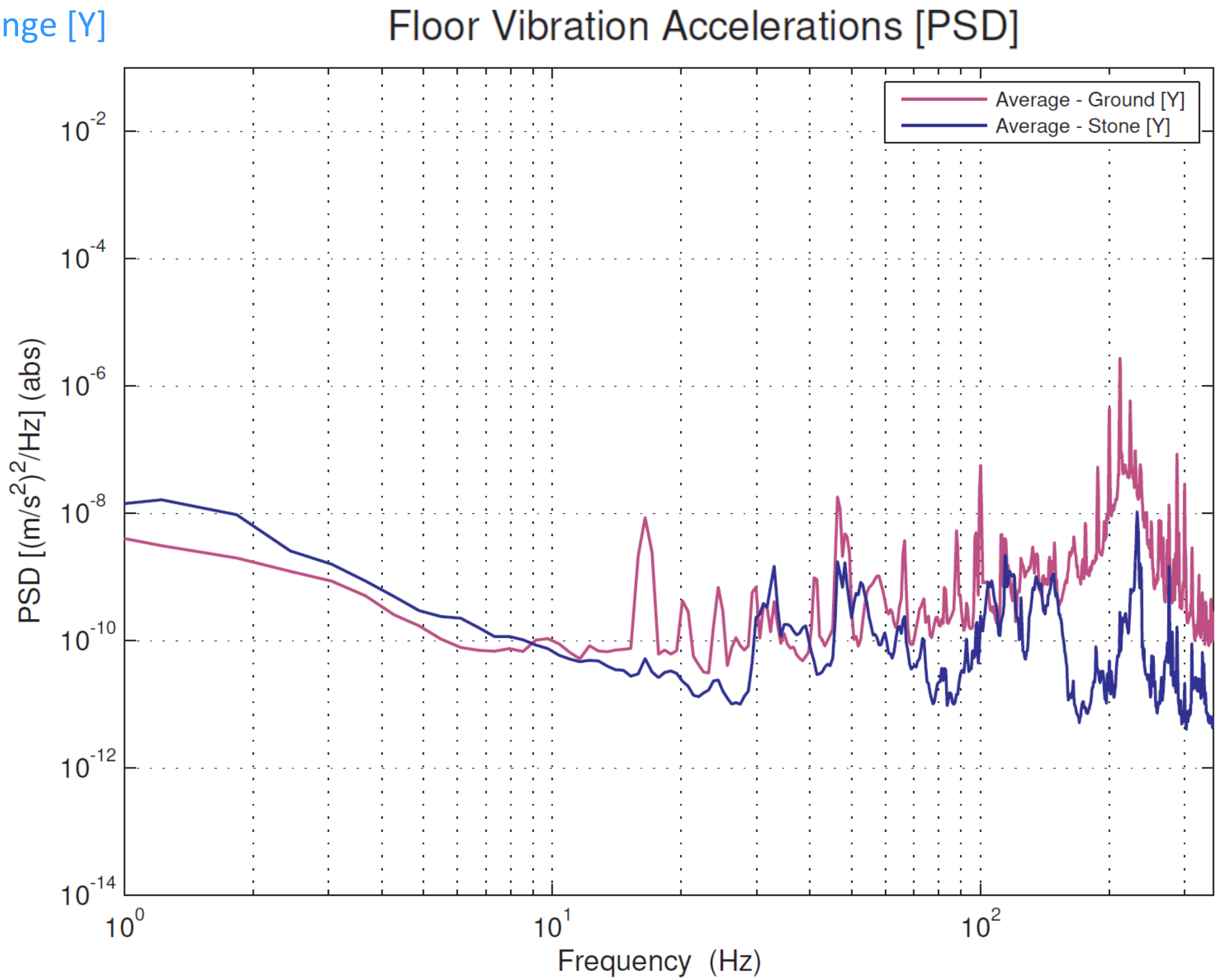

B-6: Floor Acceleration Measurements

Detailing acceleration measurement performed on the floor [XYZ] and stone [XYZ] (1st VI stage)

Floor Vibrations – design range [Z]

EXTRACT: [10 – 300 Hz]

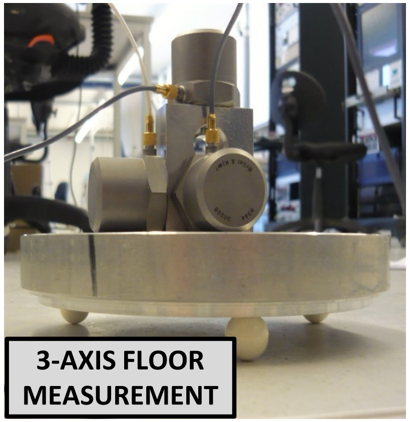

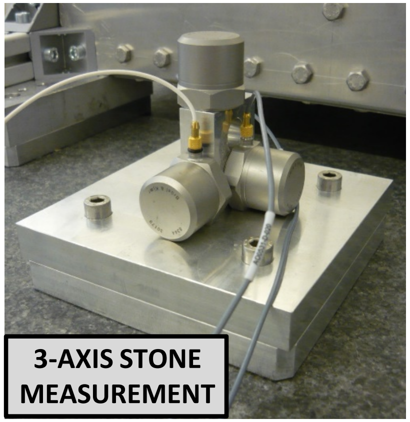

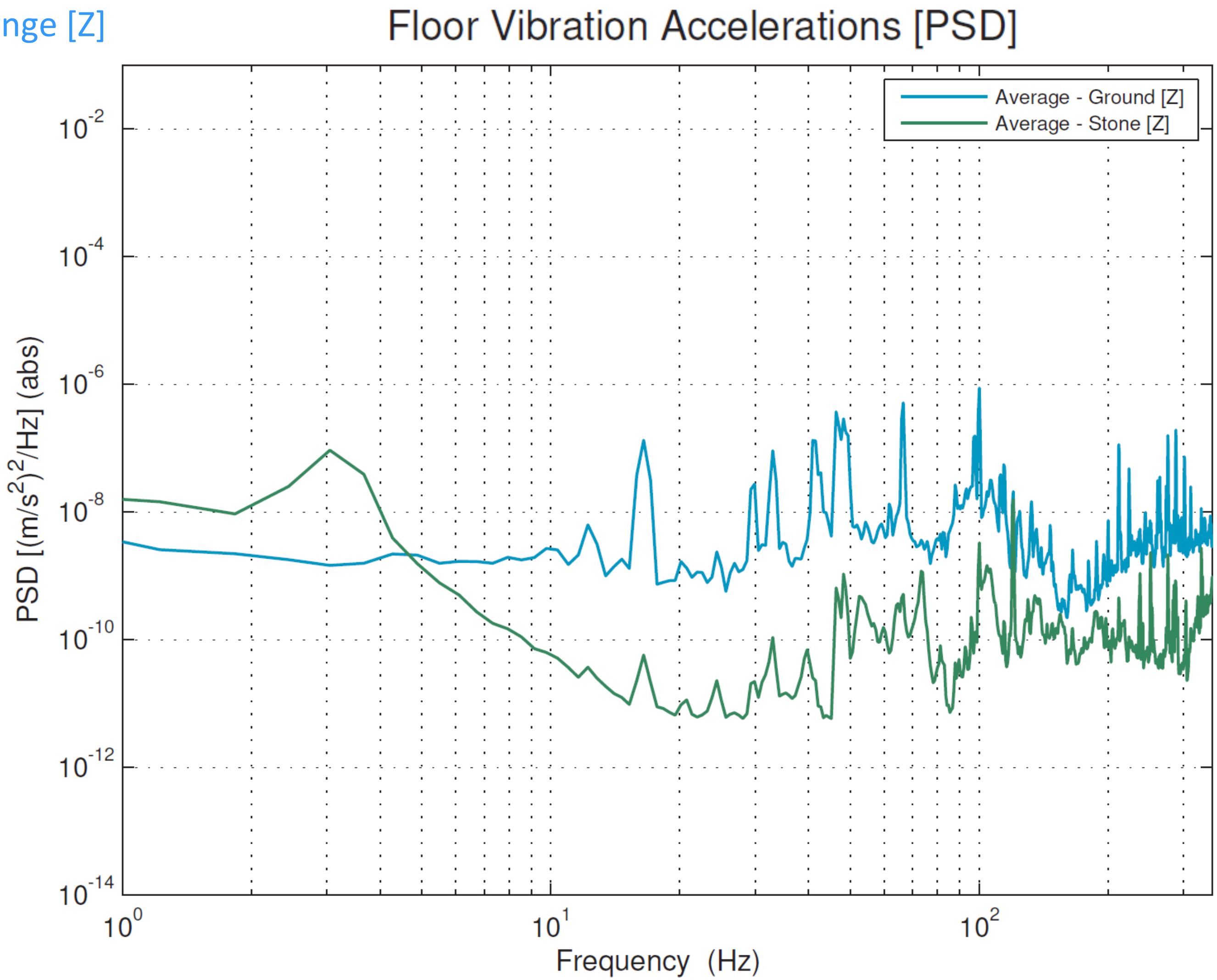

B-7: Verification Measurements

A-7.1: Additional verification measurement performed on Forcesix

SUSA Sensor Electronics – no sensors

SENSOR SIGNAL IN TIME & FREQ. DOMAIN

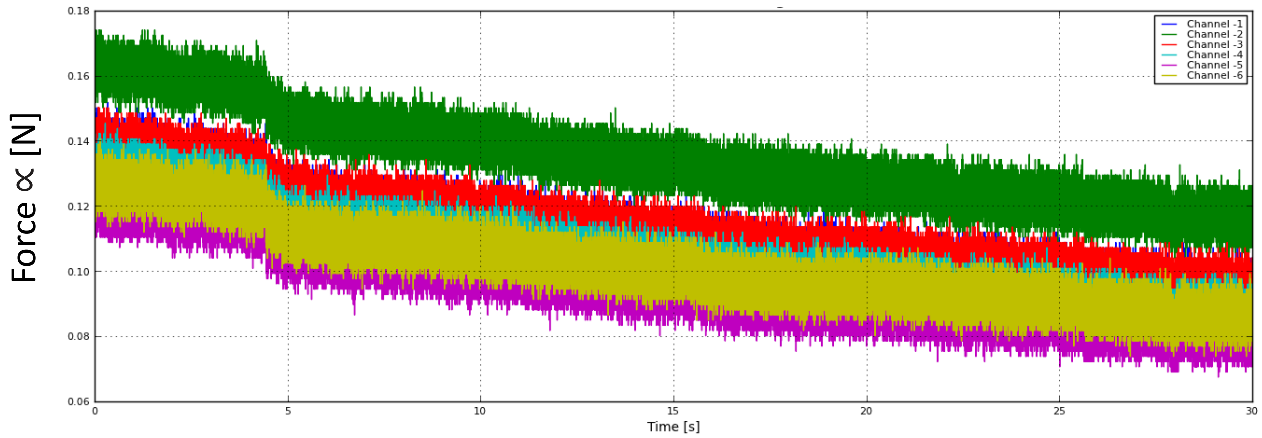

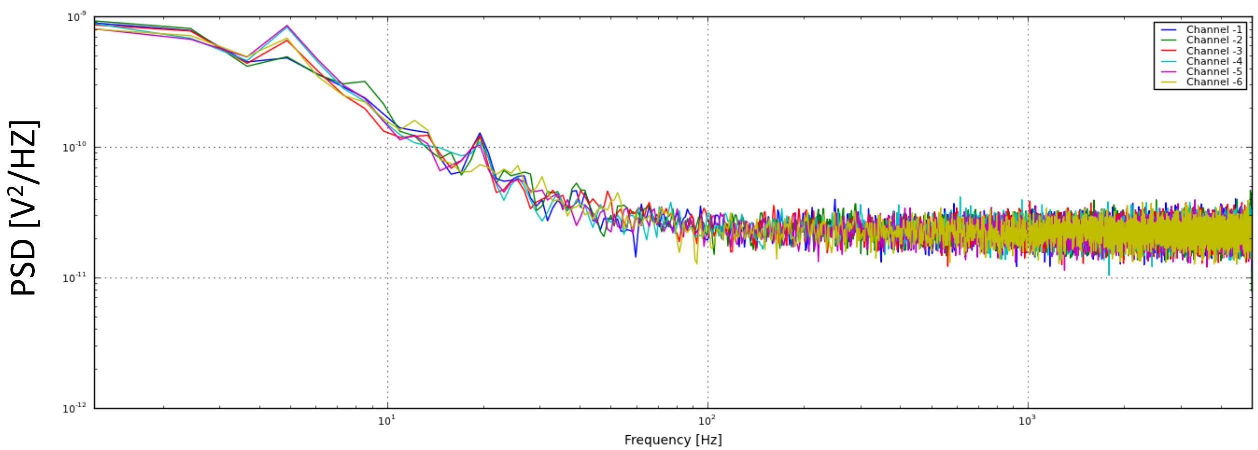

B-7: Verification Measurements

A-7.2: Additional verification measurement performed on Forcesix

Individual Piezo Sensors – prior to installation

SENSOR SIGNAL IN TIME & FREQ. DOMAIN

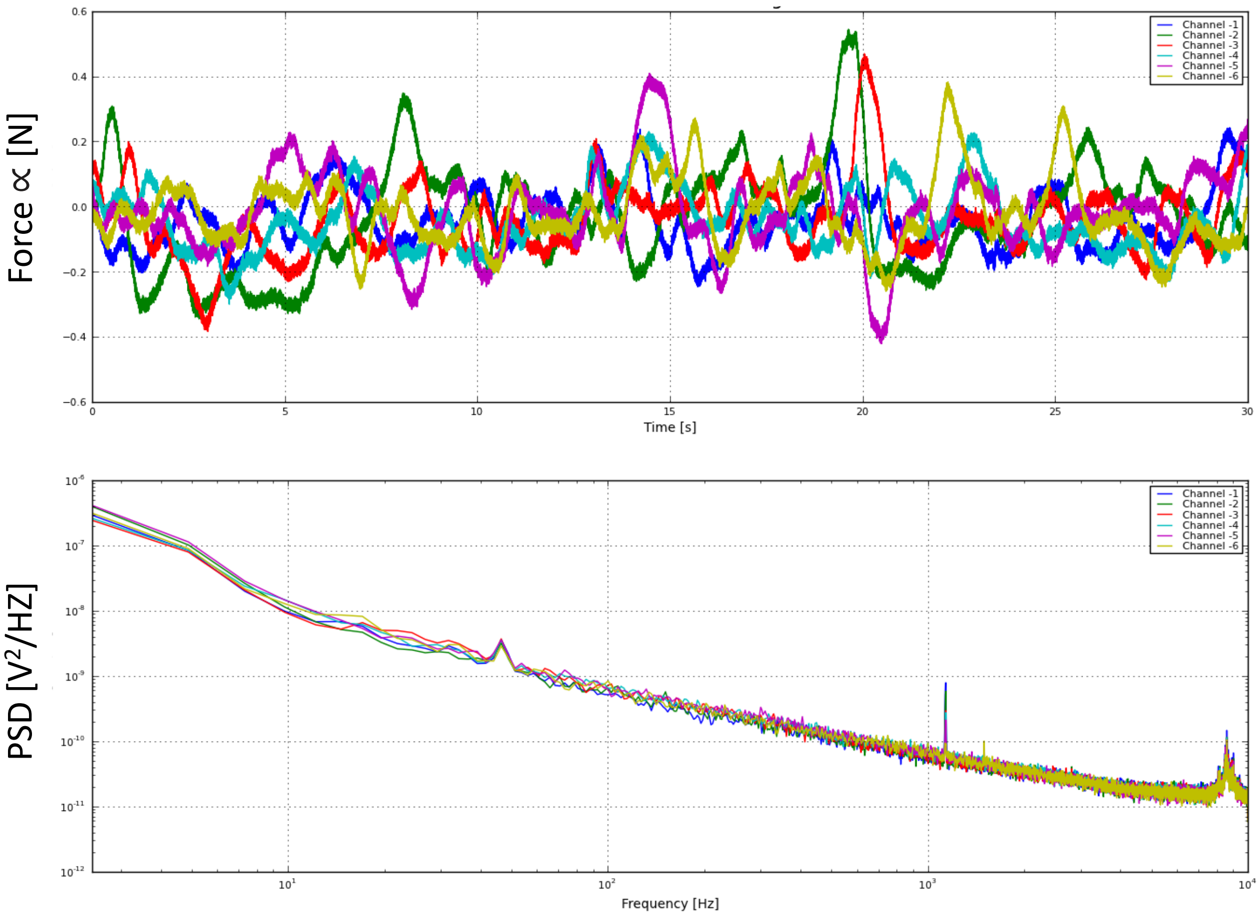

B-7: Verification Measurements

MAPPER lithography

A-7.2: Additional verification measurement performed on Forcesix

Individual Piezo Sensors – installed (no casing)

SENSOR SIGNAL IN TIME & FREQ. DOMAIN

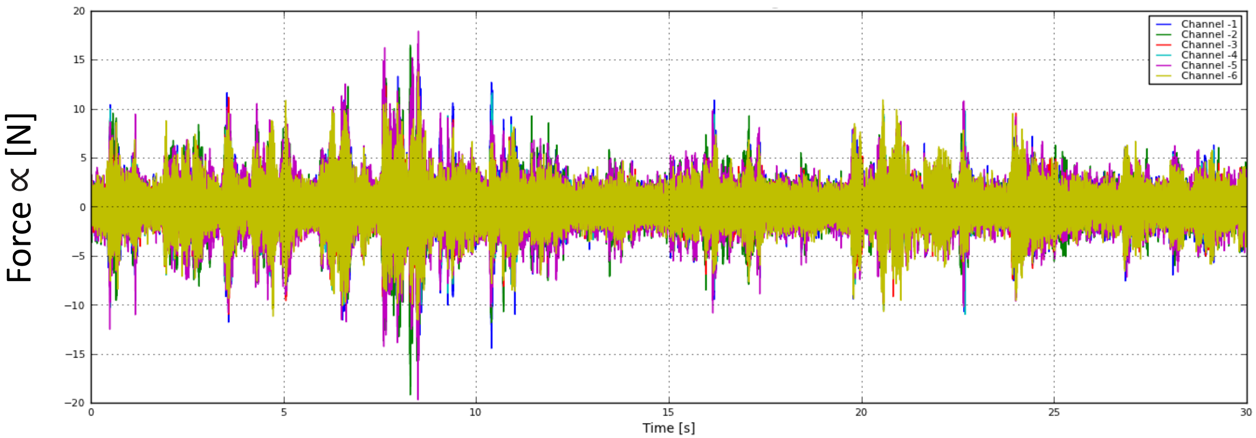

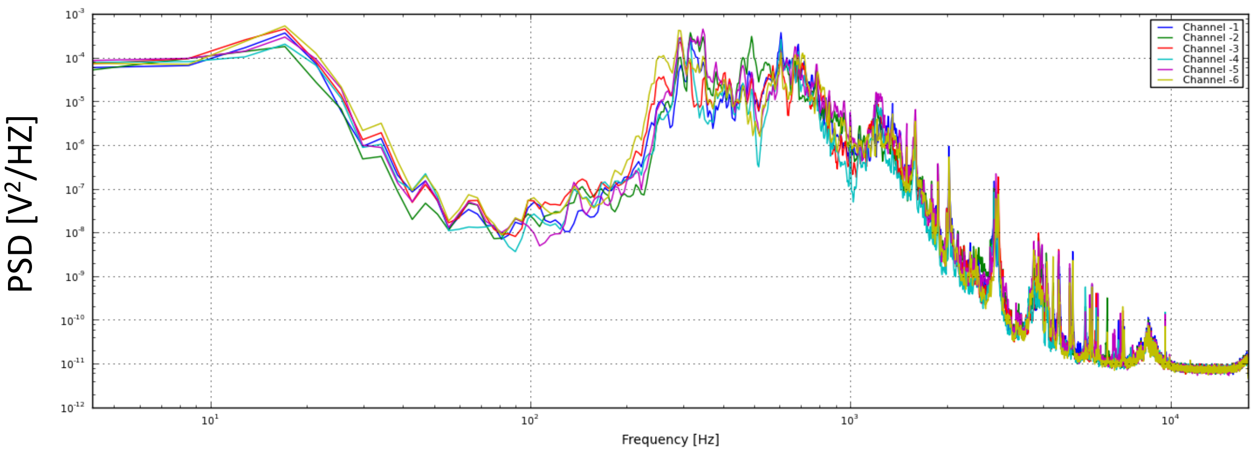

B-7: Verification Measurements

MAPPER lithography

A-7.2: Additional verification measurement performed on Forcesix

Individual Piezo Sensors – installed (casing)

SENSOR SIGNAL IN TIME & FREQ. DOMAIN

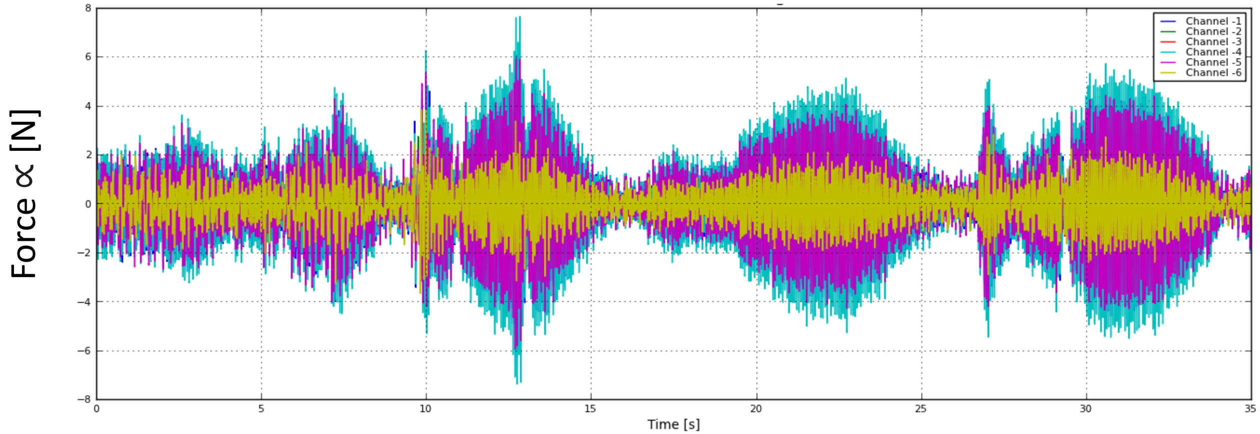

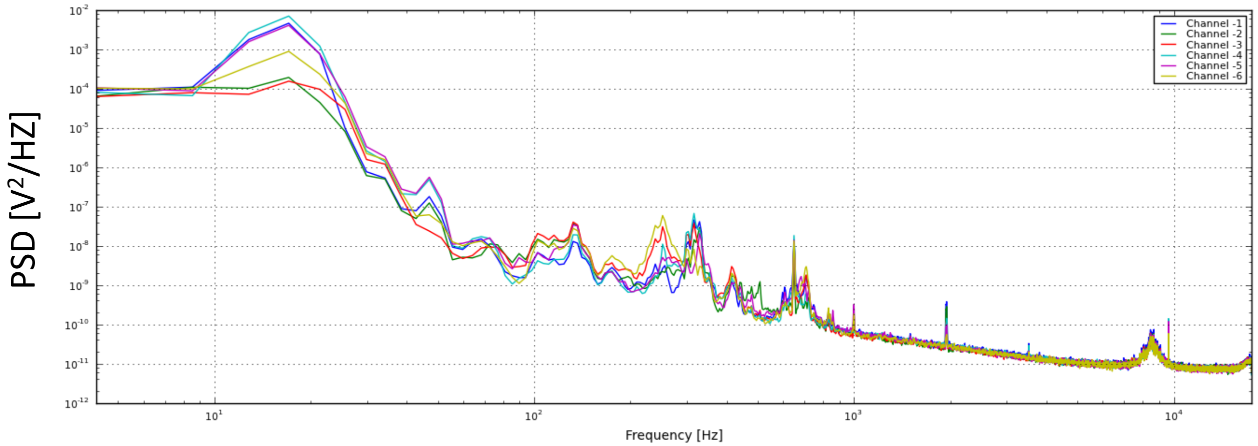

MAPPER lithography

A-7.3: Additional verification measurement performed on Forcesix

Sound pressure measurements – microphone environment

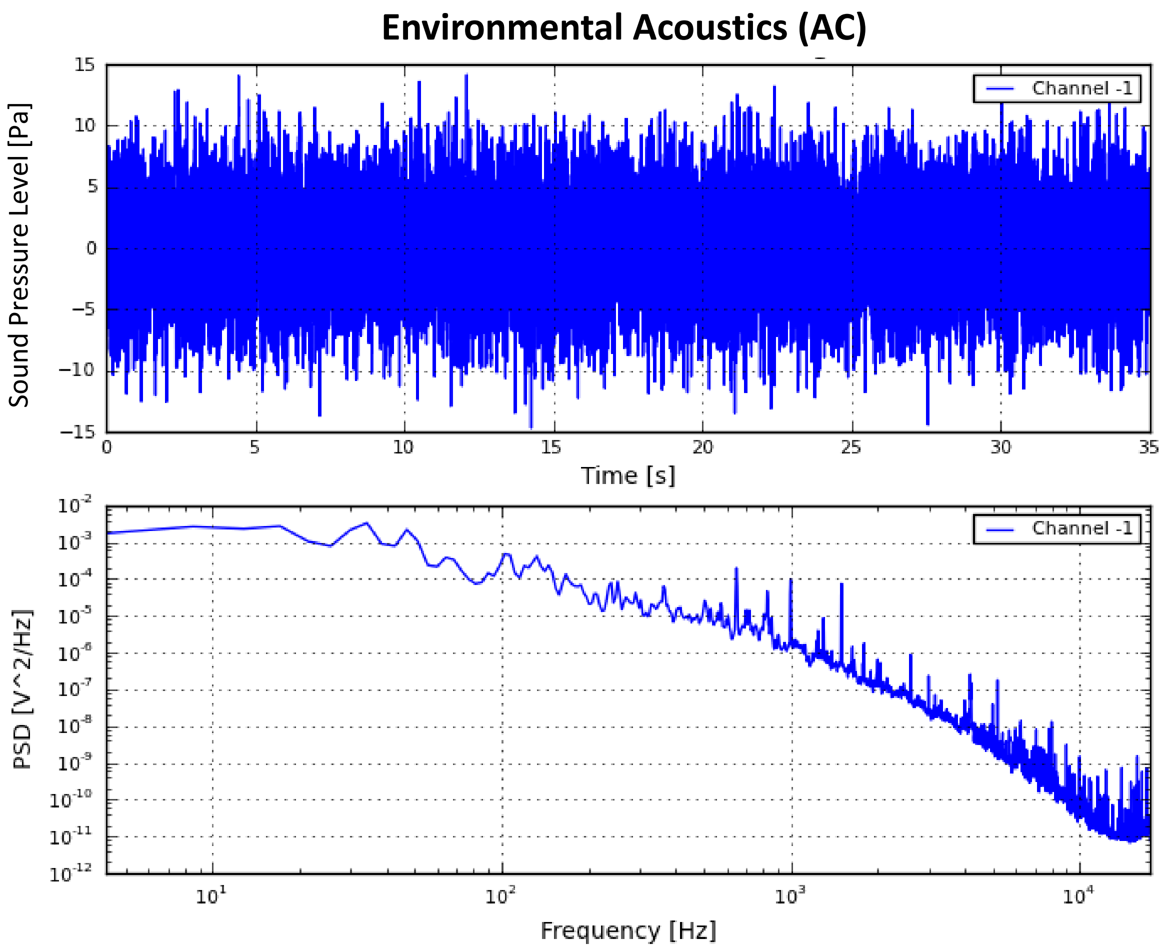

A-7.3: Additional verification measurement performed on Forcesix

Sound pressure measurements – microphone inside acoustic enclosure

Acoustic level inside Forcesix (ACi)

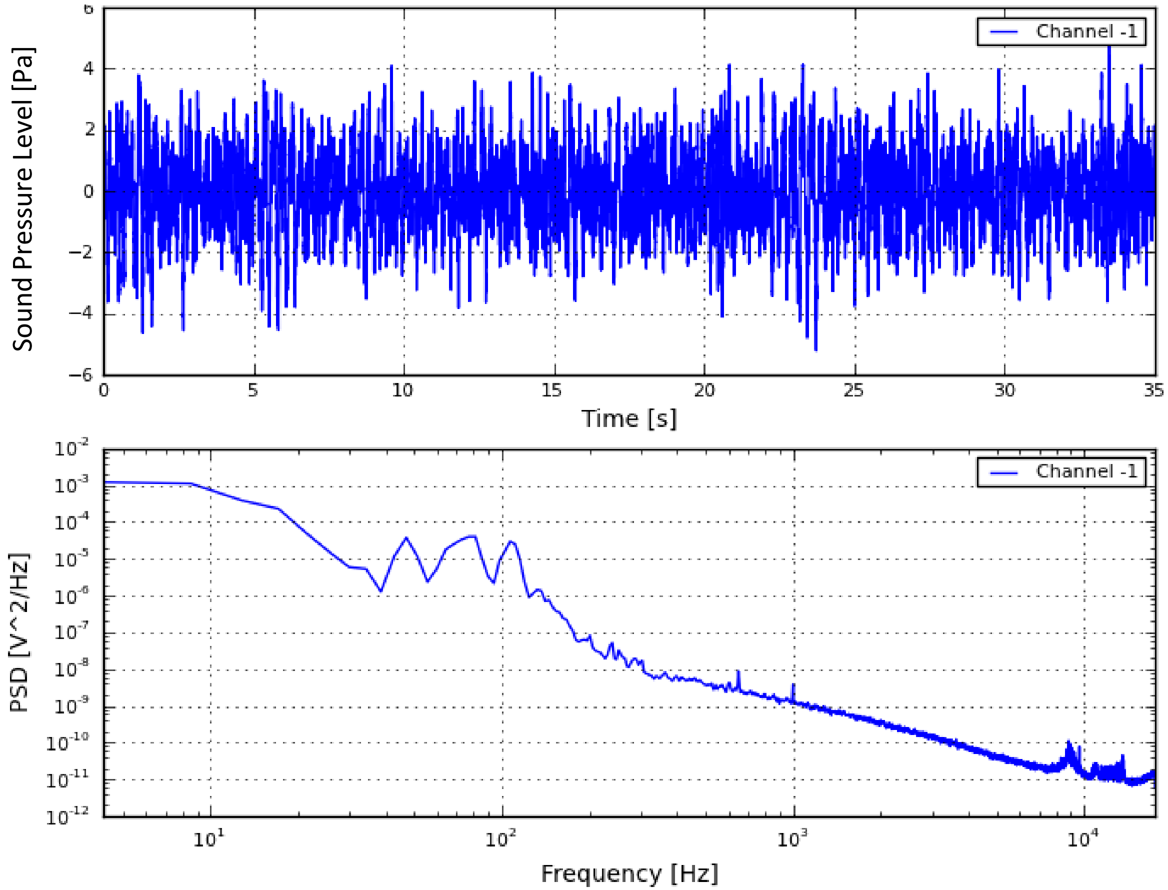

B-7: Verification Measurements

A-7.3: Additional verification measurement performed on Forcesix

Sound pressure measurements – attenuation ratio outside/inside Forcesix casing

The below graphs draw a comparison between the acoustic attenuation of the **Forcesix cage** (left plot) and the **Vibronix cage** (previous test setup, result of the work by Dennis Lakerveld; right plot) Interpretation of improvements is given here.

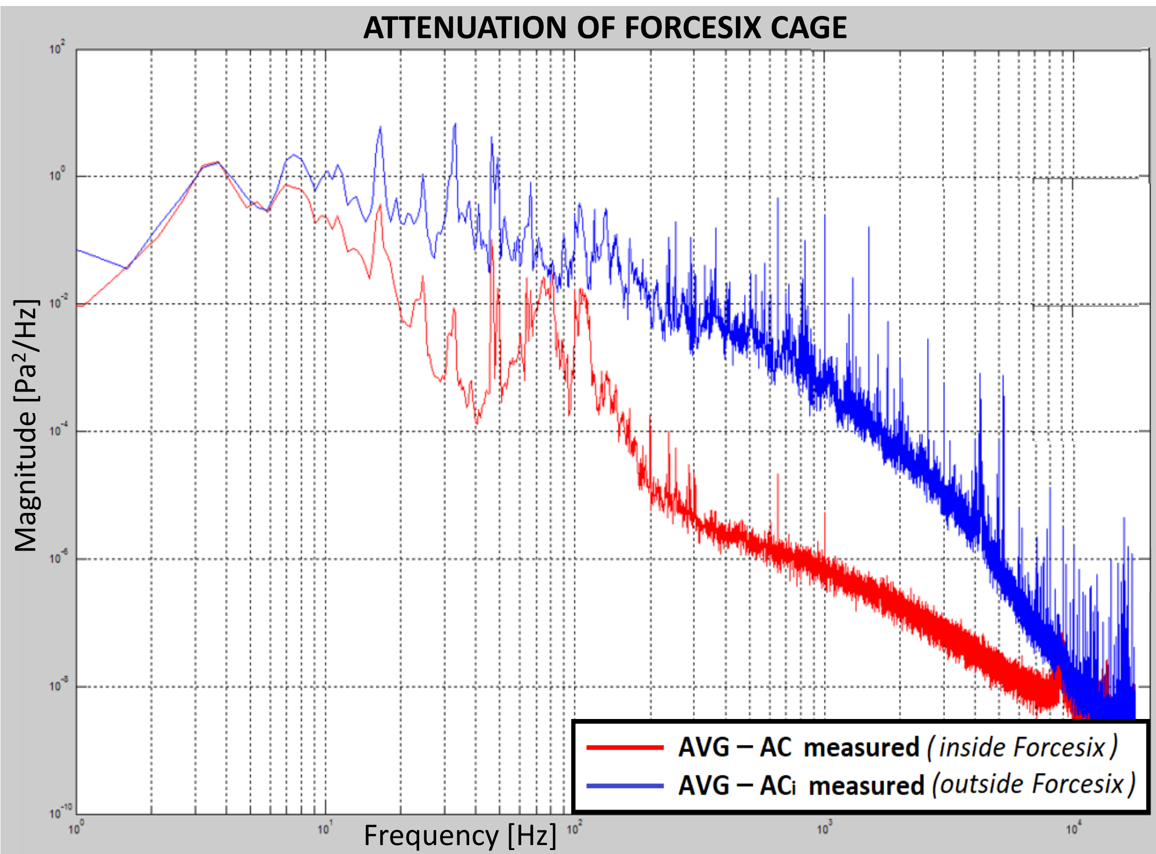

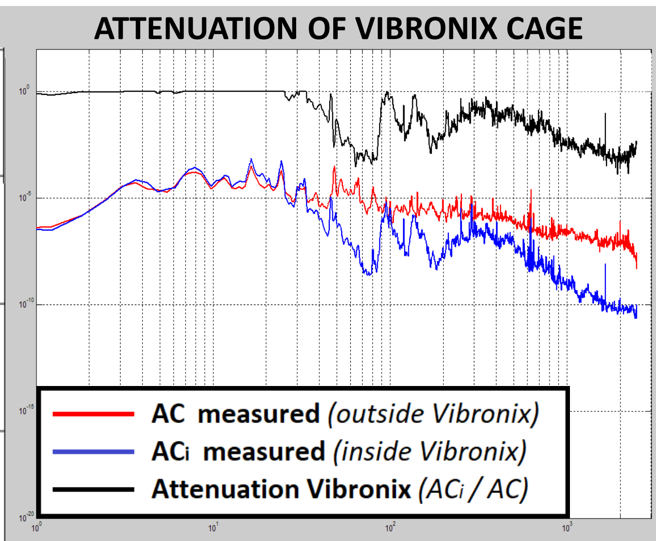

B-7: Verification Measurements

A-7.4: Additional (flow) verification measurement performed on Forcesix

POS Module Installed – hydrostatic water supply by means of pressure vessel

The below graphs show the sensor signal in the **time domain** (top graphs) and the **frequency domain** (bottom graphs) comparing **reference measurements** (no flow) with **flow measurements**. In both cases the POS module is installed whose nominal flow rate is 0.33 L/min. This is still uncorrected for sensitivity, gain, transformation matrix and unity spectral force characteristics. The clear increase in input that can be seen gives confidence that the setup can distinguish FIV forces from background noise and therefore that the measurements are reliable.

REFERENCE MEASUREMENT (no flow)

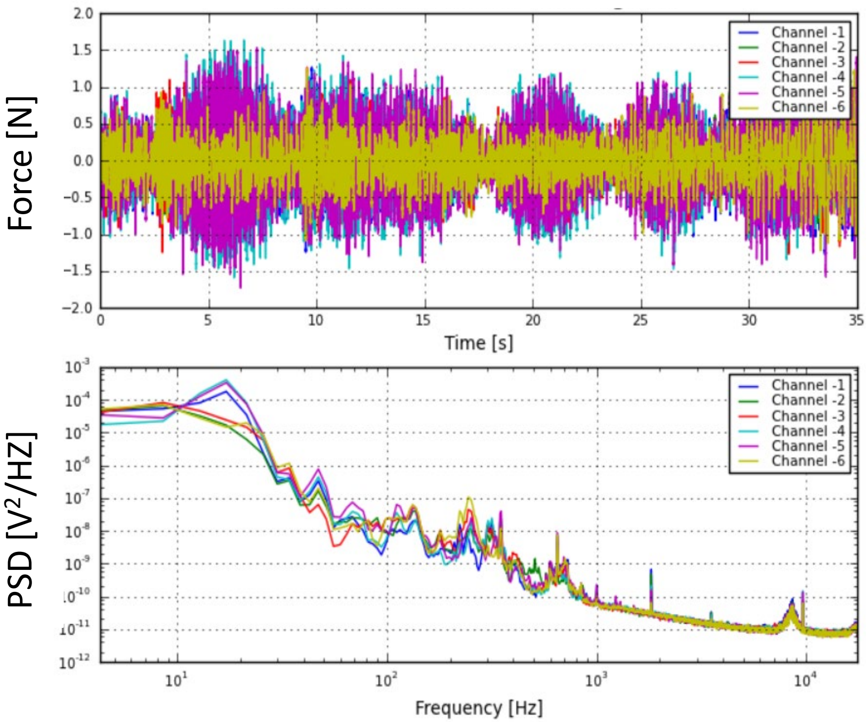

FLOW MEASUREMENT (0.1 L/min)

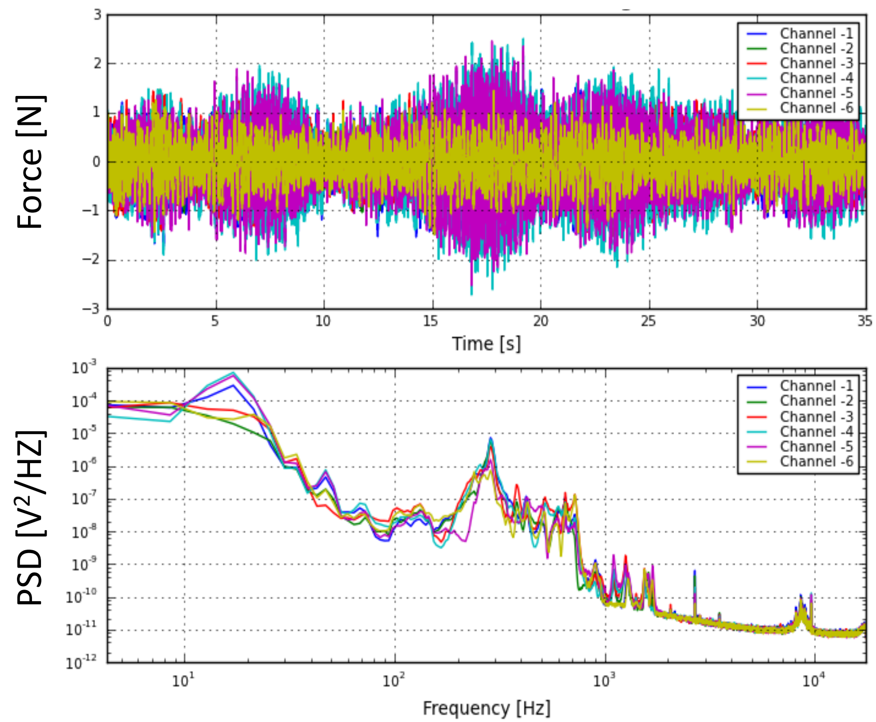

B-7: Verification Measurements

MAPPER lithography

A-7.4: Additional (flow) verification measurement performed on Forcesix

ABC Module Installed – hydrostatic water supply by means of pressure vessel

The below graphs show the sensor signal in the **time domain** (top graphs) and the **frequency domain** (bottom graphs) comparing **reference measurements** (no flow) with **flow measurements**. In both cases the ABC module is installed whose nominal flow rate is 3.0 L/min. This is still uncorrected for sensitivity, gain, transformation matrix and unity spectral force characteristics. The clear increase in input that can be seen gives confidence that the setup can distinguish FIV forces from background noise and therefore that the measurements are reliable.

REFERENCE MEASUREMENT (no flow)

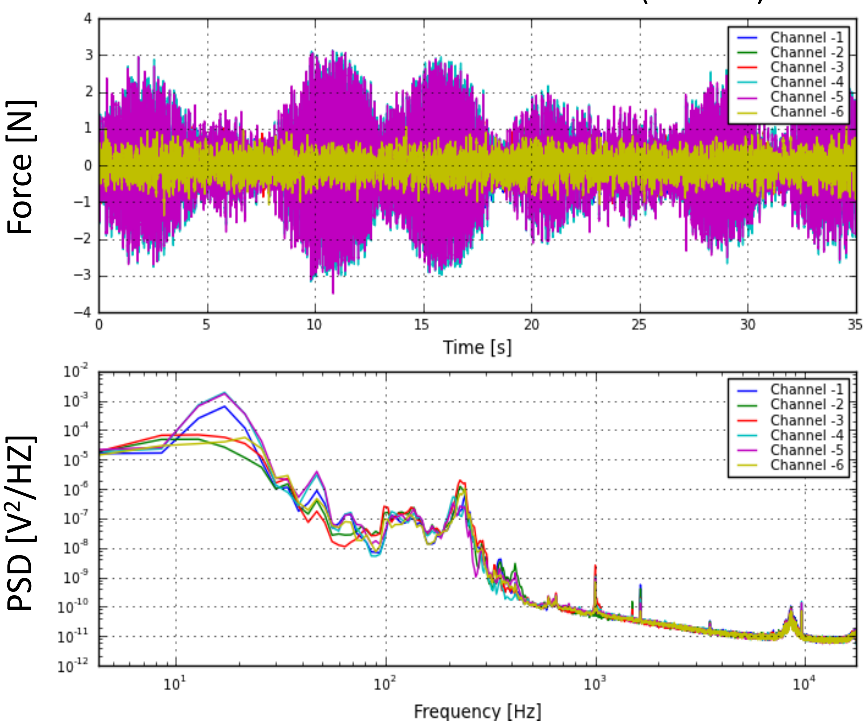

FLOW MEASUREMENT (1.5 L/min)

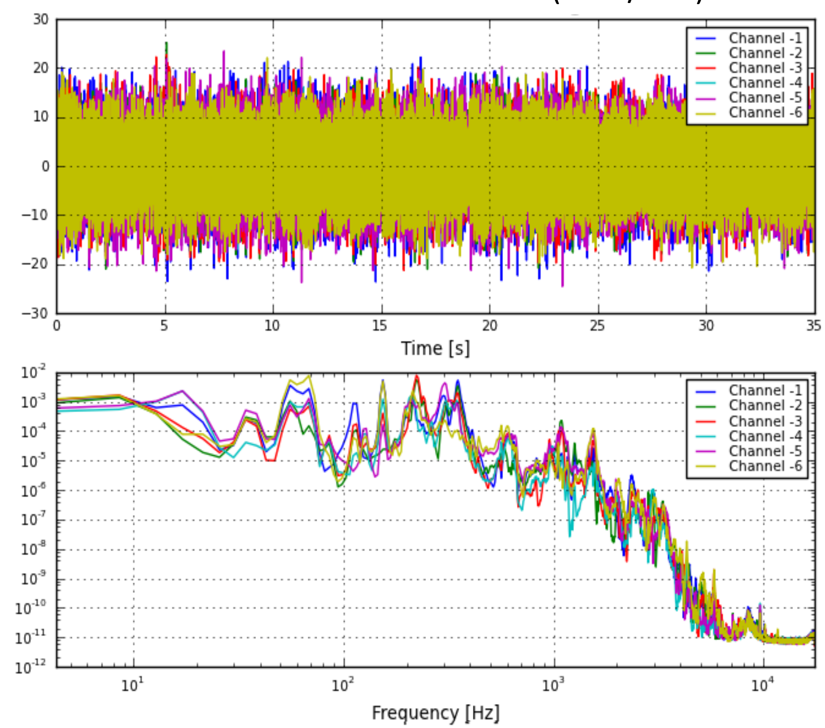

B-7: Verification Measurements

MAPPER lithography

A-7.4: Additional (flow) verification measurement performed on Forcesix

BSW Module Installed – hydrostatic water supply by means of pressure vessel

The below graphs show the sensor signal in the **time domain** (top graphs) and the **frequency domain** (bottom graphs) comparing **reference measurements** (no flow) with **flow measurements**. In both cases the BSW module is installed whose nominal flow rate is 5.2 L/min. This is still uncorrected for sensitivity, gain, transformation matrix and unity spectral force characteristics. The clear increase in input that can be seen gives confidence that the setup can distinguish FIV forces from background noise and therefore that the measurements are reliable.

REFERENCE MEASUREMENT (no flow)

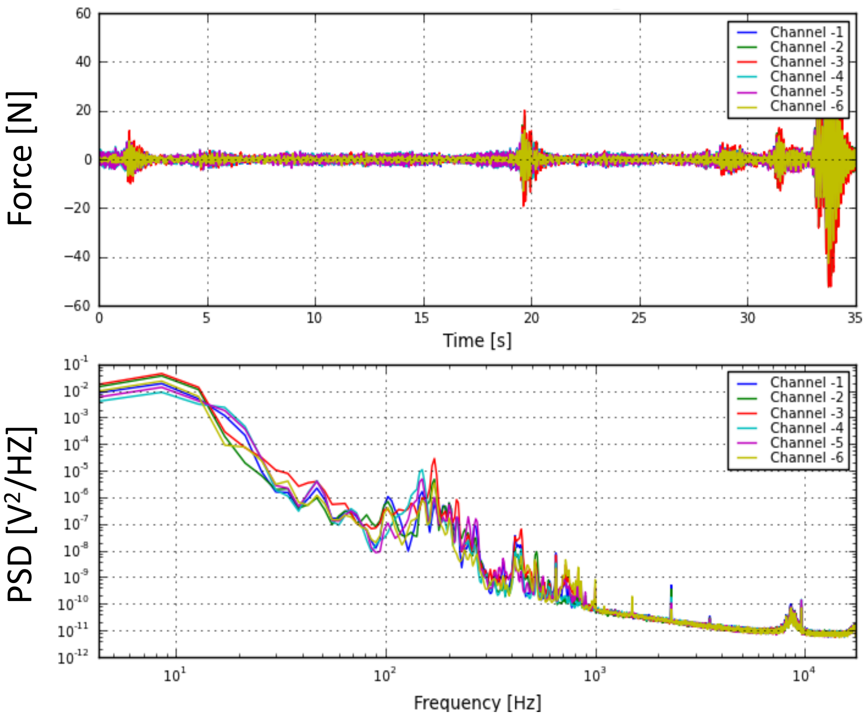

FLOW MEASUREMENT (5.2 L/min)

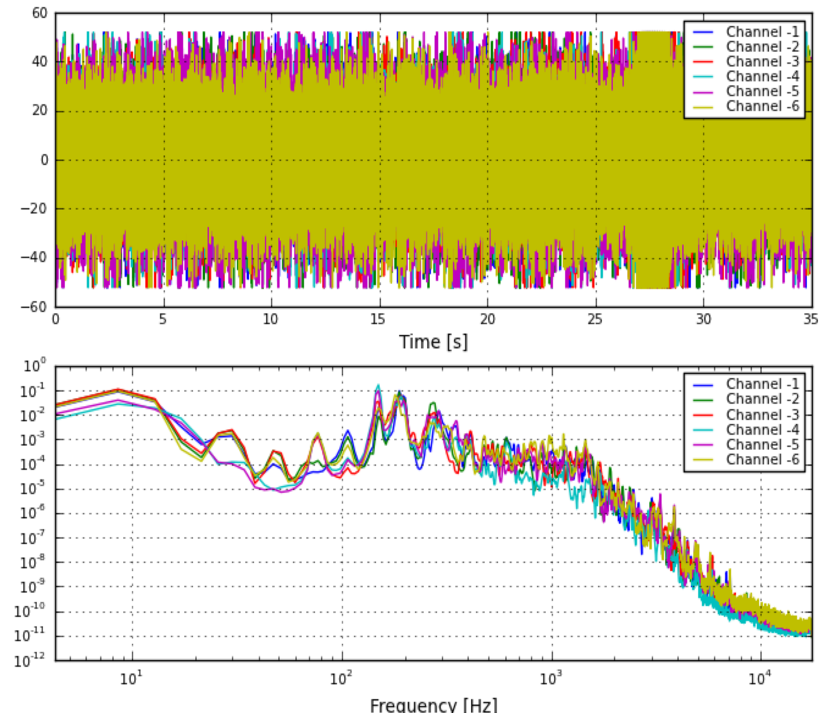

App. C

Design Details

C-1: Substantiating Design Choices

C.1.1: Modeling different mitigation strategies to limit the effect of floor vibrations

Determining the number of vibration isolation stages required for concept B

The graph below-left shows the measured forces due to ground accelerations, filtered by 0, 1 or 2 vibration isolation stages. The red line is the force-requirement spectrum (FRS) which should be observable; therefore a 2 MSD system is necessary. This is calculated with the transmissibility characteristic in Z (no crosstalk) of a single- or double MSD system (i.e. slope of -1 or -2).

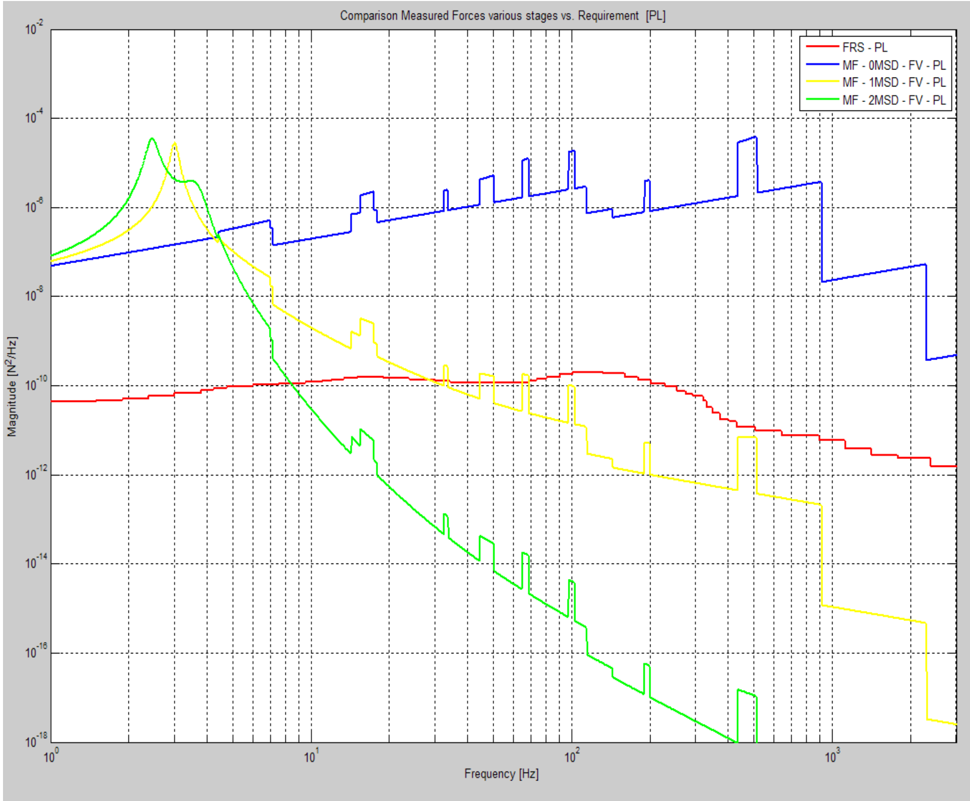

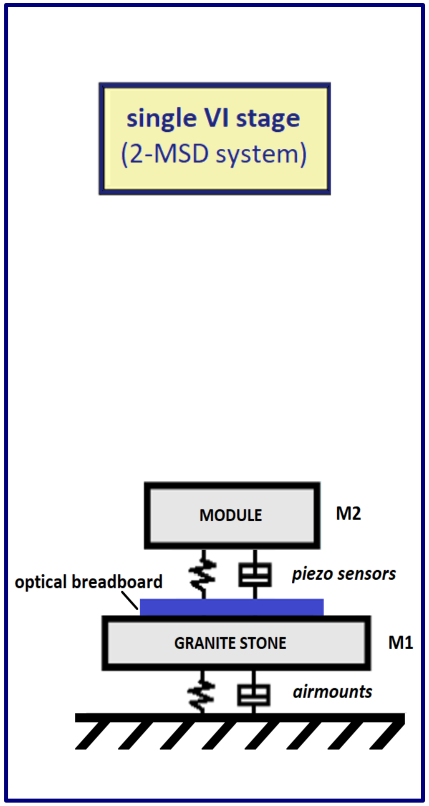

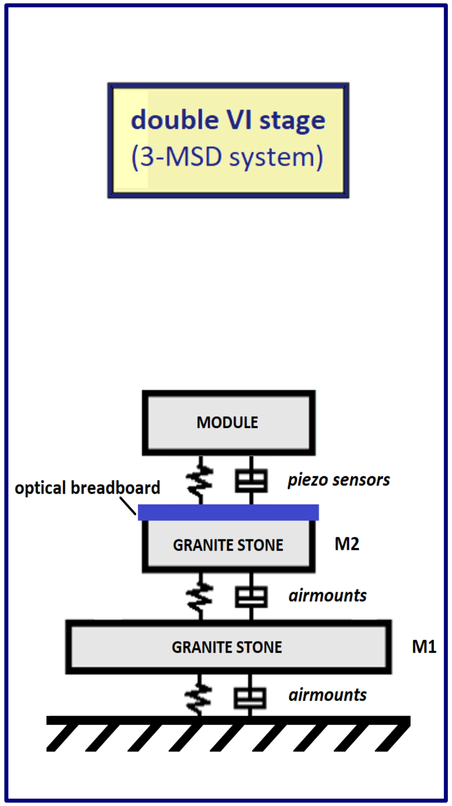

C-1: Substantiating Design Choices

C.1.2: Modeling different mitigation strategies to limit the effect of acoustics

Determining how to connect the acoustical casing for concept B

The following graphs shows the measured forces due to environmental acoustics, when an acoustical enclosure is rigidly mounted to either the top mass or the bottom mass. This is one of the vibration isolation stages to which the sound pressure input is discharged, causing it to accelerate. The **red line** is the force-requirement spectrum (FRS) for the BSW module in Z-direction i.e. the noise level that needs to be observable.

The **blue** and **green** line represent the measured forces by the piezos, only calculated different. The blue line looks at the relative displacement of a 2-MSD system and multiplies this with the piezo stiffness, whereas the green line accounts for the whole triple MSD system and parallel stiffnesses present (a more thorough approach). It can be seen that when accelerations are relatively large (high DDF), a significant difference arises and the complete system (3-MSD) needs to be considered.

Conclusion: to effectively shield-off environmental acoustics, an acoustical enclosure is required that rigidly connects to M1 (the bottom VI stage).

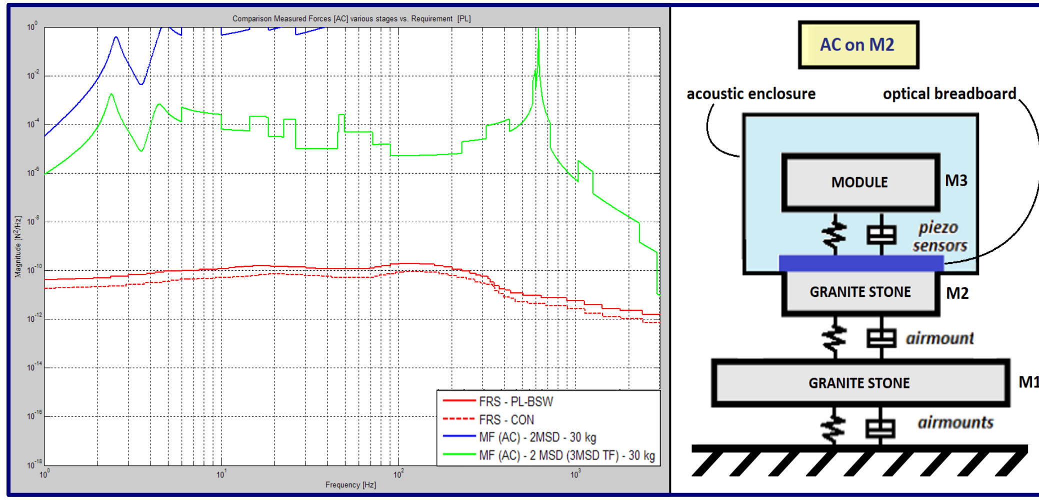

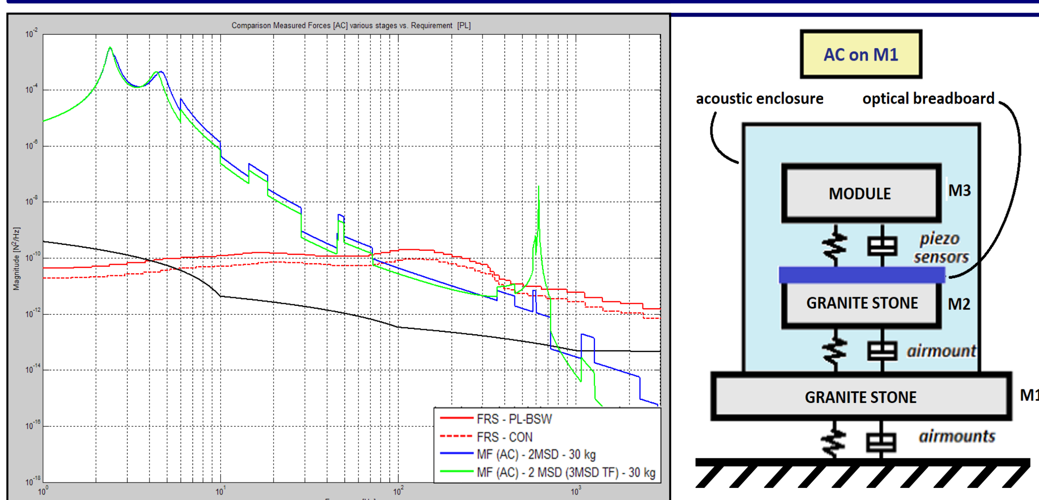

C-1: Substantiating Design Choices

MAPPER lithography

C.1.3: Modeling different mitigation strategies to limit the effect of FIV in supply tubing

Determining how to disconnect the Ariaform TPU tubing to the VI platform for concept B

Four configurations have been modeled in Matlab to investigate how the FIV induced in the supply tubing (despite all countermeasures) can be discharged most effective. Also it is looked into how best to connect the supply tubing rigidly to the various stages of the VI platform. The two most relevant systems are shown here, with model variations discussed on the next slide.

CONFIGURATION 1

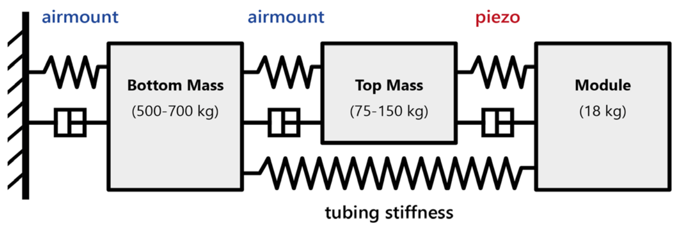

CONFIGURATION 2

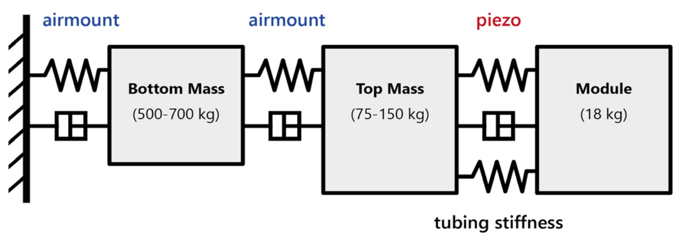

In the corresponding graphs on the right, the **red line** indicating the (unwanted) measured signal due to tubing stiffness and the **black line** the requirement that needs to be verified (FRS). The **blue line** is the result for the acceleration concept (A) which shows to be more sensitive to parasitic stiffnesses.

Clearly, #2 trumps #1 as it makes most effective use of the high axial stiffness of the piezos, whereas configuration 1 allows for a transfer path towards movement of the middle mass, affecting relative movement between M2-M3.

CONFIGURATION 1

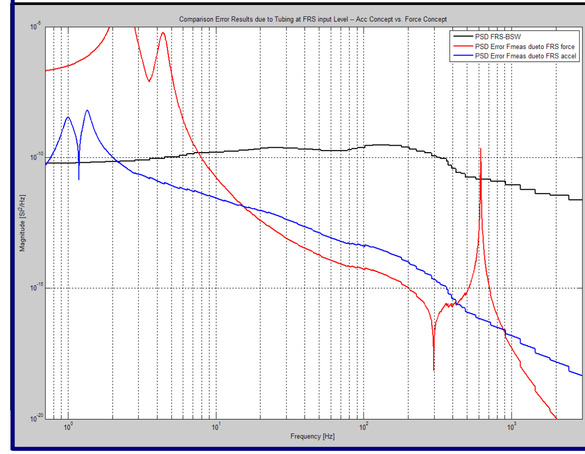

CONFIGURATION 2

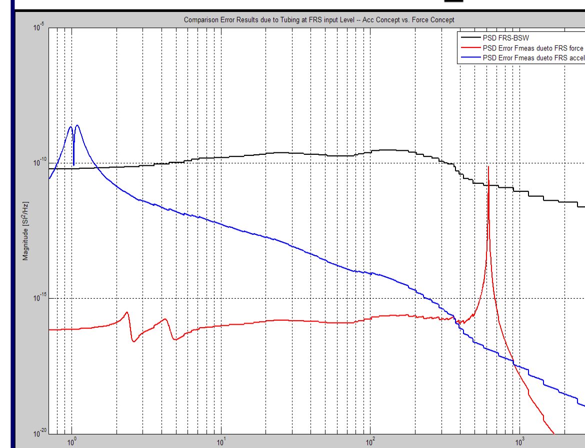

C.1.3: Modeling different mitigation strategies to limit the effect of FIV in supply tubing

.. continued ..

Configuration 3 and 4 are shown on the right, which are essentially extensions of the 3-MSD system representing the reaction-force concept (B). These options account for the mass of the water inside the flexible tubing. This would make the concept a 4-MSD system where Ktube acts between **M2-M3** or between **M3-CASE**. To model this, the cooling water has been determined to weigh about half a kilo. Also the stiffness of the (pressurized) tubing has been estimated, as follows:

- Ktube: 200 N/m (XYZ: 200 / 50 / 50 N/m)
- Mtube: 0.47 kg

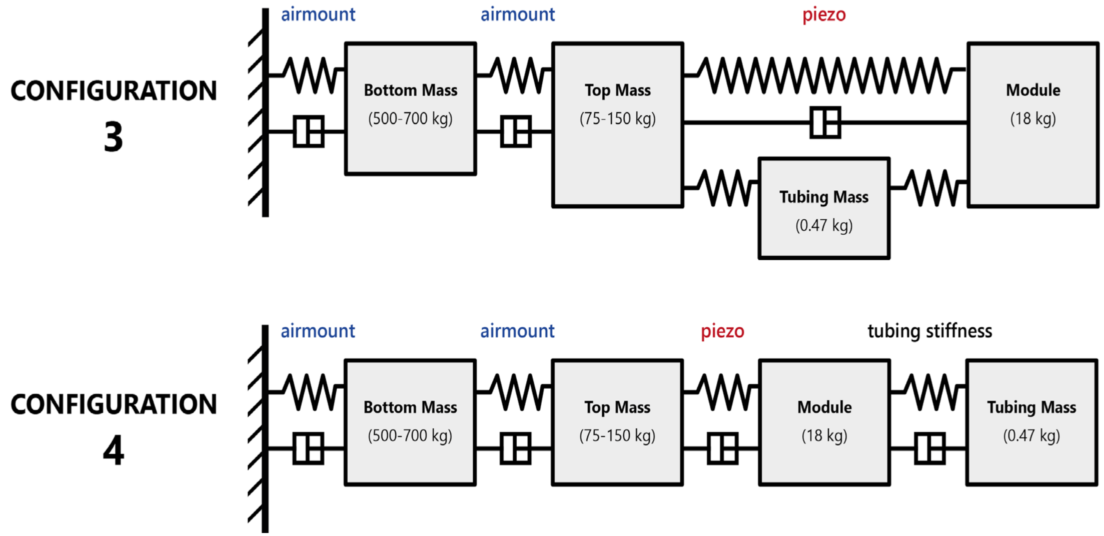

Transfer functions of these situations show that in both cases the stiffness of the tubing is insignificant to the stiffness train of the piezo that has been achieved. This mass causes spikes in the response but only becomes prominent from higher stiffness values (≥ 5000 N/m) and higher mass values (≥ 3 kg). No graphs are shown because they are identical to the response of **configuration 2**, given the relatively low mass and stiffness value achieved. Also this proofs that keeping the tubing length limited to 30 cm from M2 to the module under testing, is beneficial from a parasitic resonance point-of-view (besides obviously reducing FIV induced in the tubing)

C-2: Dynamical Behavior of Forcesix

MAPPER lithography

C.2.1: Modeling the final design as a triple mass-spring-damper system

Describing the response by analytically derived transfer functions

The above representation of the final design as a triple MSD system has been used to analytically derive transfer functions necessary to comprehend the dynamical behavior of Forcesix well. Also anomalies in the response can be timely identified.

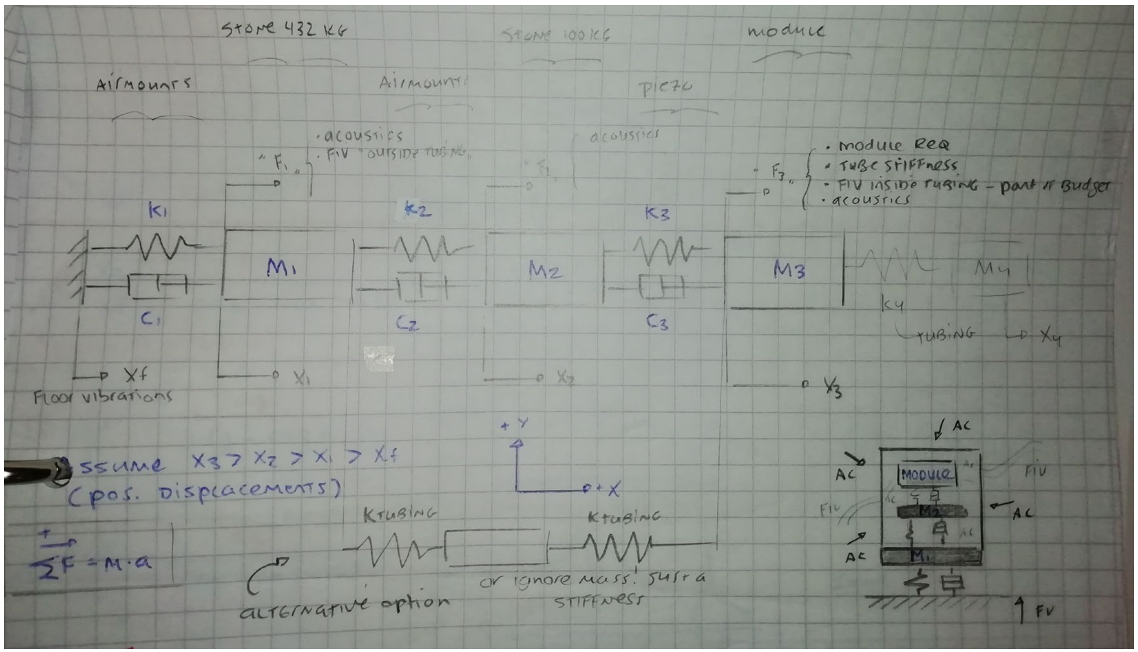

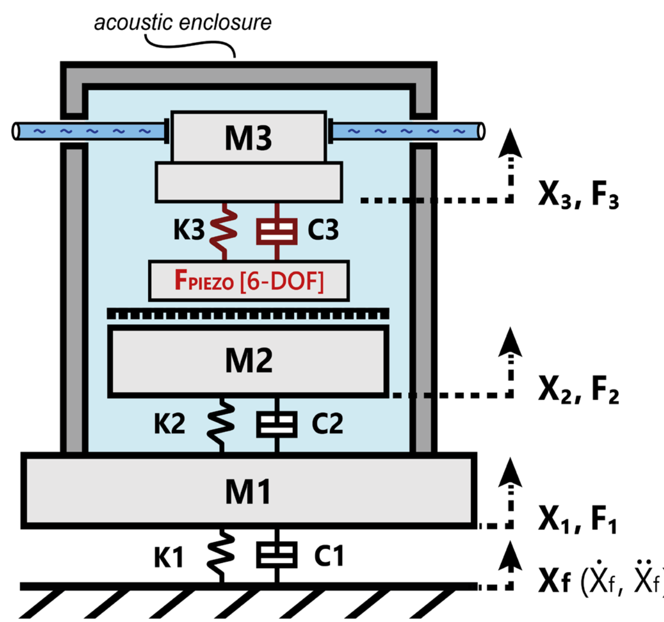

In this schematic, **M1** is the bottom granite stone + acoustic cage weighting **644.5 kg**. Next, **M2** **(113.7 kg)** stands for the 2nd stage of the vibration isolation platform i.e. a granite stone + optical breadboard + base frame. Both masses are supported by airmounts with stiffnesses k1 & k2 and verified damping values c1 & c2. Lastly, **M3** **(6.8-14.3 kg)** represents the module under testing which is rigidly attached to the Module Support Frame (MSF). This top mass is carried by 6 piezo sensors (k3, c3) that connect to M2. The free-body-diagram drawn will be used to set up the Equations of Motion (EOM) next.

C-2: Dynamical Behavior of Forcesix

MAPPER lithography

C.2.2: Manually deriving Equations of Motion (EOM)

Describing the response by analytically derived transfer functions

Using Newton's second law $\sum F = k \cdot x + c \cdot v + m \cdot a$ and assuming a net positive displacement (x3>x2>x1>xf), the following EOM can be derived in the time domain and transformed to the frequency domain using Laplace:

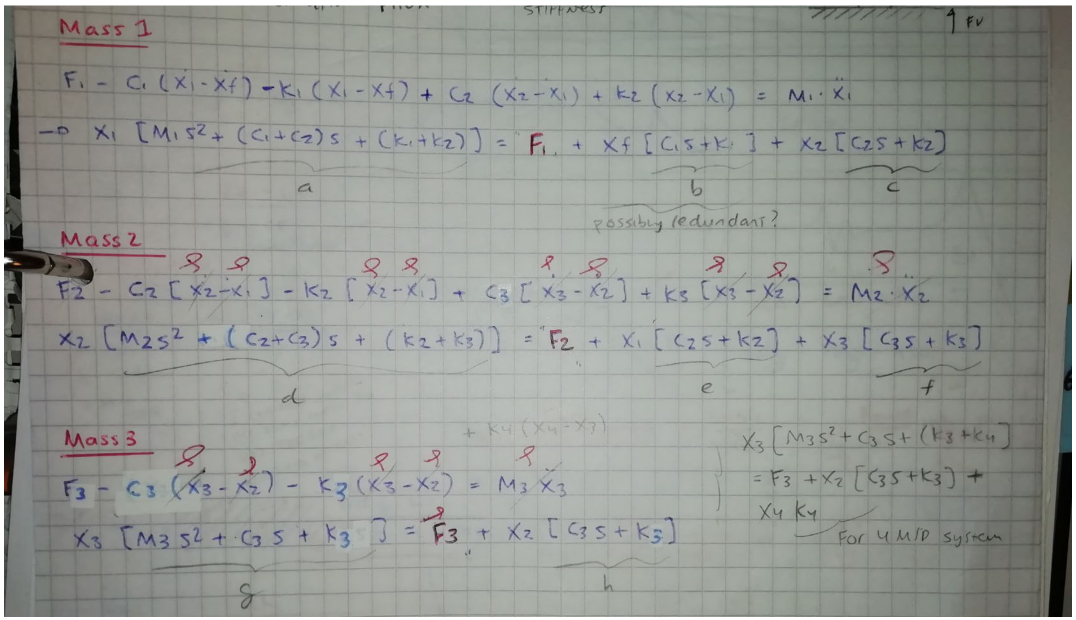

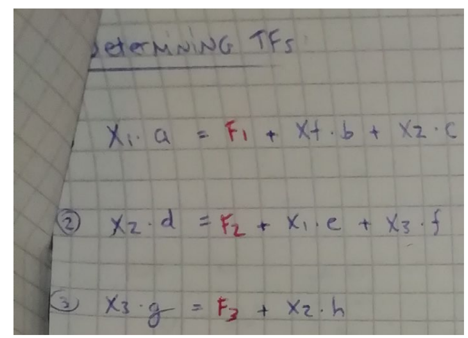

However, with 7 unknown variables and 3 EOMs, the system is undetermined. Assuming Xf = F1 = F2 = F3 = 0, the set of equations can be solved by expressing x1, x2 and x3 as a function of each other and using substitution (above right). For clarity, the letters a-h have been used to represent recurring dynamics i.e. shorten the expressions.

Note that the effect of identified disturbances which are injected at various stages has been modeled individually in § 3.4. To gain in-depth insight, the component-to-component transfer functions are derived manually here.

C-2: Dynamical Behavior of Forcesix

C.2.3: Important compliance & transmissibility transfer functions

Describing the response by analytically derived transfer functions

Using the letters a-h, it becomes possible to write out the various compliance & transmissibility relations concisely. This gives insight in the differences between elements present *only* in the numerator that lead to specific (anti)-resonances. All transfer functions have been modeled and verified in Matlab & 20-SIM as well.

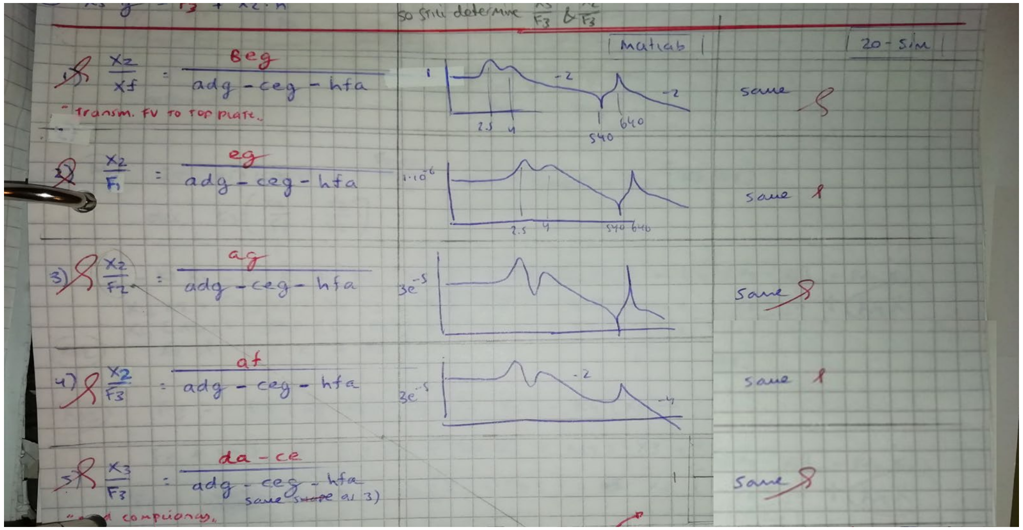

The general trend that can be observed for all responses is the low frequency cut-off of the airmounts of the VI-platform after their eigenfrequencies at 2,5 Hz & 4.0 Hz. This is followed by a decay in the response (-2 slope) until the BSW module starts to resonate on the stiffness of the piezo sensors at about 640 Hz. Apart from expressions that relate to the direct-disturbance forces (DDF) acting on the module (i.e. cooling vibrations), an anti-resonance is present at 540 Hz. This can be interpreted as isolation of the movement of the second VI-stage (M2) due to M1 and M3 acting in counterphase. The reason this only occurs at a high frequency has to do with the significant weight difference between the granite stone and the MSF+BSW. At these frequencies, the granite stones are already decoupled and thus rely on their inertia to balance the motion (F in phase with acceleration), whereas the MSF is still operating pre-resonance i.e. dominated by spring-behavior (F in phase with displacement).

C-2: Dynamical Behavior of Forcesix

MAPPER lithography

C.2.3: Important transfer functions – *measured force of floor accelerations at varying M3*

Matlab plots of analytically derived FRFs

From § 3.3 it became clear that floor vibrations and acoustics need to be sufficiently suppressed in the design. This requires good insight into the transfer paths present. The figure on the right shows the measured force in response to floor accelerations, for different values of M3.

The dashed line represents the magnitude level $10^0 = 1$ meaning that vibration levels below this line are attenuated, whilst floor accelerations above it are not only observed by the sensors but actually amplified. It can be seen that for all module masses, the graphs are below unity before intersection with y = 10 Hz i.e. start of the [10 – 300] Hz measurement range.

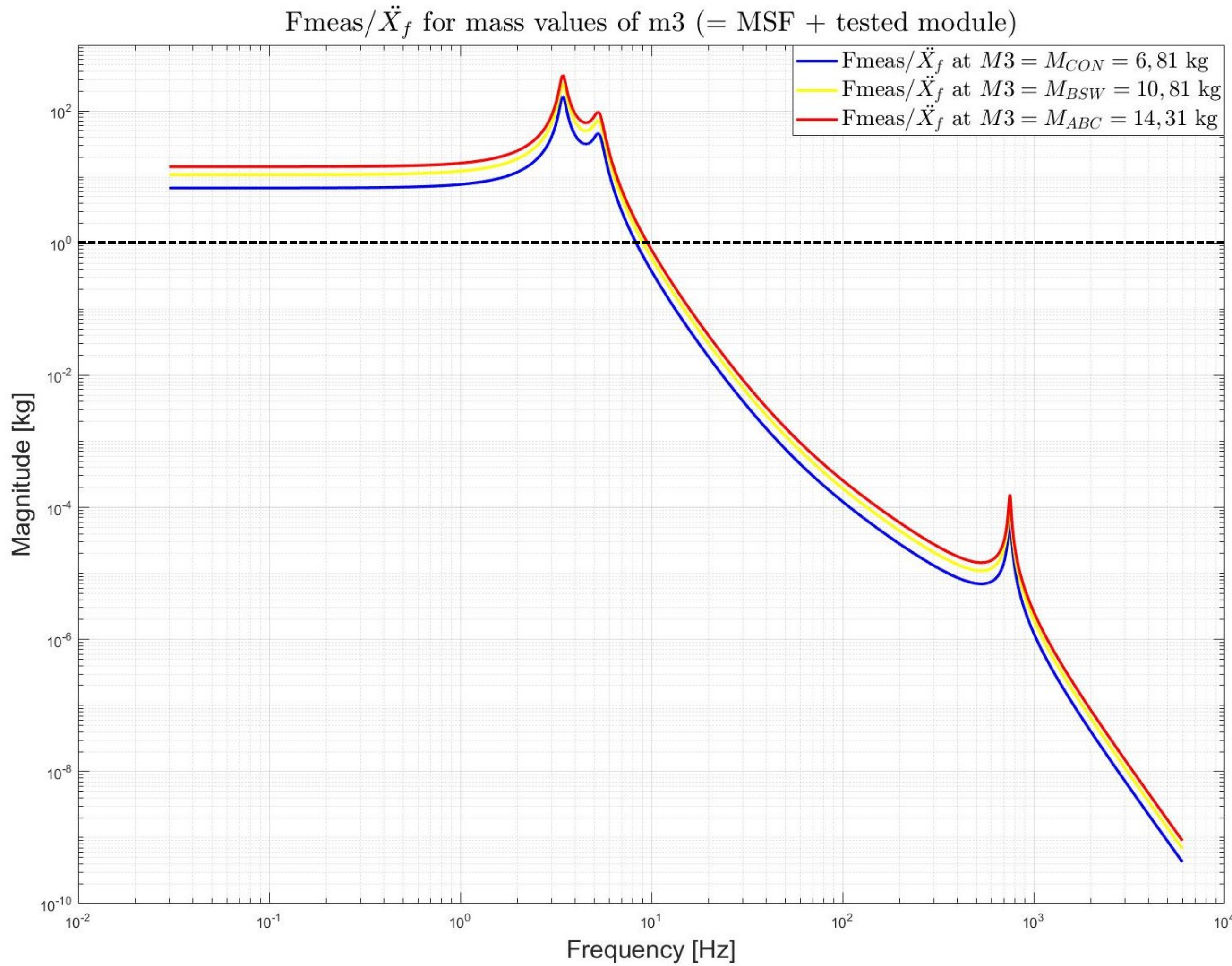

C-2: Dynamical Behavior of Forcesix

C.2.3: Important transfer functions – *compliance/mobility/accelerance responses*

Matlab plots of analytically derived FRFs

Here, the most relevant FRFs related to Forcesix's **disturbance rejection ability** are shown as discussed in § 3.4.4.2.

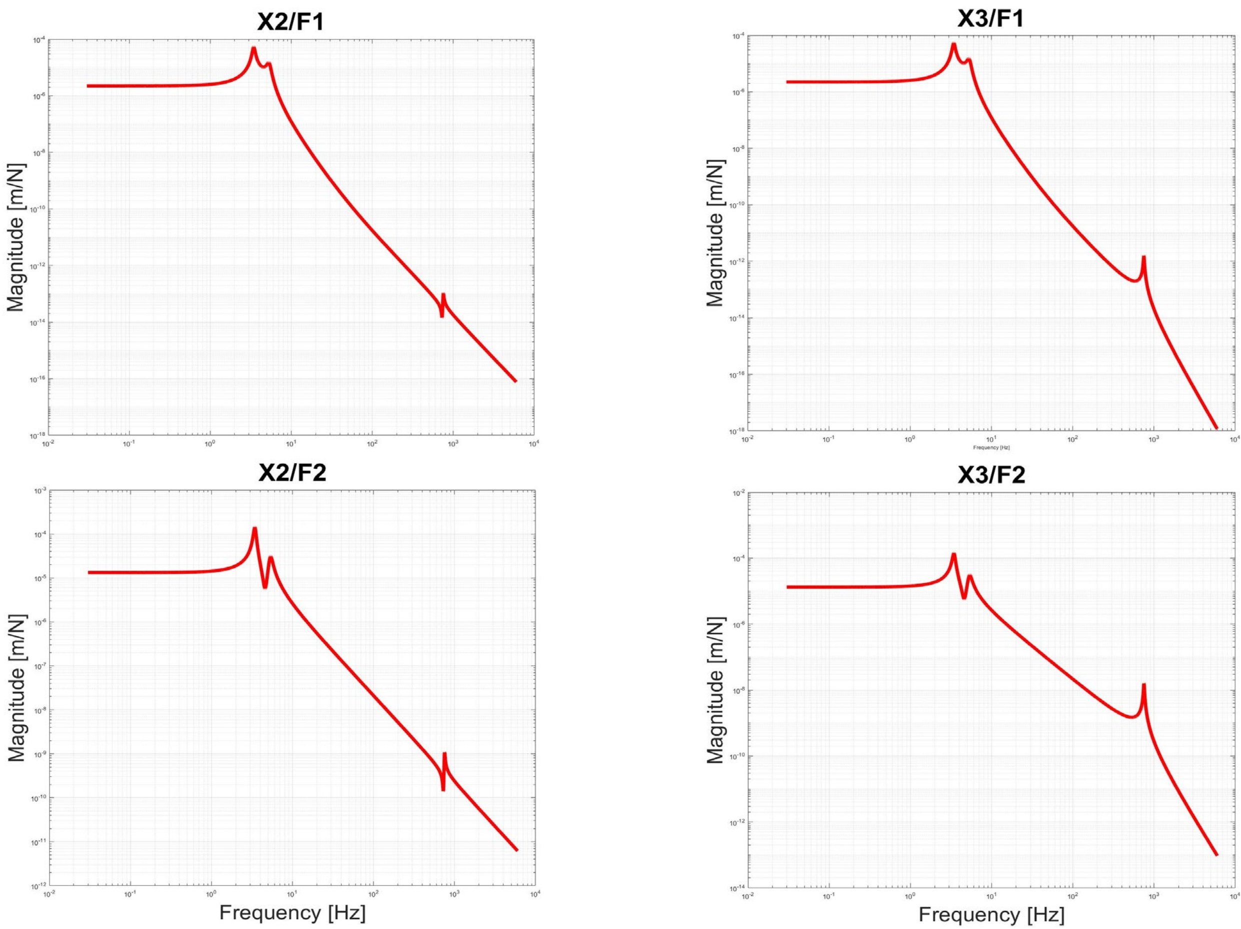

C-2: Dynamical Behavior of Forcesix

C.2.3: Important transfer functions – *compliance/mobility/accelerance responses*

Matlab plots of analytically derived FRFs

Here, the most relevant FRFs related to Forcesix's **disturbance rejection ability** are shown as discussed in § 3.4.4.2.

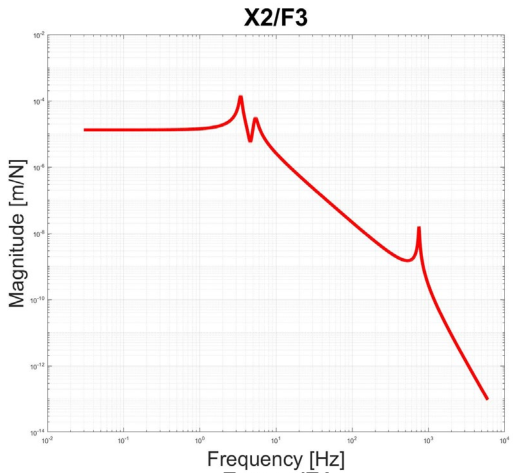

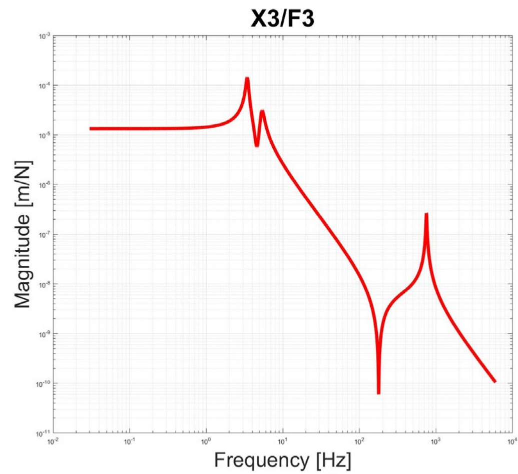

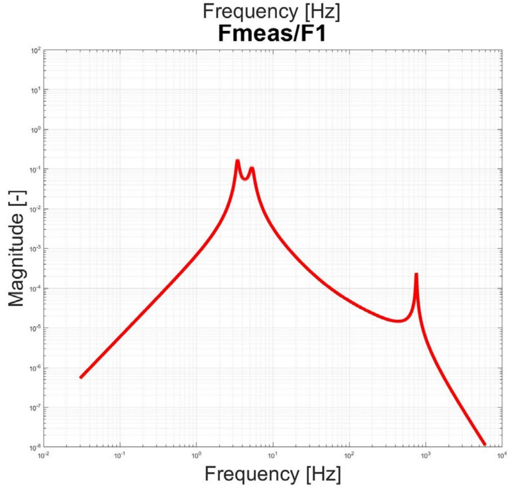

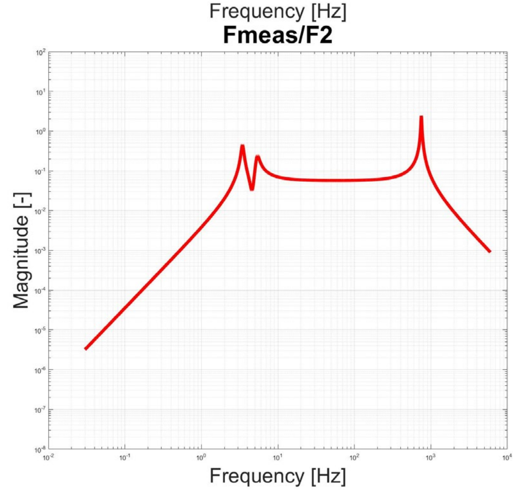

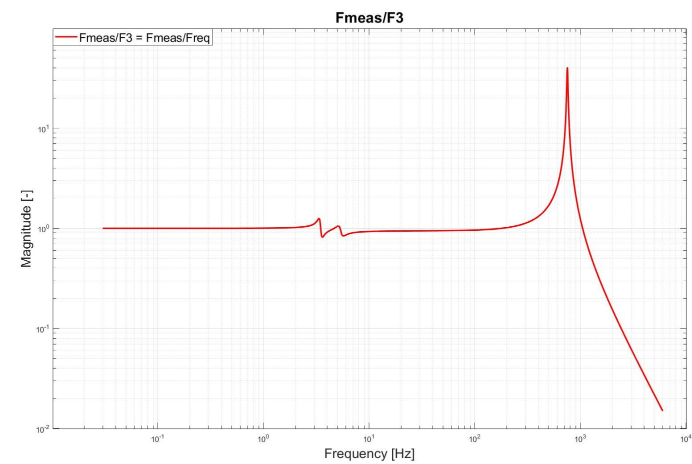

C-2: Dynamical Behavior of Forcesix

C.2.3: Important transfer functions – *input to measured force characteristics*

Matlab plots of analytically derived FRFs

The dashed line represents the magnitude level $10^0 = 1$ meaning that vibration levels below this line are attenuated, whilst input disturbances above it are amplified (severely affecting the observed sensor signal).
It can be seen that very little of the floor accelerations or forces that act on M1 make it through to the sensor signal. DDF that are exerted on M2 (such as FIV in the supply tubing and internal acoustics) have more effect, but are still suppressed by a factor 17 which is enough not to exceed FRS levels over the measurement range of Forcesix [10−300 Hz].

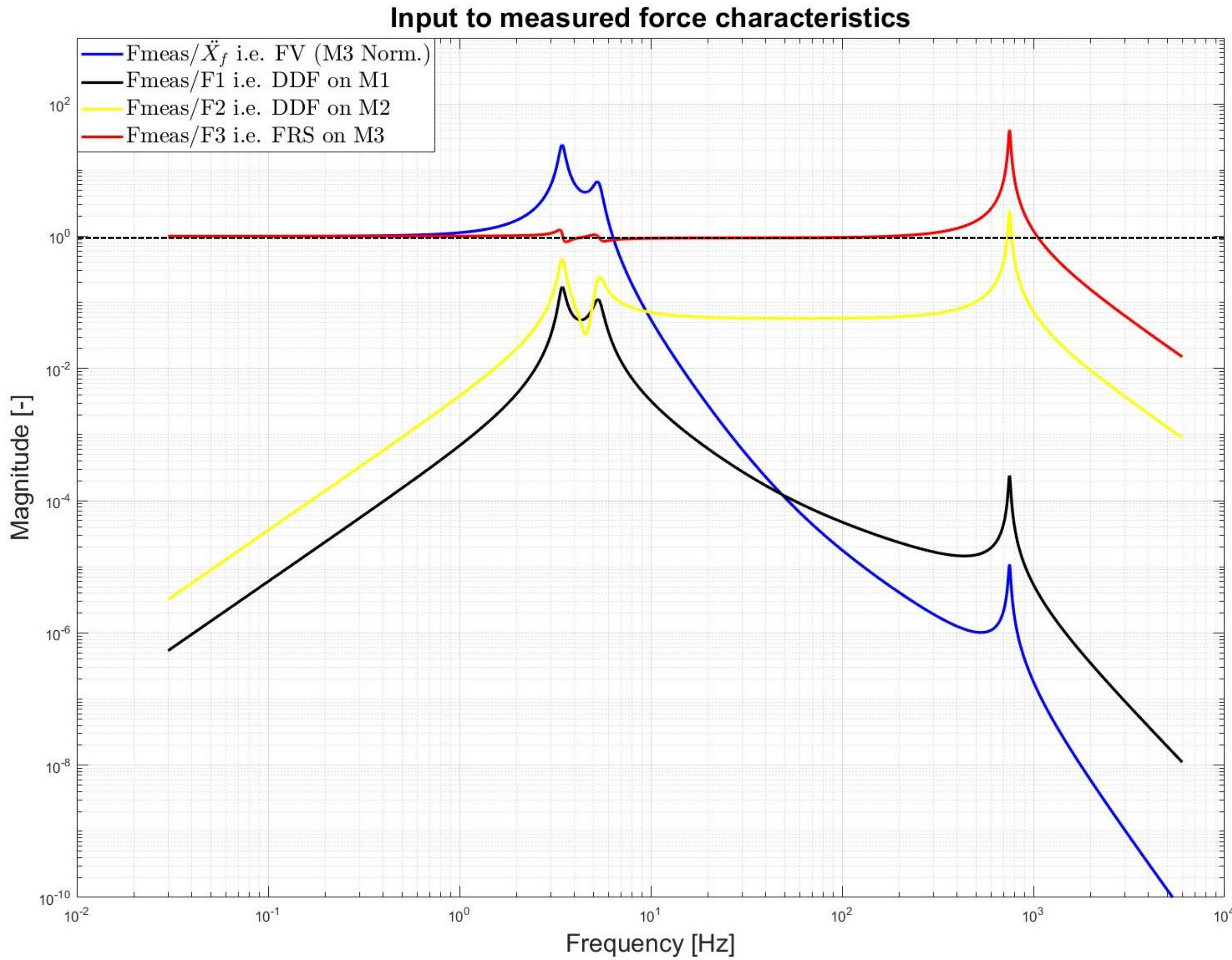

C-2: Dynamical Behavior of Forcesix

C.2.4: Complex plane representation of harmonic motion

Providing insight in the dynamic force balance pre-resonance

The below figure is taken from Rao (2004) and illustrates how the dynamic forces of the EOM that describes the system, balance each other out. It should make comprehension of the transfer functions that describe the effective measurement range of the integrated piëzos, more intuitive. The complex vectors m•a, c•v represent the inertia- and damping forces and k•x is the spring force. This diagram rotates CCW with angular frequency ω over the complex plane where a full rotation represents 2π radians or 360 degrees. Depending on the excitation frequency, the dynamic force vector F(t) is located at a different angle to the internal forces. For very low frequencies, F(t) is almost in line with k•x. Then, as the excitation frequency is increased it rotates CCW and aligns with c•v at ω_n. For frequencies above resonance, F(t) moves towards m•a where it must be noted that for every situation, the **reaction force** is directed opposite to F(t). At every frequency, the projected Re- and Im components of F bring equilibrium to the force-balance thereby satisfying the EOM. For example, at the relatively low-frequency depicted ($\omega_{exc} < \omega_n$) the excitation force is mostly in phase with displacement and spring forces dominate the response. The reaction force component $F(t)_R$ in-line with m•a, then extends this inertia force until the length of the dominant spring force k•x. At the same frequency, *the reaction force component* perpendicular to this initial component (i.e. opposite to c•v) compensates dissipative power of the damper, by balancing this damper force. At the fundamental frequency, the latter is the only force to be opposed as spring forces and inertia forces are of exactly the same magnitude (same length vector). This makes ω_n the frequency at which energy can be injected into the system with maximum efficiency. Obviously, at a high frequencies ($\omega > \omega_n$), besides the orientation of F(t), also the length of the other force-vectors change accordingly. **Dynamic measurement for forcesix takes place in the linear regime after resonance of the VI platform and well before the tested module decouples on the stiffness of the six piezo's.** *In this frequency range spring forces dominate, hence the measured force equals the stiffness of the piezo, times the relative motion between M2-M3.*

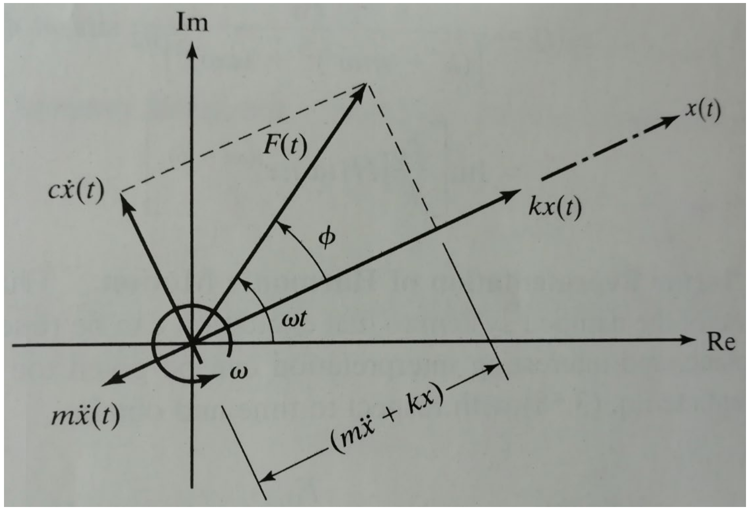

C-3.1: Overview

The strut has been designed to have a high axial/radial stiffness ratio of 693 to protect the piezos

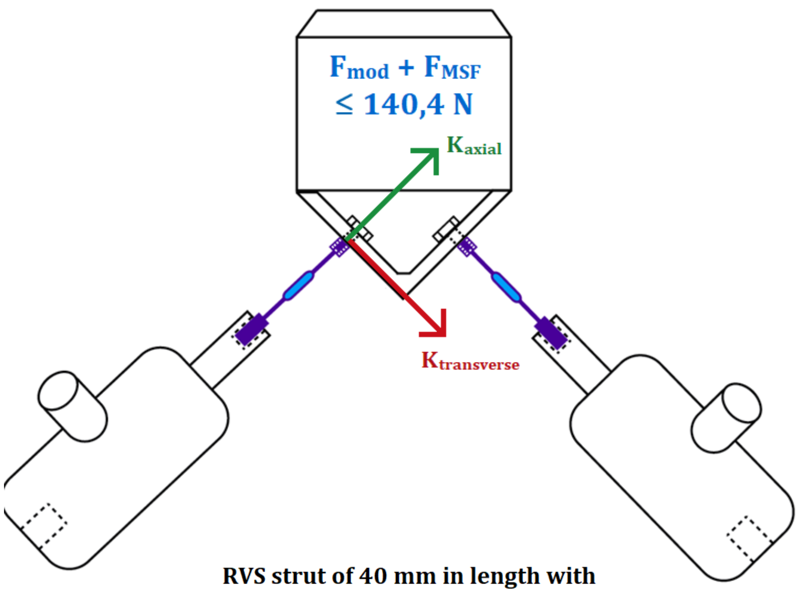

RVS strut of 40 mm in length with
a 32 mm thickened middle section

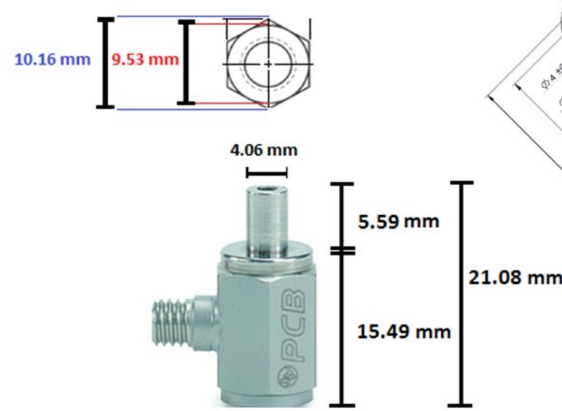

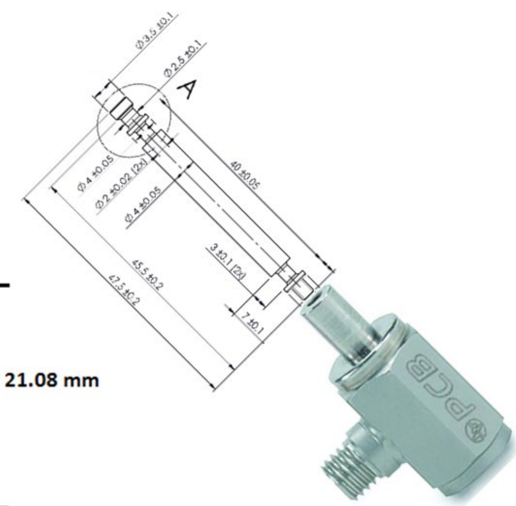

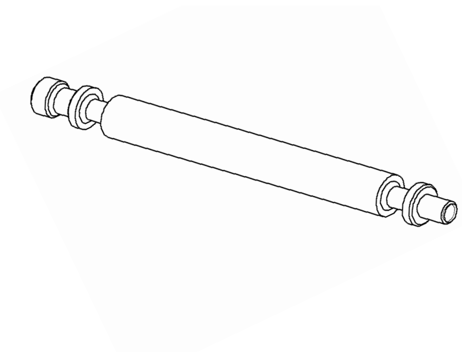

C-3: Stiff-Flexible Support Struts

C-3.2: Computation axial- and transverse force under static load

The strut has been designed to have a high axial/radial stiffness ratio of 693 to protect the piezos

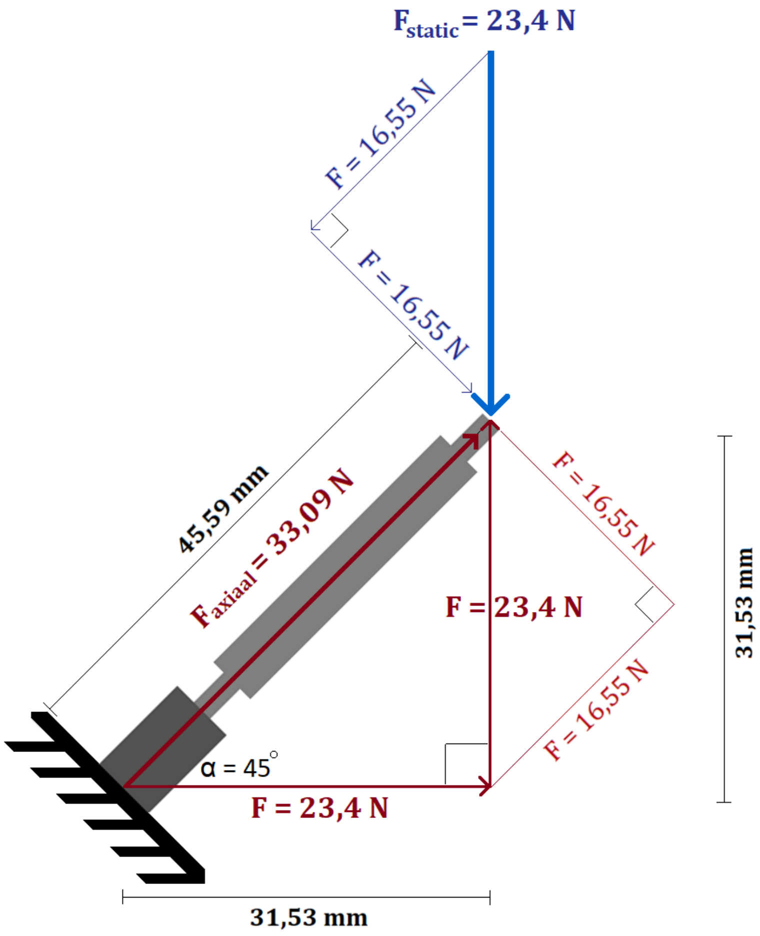

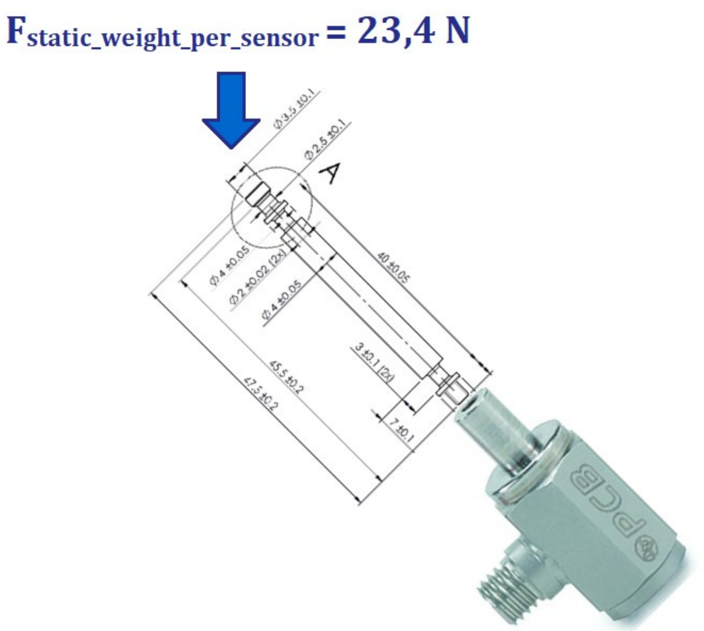

C-3: Stiff-Flexible Support Struts

MAPPER lithography

C-3.3: Computation resulting shear force and bending moment

The strut has been designed to have a high axial/radial stiffness ratio of 693 to protect the piezos

Transverse Load (unsupported)

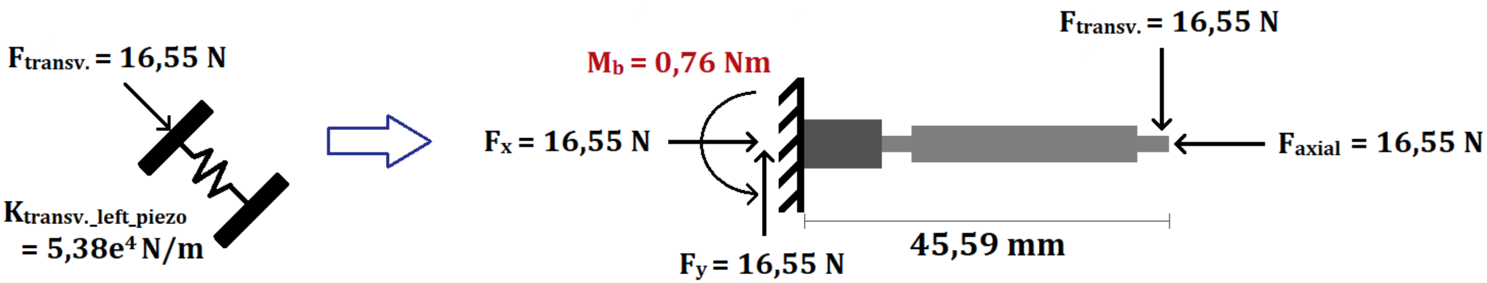

Transverse Load (supported, 45°)

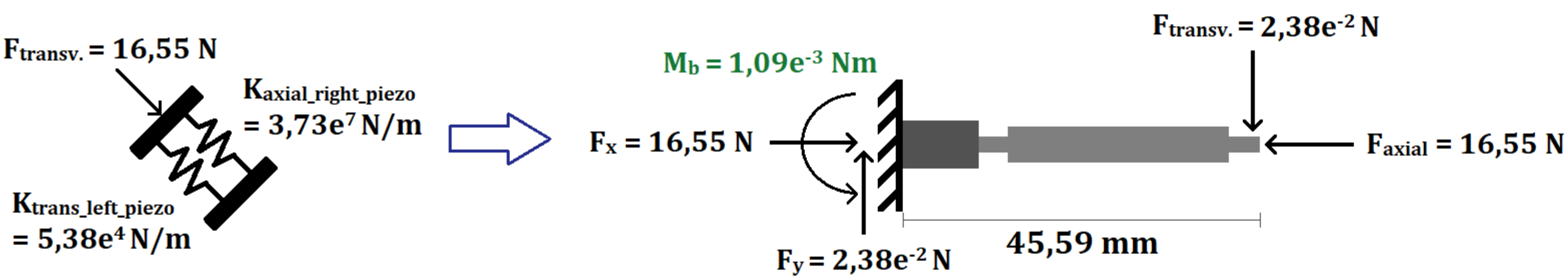

$K_{equivalent}$ = 3,74e^{7} N/m
$X_{under\_Ftransv.}$ = 0,44 mu
$F_{transv.\_actual}$ = $K_{trans\_left\_piezo}$ • $X_{under\_Ftransv.}$
$F_{transv.\_actual}$ = 2,38e^{-2} N
$M_{b\_under\_Ftransv.\_actual}$ = 1,09e^{-3} Nm

M_{b_damage} ~ 1e^{-1} Nm
$M_{b\_nonlinearity}$ ~ 1e^{-2} Nm

Sanity check: 16,55 / 2,38e^{-2} = 693,33
(matches with stiffness ratio)

C-4: Investigating Aliasing

Performing measurements under different sampling frequencies

The different parameters for effective IEPE measurement have been computed that should result in data that is not affected by digital distortion such as aliasing. To check the impact of such effects and to investigate whether the measurements have actually been executed properly, acceleration measurement have been performed under identical circumstances but with different sampling frequencies. <u>These are the results:</u>

Location 1 – **5 KHz**

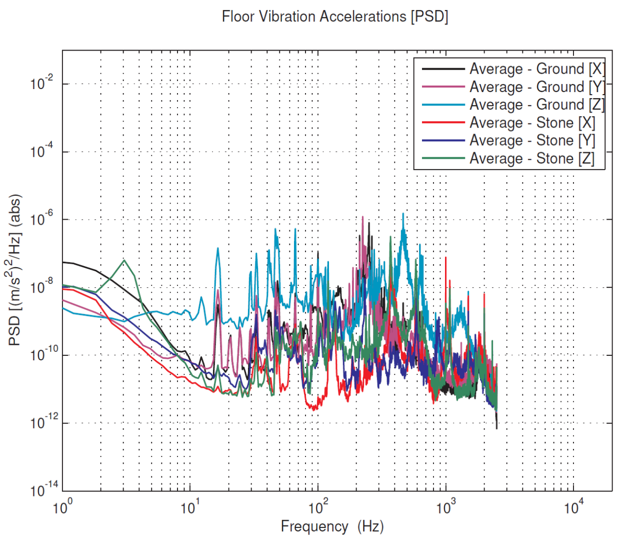

Location 1 – **25 KHz**

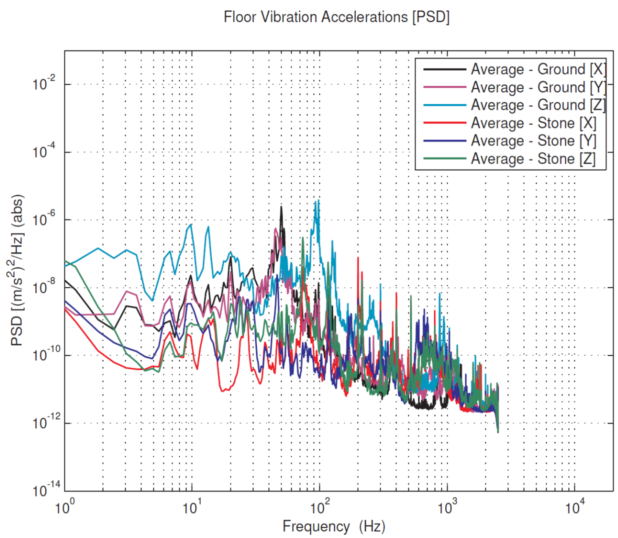

Location 1 – **50 KHz**

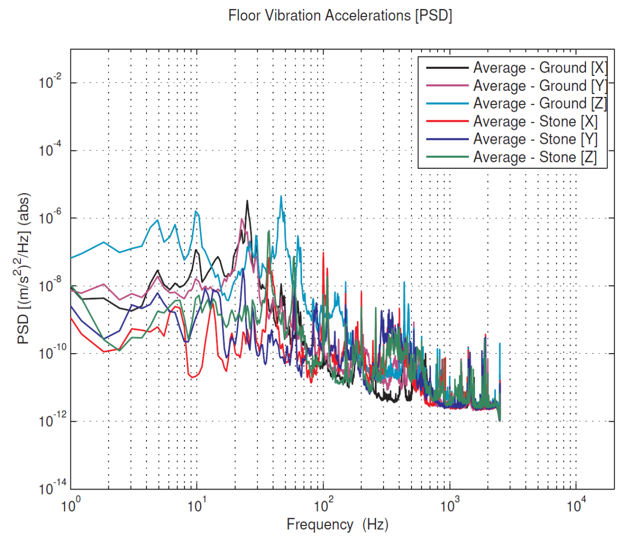

For these particular measurements, the correct sampling frequency was calculated to be 20 kHz (at Tmeas: 2m, Fres: 0.07)

It can be seen clearly that the higher the sampling frequency, the more the acceleration response seems to be shifting to the left. This is because it is mapped and 'folded back over itself'. If unaware of this phenomenon, measurement data could be affected as it results in a much lower (aliasing) frequency after filtering, from which the original signal cannot be recovered. It could appear then as if significantly higher input is present at certain frequencies than is actually the case.

C-5: Eigenmode Analysis

MAPPER lithography

C-5.1: Granite Stone (part of VI platform)

Objective for each geometry is to have its first eigenfrequency > 300 Hz

COMSOL MULTIPHYSICS®

Different locations of airmount suspension have been tested. When placed more towards the corners of the granite plate, the first eigenmode occurs below 300 Hz. An optimal location has been found that results in a fundamental frequency of 423 Hz as can be seen in the figure below left. The airmounts are connected to the granite stone(s) using threaded inserts. The bottom granite stone used in Forcesix (576 kg) measures 1.2 x 0.8 x 0.2 m and the best mounting location is found to be 25 cm from all sides, assuming a contact area of 2 x 2 cm (figure bottom right).

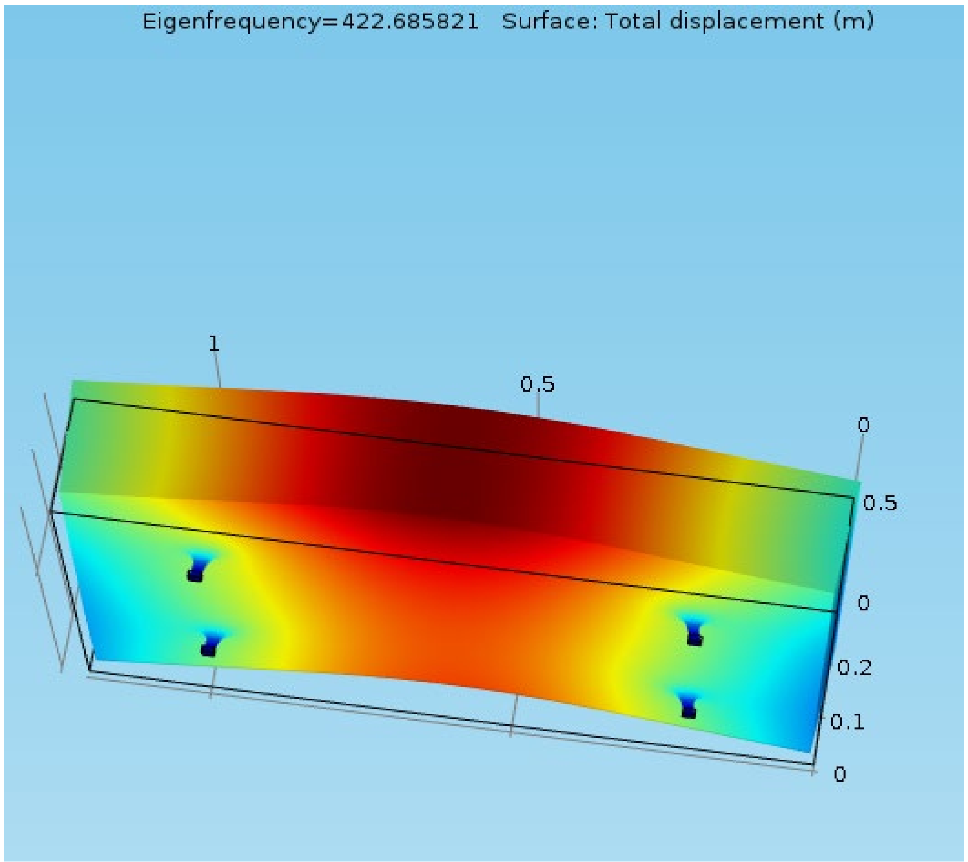

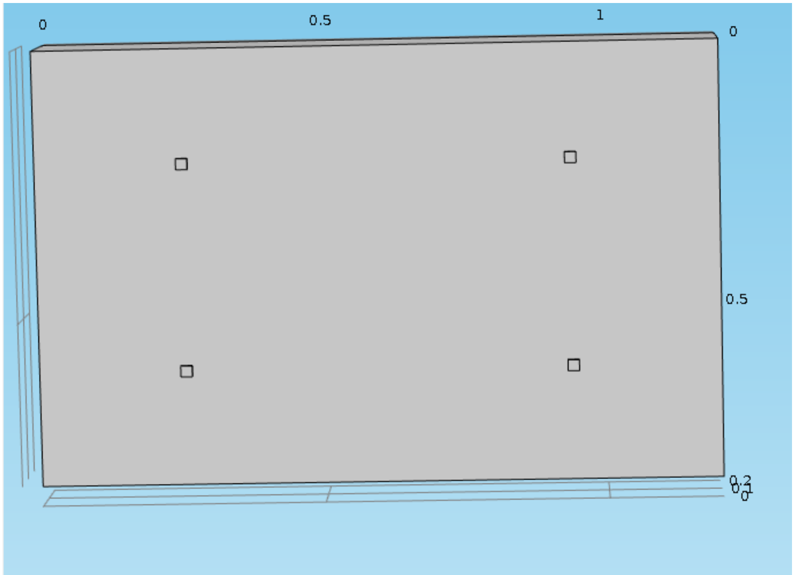

C-5.2: Optical breadboard

Objective for each geometry is to have its first eigenfrequency > 300 Hz

Different configurations to connect the optical breadboard to the granite stone have been considered. The results show that when attaching the optical breadboard on the four corners, an eigenfrequency of 105 Hz results which is too low. When the mounting location is moved away from the corners diagonally, this improves however it cannot be raised above the 300 Hz necessary for the design. The final design uses 5 threaded inserts to mount the optical breadboard to the granite stone, as indicated on the bottom left screenshot. This results in a fundamental frequency of 540 Hz and a mode shape where the center to which the base frame connects, behaves as a node. This is well sufficient for the dynamic measurement intended.

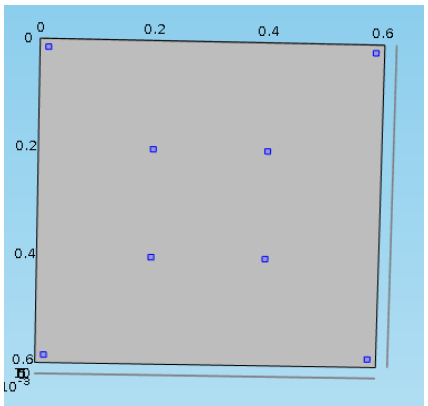

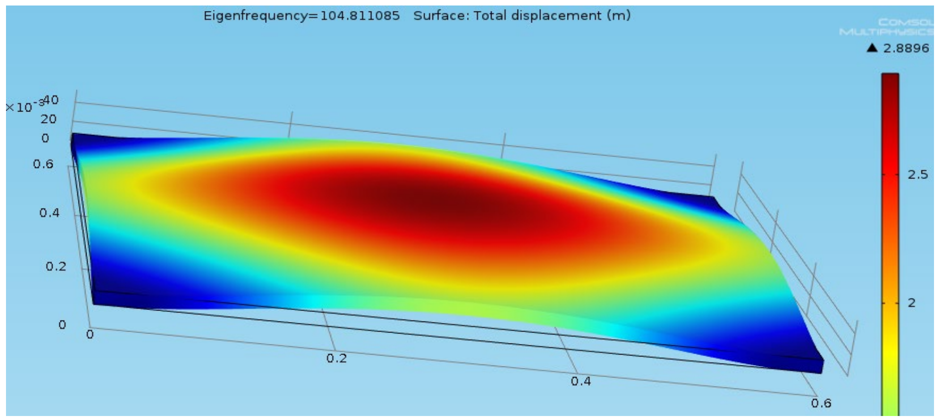

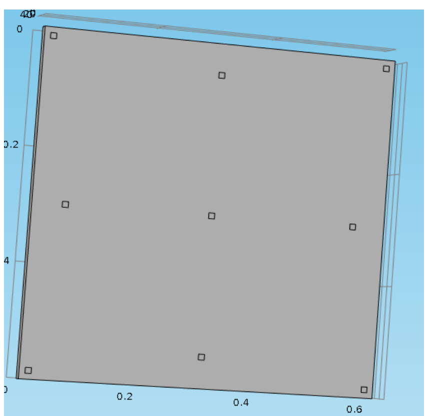

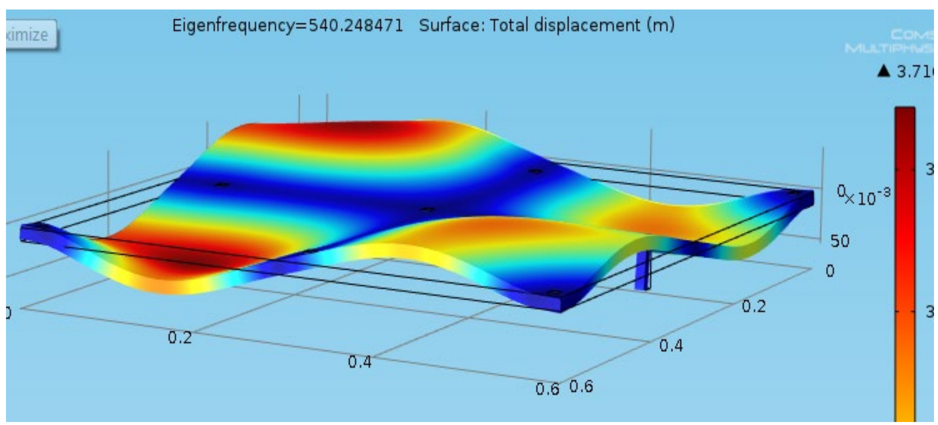

C-5: Eigenmode Analysis

C-5.3: Plating of acoustical enclosure (unsupported; insulation will provide resistance)

Objective for each geometry is to have its first eigenfrequency > 300 Hz

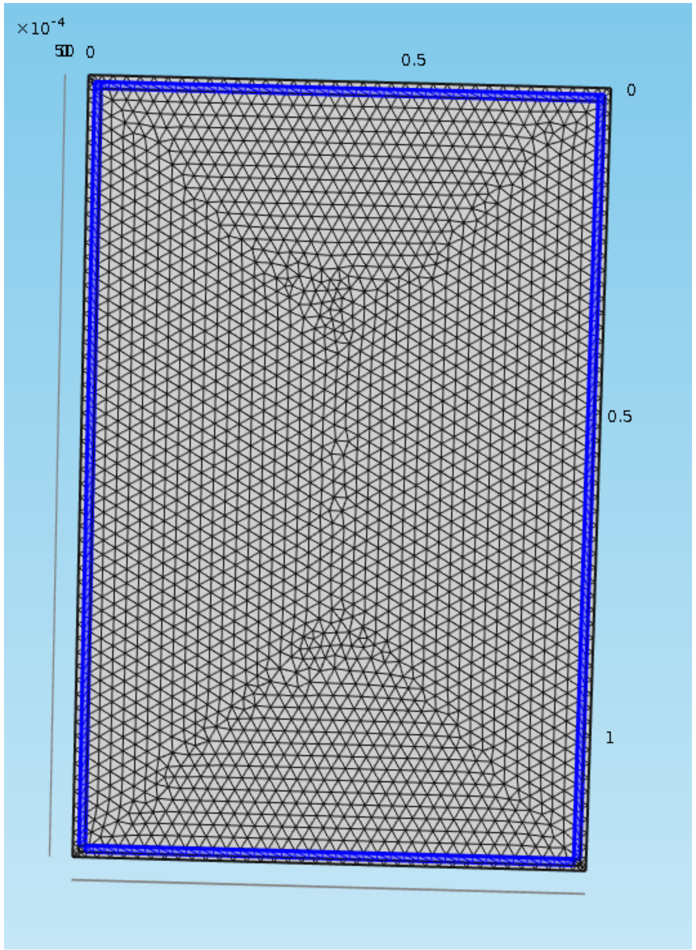

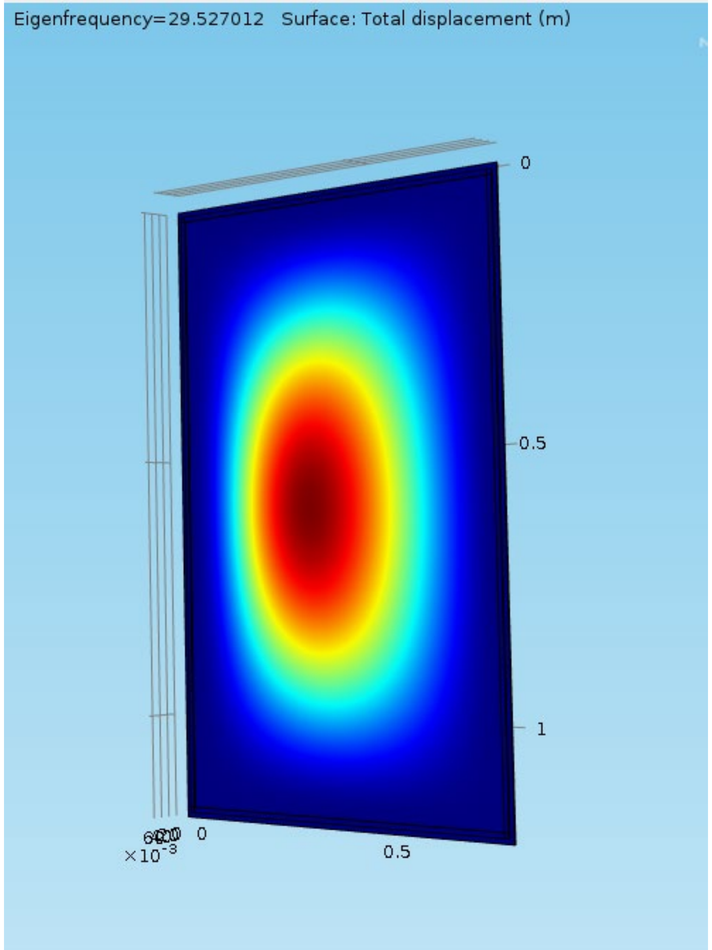

App. D

Matlab Code

D-1: Matrix Weighting Function

MAPPER lithography

6-DOF Transmissibility VIM w/cross-talk

```
%% Computing Wafer Error [6-DOF / 3-DOF]
% Author:                                 Arjan de Wildt
% Framework by:                           Rogier Ellenbroek
% Date:                                   21-06-2013
% Institute:                              Delft University of Technology
% Company:                                Mapper Lithography

% This document constitutes the simulation of the SUSA transmissibility,
% compliancy and controller sensitivity function. These are turned into a
% weighting function that is used to translate the forces as exerted on the
% MOF into wafer errors [nm].

%% Use only i,j,k for inside loops - not m and n!

%% Initialize
clear all
close all
clc

cd('C:\Users\Arjan\Documents\My Dropbox\MAPPER\Matlab\2. Stage Stability Budgeting - Matrix\Weighting Function')

%% Plot Definitions
set(0,'DefaultAxesColorOrder',[1 0 0; 0 1 0; 0 0 1],'DefaultAxesLineStyleOrder','-|:|*')
% USE DEFAULT AXES en dan de X order

%% Defining Frequency Domain
% frequency range
total_range = [0.03 6000];  % [Hz]      Total frequency range to look at [Hz]
range = [10 300];             % [Hz]      Frequency range of interest for requirements [Hz]

% Creating a logaritmic vector
log_vector = logspace(log10(total_range(1)),log10(total_range(2)),3000);  % [Hz] create a 10-based logaritmic vector
                                                                            %      from 0.03 to 6000 Hz (total_range)
                                                                            %      cut up in 3000 parts for resolution

log_vector_w = log_vector*2*pi;                        % Freq range vector in rad/s, needed for freq response

% Creating terts bands
n = max(round(log(log_vector)/log(2^(1/3))) + 3, 0);   % [-]  Terts-band numbers n [stems from definition, note t
fc = (2^(1/3)).^(n-3);                                 % [Hz] Terts band center frequency
fh = fc*2^(1/6);                                       % [Hz] Upper limit terts band
fl = fc*2^(-1/6);                                      % [Hz] Lower limit terts band

% Determine boundaries for frequency range of interest
down_lim = find(log_vector>range(1),1,'first');
up_lim = find(log_vector>range(2),1,'first');

% Create logaritmic vector for range of interest
log_vector_range = log_vector(down_lim:up_lim);        % frequency range of interest
log_vector_range_w = log_vector_range*2*pi;            % Freq range vector in rad/s, needed for freq response

% Frequency vector for integral calculation over total range
dHz = diff(log_vector);                                % determine frequency step
dHz(1,length(dHz)+1)=dHz(1,length(dHz));               % add one element to dHz for same dimension as log_vector,
dHz_cut = dHz(down_lim:up_lim);                        % taking cut at same dimension as range

%% System constants
g  = 9.81;                      % [m/s^2]   gravitiational constant
Ss = 26.7e-3;                   % [m]       EO slit size
```

I.P.

```
% T_6DOF =  X_to_X(w1)  Y_to_X(w1)  Z_to_X(w1)  Rx_to_X(w1)  ..
%           X_to_Y(w1)  Y_to_Y(w1)  Z_to_Y(w1)  Rx_to_Y(w1)  ..
%           X_to_Z(w1)     ..          ..
%             ..

%% Massaging data to get dimensions  [6x6x3000] > [36x3000]     % I could also have added all responses per row and then freq domain sweeped it.
T_6DOF = permute(T_6DOF,[1,3,2]);  %[6x3000x6] - 3D            % switch 3rd dimension with columns

% T_6DOF =  X_to_X(w1)   X_to_X(w2)   ..  X_to_X(w3000)          % with Y_to_X etc. being the 3rd dimension in the same way as X_to_X
%           X_to_Y(w1)   X_to_Y(w2)   ..  X_to_Y(w3000)
%           X_to_Z(w1)   X_to_Z(w2)   ..  X_to_Z(w3000)
%           X_to_Rx(w1)  X_to_Rx(w2)  ..  X_to_Rx(w3000)
%           X_to_Ry(w1)  X_to_Ry(w2)  ..  X_to_Ry(w3000)
%           X_to_Rz(w1)  X_to_Rz(w2)  ..  X_to_Rz(w3000)

T_6DOF_2D = zeros(36,3000);

for i=1:6;                              % [36x3000] - 2D
    for j=1:6;
        for k=1:3000;                                           % eerst lopen we all kolommen k af, dan alle
            T_6DOF_2D((j+(i-1)*6),k)=T_6DOF(j,k,i);             % rijen i, ten slotte alle 3e dimensies i
        end
```

D-1: Matrix Weighting Function

6-DOF Compliance MOF w/cross-talk

```
    end
end

% T_6DOF_2D =  1.  X_to_X(w1) X_to_X(w2) .. X_to_X(w3000)
% %            2.  X_to_Y(w1) X_to_Y(w2) .. X_to_Y(w3000)
% %            3.  X_to_Z(w1) X_to_Z(w2) .. X_to_Z(w3000)
% %                   ..         ..           ..
% %            7.  Y_to_X(w1) Y_to_X(w2) .. Y_to_X(w3000)
% %            8.  Y_to_Y(w1) Y_to_Y(w2) .. Y_to_Y(w3000)

% Transmissibility Matrix - with Crosstalk [6x3000]
T_6DOF_2D_XT = zeros(6,3000);

for i=1:6                                   % [6x3000] - 2D >> correct, matches stage stability perfectly
    for j=1:3000
        T_6DOF_2D_XT(i,j) = T_6DOF_2D(i,j) + T_6DOF_2D((i+6),j) + ...;
                            T_6DOF_2D((i+12),j) + T_6DOF_2D((i+18),j) + ...;
                            T_6DOF_2D((i+24),j) + T_6DOF_2D((i+30),j);
    end
end

%% Compliancy of VIM (6-DOF)
for i=1:6
    s = [redacted] [])
    comp [redacted] ;
end

compl_6DOF_XT = CT * compl_6DOF;                                       % MATRIx multiplication (6x6)

Resp_C = freqresp(compl_6DOF_XT,log_vector_w);                          % freq response of my functi
C_6DOF = abs(Resp_C);               % [6x6x3000]                        % take out complex values

% C_6DOF =  X_to_X(w1)  Y_to_X(w1)  Z_to_X(w1)  Rx_to_X(w1)  ..
%           X_to_Y(w1)  Y_to_Y(w1)  Z_to_Y(w1)  Rx_to_Y(w1)  ..
%           X_to_Z(w1)     ..          ..
%              ..

%% Massaging data to get dimensions  [6x6x3000] > [36x3000]            % I could also have added a
C_6DOF = permute(C_6DOF,[1,3,2]);  %[6x3000x6] - 3D                     % switch 3rd dimension with c

% C_6DOF =  X_to_X(w1)   X_to_X(w2)   ..  X_to_X(w3000)                 % with Y_to_X etc. being th
%           X_to_Y(w1)   X_to_Y(w2)   ..  X_to_Y(w3000)
%           X_to_Z(w1)   X_to_Z(w2)   ..  X_to_Z(w3000)
%           X_to_Rx(w1)  X_to_Rx(w2)  ..  X_to_Rx(w3000)
%           X_to_Ry(w1)  X_to_Ry(w2)  ..  X_to_Ry(w3000)
%           X_to_Rz(w1)  X_to_Rz(w2)  ..  X_to_Rz(w3000)

C_6DOF_2D = zeros(36,3000);

for i=1:6;                                  % [36x3000] - 2D
    for j=1:6;
        for k=1:3000;                                                   % eerst lopen we all kolomm
            C_6DOF_2D((j+(i-1)*6),k)=C_6DOF(j,k,i);                     % rijen i, ten slotte alle 36
        end
    end
end
```

```
end

% C_6DOF_2D =  1.  X_to_X(w1) X_to_X(w2) .. X_to_X(w3000)
% %            2.  X_to_Y(w1) X_to_Y(w2) .. X_to_Y(w3000)
% %            3.  X_to_Z(w1) X_to_Z(w2) .. X_to_Z(w3000)
% %                   ..         ..           ..
% %            7.  Y_to_X(w1) Y_to_X(w2) .. Y_to_X(w3000)
% %            8.  Y_to_Y(w1) Y_to_Y(w2) .. Y_to_Y(w3000)

% Compliancy Matrix - with Crosstalk [6x3000] // just take all extra entries as well, iso only the diagonal values
C_6DOF_2D_XT = zeros(6,3000);

for i=1:6                                % [6x3000] !!! - 2D >> correct, matches stage stability perfectly
    for j=1:3000
        C_6DOF_2D_XT(i,j) =  C_6DOF_2D(i,j) + C_6DOF_2D((i+6),j) + ...;
                             C_6DOF_2D((i+12),j) + C_6DOF_2D((i+18),j) + ...;
                             C_6DOF_2D((i+24),j) + C_6DOF_2D((i+30),j);
    end
end

%% System Dynamics
```

[redacted]

I.P.

D-1: Matrix Weighting Function

MAPPER lithography

6-DOF Controller Sensitivity – Transfer Functions

```
P_6DOF_tf(i,i) = [1 0 0 0]*inv(eye(4)*s - A_SS(:,:,i))*B_SS_r_c(:,:,i)*P_1_stop_roll_off;
end

Resp_P = freqresp(P_6DOF_tf,log_vector_w);          % freq response of my function to log_vecto
P_6DOF_abs = abs(Resp_P);
P_6DOF = permute(P_6DOF_abs,[1,3,2]);  %[6x3000x6] - 3D

% % P_6DOF =  X_to_X(w1)   X_to_X(w2)   ..  X_to_X(w3000)    with Y_to_X etc. being the 3rd dimens
% %           X_to_Y(w1)   X_to_Y(w2)   ..  X_to_Y(w3000)
% %           X_to_Z(w1)   X_to_Z(w2)   ..  X_to_Z(w3000)
% %           X_to_Rx(w1)  X_to_Rx(w2)  ..  X_to_Rx(w3000)
% %           X_to_Ry(w1)  X_to_Ry(w2)  ..  X_to_Ry(w3000)
% %           X_to_Rz(w1)  X_to_Rz(w2)  ..  X_to_Rz(w3000)

for i=1:6;                        % [36x3000] - 2D
    for j=1:6;
        for k=1:3000;                                  % eerst lopen we all ko
            P_6DOF_2D((j+(i-1)*6),k)=P_6DOF(j,k,i);    % rijen i, ten slotte all
        end
    end
end

% % P_6DOF_2D =  1.  X_to_X(w1) X_to_X(w2) .. X_to_X(w3000)
% %              2.  X_to_Y(w1) X_to_Y(w2) .. X_to_Y(w3000)
% %              3.  X_to_Z(w1) X_to_Z(w2) .. X_to_Z(w3000)
% %                     ..          ..           ..
% %              7.  Y_to_X(w1) Y_to_X(w2) .. Y_to_X(w3000)
% %              8.  Y_to_Y(w1) Y_to_Y(w2) .. Y_to_Y(w3000)

%% PID + Stage Controller
[redacted]
for i=1:6
    for j=1:6
        if i~=j
        D_gain(i,j)=0;
        end
    end
end
[redacted]

% Controller Transfer Function Matrix in 6-DOF
s = tf('s');

for i=1:6
    Contr_6DOF_tf(i,i) = [redacted]
end
```

```
Resp_Contr = freqresp(Contr_6DOF_tf,log_vector_w);    % freq response of my function to log_vector_w (must be in rad/s!), 6x6 for T
Contr_6DOF_abs = abs(Resp_Contr);
Contr_6DOF = permute(Contr_6DOF_abs,[1,3,2]);          %[6x3000x6] - 3D

% % Contr_6_DOF = X_to_X(w1)   X_to_X(w2)   ..  X_to_X(w3000)    with Y_to_X etc. being the 3rd dimension in the same way as X_to_X
% %               X_to_Y(w1)   X_to_Y(w2)   ..  X_to_Y(w3000)
% %               X_to_Z(w1)   X_to_Z(w2)   ..  X_to_Z(w3000)
% %               X_to_Rx(w1)  X_to_Rx(w2)  ..  X_to_Rx(w3000)
% %               X_to_Ry(w1)  X_to_Ry(w2)  ..  X_to_Ry(w3000)
% %               X_to_Rz(w1)  X_to_Rz(w2)  ..  X_to_Rz(w3000)

for i=1:6;                                           % [36x3000] - 2D
    for j=1:6;
        for k=1:3000;                                  % eerst lopen we all kolommen k af, dan alle
            Contr_6DOF_2D((j+(i-1)*6),k)=Contr_6DOF(j,k,i);   % rijen i, ten slotte alle 3e dimensies i
        end
    end
end

% % Contr_6DOF_2D =  1.  X_to_X(w1) X_to_X(w2) .. X_to_X(w3000)
% %                  2.  X_to_Y(w1) X_to_Y(w2) .. X_to_Y(w3000)
% %                  3.  X_to_Z(w1) X_to_Z(w2) .. X_to_Z(w3000)
% %                         ..          ..           ..
% %                  7.  Y_to_X(w1) Y_to_X(w2) .. Y_to_X(w3000)
% %                  8.  Y_to_Y(w1) Y_to_Y(w2) .. Y_to_Y(w3000)

%% Transfer Functions
OL_6DOF_tf = P_6DOF_tf * Contr_6DOF_tf;          % Open-Loop Transfer Function
SEN_6DOF_tf = inv(eye(6) + OL_6DOF_tf);          % Controller Sensitivity Transfer Function
PS_6DOF_tf = SEN_6DOF_tf*P_6DOF_tf;              % Process Sensitivity Transfer Function
CL_6DOF_tf = SEN_6DOF_tf*OL_6DOF_tf;             % Closed Loop Transfer Function

% Computing Responses
Resp_OL = freqresp(OL_6DOF_tf,log_vector_w);
OL_6DOF_abs = abs(Resp_OL);
OL_6DOF = permute(OL_6DOF_abs,[1,3,2]);

Resp_SEN = freqresp(SEN_6DOF_tf,log_vector_w);
SEN_6DOF_abs = abs(Resp_SEN);
SEN_6DOF = permute(SEN_6DOF_abs,[1,3,2]);

Resp_PS = freqresp(PS_6DOF_tf,log_vector_w);
PS_6DOF_abs = abs(Resp_PS);
PS_6DOF = permute(PS_6DOF_abs,[1,3,2]);

Resp_CL = freqresp(CL_6DOF_tf,log_vector_w);
CL_6DOF_abs = abs(Resp_CL);
CL_6DOF = permute(CL_6DOF_abs,[1,3,2]);

for i=1:6;                                           % [36x3000] - 2D
    for j=1:6;
        for k=1:3000;                                % eerst lopen we all kolommen k af, dan alle
            OL_6DOF_2D((j+(i-1)*6),k)=OL_6DOF(j,k,i);   % rijen i, ten slotte alle 3e dimensies i
            SEN_6DOF_2D((j+(i-1)*6),k)=SEN_6DOF(j,k,i);
            PS_6DOF_2D((j+(i-1)*6),k)=PS_6DOF(j,k,i);
            CL_6DOF_2D((j+(i-1)*6),k)=CL_6DOF(j,k,i);
        end
    end
```

D-1: Matrix Weighting Function

MAPPER lithography

Computing Wafer Error from any DDF spectrum (3 methods)

```matlab
%% Calculate Wafer Error
% Take note: you work with PSDs until the end (nm), only then transform into CPS, CAS if you want
% Take note: CPS is computed by integration, now: discrete integration i.e. cumsum((PSD.*dHz),2)!!

PSD_error_1DOF_to_DOFs=zeros(36,3000);
PSD_error_6DOF = zeros(6,3000);                          % [m^2]

% PSD - Errors per DOF_to_DOFs // per frequency [36x3000]
WF_SQ = W_cv_6DOF_2D.^2;

%      [36x3000]          =       [6x3000]           .* [36x3000]    //
%       [m^2/Hz]                   [N^2/Hz]              [m^2/N^2]

for i=1:6
    PSD_error_1DOF_to_DOFs(i,:)     = PSD_FC_cooling_6DOF(1,:) .* WF_SQ(i,:);       % X  to 6DOFs
    PSD_error_1DOF_to_DOFs(i+6,:)   = PSD_FC_cooling_6DOF(2,:) .* WF_SQ(i+6,:);     % Y  to 6DOFs
    PSD_error_1DOF_to_DOFs(i+12,:)  = PSD_FC_cooling_6DOF(3,:) .* WF_SQ(i+12,:);    % Z  to 6DOFs
    PSD_error_1DOF_to_DOFs(i+18,:)  = PSD_FC_cooling_6DOF(4,:) .* WF_SQ(i+18,:);    % Rx to 6DOFs
    PSD_error_1DOF_to_DOFs(i+24,:)  = PSD_FC_cooling_6DOF(5,:) .* WF_SQ(i+24,:);    % Ry to 6DOFs
    PSD_error_1DOF_to_DOFs(i+30,:)  = PSD_FC_cooling_6DOF(6,:) .* WF_SQ(i+30,:);    % Rz to 6DOFs
end

% Allocating Errors to single DOFs // per frequency [6x3000] -- [m^2/Hz]
for i=1:6
    PSD_error_6DOF(i,:) = PSD_error_1DOF_to_DOFs(i,:)    + PSD_error_1DOF_to_DOFs(i+6,:)  + PSD_error_1DOF_to_DOFs(i+12,:)  + ...
                                  PSD_error_1DOF_to_DOFs(i+18,:) + PSD_error_1DOF_to_DOFs(i+24,:) + PSD_error_1DOF_to_DOFs(i+30,:);
end
```

I.P.

```matlab
%% Method 3
% 3) from 6DOF PSD [m^2/Hz] into 6DOF CPS [m^2] and 6DOF CAS [m] then by CT_SLIT to 3DOF CAS [m], then CAS [m]

% CPS -- 6-DOF Error [m^2]
CPS_error_6DOF_M3=zeros(6,3000);

for i=1:6
    CPS_error_6DOF_M3(i,:) = cumsum((PSD_error_6DOF(i,:).*dHz),2);          % PSD>CPS = discrete integration -- * dHz
end

% CAS -- 3-DOF [m]
CAS_error_3DOF_M3=zeros(3,3000);                                    % {3-sigma RMS value} -- RMS is sqrt(^2) or abs()
CAS_error_6DOF_M3 = sqrt(CPS_error_6DOF_M3);

for i=1:3000
    CAS_error_3DOF_M3(:,i) = 3*abs(CT_EO_slit*CAS_error_6DOF_M3(:,i));
end

% CT_EO_slit = [ 1   0   0       0         0       S_slit/2; ...       % Rotations act over half this arm's length
%                0   1   0       0         0       S_slit/2; ...
%                0   0   1   S_slit/2  S_slit/2       0        ]

% Matrix Budgets
disp('Matrix budget is:')
SS_budget_matrix_XY = 1.8e-9                        % [m] // Overlay budget very tight (in-plane)
SS_budget_matrix_Z  = 75e-9                         % [m] // Focus budget much larger

disp('CAS error [XYZ] is:')
CAS_error_3DOF_M3(:,3000)
```

```matlab
%%% Weighting Measurement data Vibronix - Plate [X]

% Load Variables Acoustics Inside MIMO fit -- RED
% Measurement data Plate [X] - Construct: combined Endevco [0-125 Hz] + BK [125-3000 Hz]

cd('C:\Users\Arjan\Documents\My Dropbox\MAPPER\Matlab\3. Dynamic Error Budgeting\Acoustics')
load('Variables_Acoustics_Inside_MIMO_fit')

PSD_MF_Vibronix_AA  = Vibronix_Plate_X_EndBK .* (9.04^2);
PSD_MF_Vibronix_BSW = Vibronix_Plate_X_EndBK .* (29.1^2);

% Plotting Measured Cooling Forces
loglog(log_vector,PSD_MF_Vibronix_AA,'r',log_vector,PSD_MF_Vibronix_BSW,'b','LineWidth',2)
title('Measured Cooling Forces Vibronix AA & BSW')
ylabel('PSD [N^2/Hz]')
xlabel('Frequency')
axis([0 2e4 1e-13 1e-3])
legend('MF - Vibronix - AA [Z]','MF - Vibronix - BSW [Z]','location','NE');
grid on

PSD_FC_cooling = PSD_MF_Vibronix_BSW;

% PSD -- 6DOF           // [N^2/Hz]    // scaling per DOF: <1 1 10 2 2 10>
PSD_FC_cooling_6DOF = [PSD_FC_cooling; PSD_FC_cooling; PSD_FC_cooling*10; PSD_FC_cooling*2; PSD_FC_cooling*2; PSD_FC_cooling*10];

% % % % MA Vibronix turned into MF for BSW (*(19.9^2) - 300x300 optical breadboard) yields 4 nm XY and 1.2 nm Z
% % % % MA Vibronix turned into MF for BSW (*(29.1^2))- 600x600 solid aluminium) yields 5.8 nm XY and 1.8 nm Z
```

D-2: Cooling- and Floor Vibrations

MAPPER lithography

Establish Mapper spectra: cooling based on TNO research & floor vibrations from LETI, TSMC

```
end

%% Cooling Vibrations Weighting Function
% // Weighting Function // no CT

% [m/N]==[m^2/kg]  =      [-]      *  [m/N]==[m^2/kg]
W_cv_6DOF_tf        = SEN_6DOF_tf *   compl_6DOF_XT;


Resp_W_cv = freqresp(W_cv_6DOF_tf,log_vector_w);
W_cv_6DOF_abs = abs(Resp_W_cv);
W_cv_6DOF = permute(W_cv_6DOF_abs,[1,3,2]);

for i=1:6;                                              % [36x3000] - 2D
    for j=1:6;
        for k=1:3000;                                   % eerst lopen we all kolommen k af, dan
            W_cv_6DOF_2D((j+(i-1)*6),k) = W_cv_6DOF(j,k,i);  % rijen i, ten slotte alle 3e dimensie
        end
    end
end

% Weighting Function // no CT -- range  // [N^2/Hz]
% [m/N]==[m^2/kg]    : turn [36x3000] into [36x836]

for i=1:36
W_cv_6DOF_2D_range(i,1:(up_lim-down_lim+1)) = W_cv_6DOF_2D(i,down_lim:up_lim);
end

% % W_cv_6DOF_2D =  1.  X_to_X(w1) X_to_X(w2)  .. X_to_X(w3000)
% %                 2.  X_to_Y(w1) X_to_Y(w2)  .. X_to_Y(w3000)
% %                 3.  X_to_Z(w1) X_to_Z(w2)  .. X_to_Z(w3000)
% %                     ..         ..             ..
% %                 7.  Y_to_X(w1) Y_to_X(w2)  .. Y_to_X(w3000)
% %                 8.  Y_to_Y(w1) Y_to_Y(w2)  .. Y_to_Y(w3000)

for i=1:6                                 % [6x3000]!!!      D >> correct, matches stage stability perfec
    for j=1:3000
        W_cv_6DOF_2D_XT(i,j) =  W_cv_6DOF_2D(i,j) + W_cv_6DOF_2D((i+6),j) + ...;
                                W_cv_6DOF_2D((i+12),j) + W_cv_6DOF_2D((i+18),j) + ...;
                                W_cv_6DOF_2D((i+24),j) + W_cv_6DOF_2D((i+30),j);
    end
end

%% Cross-Talk Arm // Relating 6-DOF forces into 3-DOF requirements
S_slit = 26.7e-3;                                               % Beams at the end of the slit have
CT_EO_slit = [ 1    0    0          0          0        S_slit/2; ...; % Rotations act over half this arm's
               0    1    0          0          0        S_slit/2; ...;
               0    0    1   S_slit/2   S_slit/2      0            ];

%% Cooling Force Spectra (DDF)

FC_cooling = zeros(size(log_vector));
FC_cooling(n<30 | n>18) = 1e-4;
FC_cooling(n<19) = 0.4e-4;
FC_cooling(n>=30) = 0.3e-4;

% PSD -- 1DOF          // [N^2/Hz]
PSD_FC_cooling = FC_cooling.^2 ./ (log_vector.*(log(fh)-log(fl)));  % [N^2/Hz]   PSD of cooling fo
```

```
FC_cooling(n<30 | n>18) = 1e-4;
FC_cooling(n<19) = 0.4e-4;
FC_cooling(n>=30) = 0.3e-4;

% PSD -- 1DOF           // [N^2/Hz]
PSD_FC_cooling = FC_cooling.^2 ./ (log_vector.*(log(fh)-log(fl)));  % [N^2/Hz]   PSD of cooling forces - single sided but with full energy content

% ASD -- 1DOF           // [N/sqrt(Hz)]
ASD_FC_cooling = PSD_FC_cooling.^0.5;            % To verify correctness i.e. match with SS V14

% PSD -- 6DOF            // [N^2/Hz]    // scaling per DOF: <1 1 10 2 2 10>
PSD_FC_cooling_6DOF = [PSD_FC_cooling; PSD_FC_cooling; PSD_FC_cooling*10; PSD_FC_cooling*2; PSD_FC_cooling*2; PSD_FC_cooling*10];
```

```
%% Floor Vibrations (FV) - specified in velocities, subscript indicates either accelerations or displacements

% Specifiying vibration levels [RMS vibration velocity level per terts band - spectral floor velocities]
FV_VC_v = 3e-6 * ones(size(log_vector));                % [m/s]  create a FF array, the size o the log_vector
FV_VC_v(n < 6 | n > 24) = 1e-6;                         % [m/s]  and use the terts band number n to indicate
FV_VC_v(n == 15 | n == 19) = 8e-6;                      % [m/s]  the ground velocities in each band. First
FV_VC_v((n >= 16 & n < 19) | n == 20) = 6e-6;           % [m/s]  everything is made 3mu/s, then different
FV_VC_v(n == 24) = 2e-6;                                % [m/s]  values are given to certain terts band numbers n

% Turning spectral floor velocities [m/s] into floor accelerations [m/s^2]
FV_VC_x = FV_VC_v ./ (2*pi*log_vector);                 % [m]      integrating in freq dom = dividing by w (=f*2*pi)
                                                        %          by ELEMENT-wise operation
% Turning spectral floor velocities [m/s] into floor accelerations [m/s^2]
FV_VC_a = FV_VC_v .* (2*pi*log_vector);                 % [m/s^2]  integrating in freq dom = dividing by w (=f*2*pi)
                                                        %          by ELEMENT-wise operation

% Narrow band contributions
% adapting the VC-Mapper (Dansberg) spectrum with extra velocity inputs at 16.6, 33, 50, 100, 660 and 1320 Hz
% for the Turbopumps etc. this data coming from measurements performed at Leti, TSMC etc.
nNB = ones(size(log_vector));                           % creating a narrow band vector and coupling this to
nNB(abs(log_vector-16.6) < 0.5) = 2;                    % the terts band number n. identify narrowband areas
nNB(abs(log_vector-33) < 0.5) = 3;                      % i.e. determine frequency and rel. height of input
nNB(abs(log_vector-50) < 1) = 4;
nNB(abs(log_vector-100) < 2) = 5;
nNB(abs(log_vector-660) < 5) = 6;
nNB(abs(log_vector-1320) < 5) = 7;
NB = [0 5 4 1 5 2 2]*1e-6;                              % additional RMS velocity input in band
NBw = [1 1 1 2 4 10 10];                                % width of narrow-band, needed for PSD computation
FV_NB_v = NB(nNB);                                      % Linear indexing with vector nNB (1x3000) gives out a vector of that same size (1x3000) but

% PSDs of Mapper VC (Dansberg) spectrum [SI^2/Hz]
PSD_FV_VC_v = FV_VC_v.^2 ./ (log_vector.*(log(fh)-log(fl)));   % [m^2/s^2/Hz]  Taking the single-sided PSD, but /T iso 2T to still give it the full po
PSD_FV_VC_v_range = PSD_FV_VC_v(down_lim:up_lim);              % [m^2/s^2/Hz]  Select range of interest (for plots)

PSD_FV_VC_x = PSD_FV_VC_v ./ (2*pi*log_vector).^2;             % [m^2/Hz]      PSD FV_X
PSD_FV_VC_x_range = PSD_FV_VC_x(down_lim:up_lim);              % [m^2/Hz]      Select range of interest (for plots)

PSD_FV_VC_a = PSD_FV_VC_v .* (2*pi*log_vector).^2;             % [m^2/s^4/Hz]  PSD FV_A
PSD_FV_VC_a_range = PSD_FV_VC_a(down_lim:up_lim);              % [m^2/s^4/Hz]  Select range of interest (for plots)

% PSDs of Narrowband spectrum [SI^2/Hz]
PSD_FV_NB_v = FV_NB_v.^2 ./ (NBw(nNB));                        % [m^2/s^2/Hz]  Single-sided PSD of narrow band contributions, /T iso 2T so full power
PSD_FV_NB_x = PSD_FV_NB_v ./ (2*pi*log_vector).^2;             % [m^2/Hz]      PSD NB_X
PSD_FV_NB_a = PSD_FV_NB_v .* (2*pi*log_vector).^2;             % [m^2/s^4/Hz]  PSD NB_A

% PSD of total floor vibration spectrum [SI^2/Hz]
PSD_FV_TOTAL_x = PSD_FV_VC_x + PSD_FV_NB_x;                    % [m^2/Hz]      Computing PSD of total floor vibrations by adding up the separate PSDs
PSD_FV_TOTAL_v = PSD_FV_VC_v + PSD_FV_NB_v;                    % [m^2/s^2/Hz]  Computing PSD of total floor vibrations by adding up the separate PSDs
PSD_FV_TOTAL_a = PSD_FV_VC_a + PSD_FV_NB_a;                    % [m^2/s^4/Hz]  Computing PSD of total floor vibrations by adding up the separate PSDs
```

D-2: Presumed Cooling Forces

MAPPER lithography

New proposed generic shape and center frequency (based on hydrostatic measurement results)

```
load Variables_from_Weighting_Function

% Generic shape of Force Requirement Spectrum [FRS]
% based on measurement data and weighting function from stage stability V14

FRS = zeros(1,3000);            % [-] Constructing module force req spectra
FRS(n < 14 & n > 1) =  1e-5;    % [N] Indicate a constant force per terts band // note that n=[1x3000]
FRS(n == 14)         =  1.7e-5;
FRS(n == 15)         =  2.8e-5;
FRS(n == 16)         =  3.35e-5;
FRS(n == 17)         =  4.0e-5;
FRS(n == 18)         =  2.9e-5;
FRS(n == 19)         =  2.1e-5;
FRS(n == 20)         =  1.7e-5;
FRS(n == 21)         =  1.2e-5;
FRS(n == 22)         =  7.5e-6;
FRS(n == 23)         =  6.0e-6;
FRS(n == 24)         =  4.6e-6;
FRS(n == 25)         =  3.9e-6;
FRS(n == 26)         =  3.6e-6;
FRS(n == 27)         =  3.5e-6;
FRS(n == 28)         =  3.4e-6;
FRS(n == 29)         =  3.2e-6;
FRS(n == 30)         =  3.1e-6;
FRS(n > 30)          =  3.0e-6;

% Individual Force Requirement Spectra (FRS) - scaled
FRS_PL  = module_budget_PL  * FRS;      % [N]
FRS_CON = module_budget_CON * FRS;
FRS_BSW = module_budget_BSW * FRS;
FRS_BG  = module_budget_BG  * FRS;

% Measix FRS per module (order less)
M_FRS_PL  = FRS_PL  / 10;          % Measix has to be able to measure this FRS in order to verify POS
M_FRS_CON = FRS_CON / 10;          % Measix has to be able to measure this FRS in order to verify CON
M_FRS_BSW = FRS_BSW / 10;          % Measix has to be able to measure this FRS in order to verify BSW
M_FRS_BG  = FRS_BG  / 10;          % Measix has to be able to measure this FRS in order to verify ILO

% PSDs of Measix FRS // single-sided with full energy content
PSD_M_FRS_PL  = M_FRS_PL.^2  ./ (log_vector.*(log(fh)-log(fl)));  % [N^2/Hz]   POS
PSD_M_FRS_CON = M_FRS_CON.^2 ./ (log_vector.*(log(fh)-log(fl)));  % [N^2/Hz]   CON
PSD_M_FRS_BSW = M_FRS_BSW.^2 ./ (log_vector.*(log(fh)-log(fl)));  % [N^2/Hz]   BSW
PSD_M_FRS_BG  = M_FRS_BG.^2  ./ (log_vector.*(log(fh)-log(fl)));  % [N^2/Hz]   ILO

% PSDs of Measix FRS / cut over range
PSD_M_FRS_PL_range  = PSD_M_FRS_PL(down_lim:up_lim);              % [N^2/Hz]   POS
PSD_M_FRS_CON_range = PSD_M_FRS_CON(down_lim:up_lim);             % [N^2/Hz]   CON
PSD_M_FRS_BSW_range = PSD_M_FRS_BSW(down_lim:up_lim);             % [N^2/Hz]   BSW
PSD_M_FRS_BG_range  = PSD_M_FRS_BG(down_lim:up_lim);              % [N^2/Hz]   ILO

%% Calculating Transfers

% PSD of Floor Vibrations (FV) to X / for mass one
FV_RESP  = PSD_FV_TOTAL_x .* (Xf_to_X1.^2);
DDF_RESP = PSD_M_FRS_CON  .* (F_to_X1.^2);
```

```
% PSDs of Measix FRS / cut over range
PSD_M_FRS_PL_range  = PSD_M_FRS_PL(down_lim:up_lim);           % [N^2/Hz]   POS
PSD_M_FRS_CON_range = PSD_M_FRS_CON(down_lim:up_lim);          % [N^2/Hz]   CON
PSD_M_FRS_BSW_range = PSD_M_FRS_BSW(down_lim:up_lim);          % [N^2/Hz]   BSW
PSD_M_FRS_BG_range  = PSD_M_FRS_BG(down_lim:up_lim);           % [N^2/Hz]   ILO

cd 'C:\Users\Arjan\Documents\My Dropbox\MAPPER\Mapper - results [04 06 2013] on\(1)\Matlab\Stage Stability B
load Variables_from_Weighting_Function

Error_f = W_cv_6DOF_2D_XT.^2 * PSD_M_FRS_PL';      % [m/Hz] Cooling Forces filtered by Weighting Function
% Error =

%% Calculating Transfers  / always square the transfers!

% PSD of Floor Vibrations (FV) to X / for mass one
FV_RESP  = PSD_FV_TOTAL_x .* (Xf_to_X1.^2);
DDF_RESP = PSD_M_FRS_CON  .* (F_to_X1.^2);

% PSD of (parasitic) Measured Forces (MF) due to FV // with dyn force sensor, FF_A * M_module (until resonan
PSD_MF_FV_PL  = PSD_FV_TOTAL_a .* M_PL;
PSD_MF_FV_CON = PSD_FV_TOTAL_a .* M_CON;
PSD_MF_FV_BSW = PSD_FV_TOTAL_a .* M_BSW;
PSD_MF_FV_BG  = PSD_FV_TOTAL_a .* M_BG;

%% Expressions for PSD - CPS - ASD - CAS

% PSD to CPS // Use to compare perf. with spec's and determining largest error contribution
CPS = (cumsum(PSD_M_FRS_PL.*dHz));                                   % [SI^2]        RMS value (sqrt(

% PSD to CPS - via ASD and CAS
CPS_2 = (  (cumsum( (PSD_M_FRS_PL.^0.5)  .*  (dHz.^0.5) )) .^2);

% PSD to ASD // Often sensor performance is indicated at certain decades in ASD
ASD = PSD_M_FRS_PL.^0.5;                                             % [SI/sqrt(Hz)]  RMS value (sqrt(

% PSD to CAS - directly // Tells you the total outcome (often: error)
CAS_via_CPS = (cumsum(PSD_M_FRS_PL.*dHz)).^0.5;                            % [SI]          RMS value
CAS_via_ASD = cumsum((PSD_M_FRS_PL.^0.5).*(dHz));                                    % [SI]

% PSD to CAS - via CPS // Tells you the total outcome (often: error)
CAS_2 = CPS.^0.5;                                                  % [SI]          RMS value (sqrt(..
CAS_3 = sqrt(cumsum(PSD_M_FRS_PL.*dHz));
```

```
%% Shifting Center Frequency of Expected Response

clear all
close all
clc
%
% %% AA
% % AA - theory
% x=0:0.01:20;
% yt=(86/13.8)*x;
%
% % Reference
% Xr = 13.8;
% Yr = 86;
% Xdel = 17-4;
%
% % AA -- measured
% Ydel_1 = 2;
% a1 = Ydel_1/Xdel;
% b1 = 86 - (a1*Xr);
% y1 = b1 + a1*x;

% BG -- fit
Ydel_2 = 0.274989;
a2 = Ydel_2/Xdel;
b2 = 86 - (a2*Xr);
y2 = b2 + a2*x;

% BSW -- fit
Ydel_3 = 6.3236;
a3 = Ydel_3/Xdel;
b3 = 86 - (a3*Xr);
y3 = b3 + a3*x;

% POS -- fit
Ydel_4 = 65.4498;
a4 = Ydel_4/Xdel;
b4 = 86 - (a4*Xr);
y4 = b4 + a4*x;

% CON -- fit
Ydel_5 = 1.6326;
a5 = Ydel_5/Xdel;
b5 = 86 - (a5*Xr);
y5 = b5 + a5*x;
%
% % Calculate Expected Shifts
% AA                 = 13.8;  % [1/min]
% BG                 = 6;     % [1/min]
% BSW_CLBC           = 6;     % [1/min]
% BSW_BLK            = 3.8;   % [1/min]
% POS                = 0.33;  % [1/min]
% CON                = 3;     % [1/min]
%
% SHIFT_BG           = 86 - y2(601)
% SHIFT_BSW_CLBC     = 86 - y3(601)
% SHIFT_BSW_BLK      = 86 - y3(381)
% SHIFT_POS          = 86 - y4(34)
% SHIFT_CON          = 86 - y5(301)
```

D-3: Determining the FRS Spectrum

MAPPER lithography

Iterative computations to scale- and shift FRS based on TNO research and Vibronix tests

```matlab
%% Initialize
% clear all
close all
% clc

%% Import Variables
cd('C:\Users\Arjan\Documents\My Dropbox\MAPPER\Matlab\2. Stage Stability Budgeting - Matrix\Weighting Function')
load('Variables_Weighting_Function','FC_cooling','PSD_FC_cooling_6DOF','W_cv_6DOF_2D', 'W_cv_6DOF_2D_XT', 'CT_EO_slit',

%% Defining Frequency Domain
% frequency range
total_range = [0.03 6000];  % [Hz]      Total frequency range to look at [Hz]
range = [0 200];            % [Hz]      Frequency range of interest for requirements [Hz]

% Determine boundaries for frequency range of interest
down_lim = find(log_vector>range(1),1,'first');
up_lim   = find(log_vector>range(2),1,'first');
dHz_cut  = dHz(down_lim:up_lim);                        % taking cut at same dimension as range

% Create logaritmic vector for range of interest
log_vector_range   = log_vector(down_lim:up_lim);       % frequency range of interest
log_vector_range_w = log_vector_range*2*pi;             % Freq range vector in rad/s, needed for freq response

%% Define (rebudgeted) Cooling Force Budgets // error on wafer
wafer_budget_PL_3DOF   = [1.653e-10, 1.653e-10, 9.519e-10];  % [m]
wafer_budget_CON_3DOF  = [1.121e-10, 1.121e-10, 6.457e-10];  % [m]
wafer_budget_BSW_3DOF  = [6.508e-10, 6.508e-10, 3.747e-9];   % [m]
wafer_budget_BG_3DOF   = [1.637e-10, 1.637e-10, 9.424e-10];  % [m]

%% Cooling Force Spectra (DDF)

%%% USED FACTORS (Conservative Approach) (0-6000 Hz) -- PROPER WAFER ERROR COMPUTATION
factor_PL  = 1.942e-7;      % [-]   DONE - with expected force spectrum shifted ~16.76 Hz (more for lower freq than for
factor_CON = 8.896e-8;      % [-]   DONE - with expected force spectrum shifted ~6.02  Hz (more for lower freq than for
factor_BSW = 2.986e-6;      % [-]   DONE - with average flow velocity ~ that of AA and also center freq shift of +7 and
factor_BG  = 1.892e-7;      % [-]   DONE - with expected force spectrum shifted ~1.42  Hz (more for lower freq than for


% CAS_error_3DOF_M3_PL(1,3000)  = 1e-20; % [m]
% CAS_error_3DOF_M3_CON(1,3000) = 1e-20; % [m]
CAS_error_3DOF_M3_BSW(1,3000) = 1e-20; % [m]
% CAS_error_3DOF_M3_BG(1,3000)  = 1e-20; % [m]

k=0;

% Load FRS per Module
cd('C:\Users\Arjan\Documents\My Dropbox\MAPPER\Matlab\3. Dynamic Error Budgeting\Forcesix Requirements')
load Variables_PSD_FRS_PL_unscaled_shifted
load Variables_PSD_FRS_CON_unscaled_shifted
load Variables_PSD_FRS_BSW_unscaled
```

```matlab
load Variables_PSD_FRS_BSW_unscaled_proof

% Scale Force Requirement Spectrum to Height -- where wafer error matches rebudgeted budget

% while CAS_error_3DOF_M3_PL(1,3000)  <=  wafer_budget_PL_3DOF(1)
% while CAS_error_3DOF_M3_CON(1,3000) <=  wafer_budget_CON_3DOF(1)
while CAS_error_3DOF_M3_BSW(1,3000) <=  wafer_budget_BSW_3DOF(1)
% while CAS_error_3DOF_M3_BG(1,3000)  <=  wafer_budget_BG_3DOF(1)

% Increase factor every loop
% factor_PL  = factor_PL  + 1e-10
% factor_CON = factor_CON + 1e-11
% factor_BSW = factor_BSW + 1e-9;
% factor_BG  = factor_BG  + 1e-10

% % use to proof that my requirement spectrum is saver
factor_BSW_proof = factor_BSW_proof + 1e-7;

% Counter for number of Iterations
k = k + 1

%% Scaling FRS to requirement [N/Hz]
%%% Generic Shape // must be done separate for PSD calculation

PSD_FRS_PL   = factor_PL   * PSD_FRS_PL_unscaled_shifted;          % [N^2/Hz]
PSD_FRS_CON  = factor_CON  * PSD_FRS_CON_unscaled_shifted;         % [N^2/Hz]
% PSD_FRS_BSW  = factor_BSW  * PSD_FRS_BSW_unscaled;                 % [N^2/Hz]
PSD_FRS_BG   = factor_BG   * PSD_FRS_BG_unscaled_shifted;          % [N^2/Hz]

% % use to proof that my requirement spectrum is saver
PSD_FRS_BSW  = factor_BSW_proof  * PSD_FRS_BSW_unscaled_proof;                % [N^2/Hz]

% PSD -- 6-DOF  (6x3000)              // scaling per DOF: <1 1 10 2 2 10>          assumption for relation between CF DOFs
PSD_FRS_6DOF_PL  = [PSD_FRS_PL; PSD_FRS_PL; PSD_FRS_PL*10; PSD_FRS_PL*2; PSD_FRS_PL*2; PSD_FRS_PL*10];
PSD_FRS_6DOF_CON = [PSD_FRS_CON; PSD_FRS_CON; PSD_FRS_CON*10; PSD_FRS_CON*2; PSD_FRS_CON*2; PSD_FRS_CON*10];
PSD_FRS_6DOF_BSW = [PSD_FRS_BSW; PSD_FRS_BSW; PSD_FRS_BSW*10; PSD_FRS_BSW*2; PSD_FRS_BSW*2; PSD_FRS_BSW*10];
PSD_FRS_6DOF_BG  = [PSD_FRS_BG; PSD_FRS_BG; PSD_FRS_BG*10; PSD_FRS_BG*2; PSD_FRS_BG*2; PSD_FRS_BG*10];

%% Calculate Wafer Error

WF_SQ = W_cv_6DOF_2D.^2;

%% PL  - compute 6DOF PSD error by filtering with WF

PSD_error_1DOF_to_DOFs_PL=zeros(36,3000);
PSD_error_6DOF_PL = zeros(6,3000);                              % [m^2/Hz]

% PSD - Errors per DOF_to_DOFs // per frequency [36x3000]

%      [36x3000]          =       [6x3000]          .* [36x3000]
%       [m^2/Hz]                   [N^2/Hz]              [m^2/N^2]

for i=1:6
    PSD_error_1DOF_to_DOFs_PL(i,:)     = PSD_FRS_6DOF_PL(1,:) .* WF_SQ(i,:);       % X  to 6DOFs
    PSD_error_1DOF_to_DOFs_PL(i+6,:)   = PSD_FRS_6DOF_PL(2,:) .* WF_SQ(i+6,:);     % Y  to 6DOFs
    PSD_error_1DOF_to_DOFs_PL(i+12,:)  = PSD_FRS_6DOF_PL(3,:) .* WF_SQ(i+12,:);    % Z  to 6DOFs
    PSD_error_1DOF_to_DOFs_PL(i+18,:)  = PSD_FRS_6DOF_PL(4,:) .* WF_SQ(i+18,:);    % Rx to 6DOFs
```

D-3: Determining the FRS Spectrum

MAPPER lithography

Iterative computations to scale- and shift FRS based on TNO research and Vibronix tests

```
    PSD_error_1DOF_to_DOFs_PL(i+24,:)  = PSD_FRS_6DOF_PL(5,:) .* WF_SQ(i+24,:);    % Ry to 6DOFs
    PSD_error_1DOF_to_DOFs_PL(i+30,:)  = PSD_FRS_6DOF_PL(6,:) .* WF_SQ(i+30,:);    % Rz to 6DOFs
end

% Allocating Errors to single DOFs // per frequency [6x3000] -- [m^2/Hz]
for i=1:6
    PSD_error_6DOF_PL(i,:) = PSD_error_1DOF_to_DOFs_PL(i,:)    + PSD_error_1DOF_to_DOFs_PL(i+6,:)  + PSD_error_1DOF_to_DOFs_PL(i+12,:)  + ...
                             PSD_error_1DOF_to_DOFs_PL(i+18,:) + PSD_error_1DOF_to_DOFs_PL(i+24,:) + PSD_error_1DOF_to_DOFs_PL(i+30,:);
end

% ---------------------------------------------------------------------------

%% CON - compute 6DOF PSD error by filtering with WF

PSD_error_1DOF_to_DOFs_CON=zeros(36,3000);
PSD_error_6DOF_CON = zeros(6,3000);                              % [m^2/Hz]

% PSD - Errors per DOF_to_DOFs // per frequency [36x3000]

%      [36x3000]          =        [6x3000]          .* [36x3000]
%       [m^2/Hz]                    [N^2/Hz]              [m^2/N^2]

for i=1:6
    PSD_error_1DOF_to_DOFs_CON(i,:)      = PSD_FRS_6DOF_CON(1,:) .* WF_SQ(i,:);        % X  to 6DOFs
    PSD_error_1DOF_to_DOFs_CON(i+6,:)    = PSD_FRS_6DOF_CON(2,:) .* WF_SQ(i+6,:);      % Y  to 6DOFs
    PSD_error_1DOF_to_DOFs_CON(i+12,:)   = PSD_FRS_6DOF_CON(3,:) .* WF_SQ(i+12,:);     % Z  to 6DOFs
    PSD_error_1DOF_to_DOFs_CON(i+18,:)   = PSD_FRS_6DOF_CON(4,:) .* WF_SQ(i+18,:);     % Rx to 6DOFs
    PSD_error_1DOF_to_DOFs_CON(i+24,:)   = PSD_FRS_6DOF_CON(5,:) .* WF_SQ(i+24,:);     % Ry to 6DOFs
    PSD_error_1DOF_to_DOFs_CON(i+30,:)   = PSD_FRS_6DOF_CON(6,:) .* WF_SQ(i+30,:);     % Rz to 6DOFs
end

% Allocating Errors to single DOFs // per frequency [6x3000] -- [m^2/Hz]
for i=1:6
    PSD_error_6DOF_CON(i,:) = PSD_error_1DOF_to_DOFs_CON(i,:)    + PSD_error_1DOF_to_DOFs_CON(i+6,:)  + PSD_error_1DOF_to_DOFs_CON(i+12,:)  + ...
                              PSD_error_1DOF_to_DOFs_CON(i+18,:) + PSD_error_1DOF_to_DOFs_CON(i+24,:) + PSD_error_1DOF_to_DOFs_CON(i+30,:);
end

% ---------------------------------------------------------------------------

%% BSW - compute 6DOF PSD error by filtering with WF

PSD_error_1DOF_to_DOFs_BSW=zeros(36,3000);
PSD_error_6DOF_BSW = zeros(6,3000);                              % [m^2/Hz]

% PSD - Errors per DOF_to_DOFs // per frequency [36x3000]

%      [36x3000]          =        [6x3000]          .* [36x3000]
%       [m^2/Hz]                    [N^2/Hz]              [m^2/N^2]

for i=1:6
    PSD_error_1DOF_to_DOFs_BSW(i,:)      = PSD_FRS_6DOF_BSW(1,:) .* WF_SQ(i,:);        % X  to 6DOFs
    PSD_error_1DOF_to_DOFs_BSW(i+6,:)    = PSD_FRS_6DOF_BSW(2,:) .* WF_SQ(i+6,:);      % Y  to 6DOFs
    PSD_error_1DOF_to_DOFs_BSW(i+12,:)   = PSD_FRS_6DOF_BSW(3,:) .* WF_SQ(i+12,:);     % Z  to 6DOFs
    PSD_error_1DOF_to_DOFs_BSW(i+18,:)   = PSD_FRS_6DOF_BSW(4,:) .* WF_SQ(i+18,:);     % Rx to 6DOFs
    PSD_error_1DOF_to_DOFs_BSW(i+24,:)   = PSD_FRS_6DOF_BSW(5,:) .* WF_SQ(i+24,:);     % Ry to 6DOFs
    PSD_error_1DOF_to_DOFs_BSW(i+30,:)   = PSD_FRS_6DOF_BSW(6,:) .* WF_SQ(i+30,:);     % Rz to 6DOFs
end
```

```
%% PL  - turn 6DOF PSD error in 6DOF CPS and 6DOF CAS error
%        and weight 6DOF CAS error via EO_slit to 3DOF CAS error

% Method 3 -- USE!
% 3) from 6DOF PSD [m^2/Hz] into 6DOF CPS [m^2] and 6DOF CAS [m] then by CT_SLIT to 3DOF CAS [m], then CAS [m]

% CPS -- 6-DOF Error [m^2]
CPS_error_6DOF_M3_PL=zeros(6,3000);

for i=1:6
    CPS_error_6DOF_M3_PL(i,:) = cumsum((PSD_error_6DOF_PL(i,:).*dHz),2);     % PSD>CPS = discrete integration --
end

% CAS -- 3-DOF [m]
CAS_error_3DOF_M3_PL=zeros(3,3000);                                          % (3-sigma RMS value) -- RMS is sqrt
CAS_error_6DOF_M3_PL = sqrt(CPS_error_6DOF_M3_PL);

for i=1:3000
    CAS_error_3DOF_M3_PL(:,i) = 3*abs(CT_EO_slit*CAS_error_6DOF_M3_PL(:,i));
end

% ---------------------------------------------------------------------------

%% CON - turn 6DOF PSD error in 6DOF CPS and 6DOF CAS error
%        and weight 6DOF CAS error via EO_slit to 3DOF CAS error

% Method 3 -- USE!
% 3) from 6DOF PSD [m^2/Hz] into 6DOF CPS [m^2] and 6DOF CAS [m] then by CT_SLIT to 3DOF CAS [m], then CAS [m]

% CPS -- 6-DOF Error [m^2]
CPS_error_6DOF_M3_CON=zeros(6,3000);

for i=1:6
    CPS_error_6DOF_M3_CON(i,:) = cumsum((PSD_error_6DOF_CON(i,:).*dHz),2);     % PSD>CPS = discrete integration -
end

% CAS -- 3-DOF [m]
CAS_error_3DOF_M3_CON=zeros(3,3000);                                          % (3-sigma RMS value) -- RMS is sqr
CAS_error_6DOF_M3_CON = sqrt(CPS_error_6DOF_M3_CON);

for i=1:3000
    CAS_error_3DOF_M3_CON(:,i) = 3*abs(CT_EO_slit*CAS_error_6DOF_M3_CON(:,i));
end

% ---------------------------------------------------------------------------

%% BSW - turn 6DOF PSD error in 6DOF CPS and 6DOF CAS error
%        and weight 6DOF CAS error via EO_slit to 3DOF CAS error

% Method 3 -- USE!
% 3) from 6DOF PSD [m^2/Hz] into 6DOF CPS [m^2] and 6DOF CAS [m] then by CT_SLIT to 3DOF CAS [m], then CAS [m]

% CPS -- 6-DOF Error [m^2]
CPS_error_6DOF_M3_BSW=zeros(6,3000);

for i=1:6
    CPS_error_6DOF_M3_BSW(i,:) = cumsum((PSD_error_6DOF_BSW(i,:).*dHz),2);     % PSD>CPS = discrete integration -
end
```

D-4: Dynamic Error Budgeting (DEB)

MAPPER lithography

Modeling the effect of all disturbances in [Z] for concept B – *importing all computed variables*

```
%% %%%%%%%%%%%%%%%%%%%%%%%%%%%%%% Concept 2 - Direct Force [Piezo] %%%%%%%%%%%%%%%%%%%%%%%%%%%%%%%%%%%

%% Test Setup - Modeling Disturbances

% Author:                                     Arjan de Wildt
% Date:                                       07-06-2013
% Institute:                                  Delft University of Technology
% Company:                                    Mapper Lithography

% This document constitutes the simulation of a 1 DOF 1 Mass-Spring_Damper (MSD) system, in which different
% floor vibrations- and direct disturbance forces (DDF) spectra can be inputted. This with the objective of
% analyzing what FIV forces can be measured. This will determine if the set module requirements can be
% verified with Forcesix and if so quantify the performance that can be achieved.
%% Initialize
clear all
close all
clc

%% Importing Variables
% Weighting Function
cd 'C:\Users\Arjan\Documents\My Dropbox\MAPPER\Matlab\2. Stage Stability Budgeting - Matrix\Weighting Function'
load Variables_Weighting_Function

% Floor Vibrations -- Mapper VC
cd 'C:\Users\Arjan\Documents\My Dropbox\MAPPER\Matlab\3. Dynamic Error Budgeting\Floor Vibrations\VC-Mapper - Measured\50 kHz (F
load Variables_Floor_Vibrations

% Floor Vibration -- FIT
cd 'C:\Users\Arjan\Documents\My Dropbox\MAPPER\Matlab\3. Dynamic Error Budgeting\Floor Vibrations\VC-Mapper Rdam - Fitted'
load Variables_Floor_Vibrations_FIT

% Cooling Forces -- Requirement Spectra
cd 'C:\Users\Arjan\Documents\My Dropbox\MAPPER\Matlab\3. Dynamic Error Budgeting\Forcesix Requirements'
load Variables_FINAL_FRS

% Acoustics -- FIT
cd('C:\Users\Arjan\Documents\My Dropbox\MAPPER\Matlab\3. Dynamic Error Budgeting\Acoustics')
load 'Variables_Acoustics_FIT'

% Acoustics Inside -- FIT
cd('C:\Users\Arjan\Documents\My Dropbox\MAPPER\Matlab\3. Dynamic Error Budgeting\Acoustics')
load('Variables_Acoustics_inside_FIT')

% Sensor
cd('C:\Users\Arjan\Documents\My Dropbox\MAPPER\Matlab\3. Dynamic Error Budgeting\Sensors\Force')
load 'Variables_PCB209C11_Noise_Level'

% Cables
cd('C:\Users\Arjan\Documents\My Dropbox\MAPPER\Matlab\3. Dynamic Error Budgeting\Cable Noise')
load 'Variables_Cable_Noise_Force'

% DAQ
cd('C:\Users\Arjan\Documents\My Dropbox\MAPPER\Matlab\3. Dynamic Error Budgeting\DAQ Noise')
load 'Variables_DAQ_Noise_Force'
% Transfer Functions
cd('C:\Users\Arjan\Documents\My Dropbox\MAPPER\Matlab\3. Dynamic Error Budgeting\Transfer Functions')
load 'Variables_Transfer_Functions_Force'

%% Module Data
% Mass Module Keeper
M_MK = 16.88;                      % [kg]  -- tuned for M_BSW = 30 kg == overestimate, but needs to cover/hold BSW and at Wn > 300

% Mass Sensors [M86 or M731A]
M_Sensor = 0.008;                  % [kg]  -- Miniature Quartz Sensor = 8 gram (datasheet+called)
M_Bolt   = 0.010;                  % [kg]  -- connection bolt
M_Cable  = 0.012;                  % [kg]  -- SMT-100 is 1.8 kg/100 m = 1800 gram/100 m = 18 gram/m so say 12 gram for 60 cm
```

```
% Mass Modules -- have taken the undeviated value!
M_PL     = M_MK + 6*(M_Sensor+M_Bolt+M_Cable) + 3*M_Triangle + 3.05;  % [kg] 3.05 +-1.0 kg -- acc
W_PL     = M_PL*g;                                                    % [N]  // weight POS

M_CON    = M_MK + 6*(M_Sensor+M_Bolt+M_Cable) + 3*M_Triangle + 1.75;  % [kg] 1.75 +- 0.5 kg -- ac
W_CON    = M_CON*g;                                                   % [N]  // weight CON

M_BSW    = M_MK + 6*(M_Sensor+M_Bolt+M_Cable) + 3*M_Triangle + 7.5;   % [kg] 7.5 +- 0.5 kg -- acc
W_BSW    = M_BSW*g;                                                   % [N]  // weight BSW

M_BG     = M_MK + 6*(M_Sensor+M_Bolt+M_Cable) + 3*M_Triangle + 182.7; % [kg] 182.7 +- 2 kg   -- a
W_BG     = M_BG*g;                                                    % [N]  // weight ILO

M_AA     = 2*0.8 + 7.44;                                              % [kg] 7.44 kg AA + M86 (0.
W_AA     = M_AA*g;                                                    % [N]  // weight AA

%% Dynamic Inputs
%%% First MASS
m_gp = 550;                    % [kg]      granite plate
m_casing = 50;                 % [kg]      mounts + casing + tubes
% ---------------------------------------------------------------------------------------------
m1 = m_gp+m_casing;            % [kg]
% ---------------------------------------------------------------------------------------------

%%% Second MASS
% ---------------------------------------------------------------------------------------------
m2 = 115;                      % [kg]      mass of second plate
% ---------------------------------------------------------------------------------------------

%%% Third MASS
% ---------------------------------------------------------------------------------------------
% Also change FRS from ... to ...
% m3 = M_AA;                     % [kg]
% m3 = M_BG;                     % [kg]
% m3 = M_CON;                    % [kg]
% m3 = M_PL;                     % [kg]
m3 = M_BSW;                    % [kg]
% ---------------------------------------------------------------------------------------------

%%% Forth "MASS"  -- only taking the stiffness of the tubing into account right know
R_tube = 0.005;                % [m]       radius of tube of 1 cm internal diameter
L_tube = 0.5;                  % [m]       effective length of inside tubing
V_tube = pi*(R_tube^2)*L_tube;% [m^3]     volume of water in inside tube
D_water = 999;                 % [kg/m^3]  density water (20 C - 4 bar)
M_water = V_tube*D_water;      % [kg]      mass of water in tube

M_tube_p_m = 0.7;              % [kg/m]    mass of tubing only / per m (10 m flexible tubing ~ 7 kg
M_tube = M_tube_p_m*L_tube;    % [kg]      mass of this length of tubing
% ---------------------------------------------------------------------------------------------
m4 = M_water + M_tube;         % [kg]      mass of piece of internal tubing + water = EXCLUDING PLA
% m4=3;
% ---------------------------------------------------------------------------------------------
K_tube = (0.2*9.81)/0.01;      % [N/m] -- = 200 N/m (soft pillow - RMS) -- rough estimate is that 2
% K_tube = 2500;                  % [N/m] -- = 1000 N/m    (10000 N/m = car suspension / soft couch -
k4 = K_tube;                   % [N/m]     transverse stiffness of tubing
```

D-4: Dynamic Error Budgeting (DEB)

MAPPER lithography

Modeling the effect of all disturbances in [Z] for concept B – *floor vibrations* & *external acoustics*

```
%% Floor Vibrations      -- "finding out required configuration"

    %% 0-MSD // Piezo directly on Floor
%  [N^2/Hz]           =  [(m/s^2)^2/Hz]       [kg^2]
PSD_MF_FV_0MSD_PL     = PSD_FV_FIT_TOTAL_a .* (M_PL^2);        % From piezo dynamics, measured error that r
PSD_MF_FV_0MSD_CON    = PSD_FV_FIT_TOTAL_a .* (M_CON^2);
PSD_MF_FV_0MSD_BSW    = PSD_FV_FIT_TOTAL_a .* (M_BSW^2);
PSD_MF_FV_0MSD_BG     = PSD_FV_FIT_TOTAL_a .* (M_BG^2);

    %% 1-MSD // Piezo on one airmount                               % Note Xf_to_X1 = Af_to_A1!
% [(m/s^2)^2/Hz]      =  [(m/s^2)^2/Hz]        [m^2/m^2]
PSD_FV_1MSD_a         = PSD_FV_FIT_TOTAL_a .* (ONE_MSD_Xf_to_X1.^2);   % Acceleration of Plate
                                                                 % Note: for transmissibility, x_to_x = v_to_
%  [N^2/Hz]           = [(m/s^2)^2/Hz]   [kg^2]
PSD_MF_FV_1MSD_PL     = PSD_FV_1MSD_a   .*   (M_PL^2);
PSD_MF_FV_1MSD_CON    = PSD_FV_1MSD_a   .*   (M_CON^2);
PSD_MF_FV_1MSD_BSW    = PSD_FV_1MSD_a   .*   (M_BSW^2);
PSD_MF_FV_1MSD_BG     = PSD_FV_1MSD_a   .*   (M_BG^2);

    %% 2-MSD // Piezo on 2 airmounts -- using 2 MSD TFs                      % Note Xf_to_X1 = Af_to_
%%% using 2 MSD TFs

% [(m/s^2)^2/Hz]          =  [(m/s^2)^2/Hz]        [m^2/m^2]
PSD_FV_2MSD_2TF_a         = PSD_FV_FIT_TOTAL_a .* (TWO_MSD_Xf_to_X2.^2);    % Acceleration of Plate // second mass

%  [N^2/Hz]               = [(m/s^2)^2/Hz]   [kg^2]
PSD_MF_FV_2MSD_2TF_PL     = PSD_FV_2MSD_2TF_a   .*   (M_PL^2);
PSD_MF_FV_2MSD_2TF_CON    = PSD_FV_2MSD_2TF_a   .*   (M_CON^2);
PSD_MF_FV_2MSD_2TF_BSW    = PSD_FV_2MSD_2TF_a   .*   (M_BSW^2);
PSD_MF_FV_2MSD_2TF_BG     = PSD_FV_2MSD_2TF_a   .*   (M_BG^2);

    %% 2-MSD // Piezo on 2 airmounts -- using 3 MSD TFs
%  [N^2/Hz]               = [(m/s^2)^2/Hz]          [N^2/(m/s^2)^2]
PSD_MF_FV_2MSD            = PSD_FV_FIT_TOTAL_a  .* (Af_to_Fmeas.^2);    % = EXACTLY the same as PSD_FV_FIT_TOTAL x
%% Acoustics               -- "finding out required configuration"
% --- 2 MSD // Piezo on 2 airmounts                                 % Note Xf_to_X1 = Af_to_A1!

    %% AC   -- External Acoustics

        %% Case at M2                    -- force exerts at M2
%%% using 2 MSD TFs
A = 3;                                                              % [m^2] // estimated outside surface area

% [(N^2)/Hz]                = [(N/m^2)^2/Hz]     [m^4]
PSD_AC_FIT_newton           = (PSD_AC_FIT)    .*   (A^2);

% DISPLACEMENT of M2
% [(m)^2/Hz]                =     [N^2/Hz]             [m^2/N^2]
PSD_AC_2MSD_X2_dueto_F2     = PSD_AC_FIT_newton .* (TWO_MSD_F2_to_X2.^2);

% VELOCITY of M2
% [(m)^2/Hz]                =     [N^2/Hz]             [(m/s)^2/N^2]
PSD_AC_2MSD_V2_dueto_F2     = PSD_AC_FIT_newton .* (TWO_MSD_F2_to_V2.^2);    %%%% OR :
% [(m/s)^2/Hz]              =     [(m)^2/Hz]           [(1/s)^2]
PSD_AC_2MSD_V2_dueto_F2_dV= PSD_AC_2MSD_X2_dueto_F2   .* (2*pi*log_vector).^2;    % differentiating once

% ACCELERATION of M2
% [(m)^2/Hz]                =     [N^2/Hz]              [(m/s^2)^2/N^2]
PSD_AC_2MSD_V2_dueto_F2     = PSD_AC_FIT_newton .* (TWO_MSD_F2_to_A2.^2);    %%%% OR :
% [(m/s^2)^2/Hz]            =   [(m/s)^2/Hz]                 [(1/s)^2]
PSD_AC_2MSD_A2_dueto_F2_dA= PSD_AC_2MSD_V2_dueto_F2 .* (2*pi*log_vector).^2;    % differentiating once
```

```
% MEASURED FORCE (MF) BY PIEZO -- same naming as below
% [N^2/Hz]                 = [(m/s^2)^2/Hz]               [kg^2]
PSD_MF_AC_2MSD_2TF_PL      = PSD_AC_2MSD_A2_dueto_F2_dA  .*  (M_PL^2);
PSD_MF_AC_2MSD_2TF_CON     = PSD_AC_2MSD_A2_dueto_F2_dA  .*  (M_CON^2);
PSD_MF_AC_2MSD_2TF_BSW     = PSD_AC_2MSD_A2_dueto_F2_dA  .*  (M_BSW^2);
PSD_MF_AC_2MSD_2TF_BG      = PSD_AC_2MSD_A2_dueto_F2_dA  .*  (M_BG^2);

%%% using 3 MSD TFs
%  [N^2/Hz]                =      [N^2/Hz]              [N^2/N^2]
PSD_MF_AC_2MSD             = PSD_AC_FIT_newton  .*  (F2_to_Fmeas.^2);

% %%% Plotting
% % MF due to AC vs. FRS -- comparison 2 MSD TFs with 3 MSD TFs
% figure
% loglog(log_vector,PSD_FRS_6DOF_PL(3,:),'r',log_vector,PSD_FRS_6DOF_CON(3,:),'r--',log_vector,PSD_MF_AC_2MSD_2TF_
% title('Comparison Measured Forces [AC on M2] vs. Requirement - for 2MSD TF and 3MSD TF  [PL]')
% xlabel('Frequency [Hz]')
% ylabel('Magnitude [N^2/Hz]')
% axis([1e0 3e3 1e-18 1e0])
% hl(1)=legend('FRS - PL-BSW','FRS - CON','MF (AC) - 2MSD - 30 kg','MF (AC) - 2 MSD (3MSD TF) - 30 kg','location',
% grid on

         %% Case at M1, surrounding M2  -- force exerts at M1
%%% using 2 MSD TFs
A = 3;          % [m^2] // estimated outside surface area

% [(N^2)/Hz]               = [(N/m^2)^2/Hz]     [m^4]
PSD_AC_FIT_newton          = (PSD_AC_FIT)    .*   (A^2);

% DISPLACEMENT OF SECOND MASS -- force*compliancy
% [(m)^2/Hz]               =      [N^2/Hz]              [m^2/N^2]
PSD_ACi_2MSD_2TF_A2_dueto_F2    = PSD_AC_FIT_newton .* (TWO_MSD_F1_to_X2.^2);

% DISPLACEMENT OF SECOND MASS -- force*compliancy
% [(m)^2/Hz]               =      [N^2/Hz]              [m^2/N^2]
PSD_ACi_2MSD_2TF_A2_dueto_F2    = PSD_AC_FIT_newton .* (TWO_MSD_F1_to_X2.^2);

% VELOCITY OF SECOND MASS
% [(m/s)^2/Hz]             =     [(m)^2/Hz]              [(1/s)^2]
PSD_AC_2MSD_2TF_V2_dueto_F1    = PSD_ACi_2MSD_2TF_A2_dueto_F2   .* (2*pi*log_vector).^2;    % differentiating once

% ACCELERATION OF SECOND MASS
% [(m/s^2)^2/Hz]           =   [(m/s)^2/Hz]              [(1/s)^2]
PSD_AC_2MSD_2TF_A2_dueto_F1    = PSD_AC_2MSD_2TF_V2_dueto_F1 .* (2*pi*log_vector).^2;    % differentiating once

% MEASURED FORCE BY PIEZO -- same naming as above
% [N^2/Hz]                 = [(m/s^2)^2/Hz]               [kg^2]
PSD_MF_AC_2MSD_2TF_PL      = PSD_AC_2MSD_2TF_A2_dueto_F1   .*   (M_PL^2);
PSD_MF_AC_2MSD_2TF_CON     = PSD_AC_2MSD_2TF_A2_dueto_F1   .*   (M_CON^2);
PSD_MF_AC_2MSD_2TF_BSW     = PSD_AC_2MSD_2TF_A2_dueto_F1   .*   (M_BSW^2);
PSD_MF_AC_2MSD_2TF_BG      = PSD_AC_2MSD_2TF_A2_dueto_F1   .*   (M_BG^2);

%%% using 3 MSD TFs
%  [N^2/Hz]                =      [N^2/Hz]              [N^2/N^2]
PSD_MF_AC_2MSD             = PSD_AC_FIT_newton  .*  (F1_to_Fmeas.^2);

% %%% Plotting
% % MF due to AC vs. FRS -- comparison 2 MSD TFs with 3 MSD TFs
```

D-4: Dynamic Error Budgeting (DEB)

MAPPER lithography

Modeling the effect of all disturbances in [Z] for concept B – *internal acoustics* & *FRS levels*

```
%%% NOW WITH REDUCTION (calibration)
% Loading Reduced Acoustical Spectrum
cd('C:\Users\Arjan\Documents\My Dropbox\MAPPER\Matlab\3. Dynamic Error Budgeting\Acoustics')
load('Variables_Acoustics_MIMO_fit')

%%% using 3 MSD TFs
%  [N^2/Hz]               =     [N^2/Hz]              [N^2/N^2]
PSD_MF_AC_2MSD            = PSD_AC_Meas_newton_RED  .*  (F1_to_Fmeas.^2);

% %%% Plotting
% % MF due to AC vs. FRS -- comparison 2 MSD TFs with 3 MSD TFs
% figure
% loglog(log_vector,PSD_FRS_6DOF_PL(3,:),'r',log_vector,PSD_FRS_6DOF_CON(3,:),'r--',log_vector,PSD_MF_AC_2MSD_2TF_BSW,'b',
% title('Comparison Measured Forces [AC] various stages vs. Requirement  [PL]')
% xlabel('Frequency [Hz]')
% ylabel('Magnitude [N^2/Hz]')
% axis([1e0 3e3 1e-18 1e-2])
% hl(1)=legend('FRS - PL-BSW','FRS - CON','MF (AC) - 2MSD - 30 kg','MF (AC) - 2 MSD (3MSD TF) - 30 kg','location','SE');
% grid on

    %% ACi  -- Internal Acoustics
A_plate = 3.14159265*(0.2^2)*2;            % [m^2] surface area Plate (top + bottom)
A_sensor = 2*3.14159265*0.05*0.15*2;       % [m^2] surface area Sensor + Dummy (modeled as cilinder)

A_in = A_plate+A_sensor;                   % [m^2] // estimated total outside surface area

% [(N^2)/Hz]                 = [(N/m^2)^2/Hz]              [m^4]
PSD_AC_Inside_FIT_newton     = (PSD_AC_Inside_FIT)   .*  (A_in^2);

          %% 2-MSD // -- using 2 MSD TFs
% ACCELERATION OF SECOND MASS -- force*compliancy
% [(m)^2/Hz]                 =     [N^2/Hz]              [m^2/N^2]
PSD_ACi_2MSD_2TF_A2_dueto_F2 = PSD_AC_Inside_FIT_newton .* (TWO_MSD_F2_to_A2.^2);

% MEASURED FORCE BY PIEZO
% [N^2/Hz]                   = [(m/s^2)^2/Hz]              [kg^2]
PSD_MF_ACi_2MSD_2TF_PL       = PSD_ACi_2MSD_2TF_A2_dueto_F2  .*  (M_PL^2);
PSD_MF_ACi_2MSD_2TF_CON      = PSD_ACi_2MSD_2TF_A2_dueto_F2  .*  (M_CON^2);
PSD_MF_ACi_2MSD_2TF_BSW      = PSD_ACi_2MSD_2TF_A2_dueto_F2  .*  (M_BSW^2);
PSD_MF_ACi_2MSD_2TF_BG       = PSD_ACi_2MSD_2TF_A2_dueto_F2  .*  (M_BG^2);

% MEASURED FORCE BY PIEZO -- checking that the AA could have been verified!
PSD_MF_ACi_2MSD_2TF_AA       = PSD_ACi_2MSD_2TF_A2_dueto_F2  .*  (M_AA^2);

          %% 2-MSD // -- using 3 MSD TFs
% MEASURED FORCE BY PIEZO // 2 MSD using 3 TFs
% [(m/s^2)^2/Hz]             =  [(m/s)^2/Hz]              [(1/s)^2]
PSD_MF_ACi_2MSD              = PSD_AC_Inside_FIT_newton   .* (F3_to_Fmeas).^2;    % have confirmed gives identical result


% MEASURED FORCE BY PIEZO -- checking that the AA could have been verified!
PSD_MF_ACi_2MSD_2TF_AA       = PSD_ACi_2MSD_2TF_A2_dueto_F2  .*  (M_AA^2);
```

```
%%% NOW WITH REDUCTION
% Loading Reduced Internal Acoustical Spectrum
cd('C:\Users\Arjan\Documents\My Dropbox\MAPPER\Matlab\3. Dynamic Error Budgeting\Acoustics')
load('Variables_Acoustics_Internal_MIMO_fit')

% [(N^2)/Hz]                 = [(N/m^2)^2/Hz]              [m^4]
PSD_AC_Inside_FIT_newton_RED     = (PSD_AC_Inside_RED)   .*  (A_in^2);


% MEASURED FORCE BY PIEZO // 2 MSD using 3 TFs
% [(m/s^2)^2/Hz]             =  [(m/s)^2/Hz]              [(1/s)^2]
PSD_MF_ACi_2MSD              = PSD_AC_Inside_FIT_newton_RED   .* (F3_to_Fmeas).^2;    % have confirmed gives identical result

% %%% Plotting
% % MF due to ACi vs. FRS -- comparison 2 MSD TFs with 3 MSD TFs
% figure
% loglog(log_vector,PSD_FRS_6DOF_PL(3,:),'r',log_vector,PSD_FRS_6DOF_CON(3,:),'r--',log_vector,PSD_MF_ACi_2MSD_2TF_BSW,'b',log
% title('Comparison Measured Forces [ACi] various stages vs. Requirement  [PL]')
% xlabel('Frequency [Hz]')
% ylabel('Magnitude [N^2/Hz]')
% axis([1e0 3e3 1e-18 1e-2])
% hl(1)=legend('FRS - PL-BSW','FRS - CON','MF (ACi) - 2MSD - 30 kg','MF (ACi) - 2 MSD (3MSD TF) - 30 kg','location','SE');
% grid on

% Modeling ForceSix
%%% Model Measured Signal on PLATE due to various DS

    % Establish Noise Bottom at FRS level -- Combining Noise Sources (Sensor+DAQ+Cable)

Noise Level (Sensor+Cable+DAQ)
PSD_NL_Sensor_Cable_DAQ  = ((PCB209C11_noise_PSD.^2)+(Total_Cables_PSD_newton.^2)+(PSD_DAQ_total_newton.^2)).^0.5;

%%% Plotting
% Showing total noise bottom (Sensor+Cable+DAQ)
hNL(1)=figure;
loglog(log_vector,PCB209C11_noise_PSD,'r',log_vector,PSD_DAQ_total_newton,'b',log_vector,Total_Cables_PSD_newton,'g',log_vecto
title('Showing Total Noise [Sensor+DAQ+Cables]')
xlabel('Frequency [Hz]')
ylabel('Magnitude [N^2/Hz]')
axis([1e0 3e3 1e-18 1e-8])
hl(1)=legend('Noise - PCB209C11','Total Noise [CN+QN+CT] - NI4472','Total Noise [JN/SN/EN] - SMT-100','Total Noise - Combined'
grid on
%%% Comparing Spectra vs. Measured
Resp_AV_PSD_BK_Ground_Z = freqresp(AV_PSD_BK_Ground_Z,log_vector_w);
Resp_AV_PSD_BK_Ground_Z = abs(Resp_AV_PSD_BK_Ground_Z);
Resp_AV_PSD_BK_Ground_Z = permute(Resp_AV_PSD_BK_Ground_Z,[1,3,2]);

PSD_FV_2MSD_M2a          = Resp_AV_PSD_BK_Ground_Z .* (TWO_MSD_Xf_to_X2.^2);      % Stone acceleration

% ----------------------------------------------------------------------------------------------------------------
%%% AC
% Load Variables Acoustics MIMO fit-- RED
cd('C:\Users\Arjan\Documents\My Dropbox\MAPPER\Matlab\3. Dynamic Error Budgeting\Acoustics')
load 'Variables_Acoustics_MIMO_fit'

% Compensating for the fact that I have tuned AC based on a 3 m^2 surface area (Vibronix) and that I
% Expect the surface area of Forcesix to be larger 5 m^2.    : 5 m^2.

% [(N^2)/Hz]                =  % [(N^2)/Hz]        [m^2/m^2]
PSD_AC_RED_newton           = PSD_AC_RED_newton .* (5/3);


% [(m/s^2)^2/Hz]            =  [(N^2)/Hz]           ((m/s^2)^2)/(N^2)
PSD_AC_2MSD_M2a             = PSD_AC_RED_newton .* (TWO_MSD_F1_to_A2).^2;          % PLATE acceleration due to AC
```

D-4: Dynamic Error Budgeting (DEB)

MAPPER lithography

Modeling the effect of all disturbances in [Z] for concept B – *tubing stiffness* & *measured FIV*

```matlab
%%% ACi
% Load Variables Acoustics Inside MIMO fit -- RED
cd('C:\Users\Arjan\Documents\My Dropbox\MAPPER\Matlab\3. Dynamic Error Budgeting\Acoustics')
load('Variables_Acoustics_Inside_MIMO_fit')

A_breadboard = 0.6*0.6*2 + 4*0.6*0.058;          % [m^2] surface area optical breadboard (top + bottom + si
A_M731A = 2*3.14159265*(0.0625/2)*0.054*6;       % [m^2] surface area of 6 sensors - M731A
A_in = A_breadboard+A_M731A;                     % [m^2] // estimated total outside surface area -

% [(N^2)/Hz]              = [(N/m^2)^2/Hz]            [m^4]
PSD_AC_Inside_RED_newton  = (PSD_AC_Inside_RED) .* (A_in^2);

% [(m/s^2)^2/Hz]          =  [(m/s)^2/Hz]               [(1/s)^2]
PSD_ACi_2MSD_M2a          = PSD_AC_Inside_RED_newton .* (TWO_MSD_F2_to_A2).^2;    % PLATE acceleration due

% ----------------------------------------------------------------------------------------------------
%%%%% Combined Spectra - ACCELERATIONS

%%% AC+FV
% [(m/s^2)^2/Hz]                [(m/s^2)^2/Hz]               [(m/s^2)^2/Hz]
PSD_AC_FV_2MSD_M2a        = ((PSD_FV_2MSD_M2a.^2)  + (PSD_AC_2MSD_M2a.^2)).^0.5;

%%% AC+FV+ACi
% [(m/s^2)^2/Hz]               [(m/s^2)^2/Hz]          [(m/s^2)^2/Hz]             [(m/s^2)^2/Hz]
PSD_AC_FV_ACi_2MSD_M2a    = ((PSD_FV_2MSD_M2a.^2)  + (PSD_AC_2MSD_M2a.^2)  +  (PSD_ACi_2MSD_M2a.^2)).^0.5;

% ----------------------------------------------------------------------------------------------------
%%%%% Combined Spectra - FORCES

%%% FV
% [N^2/Hz]                    [(m/s^2)^2/Hz]        [kg^2]
PSD_MF_FV_2MSD            = PSD_FV_2MSD_M2a .* (m2.^2);
%%% Incorporating Tubing Stiffness [spring M1-M2]

% Load Variables
cd('C:\Users\Arjan\Documents\My Dropbox\MAPPER\Matlab\3. Dynamic Error Budgeting\Tubing Stiffness')
load('Variables_Tubing_Stiffness_Acceleration')

% Ktube
PSD_MF_Ktube_2MSD = PSD_MF_ErrorTubing_2MSD_spring_acc;          % Just renaming, was already calculated as a f

%%% AC+FV+ACi+Ktube
%          [N^2/Hz]                      [N^2/Hz]                      [N^2/Hz]
PSD_MF_AC_FV_ACi_Ktube_2MSD    = ((PSD_MF_AC_FV_ACi_2MSD.^2) + (PSD_MF_Ktube_2MSD.^2)).^0.5;

% ----------------------------------------------------------------------------------------------------
Transfer Functions
cd('C:\Users\Arjan\Documents\My Dropbox\MAPPER\Matlab\3. Dynamic Error Budgeting\Transfer Functions')
load 'Variables_Transfer_Functions_Force'

%% ACi // acting on M2
[N^2/Hz]                        [N^2/Hz]              [N^2/N^2]
PSD_MF_ACi_2MSD_M2          = PSD_ACi_M2_att_RED_newton .* (F2_to_Fmeas.^2);

%% ACi // acting on M2
[N^2/Hz]                        [N^2/Hz]              [N^2/N^2]
PSD_MF_ACi_2MSD_M3          = PSD_ACi_M3_att_RED_newton .* (F3_to_Fmeas.^2);
```

```matlab
%% ACi // Total Contribution
PSD_MF_ACi_2MSD = ((PSD_MF_ACi_2MSD_M2.^2) + (PSD_MF_ACi_2MSD_M3.^2)).^0.5;

-----------------------------------------------------------------------------------------------------
                    % Ktube [spring M2-M3]

Load Variables
cd('C:\Users\Arjan\Documents\My Dropbox\MAPPER\Matlab\3. Dynamic Error Budgeting\Tubing Stiffness')
load('Variables_Tubing_Stiffness_Force')

MF due to Ktube
PSD_MF_Ktube_2MSD  = PSD_ERROR_Fmeas_dueto_FRS_force;          % Force - Just renaming, was already calculated as a force error,

                   % FIV

                         % Measured - Straight Tube // FLOW
Load File
cd('C:\Users\Arjan\Documents\My Dropbox\MAPPER\Matlab\ii. MeasData\Hydrostatic\Hydrostatic_measurement_flow\tube_rigidly_connected\cover_closed
load All_Average_PSDs.mat

%% Obtain response of FRD object for plotting
Resp_AV_PSD_End_Stone_Flow_X = freqresp(AV_PSD_End_Stone_X,log_vector_w);
Resp_AV_PSD_End_Stone_Flow_X = abs(Resp_AV_PSD_End_Stone_Flow_X);
Resp_AV_PSD_End_Stone_Flow_X = permute(Resp_AV_PSD_End_Stone_Flow_X,[1,3,2]);

Resp_AV_PSD_End_Plate_Flow_X = freqresp(AV_PSD_End_Plate_X,log_vector_w);
Resp_AV_PSD_End_Plate_Flow_X = abs(Resp_AV_PSD_End_Plate_Flow_X);
Resp_AV_PSD_End_Plate_Flow_X = permute(Resp_AV_PSD_End_Plate_Flow_X,[1,3,2]);

%% Comparison Measured Forces [FV] vs. FRS -- [XY]'
h(9)=figure;
loglog(log_vector,Resp_AV_PSD_End_Stone_Flow_X,'r',log_vector,Resp_AV_PSD_End_Plate_Flow_X,'b','Linewidth',2)
title('MA - Straight Tubing Mounted - Flow - Stone and Plate')
xlabel('Frequency [Hz]')
ylabel('Magnitude [(m/s^2)2/Hz]')
axis([1e0 3e3 1e-18 1e-2])
hl(1)=legend('PSD - AVG - End Stone','PSD - AVG - End Plate','location','NE');
grid on

-----------------------------------------------------------------------------------------------------
                         % Measured - Straight Tube // NO FLOW
Load File
cd('C:\Users\Arjan\Documents\My Dropbox\MAPPER\Matlab\ii. MeasData\Hydrostatic\Hydrostatic_measurement_flow\tube_rigidly_connected\cover_closed
load All_Average_PSDs.mat

%% Obtain response of FRD object for plotting
Resp_AV_PSD_End_Stone_X = freqresp(AV_PSD_End_Stone_X,log_vector_w);
Resp_AV_PSD_End_Stone_X = abs(Resp_AV_PSD_End_Stone_X);
Resp_AV_PSD_End_Stone_X = permute(Resp_AV_PSD_End_Stone_X,[1,3,2]);

Resp_AV_PSD_End_Plate_X = freqresp(AV_PSD_End_Plate_X,log_vector_w);
Resp_AV_PSD_End_Plate_X = abs(Resp_AV_PSD_End_Plate_X);
Resp_AV_PSD_End_Plate_X = permute(Resp_AV_PSD_End_Plate_X,[1,3,2]);
```

MAPPER lithography

Modeling the effect of all disturbances in [Z] for concept B – *FIVo & FIVi & Wafer Error Transfer*

```
%% FIV -- FORCES
Weight Tubing
R_tube = 0.005;                                          % [m]      radius of tube of 1 cm interna
L_tube = 0.5;                                            % [m]      effective length of inside tub
V_tube = pi*(R_tube^2)*L_tube;                           % [m^3]    volume of water in inside tube
D_water = 999;                                           % [kg/m^3] density water (20 C - 4 bar)
M_water = V_tube*D_water;                                % [kg]     mass of water in tube

M_tube_p_m = 0.7;                                        % [kg/m]   mass of tubing only / per m (
M_tube = M_tube_p_m*L_tube;                              % [kg]     mass of this length of tubing

M_plate_tube  = (7.44 - 1.585) + (M_water + M_tube) - (2*0.8);  % [kg]     7.44 kg = mass Aperture Array

  [N^2/Hz]              [(m/s^2)^2/Hz]    [kg^2]
PSD_FIV_Inside_newton  = PSD_FIV_Inside * (M_plate_tube^2);

Remove crap at bottom
PSD_FIV_Inside_newton(1:index_finder(5)) = 1e-14;

%% Comparison Measured Forces [FV] vs. FRS -- [XY]'
h(9)=figure;
loglog(log_vector,Resp_AV_PSD_End_Plate_Flow_X,'r',log_vector,Resp_AV_PSD_End_Plate_X,'b',log_vector,PSD_
title('MA - Straight Tubing Mounted - Flow, No Flow and FIV isolated - Plate')
xlabel('Frequency [Hz]')
ylabel('Magnitude [(m/s^2)2/Hz]')
axis([1e0 3e3 1e-18 1e-2])
hl(1)=legend('Plate - Flow [X]','Plate - No Flow [X]','FIV - Acc [X]','FIV - Forces [X]','location','NE')
grid on

%% I have measured the FIV of a piece of tubing of 0.5 m as this is what
%% will be required to supply flow to the module from the location where
%% this tubing is disconnected to the top granite stone of the VI platform
%% under the assumption that this spectrum characteristic for a longer
%% tubing as well, and knowing that about 3-5 m of tubing will be needed
%% to connect the hydrostatic pressure vessel to M1 where the bulk of FIV
%% will be discharged, a 10x higher spectrum (5/0.5) will be used to model
%% the effect of FIVo if a) it is not discharged and transmitted to the
%% module for the most part by connecting the tubing or b) the whole FIVo
%% input spectrum is discharged on the bottom granite stone (part of M1)
%% and transmits through the F2/Fmeas compliance characteristics to the sensor.

------------------------------------------------------------------------------------------
                        % Modeled  - FIV inside  = FIVi

------------------------------------------------------------------------------------------
   [N^2/Hz]                [N^2/Hz]              [N^2/(N^2)]
PSD_MF_FIVi_2MSD  =  PSD_FIV_Inside_newton .* (F2_to_Fmeas.^2);

%% Overview used FIV spectrum, TF that weights it, resulting Measured Force vs FRS (BSW [XY])
figure
loglog(log_vector,PSD_FIV_Inside_newton,'r',log_vector,(F3_to_Fmeas.^2),'b',log_vector,PSD_MF_FIVi_2MSD,'
       log_vector,PSD_FRS_6DOF_BSW(1,:),'c','Linewidth',2);
title('Overview used FIVi spectrum, TF that weights it, resulting Measured Force')
ylabel('Magnitude [-]')
xlabel('Frequency [Hz]')
axis([1e-2 1e4 1e-20 1e0])
legend('FIV - Inside - Newton','Fmeas/F3 - incl Ktube','Measured Force (FIVi)','FRS - CON [XY]')
grid on
```

```
                        % Modeled  - FIV outside = FIVo


PSD_FIV_Outside_newton = 10 * PSD_FIV_Inside_newton;                 % [N^2/Hz]

------------------------------------------------------------------------------------------
   [N^2/Hz]                [N^2/Hz]              [N^2/(N^2)]
PSD_MF_FIVo_2MSD  =  PSD_FIV_Outside_newton .* (F1_to_Fmeas.^2);

%% Overview used FIV spectrum, TF that weights it, resulting Measured Force vs FRS (BSW [XY])
figure
loglog(log_vector,PSD_FIV_Outside_newton,'r',log_vector,(F3_to_Fmeas.^2),'b',log_vector,PSD_MF_FIVo_2MSD,'y',...
       log_vector,PSD_FRS_6DOF_BSW(1,:),'c','Linewidth',2);
title('Overview used FIVo spectrum, TF that weights it, resulting Measured Force')
ylabel('Magnitude [-]')
xlabel('Frequency [Hz]')
axis([1e-2 1e4 1e-20 1e0])
legend('FIV - Outside - Newton','Fmeas/F3 - incl Ktube','Measured Force (FIVi)','FRS - CON [XY]')
grid on
% Weighting Function Build-Up
%% ---------------------------------------------------------------
% % W_cv_6DOF_2D  =     1.  X_to_X(w1)    X_to_X(w2)    ..   X_to_X(w3000)
% %                     2.  X_to_Y(w1)    X_to_Y(w2)    ..   X_to_Y(w3000)
% % [36x3000]           3.  X_to_Z(w1)    X_to_Z(w2)    ..   X_to_Z(w3000)
% % [m/N]==[m^2/kg]     4.  X_to_Rx(w1)   X_to_Rx(w2)   ..   X_to_Rx(w3000)
% %                     5.  X_to_Ry(w1)   X_to_Ry(w2)   ..   X_to_Ry(w3000)
% %                     6.  X_to_Rz(w1)   X_to_Rz(w2)   ..   X_to_Rz(w3000)
% %                     7.  Y_to_X(w1)    Y_to_X(w2)    ..   Y_to_X(w3000)
% %                     8.  Y_to_Y(w1)    Y_to_Y(w2)    ..   Y_to_Y(w3000)
% %                     9.  Y_to_Z(w1)    Y_to_Z(w2)    ..   Y_to_Z(w3000)
% %                    10.  Y_to_Rx(w1)   Y_to_Rx(w2)   ..   Y_to_Rx(w3000)
% %                    11.  Y_to_Ry(w1)   Y_to_Ry(w2)   ..   Y_to_Ry(w3000)
% %                    12.  Y_to_Rz(w1)   Y_to_Ry(w2)   ..   Y_to_Rz(w3000)
% %                         ..            ..            ..        ..

% % So W_cv_6DOF_2D.^2 = [m^2/N^2]

% % FC_cooling_6DOF      = 1.  X(w1)      X(w2)      .. X(w3000)
% %                        2.  Y(w1)      Y(w2)      .. Y(w3000)
% % [6x3000]               3.  Z(w1)      Z(w2)      .. Z(w3000)
% % [N]                    4.  Rx(w1)     Rx(w2)     ..Rx(w3000)
% %                        5.  Ry(w1)     Ry(w2)     ..Ry(w3000)
% %                        6.  Rz(w1)     Rz(w2)     ..Rz(w3000)

% % FC_cooling_6DOF'     = 1.  X(w1)     Y(w1)     Z(w1)     Rx(w1)     Ry(w1)     Rz(w1)
% %                        2.  X(w2)     Y(w2)     Z(w2)     Rx(w2)     Ry(w2)     Rz(w2)
% % [3000x6]                   ..        ..        ..        ..         ..         ..
% % [N]                 3000.  X(w3000)  Y(w3000)  Z(w3000)  Rx(w3000)  Ry(w3000)  Rz(w3000)

% % PSD_FC_cooling_6DOF' = 1.  X(w1)     Y(w1)     Z(w1)     Rx(w1)     Ry(w1)     Rz(w1)
% %                        2.  X(w2)     Y(w2)     Z(w2)     Rx(w2)     Ry(w2)     Rz(w2)
% % [3000x6]                   ..        ..        ..        ..         ..         ..
% % [N^2/Hz]            3000.  X(w3000)  Y(w3000)  Z(w3000)  Rx(w3000)  Ry(w3000)  Rz(w3000)
```

App. E

Technical Drawings

E-1: Acoustical Enclosure

MAPPER lithography

CAD work by Arjan de Wildt - **Outside- and Inside Plating**

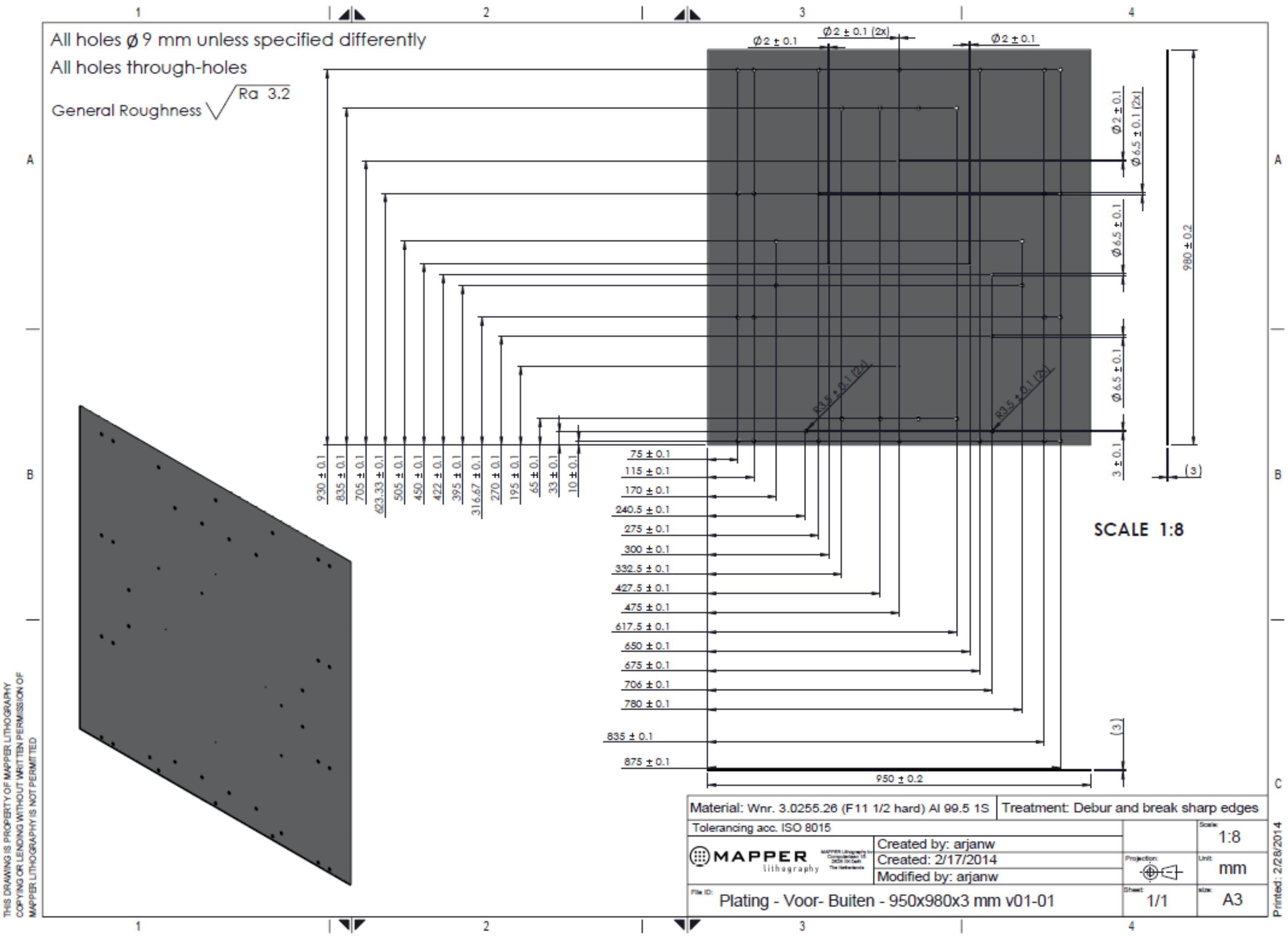

E-1: Acoustical Enclosure

CAD work by Arjan de Wildt - **Outside- and Inside Plating**

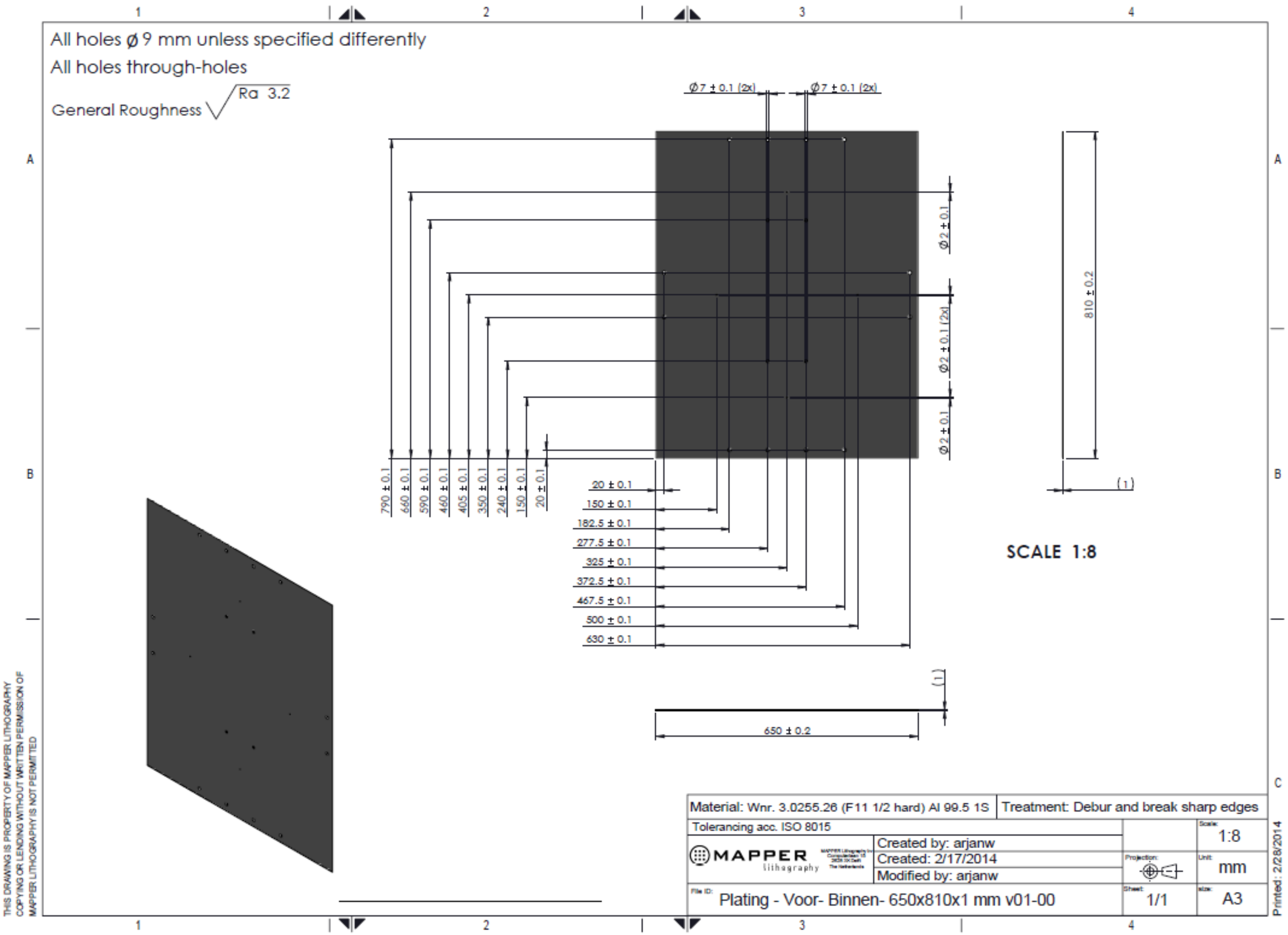

E-1: Acoustical Enclosure

MAPPER lithography

CAD work by Arjan de Wildt - **Outside- and Inside Plating**

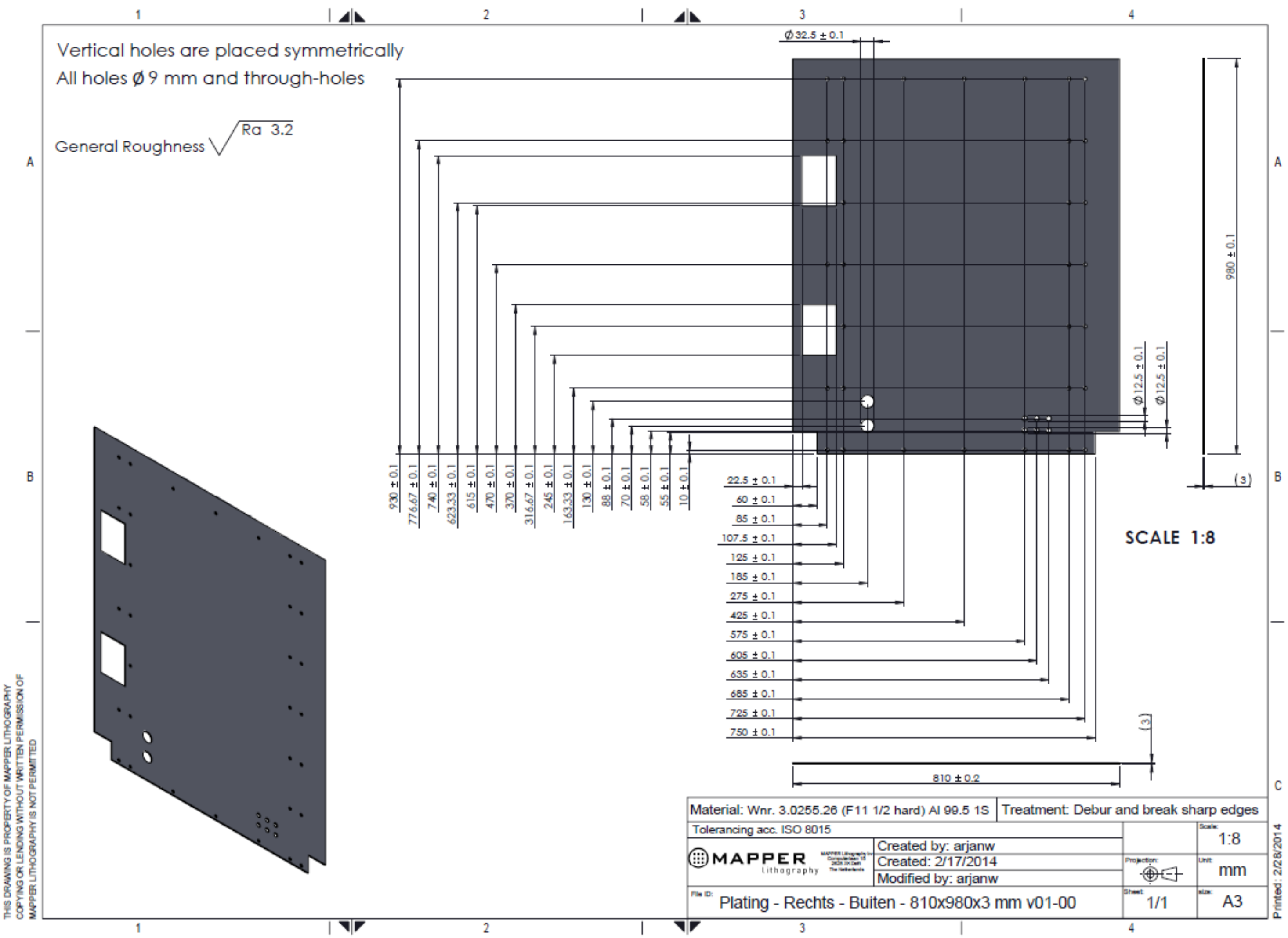

E-1: Acoustical Enclosure

MAPPER lithography

CAD work by Arjan de Wildt - **Outside- and Inside Plating**

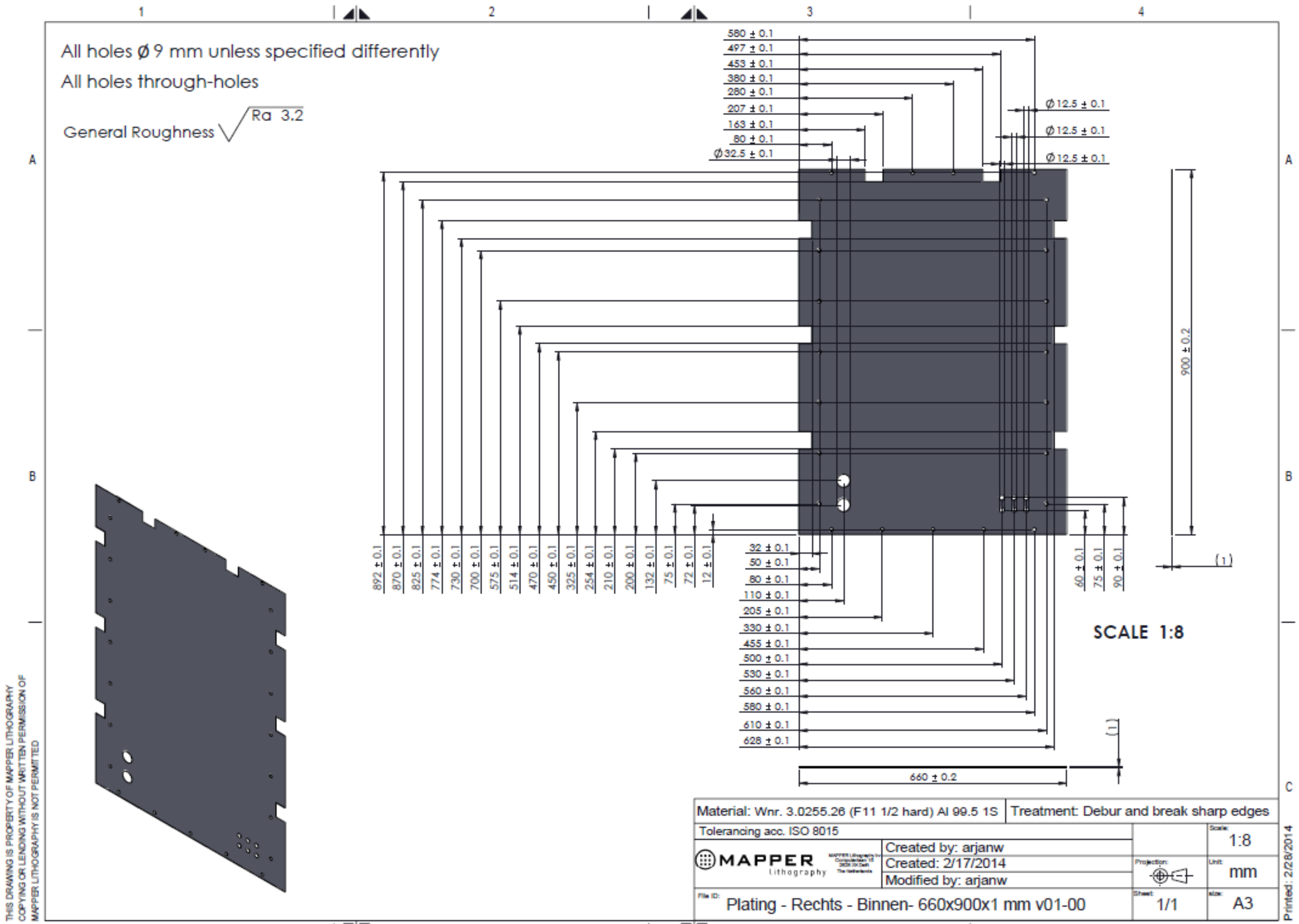

E-1: Acoustical Enclosure

CAD work by Arjan de Wildt - **Outside- and Inside Plating**

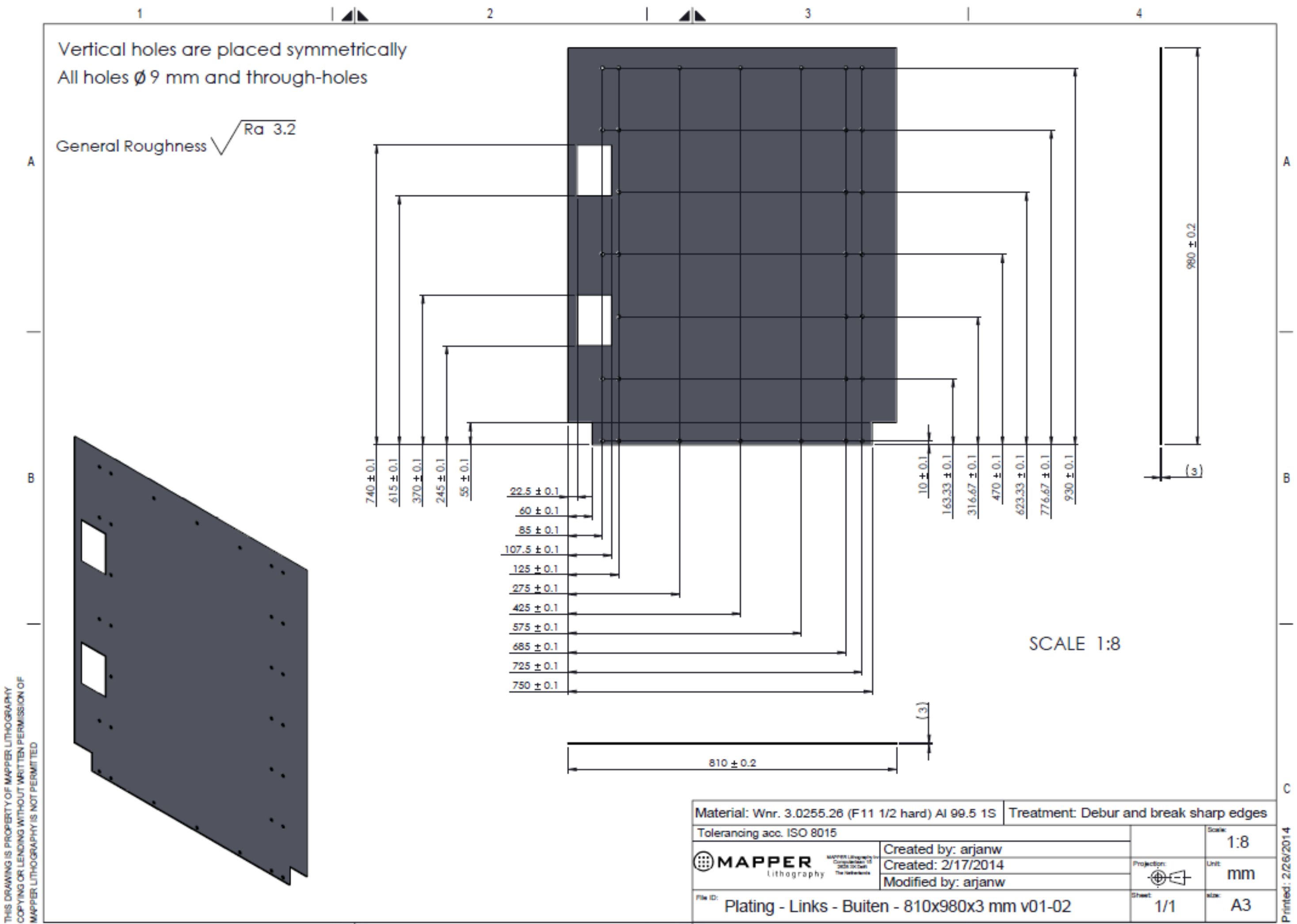

E-1: Acoustical Enclosure

CAD work by Arjan de Wildt - **Outside- and Inside Plating**

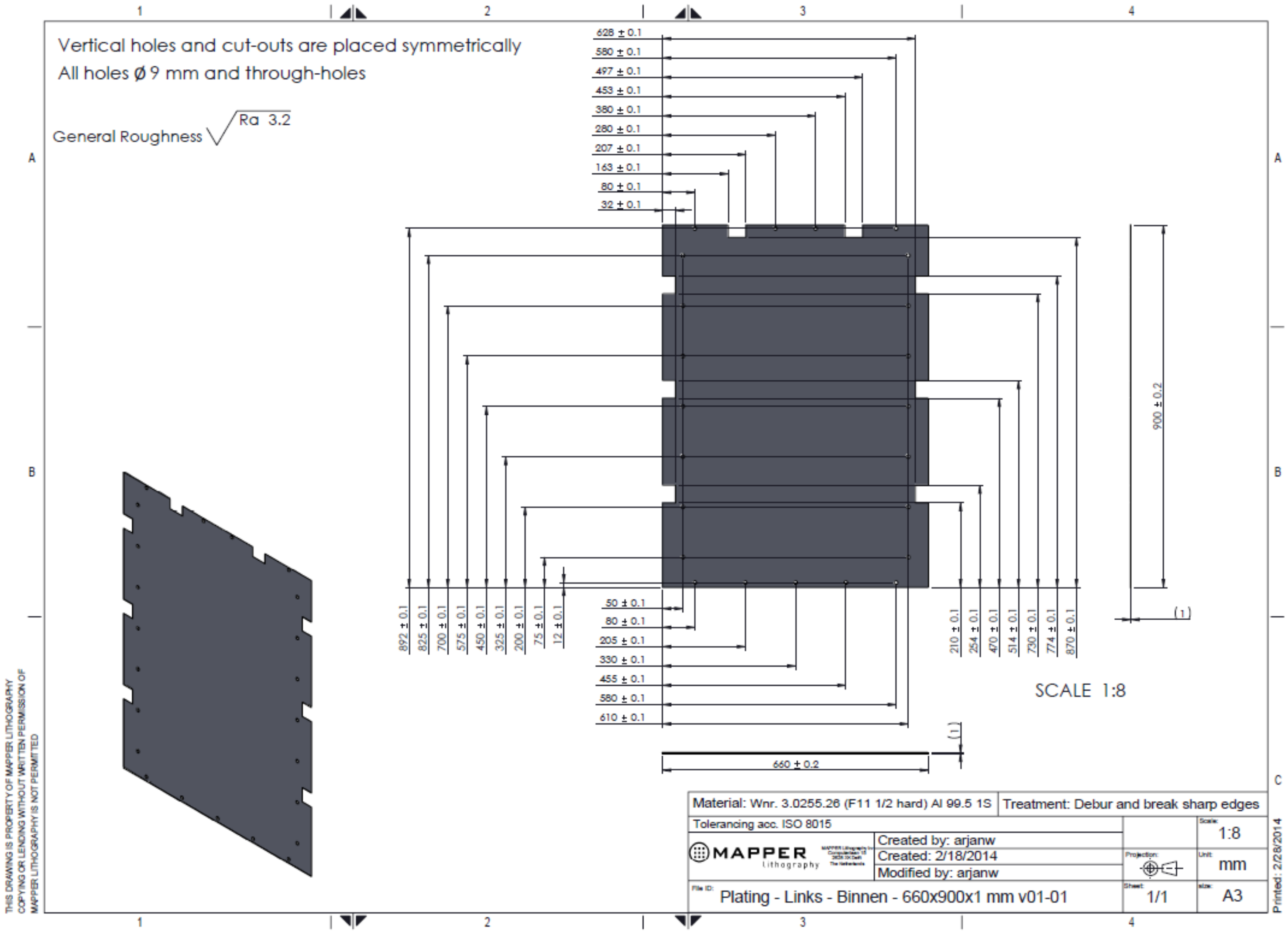

E-1: Acoustical Enclosure

MAPPER lithography

CAD work by Arjan de Wildt - **Outside- and Inside Plating**

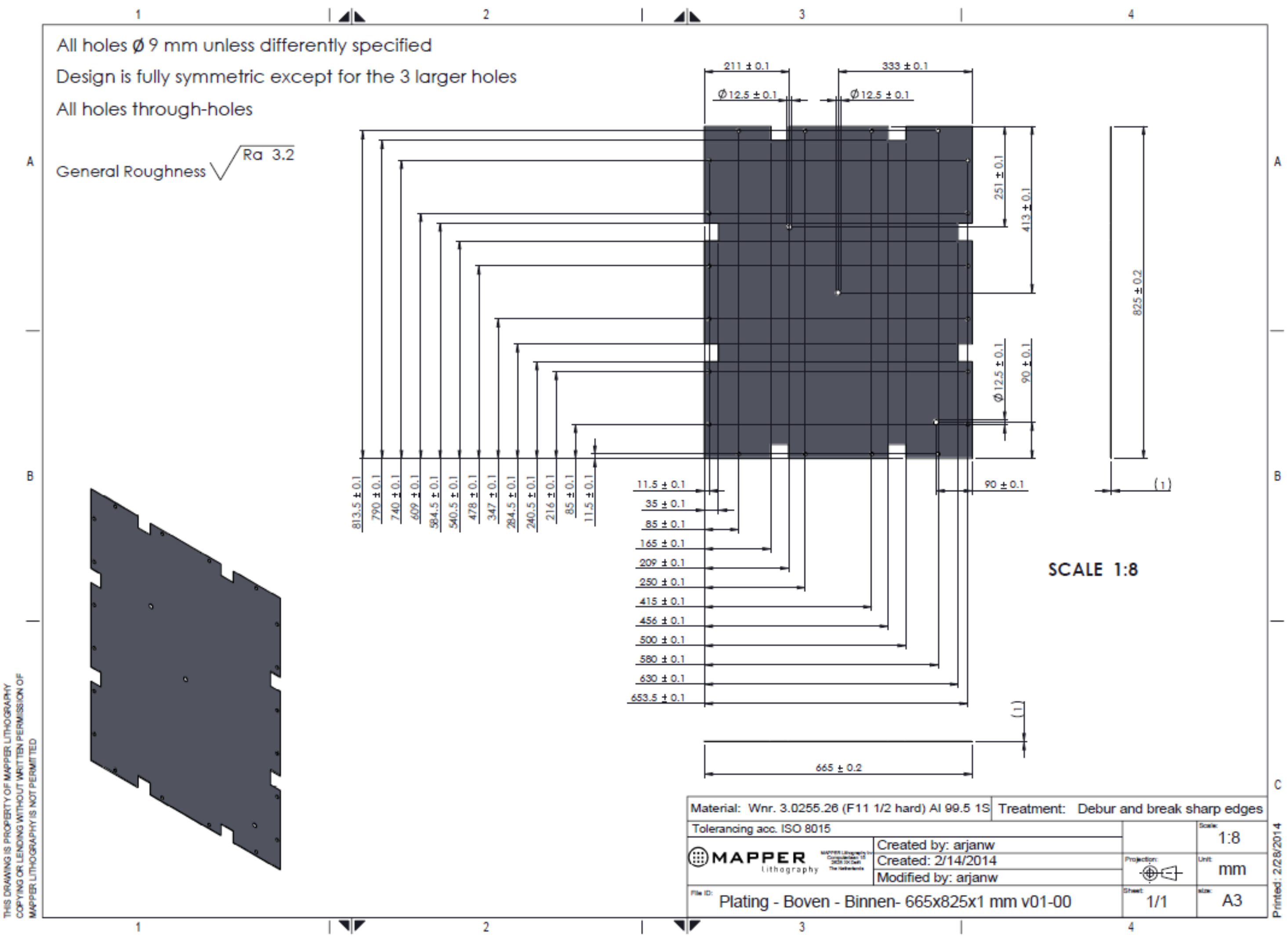

CAD work by Arjan de Wildt - **Outside- and Inside Plating**

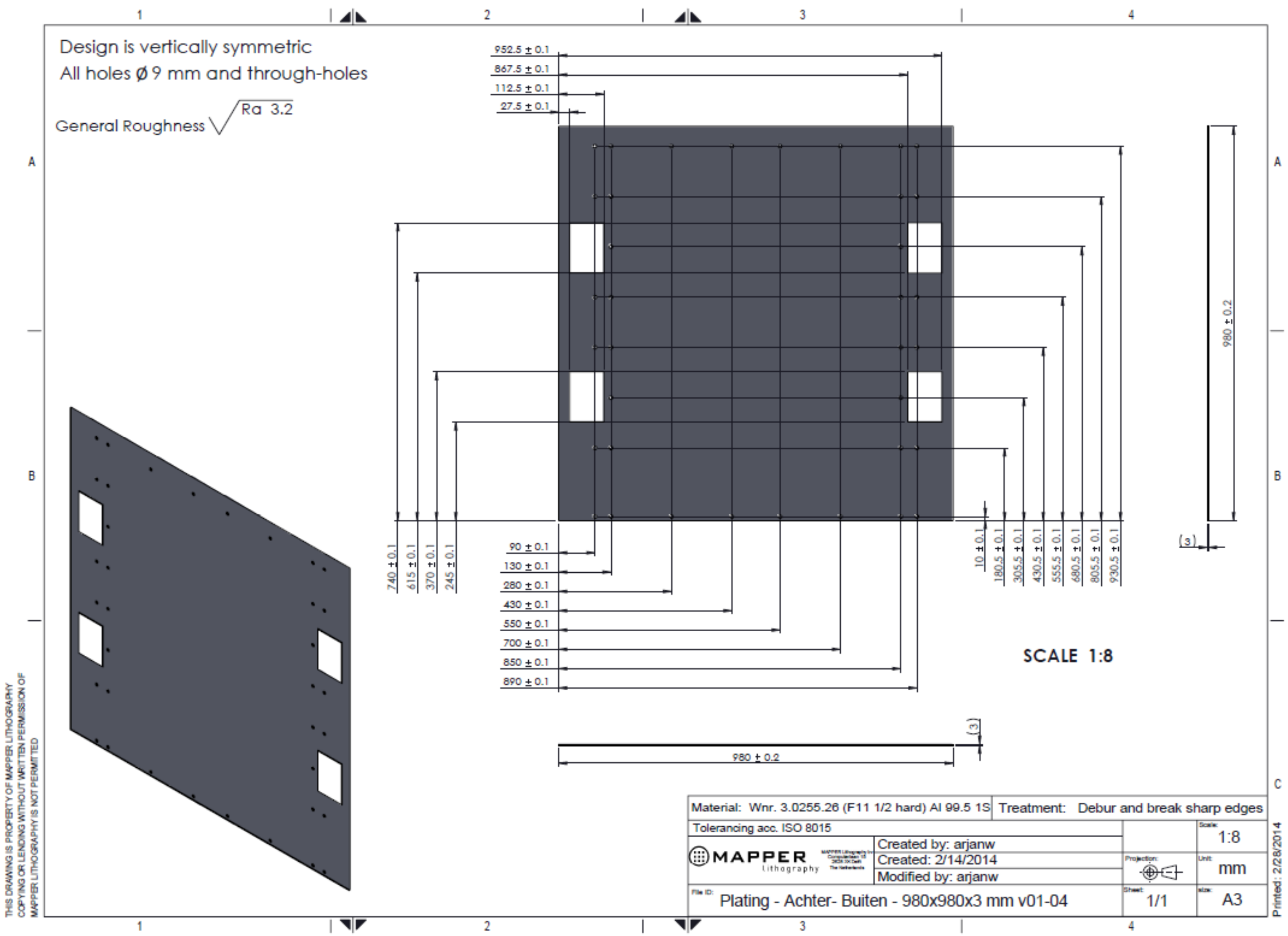

E-1: Acoustical Enclosure

MAPPER lithography

CAD work by Arjan de Wildt - **Outside- and Inside Plating**

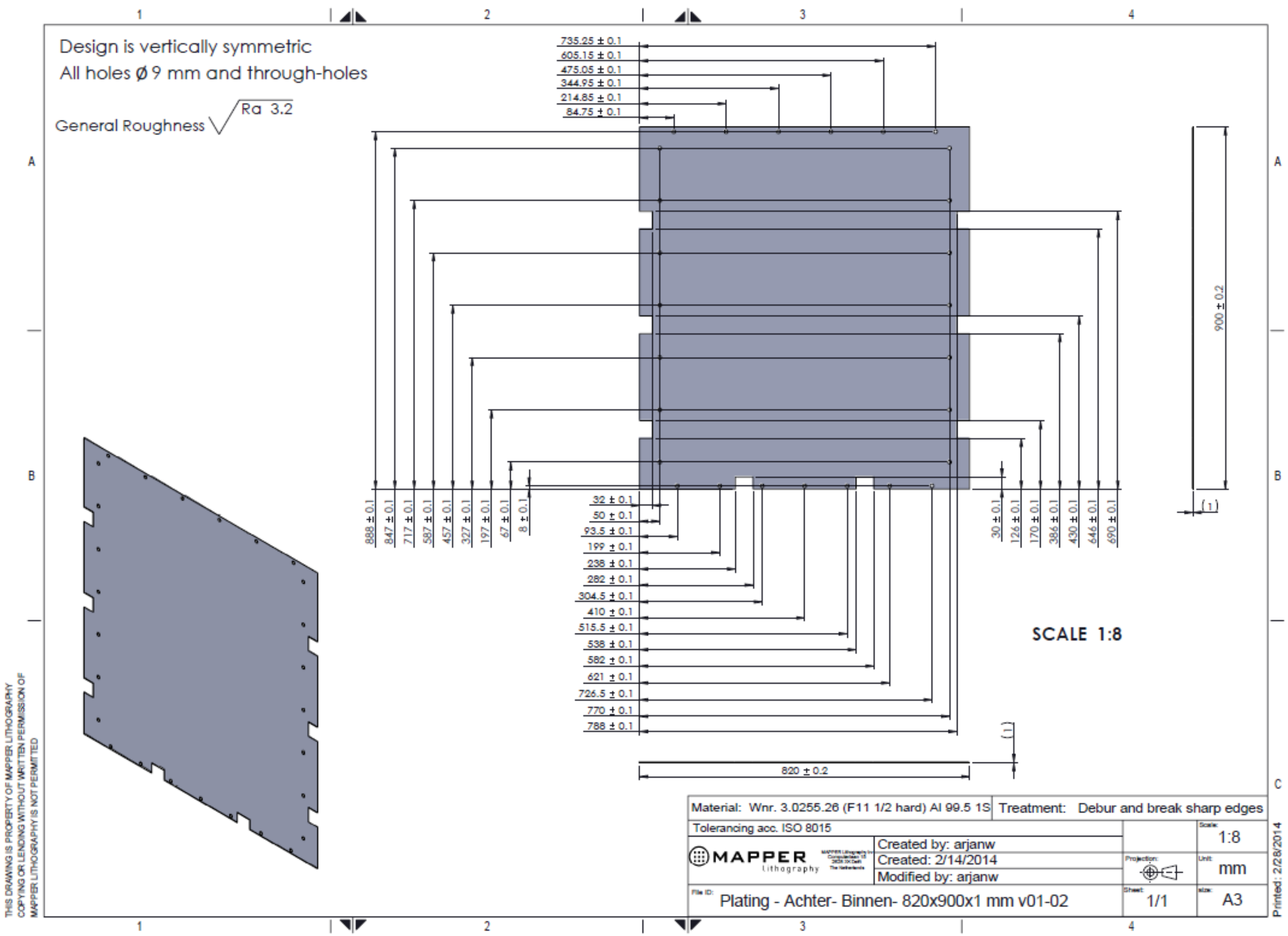

E-2: MSF mounted on BF

MAPPER lithography

E-2: Module Support Frame (MSF)

I.P.

E-2: Base Frame (BF)

I.P.

CAD work by Bart Schipper

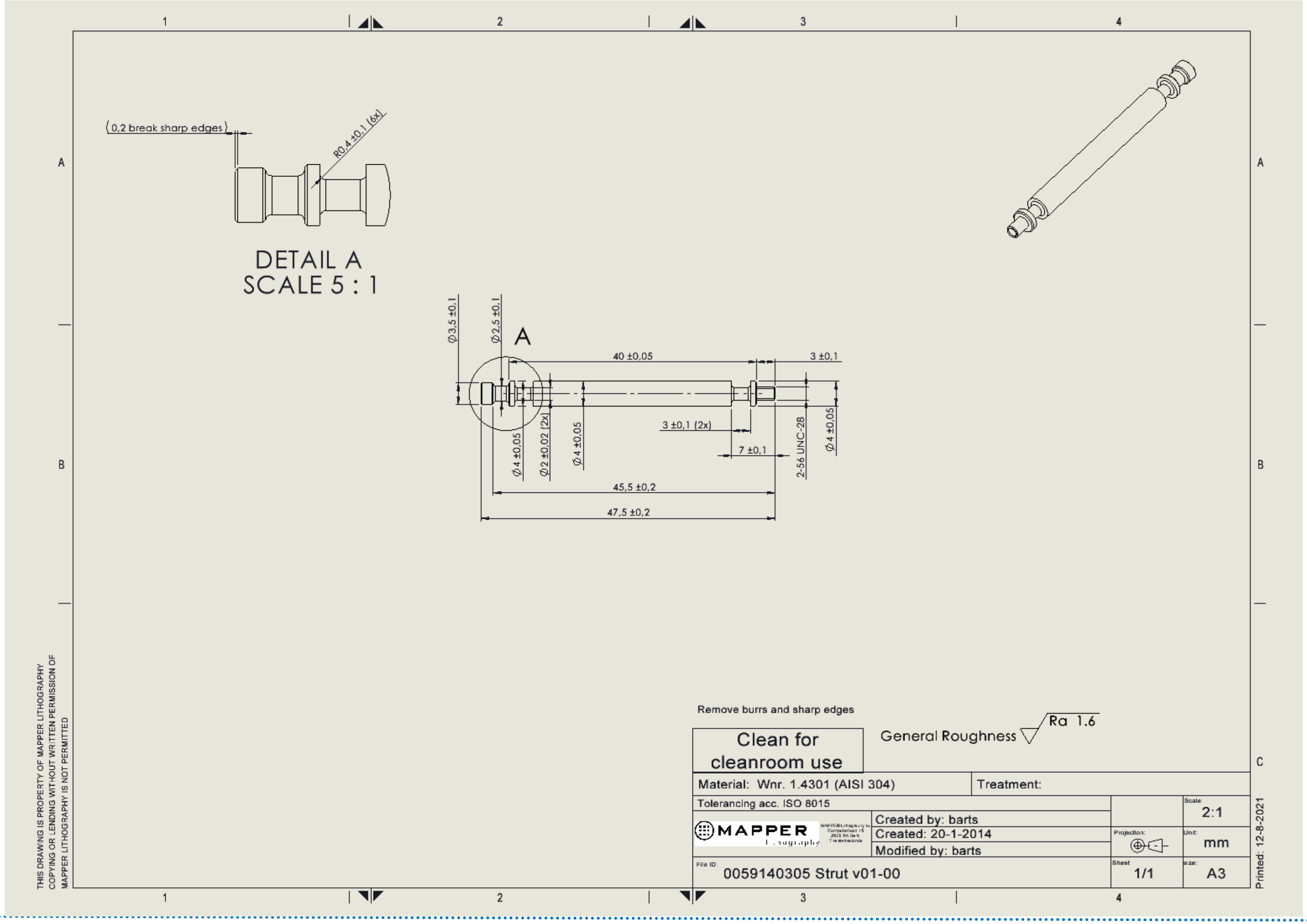

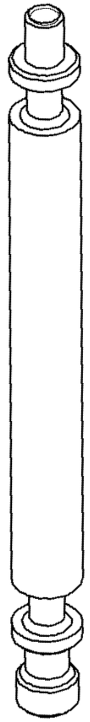

App. F

Forcesix Documentation

F-1: Forcesix – Overview

The following documents have been created:

- Forcesix - Requirements Sheet v01-05
- Forcesix - Concept Design File v01-02
- Forcesix - Detailed Design File v01-06
- Forcesix - Inventory List - v01-s05
- Forcesix - Assembly Procedure v01-06
- Forcesix - Build Sheet v03-10
- Forcesix - Verification Procedure v01-01
- Forcesix - Measurement Plan v02-01

The most relevant to be included in this report is the requirement sheet, for sake of space the others will not be shown.

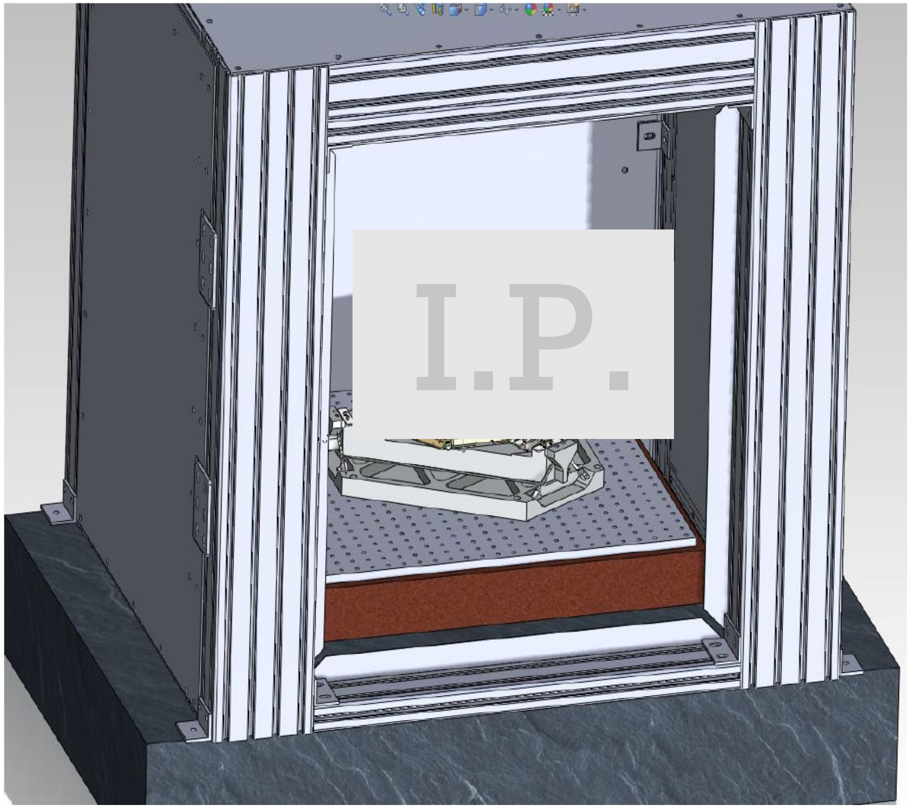

F-2: Forcesix – Requirement Sheet

MAPPER lithography

SCREENSHOT 1

Management Summary

Requirement sheet for Forcesix - the test setup designed to verify the cooling induced vibration forces of various modules (BSW / POS / ABC) in 6-DOF. Forcesix is an improved version of Vibronix which was designed solely for the Aperature Array (AA) and is only able to measure in 1-DOF.
Both setups are designed to measure forces, but where Vibronix does so by observing the resulting accelerations of a suspended mass, Forcesix makes use of the (direct) piezo-electric effect.

Open Issues

OI #	Description of Issue	Owner
	for review	

Version-Revision History

Date	Description of Change - Including Review Status	Version-Revision	Changed By
23/01/2014	initial version	v01-00	ArWi
24/01/2014	added volume, technical, mechanical, electrical, material, coordinate system, vacuum, testing - requirements	v01-01	ArWi
04/02/2014	changed mech and tech requirements and average PSD spectrum	v01-02	ArWi
10/02/2014	added mass / frequency / acoustical requirements to tech section	v01-03	ArWi
03/03/2014	added mech / vol / testing requirements	v01-04	ArWi
27/03/2014	changed mech / tech / volume requirements and changed tested requirements to PASS or FAIL.	v01-05	ArWi

Reference Documents

RD#	Item Name (including vXX-YY)	Link to item on CMT

Requirement ID	Text	Value	Unit	Justification doc	URL	Verification (plan):
FORCESIX-VOL-000	**Volume Requirements**					
FORCESIX-VOL-001	The full design of Forcesix shall fit within the allotted volume in the Labspace at the Rotterdamsweg. It shall thus fit within a volume of	2x2.5x2.5 (lxbxh)	m^3	**FloorPlan Labspace Rotterdamseweg**	http://cmt.mapper/ShowItem?docid=21216&n=1	by design
FORCESIX-VOL-002	The top part of the setup (everything from the breadboard - up) i.e. the part where the actual measurement will be conducted, shall fit in a volume of	0.55x0.55x0.75 (lxbxh)	m^3	Optical breadport (Newport) measures 0.6x0.6 m^2 and the acoustical cage surrounding this top part has an internal height (as measured from the breadboard) of 0.8 m. This is required as the RF cable + adapter from the ABC module cannot be removed. ***Update:*** *Later on it turned out that this RF cable is much less rigid than initially communicated and that it not necessary needs to be supported in its upright position. The height part of this volume requirements could therefore have been much stringent. However, for future testing purposed with POS and part of its cable assembly, strain relieves and supply tubing, this is not an unnecessary luxury. Also in view of required compliant routing of the water tubing, available height is of the essence.*		by design
FORCESIX-VOL-003	The design must be able to accommodate the following modules: ABC v01; BSW v07 s09; POS-PL-v12-05	-	-	see respective design files		by design
FORCESIX-TECH-000	**Technical Requirements**					
FORCESIX-TECH-001	In order to be able to verify the cooling budgets as allotted in [JUST DOC], the system must be able to measure the dynamic forces *(that were translated from wafer error budgets [nm] via the SUSA compliancy and the Controller Sensitivity)* induced by the coolant flow in the frequency range:	10-300	Hz	**Stage Stability Budgeting for Matrix V02-01**	http://cmt.mapper/ShowItem?docid=69295&n=2	verification measurement
FORCESIX-TECH-002	In order to being able to sufficiently distinguish the magnitude of the CF-induced forces in the frequency range as defined in **FORCESIX-TECH-001**, the combined noise level of the setup *(electrical/mechanical/thermal etc)* must, for the most criticle DOFs i.e in-plane (XY), on average be around the following level in the PSD spectrum: ***Note that this spectrum is derived from the rebudgeted water errors due to FIV*** *(also in presentation)*	=< 5e-12	N^2/Hz	For detailed overview of noise bottom lines that must be met, see slide 4 of **Forcesix - presentations - design requirements - v01-00**	http://cmt.mapper/ShowItem?	verification measurement
FORCESIX-TECH-003	The required sensitivity for the most critical DOFs (X&Y) has been defined in **FORCESIX-TECH-002**. For the other DOFs, a lower sensitivity required. The following factor relative to the XY sensitivity should be attained: <X,Y,Z,Rx,Ry,Rz> =	<1,1,10,2,2,10>	[1]	**Stage Stability Budgeting for Matrix V02-01 & Matlab Model ArWi** (Weighting Function) Sensitivities: < X, Y, Z, Rx, Ry, Rz > : < 1, 1, 10, 2, 2, 10 >	http://cmt.mapper/ShowItem?docid=69295&n=2	Verification Measurement.
FORCESIX-TECH-004	In order to being able to distinguish parasitic forces from FIV forces, the signal/noise ratio should be as high as possible, with a minimum of 100. See **FORCESIX-MECH-002, FORCESIX-MECH-003 and FORCESIX-MECH-04** for stiffness requirements.	-	-			

F-2: Forcesix – Requirement Sheet

MAPPER lithography

SCREENSHOT 2

FORCESIX-MECH-000	Mechanical Requirements					
FORCESIX-MECH-001	In order to meet **FORCESIX-TECH-001** it is required that the dynamics from each mechanical part to another of the setup (excl 4x2 airmounts) has its (first) resonance frequency above:	>= 400	Hz	**Stage Stability Budgeting for Matrix V02-01**	http://cmt.mapper/ShowItem?docid=69295&n=2	Ansys Analysis, see: http://cmt.mapper/ShowItem?docid=77752&n=1
FORCESIX-MECH-002	To ensure **FORCESIX-MECH-001** the flexible struts must have an axial stiffness of at least:	>= 5e7	N/m	Matlab model Arwi - Global Stiffness Matrix	See support drawings: **SD-1 ; Z-direction** and **SD-5**	**Modeled in Comsol:** Straight Strut: 4e7 N/m Flex Strut: 3.4e7 N/m
FORCESIX-MECH-003	To ensure **FORCESIX-MECH-001** the flexible struts may at most have a transversal stiffness of:	=< 2e5	N/m	Matlab model Arwi - Global Stiffness Matrix	See support drawings: **SD-1 ; XY-direction** and **SD-5**	**Modeled in Comsol:** Straight Strut: 3.5e5 N/m Flex Strut: 5e4 N/m
FORCESIX-MECH-004	To ensure **FORCESIX-MECH-001** all mechanical interfaces (unless specified differently) have to be mounted with a stiffness of at least:	>= 1e9	N/m	Matlab model ArWi - Dynamics Forcesix		
FORCESIX-MECH-005	To achieve the best signal/noise ratio (see **FORCESIX-TECH-003**) and to protect each piezo from being loaded by a too high transversal load (see **FORCESIX-TECH-010**) it is aimed to make the axial/transversal ratio as high as possible. This is done by optimizing the diameters of the flexible struts within the range as defined by the other requirements. The minimum axial/transversal stiffness ratio that must be attained is:	>= 200	-	Model in Comsol / Matlab.		Currently (flex strut): 680 Alternative (straight): 114
FORCESIX-MECH-006	To ensure purely elastic deformations, the material stress in the flexible struts should remain below the yield stress of stainless-steel of	=< 0.465	GPa		See support drawings: **SD-3**	
FORCESIX-MECH-007	To ensure purely elastic deformations, the different load scenarios must be modeled before construction takes place to ensure buckling of the flexible struts around their indentations is not expected.	-	-			Modeled in Comsol
FORCESIX-MECH-008	The maximum **static** axial load that each piezo-electric sensor may be subjected to in **compression** is 48.9 N = 5 kg. Given the fact that there are 6 piezo sensors that are all mounted under a 45 degree angle the maximum total weight that may be carried by all sensors together *(including module support plate i.e. everything from the struts upwards)* is 21.2 kg. That is equal to a maximum load of:	=< 208.1	N	**PCB209C11 datasheet**	http://cmt.mapper/ShowItem?docid=77748&n=1	
FORCESIX-MECH-009	The maximum **static** axial load that each piezo-electric sensor may be subjected to in **tension** is 4.45 N = 0.45 kg. Given the fact that there are 6 piezo sensors that are all mounted under a 45 degree angle the maximum total force that may be exerted in tension on the geometric center of the module support plate *(which is connected to all six sensors)* is:	=< 18.9	N	**PCB209C11 datasheet**	http://cmt.mapper/ShowItem?docid=77748&n=1	
FORCESIX-MECH-010	To protect the piezos from breaking in terms of a static (axial) overload [see FORCESIX-MECH-008], or from a mechanical bending moment [see FORCESIX-MECH-012], the maximum total weight that may be carried by the piezos is 15 kg. When also accounting for the weight of the Module Support Frame (3.1 kg), the maximum weight that may be placed on the assembly should be equal or less than:	=< 10.4	kg	**PCB209C11 datasheet**	http://cmt.mapper/ShowItem?docid=77748&n=1	
FORCESIX-MECH-011	The one-on-one mounting configuration of the sensors, together with the inclined angle of the mounting surface, ensures that **no** transverse force will act alongside the mounting surface, thereby shearing the piezo. Furthermore, in case of deflections the axial-over-transverse-stiffness ratio of 680 of each piezo (Z/X) will also prevent overloading in a shearing manner. It is the out-of-plane transverse stiffness (Y) that is not compensated and which must be limited to protect the piezo from breaking. It is therefore that the maximum total (static/dynamic) transversal load that each piezo-electric sensor may be subjected to (tension/compression) is:	=< 2	N	**PCB209C11 datasheet**	http://cmt.mapper/ShowItem?docid=77748&n=1	
FORCESIX-MECH-012	The maximum bending moment (BM) accompanying the maximum total transversal load that may be applied on the mounting location where the shaft meets the piezo should be:	=< 4.0	N*m	**Email / phone contact with PCB** (Jos Koninckx + Factory @ USA)	**See SD-8 for a schematic visual.**	BM due to transverse force: 2N*40mm = 0.08 Nm BM due to vertical load: 13.5 kg * 9.81 * 28.3mm
FORCESIX-MECH-013	The maximum **dynamic** axial load that each piezo-electric sensor may be subjected to in **compression** is 9.79 N = 1.0 kg. Given the fact that there are 6 piezo sensors that are all mounted under a 45 degree angle the maximum total weight that may be exerted dynamically on the geometric center of the module support plate *(which is connected to all six sensors)* is 4.23 kg. That is equal to a maximum dynamic load of:	=< 41.54	N	**PCB209C11 datasheet**	http://cmt.mapper/ShowItem?docid=77748&n=1	
FORCESIX-MECH-014	The maximum **dynamic** axial load that each piezo-electric sensor may be subjected to in **tension** is 4.45 N = 0.45 kg. Given the fact that there are 6 piezo sensors that are all mounted under a 45 degree angle the maximum total force that may be exerted dynamically on the geometric center of the module support plate *(which is connected to all six sensors)* is:	=< 18.88	N	**PCB209C11 datasheet**	http://cmt.mapper/ShowItem?docid=77748&n=1	
FORCESIX-MECH-015	The surface on which the bottom of the piezo will be mounted (define side of piezo with 10-32 UNF-2B threading as bottom, and side with 2-56 UNC-2B threading as the top) must have a flatness and surface finish of respectively:	0.001 TIR (~0.03 mu) & 1.6 Ra	-	**PCB209C11 datasheet**	http://cmt.mapper/ShowItem?docid=77748&n=1	by design

F-2: Forcesix – Requirement Sheet

MAPPER lithography

SCREENSHOT 3

FORCESIX-MECH-016	The angle between two piezos must be tuned for maximum in-plane sensitivity (see **FORCESIX-TECH-003**) while minimizing the effect of parasitic forces and complying with the static load requirements (**FORCESIX-MECH-007** & **FORCESIX-MECH-008**). Minimum angle required to meet **FORCESIX-TECH-002** is:	>= 42.3	degrees	Matlab model Arwi - Global Stiffness Matrix	For angle definition see support drawings: **SD-2 ; theta-y**	
FORCESIX-MECH-017	In order for the performance of this (passive) setup to meet the set requirements, proper tuning of the dynamics of the bottom part is essential. This poses requirements on the mass-damping- and stiffness (eigenfrequency) values of the granite plates, airmounts and the mounting methods of all interconnections. The following requirements have to ensure sufficient attenuation of floor vibrations (transmissibility) while at the same time allowing for direct-disturbance forces (compliancy) to be measurable.					
FORCESIX-MECH-018	The double mass-spring-damper system has been tuned such, that sufficient attenuation of floor vibrations is achieved whilst keeping a good S/N ratio. This poses the mass requirement on the bottom granite plate that it must be in the range:	450-620	kg	Matlab model ArWi - Dynamics Forcesix		**Selected:** Mytri Fine Black Graniet *(large heat capacity, temperature stable, mechanically stiff, high tolerances)*: 1200x800x200 mm = 576 kg
FORCESIX-MECH-019	The **combined** eigenfrequency of the bottom set of airmounts, under the given load, must be less than	=< 4	Hz	Matlab model ArWi - Dynamics Forcesix	**schematics SLM-12A:** http://cmt.mapper/ShowItem?docid=77834&n=1 **natural frequency / load:** http://cmt.mapper/ShowItem?docid=77836&n=1	**SLM-12A chosen:** Total load 576+2(airmounts)+117(alles daarboven zie hieronder bij SLM-3a) = 695 + casing van nog eens ~100 kg zitten we op 800 = 73.5%= of max load (4*272kg). Dan ongeveer 3.1 Hz eigenfrequency. Verify through Stone
FORCESIX-MECH-020	The double mass-spring-damper system has been tuned such, that sufficient attenuation of floor vibrations is achieved whilst keeping a good S/N ratio. This poses the mass requirement on the top granite plate that it must be in the range::	80-190	kg	Matlab model ArWi - Dynamics Forcesix		Selected: Mytri Fine Black Graniet (large heat capacity, temperature stable, mechanically stiff, high tolerances): 630x630x80 mm = 95 kg
FORCESIX-MECH-021	The **combined** eigenfrequency of the top set of airmounts, under the given load, must be less than:	=< 5	Hz	Matlab model ArWi - Dynamics Forcesix	**schematics SLM-3A:** http://cmt.mapper/ShowItem?docid=77834&n=1 **natural frequency / load:** http://cmt.mapper/ShowItem?docid=77836&n=1	**SLM-3A selected:** Total load = 95 + 12 + 10 = 117 kg = 21.7% of max load (4*135kg). Dan ongeveer 5 Hz eigenfrequency. Verify through Stone acceleration
FORCESIX-MECH-022	The acoustical attenuation spectrum (ratio / frequency band) that must be achieved over the frequency range [0-3000 Hz], should be equal or better as that of Vibronix. Slide 22 of Forcesix presentations - Concept Design v01-00: [REF] shows this previously measured spectrum. For clarity, this regards the ratio (ACi / AC) with the measured signal expressed as a Power Spectral Density (PSD) function of the sound pressure level [Pa^2/Hz]. On top of that, the attenuation in the frequency bands [80-120 Hz] and [140-170 Hz] must be significantly improved and be brought back to an average attenuation factor of at least:	=< 0.01	[-]	Matlab model ArWi - Effect of Parasitic Forces	**Forcesix presentations - Concept Design v01-00:** http://cmt.mapper/ShowItem?docid=78033&n=1	Perform measurements inside and outside the acoustical case using the following BruelKjaer microphone: **Type:** 4189-A-021 *with pre-amp* 2671
FORCESIX-MECH-023	In case of rupture of the tubing or leaking in general, both the piezo-electric sensors as well as the module under testing need to be protected against any water spills. The design of Forcesix should therefore incorporate a drip tray to account for water leaking directly onto the sensitive areas.	-	[-]			The Module Support Frame (MSF) and Base Frame (BF) have been designed such that it is very unlikely for water spills to reach the piezo-electric sensors due to their shapes and the raised edges for module interfacing. Furthermore, the orientation of the modules is such that they

MAPPER lithography

SCREENSHOT 4

FORCESIX-MECH-024	Due to the sensitive nature of the piezos [see FORCESIX-MECH-008 t/m 014] in the XY and Z direction, preventive measures shall be taken to ensure that the piezos cannot be overloaded in any of those directions. Not by static weight, nor by accidental overload / bumps / impulse forces.	-	[-]			Perform measurements inside and outside the acoustical case using the following BruelKjaer microphone: **Type:** 4189-A-021 *with pre-amp* 2671
FORCESIX-ELEC-000	**Electrical Requirements**					
FORCESIX-ELEC-001	The measurement is of the IEPE type. This means that a constant excitation voltage is required between:	18-30	V (DC)	**PCB209C11 datasheet**	**See support drawing: SD-7** http://cmt.mapper/ShowItem?docid=77748&n=1	By design
FORCESIX-ELEC-002	The measurement is of the IEPE type. This means that a constant current (bias) excitation is needed of:	2-20	mA	**PCB209C11 datasheet**	**See support drawing: SD-7** http://cmt.mapper/ShowItem?docid=77748&n=1	By design
FORCESIX-ELEC-002	Due to the non-isolated casing of the PCB209C11 and the high risk of ground loops, the pigtales (metal plated SMB connectors) are not allowed to touch each other during a measurement. Care must be taken to ensure they are electrically isolated up to:	1,00E+00	kV			Incorporated in measurement plan.
FORCESIX-ELEC-003	Due to the non-isolated casing of the PCB209C11 and the high risk of ground loops, the top and bottom of the piezo need to be lectrically isolated up to: ***Note: whatever isolation method will be used, a high mechanical stiffness as defined in FORCESIX-MECH-017, must still be achieved!***	1,00E+00	kV		See support drawings: **SD-4** and **SD-6**	**top part:** Isolate strut by pre-glueing with Loctite Hysol 9492, prior to making glue connection **bottom part:** use electrically non-conductive bus (nylon6) and ESD foil
FORCESIX-MAT-000	**Material Requirements**					
FORCESIX-MAT-001	The materials used in Forcesix will be according to [Justif. doc]	-	-	**Mapper Materials Sheet v01-05**	http://cmt/ShowItem?docid=6	Check design documents.
FORCESIX-MAT-002	The total costs of the setup shall remain below:	<= X K€	-			**Arjan:** 22.891 € 73 € 20 € 445 € 66 € **Mahmut** 2.238 € 761 € 143 € 83 € 8 € 921 € **Facilities** 300 € 100 € 5.000 € ============== 33.049 €
FORCESIX-CS-000	**Coordinate System Requirements**					
FORCESIX-CS-001	All coordinate systems must use cartesian coordinates (XYZ) using RHR.	-	-			
FORCESIX-CS-002	Modules for testing are to be placed in the test-setup in the same orientation as in Matrix. When processing results, a conversion will have to be made from the location and orientation of the CS used in Forcesix and that of Matrix (GCS). This to ensure that the measured forces are compared to the right requirements (cooling budgets).	-	-	**Galactic Coordinate System - theoretical point in Matrix.**	http://cmt.mapper/ShowItem?docid=23779&n=4	
				Matrix positions in different coordinate systems	http://cmt.mapper/ShowItem?docid=34603&n=2	
				Conversion of Coordinate Systems v01-06.xls	http://cmt.mapper/ShowItem?docid=26233&n=7	

App. G

Data Sheets

G-1: Piezoelectric Sensor

MAPPER lithography

PCB – 209C11

Model Number 209C11	FORCE SENSOR, ICP®	Revision E ECN #: 25168

Performance	ENGLISH	SI	
Sensitivity (±15 %)	2200 mV/lb	494604 mV/kN	
Measurement Range (Compression)	2.2 lb	0.00979 kN	
Measurement Range (Tension)	1.0 lb	0.00445 kN	
Maximum Static Force (Compression)	11 lb	0.0489 kN	
Maximum Static Force (Tension)	1.0 lb	0.00445 kN	
Broadband Resolution (1 to 10000 Hz)	0.00002 lb-rms	0.00009 N-rms	[1]
Low Frequency Response (-5 %)	0.5 Hz	0.5 Hz	[2]
Upper Frequency Limit	30 kHz	30 kHz	[3]
Environmental			
Temperature Range	-65 to +250 °F	-54 to +121 °C	
Temperature Coefficient of Sensitivity	≤0.05 %/°F	≤0.09 %/°C	
Electrical			
Discharge Time Constant (at room temp)	≥1 sec	≥1 sec	
Excitation Voltage	18 to 30 VDC	18 to 30 VDC	
Constant Current Excitation	2 to 20 mA	2 to 20 mA	
Output Impedance	≤100 Ohm	≤100 Ohm	
Output Bias Voltage	8 to 12 VDC	8 to 12 VDC	
Spectral Noise (1 Hz)	0.0000044 lb/√Hz	0.0000197 N/√Hz	[1]
Spectral Noise (10 Hz)	0.0000005 lb/√Hz	0.0000021 N/√Hz	[1]
Spectral Noise (100 Hz)	0.0000001 lb/√Hz	0.0000006 N/√Hz	[1]
Spectral Noise (1000 Hz)	0 lb/√Hz	0.0000002 N/√Hz	[1]
Output Polarity (Compression)	Positive	Positive	
Physical			
Stiffness	2 lb/µin	0.35 kN/µm	[1]
Size (Hex x Height)	0.375 in x 0.83 in	9.53 mm x 21.08 mm	
Weight	0.29 oz	8.2 gm	
Housing Material	Stainless Steel	Stainless Steel	
Sealing	Hermetic	Hermetic	
Electrical Connector	10-32 Coaxial Jack	10-32 Coaxial Jack	
Electrical Connection Position	Side	Side	
Mounting Thread	10-32 Female	No Metric Equivalent	
Mounting Torque (Recommended)	15 to 20	169 to 226	

CE[4]

All specifications are at room temperature unless otherwise specified.
In the interest of constant product improvement, we reserve the right to change specifications without notice.
ICP® is a registered trademark of PCB group, Inc.

Optional Versions (Optional versions have identical specifications and accessories as listed for standard model except where noted below. More than one option maybe used.)

M - Metric Mount
Supplied Accessory: Model M081A05 Mounting Stud

N - Negative Output Polarity

Output Polarity (Compression)	Negative	Negative

W - Water Resistant Cable

Electrical Connector	Sealed Cable	Sealed Cable
Electrical Connection Position	Side	Side

Notes
[1] Typical.
[2] Calculated from discharge time constant.
[3] Estimated using rigid body dynamics calculations.
[4] See PCB Declaration of Conformance PS023 for details.

Supplied Accessories
081A05 Mounting stud, 10-32 to 10-32 x 0.27" long, BeCu (H900), no shoulder (1)
084A38 Thermal boot (for Series 209) (1)

Entered: BLS	Engineer: RWM	Sales: MJK	Approved: BLS	Spec Number:
Date: 10/20/2006	Date: 10/23/2006	Date: 10/20/2006	Date: 10/24/2006	8891

PCB PIEZOTRONICS FORCE / TORQUE DIVISION
3425 Walden Avenue
Depew, NY 14043
UNITED STATES
Phone: 800-828-8840
Fax: 716-684-0987
E-mail: info@pcb.com
Web site: www.pcb.com

G-2: Seismic Accelerometer

MAPPER lithography

Endevco – M86 & Wilcoxon – 731A

Model 86
Seismic accelerometer

Endevco

Specifications

The following performance specifications conform to ISA-RP-37.2 (1964) and are typical values, referenced at +75°F (+24°C) and 100 Hz, unless otherwise noted. Calibration data, traceable to National Institute of Standards and Technology (NIST), is supplied.

Dynamic characteristics	Units	
Range	g pk	±0.5
Voltage sensitivity, ±10%	V/g	10
Frequency response (ref @ 20 Hz)		Typical
Resonance frequency (typical)	Hz	370
Amplitude response		
±1 dB	Hz	0.005 to 100
±3 dB	Hz	0.003 to 200
Transverse sensitivity	%	≤ 1
Temperature response	%	±5 from -10°C to 100°C
Amplitude non-linearity, to full scale	%	±1
Output characteristics		
Output polarity		Acceleration directed into base produces positive output
DC output bias voltage	Vdc	+9 to +13 @ 75°F (24°C)
Output impedance	Ω	≤ 10
Full scale output voltage	V	±5
Residual noise		
broadband, 0.1 Hz to 1 k Hz, typical	equiv. ng rms	100
spectral, 0.5 Hz	equiv. ng/√Hz	52
spectral, 1 Hz	equiv. ng/√Hz	39
spectral, 10 Hz	equiv. ng/√Hz	11
spectral, 100 Hz	equiv. ng/√Hz	4
Grounding		Signal ground electrically isolated from case (>50MΩ)
Power requirement		
Supply voltage	Vdc	+24 to +30
Supply current	mA	+2 to +10
Warm-up time	minutes	4
Environmental characteristics		
Temperature range	°F (°C)	-4°F to +212°F (-20°C to +100°C)
Humidity		Hermetically sealed
Base strain sensitivity at 250 μstrain	eq. g/μstrain	0.0001
Sinusoidal vibration limit	g pk	10
Shock limit	g pk	250
Physical characteristics		
Dimensions		See outline drawing
Weight	gm (lb)	771 (1.70)
Case material		Stainless Steel
Connector		Top mounted 2-pin MS 3106-10SL-4S
Calibration		
Supplied:		
Voltage sensitivity @ 10 Hz	V/g	
Maximum transverse sensitivity	%	
Frequency response	%	1 Hz to 100 Hz

Features
- Ultra high sensitivity
- Ultra low-noise electronics for clear signals at sub micro-g levels
- Low frequency capable
- Low pass filtered to eliminate high frequencies
- Reverse wiring protection

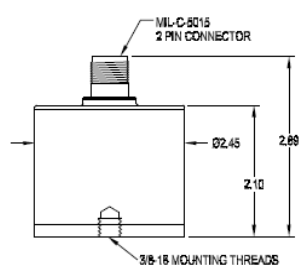

Wilcoxon Research

Model 731A
Ultra-quiet, ultra low frequency, seismic accelerometer

Dynamic	
Sensitivity, ±10%, 25°C	10 V/g
Acceleration range	0.5 g peak
Amplitude nonlinearity	1%
Frequency response:	
±10%	0.10 - 300 Hz
±3 dB	0.05 - 450 Hz
Resonance frequency	750 Hz
Transverse sensitivity, max.	1% of axial
Temperature response:	
−10°C	−12%
+65°C	+5%
Electrical	
Power requirement: voltage source	18 - 30 VDC
current regulating diode	2 - 10 mA
Electrical noise, equiv. g:	
Broadband 2.5 Hz to 25 kHz	0.5 μg
Spectral 2 Hz	0.03 μg/√Hz
10 Hz	0.01 μg/√Hz
100 Hz	0.004 μg/√Hz
Output impedance, max.	100Ω
Bias output voltage	9 VDC
Grounding	case isolated
Environmental	
Temperature range	−10 to 65°C
Vibration limit	10 g peak
Shock limit	fragile
Electromagnetic sensitivity @ 60 Hz	20 μg/gauss
Sealing	hermetic
Base strain sensitivity	0.0001 g/μstrain
Physical	
Sensing element design	PZT ceramic / flexure
Weight	775 grams
Case material	316L stainless steel
Mounting	3/8 - 16 tapped hole
Output connector	2 pin, MIL-C-5015 style
Mating connector	R6 type
Recommended cabling	J9 / J9T2A

Connector pin	Function
Shell	ground
A	power/ signal
B	common

Note: Special handling required due to sensitivity, wooden protective case included

Accessories supplied: SF7 mounting stud; calibration data (level 3)

Options: Power unit/amplifier P31

Bruel Kjaer – 8344 & 4513-002

Specifications – DeltaTron Accelerometer Type 8344

	Unit	8344*
Dynamic Characteristic		
Voltage Sensitivity (@ 159.2 Hz and 4 mA supply current)	mV/ms^{-2} (mV/g)	250±20% (2500±20%)
Measuring Range	ms^{-2} peak (g peak)	±26 (2.6)
Frequency Range (±10% limit) Amplitude Response	Hz	0.2–3000
Frequency Response		See individual Frequency Response on calibration chart
Mounted Resonance Frequency	kHz	>10
Transverse Sensitivity (@ 30 Hz, 100 ms^{-2})	%	<5 of the sensitivity of the axis in question
Transverse Resonance Frequency	kHz	3.5
Polarity		Polarity of the electrical signal is positive for an acceleration in the direction of the arrow on the drawing
Electrical Characteristics		
Bias Voltage (at full temperature and current range)	V_{dc}	13 ±1
Power Supply Constant current Unloaded Supply Voltage	 mA V	 2 to 20 +24 to +30
Output Impedance	Ω	<30
Start-up Time	s	<30
Residual Noise (RMS) Broadband noise (0.2 Hz to 3 kHz) Spectral: 1 Hz 10 Hz 100 Hz 1000 Hz	 μV (μg) $ms^{-2}/\sqrt{Hz}$ ($\mu g/\sqrt{Hz}$)	 113(45) 1.1×10^{-4} (11) 7.75×10^{-6} (0.78) 7.75×10^{-7} (0.078) 3.46×10^{-7} (0.035)
Signal Grounded		Connected to case
Environmental Characteristics		
Operating Temperature Range	°C (°F)	−50 to +100 (−58 to +212)
Temperature Coefficient of Sensitivity	%/°C	+0.05
Temperature Transient Sensitivity (3 Hz LLF, 20 dB/decade)	ms^{-2}/°C	0.001
Base Strain Sensitivity (at 250 με in base plane)	Equiv. ms^{-2}/με (g/με)	0.002 (0.0002)
Magnetic Sensitivity (50 Hz, 0.038 T)	ms^{-2}/T (g/T)	0.5 (0.05)
Max. Non-destructive Shock	ms^{-2} peak (g peak)	3500 (350)
Humidity		100% RH non-condensing
Physical Characteristics		
Case Material		Stainless steel AISI 316–L
Sensing Element		Piezoelectric, Type PZ 27
Construction		DeltaShear
Sealing		Hermetically sealed
Weight (excluding cable)	gram (oz.)	176 (6.2)
Electrical Connector		10–32 UNF
Mounting		M5
Mounting Torque	Nm (lbf-in)	Max. 3.5 (31), Min 0.5 (4.4)
Dimensions		See outline drawing

Ordering Information

Type 8344 Includes the following accessory:
- Calibration Chart

Optional Accessories*	
AO-0038-D-xxx	Teflon® super low-noise cable, 10–32 UNF to 10–32 UNF. –75 °C to +250 °C.
AO-0531-D-xxx	PVC coaxial single-screen cable. 10–32 UNF to BNC. –20 °C to +70 °C
QA-0068	Tap for M5 thread
JP-0145	Plug adaptor, BNC to 10–32 UNF
UA-0186	Extension connector for 10-32 UNF cables, set of 25
QS-0007	Tube of cyanoacrylate adhesive
YJ-0216	Beeswax for mounting
Type 4294-002	Calibration Exciter
Calibration Services	
8344-CFF	Factory Standard Calibration including programming of TEDS
8344-CAF	Accredited Calibration including programming of TEDS
8344-CAI	Accredited Initial Calibration including programming of TEDS
8344-CTF	Traceable Calibration including programming of TEDS

* Additional accessories, cables and services are available (see www.bksv.com)

CE Compliance with EMC Directive and Low Voltage Directive of the EU
Compliance with the EMC requirements of Australia and New Zealand

Specifications – General Purpose DeltaTron Accelerometers Types 4513(-B), 4513(-B)-001 and 4513(-B)-002

	Units	4513/ 4513-B	4513-001/ 4513-B-001	4513-002/ 4513-B-002
Dynamic Characteristics				
Voltage Sensitivity (@ 160 Hz)	mV/ms^{-2} (mV/g)	1 +12/–8% (10 ± 10%)	10 +12/–8% (100 ± 10%)	50 +12/–8% (500 ± 10%)
Measuring Range (±pk)	ms^{-2} (g)	4900 (500)	490 (50)	98 (10)
Frequency Response		See typical amplitude response		
Mounted Resonance Frequency	kHz	32		
Amplitude Response ±10% (typical)[a]	Hz	1 to 10000		
Residual Noise	mg	0.8	0.2	0.1
Transverse Sensitivity	%	<5		
Electrical Characteristics				
Output Impedance (typical)	Ω	20	100	200
DC Output Bias Voltage – At room temperature	V	12 ± 1		
DC Output Bias Voltage – In specified temperature range	V	8 to 16		
Power Supply	mA	2 to 20		
Start-up Time	s	1	1	3
Grounding		Insulated base		
Environmental Characteristics				
Temperature Range	°C (°F)	–51 to +121 (–60 to +250)	–51 to +100 (–60 to +212)	–51 to +100 (–60 to +212)
Humidity		Hermetically sealed		
Max. Operational Shock (peak)	g pk	5000		
Base Strain Sensitivity	Equiv. g/μ strain	0.003		
Thermal Transient Sensitivity	Equiv. %/°C (%/°F)	0.24 (0.13)		
Thermal Shock Sensitivity	g/°C	0.04		
Physical Characteristics				
Dimensions		See outline drawing		
Weight	gram (oz.)	8.6 (0.3)		
Case Material		Titanium		
Connector		10–32 UNF		
Mounting		10–32 UNF threaded hole		
Mounting Torque	Nm (lb.in.)	1.7 (15)		

a. Individual frequency response calibration up to 10 kHz
All values are typical at 25°C (77°F) unless measurement uncertainty is specified.

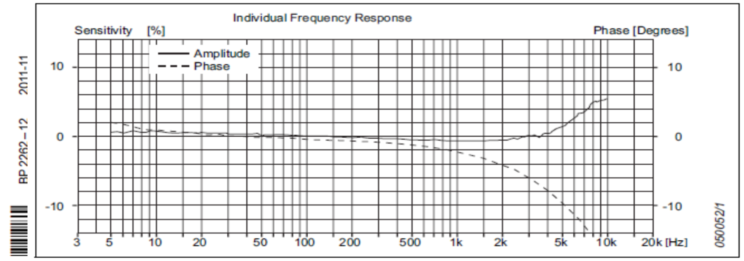

G-4: Free-field Microphone

Bruel Kjaer – 4189 A 021 w/preamp 2671

Brüel & Kjær TEDS Microphone Data

The microphones below are organised by the type of sound field that they are designed to measure.

Common Specifications

For detailed specifications please see the Product Data for the individual microphones and preamplifiers. Unless otherwise stated all specifications in this Product Data are valid under the following conditions:

CCLD input types	24 V compliance voltage
Classical input types	120 V_{DC} supply
Dynamic range low limit	Noise floor dB A
Dynamic range high limit	3% distortion limit in dB SPL RMS rounded to nearest integer The undistorted peak level will normally be 3 dB higher
Cartridge sensitivity	Nominal
TEDS microphone sensitivity	Stated as the nominal cartridge sensitivity except for small cartridges where the loaded sensitivity differs considerably from the open-circuit sensitivity

Temperature Range

The read/write temperature range of the TEDS chip is guaranteed by the chip manufacturer up to 85ºC (185ºF) only, but the TEDS chip will survive the full specified temperature range of the TEDS microphone/ preamplifier without any damage.

Standard preamplifiers (Types 2669, 2670, 2671, 2699) go to 80°C (176°F). High-temperature preamplifier Type 1706 goes to 125°C (257°C). Remember also to use cables with the correct temperature range.

Cable Length

TEDS will normally work with cables up to 100 m (328 ft).

Free-field TEDS Microphones

Free-field microphones are designed to have a flat frequency response in a free field. At higher frequencies, reflections and diffractions cause a pressure increase in front of the diaphragm. If not corrected for, this would result in an increased output voltage from the microphone, free-field optimization means that the frequency response of the microphone has been designed in such a way that a flat free-field frequency response at 0° angle of incidence is achieved.

Free-field microphones are commonly used for sound measurement in an anechoic chamber or far away from reflecting buildings, etc. Another area for free-field microphones is general electroacoustic purposes like loudspeaker and microphone measurements.

***Table1** Free-field TEDS microphones with Type 4188 ½″cartridge*

Input	Microphone	Preamplifier	mV/Pa	dB re 1 V/Pa	±2 dB Frequency Range (Hz)	Dynamic Range (dB)
Classical	Type 4188-B/C/L-001	Type 2669-B/C/L	31.6	–30	8 to 12.5 k	15.8 to 146
CCLD	Type 4188-A-021	Type 2671	31.6	–30	20 to 12.5 k	19 to 138
CCLD	Type 4188-A-031	Type 2699	31.6	–30	A-weighted	21 to 135

Type 4188 is suited for free-field measurements where an extra-robust prepolarized microphone with medium sensitivity is required
Type 4188 TEDS microphones come without a data CD and with typical frequency response on the calibration chart

***Table2** Free-field TEDS microphones with Type 4189 ½″cartridge*

Input	Microphone	Preamplifier	mV/Pa	dB re 1 V/Pa	±2 dB Frequency Range (Hz)	Dynamic Range (dB)
Classical	Type 4189-B/C/L-001	Type 2669-B/C/L	50	–26	6.3 to 20 k	15.2 to 146
CCLD	Type 4189-A-021	Type 2671	50	–26	20 to 20 k	16.5 to 134
CCLD	Type 4189-A-031	Type 2699	50	–26	A-weighted	18 to 131
CCLD	Type 4189-W-003	Type 2671-W-001	50	–26	6.3 to 20 k	16.5 to 134
CCLD	Type 4189-H-041	Type 1706	50	–26	6.3 to 20 k	16.5 to 134

Type 4189 is suited for free-field measurements where a high-sensitivity prepolarized microphone with full 20 kHz bandwidth is preferred
Type 4189 TEDS microphones come with an individual data CD and with individual frequency response on the calibration chart

G-5: DAQ Card NI

MAPPER lithography

National Instruments – PCI 4472 & PCI 6229

Specifications

Typical for 25 °C unless otherwise noted.

Analog Input

Channel Characteristics

Number of channels	
NI 4472 Series	8, simultaneously sampled
NI 4474 Series	4, simultaneously sampled
Input configuration	Unbalanced differential
Resolution	24 bits, nominal
Type of ADC	Delta-sigma
Oversampling, for sample rate (f_s):	
1.0 kS/s $\le f_s \le$ 51.2 kS/s	128 f_s
51.2 kS/s $< f_s \le$ 102.4 kS/s	64 f_s
Sample rates (f_s)	1.0 to 102.4 kS/s in 190.7 µS/s increments for $f_s >$ 51.2 kS/s or 95.36 µS/s increments for $f_s \le$ 51.2 kS/s
Frequency accuracy	±25 ppm
Input signal range	±10 V peak
FIFO buffer size	1,024 samples
Data transfers	DMA

Transfer Characteristics

Offset (residual DC)	±3 mV, max
Gain (amplitude accuracy)	±0.1 dB, max, f_{in} = 1 kHz

Amplifier Characteristics

Input impedance (ground referenced)	
Positive input	1 MΩ in parallel with 60 pF
Negative input (shield)	50 Ω in parallel with 0.02 µF
Flatness (relative to 1 kHz)	±0.1 dB, DC to 0.4535 f_s, max, DC-coupled
-3 dB bandwidth	0.4863 f_s
Input coupling	AC or DC, software-selectable
AC -3 dB cutoff frequency	
NI 4472, NI 4474	3.4 Hz
NI 4472B	0.5 Hz
Overvoltage protection	
Positive input	±42.4 V
Positive inputs protected	CH<0..7>
Negative input (shield)	Not protected, rated at ±2.5 V
Common-mode rejection ratio (CMRR)	
f_{in} < 1 kHz	>60 dB, minimum

Dynamic Characteristics

Alias-free bandwidth (passband)	DC (0 Hz) to 0.4535 f_s
Stop band	0.5465 f_s
Alias rejection	110 dB
Spurious-free dynamic range	130 dB, 1.0 kS/s $\le f_s \le$ 51.2 kS/s
	118 dB, 51.2 kS/s $< f_s \le$ 102.4 kS/s
THD, f_{in} = 1 kHz	
0 dBFS input	<-90 dB
20 dBFS input	<-100 dB
60 dBFS input	<-60 dB
IMD	<-100 dB (CCIF 14 kHz + 15 kHz)
Crosstalk[1] (channel separation), f_{in} = 0 to 51.2 kHz	
Between channels 0 and 1, 2 and 3, 4 and 5, or 6 and 7	
Shorted input	<-90 dB
1 kΩ load	<-80 dB
Other channel combinations	
Shorted input	<-100 dB
1 kΩ load	<-90 dB
Phase linearity	<±0.5 deg
Interchannel phase mismatch	<f_{in} (in kHz) x 0.018 deg + 0.082 deg
Interchannel gain mismatch	±0.1 dB
Filter delay through ADC	38.8 sample periods

Onboard Calibration Reference

DC level	5.000 V ±2.5 mV
Temperature coefficient	±5 ppm/°C maximum
Long-term stability	±20 ppm/√1,000 h

Signal Conditioning

Constant current source (software-controlled)	
Current	4 mA, ±5%
Compliance	24 V
Output impedance	>250 kΩ at 1 kHz
Current noise	<500 pA/√Hz

Triggers

Analog Trigger

Source	CH<0..7>
Level	-10 to +10 V, full scale, programmable
Slope	Positive or negative (software-selectable)
Resolution	24 bits, nominal
Hysteresis	Programmable

Digital Trigger

Compatibility	5 V TTL/CMOS
Response	Rising or falling edge
Pulse width	10 ns, minimum

Bus Interface

Type	Master, slave

Power Requirements

+3.3 VDC	
PXI	400 mA, maximum
+5 VDC	
PCI	2.6 A, maximum
PXI	2.2 A, maximum
+12 VDC	120 mA, maximum
-12 VDC	120 mA, maximum

Detailed Specifications

Specifications listed below are typical at 25 °C unless otherwise noted. Refer to the *M Series User Manual* for more information about NI 622x devices.

Analog Input	
Number of channels	
NI 6220/6221	8 differential or 16 single ended
NI 6224/6229	16 differential or 32 single ended
NI 6225	40 differential or 80 single ended
ADC resolution	16 bits
DNL	No missing codes guaranteed
INL	Refer to the *AI Absolute Accuracy Table*
Sampling rate	
Maximum	250 kS/s single channel, 250 kS/s multi-channel (aggregate)
Minimum	No minimum
Timing accuracy	50 ppm of sample rate
Timing resolution	50 ns
Input coupling	DC
Input range	±10 V, ±5 V, ±1 V, ±0.2 V
Maximum working voltage for analog inputs (signal + common mode)	±11 V of AI GND
CMRR (DC to 60 Hz)	92 dB
Input impedance	
Device on	
AI+ to AI GND	>10 GΩ in parallel with 100 pF
AI- to AI GND	>10 GΩ in parallel with 100 pF
Device off	
AI+ to AI GND	820 Ω
AI- to AI GND	820 Ω
Input bias current	±100 pA
Crosstalk (at 100 kHz)	
Adjacent channels	-75 dB
Non-adjacent channels	-90 dB[1]

Bibliography

External & Mapper

Bibliography

Anagnostopoulos, P. (2002). *Flow-Induced Vibrations in Engineering Practice*. WIT Press. ISBN: 978-1-853-12644-4. Cited on: pp. 3-12, 16-19.

ASML (2019a). "History of ASML". Available from: https://www.asml.com/en/company/about-asml/history (Accessed July 18th, 2019).

ASML (2019b). "What's next for ASML". Available from: https://www.asml.com/en/technology#whats-next (Accessed June 16th, 2019).

Belmans, R. and Binns, K. (2012). *Vibrations and Audible Noise in Alternating Current Machines*. Kluwer Academic Publishers. ISBN: 978-94-010-7767-5. Cited on: pp. 225.

Bentley, J. P. (2005). *Principles of Measurement Systems*. Pearson - Prentice Hall. ISBN: 978-0-13-043028-1 (Fourth Edition). Cited on: pp. 3-5, 12-13, 97-104, 110,120, 182-188, 219, 247-250, 477.

Cook, R. D., Malkus, D. S., Plesha, M. E., and Witt, R. J. (2002). *Concepts and Application of Finite Element Analysis*. John Wiley & Sons. ISBN: 978-0-471-35605-9 (Fourth Edition). Cited on: pp. 271-283.

EETimes (2017). "TSMC says 3nm plant could cost more than $20B". Available from: https://www.eetimes.com/report-tsmcs-3nm-fab-could-cost-20-billion (Accessed Nov 23rd, 2018).

Ellenbroek, R. (2013). "Mapper Internal Documentation - Stage Stability Budgeting for Matrix V02-01". Cited on p. 2, 6, 43.

Fish, P. (1993). *Electronic Noise and Low Noise Design*. McGraw-Hill. ISBN: 978-0-333-57309-9. Cited on: pp. 124,131,346-356,414-421.

Hisland, M. B. and Alciatore, D. G. (2012). *Introduction to Mechatronics and Measurement Systems*. McGraw-Hill. ISBN: 978-0-07-338023-0 (Fourth Edition). Cited on: pp. 232.

Intel (2012). "Process steps in chip production". Available from: https://www.youtube.com/watch?v=d9SWNLZvA8g/.

Jabben, L. (2007). "Mechatronic Design of a Magnetically Suspended Rotating Platform". Published by: Mechatronics - Dynamic Error Budgeting - Chapter 3. (Accessed Dec. 23rd, 2012).

Kaneko, S., Nakamura, T., Inada, F., and Kato, M. (2008). *Flow-Induced Vibrations - Classifications and Lessons from Practical Experiences*. Elsevier Science. ISBN: 978-0-080-44954-8. Cited on: pp. 1-7, 145-174, 189-193.

Kurzweil, R. (2006). *The Singularity Is Near - When Humans Trancend Biology*. Penguin Publishing Group. ISBN: 978-0-143-03788-0. Cited on: pp. 17-24.

Lakerveld, D. (2013). *Vibration Isolation - On the determination of direct disturbance forces*. TU Delft Repository. ISBN: 978-9-46186-110-8. Available from: http://resolver.tudelft.nl/uuid:52954fdf-82a0-4eb3-aac5-e3c5b9b2a5f9. Cited on: pp. 997-999.

Lamancusa, J. (2002). "Vibration Isolation & Noise Control". Published by: PennState University. Available from: https://www.mne.psu.edu/lamancusa/me458/12_vibration.pdf/ (Accessed Jan. 6th, 2011).

LaPedus, M. (2017). "Battling Fab Cycle Times". Available from: https://semiengineering.com/battling-fab-cycle-times/ (Accessed Dec 5th, 2018).

Lemmen, M., Pijnenburg, J., and van Wakeren, J. (2009). *Cooling Concepts Mapper Aperture Array - including vibration analysis caused by turbulence and pressure fluctuations in cooling channels*. TNO Industry & Technology. Project: 033.21136. Mapper ID: FFP-ILO-DD-007-v0. Cited on: pp. 23, 71-73, 75, 92, 113, 134.

Megens, H. (2007). "An Introduction to Photolithography Overlay". *ASML Images*, 10(3). Issue: Fall Edition 2007. Available from: https://staticwww.asml.com/doclib/productandservices/images/asml_overlay_images_fall07.pdf (Accessed Jul 17th, 2018). Cited on p.2.

Moody's (2018). "Credit Analysis". Available from: https://staticwww.asml.com/doclib/investor/misc/asml_20181212_2018-12-12_ASML_CO_Moodys.pdf (Accessed Jan 15th, 2019).

Naudascher, E. and Rockwell, D. (1994). *Flow-Induced Vibrations - An Engineering Guide*. A.A. Balkema. ISBN: 978-90-5410-131-4. Cited on: pp. 7-16, 91-104.

Pil, A. (2015). "Lithografiemachine Mapper bijna productierijp". Published by: Mechatronica Machinebouw. Available from: https://mechatronicamachinebouw.nl/artikel/asmls-multi-e-beam-metrologietool-vertraagd/ (Accessed July. 5th, 2015).

Rao, S. (2004). *Mechanical Vibrations*. Pearson - Prentice Hall. ISBN: 0-13-120768-7. Cited on: pp. 238, 479.

Schmidt, R. M., Schitter, G., and van Eijk, J. (2011). *The Design of High Performance Mechatronics*. IOS - Delft University Press. ISBN: 978-1-60750-825-0. Cited on: pp. 23-37, 70-136, 167, 551, 555, 731: design rules for precision.

Schweder, J. (2017). "Turning Out the Lights on the Factory Floor". Issue: Fall Edition 2007. Available from: https://www.automationworld.com/article/technologies/robotics/turning-out-lights-factory-floor (Accessed May 18th, 2018). Cited on p.2.

Sydenham, P. (2005). *Handbook of Measuring System Design*. John Wiley. ISBN: 9780470021439. Cited on: pp. 238, 479.

Sydenham, P. and Thorn, R. (1992). *Handbook of Measurement Science*. Wiley & Sons. ISBN: 0 471 92219 6 (Third Volume).

Tressler, J. F. (2003). "A comparison of single crystal versus ceramic piezoelectric materials for acoustic applications". Published by: The Journal of the Acoustical Society of America 113, 2311. Available from: https://ui.adsabs.harvard.edu/link_gateway/2003ASAJ..113.2311T/doi:10.1121/1.4780737 (Accessed Sept. 12th, 2011).

van Osch, M. and Smeulers, J. (2012). *Flow induced pulsation analysis inside cooling channels of Aperture Array*. TNO Industry & Technology. Project: 053.02781. TNO ID: RPT-DTS-2012-00926. Cited on: pp. 9-11, 19, 29, 43.

Vasilescu, G. (2005). *Electronic Noise and Interfering Signals - Principle and Applications*. Springer. ISBN: 3-540-40741-3 (Second Edition). Cited on: pp. 51-67, 444-478, 538, 577.

Veerapandi, R., Govindan, K., Jinu, G., and Kannaiah, R. (2019). "Experimental Study and Analysis of Flow Induced Vibration in a pipeline". *International Journal of Engineering Research & Technology (IJERT)*, 848. Available from: https://www.researchgate.net/publication/335737311_Experimental_Study_and_Analysis_of_Flow_Induced_Vibration_in_a_pipeline).

Wieland, M. (2017). "mapper: high throughput maskless lithography". Published by: CEA- Leti Alterative Lithography workshop 1. Available from: https://www.cea.fr/cea-tech/leti/Documents/%C3%A9v%C3%A9nements/Prez%20%20Leti%20Alternative%20Workshop/03%20-%20ML2%20-%20MAPPER%20-%20M%20Wieland%20-%20LETI%20WS%20SPIE%202018.pdf (Accessed Dec. 12th, 2020).

Wong, K. and Zhao, J. (2018). "Experimental investigation of flow-induced vibration of a sinusoidally rotating circular cylinder". *Journal of Fluid Mechanics*, 848. Published by: Cambridge University Press. Available from: https://doi.org/10.1017/jfm.2018.379 (Accessed Feb 12th, 2019).

Internal Mapper Documentation

MAPPER lithography

The following Reference Documents (RD) have been used to base design choices on

Internal documentation has been continuously updated; these are the versions that Forcesix is based on:

[RD.01] : Master Thesis DL – On the Determination of DDF [V01-00]

[RD.02] : UPW Cooling + Manifold PI&D Concept [V01-19]

[RD.03] : System Cooling Requirements Ultra Pure Water [V03-04]

[RD.04] : Stage Stability Budgeting for Matrix [V01-14]

[RD.05] : Report TNO Mapper Cooling concepts final

[RD.06] : Report TNO Mapper Flow Induced Pulsations inside the Aperture Array [V01-01]

[RD.07] : Estimate of Dynamic EO Position Errors caused by cooling water forces [V01-01]

[RD.08] : SUSA Tubing Flow Calculations Matrix [V01-15]

[RD.09] : ABC Pressure Drop Calculations [V01-00]

[RD.10] : SUSA Alignment Frame-Beam Generator Interface Requirements [V01-22]

[RD.11] : SUSA Alignment Frame-Projection Lens Interface Requirements [V01-18]

[RD.12] : SUSA – Beam Switcher Interface Requirements [V02-17]

[RD.13] : CON ABC - SUSA AF Interface requirements [V01-12]

[RD.14] : CLAA and IBC Cooling Concept report [V01-01]

Abbreviations

MAPPER lithography

Clustered per topic / sub-system

Matrix = **production tool developed by Mapper Lithography** *(prototype: FLX-1200)*

Forcesix = **newly designed measurement tool, objective of this Master thesis.** The constructed final design is able to: *"measure reaction forces exerted by the BSW, POS and ABC module on their environment from 10 – 300 Hz in 6-DOF"*

Vibronix = **existing measurement tool, result of thesis Dennis Lakerveld:** *"measuring 1-DOF accelerations of 1 geometry 20-90 Hz"* *(used to set requirements on the new design, flow testing insights, 'design lessons learned' and model validation purposes)*

DOF = **Degree-of-Freedom**

DEB = **Dynamic-Error-Budgeting** *(method to model the effect of various error sources acting through different transfer paths)*

DDF = **Direct-Disturbance-Forces** *(generally 'acting on a suspended mass' e.g. a pendulum or module under testing)*

FIV = **Flow-Induced-Vibrations** *(in general, as well as identified supply tubing disturbance source for the design of Forcesix)*

VI = **Vibration-Isolation** *(e.g. platform; methods to reduce the effect of transmitted floor vibrations on the sensing element)*

FV = **Floor-Vibrations** *(identified disturbance source for the design of Forcesix)*

AC = **Acoustics** *(identified disturbance source for the design of Forcesix)*

MSF = **Module-Support-Frame** *(part of M3, the top stage of Forcesix: connects rigidly to the piezos and clamps the modules)*

BF = **Base-Frame** *(part of M2, the middle stage of Forcesix: connects rigidly to the granite stone, mounting plate for piezos)*

ICP = **Integrated-Circuit-Piezoelectric** *(sensors with a built-in MOSFET microelectronic amplifier to convert the signal)*

IEPE = **Integrated-Electronics-Piezo-Electric** *(technical standard for sensors w/built-in impedance conversion electronics)*

DTC = **Discharge-Time-Constant** *(time required to discharge measured signal to 37% of its original value)*

SUSA = **Sub-System-Alignment** *(sub-system responsible for alignment of MOF w.r.t. WPS)*

VIM = **Vibration-Isolation-Module** *(suspending the MOF)*

MOF = **Metro-Optics-Frame** *(400 kg metal cage suspended from leaf springs, housing modules that produce electron beams)*

DUV / EUV = **Deep-Ultra-Violet / Extreme-Ultra-Violet**

Abbreviations

MAPPER lithography

Clustered per topic / sub-system

WPS	=	**Wafer-Positioning-System** *(system responsible for aligning the wafer underneath MOF with nanometer precision)*
WT	=	**Wafer-Table** *(part of WPS, mounted solid to the Chuck; reference of the MES interferometers)*
LS	=	**Long-Stroke Stage** *(part of WPS, responsible for the 'long stroke' to be able to step-scan the wafer over 300+150 mm)*
ShS	=	**Short-Stroke Stage** *(part of WPS, responsible for the 'short stroke' to be position the wafer with nanometer control)*
MES	=	**Metrology-System**
ALS	=	**Alignment-Sensor**
ILO	=	**Illumination-Optics** *(system responsible for creating, focusing and accelerating electron beams)*
BG	=	**Beam-Generator** *(module generating the uniform stream of electrons)*
EO	=	**Electron-Optics** *(methods to manipulate the current streams; 'optics for electron beams')*
BSW	=	**Beam-Switcher** *(module that create arrays of electron beams from the uniform electron beam created by the BG*
AA	=	**Aperture-Array** *(part of BSW module, dissipating most heat and cooled with water thus generating most FIV)*
IBC	=	**Individual-Beam-Corrector**
CL	=	**Condensor-Lense**
BLK	=	**Beam-Blanker**
BS	=	**Beam-Stop Array** *(element onto which the unnecessary current streams dissipate, part of BSW)*
BD	=	**Beam-Deflector Array** *(deflecting unnecessary beamlets, part of BSW)*
POS	=	**Projection-Optics** *(module containing the water-cooled PL that causes FIV, tested by Forcesix)*
PL	=	**Projection-Lense Array** *(fixed part of POS module, dissipating heat and water cooled thus generating FIV)*
CON	=	**Contamination sub-system** *(responsible for for cleaning MOF after exposures)*
ABC	=	**Advanced-Beam-Cleaner** *(module generating inert gas, requiring active water cooling thus generating FIV)*
WPH	=	**Wafers-Per-Hour**